The Dissertation Committee for Xi Chen Certifies that this is the approved version of the following dissertation:

Carbon Dioxide Thermodynamics, Kinetics, and Mass Transfer in Aqueous Piperazine Derivatives and Other Amines

Committee:

Gary T. Rochelle, Supervisor

Hal S. Alper

Steven L. Bryant

Brian A. Korgel

Venkat Ganesan

Carbon Dioxide Thermodynamics, Kinetics, and Mass Transfer in Aqueous Piperazine Derivatives and Other Amines

by

Xi Chen, B.E.; M.E.

Dissertation

Presented to the Faculty of the Graduate School of

The University of Texas at Austin

in Partial Fulfillment

of the Requirements

for the Degree of

Doctor of Philosophy

The University of Texas at Austin

August 2011

Dedication

To my family

Acknowledgements

I am sincerely thankful to Dr. Gary T. Rochelle for his tremendous guidance through all the three years. He is not only an incredibly knowledgeable supervisor for me, but also a great mentor and a role model. He genuinely cares about his students and is happy to see every little progress they made. His patience of teaching, passion of pursuing truth of science, dedication to learning, and desire for innovating always inspires me to be the best of myself. I didn't know that my Ph.D. study could be such a joyful and fruitful journey. Joining his research group is one of the best decisions I have ever made in my life. I am also honored and grateful to have Dr. Rochelle as the witness of my marriage.

I would like to thank the Luminant Carbon Management Program for the generous financial support for our research group over the years. Without these support, I would not be able to finish my work and have the opportunity to attend all those important conferences.

I wanted to thank all my committee members, Prof. Hal S. Alper, Prof. Steven L. Bryant, Prof. Brian A. Korgel and Prof. Venkat Ganesan, for their valuable time and insightful inputs to my research work.

I also greatly appreciate Maeve Cooney for her great contribution to the whole group. She has been very patient helping me correct any grammar mistakes in numerous reports and taking care of many requests for paperwork and reimbursement. She has made our life so much easier. I really enjoyed every little conversation with her as well.

I would like to extend my thanks to all the supporting staff in the UT-Austin community. Jim Smitherman and Butch Cunningham in the ChemE machine shop have

always given me most needed help with their tremendous skills and expertise in designing, building and modifying experimental equipment. Steve Sorey in the NMR laboratory of the Chemistry department did such an excellent job in getting all the NMR measurements done for me, and carried me through the NMR fundamentals and spectra interpretation. Mike Ronalter in the UT Glass shop is unbelievably talented in making and fixing all sorts of glass products. Randy Rife and Patrick Danielewski in the ChemE department always promptly respond to any requests on computer problems and give us a huge relief. I bothered Kevin Haynes and Eddie Ibarra for numerous times for ordering and shipping but they always took very good care of everything. Kay Costales-Swift and T Stockman have been really supportive with every trivial request for help.

I am also thankful to Dr. Isaac C. Sanchez, the greatest graduate advisor I have ever met. He gave me many valuable advices during my hard time and has been very supportive. I wanted to thank Dr. Keith P. Johnston, who taught me how to be a good graduate student in his way. I really enjoyed the class "Surface Phenomena" lectured by Dr. Roger T. Bonnecaze and "Mass Transfer" by Dr. Benny D. Freeman.

I have been really lucky to have the opportunity interacting with many great graduate students in our research group. Dr. Ross Dugas taught me how to perform the Wetted-Wall Column experiments when I was still a newbie in the group. More importantly, we spent a great amount of time together discussing various problems and solving difficulties. He has always been thoughtful and given me tons of valuable advices like an elder brother. I learned a lot from him. Stephanie Freeman is the master of various analytical apparatus in our lab, and she was always willing to spare her time patiently teaching or helping other colleagues. Her dedication to the excellence of research work and superior ability in planning and organizing experiments has always impressed me. I am really fortunate to have Fred Closmann as my labmate for three

years. He is always ready to help me with his experience of great depth and broadness in both work and life. Peter Frailie and Jorge Plaza have given many helps on my modeling works. I would also like to thank all other coworkers: Dr. Eric Chen, Dr. Tim Cullinane, Dr. Babatunde Oyenekan, Dr. Jason Davis, Dr. Andrew Sexton, Dr. Robert Tsai, David Van Wagener, Sepideh Ziaii -Fashima, Bich-Thu Nguyen, Stuart Cohen, Alex Voice, Chao Wang, Steven Fulk, Humera Rafique, Lynn Li and Omkar Namjoshi. It's really been a great pleasure working with them on a daily basis.

I also wanted to thank my best friends and former roommates Wen Li, Yang Zhang, Chaoming Zhang and Hao Ju, and my college classmates Yanghai Yu, Jun Jia, Lin Liu, and Hongfeng Ren. We shared so much pleasant time together and thank you all for the support through the years.

Finally, I wanted to thank my family, who has been the greatest support to my study abroad. My parents always encourage me to pursue whatever I choose and they truly believe that I will succeed. I am deeply indebted for their unselfish and unconditional love over the 30 years. Mom and Dad, I have not been able to be with you a lot but I love you two so much. I am so blessed to meet my wife Hui Shi and marry her. She is always able to relieve my stress and take care of everything else so that I can focus on my work. She is the best gift ever I can ask for in my life. I also wanted to thank my little sister and my parents in-law for their continuous support.

Carbon Dioxide Thermodynamics, Kinetics, and Mass Transfer in Aqueous Piperazine Derivatives and Other Amines

Xi Chen, Ph.D.

The University of Texas at Austin, 2011

Supervisor: Gary T. Rochelle

To screen amine solvents for application in CO_2 capture from coal-fired power plants, the equilibrium CO_2 partial pressure and liquid film mass transfer coefficient were characterized for CO_2-loaded and highly concentrated aqueous amines at 40 – 100 °C over a range of CO_2 loading with a Wetted Wall Column (WWC). The acyclic amines tested were ethylenediamine, 1,2-diaminopropane, diglycolamine®, methyldiethanolamine (MDEA)/Piperazine (PZ), 3-(methylamino)propylamine, 2-amino-2-methyl-1-propanol and 2-amino-2-methyl-1-propanol/PZ. The cyclic amines tested were piperazine derivatives including proline, 2-piperidineethanol, N-(2-hydroxyethyl)piperazine, 1-(2-aminoethyl)piperazine, N-methylpiperazine (NMPZ), 2-methylpiperazine (2MPZ), 2,5-trans-dimethylpiperazine, 2MPZ/PZ, and PZ/NMPZ/1,4-dimethylpiperazine (1,4-DMPZ). The cyclic CO_2 capacity and heat of CO_2 absorption were estimated with a semi-empirical vapor-liquid-equilibrium model. 5 m MDEA/5 m PZ, 8 m 2MPZ, 4 m 2MPZ/4 m PZ and 3.75 m PZ/3.75 m NMPZ/0.5 m 1,4-DMPZ were identified as promising solvent candidates for their large CO_2 capacity, fast mass transfer rate and moderately high heat of absorption.

The speciation in 8 m 2MPZ and 4 m 2MPZ / 4 m PZ at 40 °C at varied CO_2 loading was investigated using quantitative ^{1}H and ^{13}C nuclear magnetic resonance

(NMR) spectroscopy. In 8 m 2MPZ at 40 °C over the CO_2 loading range of 0 – 0.37 mol CO_2/mol alkalinity, more than 75% of the dissolved CO_2 exists in the form of unhindered 2MPZ monocarbamate, and the rest is in the form of bicarbonate and dicarbamate; 19% - 56% of 2MPZ is converted to 2MPZ carbamate at 0.1 - 0.37 mol CO_2/mol alkalinity.

A rigorous thermodynamic model was developed for 8 m 2MPZ in the framework of the Electrolyte Nonrandom Two-Liquid (ENRTL) model. At 40 °C, the reaction stoichiometry for 2MPZ and CO_2 is around 2 at lean loading but diminishes to 0 at rich loading. Bicarbonate becomes the major product at CO_2 loading greater than 0.35 mol/mol alkalinity. The predicted heat of CO_2 absorption is 75 kJ/mol at 140 °C and decreases with temperature when CO_2 loading is above 0.25.

The mass transfer rate data for 8 m 2MPZ was represented with a rate-based WWC model created in Aspen Plus®. The reaction rate was described with termolecular mechanism on an activity basis. With minor CO_2 loading adjustment and regression of pre-exponential kinetic constants and diffusion activation energy, a majority of the measured CO_2 fluxes in the WWC experiments were fitted by the model within ±20% over 40 – 100 °C and 0.1 – 0.37 mol CO_2/mol alkalinity. The diffusion activation energy for 8 m 2MPZ at the rich loading is about 28 kJ/mol. The activity-based reaction rate constant at 40 °C for 2MPZ carbamate formation catalyzed by 2MPZ is 1.94×10^{10} kmol/m^3·s. The calculated liquid film mass transfer coefficients are in close agreement with the experimental values. The liquid film mass transfer rate is dependent on the diffusion coefficients of amine and CO_2 to the same extent at lean loading and 40 °C. The sum of the powers for the two diffusivities is approximately equal to 0.5 over the loading range of 0 – 0.4 mol CO_2/mol alkalinity. The sum of the powers for the dependence of the liquid film mass transfer coefficient on the carbamate formation rate

constants ($k_{2MPZ-2MPZ}$ and $k_{2MPZCOO--2MPZ}$) approaches 0.5 at very lean loading at low temperature, but it decreases as CO_2 loading and temperature is increased. At 100 °C, the physical liquid film mass transfer coefficient is the most important factor that determines the liquid mass transfer rate. The pseudo-first order region shifts to higher range of physical liquid film transfer coefficient as temperature increases.

Table of Contents

List of Tables

List of Figures

Chapter 1: Introduction

1.1 Objectives and Scope of This Work

To significantly reduce anthropogenic CO_2 emission and battle global warming, Carbon Capture and Sequestration (CCS) needs to be implemented in a timely manner. Post-combustion capture of CO_2 (PCC) from coal-fired power plants is the one effective way to mitigate CO_2 emissions.

Acid gas treating with alkanolamine solvents is one of the most important commercial technologies for PCC because of its technical maturity and extensive operating experience in the refinery industry. However, with traditional amine solvents such as monoethanolamine (MEA) or diethanolamine (DEA), a significant energy penalty to the power plant would be incurred by heat and power required to regenerate the amine solvent and compress the CO_2. Other issues such as solvent degradation, corrosiveness and foaming also lead to considerable operating cost. To solve these problems, many efforts have been focused on development of advanced amine solvents (Puxty, Rowland et al. 2009; Singh, Brilman et al. 2009; Chowdhury, Okabe et al. 2011; Goto, Chowdhury et al. 2011). Most of these screening studies used or started with unloaded amine solvents, which are not realistic with respect to the conditions in an amine scrubbing process. The concentrations of amine solvents used are usually not high enough to meet the capacity requirements of a real process.

The key criteria for a good solvent for CO_2 capture along with the benefits are as follows:

a. High absorption/desorption rate at CO_2-loaded conditions. With same solvent flow rate, high mass transfer rate of CO_2 reduces the amount of packing required for the same percentage of CO_2 removal, which leads to

smaller absorber/stripper size and lower capital cost. High mass transfer coefficient also allows smaller driving force to be used in the absorber, which reduces exergy loss.

b. High cyclic CO_2 capacity. With higher CO_2 capacity, the circulation rate of solvent can be reduced, which in turn reduces the pump work and the sensible heat duty during temperature swing. Higher CO_2 capacity also helps reduce the size and cost of heat exchanger.

c. High heat of CO_2 absorption. Based on the study conducted by Oyenekan (Oyenekan and Rochelle 2006), although higher heat of CO_2 absorption increases the heat of regeneration of amine solvent, it leads to lower overall equivalent work due to the less energy consumption for CO_2 compression and water vaporization.

d. High resistance to degradation. Lower rate of amine loss due to degradation reduces the cost of solvent makeup and reclaiming.

e. Low volatility. Less amine loss to the vapor phase reduces the environmental impact.

f. Low corrosiveness. Cheaper construction materials such as carbon steel may be used for amine solvents with low corrosiveness.

The previous amine screening studies are valuable as they shed some light on relationships between amine activity and structure, but the results obtained from them are not ready to be used for design of a real process or estimation of process performance. Important information on liquid mass transfer rate and solvent capacity at relevant conditions was lacking. The disconnections between lab-scale testing and practical application of solvents indicate a need to screen amine solvents with a more appropriate technique at conditions relevant to realistic CO_2 capture.

The objectives of this work are to develop advanced aqueous amine solvents for removal of CO_2 from coal-fired power plants and to improve the understanding of the relationships between molecular structure, fundamental thermodynamic and kinetic properties and process performance of amine solvents. To realize these objectives, both experimental and modeling work has been performed.

Identification of advanced amine solvents suitable for CO_2 capture was accomplished by screening of conventional and novel amine solvents in a wetted wall column. Characterization of equilibrium CO_2 partial pressure and liquid mass transfer coefficients was done for 17 concentrated and CO_2 loaded amine solvents with variable temperature and CO_2 loading. Cyclic CO_2 capacity and heat of absorption were calculated from the solubility data. Amines are compared on the same basis pertaining to operating conditions. The obtained data can be directly utilized for design of the absorber and stripper. Other important amine properties such as oxidative and thermal stability and amine volatility are not included in this work.

Piperazine (PZ) has been shown to be a superior absorbent over MEA for CO_2 removal from coal-fired power plants with fast absorption/desorption rate, high cyclic CO_2 capacity and great thermal and oxidative stability (Freeman, Dugas et al. 2009). The type and position of functional groups on PZ derivatives were systematically varied in this work to study the effect of molecular structure on solvent performance. 2-methylpiperazine (2MPZ) and 2MPZ/PZ were identified as good solvent candidates for PCC and used as model solvents for further study. Important species involved in CO_2 absorption using these two solvents were identified and quantified by conducting proton and ^{13}C nuclear magnetic resonance (NMR) spectroscopic study.

CO_2 solubility data from the WWC experiments as well as the speciation data were used for the development of a rigorous and consistent thermodynamic model for

2MPZ in Aspen Plus®, which is of great importance for proper design of amine scrubbing process for CO_2 capture and predictions of performance limit.

Absorption/desorption experiments for 2MPZ in the WWC were modeled with Aspen Plus® Ratesep™ to extract information for the reaction rate constants and the diffusion coefficient of reactants and products. The experimental mass transfer data are satisfactorily represented by the developed kinetic model. The kinetic model can be incorporated into a scaled-up process simulation to predict the solvent performance in a real process.

1.2 BACKGROUND

1.2.1 Global Warming

The average global surface temperature has increased by approximately 0.74 °C over the past century and climate change becomes a growing concern (IPCC 2010). Anthropogenic greenhouse gas (GHG) into atmosphere due to human activities is believed to be the major cause of global warming. From 1750 (the start of Industrial Revolution) to 2005, the globally average concentrations of carbon dioxide (CO_2), methane (CH_4) and nitrous oxide (N_2O) have increased by 36%, 148% and 18%, respectively (IPCC 2010).

As the primary product of burning fossil fuels, CO_2 is the most important human-caused GHG. In the United States, CO_2 accounted for 83% of the total GHG emission weighted by global warming potential in 2009 (EIA 2011). The existing climate data (Etheridge, Steele et al. 1998; Hansen, Ruedy et al. 2009; Keeling, Piper et al. 2009) show that temperature anomalies parallel a continuous increase of CO_2 concentration from 280 ppm in 1850s to 380 ppm in 2009 (Figure 1.1), while historic atmospheric CO_2 concentration dating back to 800,000 years was found to only cycle between 180 ppm

and 300 ppm (Luthi, Le Floch et al. 2008). The close correlation between CO_2 level and the change of the Earth's temperature indicates that the undergoing climate change is very likely due to the dramatic increase in burning of fossil fuels in the post-industrial era (Boden, Marland et al. 2009). CO_2 emissions must be reduced to mitigate global warming.

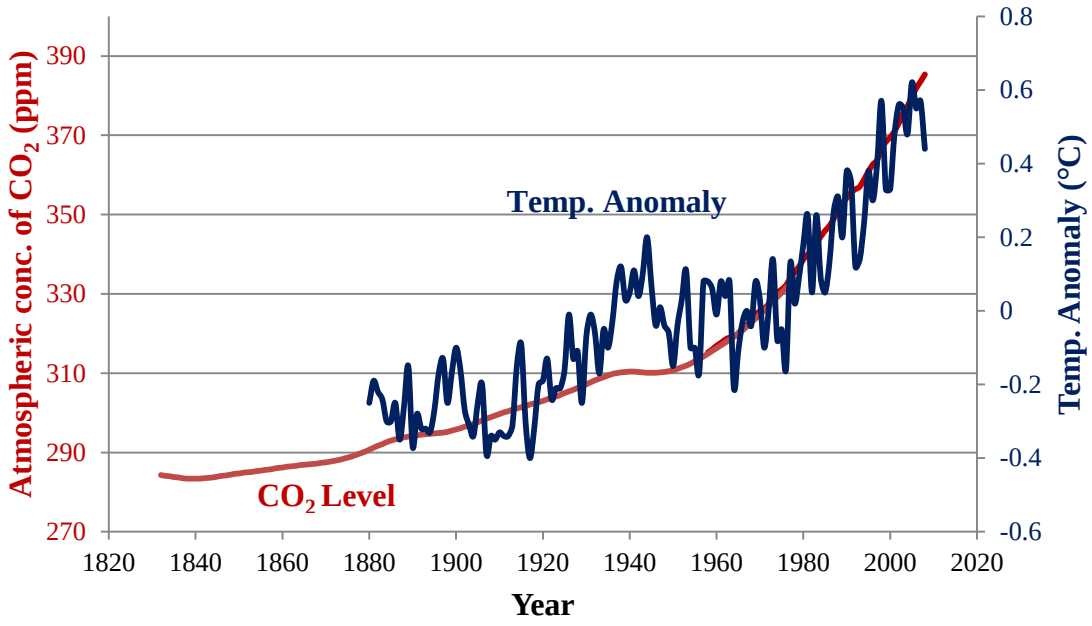

Figure 1.1: Atmospheric CO_2 concentration and temperature anomaly since 1830's (Etheridge, Steele et al. 1998; Hansen, Ruedy et al. 2009; Keeling, Piper et al. 2009).

1.2.2 Sources of CO_2 Emission

Energy-related activities are the primary sources of CO_2 emission, of which fossil fuel combustion comprises the vast majority. The level of CO_2 emission is not only determined by energy consumption, but also carbon intensity of fuel employed. Coal is the most carbon-intensive fuel. The average C content for coal is 95 Tg CO_2 Eq./QBtu,

while this number is almost halved for natural gas. In 2008, 43% of the worldwide CO_2 emissions from fuel combustion were from coal, 37% from oil and 20% from gas. Sector-wise, generation of electricity and heat, which heavily relies on burning of coal, was the largest producer of CO_2 and accounted for 41% of the total CO_2 emissions in the world (IEA 2010).

In U.S., 79% of total CO_2 emissions were from fossil fuels combustion in 2009 (EPA 2011). The annual amount of CO_2 emissions by fuel type and sector from 1990 to 2009 is shown in Table 1.1. Petroleum has been the largest CO_2 emission contributor due to the great consumption in transportation, accounting for 41.6% of the total emissions. Coal is the second-largest contributor and mainly used for electricity generation. A steady increase of natural gas in electricity generation is seen over the years.

Table 1.1: CO_2 emissions from fossil fuel combustion by fuel type and sector (Tg or million metric tons CO_2 Eq.) (EPA 2011)

Fuel/Sector	1990	2000	2005	2006	2007	2008	2009
Coal	1,718.40	2,065.50	2,112.30	2,076.50	2,106.00	2,072.50	1,841.00
Residential	3	1.1	0.8	0.6	0.7	0.7	0.6
Commercial	12	8.8	9.3	6.2	6.7	6.5	5.8
Industrial	155.3	127.3	115.3	112.6	107	102.6	83.4
Transportation	NE	NE	NE	NE	NE	NE	NE
Electricity Generation	1,547.60	1,927.40	1,983.80	1,953.70	1,987.30	1,959.40	1,747.60
U.S. Territories	0.6	0.9	3	3.4	4.3	3.3	3.5
Natural Gas	1,000.60	1,217.40	1,159.00	1,141.30	1,218.00	1,226.00	1,200.90
Residential	238	270.7	262.2	237.3	257	264.4	257.2
Commercial	142.1	172.5	162.9	153.8	164	170.2	167.9
Industrial	409.1	457.2	380.8	377.7	389	391	365
Transportation	36	35.6	33.1	33.1	35.3	36.8	36.3
Electricity Generation	175.3	280.8	318.8	338	371.3	361.9	373.1
U.S. Territories	NO	0.7	1.3	1.4	1.4	1.6	1.5

Petroleum	2,019.00	2,311.60	2,481.50	2,434.90	2,432.40	2,267.10	2,166.70
Residential	97.4	98.8	94.9	83.6	84.6	83.1	81.4
Commercial	64.9	49.6	51.3	48.5	48.7	47.4	50.3
Industrial	282.1	266.6	326.9	357.9	346	309.3	282
Transportation	1,449.90	1,773.90	1,863.50	1,845.00	1,858.70	1,753.10	1,683.40
Electricity Generation	97.5	88.4	99.2	54.4	53.9	39.2	32.9
U.S. Territories	27.2	34.2	45.7	45.5	40.4	35	36.7
Geothermal	0.4	0.4	0.4	0.4	0.4	0.4	0.4
Total	4,738.40	5,594.80	5,753.20	5,653.10	5,756.70	5,565.90	5,209.00

Figure 1.2 illustrates the contribution of different sectors to the total CO_2 emission in U.S. in 2009. Electricity generation from coal alone represents one third of the total CO_2 emissions, followed by transportation and industrial. Coal has been the most common fuel for electricity generation in U.S. because of its great abundance and low cost. In 2009, 45% of the country's nearly 4 trillion kwh of electricity was generated from coal (EIA 2010). Coal-fired power plants provide a great opportunity to effectively reduce CO_2 emission from stationary point sources.

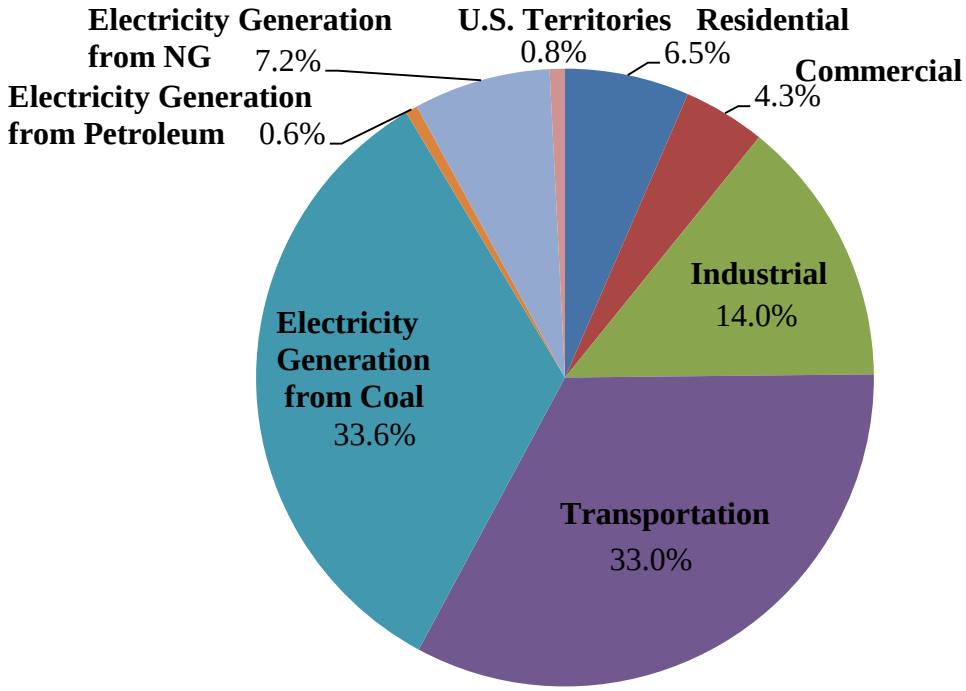

Figure 1.2: CO_2 Emissions from Fossil Fuel Combustion by sector in the U.S. in 2009 (EPA 2011) . Total Emissions = 5209 Tg CO_2 Eq.

1.3 CAPTURE OF CO_2

There are many ways to reduce CO_2 emissions, such as improving energy efficiencies, switching to less carbon-intensive fuels, and enhancing biological sinks (IPCC 2005). Renewable energy sources including wind, solar powers and biomass have also been actively pursued and the installed capacity is increasing rapidly. However, due to the constraints of current state-of-the-art technologies, alternative renewable energy sources cannot meet the requirements of ever increasing demand for power. Nuclear power is the only option that has comparable intensity of energy output as fossil fuels, but its extensive use is obstructed by great hazard potential and public

concern. As a consequence fossil fuels will continue to be the dominant power source for at least next couple of decades.

"Carbon dioxide (CO_2) capture and storage (CCS) is a process consisting of the separation of CO_2 from industrial or energy-related sources, transported to a storage location and long-term isolation from the atmosphere " (IPCC 2005). CCS is considered as a promising way to reduce CO_2 emission since it allows continuous use of fossil fuel sources while emitting no or very little CO_2 to atmosphere. It is suggested that CCS must be included as an option in the portfolio of mitigation actions to stabilize GHG concentration (IPCC 2005).

1.3.1 Capture Systems

There are three major systems for CO_2 capture: pre-combustion, oxy-combustion and post-combustion. There is also capture from industrial process streams such as purification of natural gas, production of synthesis gas and manufacture of ammonia.

1.3.1.1 Pre-combustion

Currently a promising approach for pre-combustion involves integrated gas combined cycle (IGCC) supplemented with shift conversion. In this process, coal (or other nongaseous fossil fuels) is first gasified to produce syngas (carbon monoxide (CO) and hydrogen (H_2)). The syngas is then contacted with steam and chemically shifted to CO_2 and H_2. The H_2 is separated from the CO_2 and combusted in a gas turbine. Heat is recovered from the hot exhaust gas and used to produce steam for a steam turbine which generates additional power. The advantages of pre-combustion are: 1) higher energy efficiency gained from burning of gas at higher temperature in the combined cycle, 2) simultaneous generation of electricity and H_2, 3) CO_2 is inherently generated as a separate stream with low flow rate and high concentration, leading to lower capture

cost. However, pre-combustion can only be applied to new power plants and lack of short-term flexibility, and construction cost is relatively high. Further gains could be achieved by development of high-temperature membranes allowing for simultaneous syngas shifting and H_2 separation (Haszeldine 2009).

1.3.1.2 Oxy-combustion

Oxy-combustion allows much easier CO_2 separation by burning fossil fuel with nearly pure oxygen (> 95%) mixed with recycled flue gas. In most cases a cryogenic air separation unit (ASU) would be used to supply pure oxygen to boiler. Since the currently available construction materials cannot withstand high temperatures resulting from coal combustion in pure oxygen, oxygen has to be mixed with the flue gas to maintain combustion conditions similar to those for air-fired boilers (Figueroa, Fout et al. 2008). Therefore oxy-combustion is also able to be retro-fitted to the power plants already built.

Because of the lower flue gas flow rate and higher CO_2 concentration, the cost of CO_2 capture from oxy-combustion power plant is reduced. However, a significant portion of the cost is transferred to separation of O_2 from air and recycle of flue gas. To dramatically reduce the cost of oxy-combustion, more efficient technologies for oxygen production need to be developed. To make oxy-combustion more attractive, materials need to be improved for high-temperature operation to take advantage of high-temperature combustion with oxyfuel and improve energy efficiency (Figueroa, Fout et al. 2008).

1.3.1.3 Post-combustion

Post-combustion technology captures CO_2 directly from flue gas emitted from power plants. It can be readily retro-fitted to the existing power plants, which generate

about 2/3 of the total CO_2 emission in the power sector (Figueroa, Fout et al. 2008). Therefore post-combustion provides the greatest near-term potential to reduce CO_2 emission, especially those from coal-fired power plant.

Most of the existing power plants use air for combustion, so the CO_2 concentration in the flue gas (Pressure = ~ 1 atm) is generally less than 15%, with the rest mostly being nitrogen. The small driving force for separation resulted from low CO_2 partial pressure poses a challenge for development of cost-effective capture technology for post-combustion.

1.3.2 Capture Technologies

Various technologies may be used for the CO_2 capture systems mentioned above. The selection of separation methods depends on the specific operational conditions in a power plant as well as the cost.

1.3.2.1 Absorption

In absorption, flue gas is passed through a solvent and CO_2 is selectively absorbed. The solvent is regenerated by temperature or pressure swing while CO_2 is released and collected. Depending on the reactivity of the solvent, absorption can be either physical or chemical.

For physical absorption, there is no reaction taking place between CO_2 and the solvent. It is usually applied for high CO_2 partial pressure and requires less heat for regeneration of solvent. The limitations of physical absorption are poor selectivity and low absorption rate.

In chemical absorption, CO_2 reacts with solvents. The reactions are reversed at higher temperature to regenerate solvents and release CO_2. Chemical absorption features high heat of absorption, high absorption rate and high selectivity compared to

physical absorption. In the assessment studies which compared the commercially available process technologies, absorption with chemical solvents has been shown to be the most promising choice for post-combustion CO_2 capture (PCC) (IEA 2000; IPCC 2005).

Amines have been extensively used as chemical solvents for acid gas treating. Aqueous amines are regarded as the most suitable solvents for absorption of CO_2 from flue gas in which the CO_2 partial pressure is low (Kohl and Nielsen 1997; IPCC 2005). As the focus of this work, amine scrubbing technology will be further discussed in Section 1.4.

1.3.2.2 Others

Other methods of CO_2 separation under development include adsorption, membrane, cryogenic separation, chemical looping etc. However, currently they are not ready for being implemented in large-scale test of flue gas treating due to the lack of cost-effectiveness or technical maturity. These technologies are not in the scope of this work and will not be discussed further.

1.4 TRANSPORT AND STORAGE OF CO_2

After CO_2 is separated from flue gas, it has to be compressed to high pressure (100 ~ 150 bar) to facilitate the transport to a storage site. The high density CO_2 fluid will be injected into geological formations deeper than 800 m to achieve permanent sequestration (Orr 2009).

Experience in CO_2 transport has been gained since 1970s from enhanced oil recovery (EOR). Minimizing water content in the CO_2 stream greatly reduces corrosion rate of pipelines as well as the cost of pipeline materials (Seiersten 2001). Removal of

other impurities such as N_2, O_2, H_2S and SO_3 avoids overcompression and lowers operational cost (Haszeldine 2009).

CO_2 storage in geological formation has been proved feasible based on the information and experience gained from CO_2 injection activities in previous EOR and acid gas projects as well as the existing CO_2 storage practices (IPCC 2005). The main candidates of storage sites are depleted oil/gas reservoirs, deep saline formation, and coal seams, which provide a total capacity that would be adequate for storage of CO_2 for many years into the future. To minimize the potential risks to human and ecosystem caused by CO_2 leakage, careful site selection, effective regulatory oversight and appropriate monitoring is required. Cost of CO_2 storage is highly site-specific and generally small compared to current CO_2 capture cost., which comprises 70% or more of the total cost of CCS (House, Harvey et al. 2009).

1.5 AMINE SCRUBBING TECHNOLOGY FOR CO_2 CAPTURE

Amine scrubbing is believed to be the only technology for PCC that is available to reduce CO_2 emissions from existing coal-fired power plants without shutting them down (Rochelle 2009). The technology has been extensively used in industry for natural gas sweetening for almost 80 years. As a reliable and robust technology, it has also reached commercial stage of operation for CO_2 capture.

1.5.1 Process Description

Amine scrubbing makes use of the reversible nature of the reaction between an amine and acid or sour gas. A typical commercial scrubbing process using amine solvents for removal of CO_2 from coal-fired power plant is shown in Figure 1.3.

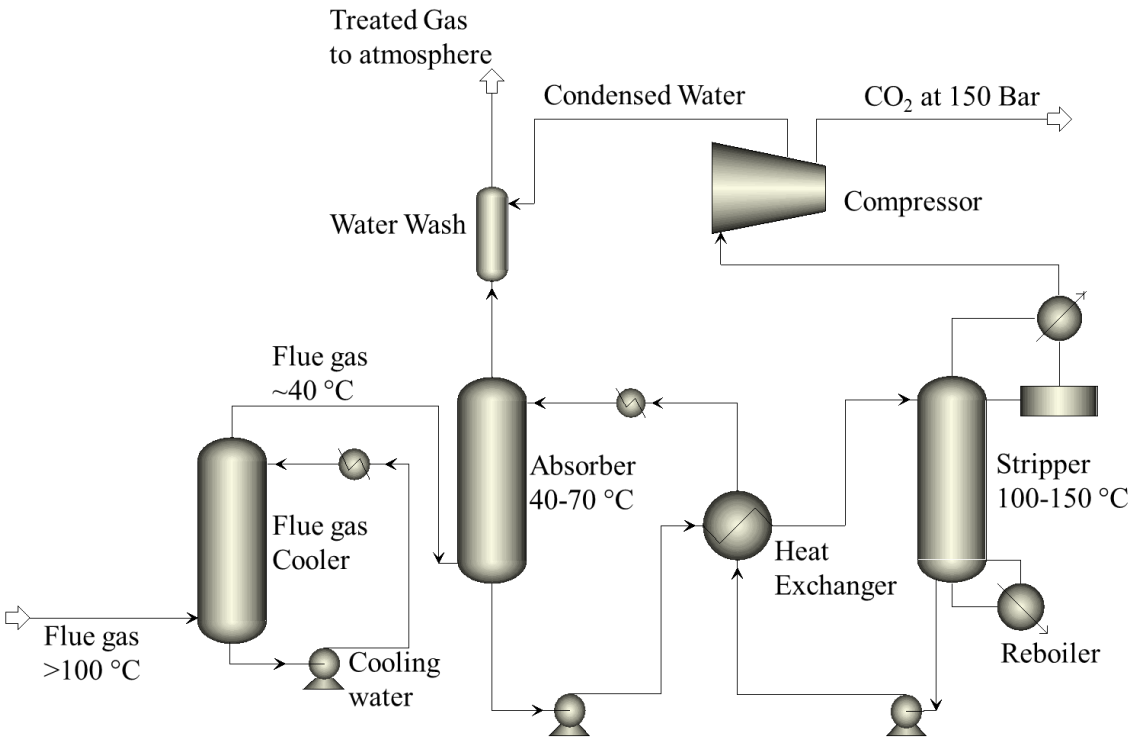

Figure 1.3: Process flow diagram of an amine scrubbing process for CO_2 recovery from coal-fired power plant flue gas.

Flue gas from power plant usually has a temperature above 100 °C and needs to be cooled down to about 40 °C to reduce the volume flow rate and increase absorption efficiency. This would be done in a direct contact cooler. NOx and SOx is contained in the flue gas. They can form heat stable salt with amine, which reduces the solvent capacity for CO_2 and increases the cost of solvent makeup. Fortunately NO_2 is the only NOx that leads to formation of stable salt and usually only accounts for less than 10% of the total NOx content in flue gas. The concentration of SOx in flues gas after a commercial desulfurization unit (commonly limestone slurry scrubber) is typically 5 - 100 ppm. Whether or not to add another FGD unit to further bring down the SO_2 level

depends on the tradeoff between the cost of solvent makeup and that of SO_2 removal (IPCC 2005).

The flue gas stream is blown to the bottom of the absorber, where it is brought into counter-current contact with lean amine solvent flowing down from the top. Most of CO_2 in the gas stream is picked up by amine with exothermal chemical reactions. Before the gas stream exits the top of the absorber, it goes through a water wash unit to reduce loss of volatile amine components. The rich amine solution exits bottom and is heated by a heat exchanger. As it goes to the stripper, the temperature is further elevated by the heat from reboiler. As a result, amine-CO_2 reaction is reversed. The released CO_2 is then collected from the top of the stripper and compressed for transportation and sequestration; the lean amine solvent is cooled by the heat exchanger and a trim cooler and pumped back to the absorber for next cycle of CO_2 absorption.

The flue gas conditions dictate the CO_2 loading of amine solvent applied. Given that flue gas from coal-fired power plants is usually at atmospheric pressure and the typical CO_2 concentration contained is 12%, the inlet CO_2 partial pressure in the absorber is about 12 kPa, and the outlet CO_2 partial pressure is 1.2 kPa if 90% of CO_2 removal is assumed. As a result, the amine solvent circulated in the process is always CO_2-loaded. To achieve a reasonably fast CO_2 mass transfer from gas to liquid, a large enough driving force should exist between them. Therefore throughout this work, the lean and rich solvents are always assumed to have an equilibrium CO_2 partial pressure at 40^{o}C of 0.5 kPa and 5 kPa, respectively.

1.5.2 Energy Requirement

The post-combustion CO_2 capture process requires considerable energy for regeneration of solvents, compression of CO_2, and to a lesser extent the electricity for

liquid pumping and the flue gas fan. A substantial fraction of steam has to be extracted from the power plant to drive the CO_2 capture system and will not be available for power generation. This results in a significant energy penalty to the power plant. The minimum work required for removal of CO_2 from coal-fired flue gas and compression to 150 bar is about 0.11 Mwh/Mt CO_2, or as much as 12% of typical power plant output (Rochelle 2009). Due to the irreversible process existing in a real absorption/stripping process, the actual energy penalty will be much greater. With the current state-of-the-art technology, the energy penalty caused by separation and compression of CO_2 is expected to be 25% to 40% of the total fuel energy of a power plant (Haszeldine 2009).

For CO_2 removal by amine scrubbing, the reduction of energy penalty to power plants is closely related to the chosen solvent system, optimization of process configuration as well as integration of capture system to power plants.

1.5.3 Capture Cost

There are two important measures for cost of post-combustion CO_2 capture for electric power plants - cost of CO_2 avoided and cost of CO_2 captured. The definitions for them are as follows (IPCC 2005):

Cost of CO_2 avoided (US\$/tCO_2)

$$= [(COE)_{capture} - (COE)_{ref}]/[(CO_2/kWh)_{ref} - (CO_2/kWh)_{capture}] \quad (1.1)$$

Cost of CO_2 Captured (US\$/tCO_2)

$$= [(COE)_{capture} - (COE)_{ref}]/(CO_{2,\ capture}/kWh) \quad (1.2)$$

where COE is levelized cost of electricity (US\$/kWh) given by

COE = [[total capital cost (US\$)]×[fixed charge factor (fraction/yr)] + [Fixed Operating Cost (US\$/yr)]]/[[net plant power (kW)]×[total hours in a typical year

(h)]*[capacity factor (fraction)]]+[variable operating costs (US$/kWh)]+[net plant heat rate (kJ/kWh)] * [unit fuel cost (US$/kJ)] (1.3)

CO_2/kWh = CO_2 mass emission rate (in tonnes) per kWh generated and $CO_{2,\ capture}$ /kWh = total mass of CO_2 captured (in tonnes) per net kWh for the plant with capture. The subscript "capture" and "ref" refer to the plant with and without CO_2 capture respectively.

Studies conducted by different authors/organizations (NETL 2002; Parsons Infrastructure & Technology Group 2002; Rao and Rubin 2002; Simbeck 2002; IEA 2004; Stobbs and Clark 2005; Rubin, Chen et al. 2007; Rochelle 2009) on new coal-fired power plants shows that cost of CO_2 avoided would be \$29-51/tCO_2 (corresponding to cost of CO_2 captured of \$23-35/tCO_2) and electricity cost would go up by 42-81% if power plants were equipped with current CO_2 capture technology. For existing power plants, the energy requirement for CO_2 capture is usually higher than that for new power plant because of less efficient heat integration (IPCC 2005). Several studies on retrofitting an amine-based CO_2 capture system to existing power plants (Alstom 2001; Simbeck 2001; Rao and Rubin 2002; Chen, Rao et al. 2003; Singh, Croiset et al. 2003; Gibbins, J. et al. 2005) shows that the average cost of CO_2 avoided is about 35% higher than for the new plants for comparable levels of about 85% CO_2 reduction per kWh (IPCC 2005).

1.5.4 Solvent Development

In most of the analyses of energy requirement and capture cost that have been done so far, monoethanolamine (MEA) has been used as the standard solvent for representing the capability of current PCC technology. However, there is still room left for improvement on amine scrubbing technology. For MEA, serious solvent

management problems rise due to oxidative and thermal degradation, resulting in significant cost of solvent consumption. Other problems associated with traditional amine solvents are precipitation, corrosion, foaming, entrainment and evaporation.

To further advance post-combustion technology and reduce energy consumption, numerous research efforts are focusing on investigation of the second or even third generation of amine solvents, in both bench-scale and pilot-scale.

Selection of amine solvents for PCC involves a great amount of work on different properties of solvent. Sometimes tradeoffs between different properties have to be compromised.

1.5.4.1 Pilot-scale Test of Amine Solvents

Currently there are two commercial amine scrubbing processes available for CO_2 capture. Fluor Daniel® Inc. developed ECONAMINE™ process which is based on formulated 30 wt% MEA with addition of corrosion inhibitor. The Kansai Electric Power Co. and Mitsubishi Heavery Industries, Ltd. developed the KEPCO/MHI Process based on a proprietary solvent KS-1, which has less corrosion and oxidation problems than MEA (Mimura, Nojo et al. 2003). A comparative study on performance assessments of power plants with PCC shows that efficiency penalty for KEPCO/MHI's CO_2 absorption process is 22% for coal fired plants, while this number is 27% for Fluor's process(IEA 2004). These two processes are representative of the state-of-the-art technologies for PCC.

A chilled ammonia process was developed and patented by Alstom for CO_2 capture. Ammonia is cheap and non-degradable. It can be also used to remove SOx and NOx from the flue gas and produce marketable fertilizer. However, due to the high volatility of ammonia, the flue gas as well as the ammonia has to be chilled below ~ 15

°C, which adds a substantial amount of cooling duty. The precipitation of ammonium bicarbonate at rich CO_2 loading needs to be handled as well (Figueroa, Fout et al. 2008). In addition, the absorption rate of CO_2 by ammonia is slow at operating conditions, which requires larger absorber size and higher capital cost. The ammonia process has been tested on scales of 5 Mw_{th} to 54 Mw_{th} for multiple coal-fired power plants (Alstom 2011). Larger demonstration projects are underway. Unfortunately, the pilot plant test results of ammonia from Alstom are not available at this time.

MEA blended with methyldiethanolamine (MDEA) was tested in a pilot plant located in the University of Regina, Canada (Idem, Wilson et al. 2005). The results showed that a huge heat duty reduction can be achieved by using MEA/MDEA blend instead of a single MEA solution at the same total molar concentration, if amine degradation could be controlled.

A new process using 40 wt% piperazine (PZ) and a simple two-stage flash for regeneration was proposed by our research group in the University of Texas at Austin as the new standard to represent the capability of PCC technology (Rochelle, Chen et al.). PZ was identified as a solvent that is faster, more stable and less corrosive than MEA. The two pilot plant campaigns show that heat duty for CO_2 recovery (MJ/tonne CO_2) for 8 m PZ is close to that reported for KS-1 (Plaza, Chen et al.).

Many other activities on pilot-scale tests of novel amine solvents for PCC for coal-fired power plants have been reported (Notz, Asprion et al. 2006; Attalla 2008; Knudsen, Jensen et al. 2009; Maloney, Gardiner et al. 2010; Mangalapally and Hasse 2011; Yokoyama, Takamoto et al. 2011). The energy consumption of these new solvents was compared to conventional amines like MEA. However, the compositions of most of the amine solvents are not disclosed, which make it difficult to extract useful information on impact of amine solvents on process performance.

1.5.4.2 Lab-scale Screening of Novel Amine Solvents

Numerous studies have been focused on screening of new amine solvents for CO_2 capture on a lab-scale. The main techniques that have been employed in these screening studies are as follows:

1. Bubbling scrubber

   The bubbling scrubber is the most commonly used screening apparatus (Puxty, Rowland et al. 2009; Singh, Brilman et al. 2009; Chowdhury, Okabe et al. 2011; Goto, Chowdhury et al. 2011). As shown in Figure 1.4, a gas scrubbing bottle is filled with an amine solvent and thermo-stated at 40 °C. A gas mixture of CO_2 and N_2 is supplied to the bottle at a fixed volumetric flow rate. The CO_2 concentration in the outlet is monitored by a CO_2 analyzer. After the solvent is saturated by CO_2, it is moved to another water bath maintained at higher temperature (70 – 100 °C) to perform desorption of CO_2 and regenerate amine solvent. The saturated CO_2 capacity and absorption/desorption rate are determined from the profile of the CO_2 concentration as a function of time at the outlet.

   The disadvantage of using this technique is that the absorption rate of CO_2 obtained from the bubbling setup is affected by area of gas-liquid interface and bubble texture, which vary from solvent to solvent because of the difference in viscosity and surface tension. Only relative and semi-quantitative absorption rate was obtained, which is hard to be translated into the mass transfer rate that is necessary for absorber design. Cyclic CO_2 capacity of solvents relevant to real operating conditions is usually not available from these studies.

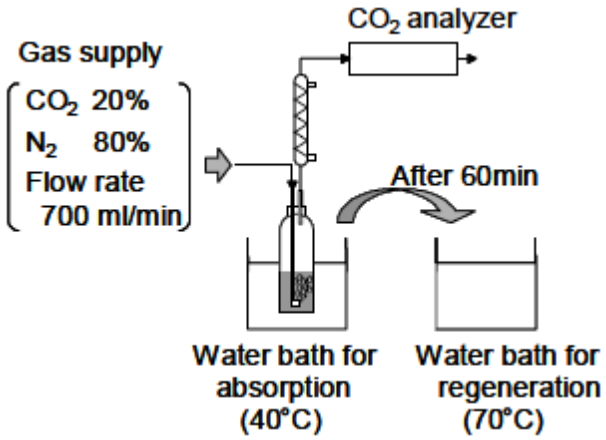

Figure 1.4: Schematic of diagram for gas bubbling screening technique (Chowdhury, Okabe et al. 2011).

2. Bench-scale absorber column (Dubois and Thomas 2011).
3. Wetted-wall column (Robinson, McCluskey et al. 2011; Rowland, Yang et al.).
4. Reaction calorimeter for measurement of heat of CO_2 absorption for various amine solvents (Goto, Chowdhury et al. 2011).
5. ^{13}C-NMR spectroscopy to identify and quantify important amine-CO_2 reaction products (Rowland, Yang et al. 2011).
6. Attenuated Total Reflectance Fourier Transform Infrared (ATR FT-IR) spectroscopy (Robinson, McCluskey et al. 2011).

Chapter 2: Literature Review

2.1 Reaction Chemistry and Kinetics

Depending on the number of substitutions on the nitrogen atom as well as the α-carbon, amines can be organized into four groups: primary amine, secondary amine, tertiary amine and hindered amine. Examples of different amines are shown in Table 2.1. Multiple amino groups of different types can also be on the same molecule (e.g. diamine or triamine). The molecular structure of the amine significantly affects the chemistry as well as the kinetics of the reaction between the amine and CO_2.

Table 2.1: Molecular structures of primary, secondary, tertiary and hindered amines.

Category	General Molecular Structure	Examples	Molecular structure
Primary Amine	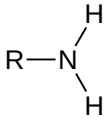	Monoethanol Amine (MEA)	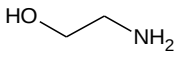
		Diglycolamine® (DGA®)	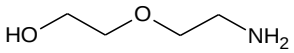
		Ethylene Diamine (EDA)	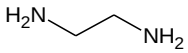
Secondary Amine	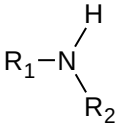	Diethanol Amine (DEA)	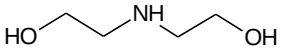
		Piperazine (PZ)	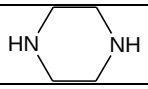
Tertiary	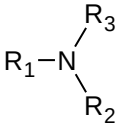	Methyldiethanol Amine (MDEA)	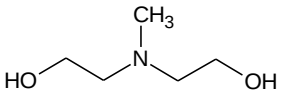

Hindered Amine	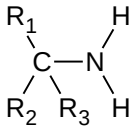	2-Amnio-2-Methyl Propanol (AMP)	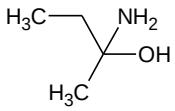
	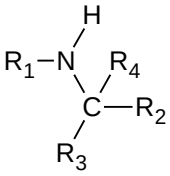	2-methylamino-2-methyl-propanol (MAMP)	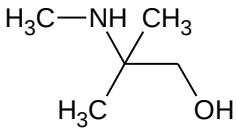
	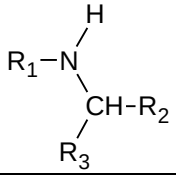	2-Piperidine Ethanol (2-PE)	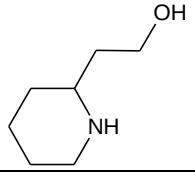

2.1.1 Primary and Secondary Amines

The reaction between primary or secondary amines and CO_2 generally results in formation of carbamate, which has been interpreted by two different reaction mechanisms – Zwitterion and Termolecule.

2.1.1.1 Zwitterion Mechanism

The zwitterion mechanism was proposed by Caplow (Caplow 1968) and introduced to chemical engineering by Danckwerts (Danckwerts 1979). This mechanism is represented by a two-step process. In the first step, amine reacts with CO_2 to form an intermediate zwitterion, which is ionic but neutrally charged:

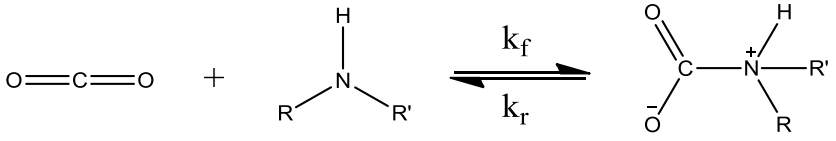

(2.1)

In the second step, a proton on the zwitterion is extracted by a base present in the system. This step is usually assumed to be irreversible.

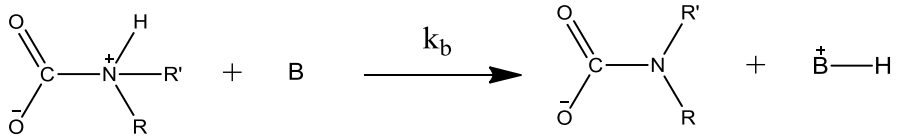

(2.2)

With the quasi-steady state assumption for the zwitterion concentration, the overall reaction rate based on the zwitterion mechanism is given by:

$$r_{CO_2} = -\frac{[Am][CO_2]}{\frac{1}{k_f} + \frac{k_r}{k_f \sum k_b[b]}} \tag{2.3}$$

where $\sum k_b[b]$ represents the total contribution to the deprotonation by all the bases present in the solution. In aqueous amine solution at lean loading, water, OH^- and free amine can act as bases (Blauwhoff, Versteeg et al. 1984; Versteeg, Van Dijck et al. 1996). In two extreme situations the reaction rate can be simplified:

1) If the deprotonation step is much faster than the reversion of zwitterion to amine, i.e. $\sum k_b[b] >> k_r$, Eq. (2.3) is simplified to

$$r_{CO_2} = -k_f[Am][CO_2] \tag{2.4}$$

This case corresponds to second-order kinetics.

2) If $\sum k_b[b] << k_r$, a more complex expression for kinetics is derived:

$$r_{CO_2} = -\frac{k_f \sum k_b[b]}{k_r}[Am][CO_2] \tag{2.5}$$

Depending upon the contribution of different bases, the reaction order with respect to amine can vary between one and two. The shifting reaction orders

was also observed experimentally for the reaction between CO_2 and primary or secondary amines (Barth, Tondre et al. 1984; Barth, Tondre et al. 1986).

If the deprotonation step (Reaction (2.2)) is reversible, the kinetics can be described with the following equation (Dugas 2009).

$$r_{CO_2} = -\frac{[Am]}{\frac{1}{k_f} + \frac{k_r}{k_f \sum k_b [b]}} \left([CO_2] - \frac{\sum \frac{k_b}{K_{eq,b}} [AmCOO^-][BH^+]}{\sum k_b [Am][B]} \right) \tag{2.6}$$

where $K_{eq,b} = \frac{[AmCOO^-][BH^+]}{[Am][CO_2]_e[B]}$ is the equilibrium constant of the overall reaction for each base. As equilibrium shifts to the products, the second term in the parenthesis will approach equilibrium CO_2 concentration, yielding near-zero reaction rate.

2.1.1.2 Termolecular Mechanism

Crooks and Donnellan (Crooks and Donnellan 1989) argued that the zwitterion mechanism could overinterpret certain experimental data and be not credible any more. They suggested a single-step termolecular mechanism to describe the reaction between amine and CO_2. The initial product of the three molecules is deemed by them as a "loosely-bound encounter complex" (Figure 2.1) and the reaction is carried out in a single step. This mechanism is supported by the ab initio study on the amine-CO_2 reaction conducted by da Silva *et al.* (da Silva and Svendsen 2006). Aboudheir *et al.* (Aboudheir, Tontiwachwuthikul et al. 2003) also showed that the termolecular mechanism is a better model than zwitterion mechanism for the modeling of CO_2 absorption into highly concentrated and highly CO_2-loaded MEA solution.

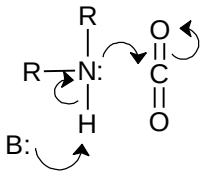

Figure 2.1: Termolecualr mechanism for amine and CO_2 reaction.(Crooks and Donnellan 1989)

The termolecular mechanism can be regarded as a zwitterion mechanism in the limiting case of $\sum k_b[b] << k_r$. It gives the identical rate expression (Eq. (2.7) and (2.8)) as that from the zwitterion mechanism (Eq. (2.5)). With the amine considered as an acting base, varying orders of reaction and equally effective representation of reaction rate can be derived, regardless which mechanism is chosen (Cullinane 2005). The termolecular mechanism is therefore preferred because of its simplicity and will be used throughout this work.

$$r_{CO_2} = -\sum_b k_{Am-b}[Am][b][CO_2] \tag{2.7}$$

$$k_{Am-b} = \frac{k_f k_b}{k_r} \tag{2.8}$$

For concentrated primary and secondary amine aqueous solution, the amine is the carbamate formation agent as well as the major base catalyst. Thus 1 mol of primary or secondary amine can only absorb 0.5 mol CO_2 theoretically, as shown by the following overall reaction:

$$2Am + CO_2 \Leftrightarrow AmCOO^- + AmH^+ \tag{2.9}$$

Primary or secondary amines generally have high heat of absorption because of the high heat of reaction in carbamate formation (Rochelle, Bishnoi et al. 2001). As CO_2 loading increases, due to the depletion of amine, the equilibrium in Reaction (2.10) is

shifted to the right-hand side. Consequently formation of bicarbonate is more significant and becomes the dominant mechanism responsible for CO_2 absorption at rich loading (typically > 0.45 mol CO_2/mol amino group), leading to a drop in heat of absorption.

$$AmCOO^- + H_2O + CO_2 \leftrightarrow Am + HCO_3^- \tag{2.10}$$

2.1.2 Tertiary Amines

Tertiary amines cannot directly react with CO_2 and form carbamate due to the extreme instability of the product. Instead, the reaction can only proceed with the presence of water. Bicarbonate is produced under the homogeneous catalysis of tertiary amine. The overall reaction is shown in (2.11), indicating that absorption of 1 mol CO_2 only consumes 1 mol tertiary amine.

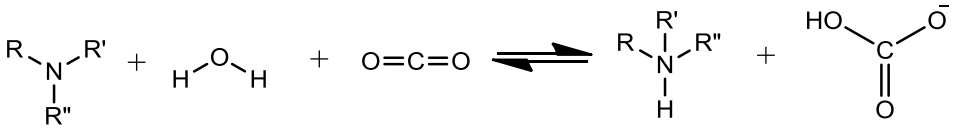

(2.11)

Following this reaction mechanism, the general expression of the reaction rate for tertiary amine and CO_2 is

$$r_2 = -k_2[Am][CO_2] \tag{2.12}$$

Since only bicarbonate is formed when tertiary amine is used as absorbent, the heat of absorption and reaction rate is usually considerably lower than for primary and secondary amine.

2.1.3 Hindered Amines

"A sterically hindered amine is defined structurally as a primary amine in which the amino group is attached to a tertiary carbon atom, or a secondary amine in which the amino group is attached to a secondary or a tertiary carbon atom" (Sartori and Savage 1983). Formation of carbamate becomes unfavorable and much slower due to the increased hindrance around the amino group. For moderately hindered amine, the

zwitterion mechanism may still contribute to the overall reaction rate. However, the subsequent decomposition of zwitterion to bicarbonate and protonated amine is likely to determine the final equilibrium (Alper 1990). The reaction mainly proceeds via bicarbonate production, as shown in the following reactions.

$$Am + CO_2 + H_2O \Leftrightarrow AmCOO^- + H_3O^+ \tag{2.13}$$

$$AmCOO^- + H_2O \Leftrightarrow AmH^+ + HCO_3^- \tag{2.14}$$

Just like tertiary amine, hindered amine has a high thermodynamic capacity for CO_2 that approaches 1 mol CO_2 / mol amine. Moderately hindered amine has a carbamate stability of intermediate or low and the overall reaction rate constant is low. Nonetheless, the fraction of free hindered amine in the CO_2 loaded solution that is available for CO_2 absorption increases with decreased carbamate stability constant, and may compensate for the lower reaction rate constant.

2.1.4 Acid and Basic Catalysis

The reaction rate constant between amine and CO_2 is not only dependent on the molecular structure of amine but also the basic strength of amine. The theory on acid and basic catalysis was first proposed by Bronsted (Bronsted 1928). In his work, the concept of acid and base was extended to any substance which accepts or donates protons.

$$A + H_2O \overset{K_A}{\leftrightarrow} B + H_3O^+ \tag{2.15}$$

$$B + H_2O \overset{K_B}{\leftrightarrow} A + OH^- \tag{2.16}$$

where A is the acid and B is the conjugate base.

In the same work Bronsted also suggested that catalytic effect from a Bronsted acid or base be proportional to the strength of the acid or base.

$$k_a = G_1 \cdot K_A^x \tag{2.17}$$

$$k_b = G_2 \cdot K_B^{1-x} \tag{2.18}$$

where k_a (k_b) and K_A (K_B) denote the catalytic and dissociation constant of the acid (base) catalyst respectively; G_1 and G_2 are constants dependent upon temperature, pressure, medium and substrate; x is a fraction value independent of acid (base) strength and has the same value for conjugate acids and bases.

The Bronsted theory has been validated for CO_2 absorption into amine. Littel *et al.* (Littel, Versteeg et al. 1992) found that in primary and tertiary amine blend, the deprotonation rate constant and the corresponding pKa value of the base followed the Bronsted correlation. Versteeg *et al.* (Versteeg and van Swaaij 1988) found that for a wide variety of alkanolamines over a wide range of temperature, the Bronsted relationship between the zwitterion–formation rate constant and the acid dissociation constant of the alkanolamines is valid. Kinetic data compiled by Rochelle *et al.* (Rochelle, Bishnoi et al. 2001) also shows that a correlation of Bronsted theory can be generalized for each category of amine: primary amine, secondary amine, hindered amine and heterocyclic amine.

For the reactions between CO_2 and amines, there are two bases involved: The amine (Am) reacting with CO_2 and the base (b) catalyzing the reaction. The reaction rate constant for the termolecular mechanism is related to the basic strength of the amine and the base by the following equation (Cullinane 2005):

$$\log_{10} k_{Am-b} = (\alpha_{Am} + \beta_{Am} pK_{a,Am}) + (\alpha_b + \beta_b pK_{a,b}) \tag{2.19}$$

For the same carbamate-formation amine, this correlation can be used to compare the catalysis effect of two bases (b_1 and b_2).

$$\log_{10} k_{Am-b_2} = \log_{10} k_{Am-b_1} + \beta_b (pK_{a,b_2} - pK_{a,b_1}) \tag{2.20}$$

2.2 MASS TRANSFER

2.2.1 Mass Transfer Without Reaction (Physical Absorption)

Without any reactive species in the solution, the absorption rate of CO_2 for unit area (CO_2 flux, N_{CO_2}) depends on the physical solubility of CO_2 in the solution (Henry's constant, H_{CO_2}) and the liquid phase mass transfer coefficient (k_l^0):

$$N_{CO_2} = k_l^0([CO_2] - [CO_2]^*) = k_l^0(\frac{P_{CO_2}}{H_{CO_2}} - [CO_2]^*) \tag{2.21}$$

k_l^0 is a function of the liquid viscosity and CO_2 diffusivity in the liquid.

The following section will briefly review several important mass transfer models that have been developed for description of the absorption mechanism regarding relationship between mass transfer coefficient and the physical properties of the gas and liquid. Although these theories are discussed in the scenario of physical absorption, they can also be applied to mass transfer with chemical reactions.

2.2.1.1 Film Theory

A two-film theory is proposed by Lewis and Whitman (Lewis and Whitman 1924) to model steady-state mass transfer between gas and liquid. As shown in Figure 2.2, as gas and liquid contact each other, there exists a gas film and a liquid film right next to the interface. They are stagnant and of finite thickness of δ_g and δ_l, respectively. The rate of absorption is determined by the diffusion of solute i through these two films while the rest of gas and liquid is well mixed and no concentration gradient exists. The

gas and liquid are assumed to be in equilibrium at the interface. With the setup of the equation of mass balance as well as proper boundary conditions, the concentration profile in the boundary layer can be derived. The mass transfer rate (flux) is then calculated with the application of the Fick's law at the interface, resulting in the following expression:

$$N = k_l^0 (C_i^* - C_i) = \frac{D_i}{\delta_l} (C_i^* - C_i) \tag{2.22}$$

where N is the flux, k_l^0 is the physical liquid mass transfer coefficient and D_i is the diffusion coefficient of the solute in the liquid.

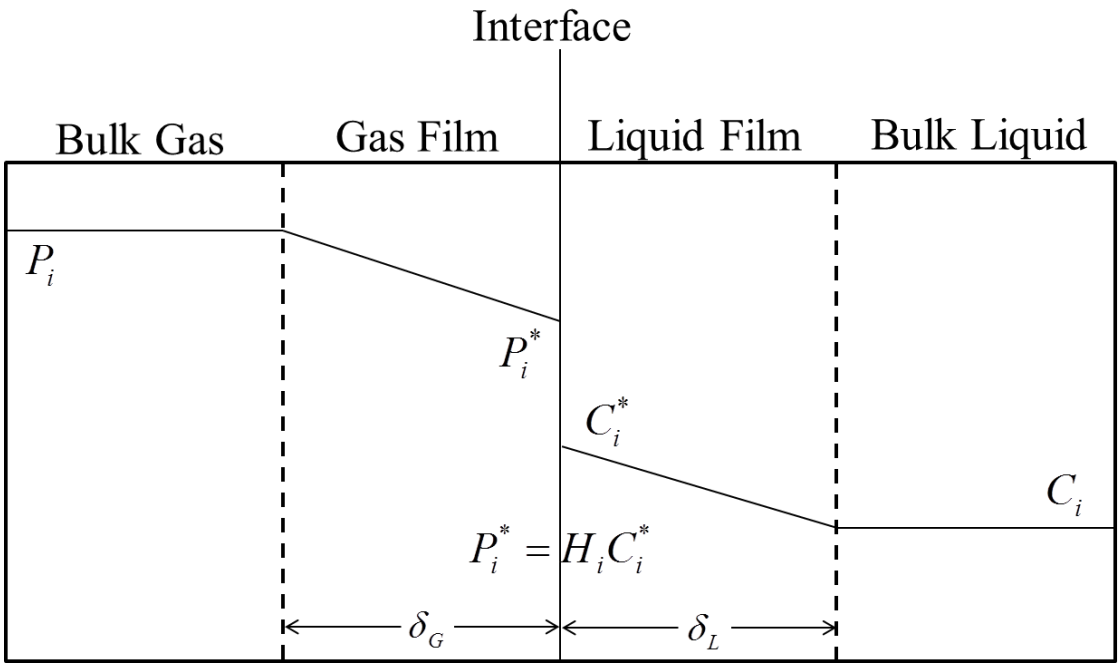

Figure 2.2: Schematic of the film theory for gas absorption into liquid.

The proportional dependence of k_l^0 on diffusivity derived from the film theory is not consistent with most experimental findings. However, the film theory is able to catch the essential feature that "gas must get into the liquid by dissolution and molecular

diffusion before it can be transported by convection" (Danckwerts 1970). Because of its simplicity the film theory is widely used in modeling of gas-liquid mass transfer. To improve the accuracy of the calculation for concentration profile within the boundary layers, especially as fast chemical reactions are involved, the films are usually further divided into segments, and mass transfer equations are numerically solved for each segment. This strategy is also implemented in the modeling software Aspen Plus® used in this work.

2.2.1.2 Penetration Theory

Higbie (Higbie 1935) argued that the film theory with its steady flow was not valid if the penetration period is of same magnitude to or even longer than the contact time between gas and liquid. Instead he proposed "Penetration Theory" to describe the real mechanism of absorption. This unsteady-state theory hypothesizes that elements of liquid at the surface is replaced by liquid from the bulk at intervals due to the turbulent motion of the liquid. Absorption only takes place when the elements of liquid are exposed to gas. The time of exposure for each element is of the same length, θ. During this time each element, which is assumed to be stagnant and infinitely deep, absorbs the same amount Q of gas per unit area. The relation between k_l^0 and θ is derived as follows:

$$k_l^0 = \frac{Q}{\theta(C_i^* - C_i)} = 2\sqrt{\frac{D_i}{\pi\theta}} \tag{2.23}$$

The square root dependence of physical mass transfer coefficient on gas diffusivity is consistent with previous experiments, in which an order of 0.5-1 on the diffusion coefficient is observed (Bishnoi 2000).

2.2.1.3 Surface Renewal Theory

The surface renewal theory is very similar to the penetration theory except the specification of the length of exposure time. Danckwerts (Danckwerts 1951) suggested that the same time of exposure for all the elements of surface is not realistic. He proposed the following stationary normal distribution of the time of exposure:

$$\phi(\theta) = se^{-s\theta} \tag{2.24}$$

where s is the mean fractional rate of replacement of any element at the surface. This distribution leads to the following dependence of k_l^0 on s:

$$k_l^0 = \sqrt{D_i s} \tag{2.25}$$

Other distributions of surface ages than the previous models have also been postulated and lead to different correlations.

2.2.1.4 Eddy Diffusivity Theory

The eddy diffusivity theory put forward by King (King 1966) postulates that the eddy diffusivity for a liquid element near or at the gas-liquid interface can be described by a power law:

$$D_E = a\delta^n \tag{2.26}$$

where δ is the distance normal to the interface. At the interface where $\delta = 0$, the eddy diffusivity is zero and the mass transfer is completely dominated by molecular diffusion. Thus the mass transfer behavior for a liquid element at the surface can be represented by the following equation:

$$\frac{\partial C_i}{\partial t} = \frac{\partial}{\partial \delta}[(D + D_E)\frac{\partial C_i}{\partial \delta}] \tag{2.27}$$

In this model a and n are independent of surface age t. If the surface age is high enough and n is sufficiently large, steady-state mass transfer will occur and k_l^0 becomes independent of t:

$$k_l^0 = a^{1/n} D_i^{1-1/n} \frac{n}{\pi} \sin\left(\frac{\pi}{n}\right) \tag{2.28}$$

The eddy diffusivity model with $n = 2$ was applied by Bishnoi (Bishnoi 2000) and Cullinane (Cullinane 2005), which corresponds to :

$$k_l^0 = \frac{2}{\pi}\sqrt{aD_i} \tag{2.29}$$

The eddy diffusivity theory allows the removal of time as a variable and simplifies solution of equations. The predictions from eddy diffusivity theory have been shown to be comparable to those from the surface renewal and penetration theory within 5% (Glasscock 1990). The main advantages of eddy diffusivity theory compared to the film theory are "the allowance for a continuous eddy diffusivity profile near the free interface ", and the avoidance of the concept of a "film" or a discontinuity in transport properties (King 1966).

2.2.2 Mass Transfer With Chemical Reaction

2.2.2.1 Instantaneous Reactions

In a limiting case the reaction between CO_2 and some highly reactive solvents like MEA and PZ at high temperature is extremely fast so equilibrium applies. With instantaneous and reversible reactions, the net result of presence of alkanolamine, to a first order approximation, is the enhancement of CO_2 solubility (Rochelle, Bishnoi et al. 2001). All dissolved forms of the gas, such as bicarbonate or carbamate, are added up to represent the total solubility of CO_2. The mass transfer rate is then given by:

$$N_{CO_2} = k_l^0([CO_2]_{i,T} - [CO_2]_T^*) = k_l^0(\frac{P_i}{H'_{CO_2}} - [CO_2]_T^*) \tag{2.30}$$

where H'_{CO_2} is the Henry's constant of CO_2 in the amine solvent; $[CO_2]_{i,T}$ is the total concentration of the dissolved CO_2 species at the gas-liquid interface that would be in equilibrium with CO_2 partial pressure in the gas phase (P_i).

2.2.2.2 Finite-Rate Reaction

Figure 2.3 is a representation of film analysis for CO_2 absorption by bulk liquid with fast chemical reaction. In this case, reaction rate is not so fast to be instantaneous while still fast enough for most of the reaction to occur within a thin boundary layer (reaction film) near gas-liquid interface. This scenario applies to most of CO_2 absorption by amine solvents. The concentration of CO_2 at the interface is now related to the chemical reaction. The rate of absorption is a function of the reaction rate constant as well as thermodynamics.

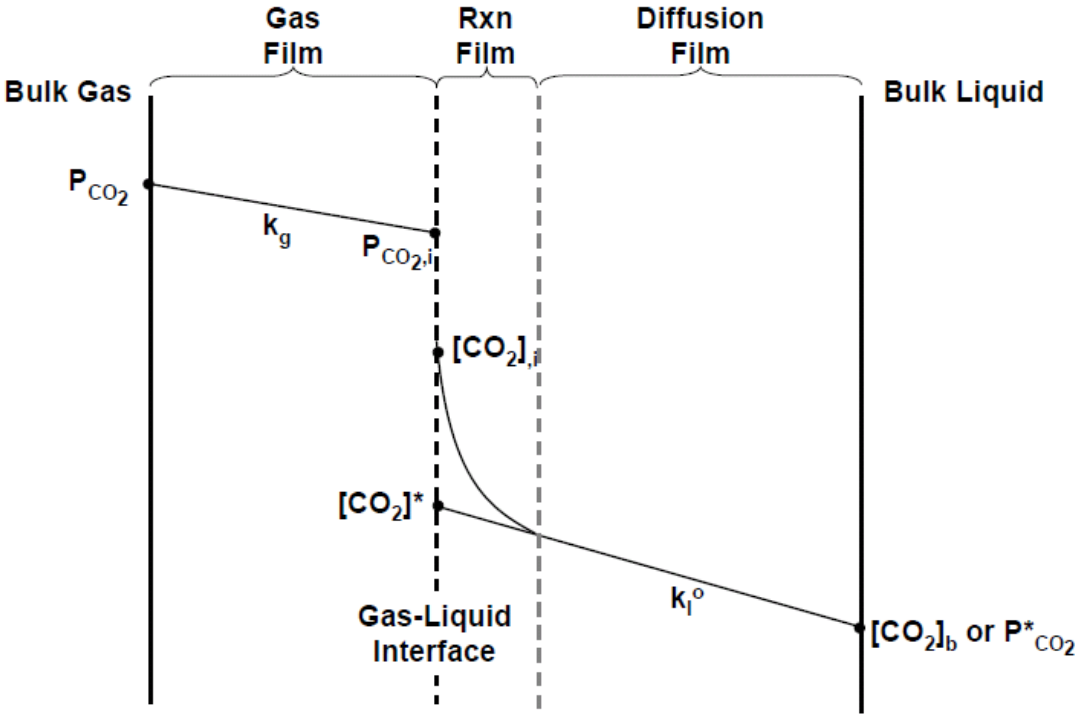

Figure 2.3: Mass transfer of CO_2 into bulk liquid with fast chemical reaction. (Cullinane 2005)

The total resistance to mass transfer consists of a series of resistances from gas film, reaction film and diffusion film, represented by the following equation:

$$\frac{1}{K_G} = \frac{1}{k_g} + \frac{H_{CO_2}}{Ek_l^0} + \frac{1}{k_{l,PROD}^0}\frac{\partial P_{CO_2}^*}{\partial [CO_2]_T} = \frac{1}{k_g} + \frac{1}{k_g^'} \tag{2.31}$$

where K_G , k_g and $k_g^'$ are the overall, gas-side and liquid-side mass transfer coefficients with driving force in gas partial pressure unit, respectively. E is the enhancement factor defined as the ratio of CO_2 flux with chemical reaction and CO_2 flux with only physical absorption. $\partial P_{CO_2}^* / \partial [CO_2]_T$ represents the slope of equilibrium curve for CO_2 in amine-CO_2-water.

CO_2 flux is usually calculated by solving the steady-state differential equation on CO_2 mass balance in the boundary layer (Eq. (2.32)), followed by applying the Fick's law to the CO_2 concentration profile at the interface (Eq. (2.33)).

$$D_{CO_2}\frac{\partial^2 [CO_2]}{\partial x^2} + r_{CO_2} = 0 \tag{2.32}$$

$$N_{CO_2} = -D_{CO_2}\frac{\partial [CO_2]}{\partial x}\Big|_{x=0} \tag{2.33}$$

Certain simplifications reduce the complexity in solving the differential equation and lead to useful analytical expressions. If the amine concentration is effectively constant across the reactive boundary layer, then the pseudo-first order (PFO) reaction assumption applies.

Irreversible Reactions

For irreversible PFO reactions, the concentration profile of CO_2 reacting with amine is given by the following differential equation:

$$D_{CO_2}\frac{\partial^2 [CO_2]}{\partial x^2} - k_1[CO_2] = 0 \tag{2.34}$$

Bishnoi (Bishnoi 2000) shows the detailed procedures for the integration of Eq. (2.34) and gave the final analytical solution:

$$[CO_2] = \frac{1}{\sinh Ha}\left[[CO_2]_B \sinh\left(x\sqrt{\frac{k_1}{D_{CO_2}}}\right) + [CO_2]_i \sinh\left(\frac{D_{CO_2}}{k_l^0} - x\right)\sqrt{\frac{k_1}{D_{CO_2}}}\right] \tag{2.35}$$

where $Ha = \sqrt{k_1 D_{CO_2}} / k_l^0$ is the Hatta number, $[CO_2]_B$ and $[CO_2]_i$ are the CO_2 concentration in the bulk and at the interface respectively.

Applying the Fick's law at the interface results in the following expression for the flux under PFO conditions:

$$N_{CO_2} = k_l^0 \left([CO_2]_i - \frac{[CO_2]_B}{\cosh Ha} \right) \frac{Ha}{\tanh Ha} \tag{2.36}$$

If the reaction is fast but not instantaneous and $1 << Ha << E^\infty$ is valid, Eq. (2.36) can be further simplified:

$$N_{CO_2} = k_l^0 Ha [CO_2]_i \tag{2.37}$$

In this case the enhancement factor is equal to the Hatta number.

The infinite enhancement factor for irreversible reaction is given by

$$E^\infty = \sqrt{\frac{D_{CO_2}}{D_{Am}}} + \frac{[Am]_B}{z[CO_2]_i} \sqrt{\frac{D_{Am}}{D_{CO_2}}} \tag{2.38}$$

where z is the stoichiometric number for amine.

Reversible Reactions

The CO_2-amine reactions concerned in this work are reversible reactions. Consider the following reaction and assume that the reaction is first order with respect to both CO_2 and amine.

$$Am + CO_2 \underset{k_r}{\overset{k_2}{\leftrightarrow}} P \tag{2.39}$$

The reaction rate

$$r_{CO_2} = -\left(k_2 [Am][CO_2] - k_r P \right) \tag{2.40}$$

The equilibrium constant for the reaction is

$$K = \frac{P}{[Am][CO_2]} = \frac{k_2}{k_r} \tag{2.41}$$

Then the reaction rate can be written as

$$r_{CO_2} = -\left(k_2[Am][CO_2] - \frac{k_2}{K} P \right) \tag{2.42}$$

The equilibrium CO_2 concentration $[CO_2]_e$ is defined as the CO_2 concentration that would be equilibrium with the actual concentration of the reactants.

$$[CO_2]_e = \frac{P}{[Am]K} \tag{2.43}$$

Subsequently the reaction rate can be expressed in the following form:

$$r_{CO_2} = -k_2[Am]([CO_2] - [CO_2]_e) \tag{2.44}$$

Thus the concentration profile of CO_2 reacting with amine is transformed to the following differential equation:

$$D_{CO_2} \frac{\partial^2[CO_2]}{\partial x^2} - k_2[Am]([CO_2] - [CO_2]_e) = 0 \tag{2.45}$$

As amine concentration in the liquid is much higher than CO_2 concentration, amine concentration is constant over the boundary layer. Hence pseudo-first order assumption can be applied. The solution to Eq. (2.45) is then given by:

$$N_{CO_2} = \frac{\sqrt{D_{CO_2} k_2 [Am]_b}}{H_{CO_2}} (P_{CO_2,i} - P^*_{CO_2}) \tag{2.46}$$

Therefore the expression for liquid mass transfer coefficient is

$$k_g^{'} \approx \frac{\sqrt{D_{CO_2} k_2 [Am]_b}}{H_{CO_2}} \tag{2.47}$$

The assumption of fast PFO reaction is usually valid for concentrated fast amine solvent at low temperature and low CO_2 loading. The following conditions generally cause the deviation from PFO (Bishnoi 2000).

1). High CO_2 partial pressure and high CO_2 flux, which causes partial or complete depletion of amine in the boundary layer.

2). Low concentration of free amine compared to CO_2 flux. At high CO_2 loading, the free amine concentration in the bulk liquid is even lower.

3). High temperature, leading to instantaneous reactions. The absorption of CO_2 becomes diffusion-controlled rather than reaction-controlled.

4). Low physical mass transfer coefficient which limits the transport of amine from the bulk to the interface and products from the interface to the bulk.

2.2.3 Literature Data on Kinetics and Mass Transfer Rate

Kinetics for reactions between CO_2 and various amines was extensively explored by many researchers. A comprehensive summary on the studies before 2001 has been given by Rochelle *et al.* (Rochelle, Bishnoi et al. 2001). The works published recently will be reviewed in this section.

2.2.3.1 Gas-Liquid Contactors

Varieties of gas-liquid contactors have been used for characterization of mass transfer coefficients as well as reaction kinetics.

Laminar Jet (LJ)

A diagram for a laminar jet is shown in Figure 2.4. The absorption chamber is filled with the absorbed gas. A jet of liquid enters the chamber through a circular nozzle, flows intact downward through the atmosphere of the gas, and then leaves through a capillary tube. The capillary tube has an internal diameter slighter larger than the diameter of the jet to prevent the jet from entraining gas-bubble or spilling liquid.

With proper design of the nozzle or orifice where the jet is formed, the behavior of the jet can be regarded as an ideal rod-like flow. The time of exposure of the liquid surface to the gas is calculated as

$$t = \frac{\pi d^2 h}{4v} \tag{2.48}$$

where h: length of the jet

d: diameter of the jet

v: volumetric flow rate of the liquid

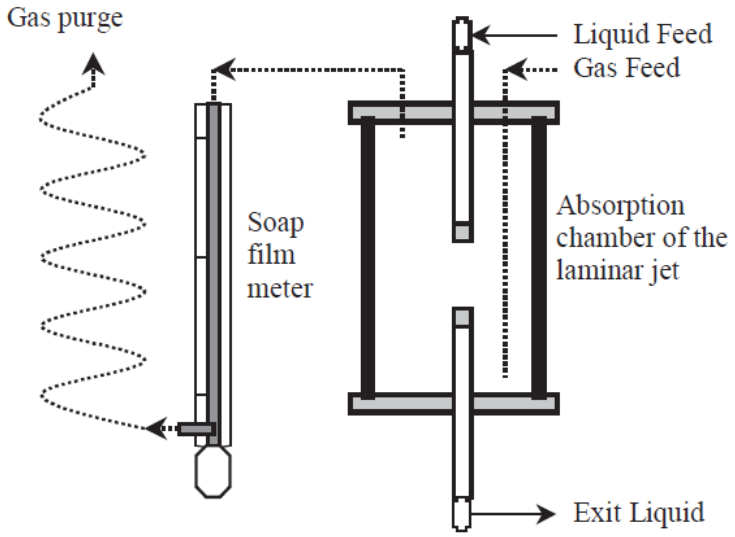

Figure 2.4: Schematic drawing of laminar jet apparatus. (Aboudheir, Tontiwachwuthikul et al. 2003)

Typically the contact-time can be varied between 0.001 - 0.01 sec by varying h and v. The total rate of absorption can be determined by taking the difference of the flow rate of the gas entering and leaving the chamber.

The laminar jet is suitable for study of very fast kinetics between gas and liquid. The free amine at the interface is not appreciably depleted at most conditions thanks to the high liquid flow rate and the short contact time. It may require a relatively large amount of liquid to finish a comprehensive study on an absorbent though.

Stirred Cell (SC)

A schematic diagram of stirred cell is shown in Figure 2.5. In a typical experiment, liquid is first loaded into the reactor, degased and thermostated at desired

temperature. Then the chamber on the top is quickly charged with gas at certain partial pressure followed by a continuous recording of gas phase pressure over time. The gas flux into the liquid is calculated based on the ideal gas law:

$$N_{CO_2} = \frac{dP_G}{dt}\frac{V_G}{A_{GL}RT_G} \tag{2.49}$$

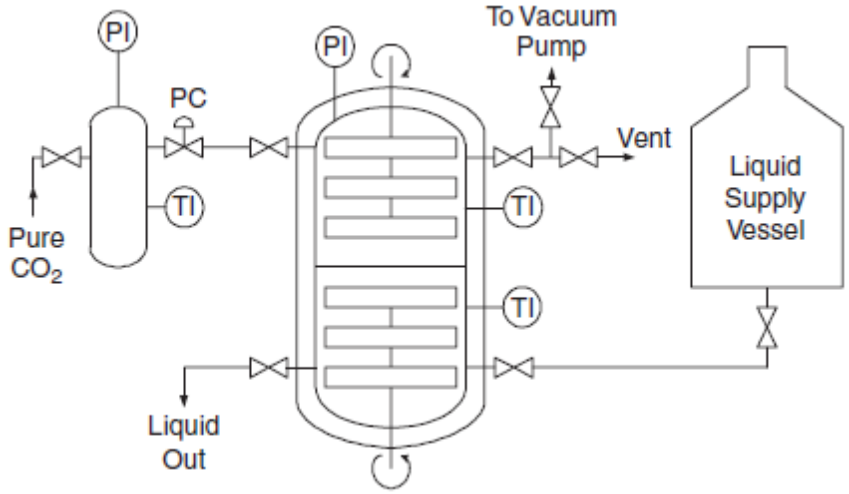

Figure 2.5: Diagram of a stirred cell setup (Derks, Kleingeld et al. 2006))

The reactor is operated batchwise with respect to liquid phase, while semi-continuous or batchwise with respect to gas phase. Derks *et al.* (Derks, Kleingeld et al. 2006) suggested semi-batchwise for gas phase operation to improve experimental accuracy. The stirred cell has proven to be a reliable method for determination of kinetics in gas-liquid systems. It offers several advantages: use of liquid with a single known composition, easiness in operation, well-defined gas-liquid contact area. However, the disadvantages are that liquid mass transfer coefficient (k_l) is relatively low, which limit its applicability in fast gas-liquid reactions; in addition, k_l is sensitive to the stirring rate and the depth and position of stirrers, which complicates the analysis of experimental results (Vaidya and Kenig 2007).

To make the absorption process fall into the pseudo-first order regime so that the absorption rate is independent of k_l, the amine concentration, the partial pressure of reactive gas components as well as the stirring speed need to be selected carefully. The following criteria have to be met:

$$2 < Ha << E^{\infty}$$

Generally a series of experiments need to be conducted to identify the PFO regime.

Wetted Wall Column (WWC)

As shown in Figure 2.6, in a WWC, the liquid passes through the center of a vertical tube or rod, forms a film on the outer surface under the influence of gravity, and then exits through an annular gap. The liquid velocity at the surface is

$$u_s = \frac{3}{2}\left(\frac{v}{\pi d}\right)^{2/3}\left(\frac{g\rho}{3\mu}\right)^{1/3} \tag{2.50}$$

And the contact time between liquid and gas is given by

$$t = \frac{h}{u_s} = \frac{2h}{3}\left(\frac{3\mu}{g\rho}\right)^{1/3}\left(\frac{\pi d}{v}\right)^{2/3} \tag{2.51}$$

h : height of the column

d : diameter of the column

v : volumetric flow rate of the liquid

μ : viscosity of the liquid

ρ : density of the liquid

Similar to the laminar jet, the absorption rate of the gas can be determined from the change in the gas flow rate in the inlet and outlet.

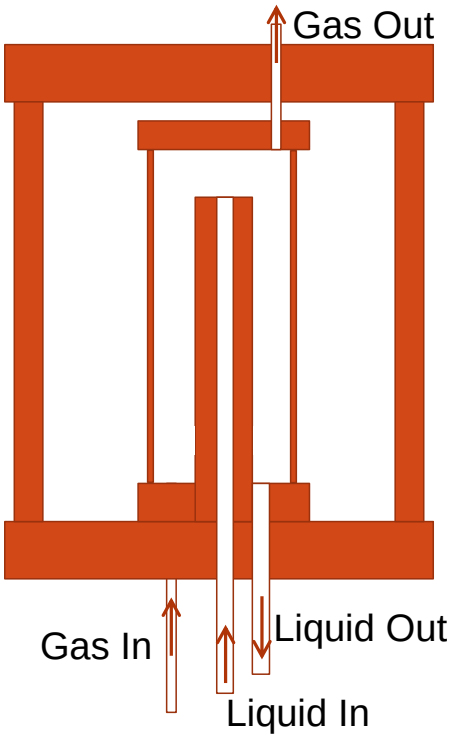

Figure 2.6: Schematic of a wetted wall column contactor.

Although there have been a number of different designs for the WWC, Danckwerts (Danckwerts 1970) pointed out a few common precautions that must be taken to reduce errors of measurements:

a. Entrance effect. The errors introduced by the different liquid velocity along the column and at the exit can be minimized by a proper design of the annular gas under the column.

b. Ripple effect. Ripples appearing on the film could enhance absorption rate. They can be eliminated by working with a shorter column or adding surface – active agents. However, the former could cause other problems such as greater end-effect, and the latter may alter the mass transfer resistance of the film.

c. Rigid film. The surface at the bottom of the column tends to be immobilized due to the accumulation of surface-active components, which reduces the rate of absorption. A grooved collar was suggested to mitigate this problem.
d. The assumption that the liquid film is infinitely deep and moving with uniform velocity also leads to errors that need to be taken into account.

String-of- Discs Column

This contactor was first introduced by Stephens and Morris (Stephens and Morris 1951). Circular disks are connected along a vertical wire and enclosed in a glass tube. The design and the range of liquid mass transfer coefficient make this apparatus a good model for a packed column. The disadvantage of using disc column is that the gas and liquid composition may change substantially over the height of the column. Therefore it is hard to characterize absorbents at defined compositions. For this reason the disk column is not suitable for fundamental studies on solvent properties.

Others

Other gas-liquid contactors such as wetted-sphere absorber, hemispherical contactor, rotating drum, string-of-sphere column etc. have been reviewed by Danckwert (Danckwerts 1970) and Vaidya *et al.* (Vaidya and Kenig 2007) and will not be discussed in this work.

For its simplicity, the wide range of applicability, versatility in data acquisition, and easiness of data interpretation, WWC is selected in this work for characterization of the mass transfer rate and kinetics between CO_2 and different amine solvents.

2.2.3.2 Historic Kinetic and Mass Transfer Data

Table 2.2 summarizes some kinetic studies that have been done for absorption of CO_2 into aqueous amine solutions since 2001. As can be seen from the table, most of

the studies focused on the absorption of CO_2 into dilute or medium concentrated amine solvent at zero or very lean CO_2 loading. There were relatively few studies for highly concentrated (> 40 wt% or > 3 M) and highly CO_2-loaded amine solvents, which are more relevant to application in CO_2 capture. Apparent second order reaction constant (k_2) is usually reported as the main result. The mass transfer data reported from stirred cell or laminar jet are usually not applicable for design of the absorber, which normally uses packing as the contactor. Besides that, most of the data were collected at temperature below 60 °C. However, it would be helpful to obtain mass transfer rate data at stripper conditions for rate-based design.

In a separate table (Table 2.3), the amine solvents that have been studied in the research group in the University of Texas at Austin using the same WWC used in this work are listed. These studies focused on measurement of kinetic data for highly concentrated and highly CO_2 loaded amine solvents in a broader range of temperature. The results obtained therefrom provide valuable information on the performance of conventional amine solvents in post-combustion CO_2 capture. 7 m MEA and 8 m PZ, as the first-generation and second-generation solvent standard respectively, will be used as baselines for evaluation of the amine solvents tested in this work.

Table 2.2: Summary of kinetic studies on aqueous amine solvents since 2001.

Type	Amine	[Am]	CO_2 loading (mol/mol amine)	Temp. (℃)	k_2 (m^3/kmol/s)	k_l (10^{-5} m/s)	Flux (10^{-3} mol/m^2/s)	Exp. Tech.	Source
Primary	MEA	5 M	0-0.5	40,60	2634 at 10 ℃	n/a	Overall K_G = 0.32-3.69 mmol/s/m^2/kPa	WWC	(Puxty, Rowland et al. 2010)
	MEA	3-9 M	0.1-0.49	20-60	Termolecular Mechanism MEA: $4.61\times10^{9}\exp\left(\frac{-4412}{T}\right)$ H_2O: $4.55\times10^{6}\exp\left(\frac{-3287}{T}\right)$	n/a	n/a	LJ	(Aboudheir, Tontiwachwuthikul et al. 2003)
	MEA	20 wt.%	0	20-51	$4.495\times10^{11}\exp\left[-\frac{4494}{R}(1/T-1/293)\right]$	n/a	n/a	SC	(Kucka, Richter et al. 2003)
	2-(1-piperazinyl)-ethylamine (PZEA)	0.083-1.226 M	0	30,40,50	$4.5\times10^{12}\exp\left(\frac{-47308}{RT}\right)$	n/a	3.1-14.5	WWC	(Paul, Ghoshal et al. 2009)
	NH_3	0.6,3,6 M	0-0.8	5,10,20	$915\exp\left[-\frac{61000}{R}(1/T-1/283)\right]$	n/a	Overall K_G 0.10-1.66 mmol/s/m2/kPa	WWC	(Puxty, Rowland et al. 2010)
Secondary	PZ	0.23-0.92 M	0.179-0.837	30.35,40	$4.49\times10^{12}\exp\left(-\frac{5712}{T}\right)$	5.52 - 6.49	4.08-9.07	WWC	(Sun, Yong et al. 2005)
	PZ	0.2-0.8 M	0	25,30,35, 40	PZ $5..8\times10^{4}\exp\left[-\frac{35000}{R}(1/T-1/298)\right]$ PZCOO- $5..95\times10^{4}\exp\left[-\frac{35500}{R}(1/T-1/298)\right]$	7.44 - 11.3	1.58-11.4	WWC	(Samanta and Bandyopadhyay 2007)
	PZ	0.6-1.5 M	0	25, 30,40	PZ: 70 at 25 ℃ PZH+: 0.28 at 25 ℃	1.4-3.0	0.8-10.9	SC	(Derks, Kleingeld et al. 2006)

	PZ	0.0025-0.1 M	0	25,30,35	21311-31061 at 30 ℃	n/a	0.6-3.3	SC	(Bindwal, Vaidya et al. 2011)
	N-(2-aminoethyl)ethanolamine (AEEA)	1.5-3.0 M	0	25,30,35	8530 at 30 ℃	n/a	8.7-31.2	SC	(Bindwal, Vaidya et al. 2011)
Tertiary	Diethylethanolamine (DEEA)	2.0-3.0 M	0	25,30,35	DEEA: 173 at 30 ℃	n/a	0.5-4.2	SC	(Vaidya and Kenig 2007)
	MDEA	10-30 wt%	0.29-0.96	20,40,60	n/a	n/a	0.04-0.64(Desorption)	SC	(Kierzkowska-Pawlak and Chacuk 2011)
Hindered	2-amino-2-methyl-1,3-propanediol (AMPD)	5-25 wt%	0.00143-0.00529	30,40,45	$1.54\times10^{9}\exp\left(-\frac{4603}{T/K}\right)$	n/a	n/a	WWC	(Yoon, Baek et al. 2003)
	AMP	0.5-2.5 M	0.01-0.971	30	n/a	2.2	3.8-10.1	SC	(Zhang, Shi et al. 2007)
	2-PE	0.14-1.13 M	0.119-0.470	30,40,50	$4.013\times10^{10}\exp\left(-\frac{45171}{RT}\right)$	5.1-8.9	11.7-40.8	WWC	(Paul, Ghoshal et al. 2008)
	2-amino-2-hydroxymethyl-1,3-propanediol (AHPD)	0.5-2.4 M	0	30,40,50	$5.08\times10^{11}\exp\left(-\frac{6465}{T}\right)$	13.2-17.1	1.22-18.64	WWC	(Bougie and Iliuta 2009)
	AHPD	0.179-1.789 M	0	30,40,50	$8.667\times10^{13}\exp\left(-\frac{65155}{RT}\right)$	n/a	0.56-4.92	WWC	(Paul, Ghoshal et al. 2009)
Amino acid	Sodium glycinate	1.07-3.47 M	0.114-0.300	30,40,50	$1.95\times10^{13}\exp\left(\frac{-7670}{T}\right)$	2.7-3.8	17-40	WWC	(Choi, Cho et al. 2007)
	Sodium glycinate	0.5-3.0 M	0	25,35,45	$3.82\times10^{12}\exp\left(\frac{-7188}{T}\right)$	0.54-0.89	3.6-21.6	SC	(Park, Son et al. 2008)
	K^+ salt of 6-aminohexanoicacid, _-alanine, l-arginine, l-glutamic, acid, dl-methionine, l-proline and sarcosine	0.5-3.0 M	0	25-60	n/a	n/a	n/a	SC	(Holst, Versteeg et al. 2009)
	K^+ salt of sarcosine	0.5 -3.8 M	0-0.46	25,30,35	22915±3050 at 25 ℃	n/a	0.1-1.5	SC	(Simons, Brilman et al. 2011)
Blend	2-amino-2-methyl-1-propanol (AMP) + Diethanolamine(DEA)	DEA: 0 – 0.425 M AMP: 2.843-3.326 M	0	40	n/a	4.83-6.92	46~60	WWC	(Mandal, Biswas et al. 2003)

PZ+AMP	PZ: 0.1-0.4M AMP: 1, 1.5 M	0.036-0.043	30.35,40	AMP: $3.13\times10^{7}\exp\left(-\frac{3034}{T/K}\right)$	3.0-4.5	3.0-4.5	WWC	(Sun, Yong et al. 2005)
MEA+AMP	MEA: 0-4.5 wt% (0-0.73M) AMP: 30-25.5 wt% (3.3-2.8 M)	0	40	AMP: $\exp\left(25.815-\frac{5801.7}{T/K}\right)$ MEA: 9500 m3/(kmols) at 313K	5.0-7.7	46-78	WWC	(Mandal and Bandyopadhyay 2006)
AHPD+PZ	PZ:0.1-0.4 M AHPD:1M	0	30,40,50	PZ: $1.353\times10^{10}\exp\left(-\frac{3706}{T/K}\right)$	10.7-14.1	1.66-2.55		(Bougie, Lauzon-Gauthier et al. 2009)
PZEA+MDEA	PZEA:0-0.3M MDEA:0.7-2.0M	0	30,40,50	PZEA: $4.16\times10^{12}\exp\left(-\frac{46943J/mol}{RT/K}\right)$ MDEA: $4.04\times10^{10}\exp\left(-\frac{56767}{RT}\right)$	n/a	0.28-7.28	WWC	(Paul, Ghoshal et al. 2009)
AMP+ Hexamethylenediamine (HMDA)	AMP: 30wt% HMDA: 1-5wt%	0	30,40,50, 70	HMDA: $3.84\times10^{10}\exp\left(-\frac{5361}{T}\right)$	n/a	n/a	SC	(Choi, Cho et al. 2007)
DEEA+PZ	DEEA: 2M PZ: 0.1-0.5M	0	25,30,35	PZ: 24450 at 30 ℃	n/a	1.5-8.7	SC	(Konduru, Vaidya et al. 2010)
AMP+PZ	AMP: 4.43-3.57M (40-32wt%) PZ: 0-0.92 M (0-8wt%)	0	30,40,50	n/a	2.8-5.5	5.4-49.8	WWC	(Dash, Samanta et al. 2011)
MDEA+PZ	MDEA:2.56-1.89 M PZ: 0-0.95 M	0	25-40	PZ: $1.75\times10^{-4}\exp\left[-\frac{87500}{R}(1/T-1/298)\right]$ PZCOO-: $1.55\times10^{-4}\exp\left[-\frac{87500}{R}(1/T-1/298)\right]$	4.2-6.4	1.32-28.8	WWC	(Samanta and Bandyopadhyay 2011)

	MDEA+MEA	MDEA: 2.3-2.0 M (23-27wt%) MEA: 0.49-1.15 M (3-7wt%)	0.1-0.14	25-60	n/a	n/a	n/a	LJ	(Edali, Aboudheir et al. 2009)
	MDEA+PZ	MDEA: 2.30-1.79 M (27-21wt%) PZ: 0.35-1.06M (3-9wt%)	0.005-0.33	30-60	PZ:4.38E5 at 60 ℃	n/a	n/a	LJ	(Edali, Idem et al. 2010)
	MEA+MDEA	MDEA: 27-23 wt% MEA: 3-7 wt%	0.005-0.15	25-60	MEA: $9.56\times10^{8}\exp\left(-\frac{3802.4}{T}\right)$ MDEA: $2.58\times10^{8}\exp\left(-\frac{3736.5}{T}\right)$	n/a	n/a	LJ	(Ramachandran, Aboudheir et al. 2006)

Table 2.3: Concentrated and CO_2-loaded aqueous amine solvents studied at The University of Texas at Austin.

Author/Year	**Solvents**	**[Amine] (molality)**	**Temp. (°C)**	**CO_2 loading (mol/mol alkalinity)**
(Dugas 2009)	MEA PZ MEA/PZ	7 ~ 13 2 ~ 12 7/2	40 ~ 100	0.2 ~ 0.5
(Cullinane 2005)	K^+/ PZ	0.0~ 6.2 /0.6 ~ 3.6	25 ~ 110	0.26 ~ 0.76
(Al-Juaied 2004)	DGA DGA / Morpholine	3.2, 17.7 14/3.5	25 ~ 60	0 ~ 0.45
(Bishnoi 2000)	MDEA/PZ	7.6 /0.2~ 0.6	25 ~ 70	0 ~ 0.31
(Pacheco 1998)	MDEA DGA MDEA/ DGA	4.5, 8.4 3.8, 11.5 0.8/10.3	25 ~ 110	0.02 ~ 0.55
(Mshewa 1995)	MDEA DEA MDEA/DEA	8.4 4.8 7.6/1.0, 4.2/4.8	40 ~ 120	0.02 ~ 0.46

Chapter 3: Experimental Methods

3.1 WETTED WALL COLUMN

Measurements of CO_2 solubility and rate of absorption and desorption in aqueous amine solutions were performed in a wetted-wall column (WWC). It was originally built by Mshewa (Mshewa 1995) and further improved by other researchers (Pacheco 1998; Bishnoi 2000; Dang 2000; Cullinane 2005; Okoye 2005; Dugas 2009). The design, operating procedure and data analysis for this WWC are described below.

3.1.1 Design

The detailed view of the WWC is shown in Figure 3.1. The stainless steel hollow column in the center is 9.1 cm in height and 1.26 cm in outer diameter (OD). The column is enclosed in a thick-walled glass tube whose inner diameter (ID) and OD is 1.83 cm and 2.54 cm, respectively. The gap between the vertical surface of the column and the inner wall of the glass tube has to be properly designed because the hydraulic diameter of the annulus affects the velocity of gas flow as well as the gas film mass transfer resistance. If the gap is too large, the gas film resistance is too high, which may make accurate measurement of liquid mass transfer coefficient more difficult; on the other hand, if the gap is too small, the liquid film on the surface will be appreciably disturbed by the fast gas flow, and it becomes harder to maintain stable operation of the WWC.

The gas enters the small chamber through a small orifice on the Teflon annular collar around the bottom of the column. The collar also serves to keep the gas from being mixed with the liquid. To make the gas flow in the glass tube more uniform, the exit point on the top for the gas is placed at the opposite side to the entrance point. It is

assumed that the composition of the gas is uniform horizontally but not vertically in experiments.

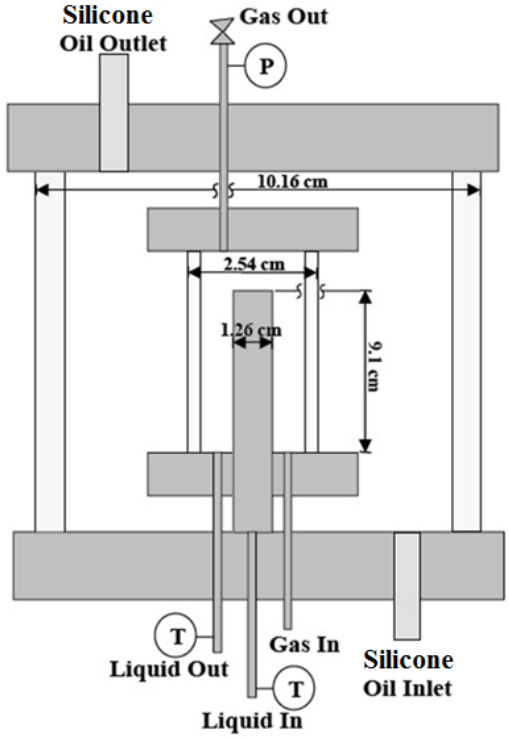

Figure 3.1: Detailed view of the WWC.

As liquid is pumped through the middle of the column, the liquid flow rate is carefully controlled so that the liquid will not overshoot from the top of the column but form a quasi-semisphere on the top and then flow down the column evenly. Adjustment of the tilt angle of the column may be necessary. The column has to be clean and free of oil, or the surface may not be evenly wetted by the amine aqueous solution. The liquid level is maintained at just slightly below the inner edge of the tilted annular surface of the collar. The space of ~ 1 mm between the column and the Teflon collar allows the liquid to be drained without carryover of the gas. For ideally formed liquid film, the total contact area between gas and liquid is calculated to be 38.52 cm^2.

The whole smaller chamber is enclosed in the larger chamber which is circulated with silicone oil to be maintained at desired temperature.

3.1.2 Operating Procedure

A schematic diagram of the entire apparatus is shown in Figure 3.2. The flow of nitrogen (N_2) and CO_2 is regulated by Brooks Mass Flow Controllers (Model #5850, Brooks Instrument, Hatfield, PA, USA). The total flow rate of the gas is kept constant at 5 standard liter (STL)/min. Variable CO_2 partial pressure in the gas mixture is achieved by altering ratio of the two inlet gases. A 20 STL/min mass flow controller is used for N_2 while three mass flow controllers (2, 0.5, 0.1 STL/min) are used for CO_2 to achieve higher accuracy in flow control. To cover a wider range of CO_2 partial pressure in gas, diluted CO_2 in N_2 (~ 5000 ppm) instead of pure CO_2 is also used. The gas mixture is first saturated with water at experimental temperature using a jacketed bubbling saturator (OD = 4 inches, ID = 3 inches, height =14 inches), and further heated by an oil bath before entering the WWC chamber from the bottom. The pressure in the WWC chamber is adjusted using a needle valve at the gas outlet, and it is measured with a standard pressure gauge (Matheson, p/n 63-3112, 0 – 100 psig) with an accuracy of 0.2 psi.

The liquid in a reservoir (one or two 1-liter stainless-steel calorimetric cells) is circulated in a closed loop at a rate of ~ 4 ml/s. The liquid volume flow rate is monitored using a rotameter. The liquid is also heated by the oil bath and then pumped into the middle of the column from the bottom. It overflows from the top, and is evenly distributed along the outer surface of the column, thus counter-currently contacting with the gas. The liquid is collected from the bottom through another liquid line and sent back to the reservoir. The temperature of liquid is measured using thermocouple probes placed at the inlet to the WWC of the liquid line. Although in this work the liquid is

recycled, the amount of the amine solvent is so large that even the greatest CO_2 flux between the gas and the solvent produced at the actual experimental conditions during the operating period of time does not significantly change the CO_2 loading of the solvent. The liquid composition remained essentially unchanged during an experimental run for each CO_2 loading and temperature. Three 3-ml liquid samples are taken at intervals through a septum on the liquid line for each temperature and CO_2 loading in order to confirm the liquid composition.

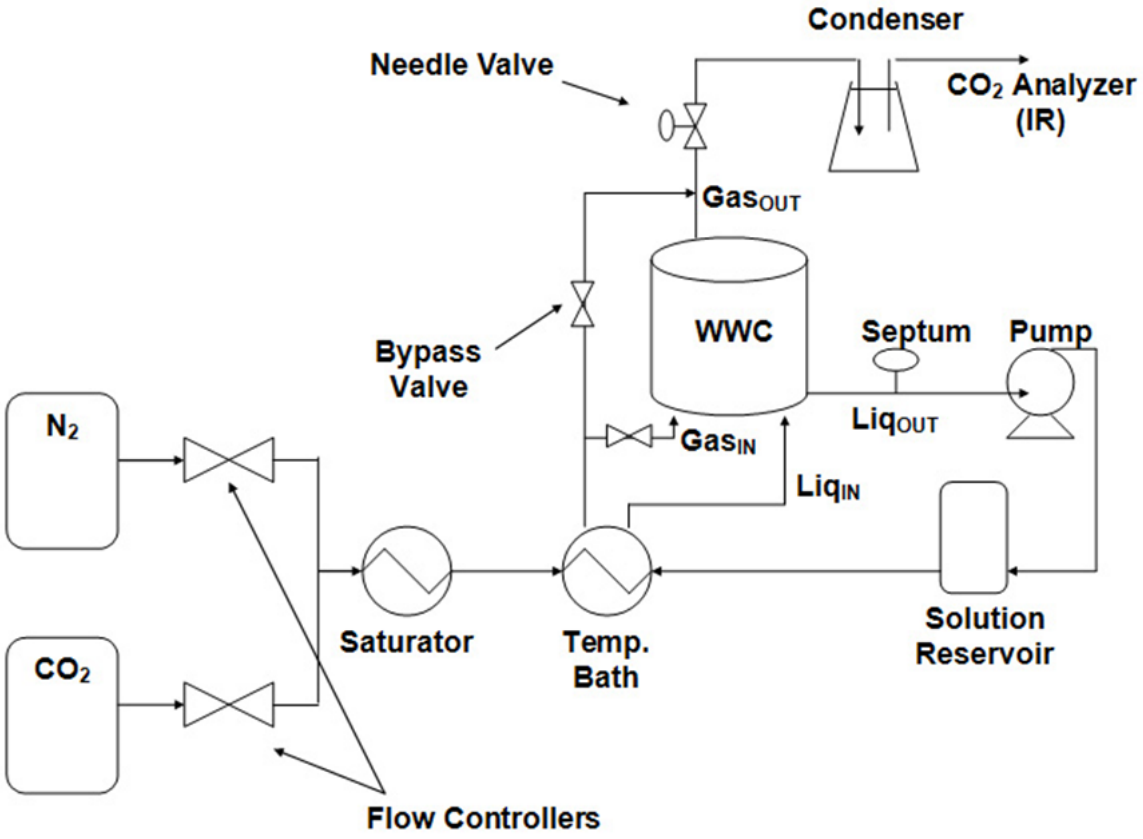

Figure 3.2: Flow diagram of the entire WWC setup.

The gas leaving from the top is passed through a condenser (a 500 ml flask immerged in an ice-water bath) and a desiccation unit (a tube filled with $CaSO_4$) to remove water and amine vapor contained. For those highly volatile amines, the amine

content in the solution is expected to slightly decrease over the course of experiments, especially at high temperature. However, the loss rate of each volatile amine is difficult to be quantified and is neglected in this work. A portion of the dried outlet gas is sent to the CO_2 analyzers while the rest is vented. There are two Horiba VIA-510 infrared analyzers available for the range of 0-1 vol% and 0-20 vol% CO_2, respectively. The analyzers are connected to a computer equipped with a PicoLog Data Acquisition program. The voltage of CO_2 response proportional to the CO_2 concentration in the gas stream is recorded continuously during an experiment.

The WWC is switched between two modes using the bypass valve: operation mode and bypass mode. In the operation mode, the gas is brought into contact with the liquid and the CO_2 concentration is measured after mass transfer; in the bypass mode, the inlet gas goes around the WWC and no mass transfer between gas and liquid occurs. The inlet CO_2 concentration is directly measured by the CO_2 analyzer. The length of time in the contact mode is always minimized to avoid unnecessary mass transfer between the gas and the liquid.

In a typical WWC experimental run, a solvent at certain CO_2 loading is prepared and loaded to the system. The equilibrium CO_2 partial pressure for the solution is estimated first by changing the CO_2 partial pressure in gas and locating the range of partial pressure where a transition from absorption and desorption occurs.

For each loading at each temperature, steady-state CO_2 fluxes and driving forces between gas and liquid for six CO_2 inlet concentrations are measured. Three of the CO_2 inlet concentrations induce absorption of CO_2 into solution and the other three correspond to desorption. The value of 0 for the CO_2 partial pressure in the gas phase (pure N_2) is always used as one of the desorption points. The maximum CO_2 partial pressure used for absorption is approximately twice of the estimated equilibrium CO_2 partial pressure of

the solvent. For each gas flow, the WWC is first bypassed to measure the inlet CO_2 concentration, which also gives the CO_2 partial pressure at the bottom of the column. Then the valve is switched and the WWC is operated at the operation mode. The CO_2 concentration in the outlet is measured to find out the CO_2 partial pressure at the top of the column.

For an amine solvent, the WWC experiments start with a lean loading, and they are carried out in the sequence of increasing temperature from 40 to 100 °C. After the experiments are finished, the solvent is taken out and loaded with more CO_2 to reach a richer loading. The procedure is then repeated. The capability of the WWC for solubility and rate measurements is limited by the maximum system pressure allowed (~ 100 psig) due to the pressure limit on the glass water saturator. The maximum measurable CO_2 concentration is also only up to 20 vol% for the CO_2 analyzer used in this work. As a result, experiments cannot be carried out for solvents at very high loading and high temperature.

3.1.3 Data Analysis

The driving force between gas and liquid is defined as the logarithmic mean of the driving force at the top and the bottom of the column.

$$\left(P_{CO_2,g} - P^*_{co_2}\right)_{LM} = \frac{(P_{co_2,top} - P^*_{co_2}) - (P_{co_2,bottom} - P^*_{co_2})}{\ln\left(\frac{P_{co_2,top} - P^*_{co_2}}{P_{co_2,bottom} - P^*_{co_2}}\right)} \tag{3.1}$$

The CO_2 flux can also be obtained given the total pressure and flow rate as well as the difference of the CO_2 concentration (molar fraction) before and after the contact with liquid.

$$N_{CO_2} = \frac{1}{A}\frac{P_t V_t}{RT}\left([CO_2]_{in} - [CO_2]_{out}\right) \tag{3.2}$$

A typical plot obtained from each run shown in Figure 3.3 illustrates the correlation between flux and driving force. A straight line can be fitted to the six points. It is known that the flux has to be zero as the driving force is zero. However, since log mean value cannot be zero, the line can only infinitely approach the origin point with the adjustment of $P^*_{co_2}$ in Eq. (3.1). The value of $P^*_{co_2}$ that makes the line almost go through the origin must be the correct equilibrium CO_2 partial pressure for the solvent. The overall mass transfer coefficient (K_g) can also be obtained by extracting the slope of the line:

$$K_g = \frac{N_{CO_2}}{\left(P_{CO_2,g} - P^*_{CO_2}\right)_{LM}} \tag{3.3}$$

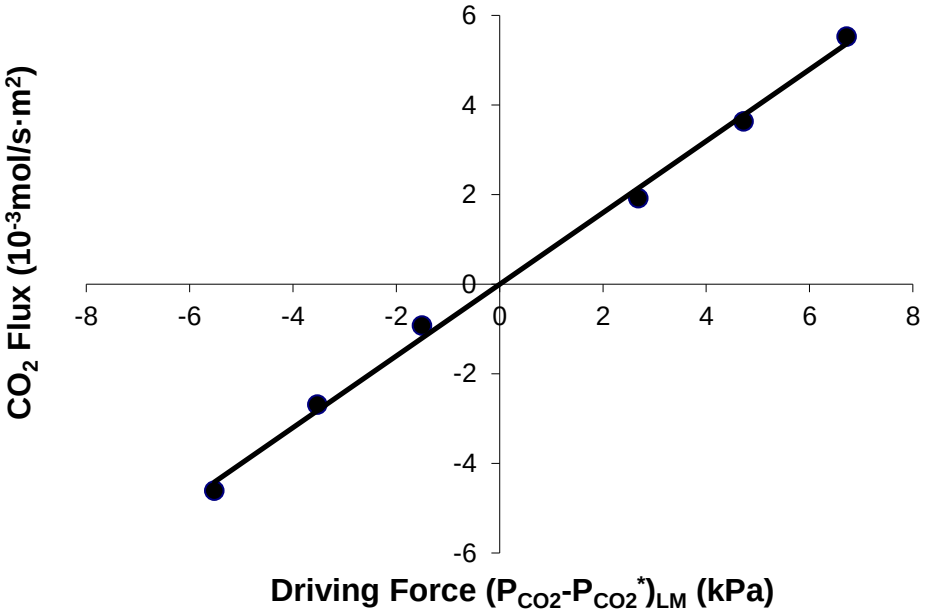

Figure 3.3: Linear correlation between CO_2 fluxes and driving force obtained from a set of measurements for 8 m 1-methylpiperazine at 60 °C and the loading of 0.20 mol CO_2/mol alkalinity in the WWC.

3.1.4 Gas Film Mass Transfer Coefficient

To separate the contribution of the liquid film and the gas film to the total mass transfer resistance, the gas film mass transfer coefficient (k_g) needs to be determined beforehand.

A dimensionless analysis to correlate k_g in laminar flow was done by Hobler (Hobler 1966), who proposed the following expression.

$$Sh = A \cdot \mathrm{Re}^B \cdot Sc^C \cdot \left(\frac{d}{h}\right)^D \tag{3.4}$$

Sh : Sherwood number

Re : Reynolds number

Sc : Schmidt number

d : the hydraulic diameter of the annulus (0.44 cm)

h : the height of the WWC (9.1 cm)

This form was adopted by Pacheco (Pacheco 1998), Bishnoi (Bishnoi 2000) and Dugas (Dugas 2009) for the development of correlations for k_g. The general principle in measuring k_g is to use a dilute gas stream and a solvent that has fast reaction rate with the gas. In this way, the mass transfer is mainly gas-film controlled. Although different solvents and gases were used to measure k_g in the WWC, the following expression was found to give a satisfactory fit to all the data.

$$Sh = 1.075\left[\mathrm{Re}\, Sc\left(\frac{d}{h}\right)\right]^{0.85} \tag{3.5}$$

The following equation allows the determination of k_g from Sh:

$$Sh = \frac{RTk_g l}{D_{CO_2}} \tag{3.6}$$

where l is the characteristic length, which is d for the WWC. k_g is therefore a strong function of the geometry of the WWC. Subsequently, the liquid mass transfer coefficient $k_g^{'}$ can be calculated from the following equation:

$$\frac{1}{k_g^{'}} = \frac{1}{K_G} - \frac{1}{k_g} \tag{3.7}$$

3.1.5 Liquid Film Physical Mass Transfer Coefficient

The liquid film physical mass transfer coefficient (k_l^0) is a property that indicates how fast a gas can be transported by a liquid without chemical reactions. For a WWC, k_l^0 can be theoretically calculated. Pigford (Pigford 1941) solved the continuity equation for gas diffusion into a falling liquid film, for which the convective transport is assumed not to affect the mass transfer in the direction perpendicular to the gas-liquid interface and only diffusive transport is important. Based on the calculation, k_l^0 is a function of the liquid flow rate (Q), the gas-liquid contact area (A) and a dimensionless driving force (Θ).

$$k_l^0 = \frac{Q}{A}(1-\Theta) \tag{3.8}$$

This model was chosen by Pacheco to represent the k_l^0 data measured from the experiments of CO_2 desorption from water (Pacheco 1998). The liquid flow rate is indicated by a rotameter. The correlation between the actual liquid flow rate and reading from the rotameter was given by Cullinane (Cullinane 2005):

$$Q(cm^3/s) = (0.4512x - 0.2901)\sqrt{\frac{7.83-\rho^2}{7.83-\rho_{T_{ref}}^2}}\sqrt{\frac{7.83-\rho_{T_{ref}}}{(7.83-0.997)\rho_{T_{ref}}}} \tag{3.9}$$

where x: rotameter reading

ρ: the density of the solution in g/cm^3

$T_{ref} = 25$ °C

By definition, the dimensionless driving force is equal to

$$\Theta = \frac{[CO_2]_i - [CO_2]_b^{out}}{[CO_2]_i - [CO_2]_b^{in}} \tag{3.10}$$

where $[CO_2]_b^{in}$ and $[CO_2]_b^{out}$ represents the CO_2 concentration in the bulk liquid at the inlet and outlet of the WWC, respectively, and $[CO_2]_i$ is the CO_2 concentration at the gas-liquid interface.

The theoretical calculation yields that for $\eta > 0.01$,

$$\Theta = 0.7857\exp(-5.121\eta) + 0.1001\exp(-39.21\eta) + 0.036\exp(-105.6\eta) + 0.0181\exp(-204.7\eta) \tag{3.11}$$

and for $\eta < 0.01$,

$$\Theta = 1 - 3\sqrt{\frac{\eta}{\pi}} \tag{3.12}$$

where $\eta = \frac{D\tau}{\delta^2}$ is a dimensionless penetration distance; $\tau = \frac{h}{u_s}$ is the time of exposure of the liquid surface, $u_s = \frac{\rho g \delta^2}{2\mu}$ is the liquid surface velocity and μ is the liquid viscosity; $\delta = \sqrt[3]{\frac{3\mu Q_{sol}}{\rho g W}}$ is the film thickness and W is the circumference of the column.

Eq. (3.12) is applicable for all of the WWC experimental conditions in this work. With substitution of Eq. (3.12), Eq. (3.8) is transformed to following expression after rearrangement (Dugas 2009):

$$k_l^0 = \left(\frac{3^{1/3}2^{1/2}}{\pi^{1/2}}\right)\left(\frac{Q^{1/3}h^{1/2}W^{2/3}}{A}\right)\left(\frac{g\rho}{\mu}\right)^{1/6} D^{1/2} \tag{3.13}$$

3.2 ANALYTICAL METHODS

The analytical methods are used to determine the amine concentrations, CO_2 loadings and viscosity for the samples taken from the WWC experiments.

3.2.1 Total Inorganic Carbon Analysis (TIC)

Quantification of CO_2 loading was realized by TIC Analysis. A 10 – 100 X dilution was prepared for each CO_2-loaded concentrated amine solution. Then a small amount of the diluted sample was injected to a tube containing 30 wt% H_3PO_4. Due to the strong acid environment, CO_2-related species, including carbamate, carbonate and bicarbonate are reversed to CO_2. The liberated CO_2 was carried by a N_2 stream to a Horiba IR-2000 infrared analyzer. Each injection generated a signal peak, which was recorded by the Picolog Data Acquisition program. The peak area was obtained via integration. At the end of each analysis a series of carbon standard (mixture of K_2CO_3/$KHCO_3$ aqueous solution, 1000 ppm) of different amount was injected to obtain a calibration curve which correlates inorganic carbon quantity and peak area.

3.2.2 Acid Amine Titration

The concentration of amine in a liquid sample was measured by titration with 0.2 N H_2SO_4. An automatic Titrando series titrator with automatic equivalence point detection (Metrohm, Riverview, FL, USA) was used. Samples of known mass were diluted ~300 times with water and titrated to a pH of 2.4. The pH value was monitored over time and all the equivalence points were recorded. The equivalence point corresponding to total neutralization of amine was used for determination of amine concentration.

3.2.3 Viscosity Measurements

The viscosity measurement was done using a Physica MCR 300 cone and plate rheometer (Anton Paar GmbH, Graz, Austria). With the increment of the angular speed of the cone, the shear rate was increased from 100 to 1000 s^{-1} over a period of 100 s. The duration of each shear rate was 10 s and the shear stress exerted on the solution was measured at the same time. The viscosities reported are the average values of the 10 measurements.

3.2.4 Density Measurements

A Mettler Toledo DE40 densiometer (Mettler-Toledo, Inc., Columbus, OH) was used in this study to measure density. 2 – 3 ml of solution is required for each measurement, and the accuracy of the measurement is up to 1/10000 g/ml. Air and water was used for calibration before any measurement was done for samples.

3.3 NUCLEAR MAGNETIC RESONANCE SPECTROSCOPY (NMR)

NMR is one of the most powerful tools for quantitative analysis of different compounds. ^{1}H and ^{13}C NMR was used in this study to obtain the equilibrium liquid composition of CO_2-loaded amine aqueous solutions. Since the abundance of ^{13}C for natural carbon nuclei is only 1.1%, $^{13}CO_2$ was used to prepare loaded amine solution to enhance responses from all the CO_2-related reaction products.

3.3.1 Material

Piperazine (Anhydrous, ≥99.0%, Aldrich-Sigma, U.S.), 2-Methylpiperazine (99%, AK Scientific Inc., U.S.), 1,4-Dioxane (99.5%, Acros Organics Inc., Belgium), ^{13}C labeled carbon dioxide ($^{13}CO_2$, 99%, Cambridge Isotope Laboratories Inc., U.S.) and Deuterium Oxide (D_2O, 99.9%, Cambridge Isotope Laboratories Inc., U.S.) were all used

as received without further purification. Deionized distilled (DDI) water generated by Direct-Q 5 ultrapure water systems (Millipore, U.S.) was used in this study.

3.3.2 Preparation of Samples

Amine was slowly added to DDI water and then heated to 60 °C to make a homogeneous unloaded concentrated aqueous solution. About 10 ml of the solution were placed in a specially designed CO_2 loader – a slim and long bubbling glass column. The feature of large length-to-diameter ratio increases the residence time of CO_2 in the amine solution and maximizes the use of expensive $^{13}CO_2$. CO_2 was introduced into the solution with a glass frit submerged well below the solution. The flow rate is precisely controlled at 0-10 ml/min by a mass flow controller to make sure that the flow is slow enough for maximum absorption. Samples at intermediate CO_2 loading were prepared by mixing unloaded solution with the highly-loaded ones. The CO_2 loading (α, mol CO_2/mol alkalinity) was determined both gravimetrically and spectroscopically.

A small amount of each amine solution (~1.5 ml) prepared from the procedure described above was transferred to an NMR sample tube (5.0 mm O.D. x 0.77 mm I.D. x 7 in. length, 300 mHz, WILMAD Labglass). ~10 % wt D_2O was added to suppress the interference of signals from water, and a known amount of 1,4-dioxane (~1% wt) was added as an internal standard.

3.3.3 Acquisition of NMR Spectra

All the sample tubes were sealed and thermostated at 40 °C before being transferred to an NMR spectrometer (VARIAN INOVA 500, 500 MHz). This apparatus is located in the Department of Chemistry and Biochemistry in the University of Texas at Austin. All the operations were carried out by Steve Sorey. ^1H and ^{13}C as well as ^1H-

^{13}C 2-dimentional correlation spectra were acquired at 40 °C. Relaxation delay of 5 times relaxation time (T1) was applied for acquisitions of quantitative ^{13}C NMR spectra.

Chapter 4: Amine Screening – Acyclic Amines

This chapter presents the amine screening results on acyclic amines, namely the amines with open-chain molecular structure. It has been mentioned in Chapter 2 that there is a need on acquiring thermodynamic and kinetic data on the amines solvents with respect to application in CO_2 capture from coal-fired power plants. In particular, the properties of aqueous amine solvents at high amine concentration and high CO_2 loading are needed. The work in this chapter is mainly targeted at fulfilling this need and improving the understanding of the relationship between the molecular structure and performance of the solvents in CO_2 absorption/desorption.

4.1 MATERIALS

The acyclic amine solvents selected for screening in this work are given in Table 4.1. DGA® and MDEA/PZ blend have been conventionally used in gas treating. The concentrations of amine in the selected solvents are mostly from 30 – 50 wt%. Higher amine concentration leads to high CO_2 capacity, but it will increase amine volatility and it will increase viscosity with an associated increase in heat exchanger area. Sometimes solid solubility problems also limit the maximum amine content in water. Therefore there exists an upper limit on amine concentration. To avoid the inconvenience caused by changes in CO_2 loading, the amine concentration is expressed in mole amine / kg H_2O (molality, or m) instead of molarity (M) throughout this work. The CO_2 loading (α) is in the unit of mol CO_2/mol alkalinity. Each amino group corresponds to one alkalinity. For example, EDA has two alkalinities on each molecule and 12 m EDA represents 24 m alkalinity.

DGA® (98%, Acros), EDA (anhydrous, certified, Fisher Chemical), MEDA (99%, Acros), AMP (99%, Acros), MAPA (99%, Alfa Aesar), MDEA (99%, Huntsman), PZ

(anhydrous, 99%, Alfa Aesar) were used without purification for preparation of aqueous solution.

Table 4.1: The acyclic amine solvents tested in this work.

Name	**Chemical structure**	**Amine Conc. (m)**	**CO_2 loading (mol/mol alkalinity)**
Ethylenediamine (EDA)	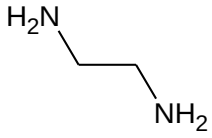	12	0.22-0.49
1,2-Diaminopropane (MEDA)	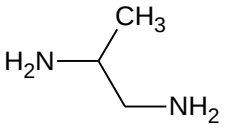	8	0.36-0.42
Diglycolamine® (DGA®)	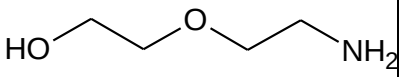	10	0.21-0.49
Methyldiethanolamine (MDEA) /Piperazine (PZ)	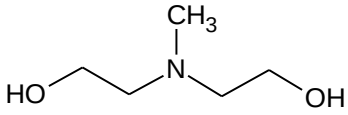	7/2	0.09-0.27
	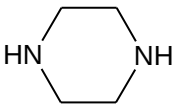	5/5	0.18-0.37

3-(methylamino)propylamine (MAPA)	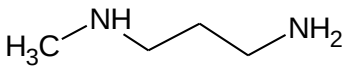	8	0.28-0.52
2-amino-2-methyl-1-propanol (AMP)	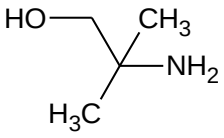	4.8	0.15-0.60

4.2 THEORY/CALCULATION

4.2.1 Calculation of CO_2 Capacity

To compare working capacity of CO_2 for each amine solvent, 5 kPa and 0.5 kPa were selected as the equilibrium CO_2 partial pressures at 40 ^oC for rich and lean amine solution respectively. These values correspond to reasonably large driving forces for CO_2 absorption at the top and bottom of an absorber for CO_2 removal from the flue gas of a coal-fired power plant. The following semi-empirical model was used in this work to fit CO_2 solubility data:

$$\ln P^*_{CO_2} = a + b/T + c\alpha + d\alpha/T + e\alpha^2 \tag{4.1}$$

Note that this model assumes that equilibrium CO_2 partial pressure of loaded amine solution ($P^*_{CO_2}$) is only dependent on temperature (T) and CO_2 loading (α). All parameters were regressed from the CO_2 solubility data. With the use of this model, the CO_2 loadings corresponding to the lean and rich CO_2 partial pressure at 40 °C are determined. Then working capacity is calculated from the difference between the lean

and rich loading with the assumption that solvent remains at constant temperature of 40 °C during absorption of CO_2.

4.2.2 Heat of CO_2 Absorption

The heat of CO_2 absorption (ΔH_{abs}) is obtained with the application of the Gibbs-Helmholtz equation:

$$\Delta H_{abs} = -R\frac{d(\ln P^*_{CO_2})}{d(1/T)} = -R\cdot(b + d\cdot\alpha) \tag{4.2}$$

The derived equation implies that within the proposed solubility model, ΔH_{abs} is independent of temperature and only a function of CO_2 loading (α). ΔH_{abs} is important as it dictates the energy requirement of regenerating amine in stripper. A previous study by Oyenekan and Rochelle (Oyenekan and Rochelle 2006) showed that for generic solvents, greater ΔH_{abs} reduces the overall energy consumption of strippers with simple or multi-pressure configurations. ΔH_{abs} at the CO_2 loading corresponding to $P^*_{CO_2}$ = 1500 Pa is reported as the average value between the lean and rich CO_2 loading.

4.3 CO_2 SOLUBILITY

CO_2 solubility data for 10 m DGA® are shown in Figure 4.1. The increase in CO_2 loading or temperature leads to higher CO_2 partial pressure or lower CO_2 solubility in the solvents. The data and solubility predictions obtained from this work show good agreement with the data reported by Martin *et al.* (Martin, Otto et al. 1978), for which a different amine concentration was used. This indicates that CO_2 solubility is not a strong function of amine concentration and the semi-empirical model is applicable.

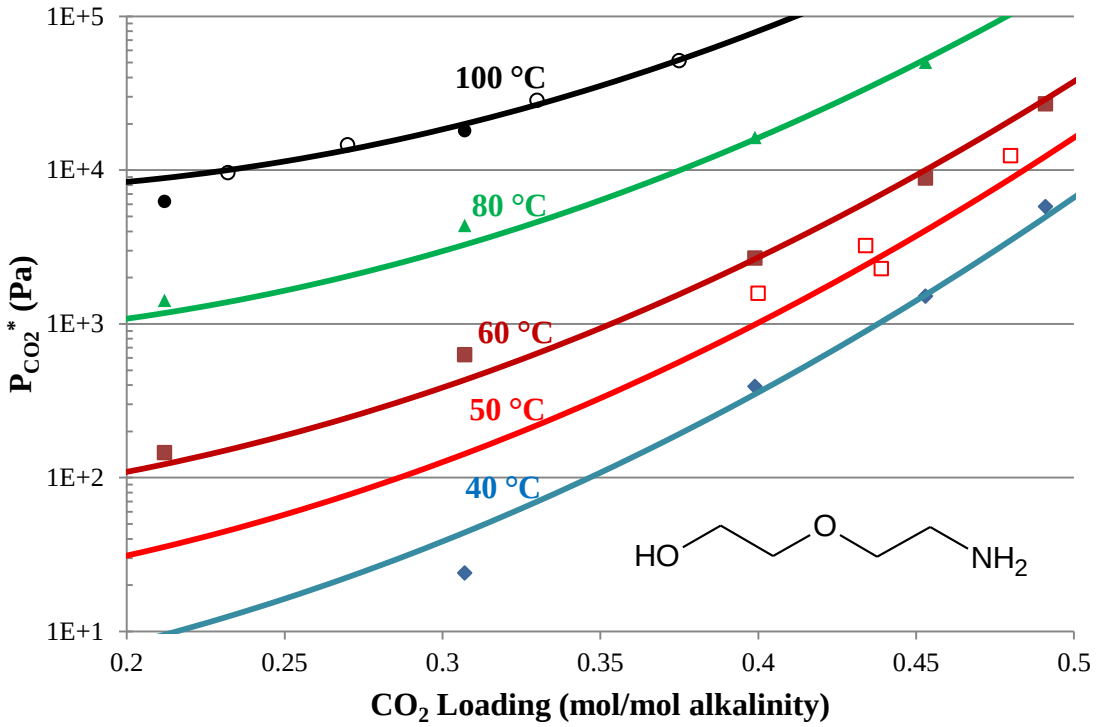

Figure 4.1: CO_2 solubility in 10 m DGA®. Filled points: experimental data; Solid lines: model prediction (Eq. (4.1)); Open points: 14.3 m DGA® at 50 °C (square) and 100 °C (circle) by Martin *et al.* (Martin, Otto et al. 1978).

The partial pressure of CO_2 above 12 m EDA is compared to the values for MEA in Figure 4.2. As CO_2 loading is less than 0.45, CO_2 has a higher solubility in EDA than in MEA, presumably because of the greater stability of EDA carbamate. Free EDA is consumed faster than MEA, so at loading above 0.45, CO_2 is more soluable in MEA.

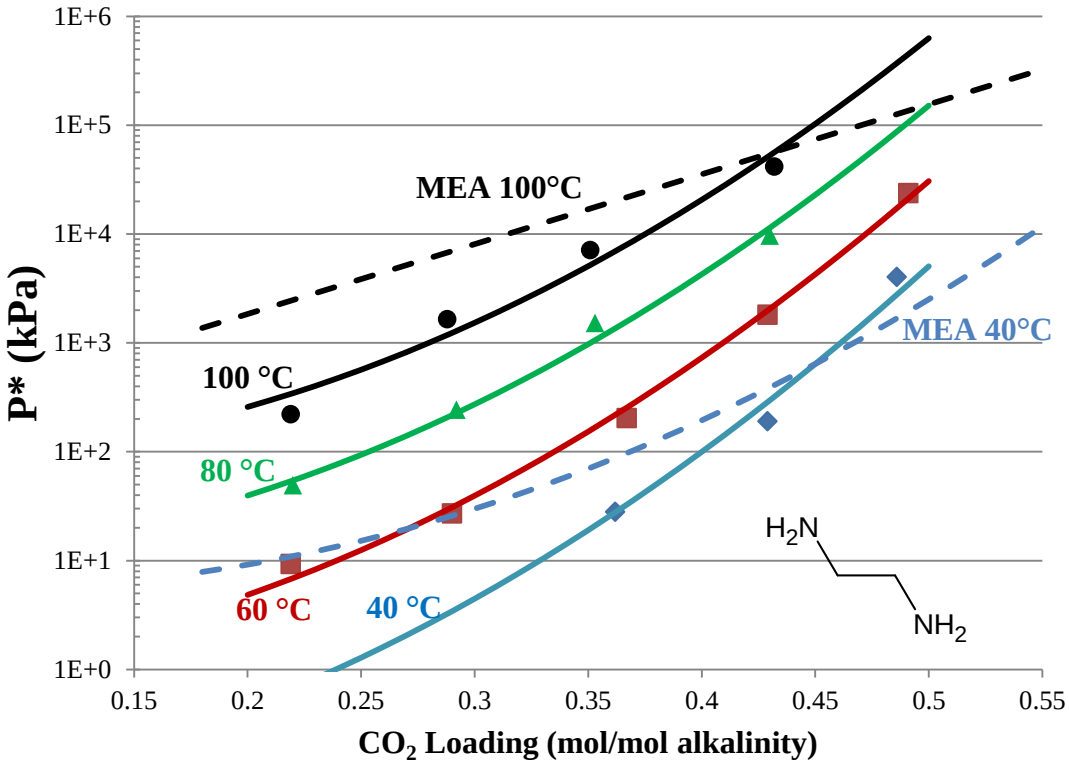

Figure 4.2: CO_2 solubility in 12 m EDA (solid lines), compared to CO_2 solubility in MEA at 40 and 100 °C (dashed line).

As shown in Figure 4.3, the solubility data for AMP from this work are consistent with the literature data within the studied loading range. The solubility model does a good job in representing the solubility over the experimental CO_2 loading range of 0.15 – 0.65 mol/mol alkalinity, but the extrapolation outside this loading range are quite different from the actual trend. This is because that the model only uses the solubility data from this study and does not take into account other data. Since the current work will be confined in the CO_2 loading range corresponding to 0.5 and 5 kPa, the solubility model is sufficient for representation of the relevant data.

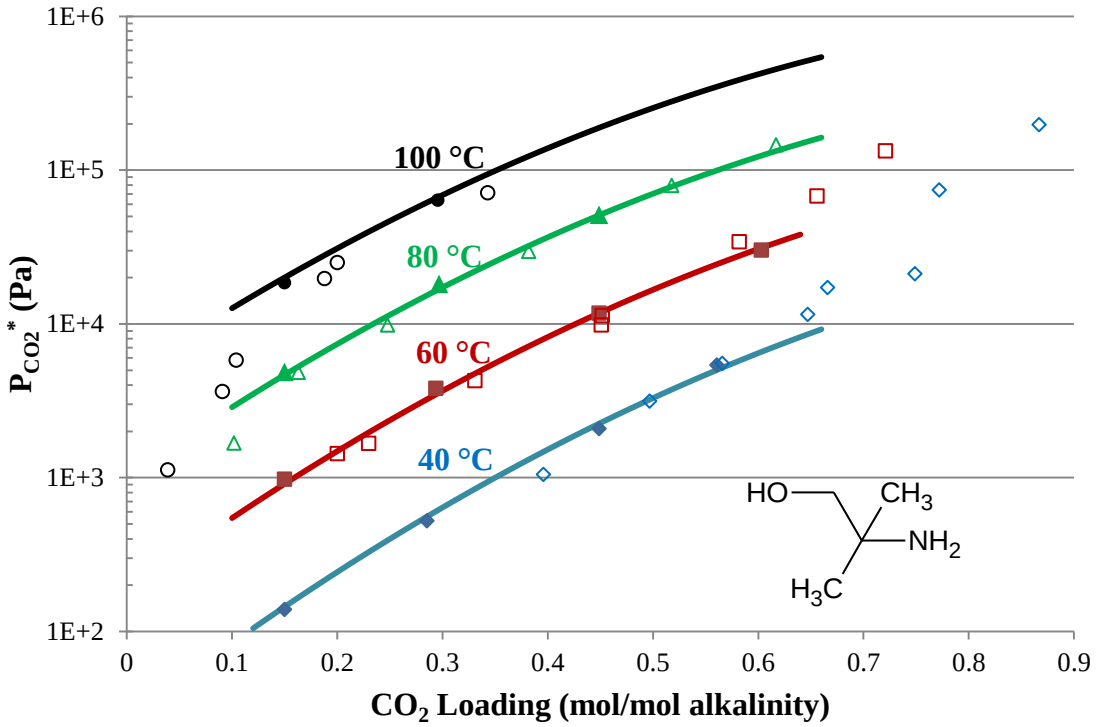

Figure 4.3: CO_2 solubility in 4.8 m AMP. Filled points: experimental data; Solid lines: model prediction (Eq. (4.1)); Open points: Li *et al.* (Li and Chang 1994).

CO_2 solubility data for MAPA are shown in Figure 4.4. In MAPA, $P^*_{CO_2}$ increases rapidly with loading as CO_2 loading approaches 0.5. This is because the free amine gets depleted at high CO_2 loading since 1 mol CO_2 absorption corresponds to 2 mol amine consumption. As a result, the intake of CO_2 by the solution is not significant as the equilibrium CO_2 partial pressure increases from 500 Pa to 5000 Pa, and the cyclic CO_2 capacity of MAPA is relatively small.

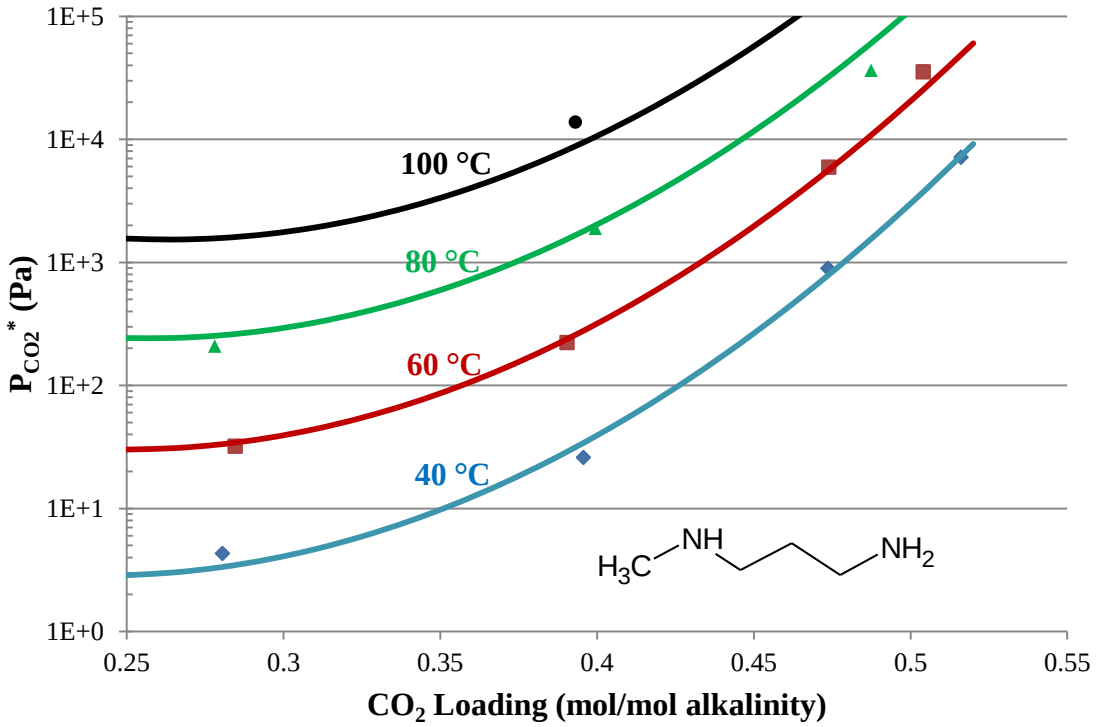

Figure 4.4: CO_2 solubility in 8 m MAPA. Filled points: experimental data; Solid lines: model prediction.

In Figure 4.5, the solubility data for 7 m/2 m and 5 m/5 m MDEA/PZ are compared to those for 7.8 m MDEA/1.2 m PZ reported by Bishnoi *et al.* (Bishnoi 2000) and Derks *et al.* (Derks, Hogendoorn et al. 2009). Increase in the fraction of PZ leads to an increase in CO_2 solubility because PZ carbamate is more stable than bicarbonate.

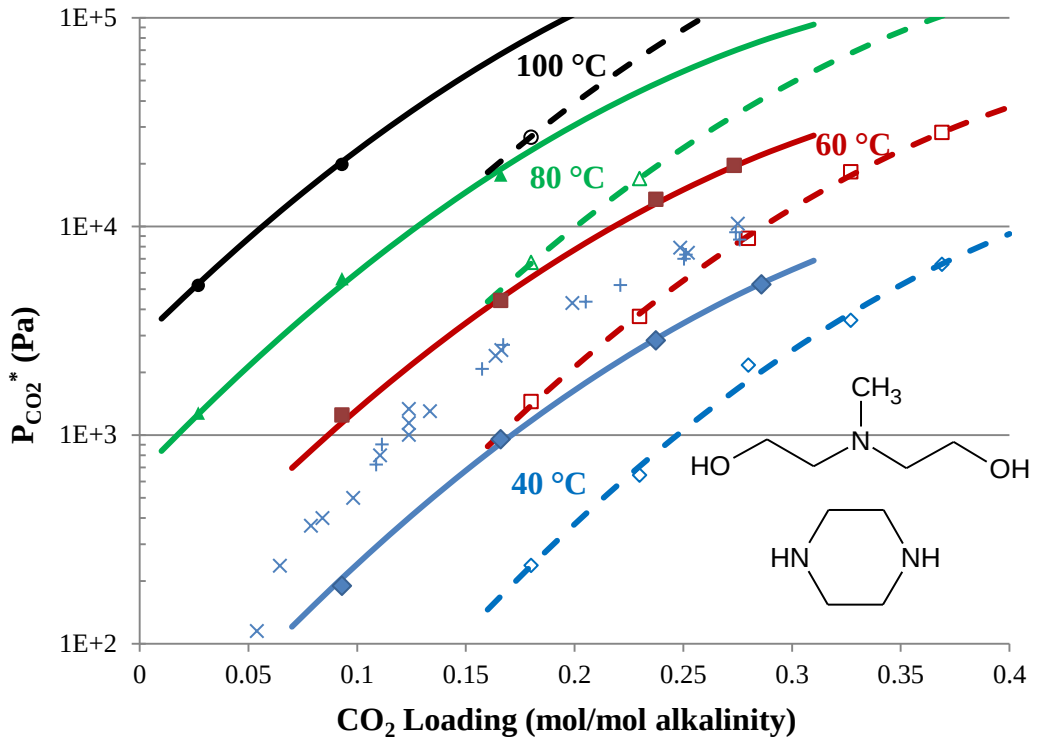

Figure 4.5: CO_2 solubility in MDEA/PZ. Filled points: experimental 7 m / 2 m; Solid lines: model 7 m / 2 m; Open points: experimental 5 m /5 m; Dashed lines: model 5/5. 7.8 m /1.2 m PZ at 40 °C by Bishnoi *et al.* (Bishnoi 2000) (×) and Derks *et al.* (Derks, Hogendoorn et al. 2009) (+).

Due to the solid solubility problem associated with MEDA solution, the CO_2 solubility was measured for only two loadings. The introduction of the methyl group to the α carbon seems to lower the critical CO_2 loading of the amine solution for precipitation to occur. The same phenomena was also observed by Hook (Hook 1997).

The parameters in the semi-empirical model (Eq. (4.1)) for different amines are given in Table 4.2.

Table 4.2: Regressed values of the parameters for the solubility model used in this work (Eq. (4.1)).

Amine	a	b	c	d	e
7 m MEA	36.61 ±2.80	-11152 ±896	-7.46 ±8.36	2389 ±2636	26.69 ±2.58
8 m PZ	34.52 ±2.09	-10676 ±683	-10.10 ±7.27	7596 ±2370	14.43 ±3.27
10 m DGA®	53.57 ±5.61	-16434 ±2081	-48.85 ±15.13	14762 ±5798	34.28 ±11.18
12 m EDA	42.82 ±6.54	-14313.4 ±2407	-29.07 ±17.01	9849 ±6419	40.94856 ±12.69
8 m MAPA	53.45 ±9.84	-14517 ±3234	-78.86 ±25.91	9035 ±8009	103.75 ±17.99
4.8 m AMP	35.47 ±0.87	-10080 ±299	1.70 ±2.80	3258 ±966	-4.89 ±1.11
7m/2m MDEA/PZ	33.94 ±0.76	-9694 ±277	2.30 ±4.98	8054 ±1918	-29.46 ±3.88
5m/5m MDEA/PZ	34.68 ±1.76	-10792 ±602	6.98 ±7.97	8746 ±2612	-31.49 ±6.39

4.4 ABSORPTION/DESORPTION RATE

The rate data for the amines are shown in Figure 4.6 through Figure 4.10. $k_g^{'}$ is shown as a function of $P_{CO_2}^*$ at 40 °C, a surrogate for CO_2 loading. In general, increase in temperature (T) leads to equal or smaller $k_g^{'}$, with the exceptions seen in AMP. This can be explained by Eq. (2.47). Although D_{CO_2} and k_2 both increase with T, H_{CO_2} increases simultaneously. The change in $k_g^{'}$ depends on how these factors offset each other. Using the $P_{CO_2}^*$ instead of CO_2 loading as the x-axis also allows direct comparison of rates on the same basis for different amines. Data for 8 m PZ and 7 m MEA at 40 °C by Dugas *et al.* (Dugas and Rochelle 2009) are shown for comparison. As can be seen, CO_2 absorption in PZ is about 1.5 to 2 times faster than MEA.

DGA® and EDA both have a comparable rate to MEA at low CO_2 partial pressure range (Figure 4.6 and Figure 4.7), presumably because that they are all unhindered primary amines. The dual amino groups in EDA do not make EDA a faster solvent than other amines, as opposed to what may be expected. The comparison of MEDA to EDA at 40 °C (Figure 4.7) shows that the rate in MEDA is slightly higher than in EDA at lean loading. This could be explained by the higher free amine concentration in MEDA solution due to the hindrance introduced by the methyl group.

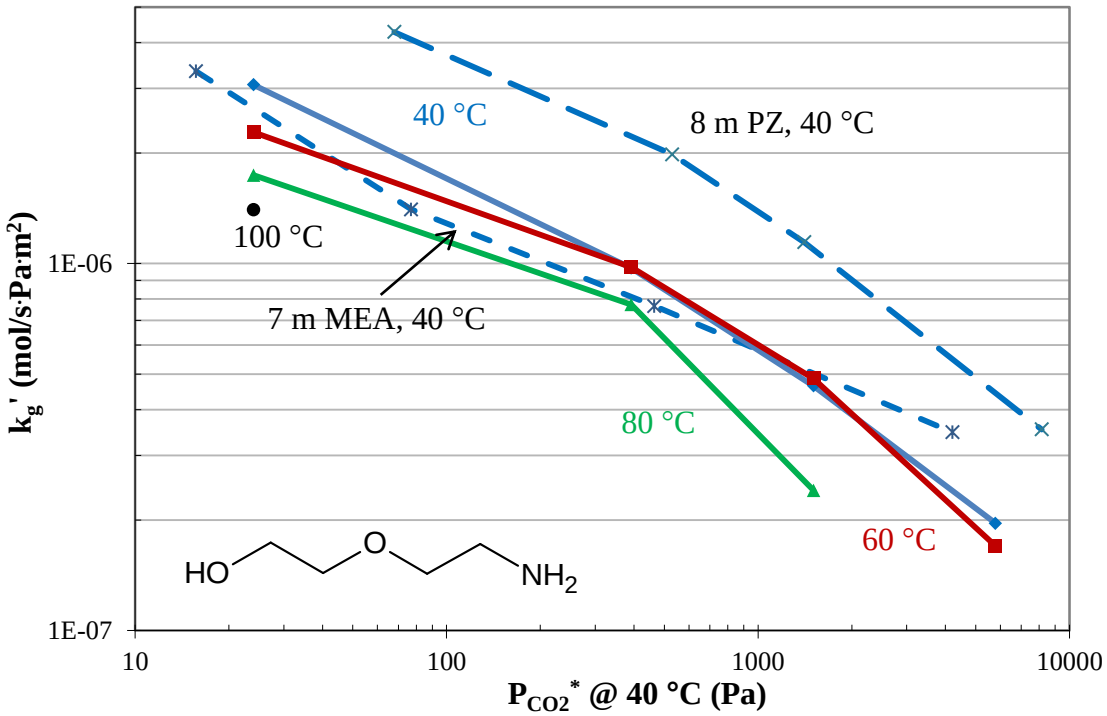

Figure 4.6: Liquid mass transfer coefficient ($k_g^{'}$) of 10 m DGA® (solid lines). The data are compared to $k_g^{'}$ for 7 m MEA (short dashed line) and 8 m PZ at 40 °C (long dashed line) (Dugas and Rochelle 2009).

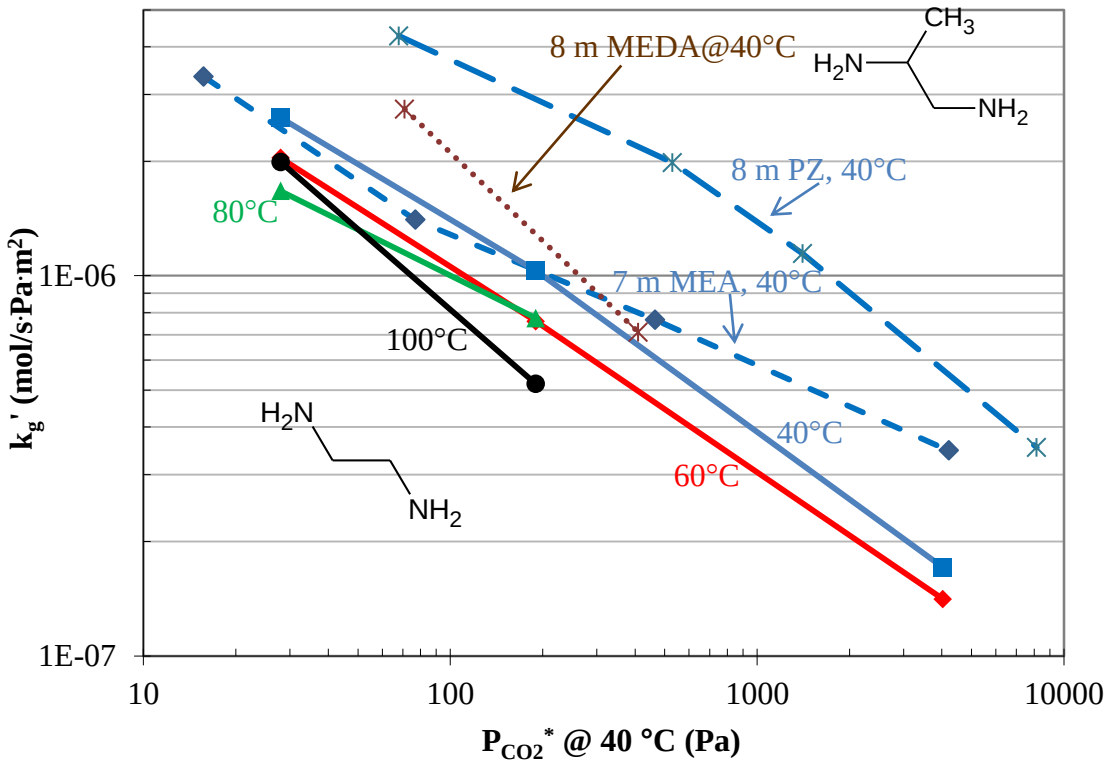

Figure 4.7: $k_g^{'}$ of 12 m EDA (solid lines) and 8 m MEDA (dotted line).

Although the reaction kinetics of AMP with CO_2 is approximately 10 times slower than MEA (Alper 1990; Saha and Bandyopadhyay 1995) due to the steric hindered amino group, CO_2 absorption rate of AMP is found to be as high as half of MEA. A stoichiometric ratio of 1 mol CO_2/mol AMP results in higher free amine concentration, which compensates for small k_2. At 40 °C, $k_g^{'}$ decreases by a factor of 4, nonetheless, the free amine concentration is only decreased by a factor of 1.4. If Equation (2.47) are considered, the drop in the amount of free amine alone is not adequate to explain the significant drop in $k_g^{'}$. It is possible that the increase in Henry's constant of CO_2 and the decrease in diffusivity of CO_2 would partially account for the remainder of the discrepancy. Nonetheless, it is postulated that the carbamate formation

between AMP and CO_2 may still play an important role in the boundary layer of the liquid film since it is a fast reaction. The dependence of $k_g^{'}$ on free amine concentration therefore could be more significant than what would be expected from Equation (2.47).

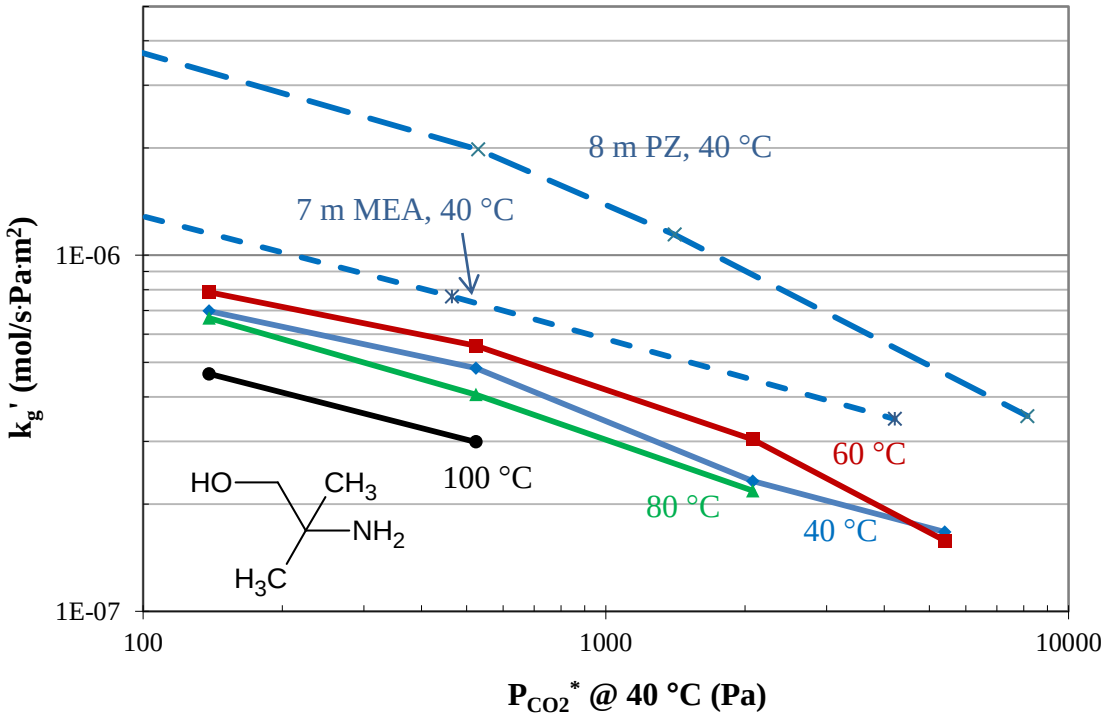

Figure 4.8: $k_g^{'}$ of 4.8 m AMP (solid lines).

$k_g^{'}$ for MAPA is a very strong function of equilibrium CO_2 partial pressure or CO_2 loading. MAPA is a faster solvent than MEA at lean CO_2 partial pressure but much slower at the rich end.

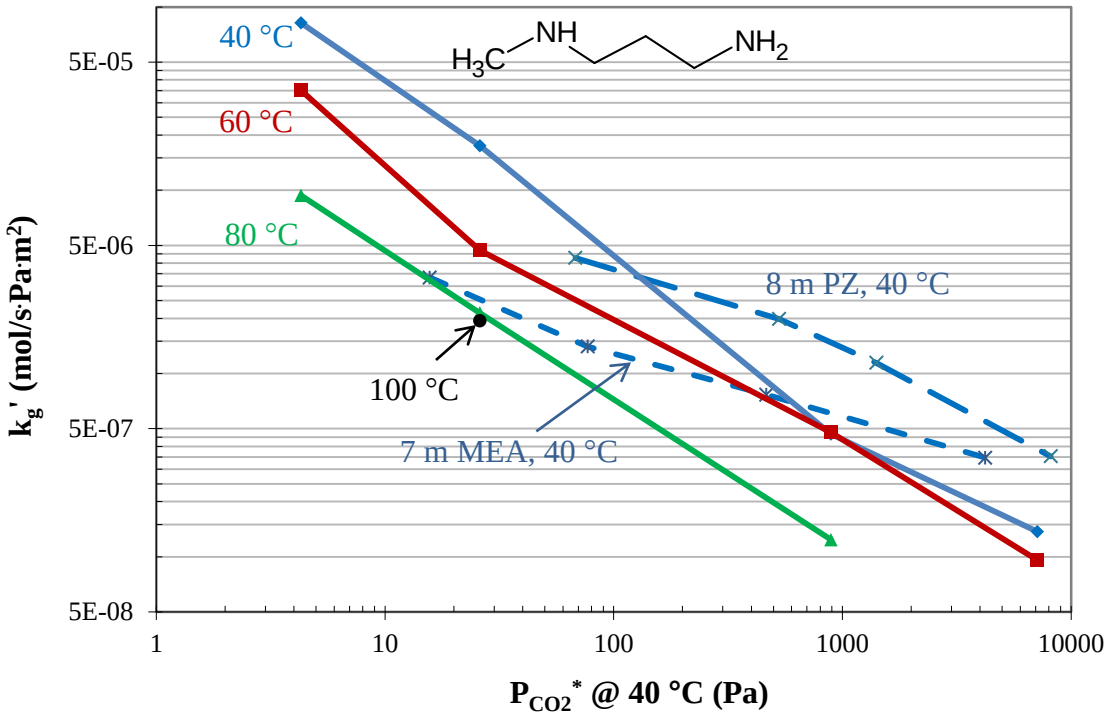

Figure 4.9: $k_g^{'}$ of 8 m MAPA (solid lines).

Figure 4.10 shows that 7 m/2 m MDEA/PZ is slightly slower than 8 m PZ at lean loading but has similar rates at rich loading. This means PZ can greatly enhance CO_2 absorption rate even at a relatively low fraction. It is inferred that MDEA is the major base which catalyzes the formation of PZ carbamate and gets protonated, therefore there is still abundant free PZ available to react with CO_2 and the solution retain high absorption rate even at high CO_2 loading. 5 m/5 m MDEA/PZ has a faster rate than 7/2 blend at all the temperatures due to the fast reaction kinetics associated with PZ. At 40 °C, the 5/5 blend outperforms 8 m PZ at medium loading but has similar rate at the rich loading. This observation is greatly related to the speciation in the blend at different loadings. $k_g^{'}$ reported by Bishnoi *et al.* for 7.8 m/1.2 m MDEA/PZ (Bishnoi 2000) is

greater than that for 7/2 blend and slightly less than that of 5/5 blend at lean loading, but slower than either 7/2 blend or 5/5 blend at rich end.

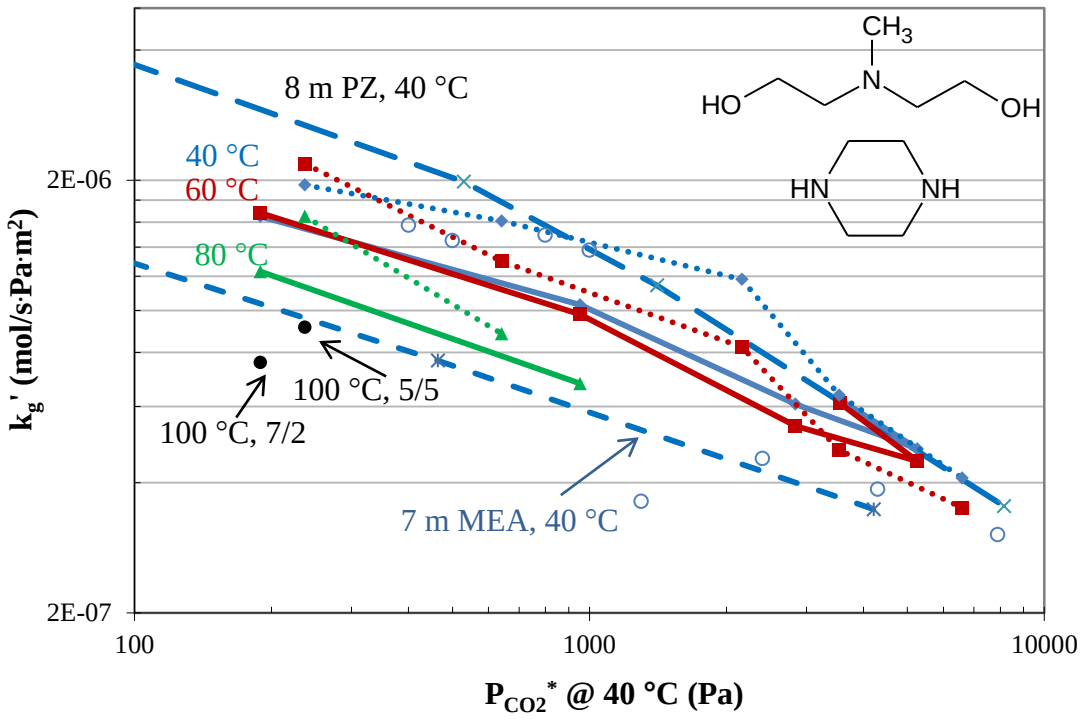

Figure 4.10: $k_g^{'}$ of 7 m/2 m (solid lines) and 5 m/5 m MDEA/PZ (dotted lines). Open circles: 7.8 m /1.2 m MDEA/PZ at 40 °C (Bishnoi 2000).

The detailed solubility and rate data for each solvent are given in Table 4.3 through Table 4.8.

Table 4.3: Equilibrium CO_2 partial pressure ($P^*_{CO_2}$) and liquid film mass transfer coefficient (k'_g) for 10 m DGA® at varied CO_2 loading (α) and temperature (T).

T (°C)	α **(mol/mol alk.)**	$P^*_{CO_2}$ **(kPa)**	k'_g **10^{-7} mol/(s·Pa·m^2)**
40	0.307	0.02	30.7
	0.399	0.39	9.7
	0.453	1.51	4.6
	0.491	5.79	2.0
60	0.212	0.15	37.1
	0.307	0.63	22.8
	0.399	2.67	9.8
	0.453	8.87	4.9
	0.491	26.9	1.7
80	0.212	1.42	31.4
	0.307	4.36	17.4
	0.399	16.3	7.7
	0.453	50.1	2.4
100	0.212	6.25	24.5
	0.307	18.0	14.0

Table 4.4: $P^*_{CO_2}$ and k'_g for 12 m EDA.

T (°C)	α **(mol/mol alk.)**	$P^*_{CO_2}$ **(kPa)**	k'_g **10^{-7} mol/(s·Pa·m^2)**
40	0.362	28	20.6
	0.429	190	26.0
	0.486	4031	10.3
60	0.219	9.3	n/a
	0.290	27	112.0
	0.367	203	20.4
	0.429	1816	7.6
	0.491	23756	1.4
80	0.220	49	n/a
	0.292	242	56.1
	0.353	1522	16.7
	0.430	9621	7.7

100	0.219	220	n/a
	0.288	1643	50.0
	0.351	7128	19.9
	0.432	41621	5.2

Table 4.5: $P^*_{CO_2}$ and $k_g^{'}$ for 4.8 m AMP.

T (°C)	α **(mol/mol alk.)**	$P^*_{CO_2}$ **(kPa)**	$k_g^{'}$ **10^{-7} mol/(s·Pa·m^2)**
40	0.150	0.14	7.0
	0.285	0.52	4.8
	0.449	2.08	2.3
	0.561	5.41	1.7
60	0.150	0.98	7.9
	0.294	3.81	5.6
	0.449	11.7	3.0
	0.603	30.2	1.6
80	0.150	4.85	6.7
	0.297	18.2	4.1
	0.449	51.0	2.2
100	0.150	18.5	4.6
	0.296	63.6	3.0

Table 4.6: $P^*_{CO_2}$ and $k_g^{'}$ for 8 m MAPA.

T (°C)	α **(mol/mol alk.)**	$P^*_{CO_2}$ **(kPa)**	$k_g^{'}$ **10^{-7} mol/(s·Pa·m^2)**
40	0.280	0.004	817.0
	0.396	0.03	175.0
	0.474	0.89	4.7
	0.516	7.12	1.4
60	0.285	0.03	350.0
	0.390	0.22	47.0
	0.474	5.92	4.8
	0.504	35.3	1.0
80	0.278	0.21	93.5
	0.399	1.89	21.4

	0.487	36.4	1.2
1000	0.393	13.8	19.4

Table 4.7: $P^*_{CO_2}$ and $k_g^{'}$ for 7 m MDEA / 2 m PZ.

T (°C)	α **(mol/mol alk.)**	$P^*_{CO_2}$ **(kPa)**	$k_g^{'}$ **10^{-7} mol/(s·Pa·m^2)**
40	0.093	0.19	16.5
	0.166	0.95	10.3
	0.237	2.84	6.1
	0.286	5.26	4.8
60	0.093	1.25	16.8
	0.166	4.41	9.8
	0.237	13.5	5.4
	0.273	19.6	4.5
80	0.027	1.27	27.6
	0.093	5.62	12.3
	0.166	17.6	6.8
100	0.027	5.21	16.3
	0.093	19.8	7.6

Table 4.8: $P^*_{CO_2}$ and $k_g^{'}$ for 5 m MDEA / 5 m PZ

T (°C)	α **(mol/mol alk.)**	$P^*_{CO_2}$ **(kPa)**	$k_g^{'}$ **10^{-7}mol/(s·Pa·m^2)**
40	0.18	0.24	19.5
	0.23	0.64	16.1
	0.28	2.16	11.8
	0.33	3.54	6.4
	0.37	6.59	4.1
60	0.18	1.45	21.8
	0.23	3.70	13.0
	0.28	8.77	8.2
	0.33	18.3	4.8
	0.37	28.2	3.5
80	0.18	6.73	16.5
	0.23	16.9	8.8
100	0.18	26.7	9.1

Table 4.9: $P^*_{CO_2}$ and $k_g^{'}$ for 8 m MEDA.

T (°C)	α (mol/mol alk.)	$P^*_{CO_2}$ (kPa)	$k_g^{'}$ 10^{-7}mol/(s·Pa·m^2)
40	0.357	0.07	27.4
	0.417	0.41	7.1
60	0.357	0.63	10.0
	0.417	3.57	7.1
80	0.357	4.07	11.4
	0.417	16.48	5.7
100	0.357	21.53	11.2

4.5 CYCLIC CAPACITY AND HEAT OF CO_2 ABSORPTION

The calculated values for lean/rich CO_2 loading, capacity, and heat of absorption are given in Table 4.10. The capacity of 7 m/2 m MDEA/PZ is the same as 8 m PZ, while that of the 5/5 blend is about 25% higher than 8 m PZ. If the total amount of alkalinity in each solvent is taken into account, it can be seen that the addition of MDEA to PZ effectively increases the CO_2 capacity while maintaining the fast kinetics associated with PZ. Tertiary amines like MDEA cannot form carbamate with CO_2. Instead, 1 mol MDEA reacts with 1 mol CO_2 to produce bicarbonate and protonated MDEA. 4.8 m AMP has a CO_2 capacity two times as great as that of MEA and about 20% higher than PZ, even at a lower amine concentration. This is attributed to the hindered nature of AMP. However the CO_2 capacity of 10 m DGA® and 8 m MAPA are only about half of 8 m PZ and slightly smaller than 7 m MEA.

The heat of CO_2 absorption for PZ and its blend with MDEA is about 70 kJ/mol CO_2. ΔH_{abs} for AMP is slightly higher than PZ. All of the primary amines, MEA,

DGA® and MAPA, have a value slightly greater than 80 kJ/mol CO_2, presumably because of the greater heat of reaction in carbamate formation.

4.6 APPLICATION OF RATE DATA

4.6.1 Design of an Isothermal Absorber

4.6.1.1 Design Basis

The accurate measurement of the liquid mass transfer coefficient for different PZ derivatives enables evaluation of their performance via a simple design of an isothermal absorber. The illustrated design (Figure 4.11) aims to remove 90% CO_2 from a flue gas stream which contains 12% CO_2 and flows at $G_{fluegas}$ m^3/s at 1 atm and 40 °C. To simplify the calculation, the absorber is assumed to be operated isothermally at 40 °C. 0.5 kPa and 5 kPa are used as the lean and rich equilibrium CO_2 partial pressure of the amine solution.

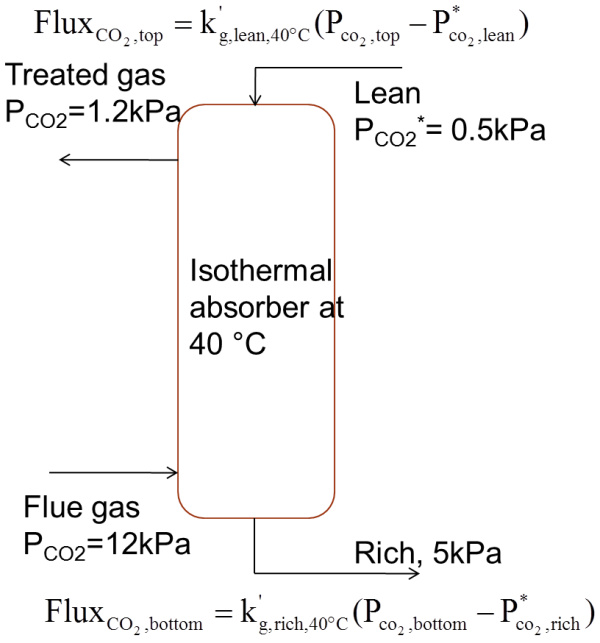

Figure 4.11: Flow sheet for design of a simple absorber

4.6.1.2 Calculation of Packing Area Required

A second-order polynomial correlation of $k_g^{'}$ to $\log_{10}$ ($P_{CO_2}^*$) at 40 °C was regressed from the experimental data points, and the $k_g^{'}$ values at $P_{CO_2}^*$ of 0.5 kPa and 5 kPa were calculated. These two values represent the rate of mass transfer at the top and bottom of an isothermal absorber operated at 40 °C. The CO_2 flux between gas and liquid is equal to $k_g^{'}$ times the driving force (Eq. (4.3) and (Eq. (4.4)). The logarithmic mean (LM) value of N_{CO2} at the top and bottom of the column is calculated to estimate average mass transfer rate between gas and liquid in the absorber (Eq. (4.5)). Note that the gas film resistance is neglected and only liquid film resistance is taken into account in this calculation.

$$N_{CO_2,top} = k_{g,lean,40°C}^{'}(P_{co_2,top} - P_{co_2,lean}^*) \tag{4.3}$$

$$N_{CO_2,bottom} = k_{g,rich,40°C}^{'}(P_{co_2,bottom} - P_{co_2,rich}^*) \tag{4.4}$$

$$N_{CO_2,LM} = \frac{N_{CO_2,top} - N_{CO_2,bottom}}{\ln(\frac{N_{CO_2,top}}{N_{CO_2,bottom}})} \tag{4.5}$$

The average value of $k_g^{'}$ is defined based on the log mean flux.

$$k_{g,avg}^{'} = \frac{N_{CO_2,LM}}{(P_{co_2,gas} - P_{co_2}^*)_{LM}} \tag{4.6}$$

where $(P_{co_2,gas} - P_{co_2}^*)_{LM}$ is the log mean driving force along the column:

$$(P_{co_2,gas} - P_{co_2}^*)_{LM} = \frac{(P_{co_2,top} - P_{co_2,lean}^*) - (P_{co_2,bottom} - P_{co_2,rich}^*)}{\ln(\frac{P_{co_2,top} - P_{co_2,lean}^*}{P_{co_2,bottom} - P_{co_2,rich}^*})} \tag{4.7}$$

$k'_{g,avg}$ reflects the average absorption rate over the whole absorber column. The packing area ($A_{packing}$) required for unit volumetric flow rate of flue gas ($G_{fluegas}$) can also be estimated with the assumption of 90 % CO_2 removal.

$$\begin{aligned}\frac{A_{packing}}{G_{fluegas}} &= \frac{90\% \times 0.12 \times P/RT}{N_{CO_2,LM}} \\ &= \frac{0.90 \times 0.12 \times 101325/(8.314 \times 313)}{N_{CO_2,LM}} \\ &= \frac{4.2}{N_{CO_2,LM}} (m^2/(m^3/s))\end{aligned} \tag{4.8}$$

A smaller value of $A_{packing}/G_{fluegas}$ corresponds to less packing height and smaller absorber, leading to less capital cost.

The average value of k'_g as well as $A_{packing}/G_{fluegas}$ are shown in Table 4.10. 8 m PZ has the fastest CO_2 mass transfer rate, corresponding to the least packing area requirement, 1800 $m^2/(m^3/s)$. 7 m MEA is only 50% as fast as PZ, which doubles the required packing area. 5 m /5 m MDEA/PZ has a similar rate to PZ, while 7/2 blend is roughly 15% slower. CO_2 absorption in 10 m DGA® and 8 m MAPA are slower than in MEA by 5–15%. 4.8 m AMP, as the slowest solvent, requires a packing area up to 6300 $m^2/(m^3/s)$.

Table 4.10: Overview of properties for all the amines tested. PZ and MEA (Dugas and Rochelle 2009) are also included.

Amine	Lean/Rich loading (mol CO_2/mol alkalinity)	Cyclic CO_2 Capacity (mol/kg (water+amine))	$-\Delta H_{abs}$ @ $P^*_{CO_2}$ =1.5kPa (kJ/mol)	$k'_{g,avg}$ @40°C ($\times 10^7$mol/s·Pa·m^2)	$\frac{A_{packing}}{G_{fluegas}}$ (10^3 m^2/(m^3/s))
8 m PZ	0.31/0.39	0.79	70	8.5	1.8
5m/5mMDEA/PZ	0.21/0.35	0.99	70	8.3	1.8
7m/2m	0.13/0.28	0.80	68	6.9	2.2
7 m MEA	0.45/0.55	0.47	82	4.3	3.5
10 m DGA®	0.41/0.49	0.38	81	3.6	4.2
8 m MAPA	0.47/0.51	0.42	84	3.1	4.8
12 m EDA	0.44/0.50	0.78	81	2.5	6.0
4.8 m AMP	0.27/0.56	0.96	73	2.4	6.3

4.7 CONCLUSIONS

The measurements of CO_2 solubility and absorption/desorption rates with the Wetted Wall Column enable the extraction and comparison of CO_2 capacity, heat of absorption, and mass transfer rates in different amine solvents. The primary amines studied, DGA® and MAPA, suffer from low CO_2 capacity and absorption rates. EDA has also a low rate but a relatively high CO_2 capacity due to high amine concentration. However, the high heat of absorption of the primary amines would benefit the overall energy consumption and could partially offset their disadvantages. 4.8 m AMP has a

high CO_2 capacity, but its application as a CO_2 capture solvent could be hindered by its low CO_2 absorption rate. MDEA blended with PZ shows great promise with its high CO_2 capacity and absorption rate, if compromised with the relatively lower heat of absorption.

The packing area for unit volume of flue gas is estimated in a simple absorber design. Fast amines such as 5 m /5 m MDEA/PZ only require 1/2 to 1/3 of the packing area that would be needed for slow solvents like DGA®, MAPA, and AMP. Therefore a fast amine would greatly reduce the column size and capital cost.

Chapter 5: Amine Screening – Cyclic Amines

This chapter presents screening of cyclic amine solvents. Concentrated aqueous piperazine (PZ) as a cyclic amine has been identified as a better solvent for CO_2 capture than monoethanolamine (MEA), because it has a higher rate of CO_2 absorption and greater CO_2 capacity. This work evaluates the effect of substitute groups on PZ performance. The WWC method was used for accurate measurement of CO_2 solubility and rate data at 40 to 100 ^oC and over the operating range of CO_2 loading for 8 m 1-methylpiperazine (1MPZ), 8 m 2-methylpiperazine (2MPZ), 3.75 m 1MPZ/3.75 m PZ/ 0.5 1,4-dimethylpiperazine (1,4-DMPZ), 4 m 2MPZ/4 m PZ, 7.7 m N-(2-hydroxyethyl)piperazine (HEP), 6 m 1-(2-Aminoethyl)piperazine (AEP), 8 m 2-piperidine ethanol (2-PE), and 2 m trans-2,5-dimethylpiperazine (2,5-DMPZ). The rate decreases as 1MPZ = PZ > 2MPZ/PZ > 2MPZ > HEP > MEA > AEP = 2-PE. Semi-empirical solubility models of CO_2 for each amine were regressed from experimental solubility data to find the lean and rich CO_2 loading corresponding to 0.5 kPa and 5 kPa CO_2 partial pressure respectively. Based on the solubility model, the operating capacity of the solvents without overstripping decreases in the sequence of 2-PE > 2MPZ > 2MPZ/PZ > 1MPZ > PZ > HEP > AEP > MEA. The enthalpy of CO_2 absorption (ΔH_{abs}) of all the piperazine derivatives is around 70 kJ/mol CO_2.

5.1 INTRODUCTION

Post-combustion capture of CO_2 by aqueous amine scrubbing will be an important alternative technology for carbon management of coal-fired power plants and other CO_2 emission sources (Rochelle 2009). Aqueous monoethanolamine (MEA) is the baseline solvent for this application. Typical power plant designs with MEA require 15 m of

absorber packing and reduce power plant output by 25 to 35%. There are additional problems with amine volatility, degradation, foaming and corrosion.

Because it has a fast reaction with CO_2, PZ has been used as a promoter with other amines or potassium carbonate for CO_2 capture (Xu, Zhang et al. 1992; Zhang, Zhang et al. 2001; Bishnoi and Rochelle 2002; Cullinane and Rochelle 2006; Samanta and Bandyopadhyay 2009). Bishnoi & Rochelle (Bishnoi and Rochelle 2000) and Derks *et al.* (Derks, Kleingeld et al. 2006) showed that the reaction rate constant of PZ with CO_2 is about one order of magnitude greater than that of MEA.

Concentrated aqueous PZ by itself is also an effective CO_2 solvent. Dugas *et al.* (Dugas 2009; Dugas and Rochelle 2009) measured the CO_2 solubility as well as the liquid film mass transfer coefficient for aqueous PZ with variable concentration and loading in a wetted wall column. His data suggested that the working CO_2 capacity of 8 m PZ is 1.5 to 2 times as large as 7 m MEA. The liquid mass transfer coefficient of aqueous PZ was also found to be 2 to 3 times greater than that of MEA. Freeman *et al.* (Freeman, Dugas et al. 2009) studied the degradation of concentrated aqueous PZ and concluded that degradation of PZ at 135 and 150 °C is negligible, while significant loss of MEA was observed at these two temperature.

However, PZ has certain disadvantages as a CO_2 absorbent. Pure PZ is only soluble in water up to 1.9 mol/kg water. Freeman studied phase behavior PZ-H_2O-CO_2 with variable temperature and loading (Freeman, Dugas et al. 2009). The result showed that, for 8 m PZ at room temperature, precipitation occurred when CO_2 loading is less than 0.2 mol CO_2/mol alkalinity (1 mol amino group is equivalent to 1 mol alkalinity). As temperature drops to 0 °C, the critical CO_2 loading to avoid crystallization is around 0.3 mol/mol alkalinity.

Several investigators have screened amines by approximate methods. Puxty and coworkers (Puxty, Rowland et al. 2009) studied 76 different amines using both micro-scale isothermal gravimetric analysis and macro-scale CO_2 absorption. They identified 7 outstanding performers in terms of capacity and initial absorption rate. Singh and co-workers (Singh, Niederer et al. 2007; Singh, Brilman et al. 2009; Singh, Niederer et al. 2009) carried out the screening experiments with bubble column reactors. Absorption of CO_2 of 10 kPa partial pressure and desorption with pure nitrogen was done to semi-quantitatively measure the absorption rate and cyclic capacity. They found increased chain length between amine group and other functional groups resulted in decreased absorption rate but increased CO_2 capacity. The effect of number of amine groups, type and position of functional groups was also investigated in their study. Ma'mun *et al.* (Ma'mun, Svendsen et al. 2006) performed a screening test by bubbling CO_2-nitrogen mixture through amine solutions. The absorption rate was determined by monitoring CO_2 concentration in the outlet stream. 2-(2-aminoethyl-amino)ethanol (AEEA) was found to have a higher CO_2 absorption rate than MEA as well as a higher cyclic capacity. Hook (Hook 1997) studied CO_2 absorption of several amino acids and compared them to MEA and 2-amino-2-methyl-1-propanol (AMP). The amount of CO_2 absorbed over time was determined by following change of CO_2 volume change at constant pressure.

Unfortunately, results obtained from the studies mentioned above are questionable in terms of accuracy. Some of the screening tests were performed by simply sparging CO_2 through amine solutions. Absorption rate obtained thereby was affected by area of gas-liquid interface and bubble size, which is specifically dependent on viscosity and surface tension of amine solutions. All the absorption rates in their studies are semi-quantitative and relative, and not directly applicable to the absorption scenarios in real packing. In addition, absolute operational CO_2 capacity of amine for practical process is

not available from these studies. Nonetheless, the previous amine screening studies are valuable as they shed light on relationships between amine activity and structure.

To further understand the relationship between structure and the performance of amine as CO_2 absorbents, several PZ derivatives were investigated in this study. The type, number and position of functional groups on PZ are varied. All the PZ derivatives except 2, 5-DMPZ showed a better solubility in water than PZ. If not specified, there were no precipitation problems observed in the range of the amine concentration, temperature and CO_2 loading studied in this work. This is one of the advantages of PZ derivatives over PZ. Accurate measurement of vapor-liquid-equilibrium (VLE) and absorption/desorption rates was made possible by using a wetted wall column, which better represents mass transfer between gas and liquid in real packing. Although some thermodynamic or kinetic studies had been reported for some of the amines (Xu, Wang et al. 1993; Paul, Ghoshal et al. 2009; Paul, Ghoshal et al. 2009), the amine concentration in this study is much higher (> 3 kmol/m^3), which is close to the practical range for industrial application. The concentration for aqueous amine solution is expressed in molality (m, mol amine/kg water) throughout this paper. Results are also compared to previous studies on PZ and MEA by Dugas (Dugas and Rochelle 2009). The impact of different substitution or molecular structure on amine performance as a CO_2 absorbent is discussed.

5.2 MATERIALS

PZ (99%, anhydrous) used in this study is a product of Alfa Aesa (MA, USA). MEA (99%), 1MPZ (99+%), HEP (98.5%), AEP (99%), 2-PE (95%) were all purchased from Acros Organics (Geel, Belgium). 2MPZ (99%), 2,5-DMPZ (98%) were supplied

by AK Sci., Inc. (Mountain View, CA). CO_2 (99.99%, Matheson Tri-Gas), nitrogen (99.9%), deionized water (Millipore, Direct-Q) were also used in this study.

The molecular structure of the cyclic amines tested in the work is shown in Table 5.1.

Table 5.1: The cyclic amine solvents tested in this work.

Name	**Chemical structure**	**Amine Conc. (m)**	**CO_2 loading (α, mol/mol alkalinity)**
N-(2-hydroxyethyl)piperazine (HEP)	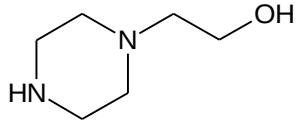	7.8	0.06 - 0.28
1-(2-Aminoethyl)piperazine (AEP)	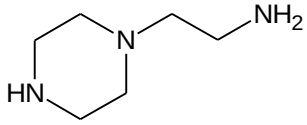	6	0.10 - 0.36
N-Methyl piperazine (1MPZ)	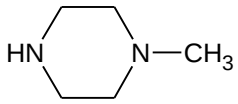	8	0.10 - 0.26

2-Methyl piperazine (2MPZ)	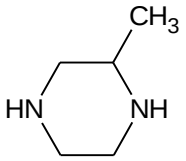	8	0.10 - 0.37
2MPZ/PZ	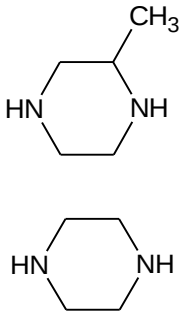	4/4	0.16 - 0.39
1MPZ/PZ/1,4-dimethylpiperazine (1,4-DMPZ)	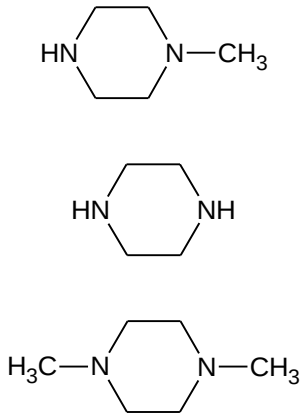	3.75/ 3.75/ 0.5	0.21 - 0.32
2,5-trans-dimethylpiperazine (2,5-DMPZ)	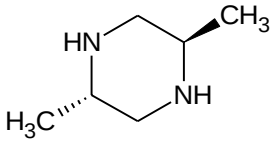	2	0.15 - 0.26
2-piperidineethanol (2-PE)	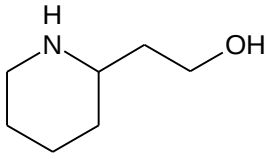	8	0.21 - 0.70

5.3 OVERVIEW

The data for CO_2 solubility, $k_g^{'}$, and viscosity are tabulated in Table 5.2. All the measurements were done at 40 to 100 °C. For each amine solvent, CO_2 loading was selectively varied to ensure that the equilibrium CO_2 partial pressure ($P_{CO_2}^{*}$) approximately covered the range of 0.5 kPa to 5 kPa at 40 °C. $k_g^{'}$ was measured for each solvent condition.

Table 5.2: Data for CO_2 solubility and $k_g^{'}$ at 40 - 100 °C and viscosity at 40 °C

Amine	**Temp (°C)**	α **(mol/mol alk.)**	$P_{CO_2}^{*}$ **(kPa)**	$k_g^{'}$ **(×10^{7}mol/s·Pa·m^2)**	**Viscosity (10^{-3}Pa·s)**
8 m 1MPZ	40	0.100	0.10	21.8	9.6
		0.150	0.35	22.1	10.5
		0.200	1.32	12.1	11.3
		0.260	5.55	4.8	12.3
	60	0.100	6.16	42.5	
		0.150	2.15	21.6	
		0.200	6.41	10.9	
		0.260	22.95	4.0	
	80	0.100	3.65	30.0	
		0.150	10.10	17.0	
		0.200	25.30	7.3	
	100	0.100	12.84	21.4	
		0.150	33.01	10.5	
8 m 2MPZ	40	0.102	0.01	191.0	10.5
		0.154	0.04	59.2	12.6
		0.203	0.12	28.1	13.6
		0.253	0.32	19.7	15.4
		0.300	0.96	8.9	16.3
		0.365	4.73	3.7	19.3
	60	0.102	0.09	91.7	
		0.154	0.29	50.2	
		0.203	0.86	24.5	
		0.253	2.26	16.8	
		0.300	4.87	9.8	
		0.365	22.41	2.8	

	80	0.102	0.59	62.8	
		0.154	1.80	41.4	
		0.203	4.06	24.5	
		0.253	9.72	13.7	
		0.300	22.06	7.4	
	100	0.102	2.68	51.2	
		0.154	7.39	29.0	
		0.203	18.65	14.9	
4 m 2MPZ/ 4 m PZ	40	0.158	0.02	250.0	10.3
		0.232	0.11	46.4	11.9
		0.281	0.33	19.3	12.8
		0.330	1.01	11.2	14.7
		0.391	5.44	4.3	15.7
	60	0.158	0.17	62.6	
		0.232	0.64	39.8	
		0.281	2.01	18.5	
		0.330	5.39	10.4	
		0.391	22.83	2.8	
	80	0.158	1.03	61.7	
		0.232	3.63	28.2	
		0.281	8.58	18.5	
		0.330	23.95	7.4	
	100	0.158	4.19	44.6	
		0.232	15.75	19.4	
7.7 m HEP	40	0.066	0.08	36.0	14.6
		0.130	0.28	19.8	15.1
		0.199	1.86	5.7	16.9
		0.289	21.12	1.1	18.8
	60	0.064	0.39	26.4	
		0.131	1.85	18.2	
		0.200	9.15	5.0	
		0.278	69.44	0.8	
	80	0.062	1.77	27.2	
		0.132	8.20	13.4	
		0.202	33.22	3.4	
	100	0.063	6.53	25.3	
		0.131	31.65	6.7	
6 m AEP	40	0.100	0.01	472.0	12.3
		0.197	0.06	30.3	17.3
		0.292	1.79	5.7	22.9
		0.361	24.95	0.8	26.2
	60	0.099	0.06	55.7	
		0.199	0.54	21.9	

		0.295	8.62	4.8	
	80	0.100	0.36	65.2	
		0.196	3.23	29.4	
		0.298	40.50	3.5	
	100	0.100	2.00	56.2	
		0.199	12.87	20.5	
8 m 2-PE	40	0.205	0.12	21.4	11.4
		0.360	0.45	9.8	14.4
		0.514	1.53	4.2	18.4
		0.684	5.38	1.9	23.5
	60	0.202	0.92	16.1	
		0.367	3.50	8.3	
		0.524	8.92	4.2	
		0.695	25.23	1.6	
	80	0.215	4.10	12.3	
		0.375	15.37	6.9	
		0.525	36.11	3.6	
		0.635	82.09	1.7	
	100	0.199	20.93	7.4	
		0.360	61.57	4.2	
2 m DMPZ	40	0.153	0.47	10.8	1.8
		0.255	1.60	6.1	1.9
	60	0.153	1.66	7.9	
		0.255	5.65	4.5	
	80	0.153	6.67	4.9	
		0.255	16.71	3.8	
	100	0.153	21.57	2.9	
3.75 m 1MPZ/3.75 m PZ/0.5 m 1,4-DMPZ	40	0.21	0.3	24.8	
		0.25	0.8	12.4	
		0.29	2.1	9.2	
		0.32	4.5	5.6	
	60	0.21	1.7	25.5	
		0.25	3.8	15.0	
		0.29	9.9	8.7	
		0.32	19.0	5.1	
	80	0.21	8.0	20.1	
		0.25	16.8	11.3	
	100	0.21	29.2	13.1	

The solvent viscosity with varied loading was measured only at 40 °C. Due to the high amine concentration, viscosity of most of the amines in this study is greater than 10 cp and monotonically increases with loading. High viscosity reduces the heat

transfer coefficient for the cross exchanger. It may also affect absorber flooding and pump work. Therefore the amine concentration might need to be further optimized before application.

Table 5.3 shows the regressed parameters of the CO_2 solubility model (Eq. (5.1)) for all of the amines. Parameter a and b are found to be in the same order of magnitude for different amines, however c, d and e change significantly from one amine to another, presumably because of different dependence of $P^*_{CO_2}$ on α.

$$\ln P^*_{CO_2}(Pa) = a + b/T(K) + c \cdot \alpha + d \cdot \alpha / T(K) + e \cdot \alpha^2 \quad (5.1)$$

Table 5.3: The values of the parameters in the solubility model (Eq. (5.1)) used in this work

Amine	a	b	c	d	e
7m MEA	36.61	-11152	-7.46	2389	26.69
8m PZ	34.52	-10676	-10.10	7596	14.43
8m 1MPZ	37.13	-11062	-16.81	14354	-10.57
8m 2MPZ	36.56	-11323	-5.12	8357	0.74
2MPZ/PZ	38.37	-11919	-16.50	10128	13.36
1MPZ/PZ/1,4-DMPZ	37.29	-11354	-16.27	11975	3.41
7.7m HEP	33.14	-9488	1.17	6176	12.88
6m AEP	38.28	-11786	-23.96	10837	42.93
8m 2-PE	37.26	-10768	-2.20	3845	-2.57

5.4 CO_2 SOLUBILITY

1MPZ

In Figure 5.1, $P^*_{CO_2}$ of 8 m 1MPZ at 40 to 100 °C is plotted against CO_2 loading. CO_2 solubility data for PZ over a range of concentration (Dugas and Rochelle, 2009) are

also shown. As can be seen, the semi-empirical model represents both sets of data well. Variation in PZ concentration did not significantly change $P^*_{CO_2}$, therefore all data points at same temperature are fitted with one single curve. When compared at the same loading and temperature, $P^*_{CO_2}$ of 1MPZ is about one order of magnitude higher than that of PZ. The methylated tertiary amino group is much less reactive with CO_2 and cannot be converted to carbamate group. Consequently at same CO_2 loading, there is more bicarbonate in 1MPZ solution than in PZ. The work of Cullinane *et al.* (Cullinane and Rochelle 2005) suggested that equilibrium constant of transformation of CO_2 to bicarbonate is much smaller than formation of PZ monocarbamate. Therefore $P^*_{CO_2}$ is expected to increase with the relative amount of bicarbonate in loaded amine solution.

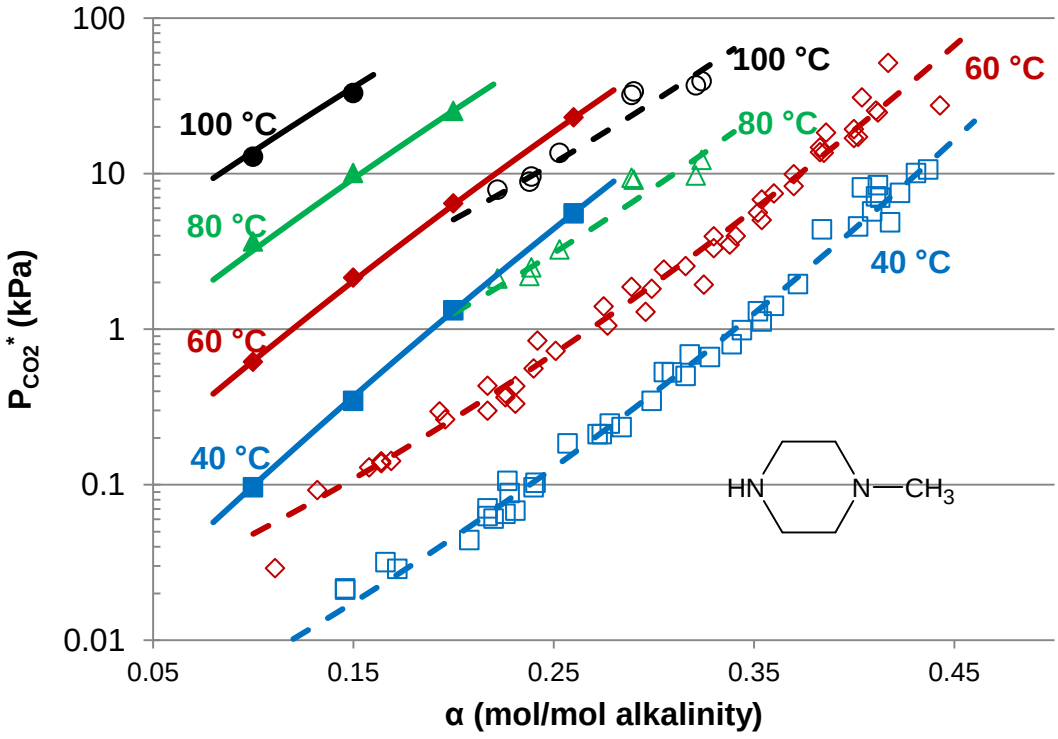

Figure 5.1: CO_2 Solubility in 8 m 1MPZ (filled points), compared with data for PZ (open points) by Dugas (Dugas and Rochelle 2009). The semi-empirical model for CO_2 solubility is represented by solid lines for 1MPZ and dashed lines for PZ.

2MPZ

CO_2 solubility in 8 m 2MPZ is shown in Figure 5.2. $P^*_{CO_2}$ of 2MPZ is about 2-3 times greater than that of PZ at same loading and temperature. It was inferred that the substitution of methyl group on 2MPZ reduces the activity of the adjacent amino group and causes destabilization of carbamate (Sartori and Savage 1983). For a moderately hindered amine like 2MPZ, there is not as much carbamate formed as seen for PZ at same CO_2 loading. At low CO_2 loading, the majority of 2MPZ monocabamate is expected to be N-carboxylic-3-methylpiperazine. Since the slope of $P^*_{CO_2}$ vs. α is about the same for 2MPZ and PZ on the semi-log plot, the stability of carbamate formed on the amino group away from methyl group is not significantly affected by the substitution.

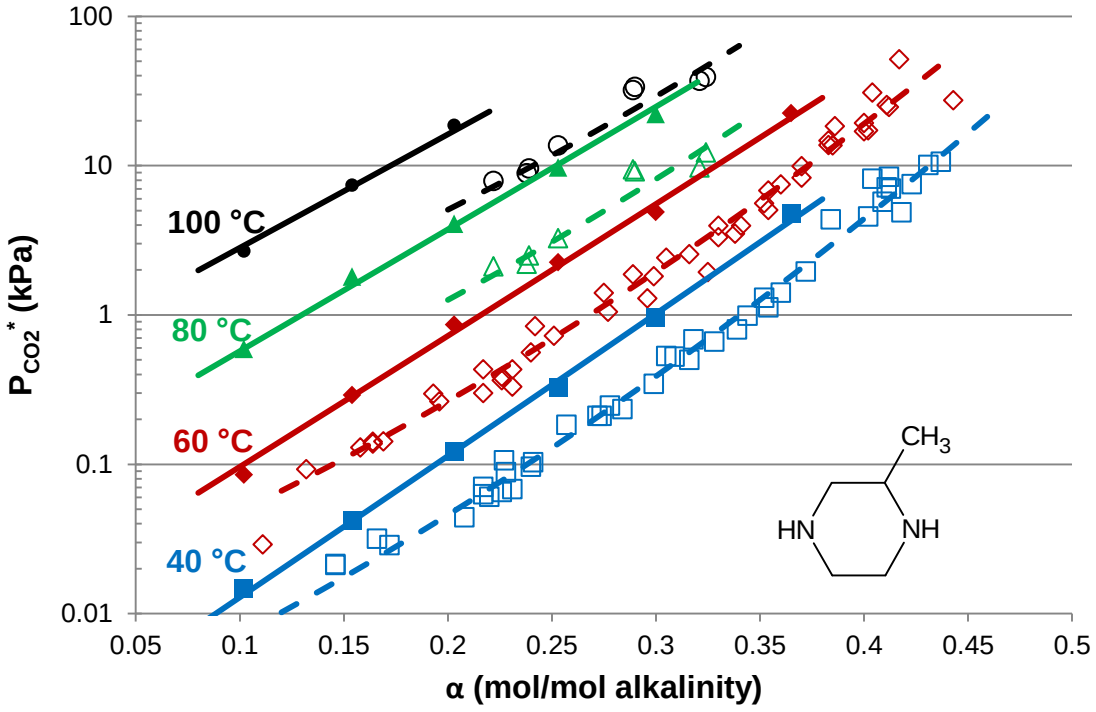

Figure 5.2: CO_2 solubility in 8 m 2MPZ. Dashed lines are models for PZ.

2MPZ/PZ

4 m 2MPZ / 4 m PZ was compared to PZ data in Figure 5.3. $P^*_{CO_2}$ of the blend is found to be only slightly higher than that of PZ. The difference also seems to increase at higher temperature, which is also observed in the case of 2MPZ alone (Figure 5.2). It is then inferred that at low temperature the stability of 2MPZ moncarbamate is comparable to PZ monocarbamate, but elevation in temperature amplifies the difference in stability of them. The methyl group on 2MPZ makes the carbamate less stable, leading to easier reversion of carbamate to bicarbonate and lower CO_2 solubility. More insight is gained from the speciation study and the modeling work discussed in the Chapter 6 & 7.

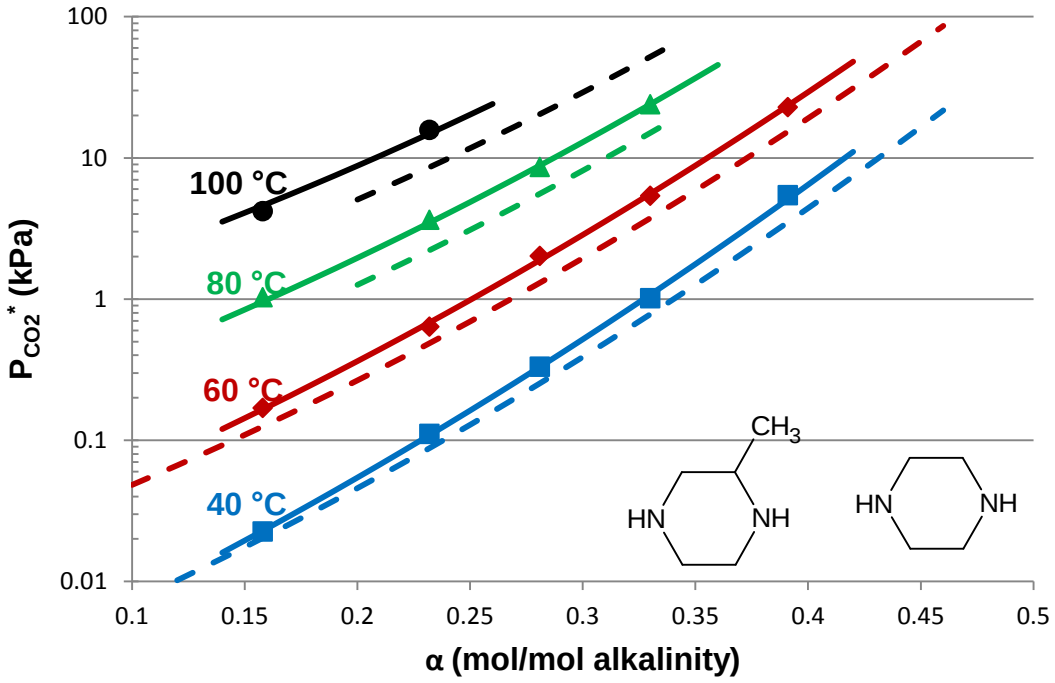

Figure 5.3: CO_2 solubility in 4 m 2MPZ /4 m PZ (points and solid line), compared with PZ (dashed line).

1MPZ/PZ/1,4-DMPZ

The thermal degradation products of 8 m 1MPZ were found to contain PZ and 1,4-DMPZ, and their concentration approaches an equilibrium ratio of 1MPZ/PZ/1,4-DMPZ = 3.75/3.75/0.5 at stripper temperature (Freeman 2011). If this particular formula is chosen, the solvent composition might stay relatively constant over time. Since equal moles of 1MPZ and PZ comprise the vast majority of the blend, the curve for the CO_2 solubility in this blend falls between those for straight PZ and straight 1MPZ at 40 °C, as seen in Figure 5.4.

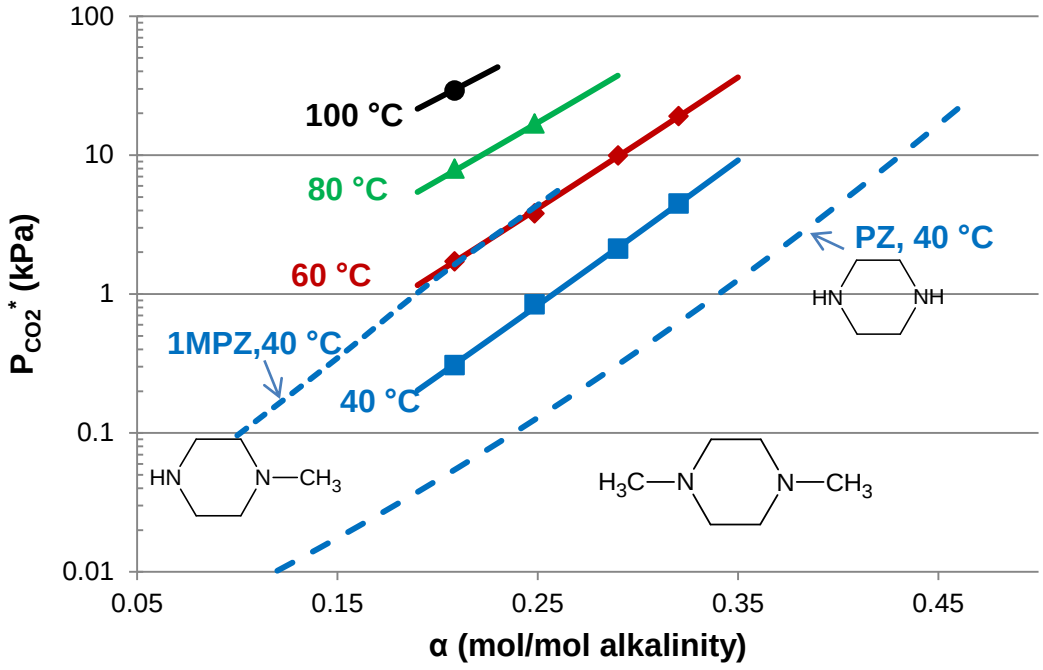

Figure 5.4: CO_2 solubility in 3.75 m PZ/3.75 m 1MPZ/0.5 m 1,4-DMPZ (solid lines), compared to 1MPZ and PZ at 40 °C.

HEP

As shown in Figure 5.5, $P^*_{CO_2}$ of loaded HEP solution is more than one order of magnitude higher than that of PZ at same loading and temperature. The increase of $P^*_{CO_2}$ with loading is also faster than PZ. Due to the attachment of the hydroxyethyl group, one of the amino groups on HEP is not able to react with CO_2 and form carbamate. Instead, this tertiary amino group can only act as a base and catalyze the formation of bicarbonate. With the assumption that the secondary amine group on HEP is comparable to that on PZ, the tertiary amino group causes more bicarbonate formation and lower CO_2 solubility.

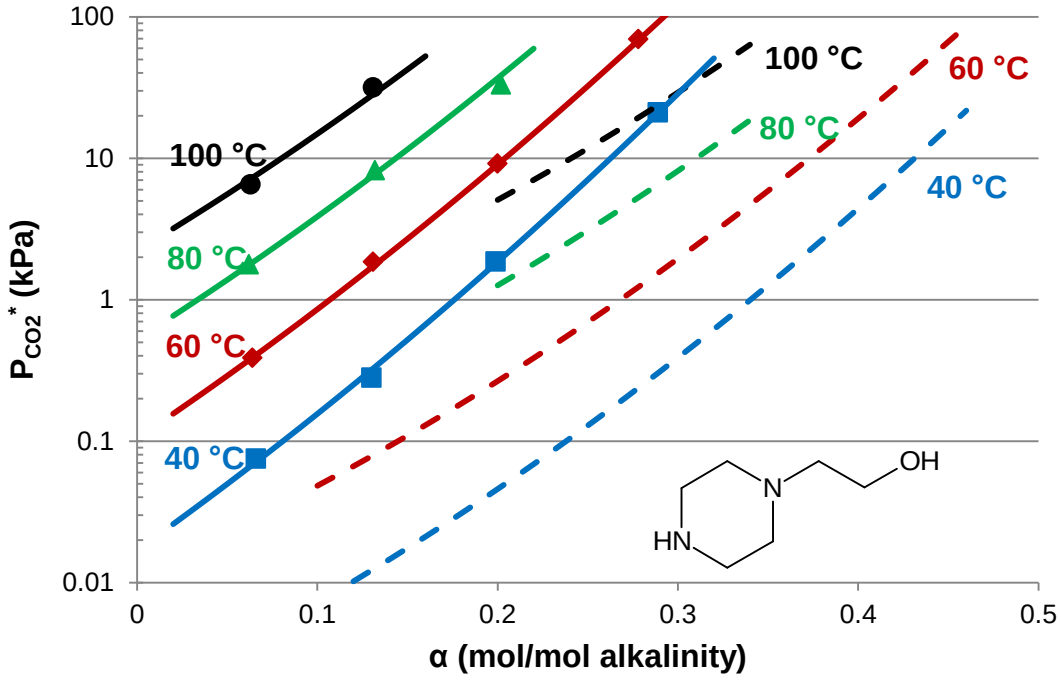

Figure 5.5: CO_2 solubility in 7.7 m HEP (solid line), compared with PZ model (dashed line).

AEP

AEP has three amino groups on its molecule, namely one primary, one secondary and one tertiary amino group. AEP was found to have a similar $P_{CO_2}^{*}$ as PZ at low temperature and low loading, as shown in Figure 5.6. This indicates that the secondary amino group on AEP is the major site which reacts with CO_2. However, as loading or temperature increases, the gap between AEP of PZ tends to increase, presumably because the other amino groups of AEP come into play and exhibit different reactivity with CO_2. Note that due to the definition of CO_2 loading in this work, the ratio of CO_2 to AEP is higher than that of CO_2 to PZ at same CO_2 loading.

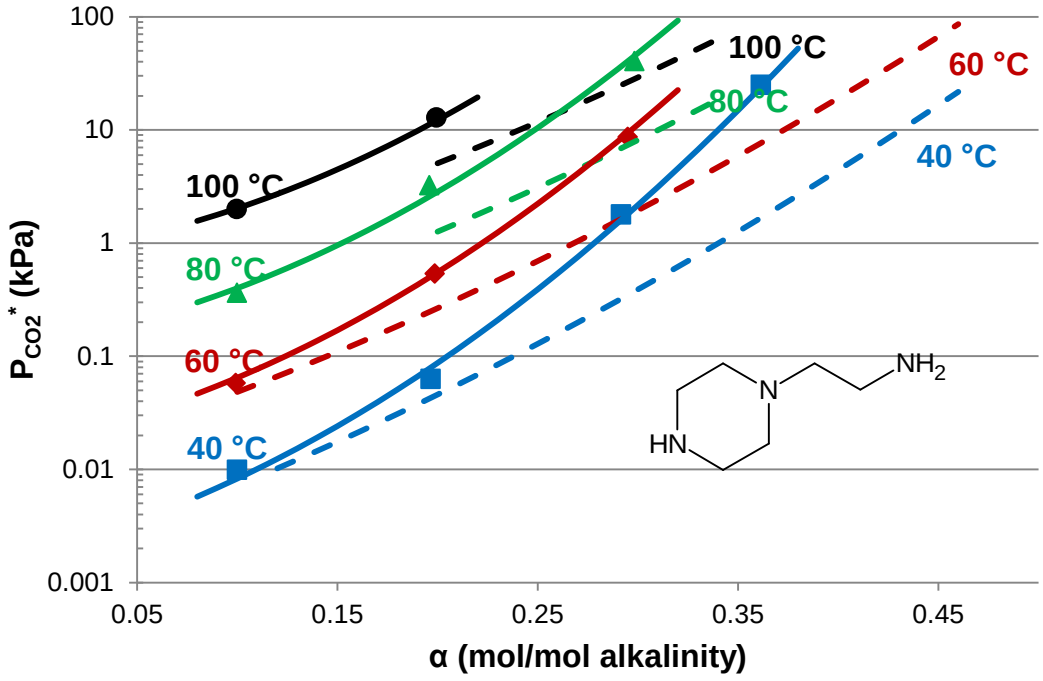

Figure 5.6: CO_2 solubility in 6 m AEP (solid line), compared with PZ model (dashed line).

2-PE

As can be seen in

Figure 5.7, the curves of $P_{CO_2}^{*}$ vs. loading for 2-PE are very different from those for the other amines. The slope of curves is less steep than other curves like PZ and $P_{CO_2}^{*}$ is increasing more slowly with CO_2 loading. $P_{CO_2}^{*}$ of 2-PE is higher than that of PZ at lean loading but becomes lower above a critical CO_2 loading. The ethanol group next to the amino group on piperidine ring introduces steric hindrance and greatly reduces the stability of carbamate. ^{13}C NMR experiments carried out by (Paul, Ghoshal et al. 2009) and Yamada (Yamada, Shimizu et al. 2010) both showed that there is no carbamate formed in CO_2-loaded 2-PE solution. The reaction proceeds through the formation of bicarbonate and 2-PE exhibits a higher $P_{CO_2}^{*}$ than PZ below the critical

loading. It is known that absorption of 1 mol CO_2 corresponds to 2 mol amine for primary or secondary amine because of the formation of stable carbamate; while for tertiary or hindered amine, only 1 mol amine is consumed for each mol CO_2. Consequently, as CO_2 loading increases, free PZ is depleted faster than 2-PE and the pH of the PZ solution drops faster as well. Above the critical loading, formation of bicarbonate dominates in the CO_2 absorption into PZ, resulting in lower CO_2 solubility than that in 2-PE.

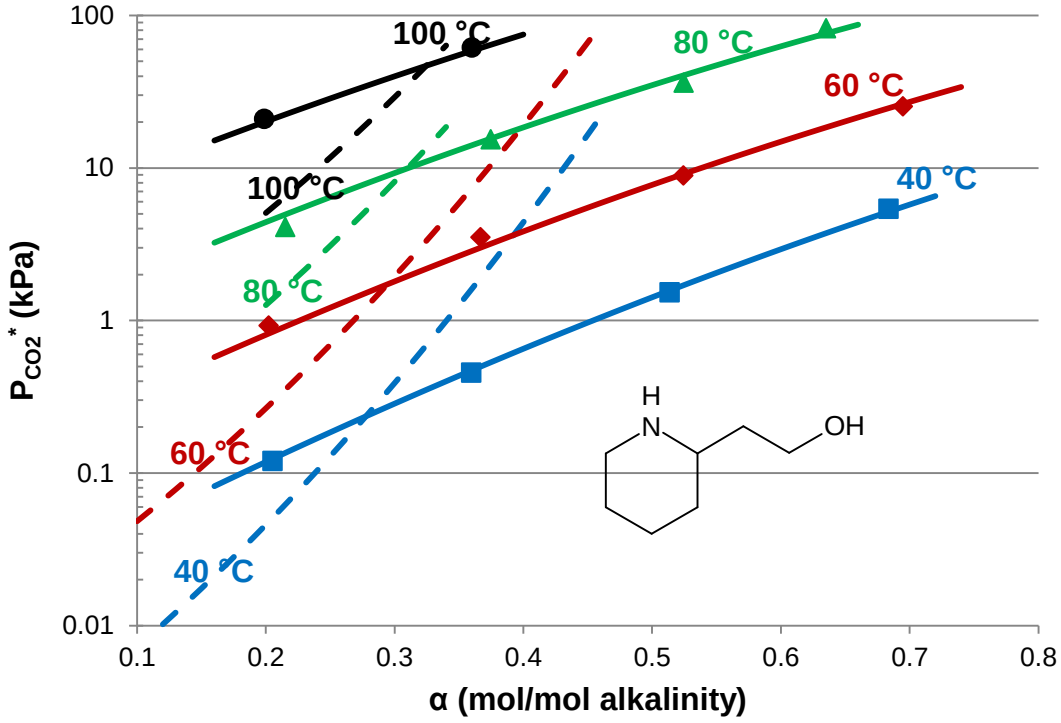

Figure 5.7: CO2 solubility in 8 m 2-PE (solid line), compared with PZ model (dashed line).

5.5 CO_2 Capacity

The working CO_2 capacity of all the amines in this study is plotted against the corresponding rich CO_2 loading in Figure 5.8. There is no defined correlation found

between rich CO_2 loading and CO_2 capacity. In other words, richer CO_2 loading does not necessarily give higher capacity and vice versa. This is opposite to what is usually thought. It is the difference between the lean and rich loading which determines the cyclic CO_2 capacity. The primary amines have high rich loading but the capacity of them is usually low. 2-PE has the greatest capacity due to the hindered amine group. 2MPZ, as a moderately hindered amine, also has a slightly higher CO_2 capacity than PZ. The capacity of 2MPZ/PZ blend, as expected, is between 2MPZ and PZ. 1MPZ has similar capacity as 2MPZ or PZ. The addition of 1,4-DMPZ to 1MPZ/PZ slightly increases the CO_2 capacity compared to just 1MPZ. Although there are three amino groups on AEP, the capacity of it is much less than other PZ derivatives.

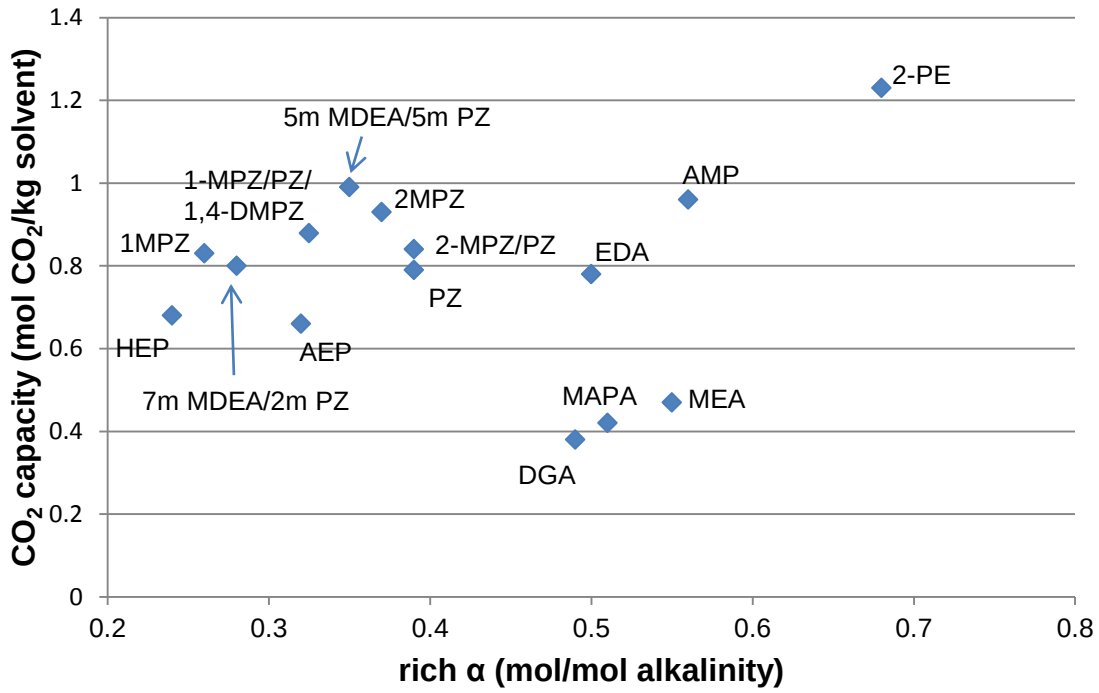

Figure 5.8: Comparison of the CO_2 capacity as a function of rich CO_2 loading (P_{CO2}^{*} = 5 kPa) for the cyclic amines.

5.6 HEAT OF CO_2 ABSORPTION

The heat of CO_2 absorption for all the amines tested in this work is presented in Figure 5.9. This plot of ΔH_{abs} vs. loading for each amine is confined within the range between the corresponding lean and rich loading. On average, all the primary amines have the highest ΔH_{abs}, ranging from 76 - 86 kJ/mol. Hindered amines have the second highest ΔH_{abs} of 68 – 77 kJ/mol; interestingly, the average ΔH_{abs} for PZ and its derivatives are all around 70 kJ/mol. The higher heat of absorption for primary amines stems from the greater heat of reaction between primary amino group and CO_2. Although there is little if any carbamate formation when the hindered amines react with CO_2, the fact that their ΔH_{abs} is greater than that of PZ may be attributed to higher heat of protonation reaction .

Due to the crystallization problem at higher loading, experimental data can only be obtained at two loadings for 2 m 2,5-DMPZ. The precipitation problem was also encountered when working with MEDA solution. Therefore CO_2 capacity and ΔH_{abs} cannot be determined for these two solvents.

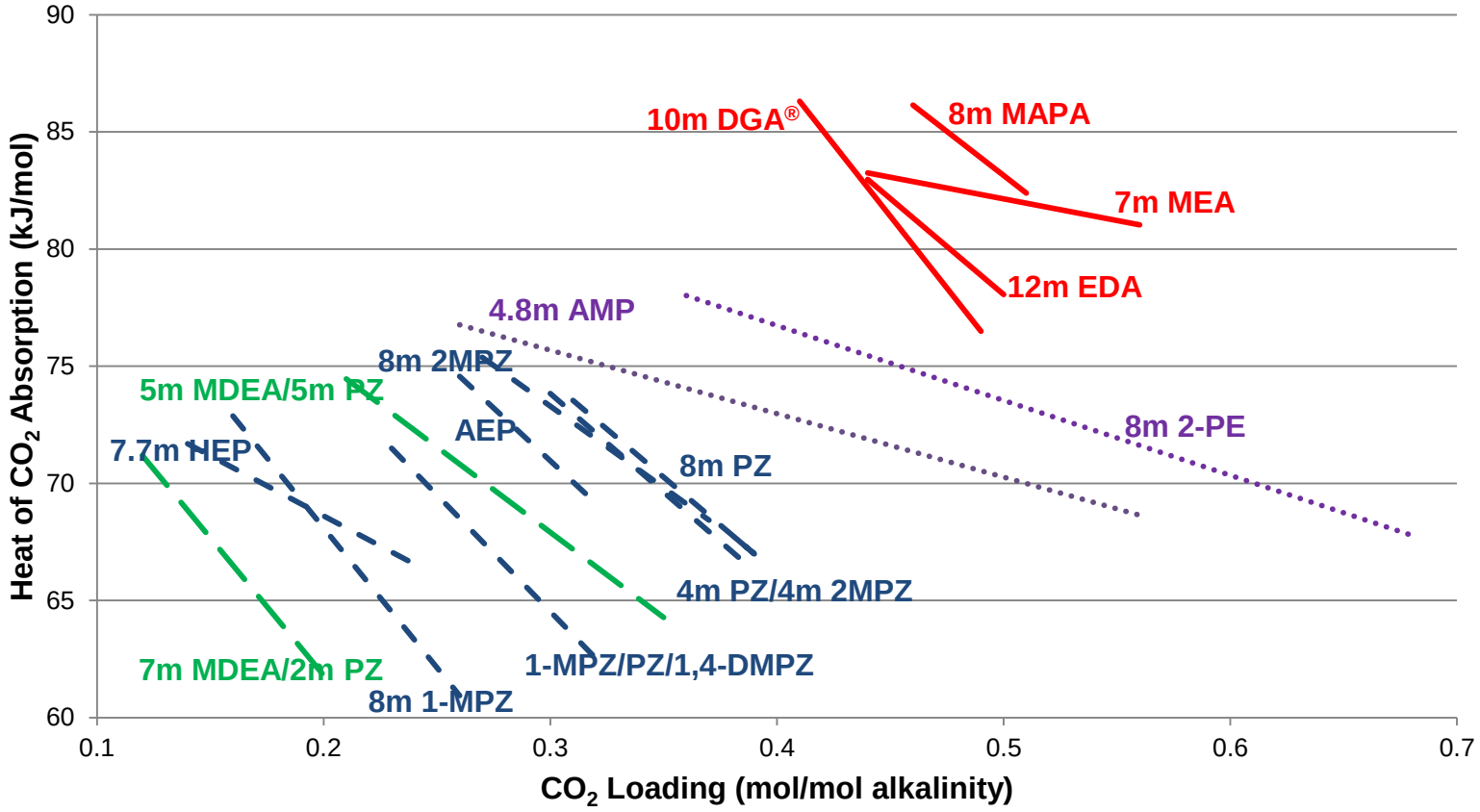

Figure 5.9: A comparison of the heat of CO_2 absorption for the screened amines over the range of the lean and rich CO_2 loading. Primary amine (red solid line), hindered amine (purple dotted line), PZ derivatives (blue short-dashed line), MDEA/PZ (green long-dashed line).

5.7 ABSORPTION/DESORPTION RATES

1MPZ

The liquid mass transfer coefficient (k_g') is plotted against $P^*_{CO_2}$ for 8m 1MPZ in Figure 5.10. Note that the abscissa refers to $P^*_{CO_2}$ at 40 °C for every set of k_g' data instead of $P^*_{CO_2}$ at the real temperature at which k_g' was measured. In this way, k_g' at different temperature can be conveniently compared. The use of $P^*_{CO_2}$ also eliminates the effect of different lean and rich loading so that amines can be compared on the same basis. For 1MPZ, except the point at 40 °C and the leanest loading, increase of temperature leads to smaller k_g' value. In other words, the amine solution becomes less effective in absorbing/desorbing CO_2 at higher temperature. This can be partially explained based on Eq. (2.47). On the numerator, D_{CO2} and k_2 increase with temperature, while H_{CO2} on the denominator goes up at the same time. Consequently the overall trend of k_g' with temperature is dependent on how these factors balance out each other. Diffusion of reactants and products also became important as kinetic rates increases at high temperature, which shift the mass transfer from kinetics-controlled regime to diffusion controlled regime. Increase in CO_2 loading also leads to lower rate, which is probably due to the depletion of free amine at the interface.

k_g' for PZ and MEA are also shown as baselines on Figure 5.10. At 40 °C and $P^*_{CO_2}$ = 0.1 kPa, 1MPZ is about two times slower than PZ, while it has very similar values of k_g' as PZ at higher $P^*_{CO_2}$. This indicates that the methyl group does not significantly affect the reactivity of the secondary amino group on 1MPZ at rich end. Interestingly enough, it seems the substitution of methyl on one of the NH groups only shifts the solubility curve while barely affected the rate when compared at same $P^*_{CO_2}$.

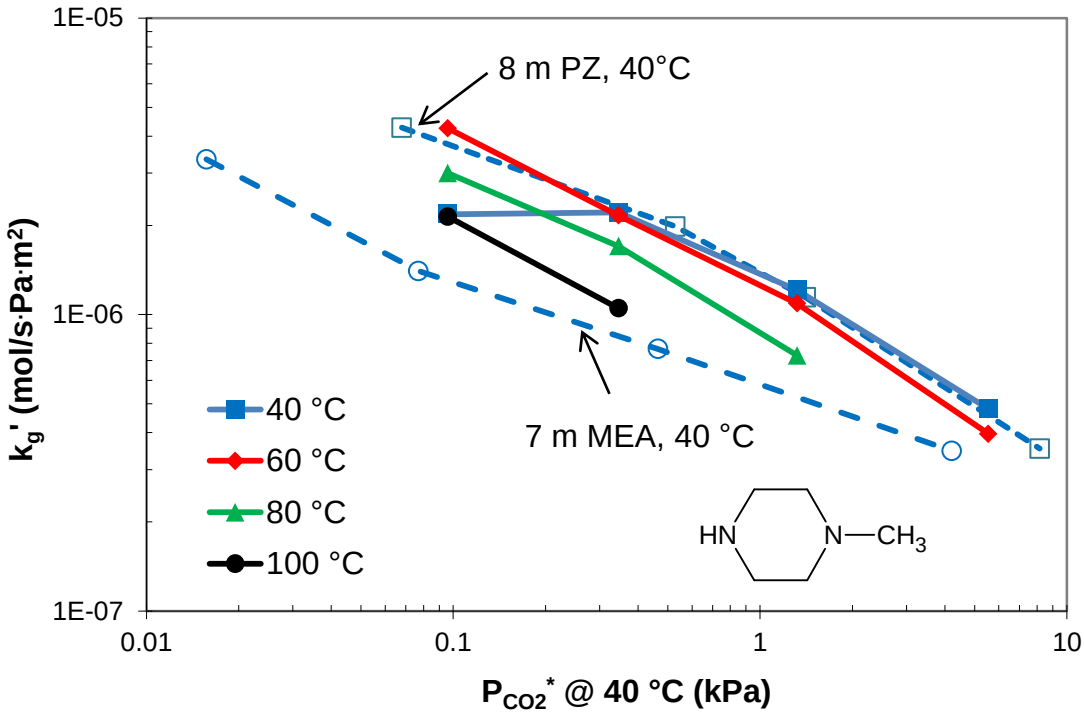

Figure 5.10: Liquid mass transfer coefficient ($k_g^{'}$) of 8 m 1MPZ. The data is compared with $k_g^{'}$ for 7 m MEA and 8 m PZ at 40 °C.

2MPZ

$k_g^{'}$ data for 2MPZ are shown in Figure 5.11. Again, $k_g^{'}$ decreases with increased temperature, but not significantly. At 40 °C and lean loading, 2MPZ seems to absorb/desorb CO_2 at comparable rates to that of PZ, but the rate drops below that of PZ at higher $P_{CO_2}^{*}$. It is inferred that at lean loading, the majority of the reaction occurs between CO_2 and the unhindered amino group, so the initial performance of 2MPZ is similar to PZ. However, as CO_2 loading increases, the slightly hindered amino group also starts to react with CO_2, dragging the overall rate down. Nonetheless 2MPZ is found to always have a higher rate than MEA.

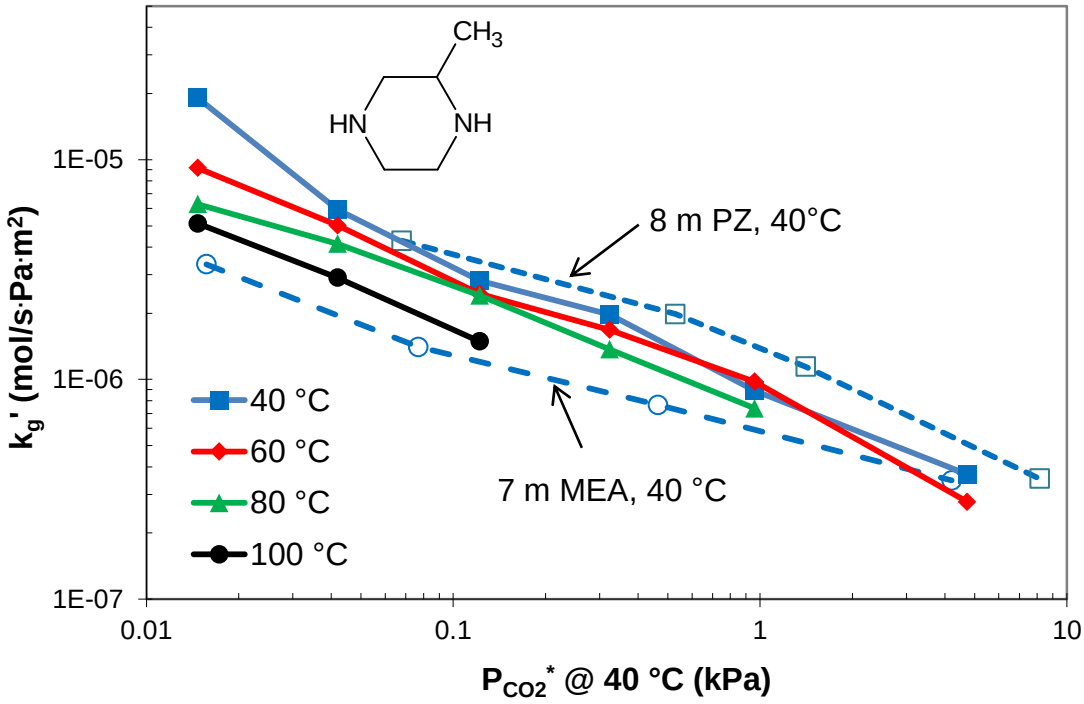

Figure 5.11: Liquid mass transfer coefficient ($k_g^{'}$) of 8 m 2MPZ (solid lines). The data is compared with $k_g^{'}$ of 7 m MEA and 8 m PZ at 40 °C.

2MPZ/PZ

As shown in Figure 5.12, at 40 °C 4 m 2MPZ/4 m PZ outperforms 8 m PZ at $P_{CO_2}^{*}$ less than 0.3 kPa. At the rich end the rate of the blend is slightly slower than PZ but greater than 2MPZ. The speciation of 2MPZ/PZ will be discussed in Chapter 6. Combined with its slightly higher CO_2 capacity than PZ, the blend is a competitive solvent for CO_2 capture.

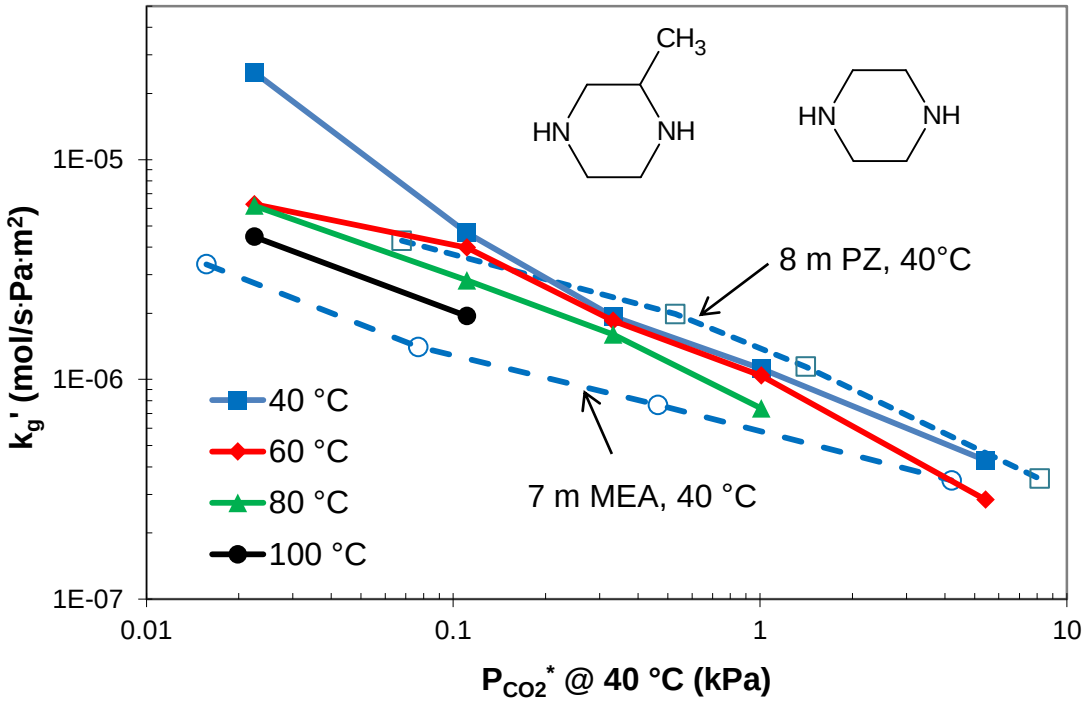

Figure 5.12: Liquid mass transfer coefficient ($k_g^{'}$) of 4 m 2MPZ /4 m PZ (solid lines). The data is compared with $k_g^{'}$ for 7 m MEA and 8 m PZ at 40 °C.

1MPZ/PZ/1, 4-DMPZ

The rate data for the blend of 1MPZ, PZ and 1,4-DMPZ are given in Figure 5.13. The blend has almost the same rates as PZ at both 40 and 60 °C. A change in temperature from 40 °C to 60 °C does not affect $k_g^{'}$ for either solvent. It has been shown that 1MPZ has a similar rate to PZ at the same CO_2 partial pressure. The blend of 1MPZ, PZ, and 1,4-DMPZ is expected to maintain the same rates as the amount of 1,4-DMPZ is much smaller than the other two components. A decrease in rate was observed at 80 and 100 °C for this blend.

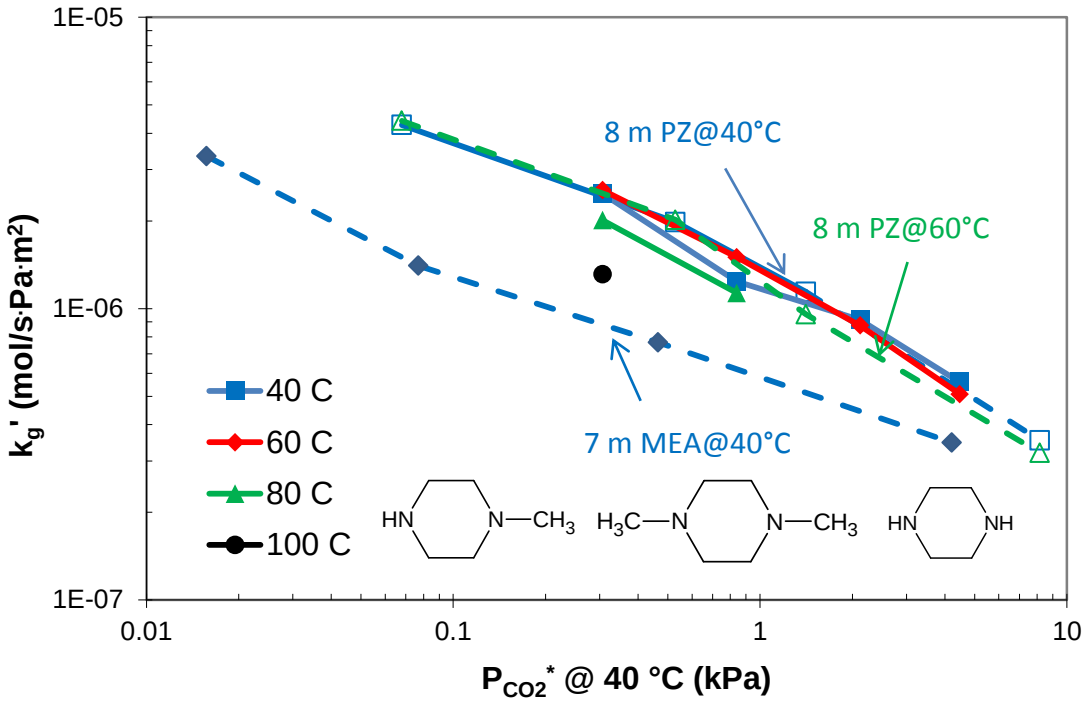

Figure 5.13: CO_2 mass transfer rate for 3.75 m PZ/3.75 m 1MPZ/0.5 m 1,4-DMPZ

HEP

As presented in Figure 5.14, the value of k_g' for HEP is consistently lower than PZ at 40 °C. The rate of HEP is faster than MEA at lean loading but it decreases more rapidly with $P_{CO_2}^*$ and becomes a slower solvent than MEA at the rich end. An increase in temperature slightly reduces the k_g'. As mentioned before, HEP has only one secondary amino group that can form carbamate with CO_2. The secondary amino group depletes more quickly for the same increase of CO_2 loading in PZ. The subsequent formation of bicarbonate catalyzed by the tertiary amino group is much slower than carbamate formation, therefore the rate of HEP decreases faster with loading.

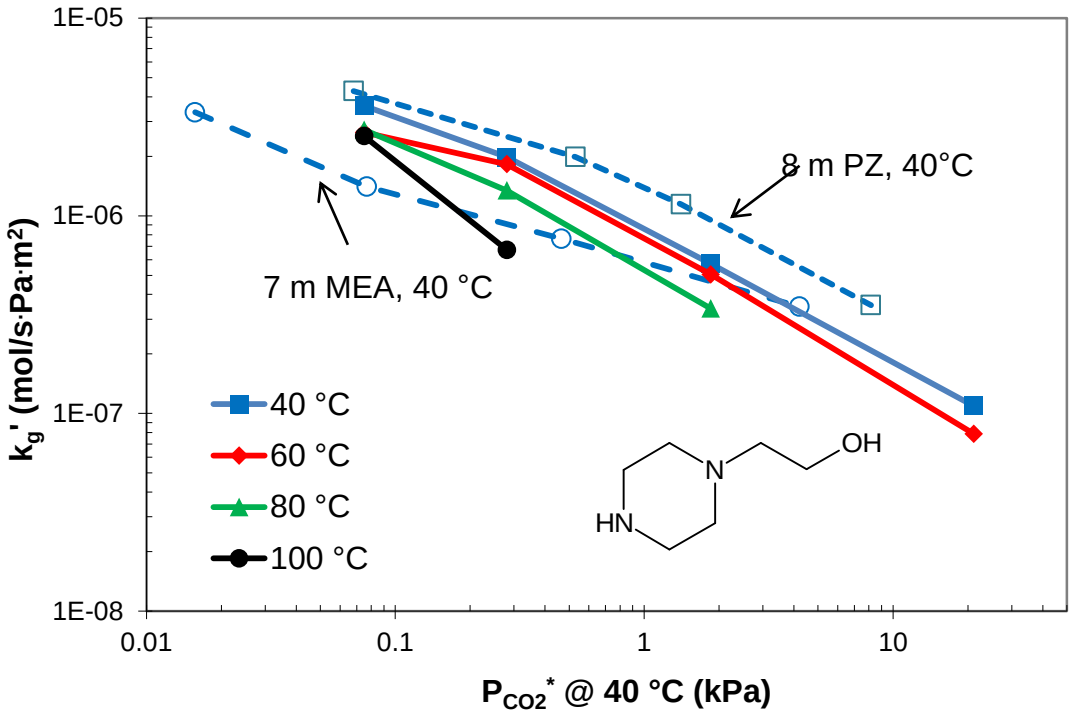

Figure 5.14: Liquid mass transfer coefficient (k_g') of 7.7 m HEP (solid lines). The data is compared with k_g' for 7 m MEA and 8 m PZ at 40 °C.

AEP

As shown in Figure 5.15, AEP, just like HEP, has a k_g' value between PZ and MEA at lean CO_2 loading, but becomes a slower solvent than MEA as $P_{CO_2}^*$ > 1 kPa. At rich CO_2 loading, the primary and secondary amino groups on AEP have probably been depleted and the absorption rate becomes considerably slower.

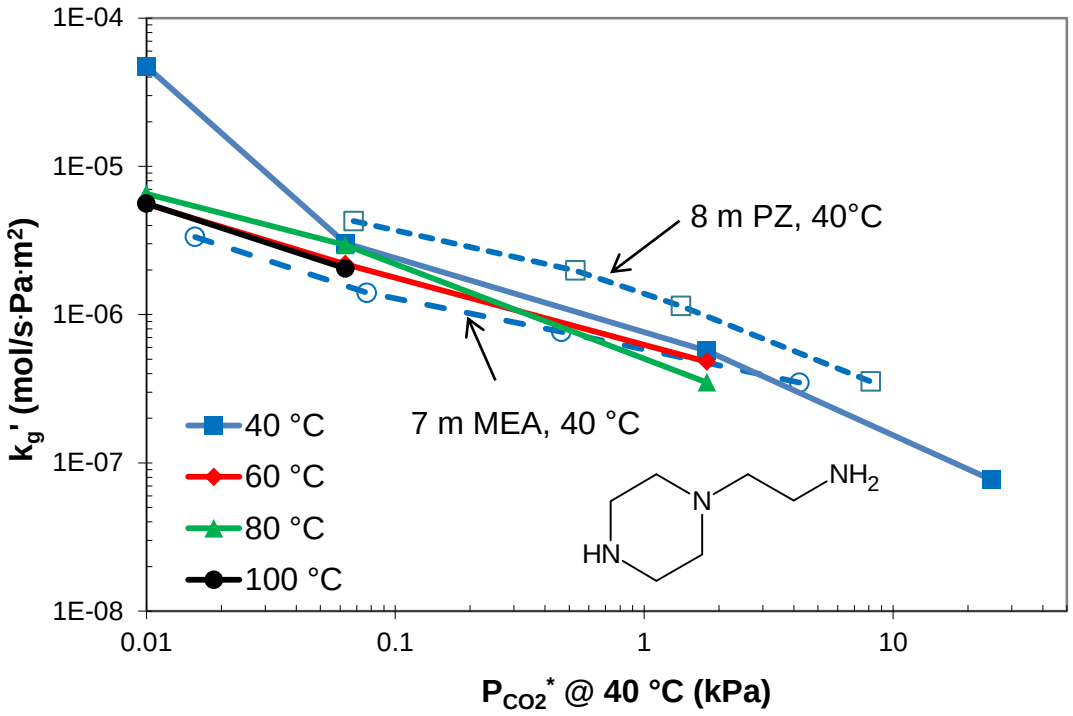

Figure 5.15: Liquid mass transfer coefficient (k_g') of 6 m AEP (solid lines). The data is compared with k_g' for 7 m MEA and 8 m PZ at 40 °C.

2-PE

At the $P_{CO_2}^*$ range of 0.5 kPa to 5 kPa, k_g' of 2-PE is only half of that of PZ, as shown in Figure 5.16. 2-PE is also found to be faster than MEA at lean loading but slower at the rich end. 2-PE is a hindered amine because of the hydroxyethyl group attached to the α-carbon, so there forms no or very little carbamate as 2-PE reacts with CO_2 (Sartori and Savage 1983). The second order reaction rate constant (k_2) of 2-PE with CO_2 was reported by Xu *et al.* (Xu, Wang et al. 1993) to be 0.6 m^3/mol·s, which is two orders of magnitude smaller than the value for PZ of 54 m^3/mol·s (Bishnoi and Rochelle 2000). However, 2-PE is not considerably slower than PZ as what would be expected from the k_2 values. The ratio of CO_2 to consumed amine is about 1:1 for

hindered amine while the ratio is 1:2 for primary and secondary amine. Therefore when compared with same concentration of PZ at same CO_2 partial pressure, 2-PE has a higher free amine concentration, which partially makes up rate of CO_2 absorption as illustrated in Eq. (2.47).

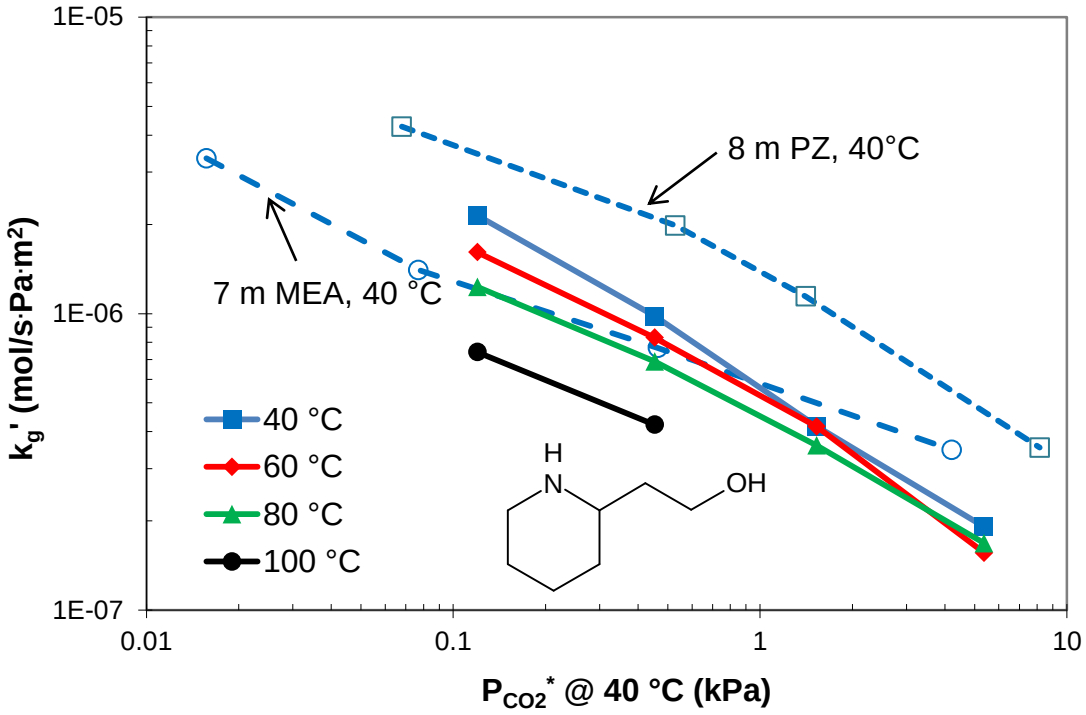

Figure 5.16: Liquid mass transfer coefficient (k_g') of 8 m 2-PE (solid lines). The data is compared with k_g' for 7 m MEA and 8 m PZ at 40 °C.

A quick analysis with Equation (2.47) shows that the decrease of k_g' with CO_2 loading cannot be simply explained by the decrease in free amine concentration. As loading is increased from 0.2 to 0.7, the free amine decreases by a factor of 1.6, however, k_g' is reduced by a factor of 10. The change in diffusivity of CO_2 and Henry's constant is not expected to account for all the discrepancy between the measured value and the predicted value by Eq. (2.47). It is therefore hypothesized that hindered amine may

undergo carbamate formation with CO_2 at the interface, and the absorption of CO_2 is facilitated by the fast chemical reaction and diffusion of 2-PE carbamate. Over the course of the diffusion to the bulk, the carbamate is reversed to bicarbonate. As the free amine concentration decreases with the loading, the interface concentration of 2-PE carbamate significantly drops, which results in a drastic drop in $k_g^{'}$. In other words, the dependence of $k_g^{'}$ on free amine concentration might be greater than what would be expected from Eq. (2.47).

2, 5-DMPZ

The rate of 2, 5-DMPZ is compared to those of 2MPZ, 1MPZ and PZ in Figure 5.17. Over the range of 0.5 kPa to 5 kPa, $k_g^{'}$ decreases in the sequence of PZ ≈ 1MPZ > 2MPZ > 2, 5-DMPZ. The reduction in $k_g^{'}$ is probably due to the introduction of steric hindrance by the methyl group next to the secondary amino groups, which slows the reaction of CO_2 with amine.

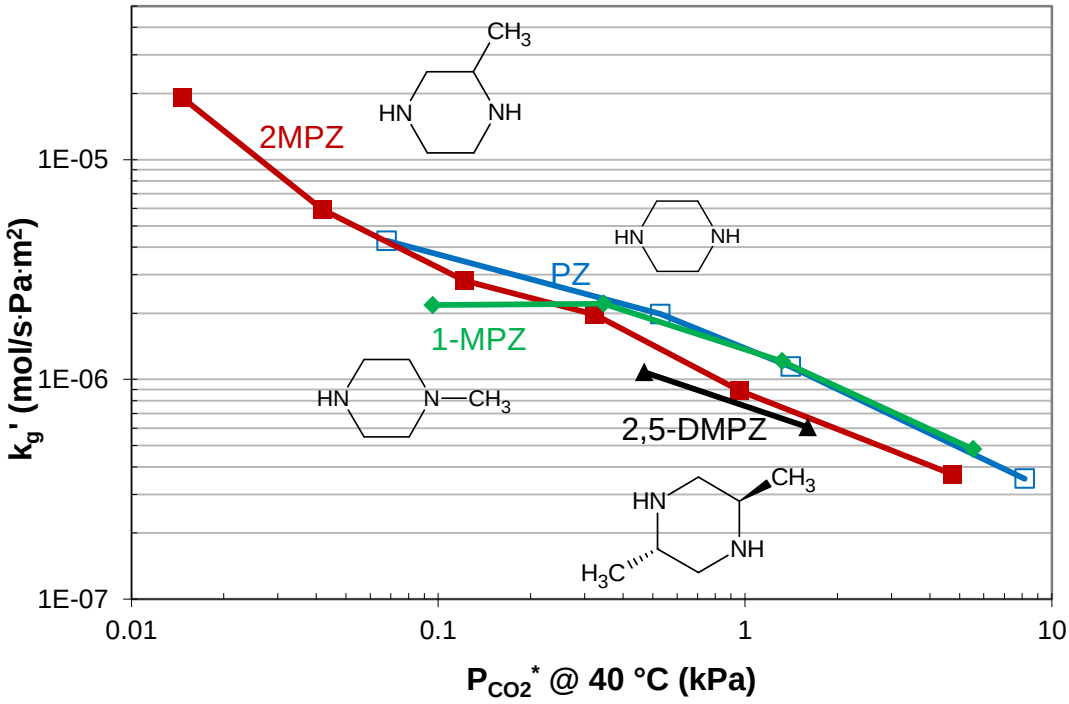

Figure 5.17: Comparison of Liquid mass transfer coefficient ($k_g^{'}$) at 40 °C between PZ, 1MPZ, 2MPZ and 2,5-DMPZ.

In Table 5.4, results for the key properties of all the solvents are summarized. The sequence of the amines is sorted by the value of $k_{g,avg}^{'}$ at 40 °C from the highest to the lowest. Lean and rich loading, capacities, heat of absorptions and $A_{packing}/G_{fluegas}$ are also presented. The value of $A_{packing}/G_{fluegas}$ increases in the same sequence of decreasing $k_{g,avg}^{'}$.

Table 5.4: Summary table for all the tested amines

Amine	m	Lean/Rich Loading	CO_2 Capacity	$-\Delta H_{abs}$ @ $P^*_{CO_2}$ =1.5kPa	$k'_{g,avg} \times 10^7$ @40 ℃
		mol_{CO2}/mol_{alka}	mol/kg solv.	kJ/mol	mol/s·Pa·m^2
PZ	8	0.31/0.39	0.79	70	8.5
1MPZ/PZ/ 1,4-DMPZ	3.75/3.75/ 0.5	0.23/0.32	0.88	67	8.5
1MPZ	8	0.16/0.26	0.83	67	8.4
2MPZ/PZ	4/4	0.30/0.39	0.84	70	7.1
2MPZ	8	0.27/0.37	0.93	72	5.9
HEP	7.7	0.15/0.24	0.68	69	5.3
MEA	7	0.45/0.55	0.47	82	4.3
AEP	6	0.26/0.32	0.66	72	3.5
2-PE	8	0.37/0.68	1.23	73	3.5

5.8 COMPARISON WITH LITERATURE

The results of CO_2 solubility from this study were compared to those reported by Singh and coworkers (Singh, Brilman et al. 2009) on PZ derivatives, as shown in Table 5.5. The CO_2 rich loading calculated for different PZ derivatives from the semi-empirical models of this study are in good agreement with those experimental values from Singh, except 1MPZ. The difference could be attributed to the sensitivity of CO_2 solubility to amine concentration and errors introduced by extrapolation to 30 °C. Singh concluded that 1MPZ had smaller cyclic loading and absorption rate than PZ. However this study found that 1MPZ had practically the same capacity and absorption rate as PZ. According to Singh, the capacity of 2MPZ is only two thirds of that of PZ, but this study found that 2MPZ has a slightly higher capacity than PZ. The difference may be

attributed to the different definitions of cyclic capacity and the errors associated with the methods used for screening. Singh used an equilibrium approach to define rich CO_2 loading but adopted a rate-controlled process to find lean CO_2 loading. However this study used thermodynamic solubility data for both lean and rich CO_2 loading. In addition, the protocols used for absorption rate measurement by Singh and this study are very different. Therefore it is hard to make a direct comparison between estimates of CO_2 capacity and rate. The conclusions for AEP relative to PZ with respect to capacity and rates from both studies agree with each other, but only qualitatively.

Table 5.5: Comparison of Singh (Singh et al. 2009) and this study

Amine	Conc. (M)		CO_2 loading at 10 kPa and 30 °C (mol CO_2/mol amine)		CO_2 capacity (mol CO_2/mol amine)		CO_2 absorption rate	
	Singh	This study	Singh	this study[a]	Singh[b]	this study[c]	Singh: Slope of absorption curve @30 °C (min^{-1})	this study: $k'_{g,avg}$ @40 °C (10^{-7} mol/s·Pa·m^2)
PZ	0.51	4.8	0.87	0.92	0.8	0.17	0.026	8.5
1MPZ	0.53	5.0	0.76	0.63	0.51	0.19	0.016	8.4
2MPZ	0.54	5.0	0.87	0.88	0.52	0.21	0.021	5.9
AEP	2.50	3.4	1.08	1.08	0.29	0.13	0.006	3.5

[a]: Calculated with the semi-empirical models for CO_2 solubility
[b]: Rich loading at 10 kPa and 30 °C, lean loading after desorption with N_2 at 90 °C
[c]: Rich and lean loading corresponding to 5 kPa and 0.5 kPa at 40 °C.

5.9 CONCLUSIONS

Accurate screening of piperazine derivatives for CO_2 capture was performed in the wetted wall column. The CO_2 solubility and absorption/desorption rate for each amine were measured. A semi-empirical solubility model was developed based on

experimental data and used for calculation of CO_2 capacity and heat of absorption. The results are compared to the previous results for PZ and MEA.

The activity of the amino group on a PZ derivative is reduced by the substitution of an alkyl group adjacent to it, while the amine capacity is increased. Cyclic CO_2 capacity of amine from $P^*_{CO_2}$ = 0.5 kPa to $P^*_{CO_2}$ = 5 kPa at 40 °C decreases in the sequence of 2-PE > 2MPZ > 1MPZ/PZ/1,4-DMPZ > 2MPZ/PZ > 1MPZ > PZ > HEP > AEP > MEA. Enthalpy of CO_2 absorption of all the piperazine derivatives is around 70 kJ/mol, substantially less than MEA.

8 m 1MPZ and 3.75 m 1MPZ/ 3.75 m PZ/ 0.5 m 1,4-DMPZ both have similar CO_2 absorption rates as 8 m PZ. 2MPZ is a slower solvent than PZ due to the moderately hindered amino group. The performance of the blend of 2MPZ and PZ is between 2MPZ and PZ. AEP and HEP both have smaller rates than PZ. 2-PE have greater capacity but lower rate than PZ and MEA.

With the use of the liquid film mass transfer coefficient measured in this study, the packing area per unit flue gas flow rate required for 90% CO_2 removal with different amine solvents was calculated based on simple design of an isothermal absorber. $A_{packing}/G_{fluegas}$ increases in the order of 1MPZ = PZ = 1MPZ/PZ/1,4-DMPZ < 2MPZ/PZ < 2MPZ < HEP < MEA < AEP = 2-PE.

Because of their high CO_2 capacity and absorption/desorption rate, 2MPZ, 2MPZ/PZ, 1MPZ/PZ/1,4-DMPZ and 2-PE are competitive CO_2 solvents.

Chapter 6: NMR and Speciation

Speciation in CO_2-loaded amine solution is of great importance for two reasons. First, the vapor-liquid equilibrium as well as the reaction kinetics between the absorbed gas and the absorbent is closely related to equilibrium liquid composition as a function of loading and temperature. Information on speciation is needed to better understand and interpret the experimental data on CO_2 solubility and liquid mass transfer rate. Second, speciation study is indispensable for development and validation of thermodynamic and kinetic models, which are to be incorporated into process simulation tools for design and optimization of real amine scrubbing process.

This chapter presents the quantitative Nuclear Magnetic Resonance (NMR) spectroscopic results for CO_2-loaded 8 m 2-methylpiperazine (2MPZ) as well as 4 m 2MPZ / 4 m Piperazine (PZ) aqueous solutions at 40 °C. ^{1}H and ^{13}C spectra as well as ^{1}H-^{13}C two-dimension correlations were acquired for determination of liquid composition in these two amine solvents at the CO_2 loading range of 0 - 0.4 mol CO_2/ mol alkalinity. All the detailed NMR spectra for each condition have been archived in Appendix B.

6.1 Literature Review

NMR spectroscopy has been widely used for exploration and quantification of substances by observing their specific resonance frequency and intensity in a magnetic field. The frequency is dependent upon the strength of the magnetic field that the nuclei sense, and the intensity is proportional to the number of the identical nuclei.

The NMR spectroscopic technique has been applied for amine-H_2O-CO_2 by many researchers. By providing detailed information on liquid composition, NMR serves to validate and refine VLE models developed solely from phase equilibrium data (Jakobsen, Krane et al. 2005). Suda *et al.* (Suda, Iwaki et al. 1996) used ^{1}H and ^{13}C NMR spectra to

quantitatively examine dissolved species during the course of CO_2 absorption into primary, secondary, tertiary and hindered amines. Ermatchkov and coworkers (Ermatchkov, Kamps et al. 2003) systematically studied speciation in PZ solutions at varied temperature and CO_2 loading, and determined the equilibrium constants for different reactions based on quantitative ^1H NMR data. Bishnoi and Rochelle quantified species in PZ (Bishnoi and Rochelle 2000) and PZ/N-methyl-diethanolamine (MDEA) (Bishnoi and Rochelle 2002), and calculated equilibrium constants for carbamate formation reactions. Cullinane (Cullinane 2005) determined the equilibrium speciation in K_2CO_3/PZ by ^1H NMR. Hilliard used $^{13}CO_2$ for preparation of amine solutions and conducted extensive quantitative speciation studies on PZ, MEA and Potassium-PZ (Hilliard 2008). More NMR studies have been summarized in Table 6.1.

This work intends to expand the knowledge of speciation in PZ derivatives as a CO_2 absorbent, for which there is little information. The obtained speciation data will be used for thermodynamic and kinetic modeling work described in the later chapters.

Table 6.1: Literature studies on amine-CO_2-H_2O using NMR techniques

Amine (Conc.)	**CO_2 Loading (mol/mol amine)**	**Temp. (°C)**	**NMR Methods**	**Author/Year**
K^+ Sarcosine (3.5 M) MAPA/Sarcosine (2.5M/2.5M)	0 – 0.5	25	Qualitative ^{13}C	(Hartono, Aronu et al. 2011)
AMP (30 wt%)	0-0.62	25	Quantitative ^{13}C	(Ciftja, Hartono et al. 2011)
Blend of two out of MEA (2M), PZ (0.3-1.2 M), N-methyl monoethanolamine (MMEA, 2M)	n/a	40	^{1}H and Quantitative ^{13}C	(Ballard, Bown et al. 2011)
DEA (0.667 M), MDEA (1.33 M), AMP (2.00 M)	n/a	20	Quantitative ^{13}C	(Barzagli, Mani et al. 2010)
MAE (2-(methylamino)ethanol), AMP	MAE: 0.59 ; AMP: 0.68	22	Quantitative ^{13}C	(Yamada, Shimizu et al. 2010)
2-Piperidine ethanol (2-PE) (Concentration n/a)	n/a	n/a	^{13}C	(Paul, Ghoshal et al. 2009)

MEA (4 M)	n/a	25, 40	Quantitative ^{13}C	(Yang, Bown et al. 2009)
2-[(2-aminoethyl)amino]-ethanol (AEEA, 5 wt%)	0 -0.8	20	^{1}H and ^{13}C	(Jakobsen, da Silva et al. 2008)
MEA (5M)	0-0.55	22.5	^{1}H and ^{13}C	(Fan, Wee et al. 2009)
MEA (4.1 m) DEA (4.1 m)	0 – 1.01	20-80	^{1}H and ^{13}C	(Böttinger, Maiwald et al. 2008)
MDEA(2.1,3.1,5.6 m) MDEA-PZ (4.2 m – 1.9 m)	0-1.4	20-60	^{1}H and ^{13}C	(Bottinger, Maiwald et al. 2008)
MEA (15 wt%, 30 wt%) butyl-ethanolamine (BEA, 9 wt%, 30wt%) MDEA (23 wt%)	0.1-1	20, 40	Quantitative ^{13}C	(Jakobsen, Krane et al. 2005)
MEA (10 wt%) 2-amino-2-hydroxymethyl-1,3-propanediol (AHPD, 10wt%)	0-1	25	Quantitative ^{13}C	(Park, Yoon et al. 2003)

MEA, AMP, 2-amino-2-methyl-1,3-propanediol (AMPD), 2-amino-2-ethyl-1,3-propanediol (AEPD) (All 20 wt%)	0.723, 1.200 0.966, 0.947	25	^{15}N NMR, ^{13}C NMR	(Yoon and Lee 2003)

6.2 SPECIES AND CHEMICAL EQUILIBRIUM

The chemistry of PZ-CO_2-H_2O has been well studied (Ermatchkov, Kamps et al. 2003; Hilliard 2008), as illustrated in Figure 6.1. There are five PZ compounds present in the system.

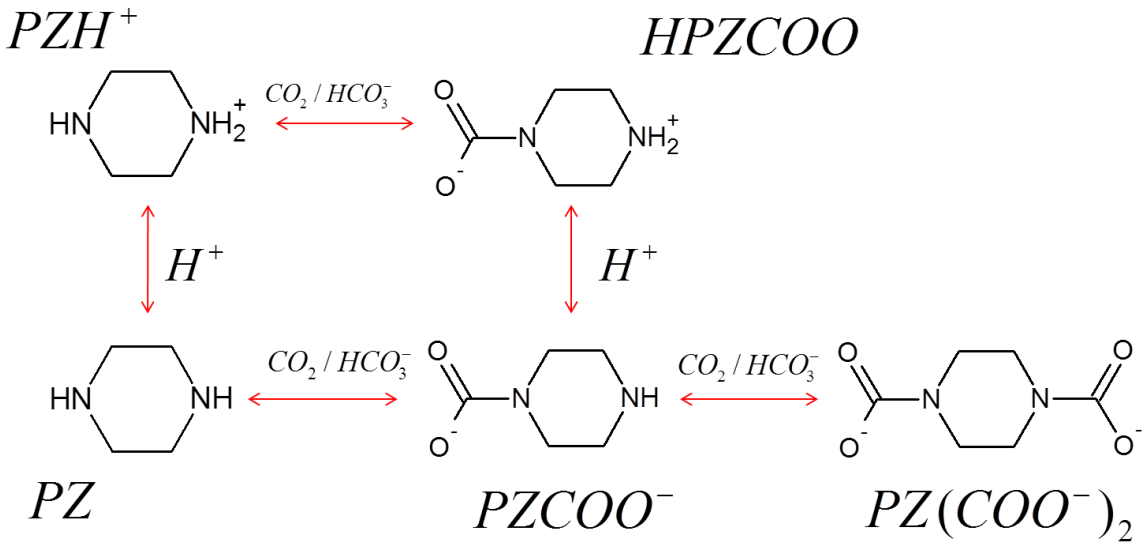

Figure 6.1: The species and reaction scheme in 2MPZ-CO_2-H_2O.

The reaction products between CO_2 and 2MPZ can be deduced based on the reaction scheme for PZ. Figure 6.2 shows the possible reactions and compounds in 2MPZ-H_2O-CO_2. There are seven possible 2MPZ species in 2MPZ CO_2-loaded solution instead of just five as in PZ solution. The two amino groups on 2MPZ are not equivalent due to the substitution of the methyl group, which introduces moderate hindrance to the adjacent amino group. As a consequence, there are two types of monocarbamate that can be formed. Formation of hindered monocarbamate ($^-$OOC2MPZ) is expected to be less energetically favorable than unhindered monocarbamate (2MPZCOO$^-$). However, the electron-donating methyl group is expected to stabilize the positive charge on the

neighboring amino group so the protonation is projected to occur first on the hindered amino group. The 2MPZ monocarbamates can either be protonated and form zwitterions (H2MPZCOO and OOC2MPZH), or react with one more mole CO_2 to form dicarbamate ($2MPZ(COO^-)_2$).

The second pKa values of 2MPZ and PZ were reported to be around 5 at 25 – 50 °C (Khalili, Henni et al. 2009), and the normal pH value in CO_2-loaded amine solution at the rich loading is typically well above 8 (Yamada, Shimizu et al. 2010). Therefore the amount of di-protonated 2MPZ or di-protonated PZ is extremely small in loaded solutions and they are excluded from consideration in this work.

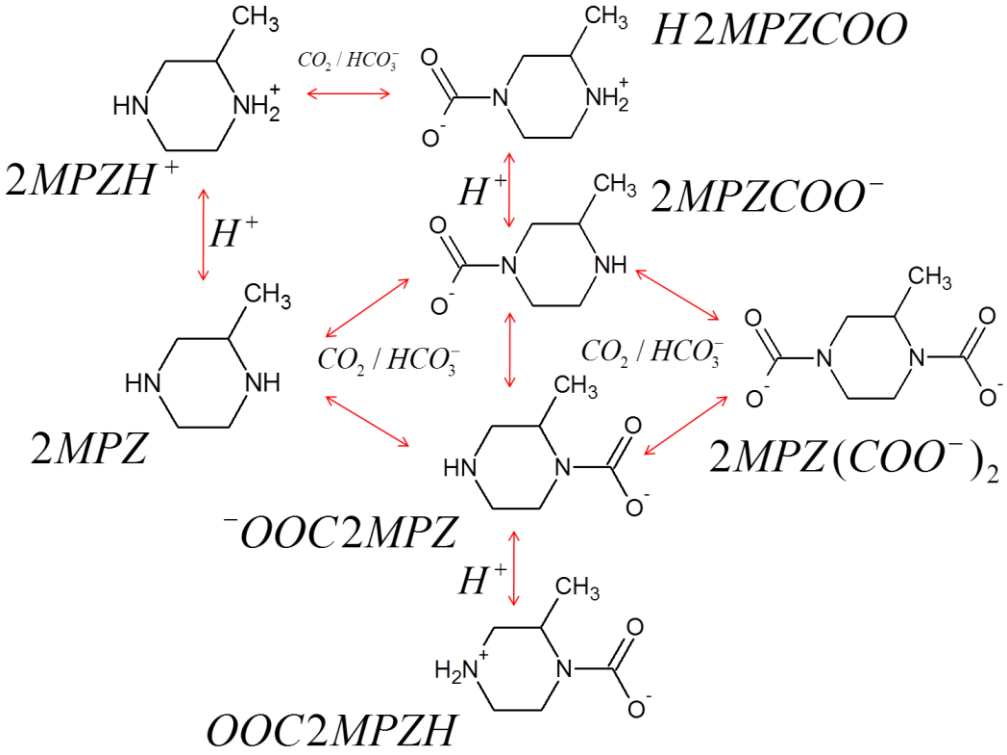

Figure 6.2: The species and reaction scheme in 2MPZ-CO_2-H_2O.

To differentiate the carbon and proton nuclei with different electronic environments, they are numbered for different species present in 2MPZ-H_2O-CO_2 and PZ-H_2O-CO_2, as shown in Table 6.2. The same number is assigned to a ^{13}C nucleus and the protons attached to it. Due to the rapid exchanging rate of protons, a protonated species and the unprotonated counterparts cannot be differentiated by the NMR spectroscopy used in this study. Therefore it is the sum of them which was quantified from the NMR spectra.

Table 6.2: Molecular structure of the compounds in CO_2-loaded 2MPZ and PZ aqueous solutions.

Name	Molecular Structure
2MPZ/2MPZH$^+$	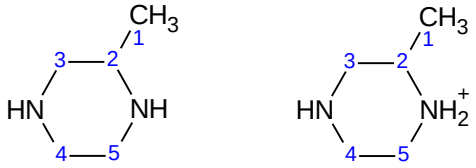
2MPZCOO$^-$/H2MPZCOO	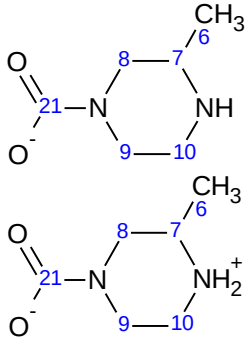
$^-$OOC2MPZ/OOC2MPZH	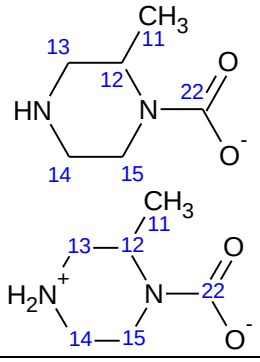

2MPZ(COO^-)$_2$	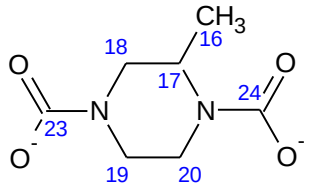
PZ/PZH^+	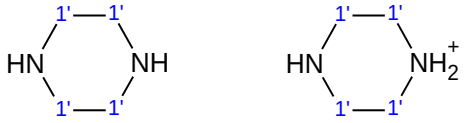
PZCOO^-/HPZCOO	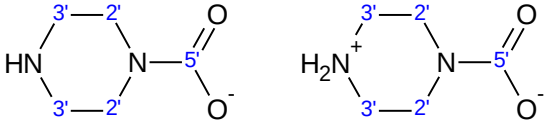
PZ(COO^-)$_2$	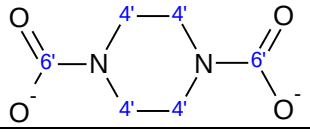
HCO_3^-/CO_3^{2-}	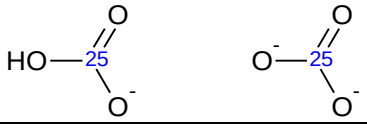

In addition to the species listed in Table 6.2, CO_2 is also expected to be present in the system. However, the amount of free CO_2 in the amine solutions is well below the detection limit of the NMR spectroscopy and will not be accounted for.

6.3 NMR DATA ANALYSIS

To quantitatively analyze NMR data, 1,4-dioxane was used as the internal standard because it has a symmetric cyclic molecular structure similar to PZ. A sensitivity analysis conducted by Hilliard (Hilliard 2008) shows that the minimal amount of 1,4-dioxane needed for accurate determination of liquid composition is 1-5 wt%. In this work, the method employed by Hilliard (Hilliard 2008) was also followed to quantify different species based on the known amount of the standard. In this method, a universal ratio is determined:

$$R_b = \frac{\varphi_{ref} \cdot C_{ref}}{A_{ref}} \tag{6.1}$$

where R_b is the number of moles of dioxane/kg H_2O per unit area; φ_{ref} is the number of active protons or carbons in dioxane; C_{ref} is the experimental dioxane molality based on the batch solution; A_{ref} is the experimental integrated area for the dioxane reference peak.

With the R_b calculated, the molality of other species in the same sample can be determined by the following equation

$$C_i = \frac{A_i \cdot R_b}{\varphi_i} \tag{6.2}$$

where A_i and φ_i are the experimental integrated peak area for species i and the number of active protons or carbons in species i respectively. The CO_2 loading in the solution can also be determined from the NMR method by dividing the total CO_2 species concentration by the equivalents of total amine. The values will be compared to those calculated by the gravimetric method.

6.4 2MPZ-CO_2-H_2O

Samples of 2MPZ-CO_2-H_2O were prepared at variable CO_2 loading (α). The apparent liquid composition in molality as well as the CO_2 loading determined gravimetrically for these samples is shown in Table 6.3. Note that D_2O is not considered as equivalent to water and is not included for the determination of molality.

Table 6.3: Apparent liquid composition of 2MPZ-CO_2-H_2O samples based on gravimetric preparation.

Loading (mol/mol alkalinity)	**Apparent concentration (mole/kg H_2O)**			
	2MPZ	**$^{13}CO_2$**	**1,4-Dioxane**	**D_2O**
0	8.009	0	0.2397	10.40

0.105	8.009	1.676	0.2341	11.67
0.299	8.009	4.784	0.3055	14.07
0.361	8.009	5.775	0.4278	15.36

6.4.1 Peak Identification

6.4.1.1 ^1H NMR

The proton NMR spectra for 8 m 2MPZ at varied loading are shown in Figure 6.3. Note that the reported values of α were determined from the NMR spectra, and they are slightly different from those obtained by gravimetric preparation. The details for quantitative NMR analysis will be discussed later. The peaks at 3.5 ppm are from 1,4-Dioxane.

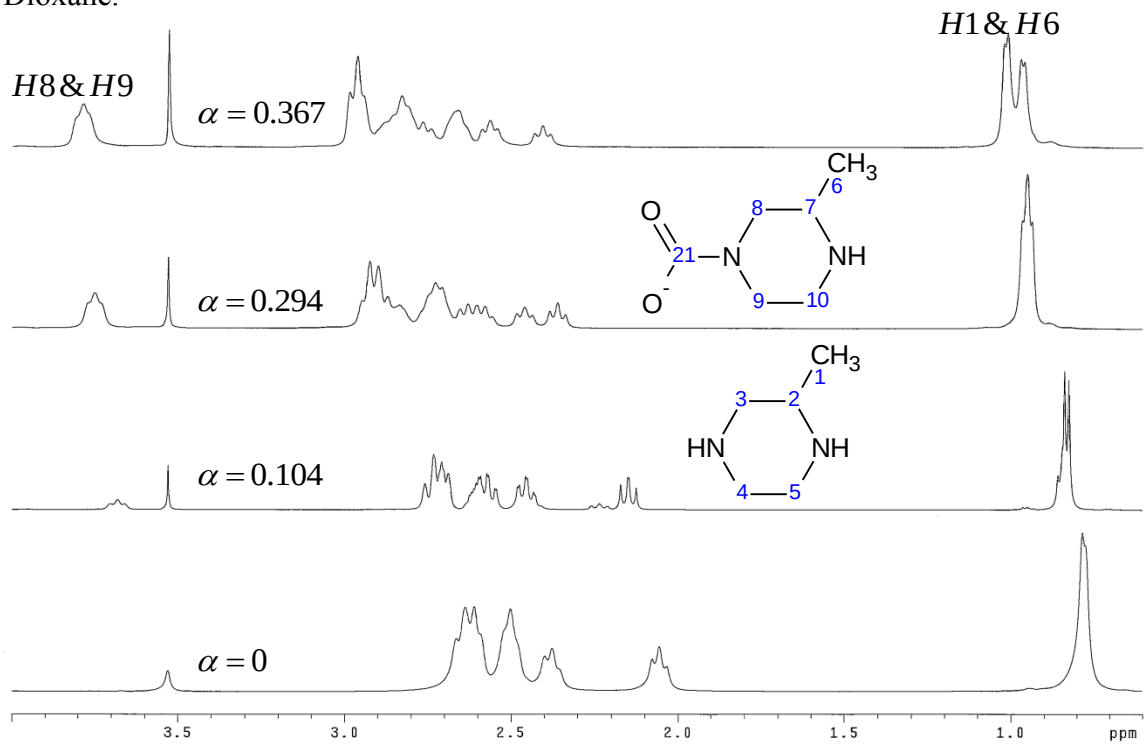

Figure 6.3: ^{1}H NMR spectra for 8 m 2MPZ at 40 °C and varied loading.

It is relatively easier to interpret the spectrum and perform the peak assignment for the unloaded sample. The online spectral database for organic compounds (SDBS 2011) gives the chemical shifts (δ) of the peaks in the ^{1}H-NMR spectrum at 400 MHz as well as in the ^{13}C NMR spectrum for 2MPZ in $CDCl_3$, as shown in Table 6.4 and Table 6.5, respectively. The SDBS database suggests that 2MPZ assumes a three-dimension molecular configuration rather than a flat one, and the electronic environment of one proton is therefore slightly different from another, which causes different resonance frequency. The numbering of the proton and carbon nuclei on 2MPZ has been shown in Figure 6.4. Note that the convention of numbering for carbon nuclei is kept the same as shown in Table 6.2. However, the numbering of proton is temporarily changed from numbers to letters to better differentiate the protons.

With the assumption that the relative position of the carbon peaks is not affected by the solvent, the ^{13}C NMR peaks observed for the unloaded 2MPZ aqueous solution in this study are assigned to different ^{13}C nuclei on 2MPZ based on the peak assignment from the SDBS database (Table 6.5). The assignment of the proton peaks in this work was accomplished by referring to ^{1}H-^{13}C two-dimension (2D) spectrum (Figure 6.5), which correlates the ^{13}C to the mutually bonded ^{1}H. Clearly the 2D spectrum indicates that each carbon is correlated to two protons except C2, which is consistent with the actual molecular structure. The assignment of the peaks for the two protons on a same carbon is again based on the relative peak position found in the SDBS database. This results in a similar sequence of chemical shift from low to high for the protons, with the exception of ^{A}H, ^{B}H and ^{C}H, , as shown in Table 6.4. The peaks for ^{D}H and ^{E}H are also found to overlap each other. The small change in relative chemical shifts of these proton peaks might be attributed to the change in solvent polarity ($CDCl_3$ vs. H_2O).

Table 6.4: Chemical shift and peak assignment in the ^{1}H NMR spectrum for 2MPZ in $CDCl_3$ (SDBS 2011) and H_2O (this work).

^{1}H Assignment	Count of protons	δ (ppm) (SDBS)	δ (ppm) (this work)
K	3	1.001	0.0778, 0.0785
J	2	1.96	n/a
G	1	2.346	2.038,2.059,2.081
F	1	2.707	2.361, 2.381, 2.404
E	1	2.743	2.505
D	1	2.823	2.505
C	1	2.89	2.672
B	1	2.90	2.643
A	1	2.95	2.615

Table 6.5: Chemical shift and peak assignment in the ^{13}C NMR spectrum for 2-MPZ in $CDCl_3$ (SDBS 2011) and H_2O (this work).

^{13}C Assignment	Count of ^{13}C	δ (ppm) (SDBS)	δ (ppm) (this study)
1	1	20.02	18.793
2	1	51.74	50.230
3	1	54.03	51.793
4	1	47.32	45.243
5	1	46.34	44.307

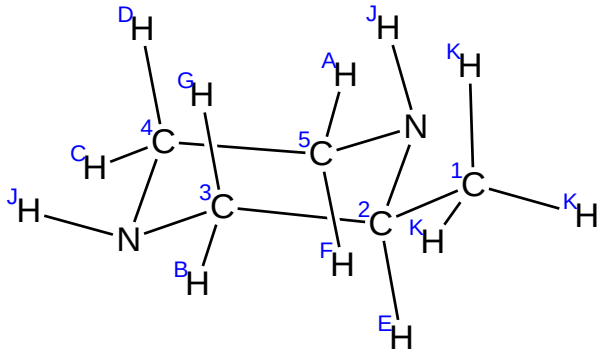

Figure 6.4: The 3D configuration of 2MPZ molecule and the numbering of carbon and proton nuclei.

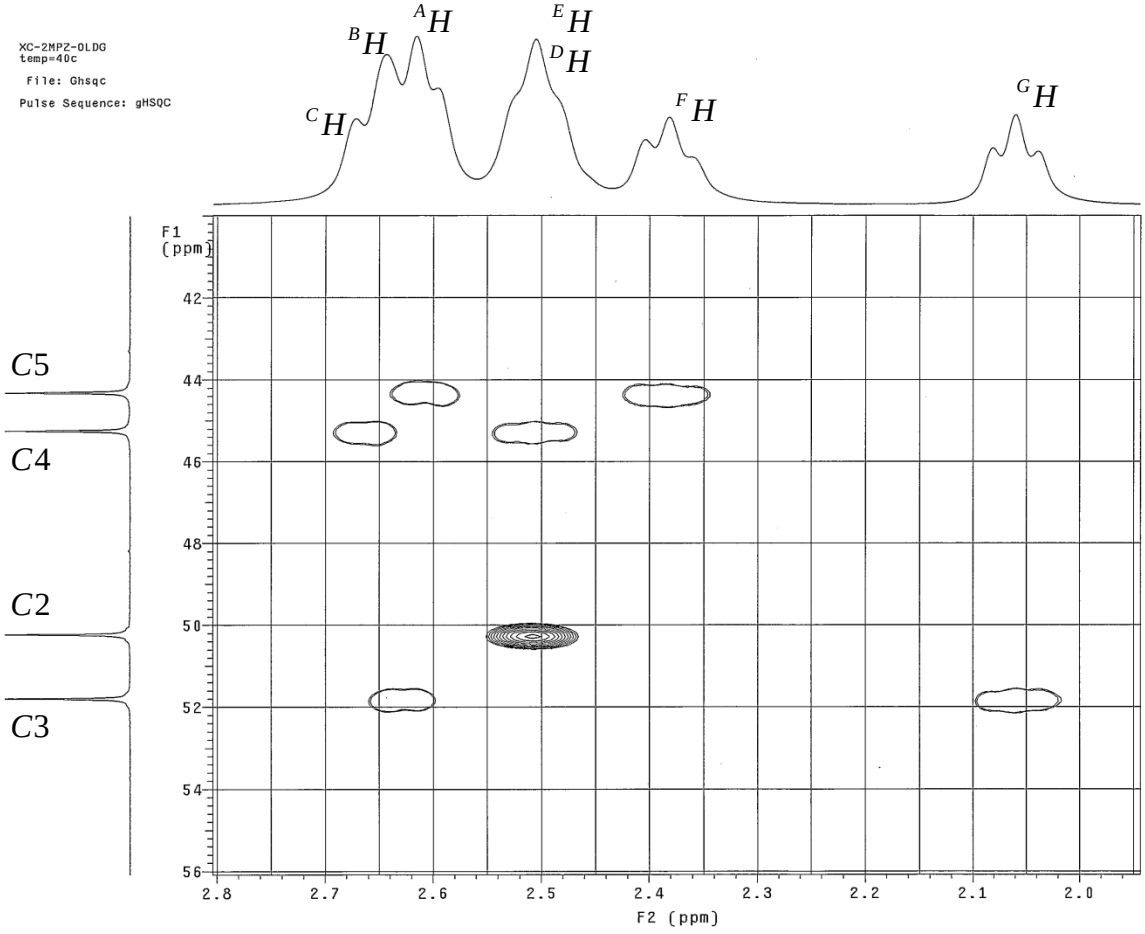

Figure 6.5: ^{1}H-^{13}C 2D correlation spectrum for unloaded 8 m 2MPZ at α = 0 mol/mol alkalinity and 40 °C.

As CO_2 is loaded to 2MPZ solutions, the additional ionic products considerably complicate the ^1H NMR spectra. The shift of the proton peaks due to the introduction of carbonyl group is relatively small, so they partially overlap with the original peaks from the amine itself. As a result, most of the peaks at the proximity of δ=2.5 ppm are confounded to a great extent at high CO_2 loading. The split of proton peaks makes it even harder to identify all the peaks.

There appear only two distinct peaks, which grow with CO_2 loading and shift between 3.6-3.8 ppm and 2.2-2.5 ppm respectively. With the help from the 2-D correlations (shown later in Figure 6.9 through Figure 6.11), the peak on the far left side corresponds to H8 and H9, while the other is identified as H3. These two peaks are the only ones that can be directly used for quantification of $2MPZCOO^-$/H2MPZCOO. Unfortunately, the peaks for hindered carbamate and dicarbamate cannot be determined from the proton NMR spectra. As a result, the peaks that are well separated from the others are not sufficient to represent the complete speciation.

Conclusively, the splitting and insufficient separation of proton peaks from 2MPZ and 2MPZ products poses a great challenge for peak identification and independent integration. Consequently using ^1H NMR spectra for determination of liquid composition in 8 m 2MPZ is not feasible, and the quantification of species is mainly accomplished by analyzing ^{13}C NMR spectra in this work.

6.4.1.2 ^{13}C NMR

The ^{13}C NMR spectra for 8 m 2MPZ at varied CO_2 loading and 40 °C in the upfield are shown in Figure 6.6. The peaks at δ = 66.5 ppm are from 1,4-dioxane. The ^{13}C peaks have been identified for the unloaded solution. As CO_2 was loaded to the amine solution, additional peaks emerge near the original peaks for 2MPZ. The intensity

of the new peaks also grows with CO_2 loading, whereas the peaks for C1 through C5 shrink. The position of the peaks also shifted toward upfield slightly with CO_2 loading. Since the most probable products of 2MPZ with CO_2 are the unhindered carbamate or its protonated form, the new peaks in the spectra are assigned to $2MPZCOO^-$/H2MPZCOO. The peaks for the carbamate seem to be more apart from the peaks for 2MPZ as loading increases. At $\alpha = 0.367$, it can be clearly seen that there appears one new peak for each original peak. However, there are no separate ^{13}C peaks observed for $^-$OOC2MPZ/OOC2MPZH or $2MPZ(COO^-)_2$, presumably because these species exist in very small amount and are below the detection limit, or they might be merged into other large peaks.

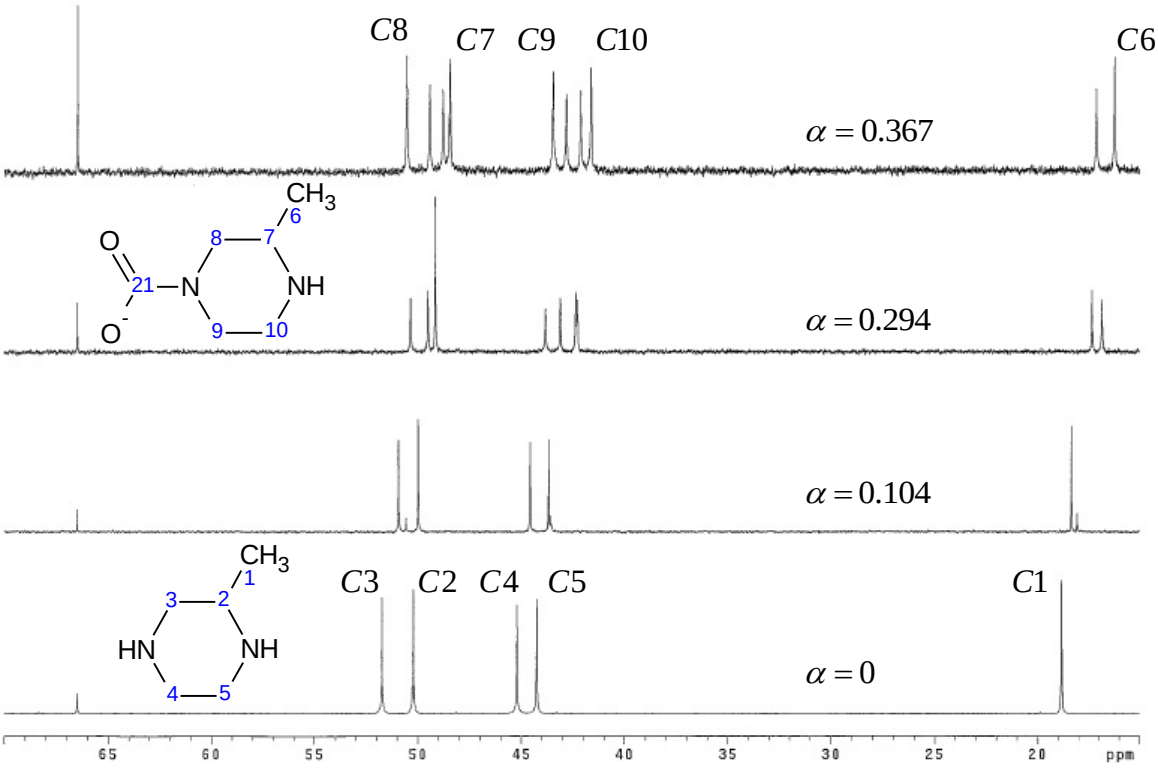

Figure 6.6: ^{13}C NMR spectra (upfield, δ = 15 – 70 ppm) for 8 m 2MPZ at 40 °C and varied loading.

Most of the enriched $^{13}CO_2$ is converted to carboxyl groups after being absorbed, so the downfield (166 < δ <160 ppm) spectra (Figure 6.7) is where all the CO_2-related reaction products should be seen. The largest peak is assigned to $2MPZCOO^-$ /H2MPZCOO, which shifts slightly toward upfield as CO_2 loading increases. The shift is attributed to the change in the ratio of the monocarbamate and its protonated forms, as the pH of the loaded solution drops with CO_2 loading. The second largest peak is deemed to come from HCO_3^-/CO_3^{2-}, the chemical shift of which changes significantly with loading. Previous NMR studies on two hindered amines, AMP (Chakraborty, Astarita et al. 1986; Yamada, Shimizu et al. 2010) and 2-PE (Paul, Ghoshal et al. 2009)

have shown that there is no or very little carbamate found in CO_2 loaded aqueous solutions. Another speciation study on another hindered amine, AHPD (Park, Yoon et al. 2003) indicated that there is much less carbamate formed than bicarbonate/carbonate at relatively high CO_2 loading and 25 °C. These studies suggest that hindered carbamate is thermodynamically unstable and much less likely to be formed in a loaded solution than bicarbonate/carbonate. If there was any hindered 2MPZ monocarbamate formed, it should exist in a much less amount than HCO_3^-/CO_3^{2-}.

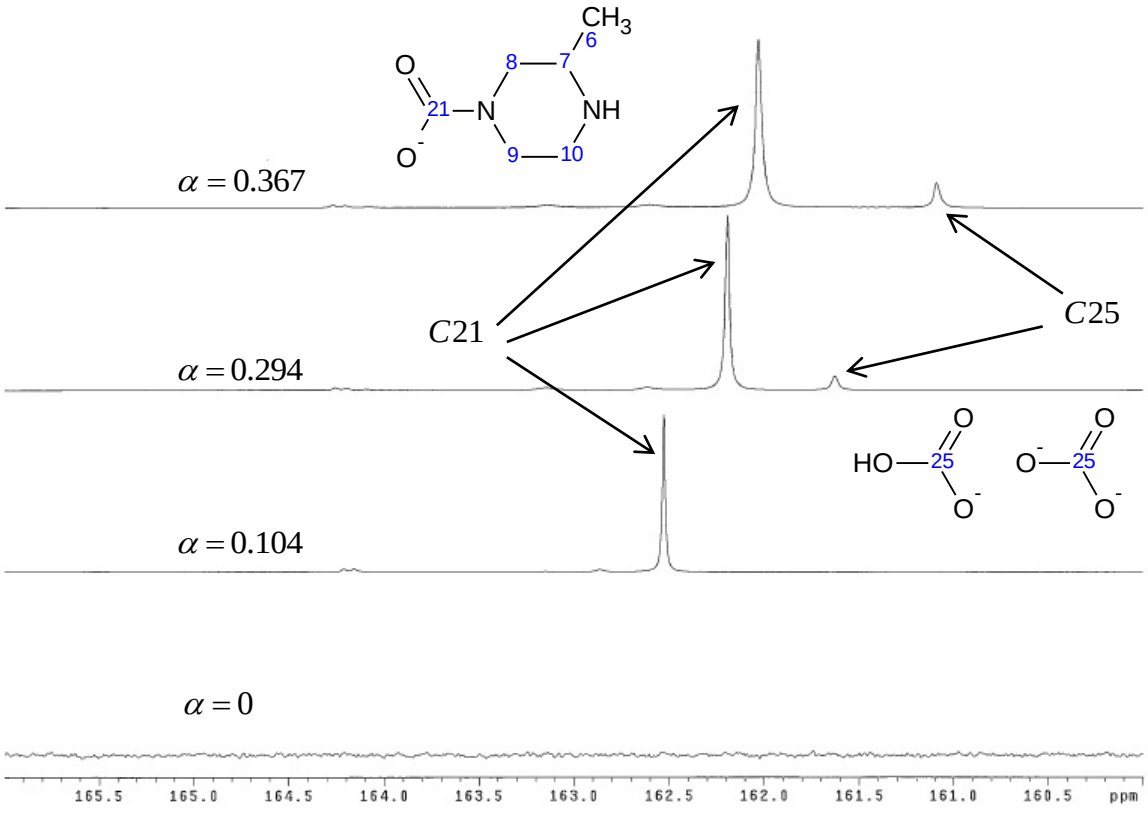

Figure 6.7: ^{13}C NMR spectra (downfield, δ = 160 – 166 ppm) for 8 m 2MPZ at 40 °C and varied loading.

The downfield spectra was expanded and shown in Figure 6.8 to have a close look at the small peaks. The two peaks of similar size correspond to the two carbonyl groups on 2MPZ(COO^-)$_2$. The dicarbamate cannot be protonated, so the positions of the two peaks remain almost constant at varied loading. The four tiny peaks on the far left side are suspected to be the carbamate of impurity amines in the 2MPZ samples since their peak position and size remains essentially unchanged with loading. Ethylene diamine could possibly be one of the impurity amines since it might be a byproduct from 2MPZ production. Fortunately, these peaks from impurities are relatively small, and neglecting them should not significantly affect the quantitative analysis on other species and the conclusions drawn therefrom. Again there are no separate peaks found for the hindered 2MPZ monocarbamate in the spectra even at the highest loading. The fact that the dicarbamate is observed but the monocarbamate is not indicates that the formation of carbamate on the unhindered amino group increases the stability of the other carbamate on the hindered amino group.

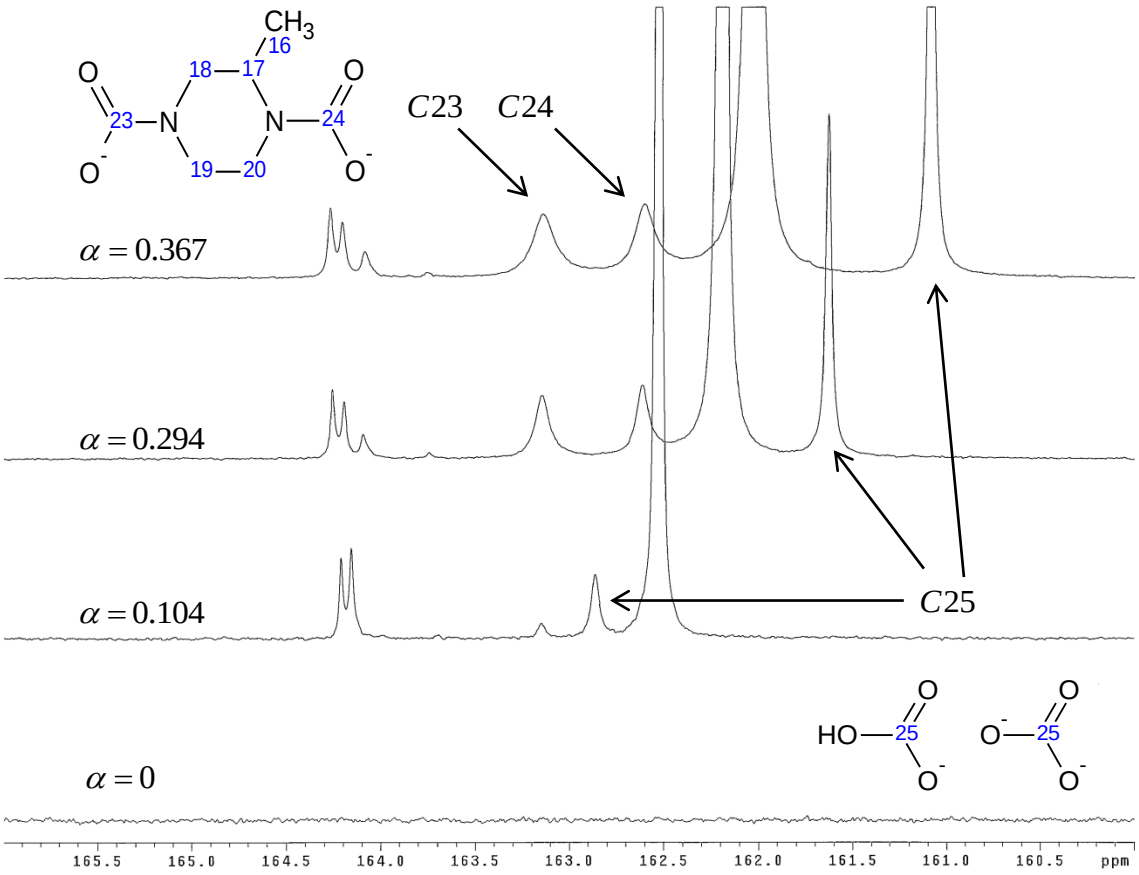

Figure 6.8: Expanded ^{13}C NMR spectra (downfield, δ = 160 – 166 ppm) for 8 m 2MPZ at 40 °C and varied loading.

6.4.1.3 ^{1}H-^{13}C Correlation

It has been shown that the one-dimension (1D) proton spectra are somewhat too complex for peak identification, so the 2D heteronuclear single quantum correlations (HSQC) were acquired for 8 m 2MPZ at varied CO_2 loading of 0.1 – 0.3 mol CO_2/mol alkalinity, as shown in Figure 6.9 through Figure 6.11. The 2D spectra correlate ^{13}C to the directly chemically bonded protons and facilitate peak identification as peaks are separated by chemical shifts of two nuclei. The use of 2D NMR spectra for species quantification is feasible but involves extra complexity due to the variation of coupling

values and relaxation effect etc. (Koskela and Vaananen 2002), which are beyond the capability and scope of this work and therefore will not be pursued any further.

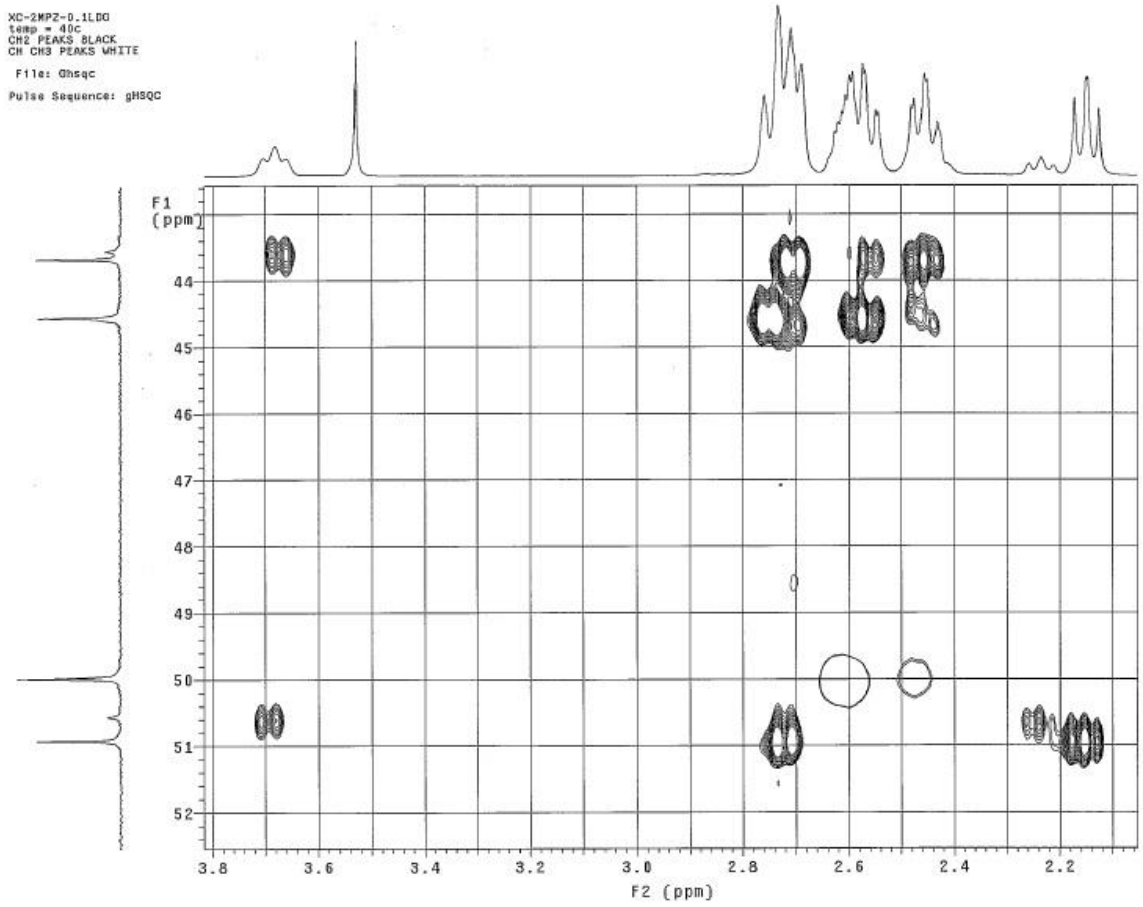

Figure 6.9: ^{1}H-^{13}C 2-D correlation spectrum for 8 m 2MPZ at α = 0.104 mol/mol alkalinity and 40 °C.

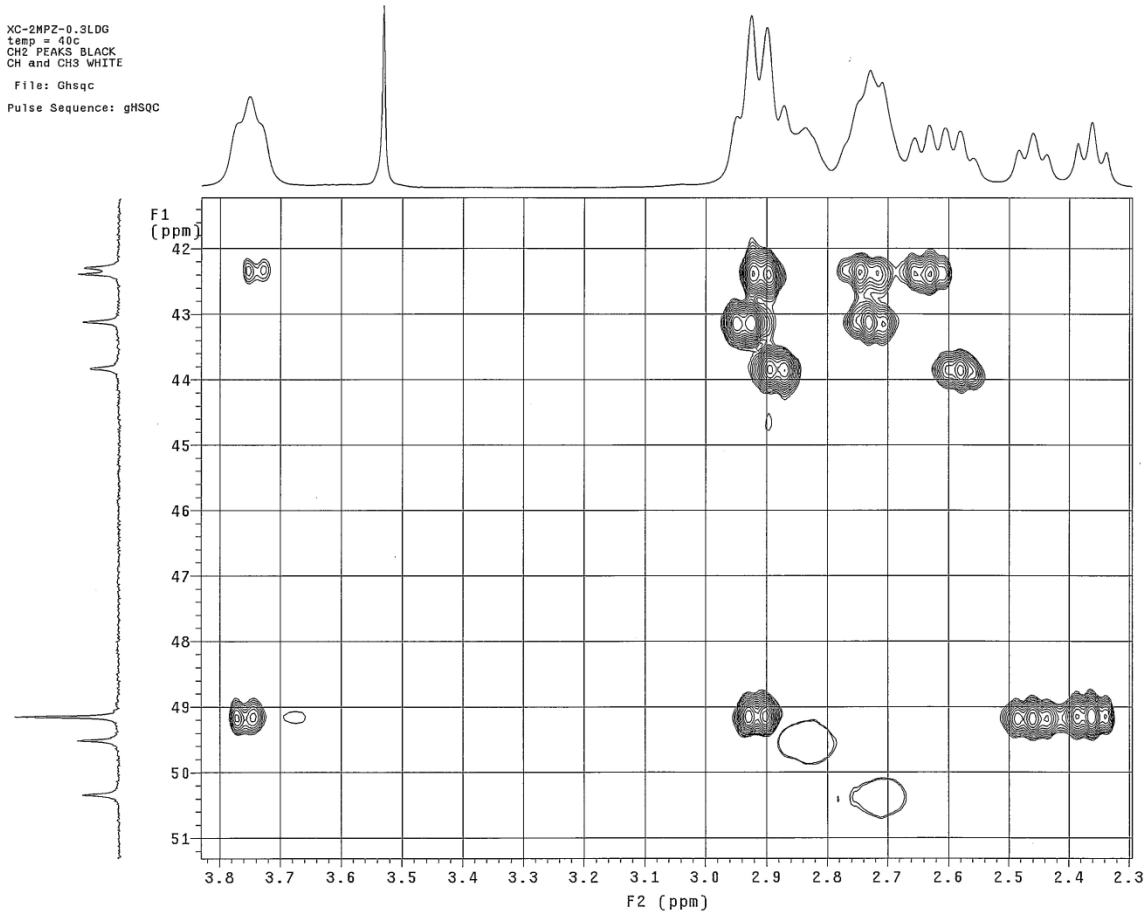

Figure 6.10: ^{1}H-^{13}C 2-D correlation spectrum for 8 m 2MPZ at α = 0.294 mol/mol alkalinity and 40 °C.

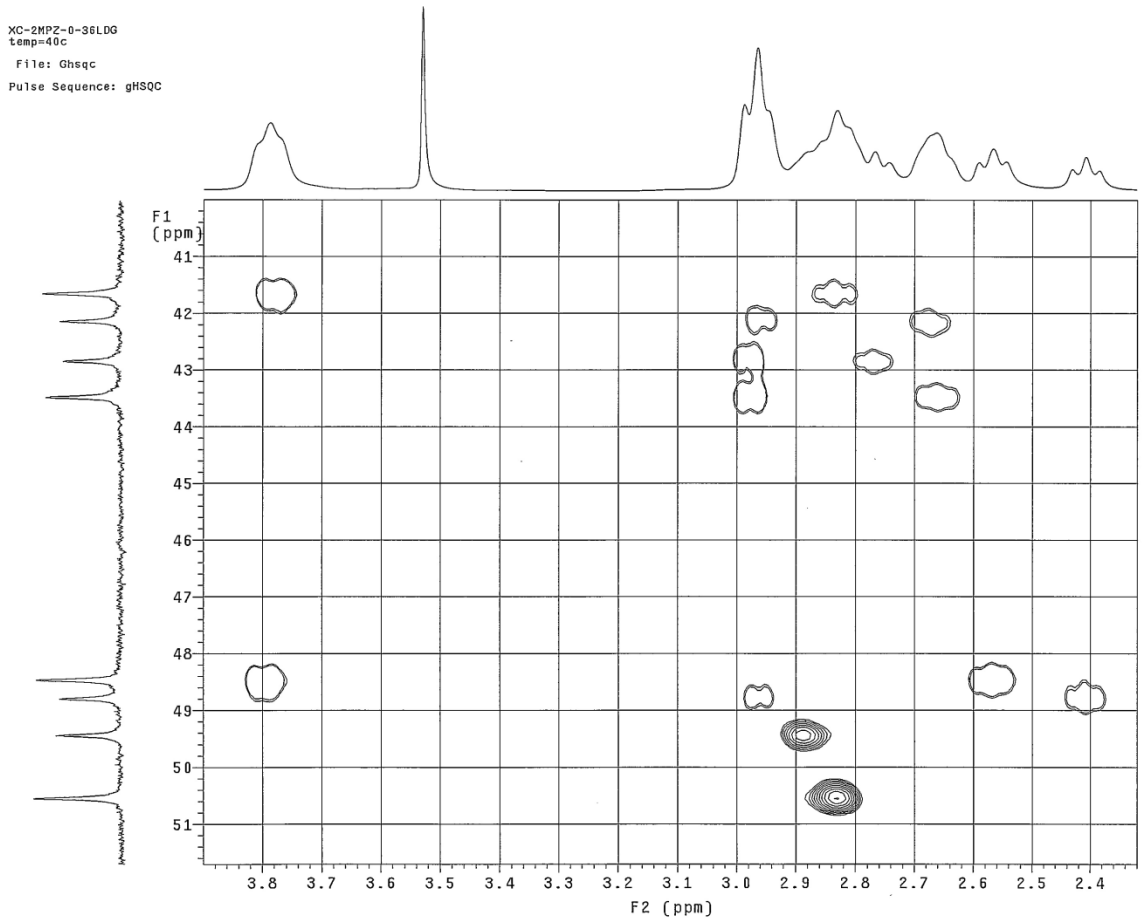

Figure 6.11: ^{1}H-^{13}C 2-D correlation spectrum for 8 m 2MPZ at α = 0.367 mol/mol alkalinity and 40 °C.

6.4.2 Species Quantification

Theoretically, the peaks from down field (~ 160 ppm) and from the upfield (~ 40 - 60 ppm) can both be used for quantification of H2MPZCOO/2MPZCOO^{-}. However, the peak for the standard, 1,4-dioxane shows up only in the upfield, and its height and area is only comparable to the peaks in the upfield for H2MPZCOO/2MPZCOO^{-}. The peaks in the downfield are from enriched ^{13}C, so their peak height is much greater than those in the upfield. It is suggested that the ratio of the areas of the peaks with similar size and position yields better accuracy in quantification (Shoulder 2011), therefore the

upfield peaks should be used to determine the amount of the unhindered carbamate species. Since the peaks for HCO_3^-/CO_3^{2-} and $2MPZ(COO^-)_2$ cannot be observed in the upfield, the amount of them has to be determined through the ratio of their peak areas in the downfield to the downfield peak area of H2MPZCOO/2MPZCOO$^-$.

The concentration of different species was determined for 8 m 2MPZ at the loading of 0.367 with the application of Eq. (6.1) and Eq. (6.2), and the results have been shown in Table 6.6. For any species that can be represented by multiple carbon peaks, the average value of the peak areas was used.

Table 6.6: Summary of peak position, integrated area and species concentration for 8 m 2MPZ at 40°C, α = 0.367 mol/mol alkalinity. (N: Natural ^{13}C; E: Enriched ^{13}C).

Peaks	ID	Type of ^{13}C	# of C	δ (ppm)	A_{ref}	R_b
Dioxane	Ref	N	4	66.500	1.00	1.7110
					A_i	C_i
2MPZ/2MPZH$^+$	C1	N	1	17.143	1.65	2.8232
	C2	N	1	48.794	1.81	3.0970
	C3	N	1	49.439	1.90	3.2510
	C4	N	1	42.837	1.86	3.1825
	C5	N	1	42.135	1.86	3.1825
2MPZCOO$^-$ /H2MPZCOO	C6	N	1	16.238	2.18	3.7301
	C7	N	1	48.463	2.45	4.1921
	C8	N	1	50.548	2.62	4.4829
	C9	N	1	43.476	2.66	4.5514
	C10	N	1	41.645	2.47	4.2263
-	C11	N	1	-	-	-
	C12	N	1	-	-	-

OOC2MPZ/OOC2MPZH	C13	N	1	-	-	-
	C14	N	1	-	-	-
	C15	N	1	-	-	-
	C16	N	1	-	-	-
	C17	N	1	-	-	-
$2MPZ(COO^-)_2$	C18	N	1	-	-	-
	C19	N	1	-	-	-
	C20	N	1	-	-	-
$2MPZCOO^-$ /H2MPZCOO	C21	E	1	162.034	258.89	442.9728
$^-$OOC2MPZ/ OOC2MPZH	C22	E	1	-	-	-
$2MPZ(COO^-)_2$	C23	E	1	162.605	14.86	25.4261
$2MPZ(COO^-)_2$	C24	E	1	163.143	14.86	25.4261
HCO_3^-/ CO_3^{2-}	C25	E	1	161.092	42.47	72.6681
Unknown		E		>164	8.86	7.5799

The species concentration determined from the enriched ^{13}C shown in Table 6.6 has to be further adjusted. The amount of 2MPZCOO-/H2MPZCOO determined from C6 through C10 (the average value) and C21 respectively render a ratio which correlates the amounts determined from natural ^{13}C atoms and enriched ^{13}C atoms. This number is in turn used to determine the amount of the other species showing up in the downfield. The composition of 2MPZ-related and CO_2-related species calculated for varied CO2 loading is shown in Table 6.7.

The total concentration of 2MPZ is the sum of the different 2MPZ species:

$$[2MPZ]_t = \left([2MPZ]+[2MPZH^+]\right)+\left([2MPZCOO^-]+[H2MPZCOO]\right)+\left([^-OOC2MPZ]+[OOC2MPZH]\right)+[2MPZ\left(COO^-\right)_2] \quad (6.3)$$

Table 6.7: The liquid composition determined from the ^{13}C NMR spectra for 8 m 2MPZ at 40 °C and varied loading.

	CO_2 Loading (mol CO_2/mol alkalinity)								
	α = 0.104			α = 0.294			α = 0.367		
Component	Conc. (m)	% of $[2MPZ]_t$	Dev.*	Conc. (m)	% of $[2MPZ]_t$	Dev.*	Conc. (m)	% of $[2MPZ]_t$	Dev.*
2MPZ/$2MPZH^+$	6.654	81.3	-	4.767	50.7	-	3.107	41.0	-
$2MPZCOO^-$/H2MPZCOO	1.517	18.5	-	4.437	47.1	-	4.237	55.8	-
$^-$OOC2MPZ/OOC2MPZH	0	0	-	0	0	-	0	0	-
$2MPZ(COO^-)_2$	0.013	0.2	-	0.207	2.2	-	0.243	3.2	-
HCO_3^-/ CO_3^{2-}	0.067	-	-	0.509	-	-	0.695	-	-
Unknown	0.085	-	-	0.166	-	-	0.145	-	-
$[2MPZ]_t$	8.184	100.0	2.19%	9.411	100.0	17.51%	7.587	100.0	-5.27%
$[CO_2]_t$	1.695	-	1.13%	5.526	-	15.51%	5.563	-	-3.67%
α (mol/mol alkalinity)	0.104	-	-0.95%	0.294	-	-1.67%	0.367	-	-1.66%

Dev.*: Deviation from the gravimetric value.

The total concentration of dissolved CO_2 is determined from the following equation:

$$[CO_2]_t = \left([2MPZCOO^-]+[H2MPZCOO]\right)+\left([^-OOC2MPZ]+[OOC2MPZH]\right) + 2\times[2MPZ\left(COO^-\right)_2]+[unknown] \tag{6.4}$$

The unknown peaks are included to get a more accurate result on the total CO_2 content. The CO_2 loading based on the spectra is calculated as

$$\alpha = \frac{[CO_2]_t}{2\times[2MPZ]_t} \tag{6.5}$$

It can be seen that as α increases from 0.104 to 0.367, the percentage of $2MPZCOO^-/H2MPZCOO^-$ out of the original 2MPZ increases from 18.5% to 55.8%, while only about 0.2 - 3.2% of 2MPZ is converted to $2MPZ(COO^-)_2$.

$[2MPZ]_t$, $[CO_2]_t$ and α determined from the NMR spectra is different from the nominal concentration shown in Table 6.3. The deviation is relatively small (<5%) for the α = 0.104 and 0.367, which are well in the range of NMR experimental error. At α = 0.294, the deviation between the spectroscopic value and gravimetric value for $[2MPZ]_t$ and $[CO_2]_t$ is significant. Other than the errors associated with peak areas, the determined concentration of 1,4-dioxane in this sample might be inaccurate and leads to considerable deviation. However, the calculation for the CO_2 loading is in a good agreement with the nominal value with the deviation equal to -1.67%. Therefore the calculation of the fraction or ratio of different species in the liquid is not affected by the absolute value of the concentrations.

The distribution of the total absorbed CO_2 in different reaction products as a function of CO_2 loading is shown in Figure 6.12. As loading is very close 0, it is assumed that all the CO_2 goes to $2MPZCOO^-/H2MPZCOO^-$ since it is presumably the

most stable reaction product. The results from NMR data are used for the nonzero loading. Although 2MPZCOO$^-$/H2MPZCOO is the major sink for CO_2 at lean loading, the amount of dissolved CO_2 in the form of 2MPZCOO$^-$/H2MPZCOO decreases significantly with increased CO_2 loading. The share of HCO_3^-/ CO_3^{2-} and 2MPZ$(COO^-)_2$ steadily increases with loading. At the rich loading of 0.367, 12% and 9% of the total absorbed CO_2 is converted to HCO_3^-/ CO_3^{2-} and 2MPZ$(COO^-)_2$, respectively.

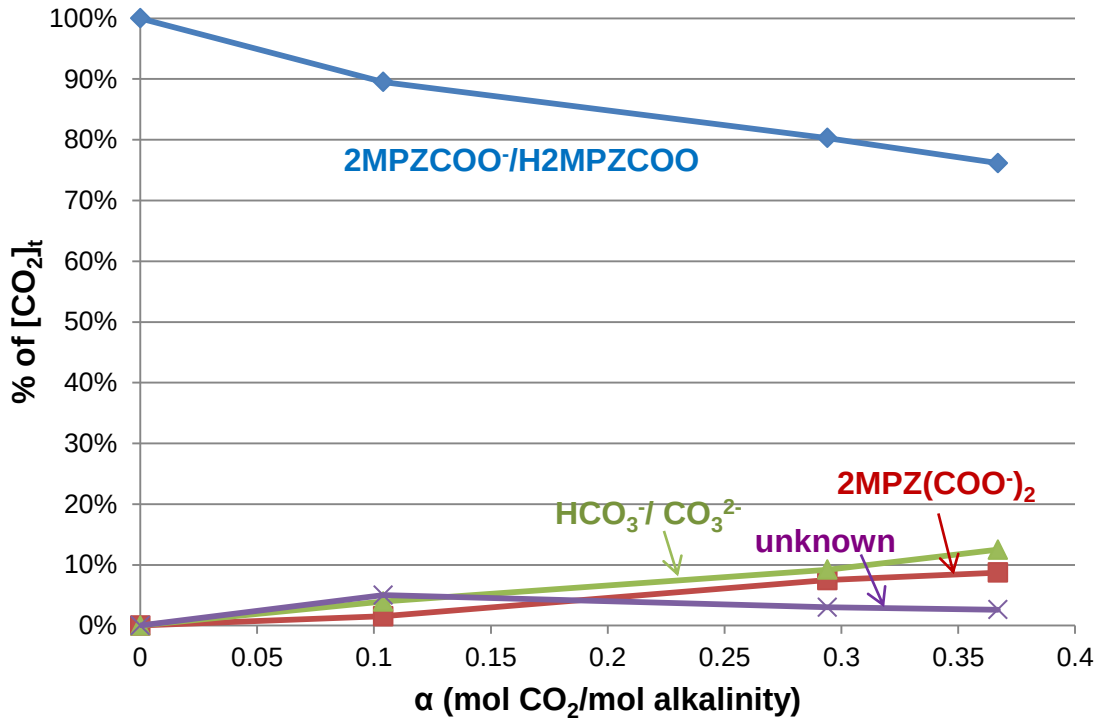

Figure 6.12: The distribution of CO_2 in different reaction products as a function of loading in 8 m 2MPZ at 40 °C.

6.5 2MPZ-PZ-CO_2-H_2O

The apparent liquid composition in molality determined gravimetrically for the samples of 2MPZ/PZ loaded solutions is shown in Table 6.8.

Table 6.8: Apparent liquid composition determined gravimetrically for the samples of 4 m 2MPZ / 4 m PZ.

Loading (mol/mol alk)	Apparent concentration (mol/kg H_2O)				
	2MPZ	**PZ**	**$^{13}CO_2$**	**1,4-Dioxane**	**D_2O**
0	3.996	3.996	0	0.352	10.71
0.143	3.996	3.996	2.284	0.354	10.84
0.219	3.996	3.996	3.496	0.358	10.86
0.300	3.996	3.996	4.798	0.359	11.03
0.440	3.996	3.996	7.037	0.363	11.09

6.5.1 Peak Identification

6.5.1.1 ^1H NMR

The ^1H NMR spectra for 4m 2MPZ/4m PZ at varied loadings are presented in Figure 6.13. The largest peak in the spectra corresponds to H1' of PZ/PZH^+. The resonance frequency from PZ and PZ carbamate is superimposed on those for 2MPZ and 2MPZ carbamate, which significantly complicates the identification of each peak, especially at rich loading. As loading increases, the only additional peaks that stay clear of the others show up in the regime of $\delta > 3.0$ ppm. Specifically, the peak at $\delta = 3.1$ ppm does not shift with loading, so it should be from the $PZ(COO^-)_2$. With the reference to the ^1H NMR for 2MPZ as well as ^1H-^{13}C 2D correlation for 2MPZ/PZ shown in Figure 6.17 through Figure 6.20, the peak which shifts from 3.160 to 3.404 ppm corresponds to $PZCOO^-$/HPZCOO, and the peak on the far left side is due to H8 and H9 on $2MPZCOO^-$ /H2MPZCOO. Due to the overwhelming number of species present in the solution, it is

hardly feasible to separate and identify all the peaks for the loaded solutions. Therefore the ^{1}H NMR spectra can only be used for quantification of the species mentioned above.

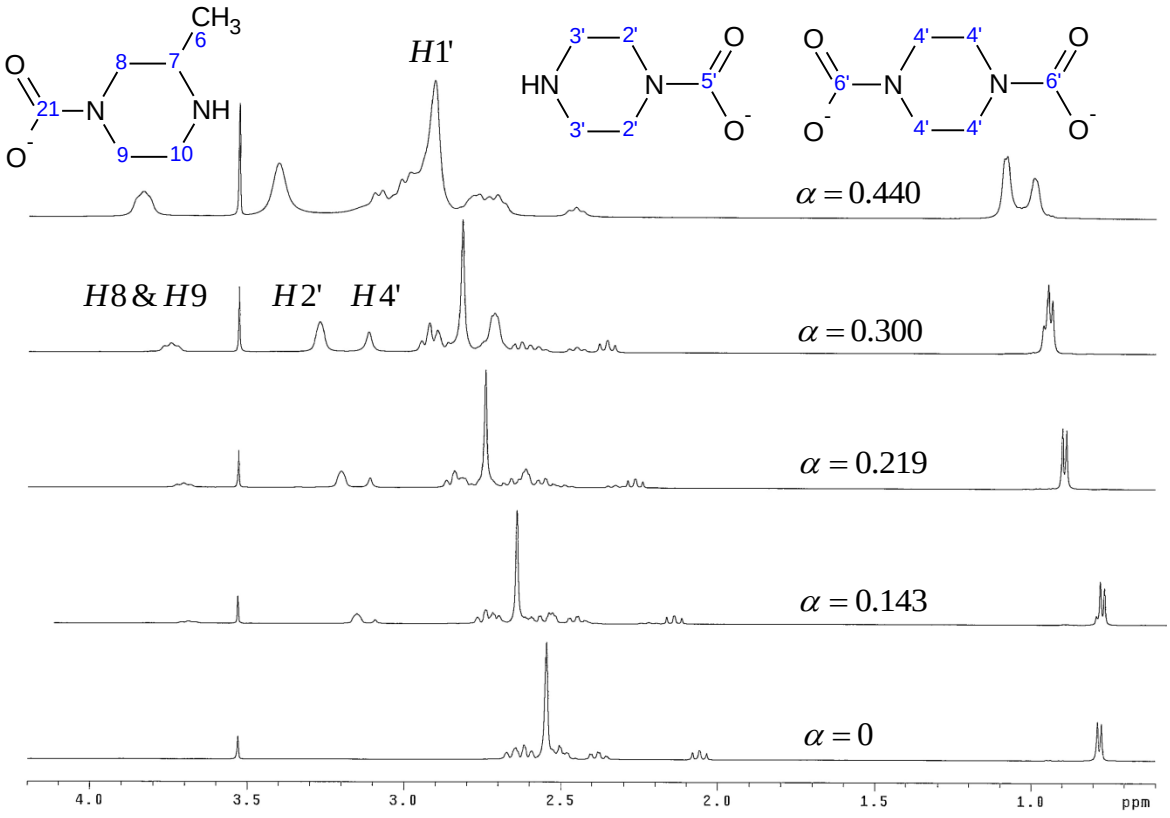

Figure 6.13: ^{1}H NMR spectra for 4m 2MPZ/4m PZ at α = 0 – 0.44 mol/mol alkalinity and 40 °C.

6.5.1.2 ^{13}C NMR

The ^{13}C NMR spectra in the upfield and downfield for 2MPZ/PZ at varied CO_2 loading are shown in Figure 6.14 and Figure 6.15 respectively.

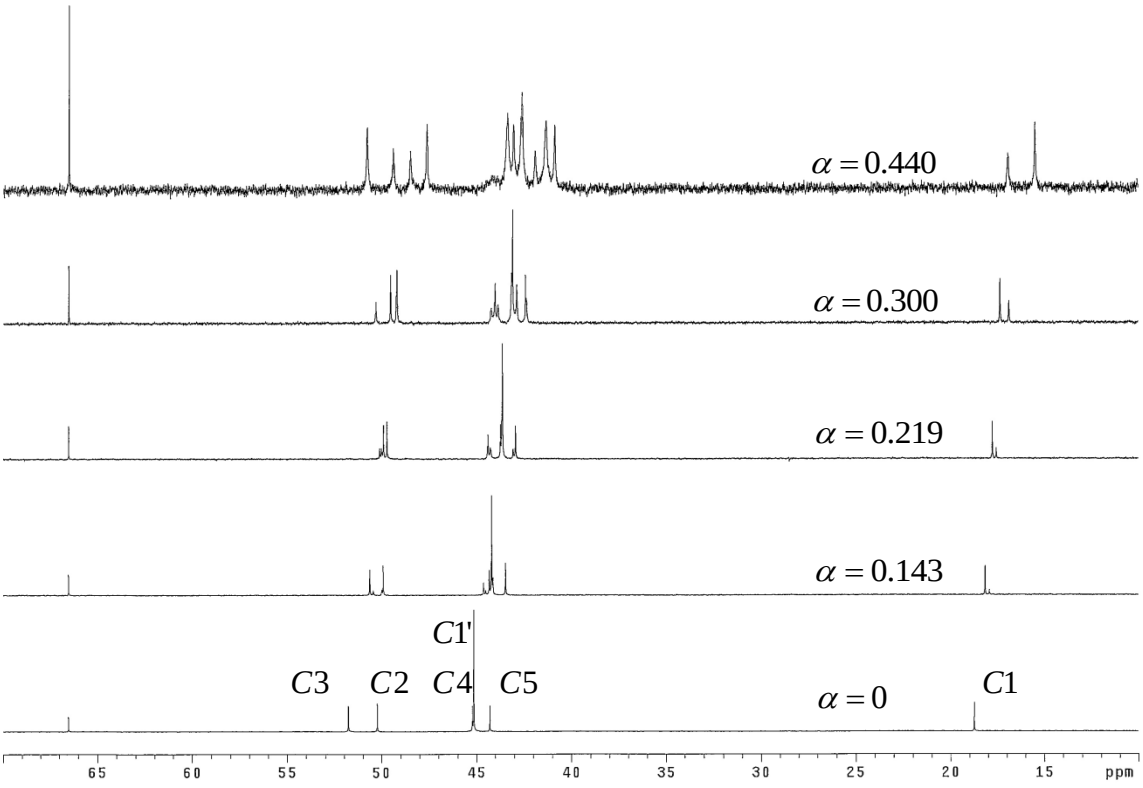

Figure 6.14: ^{13}C NMR spectra for 4m 2MPZ/4m PZ (upfield, δ = 10 – 70 ppm) at α = 0 – 0.44 mol/mol alkalinity and 40 °C.

The existence of a number of species makes the spectra for the blend more complex than that of straight 2MPZ. For the unloaded solution in the upfield, the PZ peak (C1') overlap with one of the 2MPZ peaks, C4. The overlap is more severe at higher loading with the appearance of additional peaks at 40 ppm < δ < 45 ppm. Even if all the peaks for the PZ compounds could be identified, separate integration for each of them is not possible. Therefore the usefulness of ^{13}C NMR spectra in the upfield for quantification of PZ species is very limited.

In Figure 6.15, the peaks for the blend in the downfield were identified and labeled. The peak identification was based on the size as well as the position of the peaks as a function of loading. The spectra for straight 2MPZ and straight PZ loaded

solution are also able to provide information on the chemical shift for different species, even though the chemical shifts of the peaks in these spectra are not exactly the same.

The highest peak is from $PZCOO^-$/HPZCOO (C5') since there is no hindrance on PZ and it is expected to be more reactive with CO_2 than 2MPZ. This is also consistent with the ^1H NMR spectra (Figure 6.13) in which the peak for PZ carbamate is larger than that of unhindered 2MPZ carbamate. The second largest peak corresponds to $2MPZCOO^-$/$H2MPZCOO^-$ (C21). The peaks for 2MPZ monocarbamate and PZ monocarbamate get closer at higher CO_2 loading, where it is not possible to separately determine the amount of $PZCOO^-$/HPZCOO and $2MPZCOO^-$/$H2MPZCOO^-$.

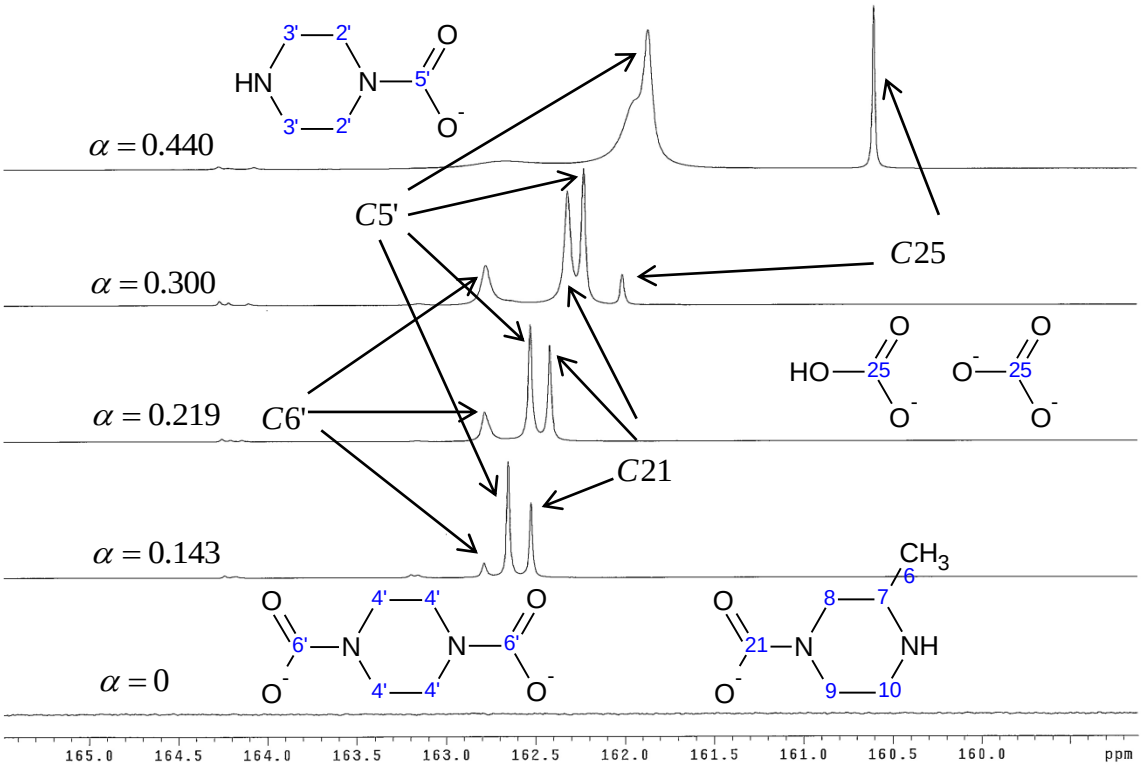

Figure 6.15: ^{13}C NMR spectra for 4m 2MPZ/4m PZ (downfield, δ = 160 – 166 ppm) at α = 0 – 0.44 mol/mol alkalinity and 40 °C.

The peak at 162.8 ppm is not shifting with CO_2 loading, and it must be $PZ(COO^-)_2$ (C6') since $PZCOO^-$ has a higher reactivity with CO_2 than $2MPZCOO^-$ does. The peak for $PZ(COO^-)_2$ grows with CO_2 loading of 0 to 0.30 mol/mol alk, but diminishes at $\alpha = 0.44$. The peak shifting from the left to the far right is from the signal for HCO_3^-/ CO_3^{2-}.

To more closely examine all the peaks in the downfield, the spectra are expanded and shown in Figure 6.16. The peak at 163.1 ppm is not moving with CO_2 loading and therefore comes from $2MPZ(COO^-)_2$. The peak position is also similar to that in 8 m 2MPZ. The other peak for $2MPZ(COO^-)_2$ (C23) probably overlaps with the peak for $PZ(COO^-)_2$ due to the similar electronic environment. Similar to 8 m 2MPZ, there is no signal for $^-$OOC2MPZ/OOC2MPZH found in the spectra.

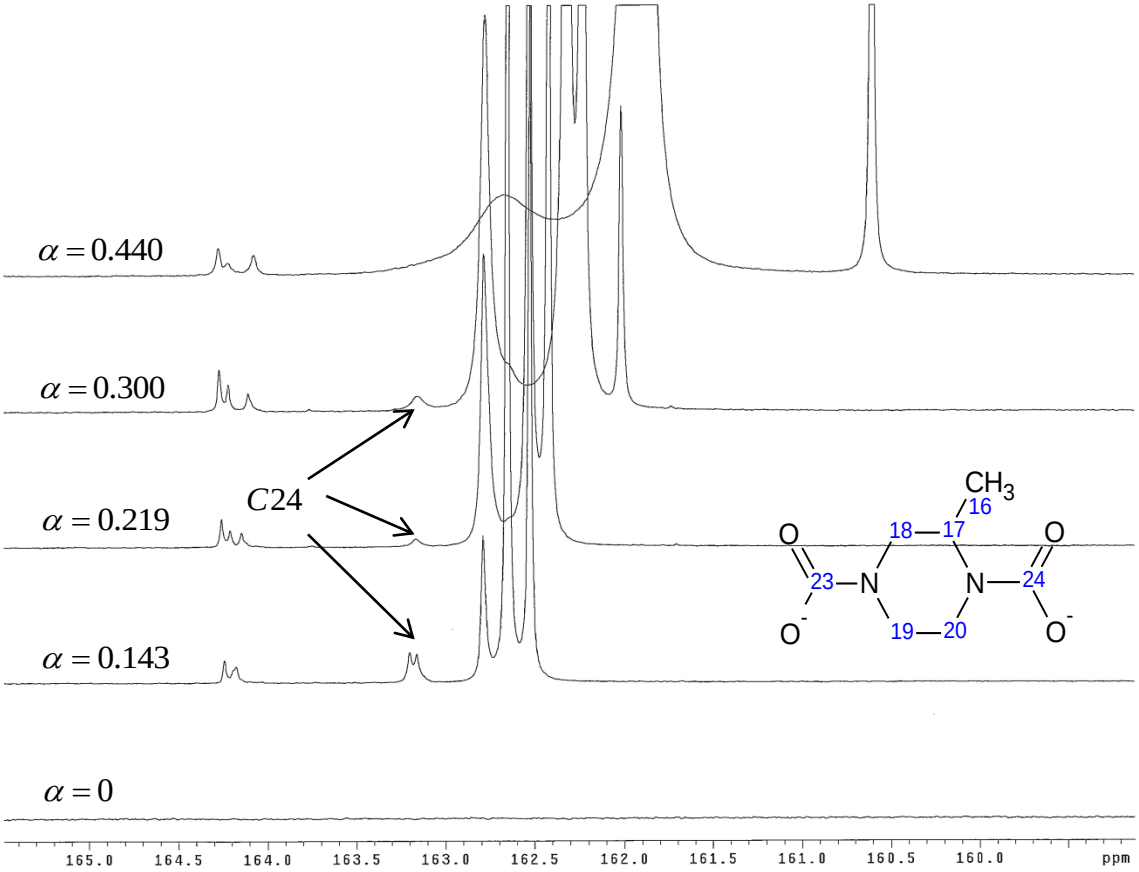

Figure 6.16: Expanded ^{13}C NMR spectra for 4m 2MPZ/4m PZ (downfield, δ = 160 – 166 ppm) at α = 0 – 0.44 mol/mol alkalinity and 40 °C.

6.5.1.3 ^{1}H-^{13}C Correlation

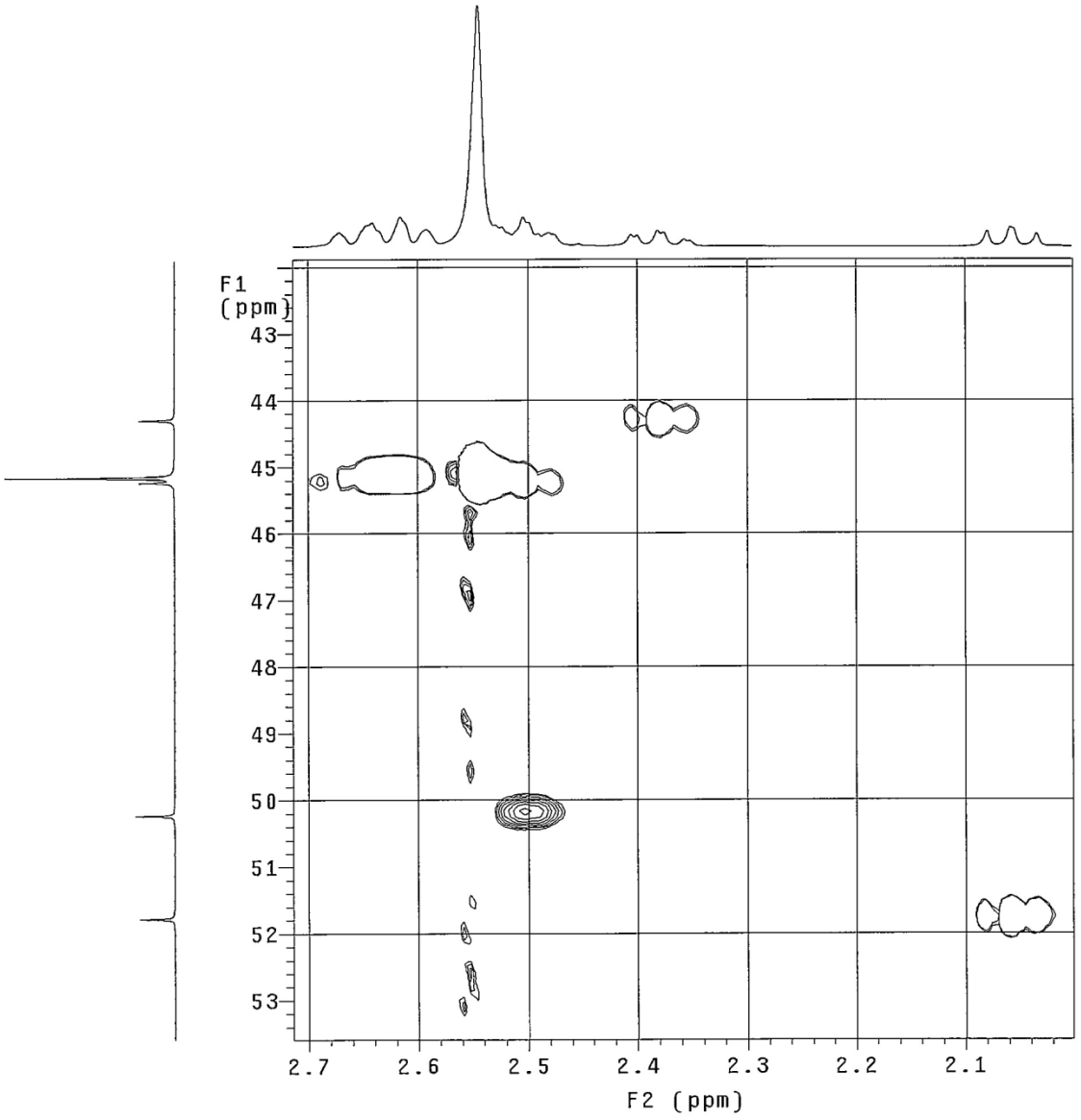

Figure 6.17: ^{1}H-^{13}C 2D correlation spectrum for unloaded 4m 2MPZ/4m PZ at 40 °C.

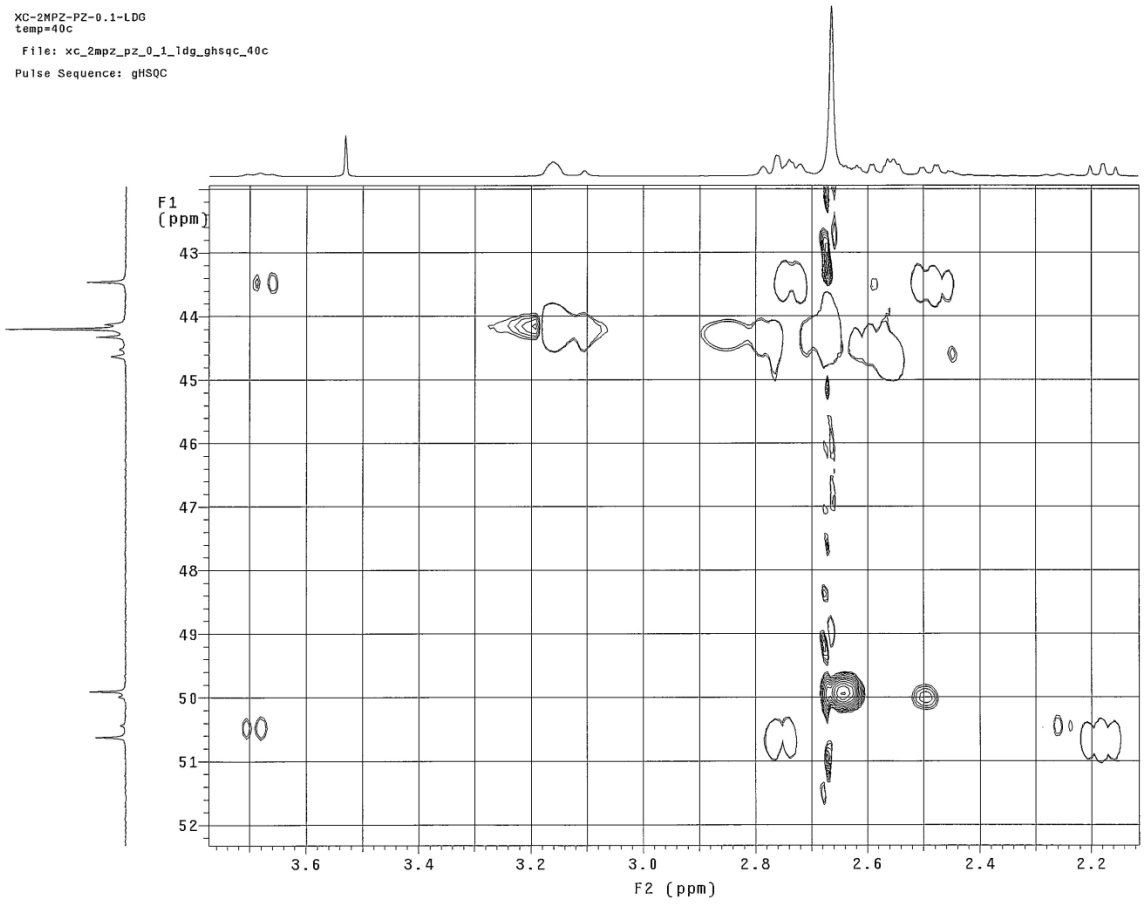

Figure 6.18: ^{1}H-^{13}C 2D correlation spectrum for 4m 2MPZ/4m PZ at α = 0.143 mol/mol alkalinity and 40 °C.

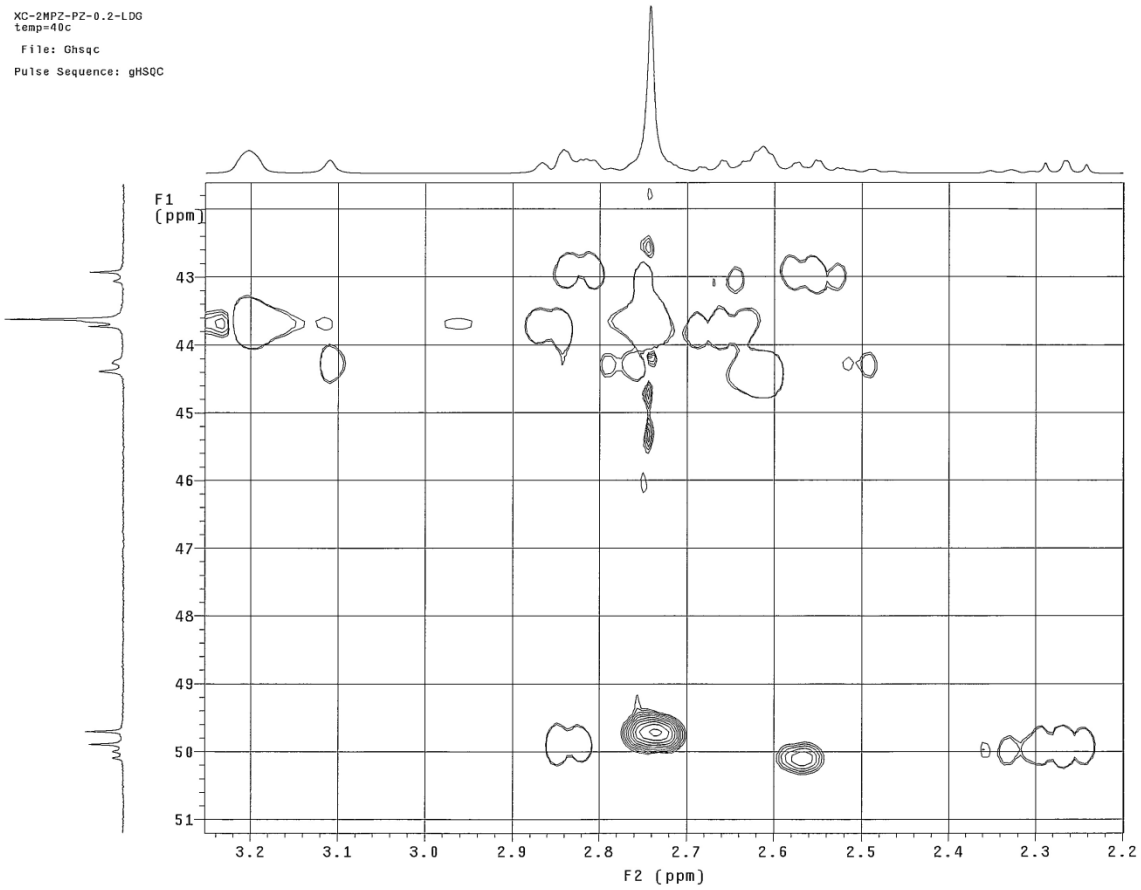

Figure 6.19: ^{1}H-^{13}C 2D correlation spectrum for 4m 2MPZ/4m PZ at α = 0.219 mol/mol alkalinity and 40 °C.

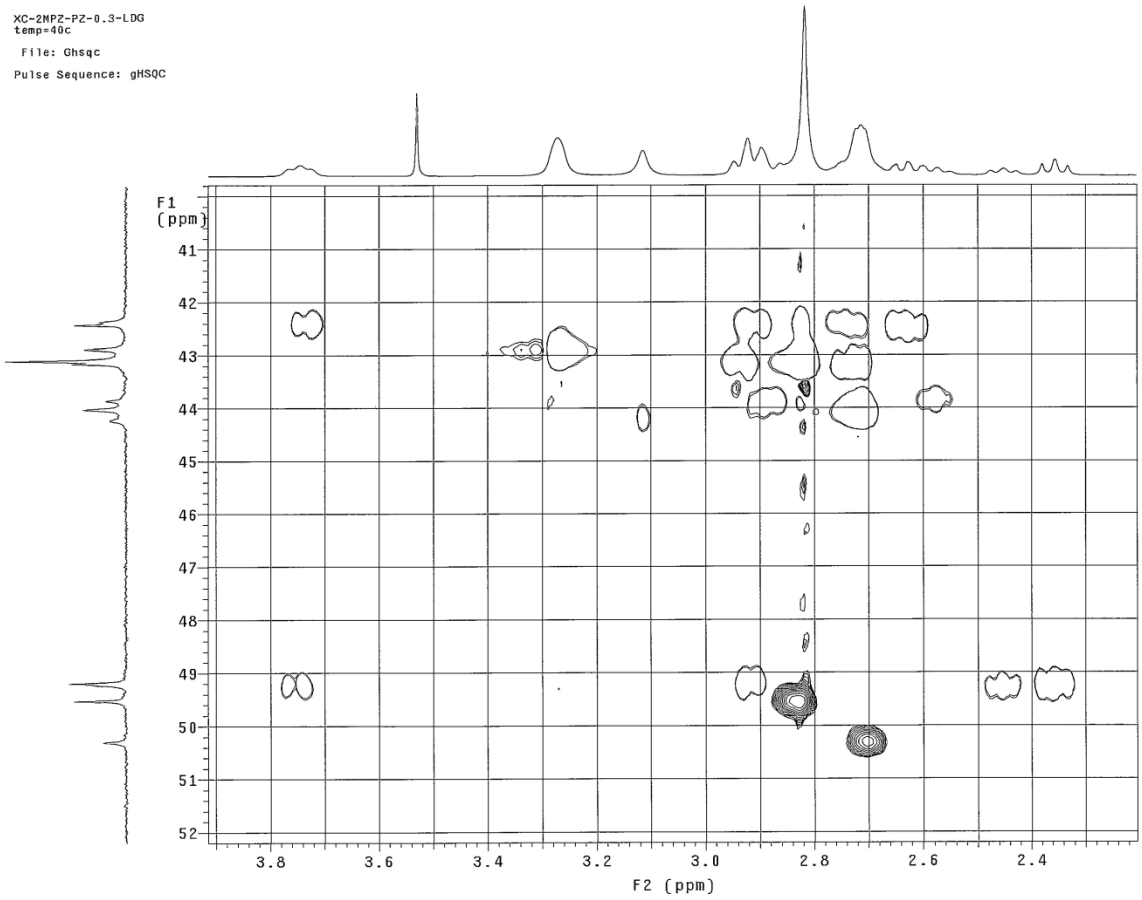

Figure 6.20: ^{1}H-^{13}C 2D correlation spectrum for 4m 2MPZ/4m PZ at α = 0.300 mol/mol alkalinity and 40 °C.

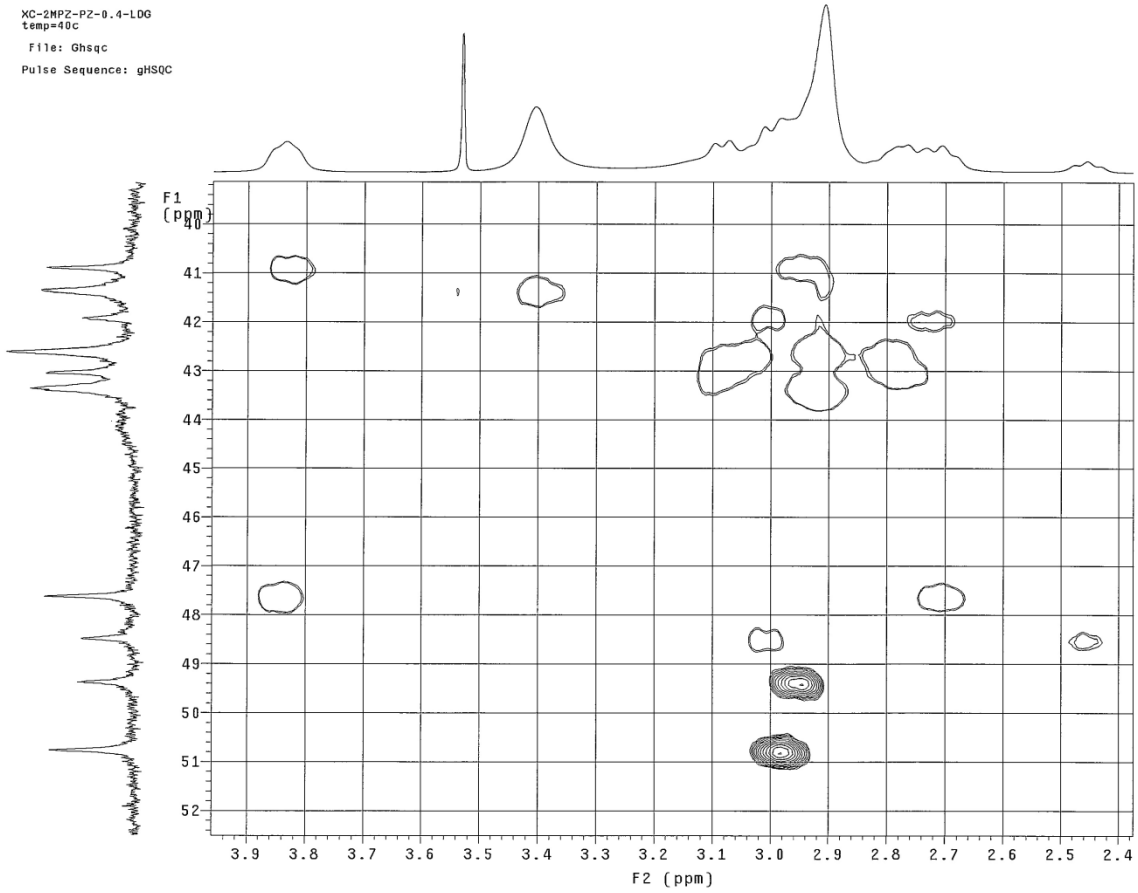

Figure 6.21: ^{1}H-^{13}C 2D correlation spectrum for 4m 2MPZ/4m PZ at α = 0.440 mol/mol alkalinity and 40 °C.

Based on the peak identification discussed above, the peak positions as a function of loading for all the species are shown in Figure 6.23 for 8 m 2MPZ, 8 m PZ (and 4 m 2MPZ / 4 m PZ. The same species have similar peak position as well as similar peak shift as a function of loading in different solvents, which confirms the peak identification. The peak for HCO_3^-/CO_3^{2-} more significantly changes with loading than those peaks for carbamate indicates that the ratio of HCO_3^-/CO_3^{2-} may change more dramatically than that of carbamates and their protonated form. The relatively large shift for HCO_3^-/CO_3^{2-} peak was also reported by Park *et al.* for MEA-CO_2-H_2O (Park, Yoon et al. 2003).

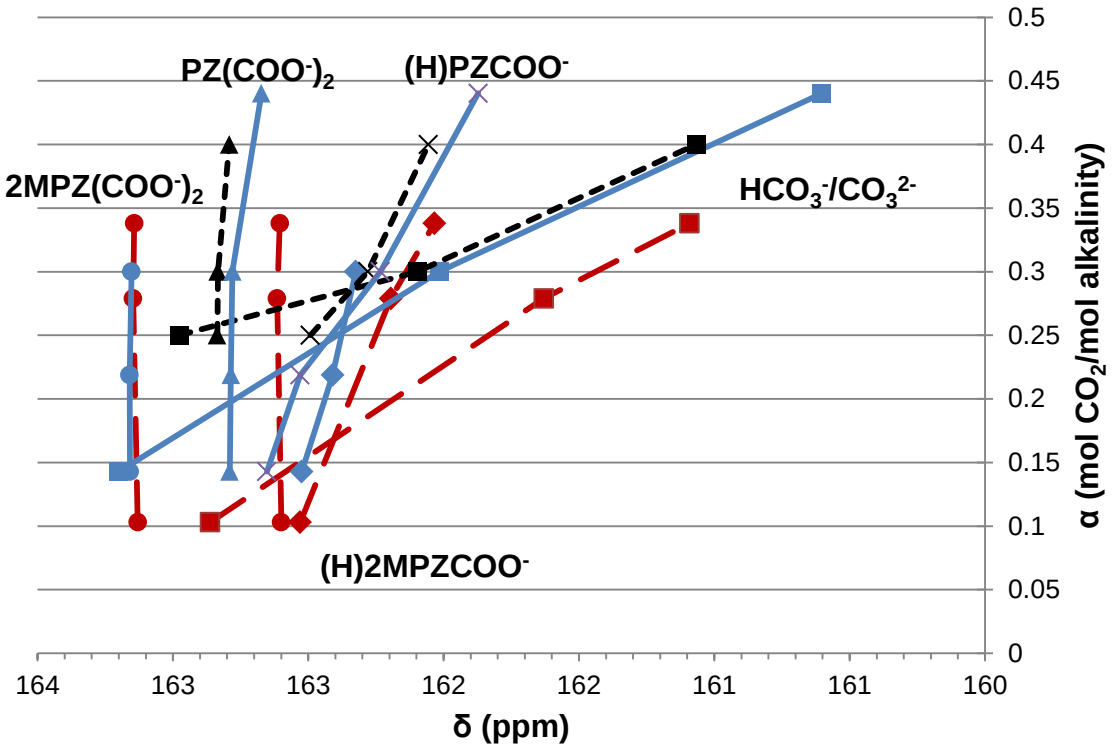

Figure 6.22: Peak shift as a function of CO_2 loading for carbamate and bicarbonate/carbonate species in 8 m 2MPZ (red long-dash line), 8 m PZ (black short-dash line) and 4 m 2MPZ / 4 m PZ (blue solid line). $PZCOO^-$ /HPZCOO (×),$PZ(COO^-)_2$ (▲), $2MPZCOO^-$/H2MPZCOO (♦), $2MPZ(COO^-)_2$ (●),HCO_3/CO_3^{2-} (■).

6.5.2 Species Quantification

The PZ carbamate, dicarbamate and 2MPZ unhindered carbamate was first quantified by using the ^1H NMR spectra. The results are shown in Figure 6.23. The concentration of $PZCOO^-$/HPZCOO is always higher than 2MPZCOO-/H2MPZCOO and $PZ(COO^-)_2$, which indicates higher reactivity of PZ with CO2 than 2MPZ. This is also consistent with the peak assignment for the ^{13}C NMR spectra in the downfield. 2MPZ

dicarbamate and HCO_3/CO_3^{2-} cannot be quantified using the ^1H NMR spectra since separate peaks for them are absence.

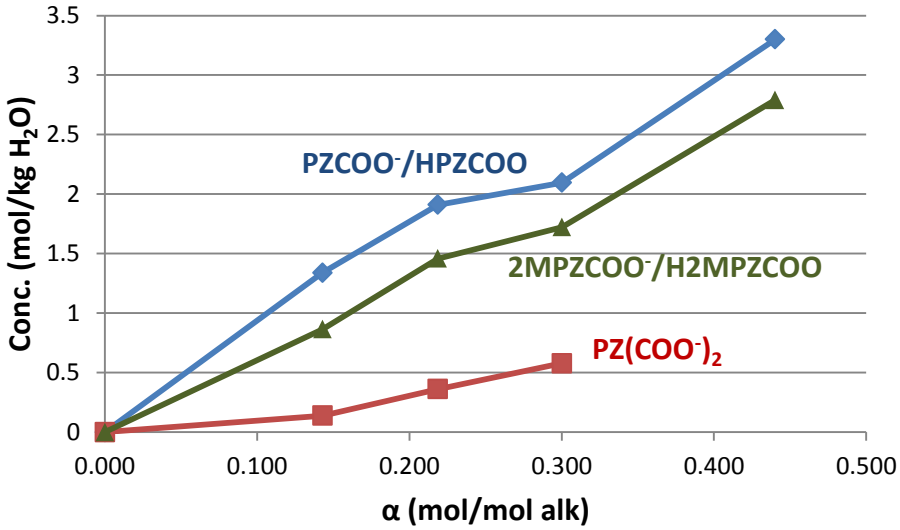

Figure 6.23: PZ carbamate and 2MPZ carbamate as a function of CO_2 loading based on ^1H NMR spectra in 4m 2MPZ/4m PZ at 40 °C.

$2MPZ(COO^-)_2$ and HCO_3/CO_3^{2-} can only be seen in ^{13}C NMR in the downfield, therefore ^{13}C NMR spectra in the downfield are used in this work to quantify all the CO_2-related species in the 4m 2MPZ/4m PZ loaded solution. Because it is not possible to quantify $2MPZ/2MPZH^+$ and PZ/PZH^+ with either ^1H NMR or ^{13}C NMR spectra, the total amount of 2MPZ cannot be obtained from the spectra. The CO_2 loading can only be determined based on the gravimetric measurement during sample preparation.

The chemical shift and peak area of various species in the downfield of ^{13}C NMR has been summarized in Table 6.9. The merge of the peaks for PZ carbamate and 2MPZ carbamate at rich loading makes it difficult to get separate peak area for each species. The ratios between other species and $2MPZCOO^-$/H2MPZCOO are determined from both the ^1H NMR and ^{13}C NMR spectra. The values from these two methods are mostly very

close to each other. At the lean loading range where the ratios are available, HCO_3/CO_3^{2-} and $2MPZ(COO^-)_2$ are negligible, so it can be concluded that about half of the CO_2 absorbed reacts with PZ, while approximately 40% and 10% of them reacts with 2MPZ and $PZCOO^-$ respectively.

Table 6.9: Chemical shift and peak areas of CO_2-related species in the downfield of ^{13}C NMR spectra for 4m 2MPZ/4m PZ at 40 °C.

α = 0.143 mol/mol alk				
Component	**δ (ppm)**	**A_i**	**Ratio to [2MPZCOO-/H2MPZCOO-]**	**Ratio from ^{1}H NMR**
$PZCOO^-$/HPZCOO	162.653	89.94	1.54	1.55
$PZ(COO^-)_2$	162.790	16.41	0.141	0.160
$2MPZCOO^-$/H2MPZCOO	162.524	58.36	1	1
HCO_3^-/CO_3^{2-}	163.199	n/a	n/a	n/a
$2MPZ(COO^-)_2$	163.159	n/a	n/a	n/a
α = 0.219 mol/mol alk				
Component	**δ (ppm)**	**A_i**	**Ratio to [2MPZCOO-/H2MPZCOO-]**	**Ratio from ^{1}H NMR**
$PZCOO^-$/HPZCOO	162.530	143.96	1.31	1.31
$PZ(COO^-)_2$	162.786	67.33	0.307	0.248
$2MPZCOO^-$/H2MPZCOO	162.419	109.69	1	1
HCO_3^-/CO_3^{2-}	n/a	n/a	n/a	n/a
$2MPZ(COO^-)_2$	163.16	2.21	0.020	n/a

α = 0.300 mol/mol alk				
Component	**δ (ppm)**	**A_i**	**Ratio to [2MPZCOO-/H2MPZCOO-]**	**Ratio from ^{1}H NMR**
$PZCOO^-$/HPZCOO	162.233	n/a	n/a	1.22
$PZ(COO^-)_2$	162.780	102.74	n/a	0.335
$2MPZCOO^-$/H2MPZCOO	162.324	n/a	1	1
HCO_3^-/CO_3^{2-}	162.016	31.77	n/a	n/a
$2MPZ(COO^-)_2$	163.153	5.81	n/a	n/a
α = 0.440 mol/mol alk				
Component	**δ (ppm)**	**A_i**	**Ratio to [2MPZCOO-/H2MPZCOO-]**	**Ratio from ^{1}H NMR**
$PZCOO^-$/HPZCOO	161.872	n/a	n/a	1.18
$PZ(COO^-)_2$	162.673	n/a	n/a	n/a
$2MPZCOO^-$/H2MPZCOO	n/a	n/a	1	n/a
HCO_3^-/CO_3^{2-}	160.602	107.44	n/a	n/a
$2MPZ(COO^-)_2$	n/a	n/a	n/a	n/a

6.6 CONCLUSIONS

The liquid composition of 8 m 2MPZ at varied loading was determined from the ^{13}C NMR quantitative results. ^{1}H NMR spectra is not very useful due to the heavy overlap of signals. At the loading range of 0.10-0.37 mol CO_2/mol alkalinity, $2MPZCOO^-$/H2MPZCOO comprise more than 75% of the total CO_2-related reaction products, while the amount of HCO_3^-/CO_3^{2-} and $2MPZ(COO^-)_2$ is relatively small but

steadily increases with CO_2 loading. The fraction of the original 2MPZ that is converted to 2MPZCOO$^-$/H2MPZCOO increases from 19% at α=0.104 loading to 56% at α=0.367.

The use of quantitative NMR data for determination of complete liquid composition for the 4 m 2MPZ / 4 m PZ is limited by the extensive overlap of peaks. The equilibrium species distribution can only be determined for PZCOO$^-$/HPZCOO, 2MPZCOO$^-$/H2MPZCOO and PZ(COO$^-$)$_2$ at lean loading. The ratios between them determined from ^{1}H NMR are similar to the values from ^{13}C NMR spectra. At lean loading, PZCOO$^-$/HPZCOO, 2MPZCOO$^-$/H2MPZCOO and PZ(COO$^-$)$_2$ are also the major CO_2 sinks, contributing to roughly 50%, 40% and 10% of the total CO_2 absorption, respectively.

Chapter 7: Thermodynamic Modeling of PZ Derivatives

Design and simulation of CO_2 capture process using amine scrubbing technology requires accurate representation of thermodynamic properties of aqueous amine solutions at operating conditions. The Electrolyte Nonrandom Two-Liquid (ENRTL) model is adopted in this work to develop a rigorous and thermodynamically consistent model for 8 m 2MPZ. Relevant parameters required by the model were obtained by sequential data regression by the Data Regression System (DRS) in Aspen Plus®. The available data for the binary system (2MPZ-H_2O) are the amine volatility data and pK_a data; for the ternary (2MPZ-CO_2-H_2O) systems, the CO_2 solubility data and NMR spectroscopic data were used. Based on the developed 2MPZ model, predictions of speciation as a function of loading and temperature, activity coefficient, reaction stoichiometry and heat of absorption are presented.

7.1 Literature Review

Solubility of acid gas in amine solution has been modeled with a number of models, of which the ENRTL model is a most widely applied one. Unlike the non-rigorous models such as the Kent-Eisenberg model (Kent and Eisenberg 1976), the ENRTL model is based on the excess Gibbs free energy method to calculate activity coefficients and thus can be used for development of rigorous thermodynamic correlations. Compared to other models such as the Pitzer's equation (Pitzer 1973) using the same method, the ENRTL model is capable of handling electrolyte solutions up to very high concentration (Chen, Britt et al. 1982; Chen and Evans 1986).

The thermodynamic properties of a variety of aqueous amine solutions as CO_2 absorbents have been modeled with the ENTRL model. The solubility of CO_2 in MEA and DEA (Austgen, Rochelle et al. 1989), MDEA and DEA (Posey 1996), MEA (Liu,

Zhang et al. 1999), MDEA, PZ and PZ/MDEA (Bishnoi and Rochelle 2000), MDEA and AMP (Aroua, Haji-Sulaiman et al. 2002), PZ/K_2CO_3 (Cullinane and Rochelle 2005), DEA and Morpholine (Al-Juaied and Rochelle 2006), has been successfully correlated with the ENRTL model. Speciation and heat of absorption have also been calculated in some of these works.

With the availability of more thermodynamic data, the old models were also modified and updated over time to account for additional properties. Zhang *et al.* (Zhang and Chen 2011) incorporated a comprehensive set of literature data including VLE, heat of absorption and heat capacity, and developed a more accurate ENRTL model for MDEA-CO_2-H_2O system. Frailie *et al.* (Frailie, Plaza et al. 2011) developed PZ and PZ/MDEA models based on Hilliard's work (Hilliard 2008) to better fit the high temperature VLE, heat capacity data. Hessen took into account multiple types of data for MEA and MDEA, and developed a refined ENRTL model for them (Hessen, Haug-Warberg et al. 2011).

7.2 MODEL DESCRIPTION

7.2.1 Chemical Equilibrium

The following chemical equilibrium reactions are taken into account in this study:

$$H_2O \leftrightarrow H^+ + OH^- \tag{7.1}$$

$$CO_2 + H_2O \leftrightarrow HCO_3^- + H^+ \tag{7.2}$$

$$HCO_3^- + H_2O \leftrightarrow CO_3^{2-} + H^+ \tag{7.3}$$

$$2MPZ + HCO_3^- \leftrightarrow 2MPZCOO^- + H_2O \tag{7.4}$$

$$2MPZCOO^- + HCO_3^- \leftrightarrow 2MPZ(COO^-)_2 + H_2O \tag{7.5}$$

$$2MPZH^+ \leftrightarrow 2MPZ + H^+ \tag{7.6}$$

$$H2MPZCOO \leftrightarrow 2MPZCOO^{-} + H^{+} \tag{7.7}$$

Based on the NMR speciation study, there is no hindered monocarbamate of 2MPZ present in the system, therefore it is excluded from consideration in the chemical equilibria. Diprotonated 2MPZ is also neglected due to the extremely small amount of it at the loading range under study.

To calculate the species distribution in CO_2-loaded amine solution, the equilibrium constants for various chemical reactions in the liquid phase must be determined. In this work, the definition of chemical equilibrium constant is activity-based as shown in the following expression

$$K_j = \prod_i a_i^{v_{ij}} = \prod_i (x_i \gamma_i)^{v_{ij}} \tag{7.8}$$

where K_j is the equilibrium constant for reaction j; a_i is the activity of component i; v_{ij} is the stoichiometric coefficient of component i in reaction j; x_i and γ_i is the mole fraction and the activity coefficient of component i, respectively.

The symmetric convention for definition of activity coefficient is applied for water as a solvent

$$\gamma_w \to 1 \text{ as } x_w \to 1 \tag{7.9}$$

whereas for other molecular and ionic species, the unsymmetric reference state is used, which is infinite dilution in water at the temperature and pressure of the mixture.

$$\gamma_i^* \to 1 \text{ as } x_i \to 0 \tag{7.10}$$

According to the second thermodynamic law, the Gibbs free energy of a closed system is at its minimum when equilibrium is reached at constant temperature and pressure. The minimization of the Gibbs free energy dictates the reaction equilibrium as well as the equilibrium speciation. The chemical equilibrium constant is related to the difference in the standard free energy of formation of reactants and products by:

$$K_j = \exp\left(-\frac{\Delta G_j^0}{RT}\right) \tag{7.11}$$

where ΔG_j^0 is the change of the standard free energy of formation in reaction j.

$$\Delta G_j^0 = \sum_i v_{ij} G_i^0 \tag{7.12}$$

G_i^0 is the standard free energy of formation of component i. With the substitution of Eq. (7.13) through (7.15) and algebraic rearrangements, Eq. (7.11) is transformed to (7.16):

$$\Delta G = \Delta H - T\Delta S \tag{7.13}$$

$$\Delta H = \Delta H_0^0 + R\int_{T_0}^{T} \frac{\Delta C_p^0}{R} dT \tag{7.14}$$

$$\Delta S = \Delta S_0^0 + R\int_{T_0}^{T} \frac{\Delta C_p^0}{RT} dT \tag{7.15}$$

$$-\ln K_j = \frac{\Delta G_j^0}{RT} = \frac{\Delta G_{0,j}^0 - \Delta H_{0,j}^0}{RT_0} + \frac{\Delta H_{0,j}^0}{RT} + \frac{1}{T}\int_{T_0}^{T} \frac{\Delta C_{P,j}^0}{R} dT - \int_{T_0}^{T} \frac{\Delta C_{P,j}^0}{R} \frac{dT}{T} \tag{7.16}$$

The equation shown above is the origin of the conventional expression that was commonly used and reported in literature.

$$-\ln K_j = A + \frac{B}{T} + C\ln T + DT \tag{7.17}$$

Eq. (7.16) rather than (7.17) is used in this work for calculation of chemical equilibrium constant because it assures the developed thermodynamic model is inherently consistent to the definition of thermodynamic properties.

7.2.2 Vapor-Liquid Equilibrium Calculations

As the vapor and the liquid phase reach equilibrium with each other, the fugacity in each phase should be equal

$$\hat{f}_i^v = \hat{f}_i^l \tag{7.18}$$

In the vapor phase,

$$\hat{f}_i^v = y_i \hat{\phi}_i^v P \tag{7.19}$$

The fugacity coefficient of component i in the vapor phase is calculated from an equation of state:

$$\hat{\phi}_i^v = -\frac{1}{RT}\int_{\infty}^{V}\left[\left(\frac{\partial P}{\partial n_i}\right)_{T,V,n_{j\neq i}} - \frac{RT}{V}\right]dV - \ln Z_m \tag{7.20}$$

For the solvent in the liquid phase

$$\hat{f}_i^l = x_i\gamma_i \hat{\phi}_i^0 P_i^0 \exp\left[\frac{V_i^l\left(P - P_i^0\right)}{RT}\right] \tag{7.21}$$

For the molecular solute modeled as Henry's components, the Henry's law is applicable.

$$\hat{f}_i^l = x_i\gamma_i\left(\frac{H_i}{\gamma_i^{\infty,aq}}\right)\exp\left[\frac{V_i^{\infty,aq}\left(P - P_{H_2O}^0\right)}{RT}\right] \tag{7.22}$$

The conventional symmetric definition of reference state for amines is not used for PZ and 2MPZ in this work. Instead, they are modeled as Henry's components just like CO_2. This treatment allows a more convenient handling of these two components as molecular solutes with the reference state of infinite dilution in water. Although PZ and 2MPZ are not truly supercritical components in the liquid, when it comes to calculate the vapor-liquid equilibrium, whether to model them as subcritical solutes or Henry's components makes little difference since the dependence of Henry's constant on temperature (Eq. (7.23)) is very similar to that of vapor pressure in the vapor pressure models (e.g. extended Antoine Equation (Eq. (7.24)) in Aspen Plus®.

$$\ln H_{i,H_2O}\left(T, P_{H_2O}^{*l}\right) = a_i + b_i/T + c_i \ln T + d_i T + e_i/T^2 \tag{7.23}$$

where H_{i,H_2O} is the Henry's constant of solute i in water.

$$\ln P_i^{*,l} = C_{1i} + \frac{C_{2i}}{T + C_{3i}} + C_{4i}T + C_{5i}\ln T + C_{6i}T^{C_{7i}} \tag{7.24}$$

where $P_i^{*,l}$ is the vapor pressure of component i.

H2MPZCOO is a zwitterion species so it is treated as a nonvolatile Henry's component in the liquid phase. The equilibrium constant reported in literature is usually referenced to infinite dilution in water, which is consistent with the activity coefficient convention used in this work for the solutes.

7.2.3 Vapor Phase Model

The Redlich-Kwong-Soave (RKS) equation of state (Soave 1972) is used in this work for representation of vapor phase. The RKS equation is given in the following expression explicit in pressure:

$$P = \frac{RT}{V_m - b} - \frac{a\alpha(T,\omega)}{V_m(V_m + b)} \tag{7.25}$$

where

$$a = 0.42748\frac{R^2T_c^2}{P_c}$$

$$b = 0.08664\frac{RT_c}{P_c}$$

$$\alpha = \left[1 + \left(0.48508 + 1.55171\omega - 0.15613\omega^2\right)\left(1 - T_r^{0.5}\right)\right]^2$$

$$\omega = -\log_{10}\left(P_r^{sat}\right) - 1 \text{ at } T_r = T/T_c = 0.7$$

T_c : critical temperature

P_c : critical pressure

For a multiple-component vapor phase,

$$(a\alpha)_m = \sum_i \sum_j y_i y_j \left[\left(a_i\alpha_i a_j\alpha_j\right)^{0.5}\left(1 - k_{ij}\right)\right]$$

$$b = \sum_i y_i b_i$$

$k_{ij} = k_{ji}$ are binary interaction parameters

7.2.4 Activity Coefficient Model

To calculate activity coefficient and model liquid thermodynamic properties, the interactions between different species in the solution have to be represented with an appropriate model. There are two methods available for calculation of activity coefficient: excess Gibbs free energy and equation of state. The former method is implemented in the ENTRL model. The following section briefly reviews the ENRTL theory.

The molar Gibbs free energy (g^*) is calculated in Aspen Plus® by the following equation:

$$g^* = x_w \mu_w^* + \sum_k x_k \mu_k^\infty + \sum_j x_j \ln x_j + g^{*,ex} \tag{7.26}$$

where μ_w^*: chemical potential of water;

μ_k^∞ : chemical potential of solute k ;

$\sum_j x_j \ln x_j$: free energy of ideal mixing;

The "*" denotes that the reference state is infinite dilution in water. Molar excess Gibbs free energy ($g^{*,ex}$) is a convenient property that is used to represent the deviation from ideal solution. The molar excess Gibbs free energy stems from the nonzero interactions between molecules and molecules, molecules and ions or ions and ions. The relationship between $g^{*,ex}$ and activity coefficient γ is as follows:

$$\frac{g_i^{ex^*}}{RT} = \ln \gamma_i \tag{7.27}$$

Therefore activity coefficient can be determined from excess Gibbs free energy.

Both long-range interactions and short-range interactions contribute to the molar excess Gibbs free energy

$$\frac{g_i^{ex^*}}{RT} = \frac{g_{LR,i}^{ex^*}}{RT} + \frac{g_{SR,i}^{ex^*}}{RT} = \left(\frac{g_{PDH,i}^{ex^*}}{RT} + \frac{g_{Born,i}^{ex}}{RT} \right) + \frac{g_{NRTL,i}^{ex^*}}{RT} \tag{7.28}$$

Accordingly,

$$\ln \gamma_i = \ln \gamma_i^{PDH} + \ln \gamma_i^{Born} + \ln \gamma_i^{NRTL} \tag{7.29}$$

The importance of the two types of interaction varies with the concentration of the solute. In dilute solutions, molecules or ions are far apart from each other so the long-range interactions are dominant to the excess Gibbs free energy; in concentrated solution, molecule or ions get closer to each other and short-range interactions become significant.

The contribution to Gibbs free energy from the long-range interactions can be described by the Pitzer-Debye-Huckel model:

$$g_{PDH,i}^{ex^*} = -RT\left(\sum_k x_k \right)\left(\frac{1000}{M_s} \right)^{0.5}\left(\frac{4A_\phi I_x}{\rho} \right)\left(\ln 1 + \rho I_x^{0.5} \right) \tag{7.30}$$

where x_i : the mole fraction of component i,

M_s : the molecular weight of the solvent,

I_x : the ionic strength calculated based on mole fraction,

$I_x = \frac{1}{2}\sum_i x_i z_i^2$

ρ : the parameter of closest approach,

A_ϕ is the Debye-Huckel parameter given by the following expression

$$A_\phi = \frac{1}{3}\left(\frac{2\pi N_0 \rho_s}{1000} \right)^{0.5}\left(\frac{e^2}{D_s kT} \right)^{1.5} \tag{7.31}$$

where N_0 : Avogadro's number,

ρ_s : the solvent density,

e : the charge of an electron,

k : the Boltzmann constant,

$D_s = \sum_j w_j D_{sj}$: The dielectric constant of the solvent mixture

w_j : The mass fraction of solvent j

The Born equation is introduced to account for the change in the dielectric constants when solvent is changed from water to mixed solvent. Thus the reference state for ions is maintained as infinite dilution in water.

$$g_{Born}^{ex} = RT\left(\frac{e^2}{2kT}\right)\left(\sum_i \frac{x_i z_i^2}{r_i}\right)\left(\frac{1}{D_m} - \frac{1}{D_w}\right) \tag{7.32}$$

where r_i is the Born radius, and D_m and D_w is the dielectric constant of the mixed solvent and water, respectively.

The NRTL model, which was developed by Renon *et al.* (Renon and Prausnitz 1968) on the basis of Wilson's work on excess free energy of mixed nonelectrolytes system (Wilson 1964), was extended by Chen *et al.* (Chen, Britt et al. 1982; Chen and Evans 1986) to describe local interactions in electrolyte systems. In the ENRTL model, the distribution of molecules around a central molecule is described by the following equation

$$\frac{x_{ji}}{x_{ii}} = \left(x_j / x_i\right) G_{ji} \tag{7.33}$$

$$G_{ji} = \exp\left(-\alpha \tau_{ji}\right) \tag{7.34}$$

$$\tau_{ji} = \left(g_{ji} - g_{ii}\right) / RT \tag{7.35}$$

where α is the non-randomness parameter, typically ranging from 0.1 to 0.4; g_{ji} is the interaction energy between species i and j and is inherently symmetric; τ_{ji} is the binary interaction parameter for i and j.

The ENRTL model assumes that there are three types of cells: molecules (m), cations (c) and anions (a). The developed local composition model for excess Gibbs free energy is based on two fundamental assumptions: like-ion repulsion and local electroneutrality. As a result, there are three types of interactions needed to be taken into account: m – m, m – ca, ca – ca. The total excess Gibbs free energy calculated from the ENRTL model is as follows:

$$\frac{g^{ex}_{NRTL}}{RT} = \sum_m X_m \frac{\sum_j X_j G_{jm}\tau_{jm}}{\sum_k X_k G_{km}} + \sum_c X_c \left(\sum_{a'} \left(\frac{X_{a'} \sum_j G_{jc,a'c}\tau_{jc,a'c}}{\sum_{a''} X_{a''} \sum_k X_k G_{kc,a'c}} \right) \right) + \sum_a X_a \left(\sum_{c'} \left(\frac{X_{c'} \sum_j G_{ja,a'c}\tau_{ja,a'c}}{\sum_{c''} X_{c''} \sum_k X_k G_{ka,a'c}} \right) \right) \tag{7.36}$$

where

$$G_{cm} = \frac{\sum_a X_a G_{ca,m}}{\sum_{a'} X_{a'}}, \quad G_{am} = \frac{\sum_c X_c G_{ca,m}}{\sum_{c'} X_{c'}}$$

$$\alpha_{cm} = \frac{\sum_a X_a \alpha_{ca,m}}{\sum_{a'} X_{a'}}, \quad \alpha_{am} = \frac{\sum_c X_c \alpha_{ca,m}}{\sum_{c'} X_{c'}}$$

$$G_{jc,a'c} = \exp(-\alpha_{jc,a'c}\tau_{jc,a'c}), \quad G_{ja,c'a} = \exp(-\alpha_{ja,c'a}\tau_{ja,c'a})$$

$$G_{im} = \exp(-\alpha_{im}\tau_{im}), \quad G_{ca,m} = \exp(-\alpha_{ca,m}\tau_{ca,m})$$

$$\tau_{ma,ca} = \tau_{am} - \tau_{ca,m} + \tau_{m,ca}, \quad \tau_{mc,ac} = \tau_{cm} - \tau_{ca,m} + \tau_{m,ca}$$

$$X_j = x_j C_j \quad (C_j = Z_j \text{ for ions and } C_j = 1 \text{ for molecules}$$

In Aspen Plus®, the temperature dependence of the ENRTL parameters is expressed in the following relationships:

Molecule-Molecule Binary Parameters

$$\tau_{mm'} = A_{mm'} + \frac{B_{mm'}}{T} + F_{mm'} \ln(T) + G_{mm'} T \tag{7.37}$$

Electrolyte-Molecule Pair Parameters

$$\tau_{ca,m} = C_{ca,m} + \frac{D_{ca,m}}{T} + E_{ca,m}\left[\frac{\left(T_{ref} - T\right)}{T} + \ln\left(\frac{T}{T_{ref}}\right)\right] \tag{7.38}$$

Molecule-Electrolyte Pair Parameters

$$\tau_{m,ca} = C_{m,ca} + \frac{D_{m,ca}}{T} + E_{m,ca}\left[\frac{\left(T_{ref} - T\right)}{T} + \ln\left(\frac{T}{T_{ref}}\right)\right] \tag{7.39}$$

where $T_{ref} = 298.15K$. The default values for A, B, F, D, G and E are zero, and the default values for $C_{ca,m}$ and $C_{m,ca}$ are set at -8 and 15 respectively in this work if not specified otherwise. If the molecule is water then the default values are -4 and 8. The interaction between ion pair-ion pair is neglected ($\tau_{c'a',ca} = 0$). For molecule-molecule interaction, the non-randomness parameter $\alpha = 0.3$; for molecule-ion pair interaction or ion pair-ion pair interaction, $\alpha = 0.2$. As electrolyte concentration approaches zero, the ENRTL model is reduced to the NRTL model.

7.2.5 Data Regression and Parameter Settings

The data regression system (DRS) incorporated into Aspen Plus® was used in this study for regression of relevant parameters based on the existing experimental data sets. Standard-state property parameters and binary interaction parameters were manipulated in DRS with Britt-Luecke algorithm to minimize the Maximum Likelihood objective function, in which errors in all measured variables are taken into account.

The thermodynamic model built for 2MPZ in this work is based on the model for PZ ("Guy Fawkes" model) developed by Frailie *et al.* (Frailie, Plaza et al. 2011). As there is no data available for 2MPZ in the Aspen databank, 2MPZ was added as a new component by providing the molecular structure and boiling point. The standard free energy of formation and the standard enthalpy of formation for 2MPZ share the same

values for PZ, since it is the difference of the state properties of reactants and products which matters. All other 2MPZ-related species are then referenced to 2MPZ. The values for the reference state properties are given in Table 7.1.

Table 7.1: Parameters for the reference state properties used in this work (Unit: kJ/mol). All but those for 2MPZ and $2MPZH^+$ are based on Aspen Databank.

Component i	$\Delta_f G_i^{ig}$	$\Delta_f H_i^{ig}$	$\Delta_f G_i^{\infty,aq}$	$\Delta_f H_i^{\infty,aq}$
2MPZ	170.1139	16.41096	-	-
$2MPZH^+$	-	-	826.0	-107.0
H_2O	-228.743	-241.976	-	-
CO_2	-394.648	-393.773	-	-
HCO_3^-	-	-	-586.770	-587.333
CO_3^{2-}	-	-	-527.810	-528.336
OH^-	-	-	-157.244	-157.403

$\Delta_f G_i^{ig}$: Ideal gas free energy of formation at 298.15K

$\Delta_f H_i^{ig}$: Ideal gas enthalpy of formation at 298.15K

$\Delta_f G_i^{\infty,aq}$: Aqueous phase free energy of formation at infinite dilution and 298.15K.

$\Delta_f H_i^{\infty,aq}$: Aqueous phase heat of formation at infinite dilution and 298.15K

For the Henry's components, $\Delta_f G_i^{\infty,aq}$ is related to $\Delta_f G_i^{ig}$ by

$$\Delta_f G_i^{\infty,aq} = \Delta_f G_i^{ig} + RT \ln\left(\frac{H_{i,H_2O}}{P^{ref}}\right) \tag{7.40}$$

where H_{i,H_2O} is the Henry's constant of solute i in water and P^{ref} is the reference pressure of 1 bar. $\Delta_f H_i^{\infty,aq}$ is correlated to $\Delta_f H_i^{ig}$ with the following equation:

$$\Delta_f H_i^{\infty,aq} = \Delta_f H_i^{ig} - RT^2 \frac{\partial \ln H_{i,H_2O}}{\partial T} \tag{7.41}$$

The values for heat capacity parameters for 2MPZ-CO_2-H_2O system are not regressed in this work and are assumed to have the same values as the similar species in the Fawkes PZ model. The values for heat capacity model parameters used in this work have been summarized in Table 7.2.

Table 7.2: Coefficients for ideal gas heat capacity[a] (C_p^{ig} for molecules, kJ/(mol·k)) and aqueous infinite dilution heat capacity[b] ($C_p^{\infty,aq}$ for ions, kJ/(mol·k)).

Comp.	Parameters[c]					
	C_0	C_1	C_2	C_3	C_4	C_5
2MPZ	-3.60E-2	7.25E-4	0	0	0	0
$2MPZH^+$	2.21E-1	0	0	0	0	0
$2MPCOO^-$	1.07E-1	6.04E-4	0	0	0	0
H2MPZCOO	-2.55E-1	0	0	0	0	0
$2MPZ(COO^-)_2$	-1.41E+0	4.07E-3	0	0	0	0
CO_2	1.98E-2	7.34E-5	-5.60E-8	1.72E-11	0	0
H_2O	3.37E-2	-7.02E-6	2.73E-8	-1.67E-11	4.30E-15	-4.17E-19
OH^-	-1.49E-1	0	0	0	0	0
HCO_3^-	2.11E-1	-8.82E-4	8.75E-07	-1.88E+1	0	0
CO_3^{2-}	1.33E+0	-5.56E-3	5.19E-06	-1.19E+2	0	0

a: $C_p^{ig} = C_0 + C_1 T + C_2 T^2 + C_3 T^3 + C_4 T^4 + C_5 T^5$

b: $C_p^{\infty,aq} = C_0 + C_1 T + C_2 T^2 + \frac{C_3}{T} + \frac{C_4}{T^2} + \frac{C_5}{\sqrt{T}}$

c: Values for 2MPZ-related species are from the Fawkes model (Frailie, Plaza et al. 2011) and the others are from Aspen databank.

The Fawkes model for PZ also fits the measured γ_{CO_2} in 8 m PZ at multiple temperature. To reasonably represent γ_{CO_2} in 8 m 2MPZ, it is assumed that γ_{CO_2} has the same values to that in 8 m PZ, and the binary interaction parameters for CO_2 with other molecular and ionic species in aqueous 2MPZ are taken from the Fawkes model for PZ.

7.3 BINARY SYSTEM 2MPZ-H_2O

7.3.1 Volatility of 2MPZ in Water

Since 2MPZ is modeled as a Henry's component in this work, Henry's law is applied to calculate the vapor pressure of 2MPZ. The vapor pressure of 2MPZ above 1 m 2MPZ aqueous solution from 40 – 70 °C measured by Thu Nguyen (Nguyen 2010) was used for data regression. It is found that only the first two coefficients in the Henry's constant model (Eq. (7.23)) are needed to fit the data. The regression results are given in Table 7.3 along with the parameters in the Henry's constant model for CO_2 and H2MPZCOO. H2MPZCOO is a zwitterion and thus not volatile, so an extremely small Henry's constant is assigned to H2MPZCOO.

Table 7.3: Coefficients for Henry's Constant in H_2O:
$\ln H = a + b/T + c\ln T + dT + e/T^2$ (Unit: Pa)

Solute	*a*	*b*	*c*	*d*	*e*	Source
2MPZ	33.1 ± 0.6	-9180± 205	0	0	0	This work
CO_2	170.7	-8478	-21.96	5.78E-3	0	Aspen Databank
H2MPZCOO	-10	0	0	0	0	This work

The calculation results for the vapor pressure of 2MPZ in unloaded 2MPZ aqueous solutions are compared to the experimental data in Figure 7.1. The calculated values from the model agree well with the experimental data for 1 m 2MPZ. Since there are no data available for 2 m and 8 m 2MPZ, the predictions for 2MPZ at these two concentrations are compared to 2 m PZ and 8 m PZ, respectively. Because of the additional methyl group, 2MPZ is expected to be less hydrophilic and more volatile than PZ at the same concentration, which is what is predicted by the model above 50 °C.

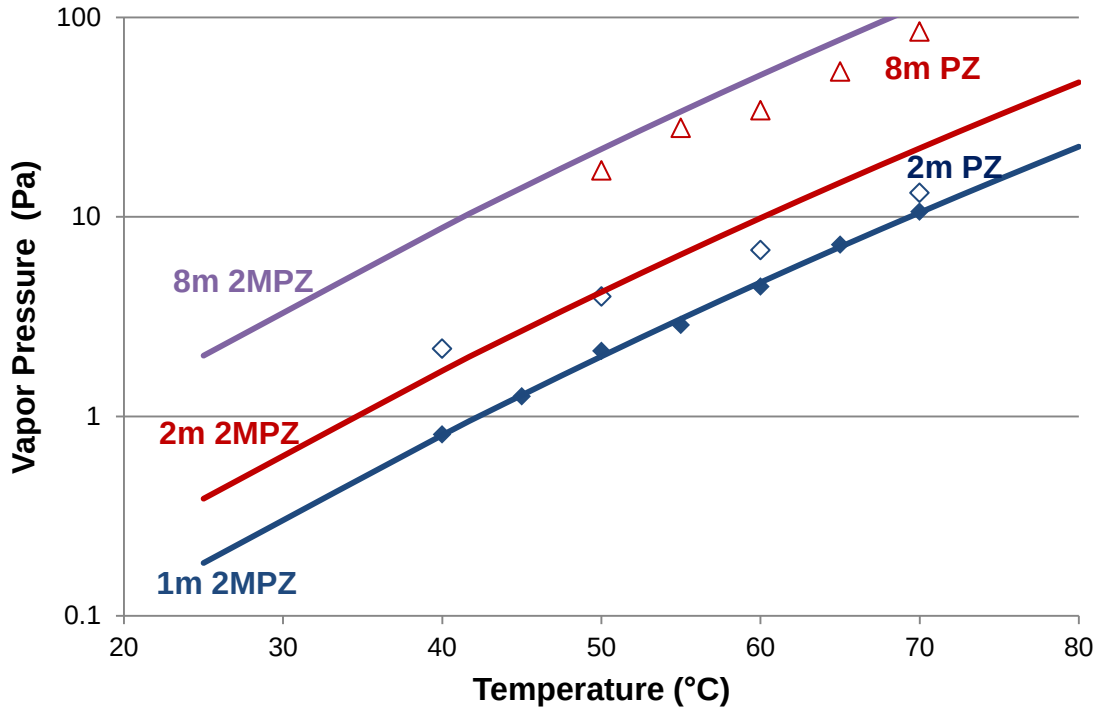

Figure 7.1: 2MPZ vapor pressure predicted by the model compared with experimental data for 1 m 2MPZ, 2 m PZ, and 8 m PZ with no CO_2 loading. Filled Points: Measurements for 1 m 2MPZ. Open Points: Measurements for 2 m and 8 m PZ (Nguyen, 2010); Solid lines: Model prediction from this work.

7.3.2 pKa Values for Dissociation of 2MPZH$^+$

$\Delta_f G_i^{\infty,aq}$, $\Delta_f H_i^{\infty,aq}$ for 2MPZH$^+$ were manually adjusted to fit the pKa data reported by Khalili and coworkers (Khalili, Henni et al. 2009). Figure 7.2 shows that experimental pKa data from 25 to 50 °C are represented well by the calculated correlation from the model.

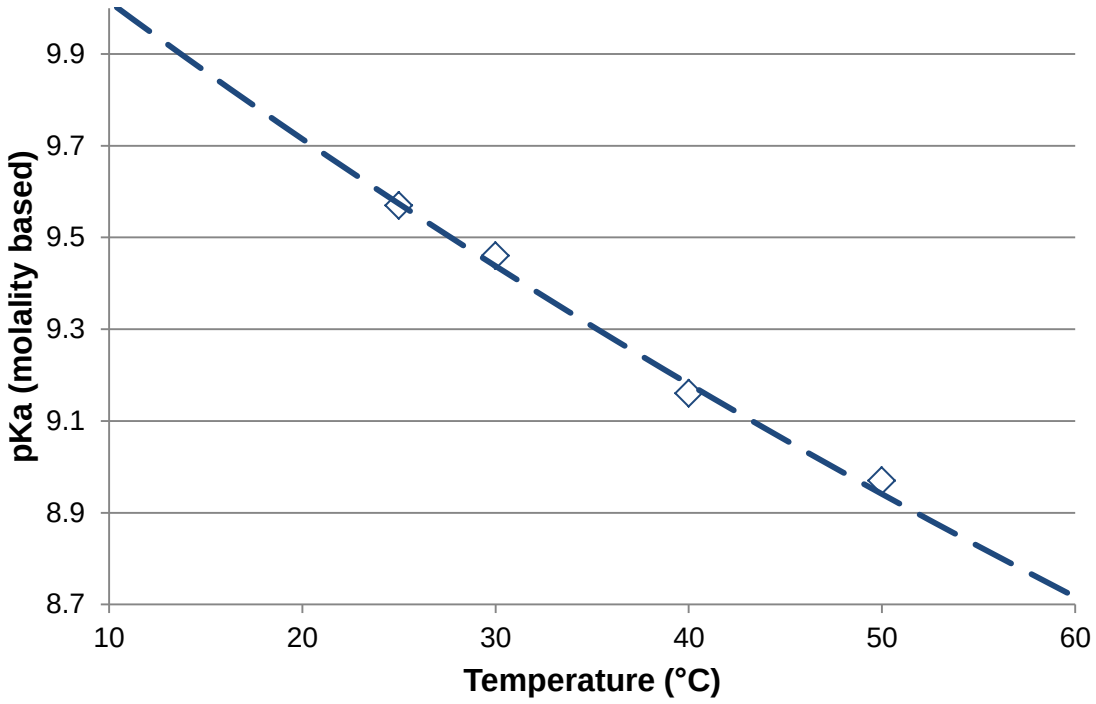

Figure 7.2: pKa of dissociation of 2MPZH$^+$ as a function of temperature. Solid line: Model prediction; Points:(Khalili et al., 2009).

7.4 TERNARY SYSTEM 2MPZ-CO_2-H_2O

The equilibrium partial pressure of CO_2 for 8 m 2MPZ has been measured with the WWC at temperatures up to 100 °C as well as through the total pressure method from

100 °C to 160 °C by Xu *et al.* (Xu and Rochelle 2011). These two sets of data along with the ^{13}C NMR speciation data at 40 °C were used for data regression.

Table 7.4 summarizes the regression results for the selected parameters. A total of 8 parameters were picked for regression, which include reference state properties for 2MPZ carbamate species and binary interaction parameters. Except $\Delta_f H_i^{ig}$ for 2MPZ(COO^-)$_2$, all the estimated values are significantly greater than the standard deviation, which suggests a high confidence level in the estimates. The parameters regressed for 2MPZ(COO^-)$_2$ have a relatively larger uncertainty because it is never a significant species throughout the CO_2 loading range,.

Table 7.4: Parameters and results for the simultaneous regression of the CO_2 solubility and NMR data for 8 m 2MPZ.

#	Parameter	Component i	Component j	Value (kJ/mol)	Std. Dev. (kJ/mol)
1	$\Delta_f G_i^{\infty,aq}$	2MPZCOO$^-$	-	-219.5	3.4
2	$\Delta_f H_i^{\infty,aq}$			-500.7	30.3
3	$\Delta_f G_i^{\infty,aq}$	2MPZ(COO^-)$_2$	-	-564.9	40.0
4	$\Delta_f H_i^{\infty,aq}$			-928.2	808.2
5	$\Delta_f G_i^{ig}$	H2MPZCOO	-	-229.1	15.2
6	$\Delta_f H_i^{ig}$			-564.4	23.1
#	**Parameter**	**Component i**	**Component j**	**Value**	**Std. Dev.**
$\tau_{ca,m} = C_{ca,m} + \frac{D_{ca,m}}{T} + E_{ca,m}\left[\frac{(T_{ref} - T)}{T} + \ln\left(\frac{T}{T_{ref}}\right)\right]$					
7	$C_{ca,m}$	(2MPZH$^+$,2MPZCOO$^-$)	H2MPZCOO	-10.42	5.75
8		(2MPZH$^+$,HCO_3^-)	H2MPZCOO	-11.46	4.90

The correlation matrix for the parameters regressed in the 2MPZ model is calculated and shown in Table 7.5. The correlation coefficient is a number between -1 and 1 and indicates the extent of correlation between two parameters. If the coefficient is 0, the two parameters are independent of each other; if the coefficient is close to -1 or 1, the two is then highly correlated. The diagonal elements in the matrix are all 1 since a parameter is always linearly related to itself. As shown in the table, most of the parameters regressed are not highly correlated to each other, and therefore not significantly affected by other parameters. The exceptions are that Parameter 3 ($\Delta_f G_i^{\infty,aq}$ of 2MPZ(COO^-)$_2$) is strongly related to Parameter 4 ($\Delta_f H_i^{\infty,aq}$ of 2MPZ(COO^-)$_2$), and Parameter 5 ($\Delta_f G_i^{ig}$ of H2MPZCOO) is also interfered by Parameter 7 (the τ parameter for ($2MPZH^+$/2MPZCOO^-, H2MPZCOO)). However, elimination of any one of them from the regression leads to a significant drop in the quality of fit to the VLE and NMR data, therefore they are all kept in the regression.

Table 7.5: Correlation matrix of the regressed parameters for 8 m 2MPZ.

Parameter	**1**	**2**	**3**	**4**	**5**	**6**	**7**	**8**
1	1.00							
2	0.82	1.00						
3	-0.11	-0.53	1.00					
4	-0.22	-0.61	0.99	1.00				
5	-0.33	-0.08	-0.30	-0.24	1.00			
6	0.54	0.42	0.13	0.05	-0.03	1.00		
7	0.38	0.10	0.45	0.38	-0.94	0.23	1.00	
8	0.52	0.34	-0.03	-0.12	-0.85	0.33	0.77	1.00

CO_2 Solubility

The comparison of the model prediction and the experimental data for CO_2 solubility in 8 m 2MPZ is presented in Figure 7.3. The dependence of CO_2 partial pressure ($P_{CO_2}^*$) on loading and temperature is satisfactorily represented by the model

except the data point at 100 °C and the highest loading. It can also be seen from the chart that the lean and rich CO_2 loading, which correspond to $P^*_{CO_2}$ = 500 and 5000 Pa at 40 °C, are 0.27 and 0.37 mol CO_2/mol alkalinity, respectively.

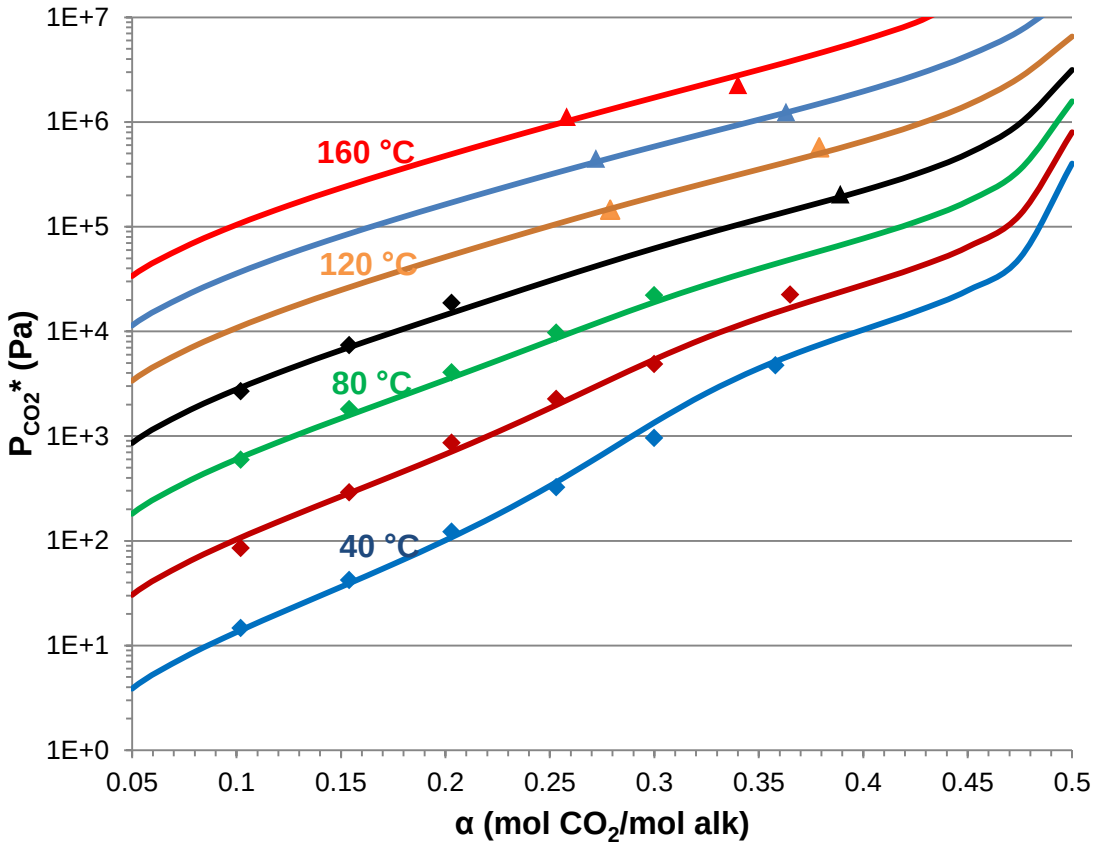

Figure 7.3: CO_2 solubility in 8 m 2MPZ from 40 to 160 °C. Solid line: model prediction; Diamond Points: Measurements in the WWC; Triangle Points: (Xu and Rochelle 2011)

All measured values including the content of total amine and CO_2 were also adjusted by Aspen Plus® during data regression. The parity plot of the calculated CO_2 partial pressure at varied CO_2 loading after adjustment versus the experimental values is given in Figure 7.4. It can be seen that the partial pressure data is well matched by the

model. This is partially attributed to the adjustment in CO_2 loading at rich end, as shown in the parity plot for CO_2 loading in Figure 7.5. The data at this rich loading is from the total pressure method, which features a batch process at high temperature and typically has a higher uncertainty in the actual CO_2 loading. This explains the larger deviation in CO_2 loading at rich end. The absolute average relative deviation for all the calculated CO_2 loading is only 2.4% though, which is well within the error in experimental CO_2 loading measurements.

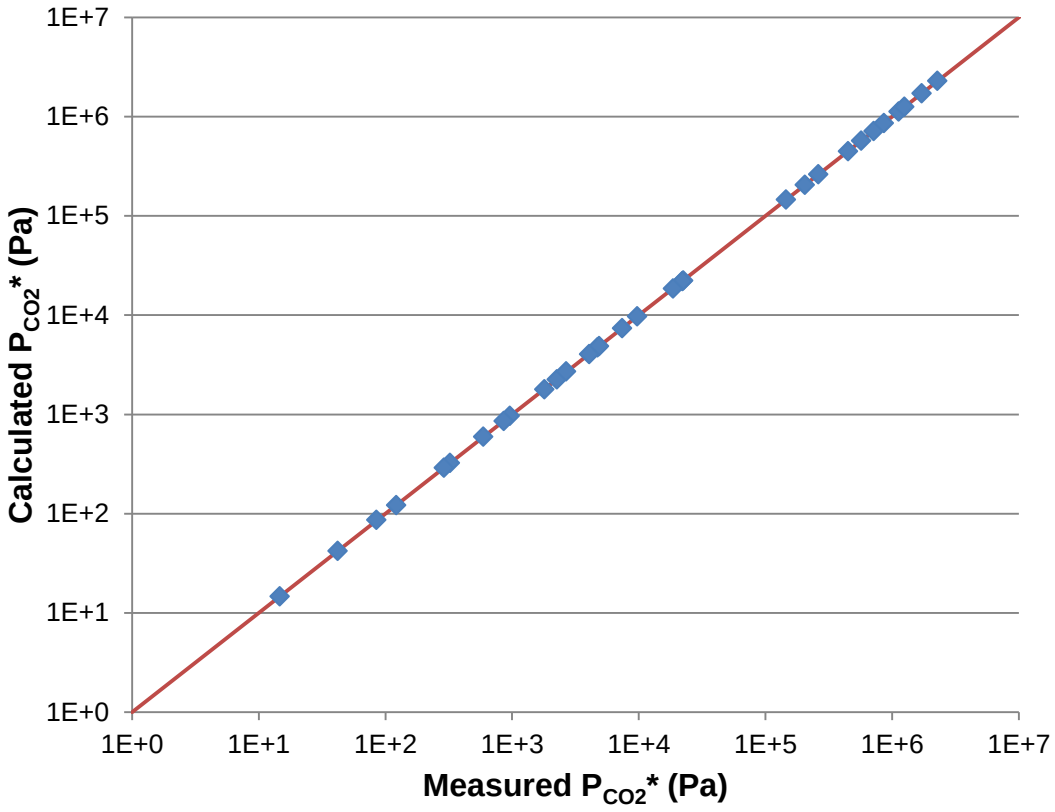

Figure 7.4: Parity plot for equilibrium CO_2 partial pressure for 8 m 2MPZ. The calculated P_{CO2}^* corresponds to the CO_2 loading value after adjustment.

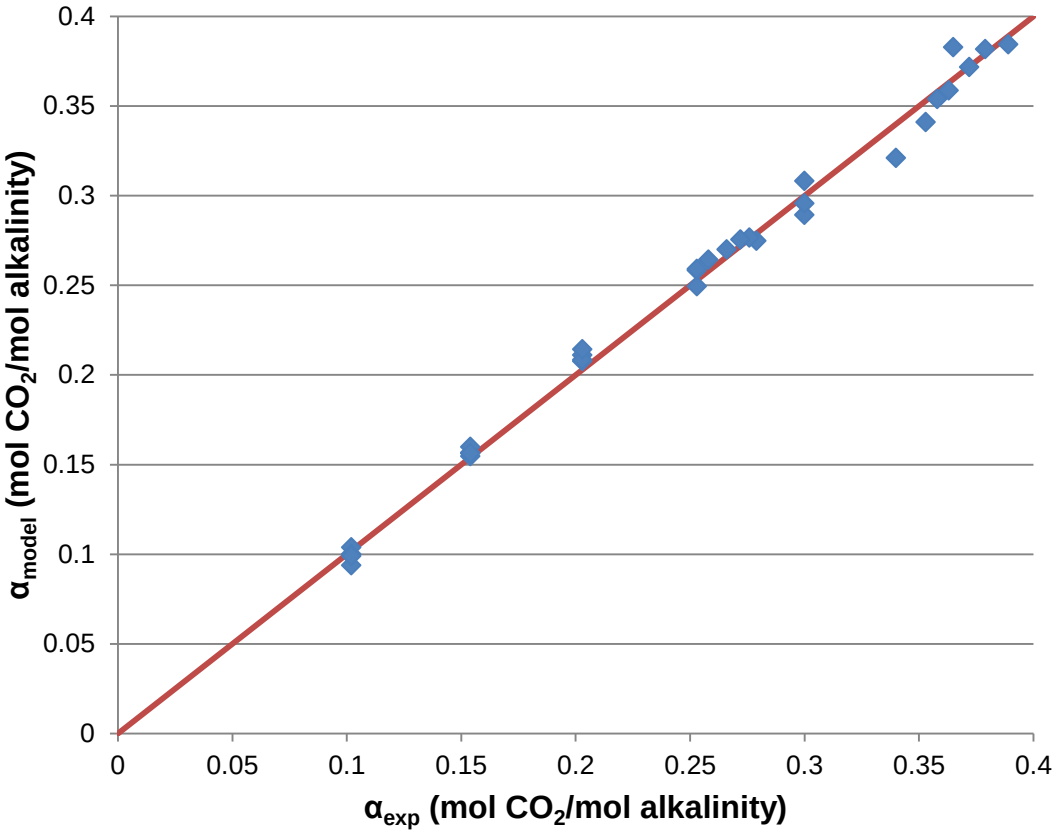

Figure 7.5: Parity plot for the CO_2 loading of 8 m 2MPZ. α_{model} is the ratio of the adjusted total CO_2 concentration and the total alkalinity in the solution; α_{exp} is the experimental value of CO_2 loading.

NMR and Speciation

The distribution of the total absorbed CO_2 in different CO_2-related species as a function of loading has been shown in Figure 7.6. The prediction of the model is in good agreement with the experimental NMR measurements, except that the amount of bicarbonate at rich loading is slightly overpredicted by the model. As can be seen from the chart, the fraction of CO_2 in the form of monocarbamate decreases from about 95% at very lean loading to 50-60% at rich loading. The initial drop in the contribution of HCO_3^-/CO_3^{2-} at the lean end is due to the slight increase in the contribution of

monocarbamate, which replaces CO_3^{2-} as the major CO_2 sink at very lean loading. Due to the depletion of free amine, the bicarbonate production keeps increasing with CO_2 loading and accounts for about 40% of the total at the loading of 0.5 mol CO_2/mol alkalinity. The share of 2MPZ dicarbamate as a CO_2 sink increases with loading until the CO_2 loading is above 0.33, presumably because the dicarbamate is not very stable and is converted to bicarbonate at rich loading.

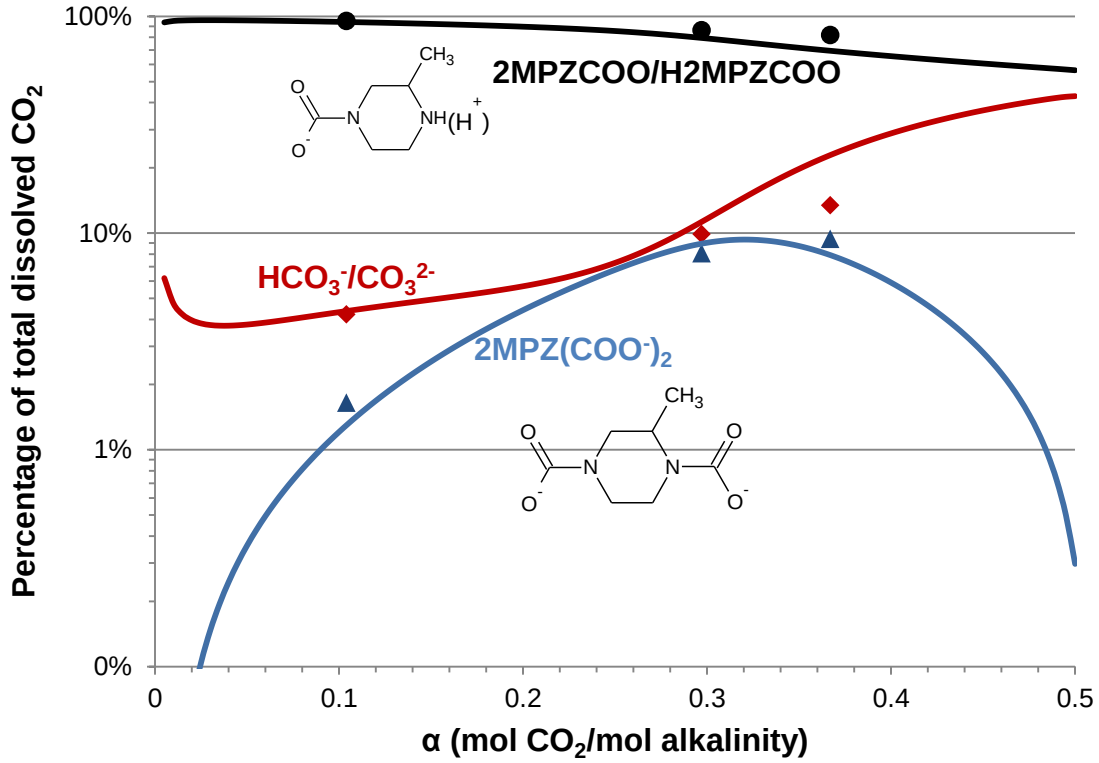

Figure 7.6: Distribution of CO_2 in difference reaction products. Points: quantitative ^{13}C NMR data; Lines: model prediction in this work.

A complete speciation chart was generated by the model for 8 m 2MPZ at 40 °C, as shown in Figure 7.7. Free 2MPZ decreases drastically with CO_2 loading and is almost completely depleted at α = 0.4 mol/mol alkalinity. $2MPZH^+$ and $2MPZCOO^-$ are the two major products in the lean loading range, indicating that the reaction of 2MPZ and

CO_2 is catalyzed by 2MPZ itself. As CO_2 loading increases, the amount of H2MPZCOO is more and more significant. The increase in H2MPZCOO is partially attributed to the protonation of $2MPZCOO^-$ as $2MPZCOO^-$ starts to decrease as loading is above 0.26. At $\alpha = 0.5$, there is no $2MPZCOO^-$ left and the concentration of H2MPZCOO is close to 5 m, which indicates that about 60% of the total 2MPZ is converted to H2MPZCOO and the rest is converted to $2MPZH^+$. There is little $2MPZ(COO^-)_2$ at lean loading, and at $\alpha = 0.33$ it reaches the maximal concentration which is still more than one order of magnitude lower than $2MPZH^+$ and H2MPZCOO. The amount of HCO_3^- increases with CO_2 loading and it becomes a significant species as loading above 0.3. The concentration of HCO_3^- is slightly more than 3.5 m at $\alpha = 0.5$. CO_3^{2-} and free CO_2 are not significant species in the solution across the entire CO_2 loading range.

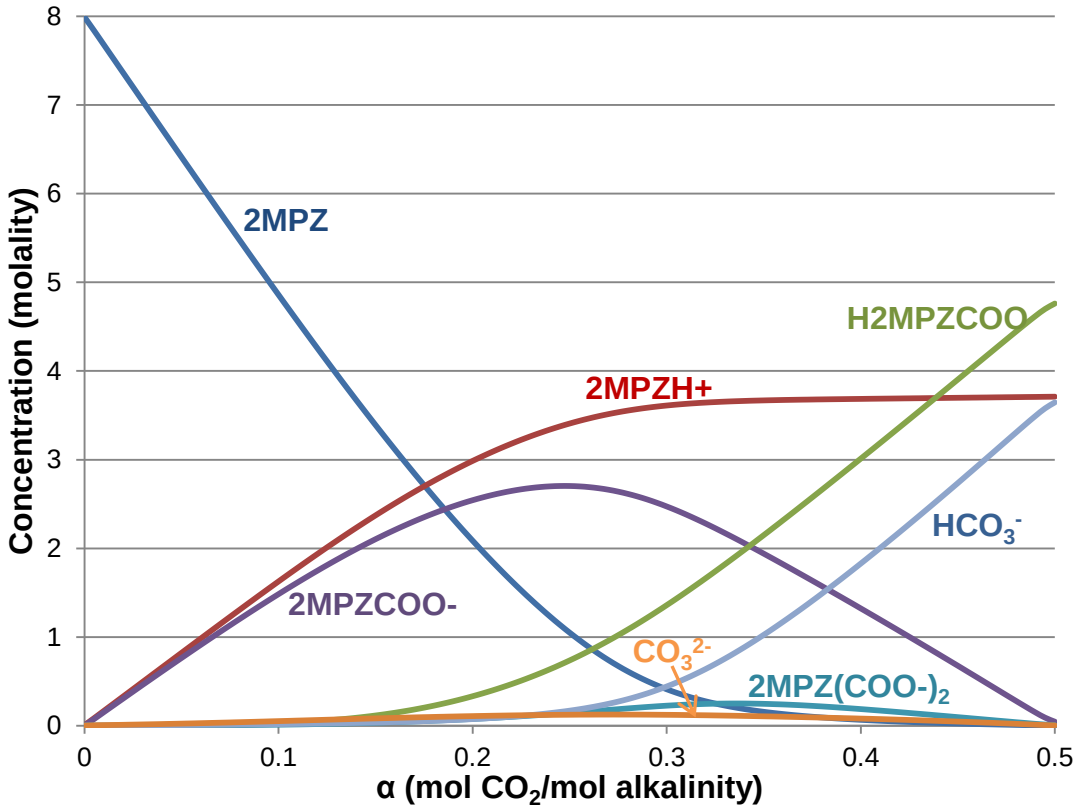

Figure 7.7: Speciation in 8 m 2MPZ at 40 °C.

The temperature dependence of species concentration at the rich condition from 40 to 160 °C is presented in Figure 7.8. The amount of $2MPZH^+$ and $2MPZCOO^-$ is found to be relatively stable despite the change in temperature. The concentrations of free 2MPZ, HCO_3^{2-} and CO_2 all increase with temperature while those of H2MPZCOO, $2MPZ(COO^-)_2$ and CO_3^{2-} decrease since they are less stable as temperature is elevated. An increase of more than two orders of magnitude in free CO_2 concentration is also observed, which indicates a stronger tendency for CO_2 to leave the solution.

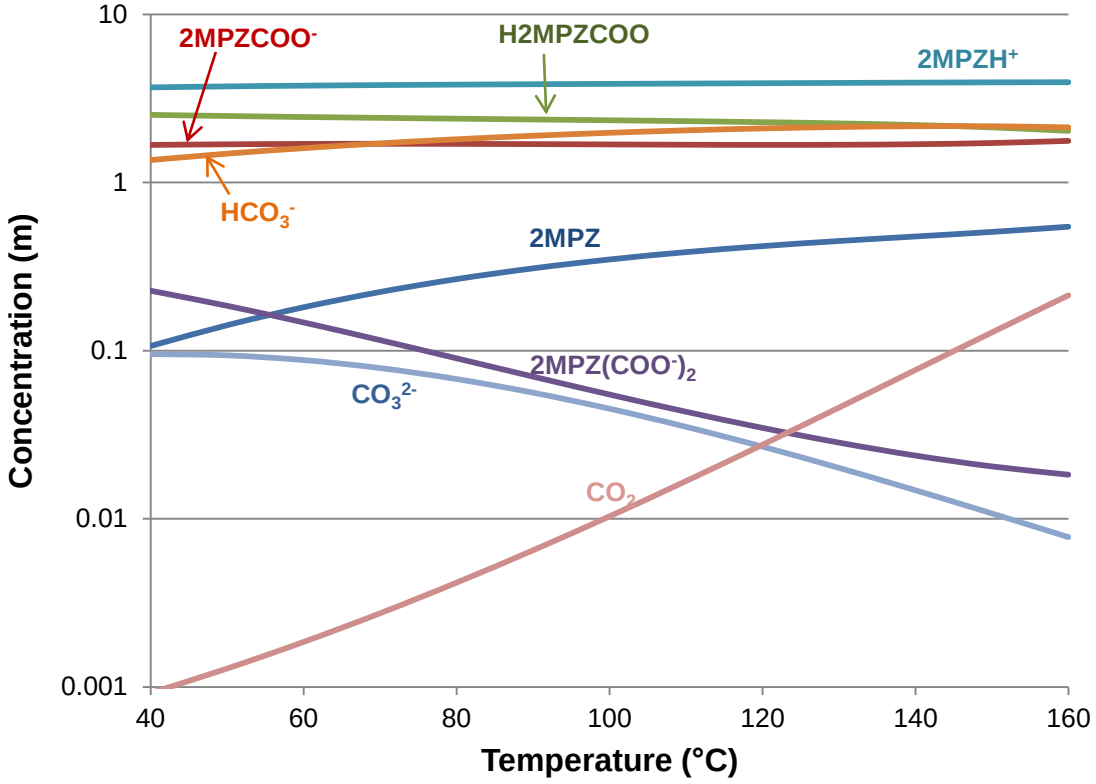

Figure 7.8: Temperature dependence of speciation for 8 m 2MPZ at α = 0.37 mol CO_2/mol alkalinity, P_{CO2}^* = 5000 Pa at 40 °C.

Activity Coefficient

As a rigorous thermal model, the ENTRL model also calculated the activity coefficients (γ) of different species in the liquid. However, it is not possible to validate the predictions for γ since there are no experimental data available for 8 m 2MPZ. The variation of γ with loading for 8 m 2MPZ at 40 °C is shown in Figure 7.9. γ of 2MPZ and CO_2 are both greater than 1 and slightly increase with loading. The values and the behavior with loading are consistent with the experimental results from the Henry's constant measurement for PZ (Hilliard 2008) in CO_2-loaded aqueous PZ and that for N_2O in CO_2-loaded concentrated aqueous monoethanolamine (Hartono 2009). The increase in CO_2 loading leads to higher ionic strength of the solution, which salts out the molecular species. γ of all the ionic species, on the other hand, is found to decrease with loading. The charged species are expected to have a favorable interaction with more polar liquid phase and thus have lower activity coefficient. The dependence of γ of HCO_3^-, $2MPZH^+$ and $2MPZCOO^-$ on CO_2 loading is similar, presumably because that they are all singly-charged species. γ of CO_3^{2-} is found to have exactly the same trend as shown for $2MPZ(COO^-)_2$. H2MPZCOO has the smallest γ throughout the CO_2 loading range. This might be attributed to the zwitterion nature of H2MZPCOO, which make it favorably interact with both cations and anions in the solution. It has been mentioned that $\Delta_f G_i^{ig}$ of H2MPZCOO is strongly correlated with the binary interaction parameters for H2MPZCOO, so the value of γ is also affected by the final estimates for $\Delta_f G_i^{ig}$ of H2MPZCOO.

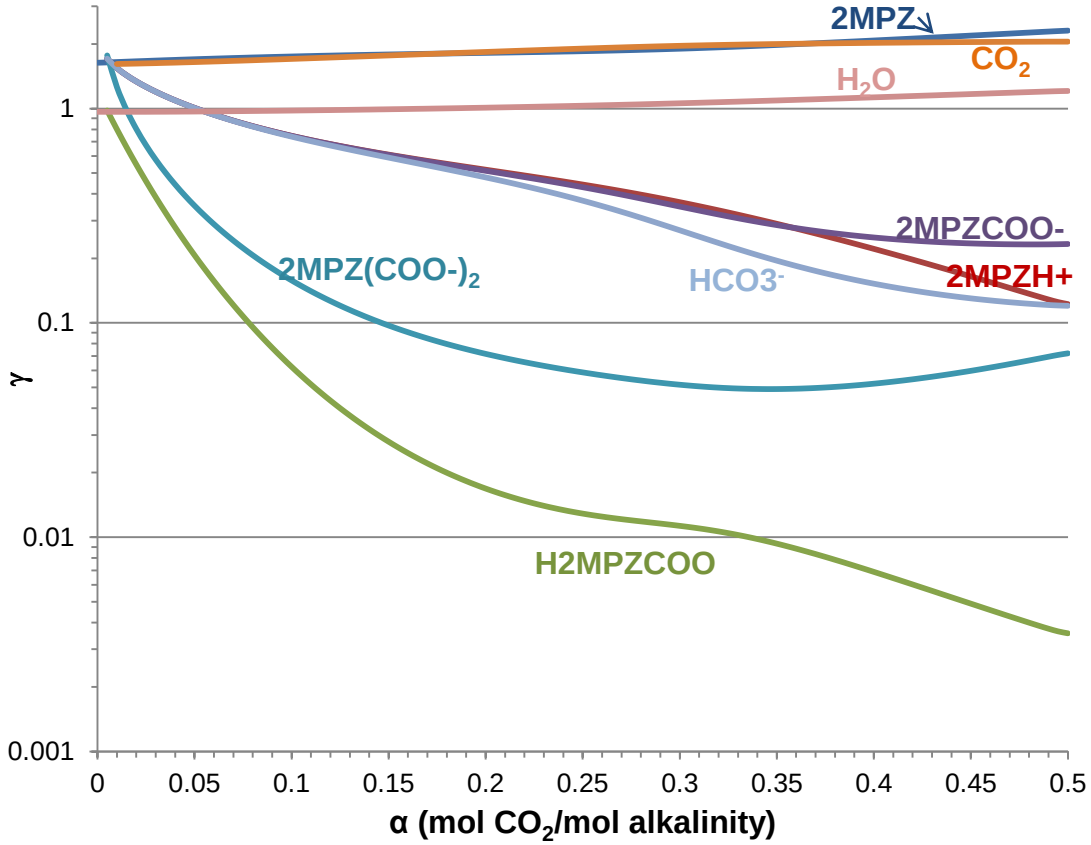

Figure 7.9: Predicted activity coefficients by the ENRTL model for 8 m 2MPZ at 40 °C.

Reaction Stoichiometry

The reaction stoichiometry is calculated for 8 m 2MPZ at 40 °C and shown in Figure 7.10. The amount of reactant and product is normalized to the amount of CO_2 absorbed. 2MPZ is the major reactant responsible for CO_2 absorption up to the lean loading. At loading less than 0.1, the reaction stoichiometric ratio between 2MPZ and CO_2 is around 2, and the major products are 1 mol $2MPZCOO^-$ and 1 mol $2MPZH^+$. This indicates that the overall absorption is mainly driven by the carbamate formation reaction between 2MPZ and CO_2. The importance of this reaction diminishes with CO_2 loading as the stoichiometric number decreases, and in parallel is an increase in the production of H2MPZCOO. A transition from positive to negative in the $\Delta n_i/\Delta n_{CO2}$ for

2MPZCOO- occurs around 0.25 loading, where the HCO_3^- becomes an important product. Between the lean and rich loading, the similar stoichiometric numbers (with different signs) for $2MPZCOO^-$, HCO_3^{2-} and H_2O indicate that 2MPZCOO- acts as a base and catalyzes the hydrolysis of CO_2. At loading above 0.38, bicarbonate and H2MPZCOO have similar stoichiometric number and they are the dominant products of CO_2 absorption with H_2O and $2MPZCOO^-$ as the main reactants. Production of $2MPZH^+$ diminishes to 0 at the rich loading, which corresponds to the depletion of free 2MPZ. Half of the additional CO_2 absorbed at 0.5 loading stays in the free form, which also seems to be the most abundant product at $\alpha > 0.5$. CO_3^{2-} and $2MPZ(COO^-)_2$ are never significant products throughout the entire loading range. The reaction stoichiometry from this study resembles that for 1.8 PZ at 25 °C given by Cullinane (Cullinane 2005).

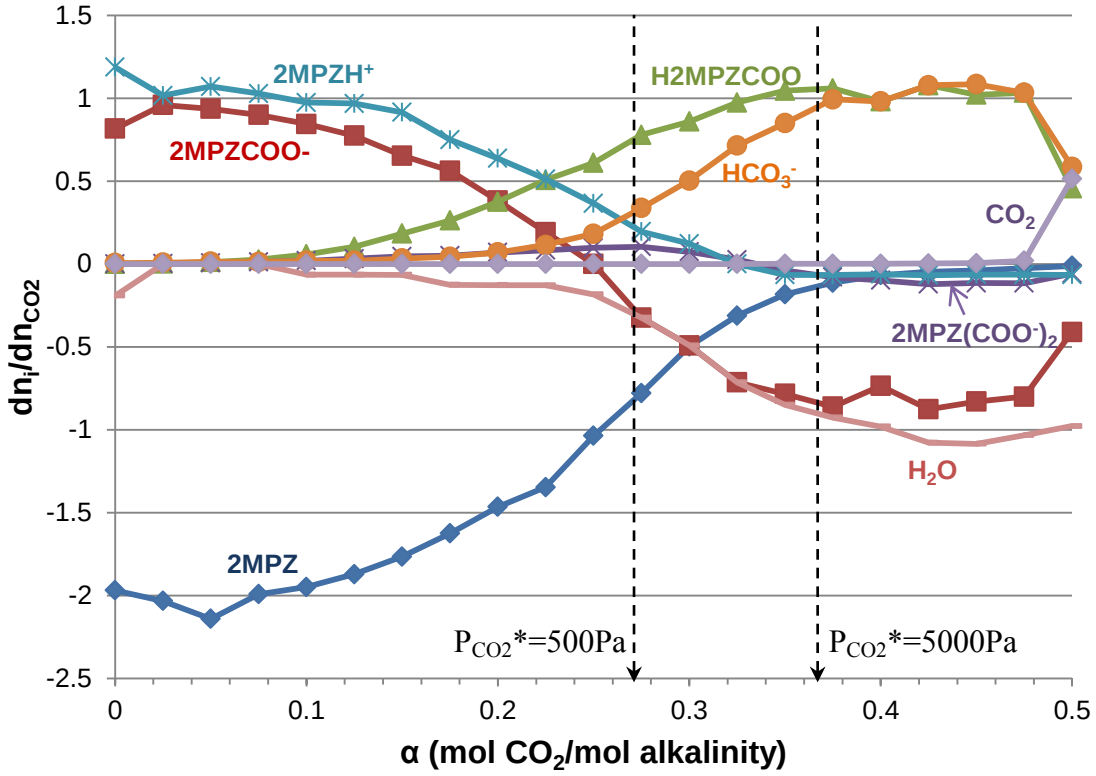

Figure 7.10: Reaction stoichiometry for 8 m 2MPZ at 40 °C.

Heat of Absorption

The heat of absorption (ΔH_{abs}) is an important thermodynamic property that represents the thermal effect as CO_2 is absorbed into an amine solvent. It is also equivalent to the minimal heat duty required to reverse the CO_2 absorption reactions and desorb CO_2 from the solvent. Therefore ΔH_{abs} is critical for estimation of energy performance for an amine solvent.

The calculation of ΔH_{abs} is done by applying Gibbs-Helmholtz equation (Eq. (4.2)) to the CO_2 fugacity ($f^*_{CO_2}$) predicted from the ENRTL model. A small change (0.1 K) in temperature (T) was introduced and the $f^*_{CO_2}$ value is calculated, and the

differential of $\ln f^*_{CO_2}$ with respect to $1/T$ is approximated by $\Delta\left(\ln f^*_{CO_2}\right)/\Delta(1/T)$. The heat absorption calculated in this way for 8 m 2MPZ at varied temperature is shown in Figure 7.11.

As CO_2 loading goes higher, bicarbonate formation, which comes with a low heat of reaction, gradually takes over the role of carbamate formation and starts to dominate CO_2 absorption due to the depletion of free amine, as shown in the reaction stoichiometry plot (Figure 7.10). As a result of that, the apparent ΔH_{abs} decreases dramatically with CO_2 loading. However, ΔH_{abs} is decreasingly dependent on CO_2 loading as temperature increases. At loading less than 0.25, ΔH_{abs} decreases slightly with temperature. This trend is reversed as loading is above 0.25 and ΔH_{abs} is greater at higher temperature. An analysis of the reaction stoichiometry at 140 °C and rich loading shows that 2MPZ concentration and the stoichiometric number for 2MPZ are higher than at 40 °C, and bicarbonate reaction is less important. This might explain the higher heat of absorption at higher temperature. Between the lean and the rich loading, ΔH_{abs} varies between 70 and 75 kJ/mol at 120 - 140 °C, which is expected to be the range of stripper temperature.

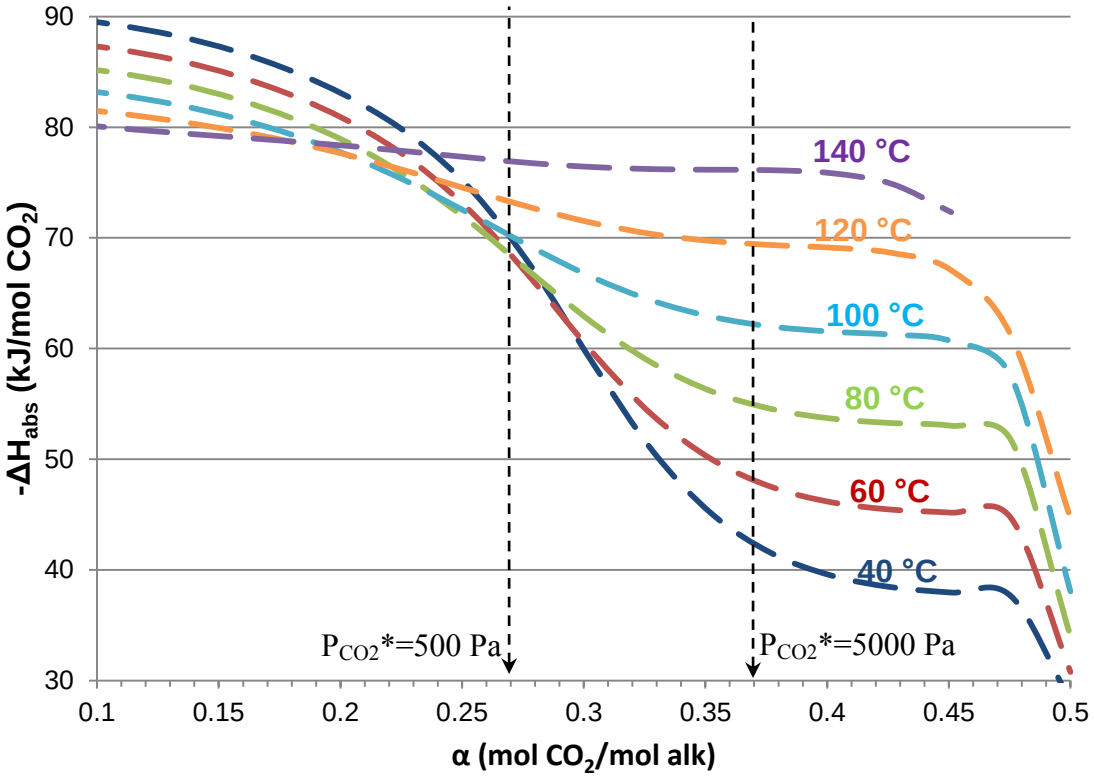

Figure 7.11: Heat of absorption calculated by the ENRTL model for 8 m 2MPZ.

7.5 CONCLUSIONS

A thermodynamic model was successfully developed for 8 m 2-methylpiperazine by sequential data regression in the framework of the ENRTL model. 2MPZ is modeled as a Henry's component instead of a solvent. pKa and volatility of 2MPZ in water is well represented by the model.

The prediction for CO_2 solubility and speciation is in good agreement with the experimental data. The standard free energy of formation, the standard enthalpy of formation for all carbamate species as well as binary interaction parameters included in the data regression were mostly slightly or moderately correlated to each other and have

small standard deviations compared to the final estimates. Additional small adjustment in rich CO_2 loading is necessary to properly represent the VLE data.

In 8 m 2MPZ at 40 °C, 2MPZ is depleted at CO_2 loading of 0.4. $2MPZCOO^-$ reaches maximum concentration around loading of 0.25 and decreases at the rich end. About 40% of the original 2MPZ is in the form of $2MPZH^+$ and the remainder is H2MPZCOO at 0.5 loading. Bicarbonate is an important species starting at $\alpha = 0.3$ and reaches 3.6 m at 0.5 loading, accounting for about 40% of the total dissolved CO_2.

The activity coefficients of 2MPZ and CO_2 slightly increase with CO_2 loading, while those of the ionic species decrease. H2MPZCOO has the lowest activity coefficient among all the species, which might be related to the property of a zwitterion ion but is more likely a consequence of the strong correlation of its standard Gibbs free energy of formation with the activity coefficient parameters.

Reaction stoichiometry shows that 2MPZ is the major reactant at lean loading and is consumed at 2:1 ratio when normalized to CO_2, resulting in the formation of equal mole carbamate and protonated 2MPZ. This ratio drops as CO_2 loading increases and the bicarbonate formation buffered by 2MPZ and $2MPZCOO^-$ becomes the major reaction above the lean loading.

Heat of absorption for 8 m 2MPZ decreases with CO_2 loading, but the dependence of it on CO_2 loading decreases as temperature increases. ΔH_{abs} is relatively constant at temperature from 120 – 140 °C, ranging from 70 – 75 kJ/mol in the operating CO_2 loading range. The dependence of heat of absorption on temperature is reversed at loading of 0.25.

Chapter 8: Kinetic Modeling of CO_2 Absorption into 2-Methylpiperazine

In a real amine scrubbing process, thermodynamic equilibrium is rarely encountered, and the assumption of instantaneous reactions is usually not valid except at very high temperature. Most of reactions proceed at a finite rate at absorber conditions. At stripper conditions, although the reversion of carbamate or bicarbonate to free CO_2 occurs at a very fast rate, mass transfer rate is limited by the diffusion of reactants and products. Therefore creation of rigorous rate-based kinetic models for CO_2 absorption into amine solvents is of critical importance for design and simulation of CO_2 capture process.

8.1 Literature Review

A number of efforts in developing kinetic models for CO_2 absorption into amine solvents have been reported. Freguia *et al.* (Freguia and Rochelle 2003) created a rate model for MEA on the basis of the thermodynamic model created by Austgen (Austgen, Rochelle et al. 1989). The kinetic constant for carbamate formation was obtained by matching pilot plant test data. Aboudheir *et al.* (Aboudheir, Tontiwachwuthikul et al. 2003) used the termolecular mechanism to interpret the kinetic data from measurements in a laminar jet for CO_2-loaded and concentrated MEA solution, and obtained rate constants through data regression. These kinetic data were also used by Plaza (Plaza, Wagener et al. 2009) to extract kinetic constants and develop a rigorous model for MEA in Aspen Plus®. Kucka (Kucka, Muller et al. 2003) created a numerical model for reactive absorption of CO_2 into MEA, and validated this model by implementing it to Aspen Custom Modeler. Culliane (Cullinane 2005) regressed kinetic constants based on the mass transfer data for absorption of CO_2 into PZ/K_2CO_3 in a Wetted Wall Column

and developed a rate model. Tobiesen (Tobiesen, Svendsen et al. 2007) developed a rigorous rate model for CO_2 absorption into MEA based on literature data and validated it against experimental results from a laboratory pilot plant.

Most of the previous kinetic modeling works were focused on the traditional amine solvent, MEA. The current study aims to develop a kinetic model for the novel amine solvent, 2MPZ, screened in this work. The kinetic characteristics of 8 m 2MPZ are investigated by fitting the wetted wall column (WWC) model created in Aspen Plus® to the mass transfer data obtained from the WWC experiments at 40 – 100 °C. The Bronsted theory is applied to correlate the rate constants of different reactions. Through regression of only two kinetic reaction rate constants and one diffusion activation energy, a majority of the measured CO_2 fluxes were fitted within ±20%. Sensitivity of the calculated liquid mass transfer coefficient to kinetic rates, diffusion coefficients and physical liquid mass transfer coefficient is analyzed. The liquid film concentration profiles are also examined for the lean and rich conditions at 40 and 100 °C.

8.2 MODEL DESCRIPTION

8.2.1 Flow Sheet

A Ratesep™ model was created in Aspen Plus® to simulate the experimental WWC. The flow sheet of this model is shown in Figure 8.1, which resembles the real flow diagram for the WWC (Figure 3.2).

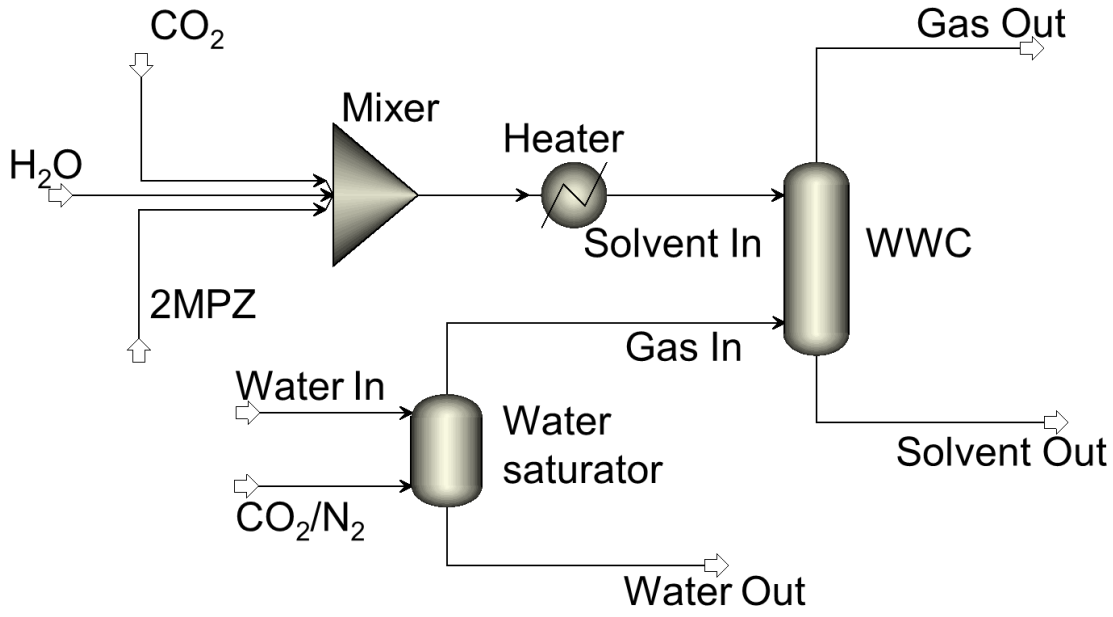

Figure 8.1: The flow sheet for the WWC model in Aspen Plus®.

CO_2, H_2O and the pure amine are mixed via a mixer to generate CO_2-loaded aqueous amine solution at desired amine concentration. The pressure and temperature of the solvent is varied by changing the operating conditions of the heater. The gas stream consisting of CO_2 and N_2 is contacted with water stream in a flash tank (water saturator) to be saturated with water vapor at experimental temperature. The saturated gas is then sent to the WWC and counter-currently contacted with the solvent entering from the top. The WWC is modeled as a three-stage Radfrac column equipped with an arbitrary type of random packing -- CMR. The Radfrac column has the same height (0.091 meter) as the WWC but the diameter of it is 100 times larger than that of the WWC. The same area/volume value is specified for the column model via a Fortran subroutine. As a result, the total contact surface area for gas and liquid is 10,000 times that of the experimentally used WWC (38.52 m^2 vs. 38.52 cm^2). To maintain the same gas and liquid velocity as in the WWC, the molar flow rate of the gas and liquid in the model are

10,000 times the gas and liquid molar flow rate in the WWC, respectively. The gas film mass transfer coefficient (k_g) and physical liquid film mass transfer coefficient (k_l^0) for the column in the model is also calculated with a Fortran subroutine, which uses the same correlations that were experimentally determined for the real WWC (Eq. (3.6) and (3.13)). The Chilton and Colburn analogy (Chilton and Colburn 1934) is used in this work for heat transfer coefficient correlation. The change in the temperature of gas and liquid stream is normally very small because of the excessive liquid flow rate compared to the gas flow rate. The absorption/desorption can thus be regarded as isothermal.

As described in Experimental Methods (Chapter 3), for a solvent at each loading and temperature, six inlet gas compositions corresponding to six values of CO_2 partial pressure were used to give both absorption and desorption CO_2 fluxes between the gas and the solvent. In order to simultaneously calculate all the desorption / absorption fluxes with the same solvent, six identical WWC were created in the same flow sheet. The inlet solvent stream for each is identical in each run of simulation, but the composition of the inlet gas is all different, corresponding to the six different inlet gas compositions used in the experiments. The inputs to the WWC model are measured variables including temperature, system pressure, liquid and gas flow rate and apparent liquid and gas composition. Chemical and physical properties including kinetic constants and diffusion coefficients are adjusted through the "Data Fit" block in Aspen Plus® to match the measured CO_2 flux data. The difference between the predicted fluxes y_i and the experimentally determined fluxes (y_{im}) weighted by the standard deviation (σ_{iy}), as well as the deviation between the reconciled inputs (x_i) and the measured inputs (x_{im}) weighted by σ_{ix} are taken into account in the objective function to be minimized, as shown in the following equation:

$$F_{obj} = \frac{1}{2}\left\{\sum\left[\left(x_i - x_{im}\right)/\sigma_{ix}\right]^2 + \sum\left[\left(y_i - y_{im}\right)/\sigma_{iy}\right]^2\right\} \quad (8.1)$$

The only input allowed to be adjusted in this work is CO_2 loading. The adjustment in CO_2 loading is done through varying the flow rate of the CO_2 stream going to the mixer, and is specified to be no more than 5%.

8.2.2 Physical Properties

8.2.2.1 Density

The molar volume or the density is required for conversion of molar flow rate to volume flow rate, and thus affects the calculation of liquid velocity in the column and liquid-gas contact time. The density data for 8 m PZ and 4 m 2MPZ / 4 m PZ have been reported by Freeman (Freeman 2011), who also developed a correlation for density as a function of temperature and CO_2 loading:

$$\rho / \rho_{H_2O} = a + b[CO_2] + c[Am] \quad (8.2)$$

where ρ is the density of the aqueous amine solution, and ρ_{H_2O} is the water density at the experimental temperature. The concentration of total CO_2 and amine are in the unit of mol/kg solvent. The density of 8 m 2MPZ at variable loading was measured in this work. The empirical model as shown in Eq. (8.2) is applied to the amine solvents mentioned above and the regression results for the coefficients are shown in Table 8.1. Since the density measurement was done at just one concentration for PZ/2MPZ and 2MPZ, the dependence on amine concentration cannot be determined (c = 0).

Table 8.1: Coefficients of the empirical density model (Eq. (8.2)) for 8 m PZ, 8 m 2MPZ and 4 m 2MPZ / 4 m PZ.

Amine	*a*	*b*	*c*
8 m PZ (Freeman 2011)	0.991	0.0407	0.008

8 m 2MPZ	1.018	0.0408	0
4 m 2MPZ/ 4 m PZ	1.025	0.0404	0

The comparison of the experimental density data to the calculation results from Eq. (8.2) for the three solvents are shown in Figure 8.2 through Figure 8.4. The model seems to slightly underestimate the density at 20 °C, however it represents the data at 40 and 60 °C very well.

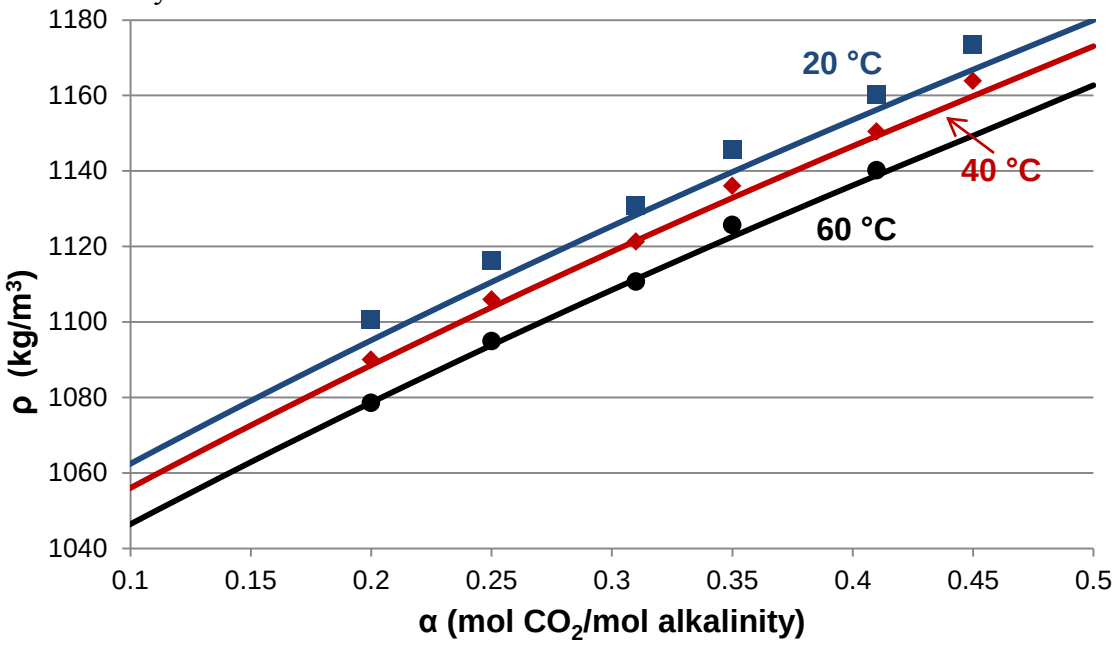

Figure 8.2: Comparison of the density model (lines) and the experimental density data for 8 m PZ from 20 to 60 °C (Freeman 2011).

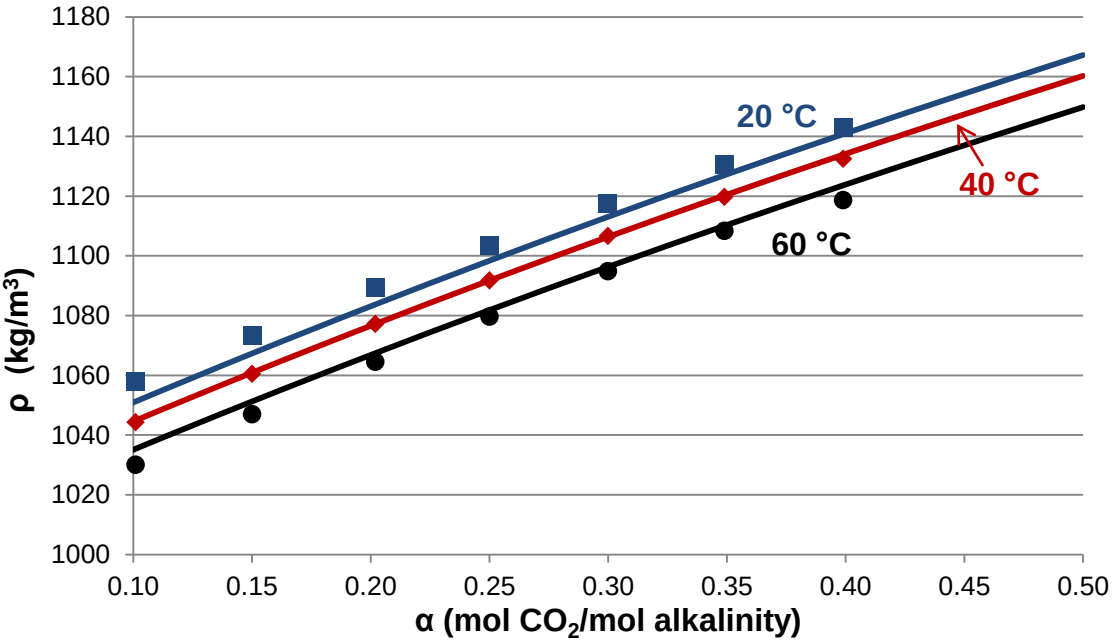

Figure 8.3: Comparison of the density model (lines) and the experimental density data for 8 m 2mPZ from 20 to 60 °C.

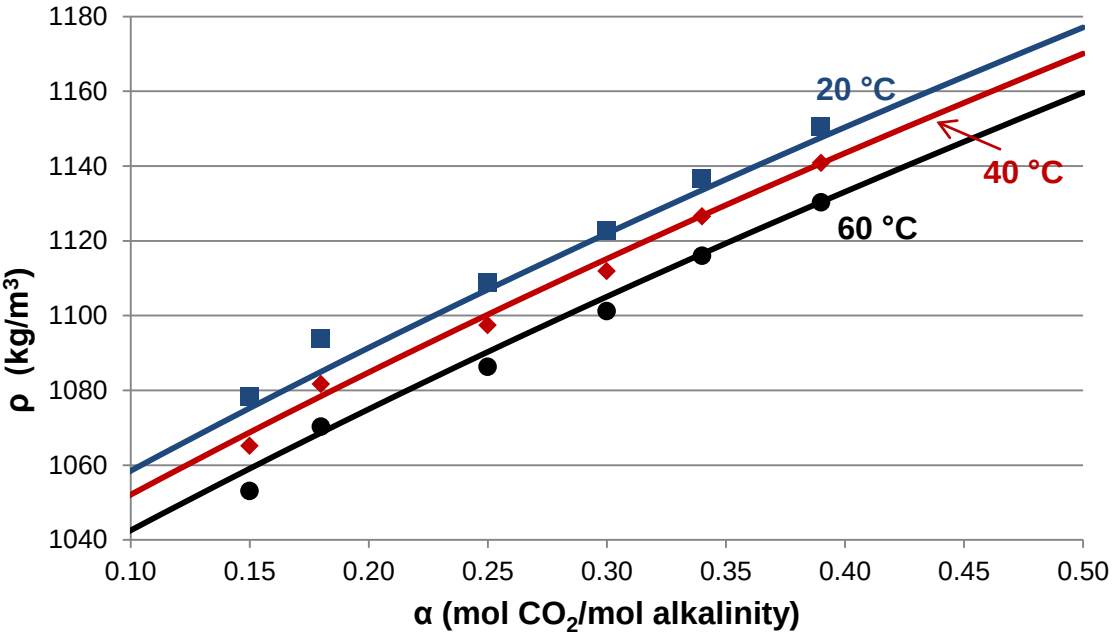

Figure 8.4: Comparison of the density model (lines) and the experimental density data for 4 m 2mPZ / 4 m PZ from 20 to 60 °C.

8.2.2.2 Viscosity

Proper representation of viscosity as a function of temperature and CO_2 loading is important for kinetic modeling since diffusion coefficient is strongly dependent on viscosity. The viscosity model used by Freeman for concentrated PZ (Eq. (8.3)) is taken for correlating the viscosity of 8 m 2MPZ and 4 m 2MPZ / 4 m PZ to the content of CO_2 and amine, as shown in the following equation:

$$\ln\left(\eta / \eta_{H_2O}\right) = a + \left(b_1 + \frac{b_2}{T}\right)[CO_2] + \left(c_1 + \frac{c_2}{T}\right)[Am] + \left(d_1 + \frac{d_2}{T}\right)[CO_2][Am] \quad (8.3)$$

where η is the viscosity of the aqueous amine solution, and η_{H_2O} is the water viscosity at the experimental temperature. The concentration of the total CO_2 and amine are in the unit of mol/kg solution. The parameter values for 8 m PZ, 8 m 2MPZ and 4 m 2MPZ / 4 m PZ are shown in Table 8.2. Comparisons of the model predictions to the experimental data shown in Figure 8.5 through Figure 8.7 demonstrate that the model is capable of adequately representing the viscosity of 8 m PZ, 8 2MPZ and 4 m 2MPZ / 4 m PZ at experimental conditions.

Table 8.2: Coefficients in the empirical viscosity model (Eq. (8.3)) for 8 m PZ, 8 m 2MPZ and 4 m 2MPZ / 4 m PZ.

Amine	a	b_1	b_2	c_1	c_2	d_1	d_2
8 m PZ (Freeman 2011)	1.723	2.63	-778	-1.019	355.2	-0.527	169.3
8 m 2MPZ	-4.634	-3.765	1587	0	506.1	1.171	-411.0
4 m 2MPZ/ 4 m PZ	-3.434	25.58	-7124	0	407.0	-5.75	1636

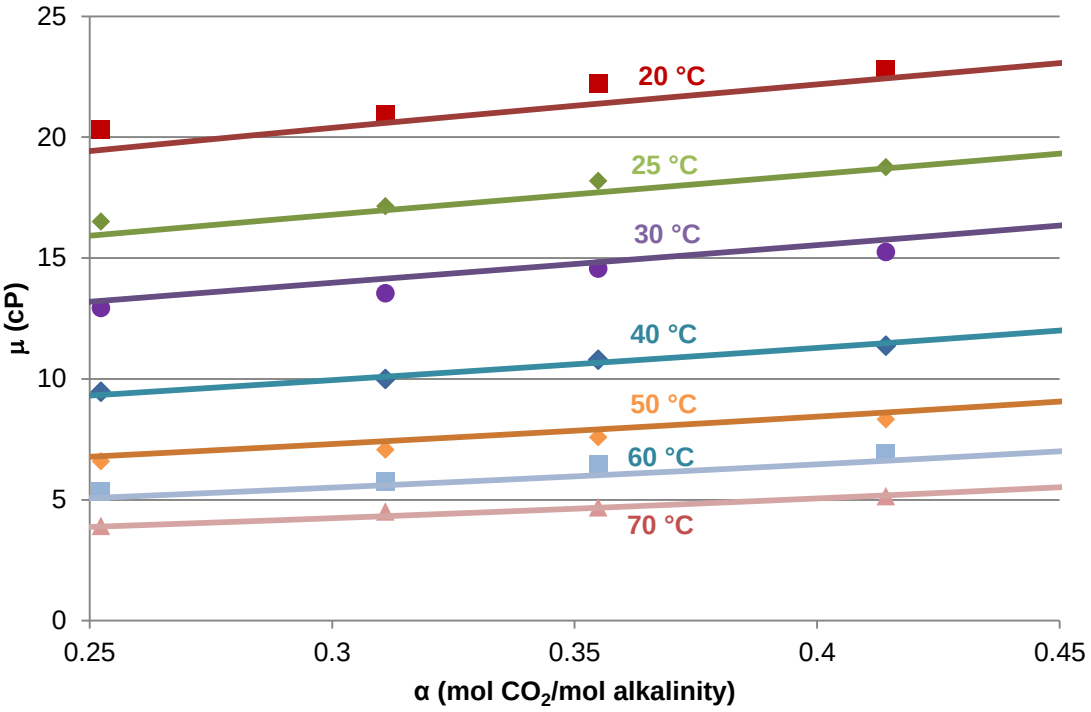

Figure 8.5: Comparison of the empirical viscosity model (lines) and the experimental viscosity data for 8 m PZ from 20 to 70 °C (Freeman 2011).

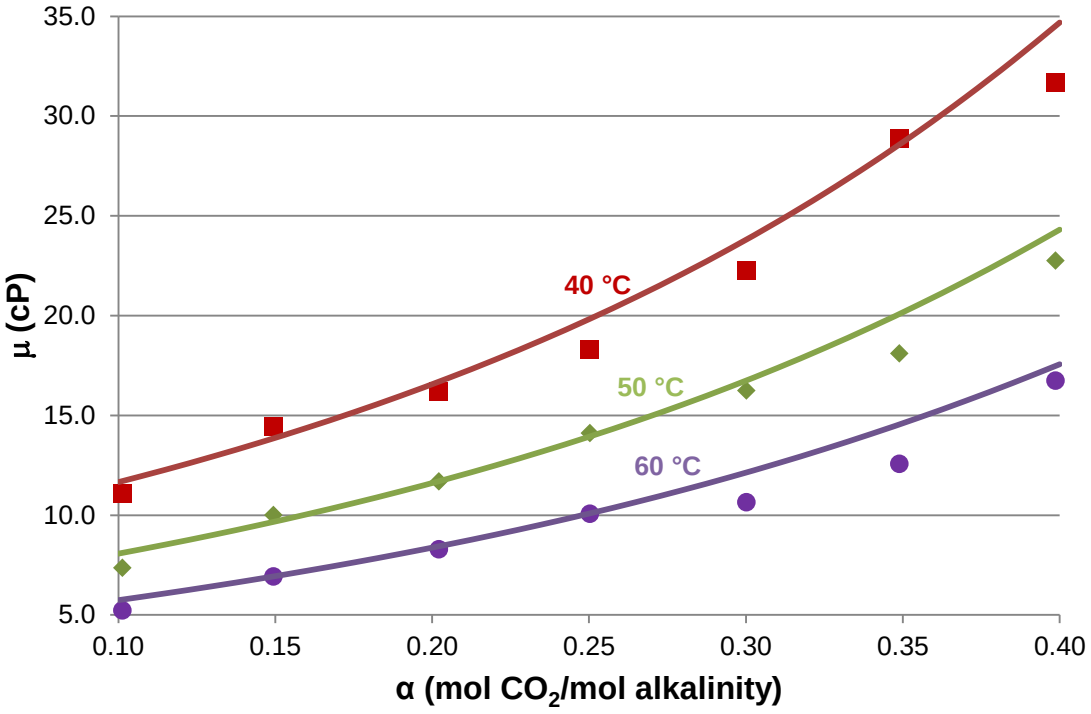

Figure 8.6: Comparison of the empirical viscosity model (lines) and the experimental viscosity data for 8 m 2MPZ from 40 to 60 °C.

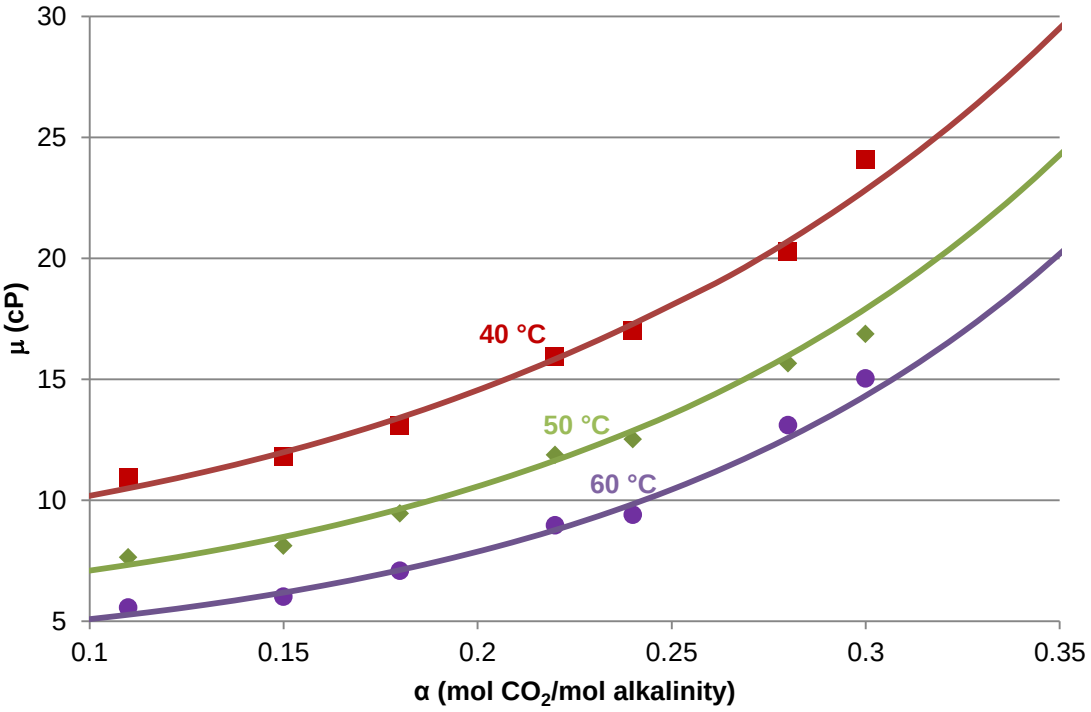

Figure 8.7: Comparison of the empirical viscosity model (lines) and the experimental viscosity data for 4 m 2MPZ / 4 m PZ from 40 to 60 °C (Freeman 2011).

8.2.2.3 Diffusion Coefficients

Because of the high reactivity of CO_2 with amine, it is not possible to directly measure the diffusivity of CO_2 in an amine solvent. This difficulty was overcome by using nonreactive N_2O as a CO_2 analogy because of their similarities in molecular volume, configuration and electronic structure (Versteeg and Van Swaalj 1988). A general correlation for the dependence of the CO_2 diffusivity in aqueous alkanolamine solutions on the solvent viscosity was derived by Versteeg and coworks (Versteeg and Van Swaalj 1988):

$$\left(\eta^{0.8} D_{CO_2}\right)_{Am} = \left(\eta^{0.8} D_{CO_2}\right)_{water} = Const. \tag{8.4}$$

The diffusivity of CO_2 in water has been well studied and can be described by the following equation (Versteeg and Van Swaalj 1988):

$$D_{CO_2} = 2.35\times10^{-6}\exp(-2119/T) \quad m^2/s \tag{8.5}$$

Equation (8.4) and (8.5) was adopted in this work for representation of the binary diffusion coefficients of CO_2 in any other components. This ensures the effective CO_2 diffusivity in the solution equal to the reported experimental value.

Dugas measured the effective diffusivity of all the species in loaded MEA and PZ aqueous solution at 30 °C with a diaphragm cell (Dugas 2009). The measured diffusivity was correlated to solution viscosity (η, cP) and temperature (T, K) as shown in Eq. (8.6). The measurements were done at only one temperature, and the temperature dependence of the diffusion coefficient in his correlation is taken from the Wilke-Chang correlation for dilute solution (Wilke and Chang 1955).

$$D_{Am}(m^2/s) = 8.2\times10^{-10}\eta^{-0.72}\left(\frac{T}{303.15}\right) \tag{8.6}$$

The binary diffusivity of all molecular and ionic species other than CO_2 (D_{Am}) in any other species in loaded 2MPZ at 30 °C is assumed to have the same value as reported by Dugas for MEA and PZ solution. However, the dependence of the diffusivity on temperature is expressed in a different form as shown in Eq. (8.7), which is similar to that used for CO_2 diffusivity in Eq. (8.5).

$$D_{Am} = 8.2\times10^{-10}\eta^{-0.72}\exp\left(-\frac{A}{R}\left(\frac{1}{T}-\frac{1}{303.15}\right)\right) \tag{8.7}$$

A is used as an adjustable parameter in this work to take into account the unknown dependence of D_{Am} on temperature. It is similar to but different from diffusion activation energy (E_D). The effect of temperature on the diffusivity in loaded amine solution is still not clear since there has been very few data reported in the currently available literature. The exponent term in Eq. (8.7) basically accounts for the additional impact of temperature on diffusivity other than the effect of changing viscosity. Snijder and coworkers (Snijder, te Riele et al. 1993) measured the diffusion coefficient for

several aqueous amines, and found that the dependence of the diffusivity of amine in water on temperature can be represented well with the exponential function. The same form was used by Chang *et al.* (Chang, Lin et al. 2004) to describe their diffusivity data as a function of temperature for aqueous amine at 30 – 70 °C. However, both works did not include viscosity in their correlations.

The correlations for the physical properties mentioned above are input to Aspen Plus® through Fortran subroutines. All the subroutines used in this work have been documented in Appendix E.

8.2.3 Multicomponent Mass Transfer

The average diffusion coefficient of a component in a mixture calculated from certain mixing rule does not have quantitative application in Aspen Plus®. Instead, a rigorous multicomponent mass transfer theory (Krishna and Standart 1976; Krishna 1977; Krishna and Wesselingh 1997) involving the Maxwell-Stephan equation is employed by Aspen Rate-Based model to evaluate multicomponent mass transfer rates (component number = n), as shown in the following equation:

$$([N]-N_t[x])=[R]^{-1}\left[[\Gamma]([x^I]-[x])+\Delta\phi^E([x][z])\right] \tag{8.8}$$

where $[N]$, $[x]$ and $[x^I]$ are the column vectors of length (n-1) for flux, bulk composition and interfacial composition, respectively. $N_t=\sum_{i=1}^{n}N_i$ is the total mass transfer flux. If electrolyte is present in the solution, $\Delta\phi^E([x][z])$ is the driving force caused by electric potential which is adjusted to satisfy electroneutrality. $[\Gamma]$ is a (n-1) × (n-1) matrix correcting for the non-ideal thermodynamic behavior.

$$\Gamma_{ik}=\delta_{ik}+x_i\left.\frac{\partial\ln\gamma_i}{\partial x_k}\right|_{T,P,x_{j\neq k=1,2,\ldots,n-1}} \tag{8.9}$$

where δ_{ik} = 0 if $i \neq k$ and δ_{ik} = 1 if $i = k$. In this work, non-ideality correction is not applied, so $[\Gamma]$ is replaced by the identity matrix.

$[R]$ has a dimension of (n-1) × (n-1) as well, whose elements is described by the following equation:

$$R_{ii} = \frac{x_i}{\bar{\rho}\kappa_{in}} + \sum_{\substack{k=1 \\ k\neq i}}^{n} \frac{x_k}{\bar{\rho}\kappa_{ik}} \quad \text{for i=1, 2, …, n-1}$$

$$R_{ik} = -x_i\left(\frac{1}{\bar{\rho}\kappa_{ik}} - \frac{1}{\bar{\rho}\kappa_{in}}\right) \quad \text{for i=1, 2, …, n-1, i≠k} \tag{8.10}$$

in which $\bar{\rho}$ is the average molar density and κ_{ik} represents the binary mass transfer coefficients in a multicomponent mixture.

If the electric potential driving force is neglected, Eq. (8.8) can be further simplified to

$$[N] = [k][\Delta x] + N_t[x] \tag{8.11}$$

in which $[k]$ is a (n-1)×(n-1)-dimensional matrix of multicomponent mass transfer coefficients:

$$[k] = [R]^{-1}[\Gamma] = [R]^{-1} \tag{8.12}$$

$[\Delta x]$ is composition difference driving force:

$$[\Delta x] = [x^I] - [x] \tag{8.13}$$

The binary mass transfer coefficient κ_{ik} in this work is calculated from the binary diffusion coefficient D_{ik} using the following equation:

$$\kappa_{ik} = k_j^0 D_{ik}^{\alpha} = \left(\frac{3^{1/3}2^{1/2}}{\pi^{1/2}}\right)\left(\frac{Q^{1/3}h^{1/2}W^{2/3}}{A}\right)\left(\frac{g\rho}{\mu}\right)^{1/6} D_{ik}^{0.5} \tag{8.14}$$

This correlation is similar to Eq. (3.13).

In this work, since $D_{ik} = D_{ij}$ for $k \neq j$, $\kappa_{ik} = \kappa_{ij}$ for $k \neq j$. Therefore,

$$R_{CO_2,CO_2} = \frac{x_i}{\bar{\rho}\kappa_{in}} + \sum_{\substack{k=1 \\ k\neq i}}^{n} \frac{x_k}{\bar{\rho}\kappa_{ik}} = \frac{1}{\bar{\rho}\kappa_{CO_2}} \quad \text{and} \quad R_{CO_2,k} = -x_i\left(\frac{1}{\bar{\rho}\kappa_{ik}} - \frac{1}{\bar{\rho}\kappa_{in}}\right) = 0 \tag{8.15}$$

$$k_{CO_2,CO_2} = \overline{\rho}\kappa_{CO_2} \text{ and } k_{CO_2,k} = 0 \tag{8.16}$$

The flux for CO_2 can be calculated from Eq. (8.11)

$$N_{CO_2} = \overline{\rho}\kappa_{CO_2}\left(x^I_{CO_2} - x_{CO_2}\right) + x_{CO_2}N_t \tag{8.17}$$

Computation of N_{CO_2} requires an iterative procedure since N_{CO_2} is needed for calculation of N_t. If x_{CO_2} has a very small value (e.g. at very lean loading), N_{CO_2} is proportional to κ_{CO_2} and $D^{0.5}_{CO_2}$.

8.2.4 Reactions

The single-step termolecular reaction mechanism is used in this work to model the reaction rate between CO_2 and amine solvents, as shown in the following reaction:

$$Am + CO_2 + B \leftrightarrow AmCOO^- + BH^+ \tag{8.18}$$

The reaction rate is expressed in the form of the product of the kinetic rate constant and the activity of reactants. As an example, the following forward and reverse reaction rates with respect to CO_2 can be written for Reaction (8.18):

$$r_f = -k_f a_{Am} a_{CO_2} a_B \tag{8.19}$$

$$r_r = k_r a_{AmCOO^-} a_{BH^+} \tag{8.20}$$

where k_f and k_r are the forward and reverse rate constant, respectively. They are correlated to each other by the equilibrium constant (K_{eq}):

$$k_r = \frac{k_f}{K_{eq}} \tag{8.21}$$

K_{eq} can be obtained from the equilibrium composition and activity coefficients of reactants and products calculated from the thermodynamic model, as shown in Eq. (7.8). The overall reaction rate is therefore equal to

$$r_{CO_2} = r_f + r_r = -\left(k_f a_{Am} a_{CO_2} a_B - k_r a_{AmCOO^-} a_{BH^+}\right) = -k_f\left(a_{Am} a_{CO_2} a_B - \frac{a_{AmCOO^-} a_{BH^+}}{K_{eq}}\right) \tag{8.22}$$

In Aspen Plus®, a power-law kinetic expression is implemented to represent the temperature effect on reaction rate constant:

$$k = k_0\left(\frac{T}{T_0}\right)^n \exp\left[-\frac{E}{R}\left(\frac{1}{T}-\frac{1}{T_0}\right)\right] \tag{8.23}$$

where k_0 is the pre-exponential constant; T_0 is the reference temperature; E is the reaction activation energy. $T_0 = 313.15$ K and $n = 0$ is used throughout this work.

Based on the speciation study and the thermodynamic model discussed in Chapter 7, the species in aqueous 2MPZ that are capable of forming carbamate with CO_2 include $2MPZ$, $2MPZCOO^-$ and $2MPZH^+$. Consequently the following kinetic reactions are taken into account:

$$2MPZ + CO_2 + B \leftrightarrow 2MPZCOO^- + BH^+ \tag{8.24}$$

$$2MPZCOO^- + CO_2 + B \leftrightarrow 2MPZ(COO^-)_2 + BH^+ \tag{8.25}$$

$$2MPZH^+ + CO_2 + B \leftrightarrow H2MPZCOO + BH^+ \tag{8.26}$$

The bases (B) included in the reaction set above are $2MPZ$, $2MPZCOO^-$ and H_2O. The concentration of OH^- as a base is very small and has a negligible effect on the total reaction rate, therefore it is excluded from consideration. The pK_a value for $2MPZH^+$ is very low, leading to a very small reaction rate compared to other stronger bases, so $2MPZH^+$ is not accounted for as a base in this work.

$2MPZ$ and $2MPZCOO^-$ can also catalyze the hydrolysis of CO_2 as shown in the following reactions:

$$2MPZ + CO_2 + H_2O \leftrightarrow HCO_3^- + 2MPZH^+ \tag{8.27}$$

$$2MPZCOO^- + CO_2 + H_2O \leftrightarrow HCO_3^- + H2MPZCOO \tag{8.28}$$

Because of the large number of possible kinetic reactions, it is not feasible to independently regress each reaction rate constant in a statistically meaningful manner. To simplify the problem, the Bronsted theory is used in this work to correlate the rate constants to the pKa of the participating amines and bases. Cullinane (Cullinane 2005)

regressed reaction rate constants for aqueous PZ and found that the following Bronsted correlation hold true for carbamate formation reactions with respect to termolecular mechanism:

$$\ln k_{Am-b_2} = \ln k_{Am-b_1} + 0.457(pK_{a,b_2} - pK_{a,b_1}) \tag{8.29}$$

Based on the correlation above, the natural logarithm value of the reaction rate constant involving PZ species with CO_2 is proportionally related to the pKa value of the catalyzing base with a slope of 0.457. Analysis done by Cullinane in the same work also suggested that a similar relationship between base strength and rate constants is applicable for other amines with the Bronsted slope close to 0.5. Due to the similar ring structure of PZ and 2MPZ, Eq. (8.29) is assumed to be applicable as well to the reactions involving 2MPZ species.

For the different amines catalyzed by the same base, if the amine structure is very close to each other, the same factor of 0.457 is applied to account for the effect of the basic strength of amine on rate constant, as shown in the following equation:

$$\ln k_{Am_2-b} = \ln k_{Am_1-b} + 0.457(pK_{a,Am_2} - pK_{a,Am_1}) \tag{8.30}$$

Eq. (8.30) is used to quantify the change in the carbamate formation rate as 2MPZ is protonated to $2MPZH^+$.

Versteeg *et al.* (Versteeg and Van Swaaij 1988) summarized the kinetic data for the reactions between tertiary amines and CO_2, and correlated the reaction rate of hydrolysis of CO_2 to the basic strength of the catalyzing base with a linear relationship:

$$\ln k_2 = pKa - 14.24 \tag{8.31}$$

Eq. (8.31) is adapted in this work to correlate the bicarbonate formation rate catalyzed by different bases except $2MPZCOO^-$, as shown by the following equation:

$$k_{2,b_1} / k_{2,b_2} = \exp\left(pKa_{b_1} - pKa_{b_2}\right) \tag{8.32}$$

The pKa values for the bases existing in the system and the ratio of reaction rate constants according to Eq. (8.29), (8.30) and (8.32) are shown in Table 8.3. The contribution of H_2O, OH^- and CO_3^{2-} to the overall bicarbonate formation reaction is found to be negligible and thus excluded from the reaction set. The pKa value predicted for 2MPZCOO$^-$ from the thermodynamic model is subject to an uncertainty of as high as ±2.5 due to the standard deviation of the obtained standard property values for 2MPZCOO$^-$ and H2MPZCOO, so the model predicted value is not used. Instead, the difference in the pKa of 2MPZCOO$^-$ and that of 2MPZ is assumed to be equal to the difference between the pKa of PZ (Hetzer, Robinson et al. 1968) and PZCOO$^-$ (Ermatchkov, Kamps et al. 2003), and the estimated pKa value for 2MPZCOO$^-$ is 8.87. Even though the ratio of bicarbonate formation rate constant is calculated from Eq. (8.32) for 2MPZCOO$^-$ as listed in Table 8.3, the rate constant for bicarbonate formation reaction with 2MPZCOO$^-$ (Reaction (8.34)), $k_{2,2MPZCOO^-}$, is not linked to that for bicarbonate formation with 2MPZ, $k_{2,2MPZ}$ (Reaction (8.33)) through the Bronsted Theory. They will be independently determined. The hypothesis is that, as a hindered amine, 2MPZCOO$^-$ could catalyze the formation of bicarbonate with formation of dicarbamate followed by hydrolysis, which would possibly have a much higher rate than what would be expected.

$$2MPZ + CO_2 + H_2O \leftrightarrow HCO_3^- + 2MPZH^+ \tag{8.33}$$

$$2MPZCOO^- + CO_2 + H_2O \leftrightarrow HCO_3^- + H2MPZCOO \tag{8.34}$$

For each amine, the carbamate formation reactions having 2MPZ as the catalyzing base are used as the reference case. The reaction rate constants are ratioed to that of one of the following two reactions:

$$2MPZ + CO_2 + 2MPZ \leftrightarrow 2MPZCOO^- + 2MPZH^+ \tag{8.35}$$

$$2MPZCOO^- + CO_2 + 2MPZ \leftrightarrow 2MPZ(COO^-)_2 + 2MPZH^+ \tag{8.36}$$

Table 8.3: Molality-based pKa of the bases and the ratio of kinetic reaction constants used in this work for 8 m 2MPZ.

		Bases				
		$2MPZ$	$2MPZCOO^-$	H_2O	OH^-	CO_3^{2-}
pKa		9.16 [a]	8.87 [b]	-1.74	15.74	10.33
Bicarbonate formation $k_{2,b}$ [c]		1	0.75	1.8E-5	7.2E+2	3.2
	Amine					
Carbamate formation reaction rate k_{Am-b}	$2MPZ$ [d]	1	0.88	6.9E-3	2.0	1.7
	$2MPZH^+$ [d]	0.14	0.13	9.9E-4	2.9	0.25
	$2MPZCOO^-$ [e]	1	0.88	6.9E-3	2	1.7

a: (Khalili, Henni et al. 2009)
b: Estimated from pka of 2MPZ, PZ and $PZCOO^-$.
c: Ratio to $k_{2,2MPZ}$ for Reaction (8.33) based on Eq. (8.31).
d: Ratio to $k_{2MPZ-2MPZ}$ for Reaction (8.35).
e: Ratio to $k_{2MPZCOO^- -2MPZ}$ for Reaction (8.36).

CO_2 can also directly react with H_2O and OH^- and form bicarbonate.

$$CO_2 + H_2O \leftrightarrow HCO_3^- + H^+ \tag{8.37}$$

$$CO_2 + OH^- \leftrightarrow HCO_3^- \tag{8.38}$$

However, the contribution of these two reactions is usually negligible. Reaction of CO_2 with H_2O is much slower than other reactions involving amine. This can be also seen from the $k_{2,b}$ value for H_2O in Table 8.3. The contribution of OH^- has been shown to be unimportant as well due to the severe depletion at the interface of gas and liquid. (Glasscock and Rochelle 1989; Littel, Van Swaaij et al. 1990). Therefore Reaction (8.37) and (8.38) are not taken into account in the kinetic model of this work.

In addition to the kinetic reactions mentioned above, the following reactions are accounted for in the model as equilibrium reactions since they involve exchange of proton only.

$$2H_2O \leftrightarrow H_3O^+ + OH^- \tag{8.39}$$

$$HCO_3^- + H_2O \leftrightarrow CO_3^{2-} + H_3O^+ \tag{8.40}$$

$$2MPZH^+ + H_2O \leftrightarrow 2MPZ + H_3O^+ \tag{8.41}$$

$$H2MPZCOO + H_2O \leftrightarrow 2MPZCOO^- + H_3O^+ \tag{8.42}$$

8.2.5 Film Discretization

To more accurately calculate the concentration profile across the boundary layer next to the interface of gas and liquid, the liquid film is usually further divided into multiple segments or regions (i.e. film discretization). The mass balance and energy balance is applied to each segment.

The steady state equation of continuity along with the Maxwell-Stephan equation is solved by Aspen Plus® for each component in each film segment.

$$\nabla \cdot N_i = r_i \text{, i = 1, 2, …, n-1} \tag{8.43}$$

The reaction rate and mass transfer coefficient are evaluated at a point within each film segment, the position of which is adjusted with reaction condition factor and the transfer condition factor, respectively. These two factors are defaulted at 0.5.

Film discretization is important for modeling the mass transfer enhanced by fast chemical reaction, in which the concentration of CO_2 changes dramatically in the boundary layer. The choice of the number of segments as well as the relative thickness of each segment is critical. Too many segments would adversely affect the computation time and convergence stability. Asprion *et al.* (Asprion and Pantelides 2006) suggested

that most of the film segmentation should be placed at the region where the sharpest change in concentration occurs.

The film discretization implemented in this work is presented in Table 8.4.

Table 8.4: Film discretization used in this work. δ: the dimensionless distance from the interface of a segmentation point.

Point	δ	Point	δ	Point	δ
1	1.00E-06	18	0.000476	35	0.0106
2	2.00E-06	19	0.000571	36	0.0127
3	4.00E-06	20	0.000685	37	0.0152
4	8.00E-06	21	0.000822	38	0.0182
5	1.60E-05	22	0.000986	39	0.0219
6	3.20E-05	23	0.00118	40	0.0263
7	6.40E-05	24	0.00142	41	0.0315
8	7.68E-05	25	0.0017	42	0.0378
9	9.22E-05	26	0.00204	43	0.0454
10	0.000111	27	0.00245	44	0.059
11	1.33E-04	28	0.00294	45	0.0826
12	0.000159	29	0.00353	46	0.124
13	1.91E-04	30	0.00424	47	0.198
14	0.000229	31	0.00509	48	0.317
15	2.75E-04	32	0.00611	49	0.507
16	0.00033	33	0.00733	50	0.862
17	3.96E-04	34	0.00879	51	1.0

A liquid film typically has a thickness of 1 – 2 mm (10^{-3} m), and the dimension for a gas molecule is in the order of magnitude 1 – 10 Angstrom (10^{-10} -10^{-9} m). Hence 1E-6 of the film thickness is approaching the size of the molecule and should be the lower limit of the film thickness used. The region between 1E-1 and 1 is very close to the bulk of the solution and there should not be dramatic change. If the diffusion of molecules is taken into account, the region between 1E-4 to 1E-1 is approximately where the steepest variation in concentration is expected to happen. The visualized distribution of the film discretization in Figure 8.8 shows that a high portion of the film is placed in

the region of 1E-4 to 1E-1 to correctly capture the concentration variation. The concentration profile for different operating conditions will be shown later to examine the validity of this film discretization.

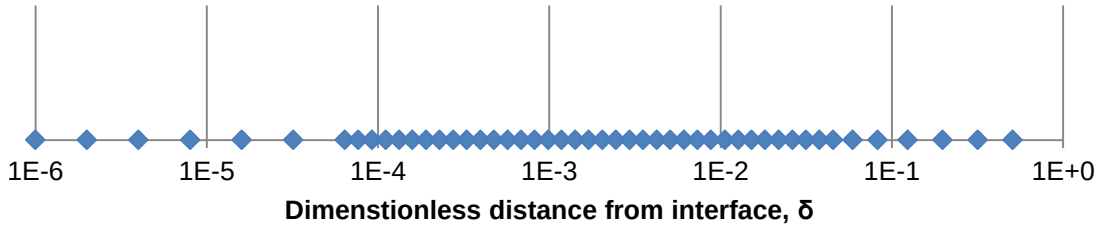

Figure 8.8: The grid distribution in the liquid film. 0 represents the interface and 1 represents the bulk.

8.3 MODEL RESULTS

8.3.1 Regression Results

The experimental WWC data for 8 m 2MPZ over the loading range of 0.10 – 0.37 mol CO_2 / mol alkalinity and the temperature range of 40 – 100 °C were used for data regression.

The reaction rate constant at 40 °C for $k_{2,2MPZ}$ (Reaction (8.33)) is estimated from the results reported by Ko and coworkers for MDEA (Ko and Li 2000) since their results are representative of previous kinetic measurements for MDEA. The kinetic rate was further corrected with the Bronsted theory using Eq. (8.32) to be used for 2MPZ. The pKa value for MDEA was taken from the result reported by Hamborg *et al.* (Hamborg, Niederer et al. 2007), and the first pKa for 2MPZ is based on the value reported by Khalili *et al.* (Khalili, Henni et al. 2009). Conversion from concentration-based reaction rate to activity based reaction rate is also necessary. $k_{2,2MPZCOO^-}$ for reaction (8.34) is one of the parameters included in data regression. The activation

energy for Reaction (8.33) and Reaction (8.34) is approximated with the value reported for MDEA (Ko and Li 2000).

Studies by Bishnoi (Bishnoi and Rochelle 2000) and Cullinane (Cullinane 2005) showed that the activation energy for the PZ carbamate formation reaction has a value of ~ 35 kJ/mol. This value was used by Dugas in the development of a spreadsheet model for absorption of CO_2 into PZ (Dugas 2009). The same activation energy (E) of 35 kJ/mol is also used in this work for the carbamate formation with 2MPZ (Reaction (8.35)) and the dicarbamate formation reaction (8.36). All the other reactions are assumed to have the same activation energy as the corresponding reaction that they are referenced to.

The parameters that were included for regression are k_f at 40 °C for Reaction (8.34), (8.35), (8.36), and the quasi-diffusion activation energy A in Eq. (8.7) for the diffusivity of all the non-CO_2 species. The default values and the regressed values for different parameters are summarized in Table 8.5.

Table 8.5: Default and regressed parameters in the regression of the WWC data for 8 m 2MPZ at 40 – 100 °C and 0.102 - 0.365 mol CO_2 / mol alkalinity.

Parameters	Estimates	Std. Dev.	Source
$k_{2MPZ-2MPZ}$ (kmol/m^3·s)	1.94E+10	4.0E+4	Regression in this work
$k_{2MPZCOO^--2MPZ}$ (kmol/m^3·s)	6.19E+10	1.1E+9	Regression in this work
$k_{2,2MPZCOO^-}$	1.65E+8	1.1E+7	Regression in this work
A (kJ/mol)	2.0	0.1	Regression in this work
$k_{2,2MPZ}$ (kmol/m^3·s)	9.83E+4	n/a	(Ko and Li 2000)
$E_{2MPZ-2MPZ}$ (kJ/mol)	35.0	n/a	PZ (Cullinane 2005; Dugas 2009)
$E_{2,2MPZ}$ (kJ/mol)	44.9	n/a	(Ko and Li 2000)

As can be seen from the table, the regression returns estimates for all the regressed parameters and relatively small standard deviations. The calculation of the covariance matrix for the regression shows that all the regressed parameters are very weakly correlated to each other. The greatest correlation is -0.65 for $k_{2,2MPZCOO^-}$ with $k_{2MPZCOO^--2MPZ}$.

The value obtained for $k_{2MPZ-2MPZ}$ at 40 °C is 1.94×10^{10} kmol/m^3·s, which has the same order of magnitude as the value of 6.12×10^{10} kmol/m^3·s for the carbamate formation reaction rate constant k_{PZ-PZ} for 8 m PZ obtained by Frailie (Frailie 2011). From the view point of the number of available unhindered amino group on each molecule, kinetics for 2MPZ is expected to be slightly slower than that for PZ. Cullinane *et al.* (Cullinane and Rochelle 2006) used concentration-based rate expression

and obtained a value of 7.0×10^4 $m^6/kmol^2\cdot s$ for k_{PZ-PZ} at 25 °C for dilute PZ solution by data regression. After being converted to activity based rate constant, this value turns out to be 2.4×10^{10} $kmol/m^3\cdot s$ at 40 °C. Bishnoi (Bishnoi 2000) reported the second-order rate constant of for PZ, which is equal to 3.2×10^{10} $kmol/m^3\cdot s$ at 40 °C after the amine concentration is taken into account. The values from both the studies compare favorably with the value of $k_{2MPZ-2MPZ}$ from this work.

The result that $k_{2MPZCOO^--2MPZ}$ has a higher value than $k_{2MPZ-2MPZ}$ might be related to its activity coefficient. As shown in the previous chapter, the calculated activity coefficient of $2MPZCOO^-$ at rich CO_2 loading is about one order of magnitude lower than that of 2MPZ. Since activity-based kinetics is used in this work, the kinetic rate constant has to be higher to compensate lower activity coefficient. Concentration-based rate constant for Reaction (8.36) still has a lower rate than Reaction (8.35).

The value of $k_{2,2MPZCOO^-}$ is about one order of magnitude higher than what would be predicted from the rate measured for another hindered amine, 2-piperidine ethanol (2-PE) (Paul, Ghoshal et al. 2009) corrected by the Bronsted theory. This might be because that the hindrance around the hindered amino group on $2MPZCOO^-$ is not as severe as that on 2-PE, therefore the bicarbonate formation under the catalysis of $2MPZCOO^-$ could be a result of a faster carbmate formation followed by hydrolysis. It is found that the adjustment in $k_{2,2MPZCOO^-}$ is necessary to account for the CO_2 fluxes data at rich loading.

If the viscosity term in Eq. (8.7) is expressed in an exponential function of temperature, the diffusivity activation energy can be calculated for 8 m 2MPZ. The calculated values are compared to literature data for unloaded amine solutions in Table 8.6. According to the results by Snijder *et al.* (Snijder, te Riele et al. 1993), the diffusion activation energy increases with liquid viscosity. The slightly higher value for E_D

obtained in this work compared to the literature values is presumably due to the higher viscosity of either unloaded or loaded 8 m 2MPZ.

Table 8.6: Comparison of the diffusion activation energy for 8 m 2MPZ with literature values for aqueous MDEA.

Amine	**Am Conc. (Molarity)**	**CO_2 loading (mol/mol alk)**	**Viscosity at 60 °C (cP)**	E_D **(kJ/mol)**	**Source**
2MPZ	4.5	0	4.1	25.6	This work
	4.4	0.35	12.6	27.9	This work
MDEA	1.0	0	0.6	17.8	(Snijder, te Riele et al. 1993)
	4.0	0	2.3	23.1	

A parity plot comparing the calculated fluxes from the model with the experimental values is shown in Figure 8.9. It can be seen that most of the points essentially fall on the parity line except a few outliers. The absolute average relative deviation (AARD) between the calculated fluxes and the measured fluxes, as calculated by the following equation, is 11%.

$$\text{AARD (\%)} = \frac{100}{N}\sum_{N}\frac{\left|Flux_{cal} - Flux_{\exp}\right|}{Flux_{\exp}} \tag{8.44}$$

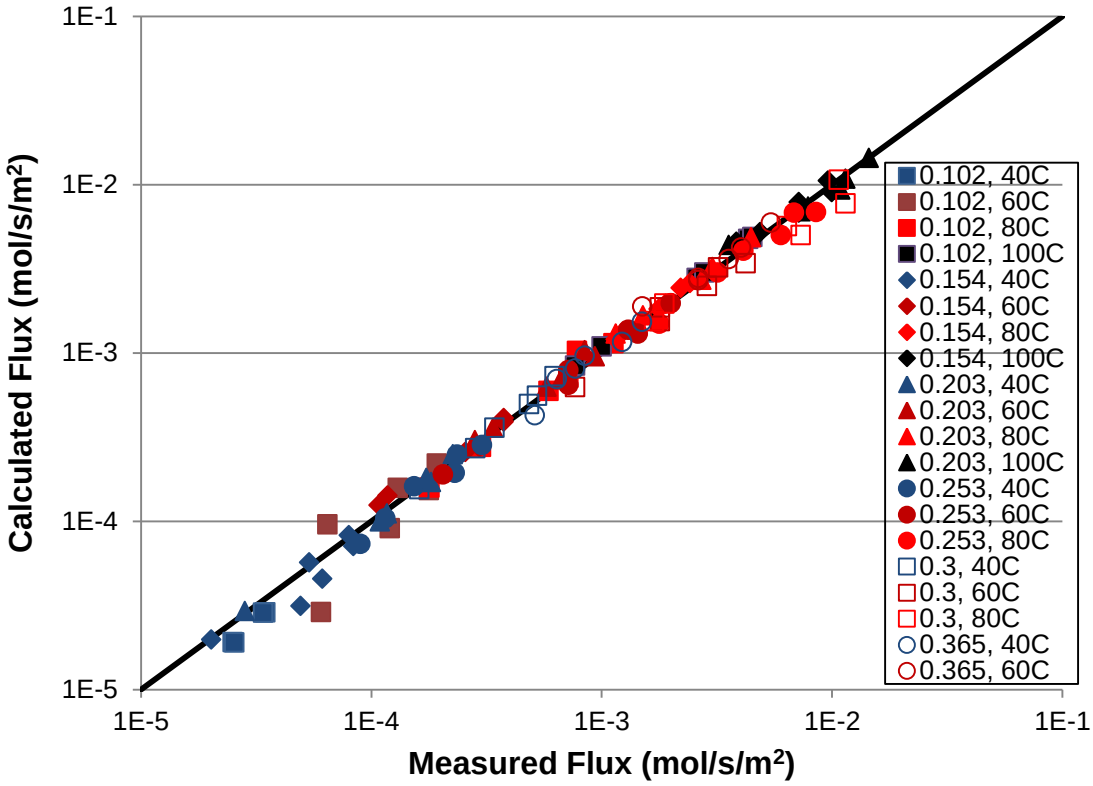

Figure 8.9: Parity plot of the calculated fluxes from the model versus the experimental measurements for 8 m 2MPZ at 40 – 100 °C and loading range of 0.102 – 0.365 mol CO_2 / mol alkalinity.

The relative deviations between the model and the measurements for each experimental CO_2 loading, as shown in Figure 8.10, are found to be mostly within ±20%. This is considered as a good fit because the experimental flux values span more than three orders of magnitude over the studied loading range. As a comparison, the spreadsheet model developed by Dugas *et al.* (Dugas 2009) fitted the WWC data for 2 – 12 m PZ within ±50%; the relative deviation between the predictions from Cullinane's model (Cullinane 2005) and the measured fluxes for PZ/K_2CO_3 in the WWC is ±30%. There is no obvious systematic error associated with CO_2 loading based on the deviation plot.

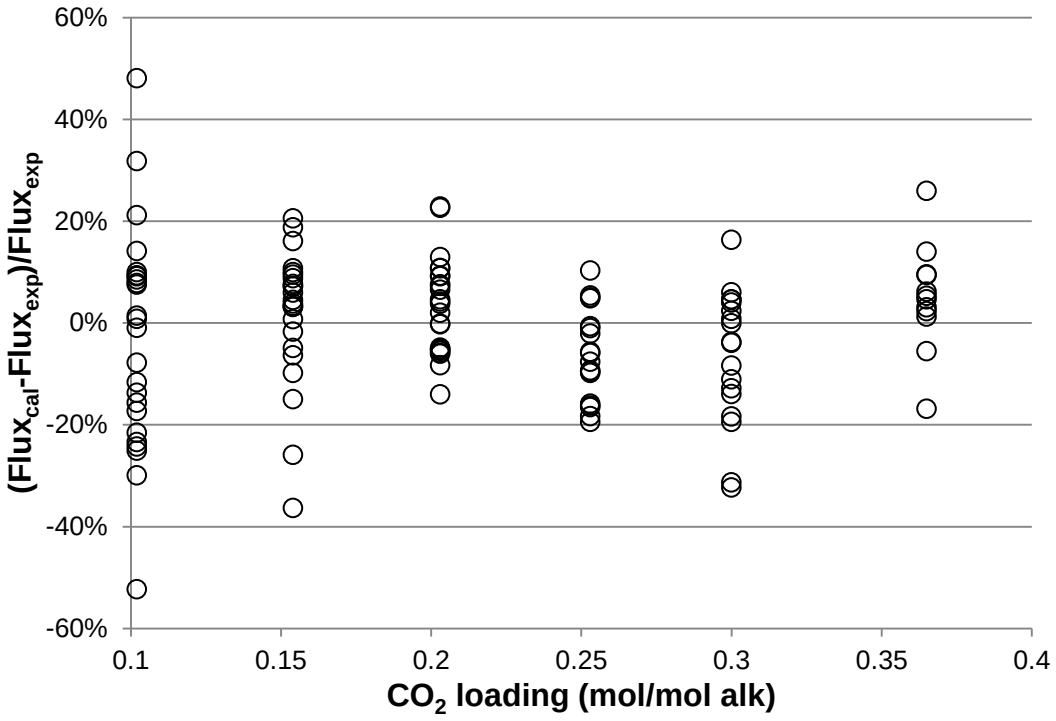

Figure 8.10: Relative deviation of the calculated fluxes from the experimental measurements as a function of CO_2 loading for 8 m 2MPZ over the loading range of 0.102 – 0.365 mol CO_2/mol alkalinity.

The relative deviation of the calculated fluxes is plotted against temperature in Figure 8.11. The positive and negative relative deviations are evenly distributed, and there is no systematic error associated with temperature. The fit seems to be better at higher temperature, which is because there are fewer points and there may be less complexity caused by the kinetic factors.

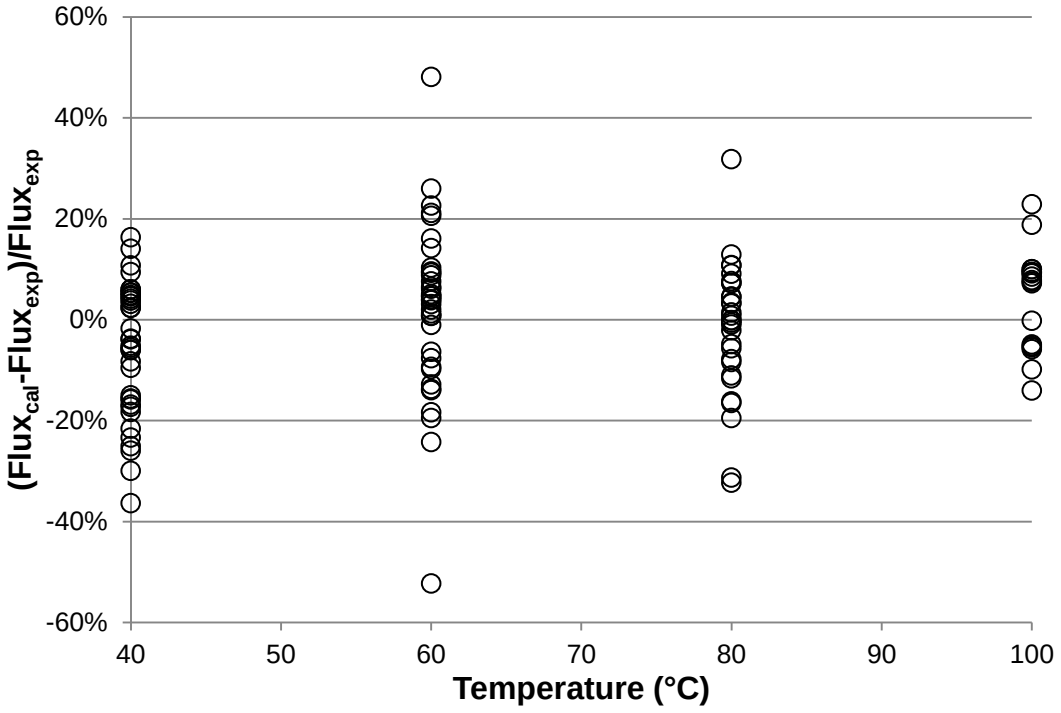

Figure 8.11: Deviation of the calculated fluxes from the experimental measurements as a function of temperature for 8 m 2MPZ over the loading range of 0.102 – 0.365 mol CO_2/mol alkalinity.

Adjustment in CO_2 Loading

Because the equilibrium CO_2 partial pressure is not exactly represented by the thermodynamic model developed for 2MPZ, if the same CO_2 loading values from the WWC experiments are used in the model, the driving force exerted between the gas and liquid would deviate from the real driving force. In some cases, the sign of the driving force can even change from positive to negative, or vice versa. To solve this problem, CO_2 loading is allowed to be reconciled by Aspen during the data fit. A standard deviation of 0.5% is put on CO_2 loading data to control the extent of the reconciliation and avoid wild adjustment. All the adjustments for varied CO_2 loading are thus restricted to be less than 5%, which is the typical uncertainty range for experimentally

determined CO_2 loading. The final results on the reconciled CO_2 loading at varied temperature and loading is shown in Figure 8.12. The average absolute adjustment in CO_2 loading is found to be 2.8%, which is well in the range of experimental error. Most of the calculated equilibrium CO_2 partial pressure at the adjusted loading is found to closely match the measured equilibrium CO_2 partial pressure.

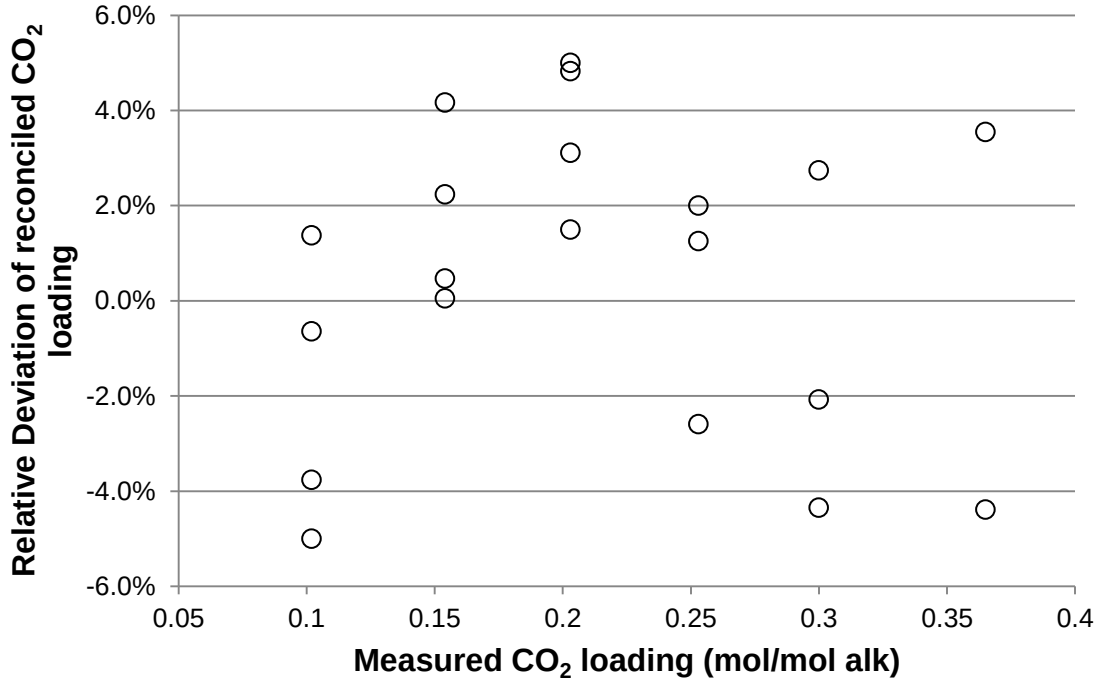

Figure 8.12: Relative deviation of the reconciled CO_2 loading from the measured CO_2 loading in the regression of CO_2 fluxes for 8 m 2MPZ at 40 °C.

8.3.2 Liquid Film Mass Transfer Coefficient

Given that the model represents the experimental CO_2 fluxes well, it was used to calculate the values for the liquid film mass transfer for 8 m 2MPZ at 40 - 100 °C. Similar to the method used in obtaining the experimental values for $k_g^{'}$ (Eq. (3.3) and (3.7)), the model value for $k_g^{'}$ is calculated from the modeling results for the difference of CO_2 concentration in the inlet and outlet gas stream and the logarithmic mean of

partial pressure driving force. The reported value for k_g' calculated at each temperature and CO_2 loading is an average of the calculated k_g' at varied driving force, corresponding to the CO_2 partial pressure in the gas phase (P_{CO2}) equal to 0, 0.3, 0.6, 1.4, 1.7 and 2 times the equilibrium CO_2 partial pressure of the solvent (P_{CO2}^*). In this way, the experimental conditions are approximately matched. The model values are compared to the measured values in Figure 8.13. As can be seen from the figure, the model is able to satisfactorily capture the trend of k_g' with both loading and temperature, and agrees satisfactorily with the experimental measurements. At very lean loading at 40 °C, the predictions are somewhat lower, which could be partially due to the greater uncertainty in the measurements at very lean loading. At very lean loading, the resistance of liquid film is much less than gas film resistance and the latter dominates the overall mass transfer. A small error in the measured overall mass transfer coefficient would be amplified to greater error in k_g' value. The model also overestimates k_g' at 80 °C at lean loading but agrees well with experimental results for $P_{CO2}^* > 100$ Pa.

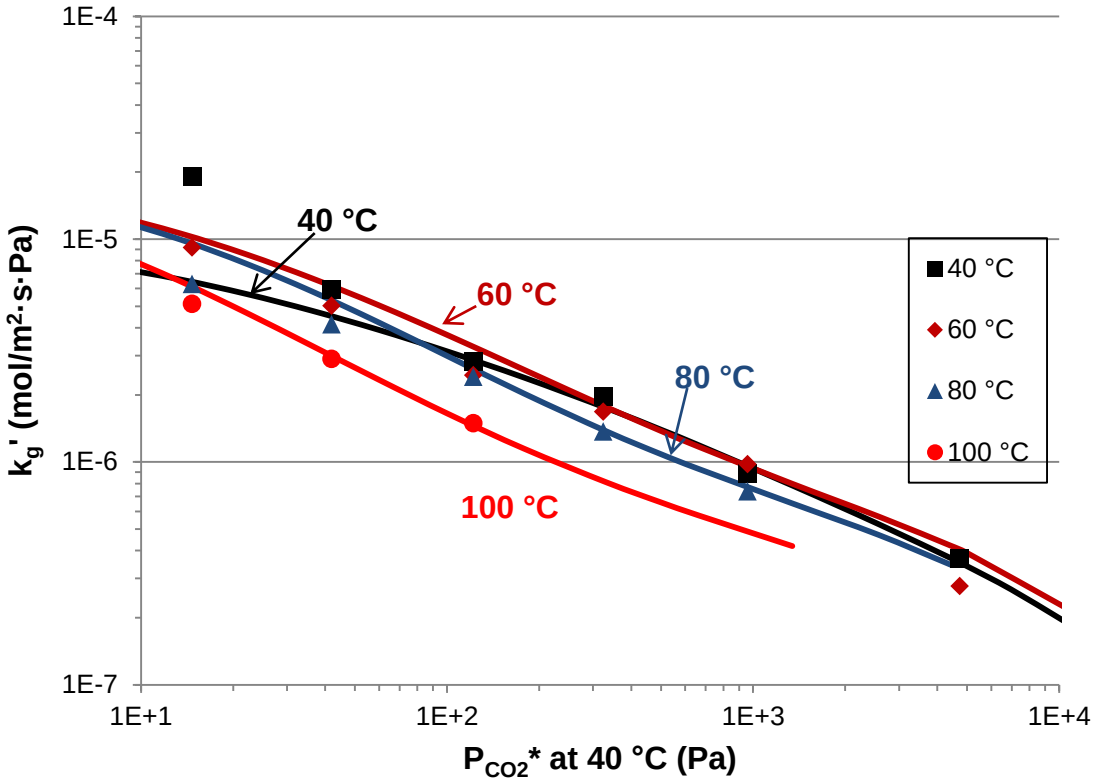

Figure 8.13: Liquid mass transfer coefficient for 8 m 2MPZ. Solid lines: model calculations; Points: measurements.

The liquid film resistance is comprised of two components, the reaction resistance and the diffusion resistance, as shown in the following equation.

$$\frac{1}{k_g^{'}} = \frac{H_{CO_2}}{Ek_l^0} + \frac{1}{k_{l,PROD}^0}\frac{\partial P_{CO_2}^*}{\partial [CO_2]_T} \tag{8.45}$$

The first term on the right-hand side in Eq. (8.45) represents the reaction resistance. At lean loading and low temperature, free amine concentration is much higher than CO_2 and remains almost constant across the boundary layer. As a result of that, the diffusion of reactant from the bulk to the interface and products from the interface to the bulk is fast enough to keep up with the reaction rate. In this case, the pseudo-first-order (PFO) assumption applies and reaction resistance dominates the overall mass transfer. At high

CO_2 loading, the slope of the CO_2 solubility curve increases as amine gets depleted. If this is coupled with increased reaction rate at high temperature, the mass transfer in liquid film becomes diffusion-controlled, and the second term in Eq. (8.45) is more significant.

When PFO assumption is applicable and the amine-catalyzed carbamate formation reaction is interpreted with termolecular mechanism, the liquid film mass transfer coefficient can be approximated by the following equation according to Dugas (Dugas 2009):

$$k'_{g,PFO} \approx \frac{\sqrt{D_{CO_2} k[Am]^2 \gamma_{Am}^2}}{\gamma_{CO_2}^{0.5} H_{CO_2}} \tag{8.46}$$

In the expression above, the unit for concentration is molarity and the unit for H_{CO_2} is Pa·m^3/mol, however this work uses activity-based reaction based on mole fraction. Therefore Eq. (8.45) is adapted into the following form to be used in this work:

$$k'_{g,PFO} \approx \frac{\sqrt{D_{CO_2} \left(k x_{2MPZ}^2 \gamma_{2MPZ}^2 + k x_{2MPZ} \gamma_{2MPZ} x_{2MPZCOO^-} \gamma_{2MPZCOO^-}\right)/V_m}}{\gamma_{CO_2}^{0.5} H_{CO_2}} \tag{8.47}$$

where V_m is the molar volume of the amine solution (m^3/mol), H_{CO_2} is the Henry's constant of CO_2 in water (Pa), k is the kinetic reaction rate constant (mol/m^3·s) and D_{CO_2} is the diffusivity of CO_2 in the amine solution (m^2/s) . The contribution of two amines (2MPZ and 2MPZCOO$^-$) is taken into account in the equation above.

The calculated $k'_{g,PFO}$ according to Eq. (8.47) is compared to k'_g calculated by the model at 40 °C and 100 °C in Figure 8.14. At 40 °C, the prediction from the Aspen model is close agreement with the result based on the PFO approximation, which indicates that the PFO is adequately valid to represent the mass transfer at low temperature and even up to rich loading. However, at 100 °C the deviation between $k'_{g,PFO}$ and k'_g is significant due to the dominance of diffusion-controlled mass transfer at high temperature. Calculation of $1/k'_{g,PFO}/(1/k'_g)$ yields a fraction number, which

indicates that the contribution of the mass transfer resistance from reaction to the overall liquid film resistance decreases to 10% at the operating CO_2 loading range from 43% at very lean loading.

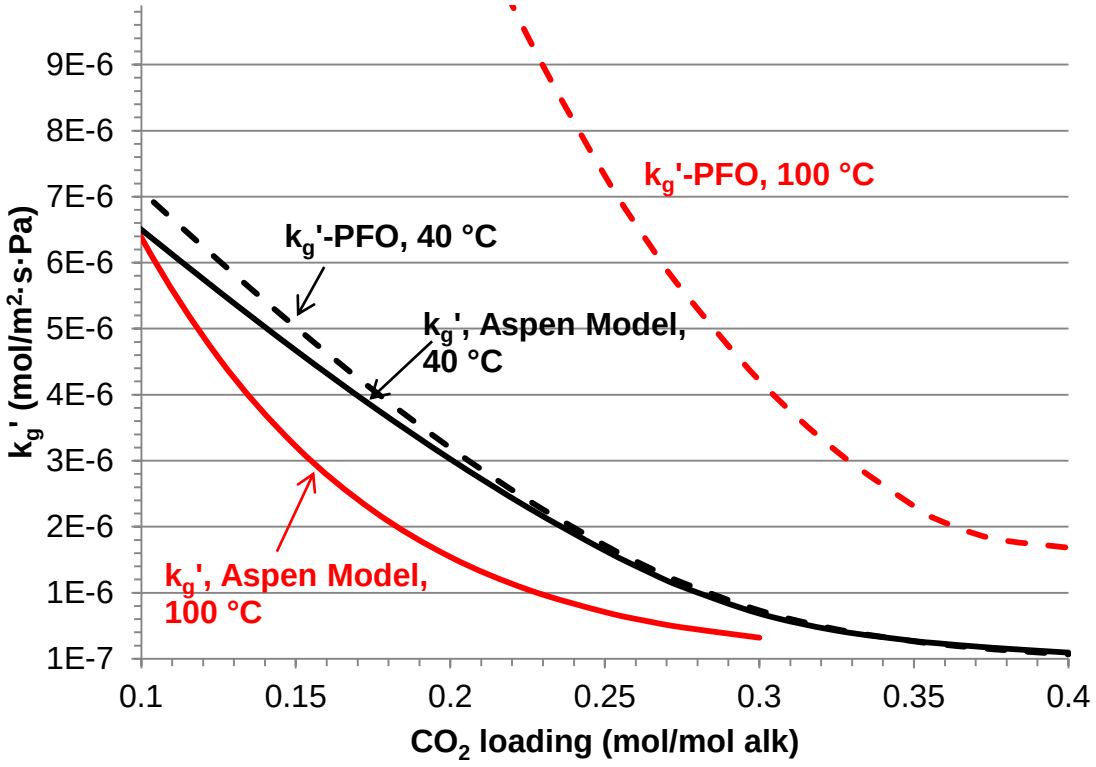

Figure 8.14: Comparison of the liquid film mass transfer coefficient from the model to that calculated from pseudo first order assumption (Eq. (8.47)) for 8 m 2MPZ at 40 and 100 °C.

Parameter Significance Analysis

The effect of the change in the relevant parameters on liquid film mass transfer coefficient as CO_2 loading is increased from the lean loading to the rich loading is examined in Table 8.7. H_{CO_2} and k remain constant at same temperature and are therefore not shown. It can be seen from the table that at either 40 °C or 100 °C the vast majority of the decrease in $k_g^{'}$ is caused by the decrease in free amine concentration.

This conclusion is consistent with the analysis done by Dugas (Dugas 2009) for concentrated PZ.

Table 8.7: Calculated change in different parameters from the lean loading (0.265 mol CO_2 / mol alkalinity, P_{CO2}^* = 500 Pa) to the rich loading (0.356 mol CO_2 / mol alkalinity, P_{CO2}^* = 5000 Pa) for 8 m 2MPZ at 40 °C and 100 °C.

Temp.	Parameter	@Lean loading	@Rich loading	Factor of change
40 °C	k_g' (mol/m^2·s·Pa)	1.4E-6	3.4E-7	4.1
	[Am]	1.3E-2	2.2E-3	5.9
	γ_{Am}	1.9	2.0	0.9
	D_{CO2} (m^2/s)	1.7E-10	1.3E-10	1.3
	γ_{CO2}	1.9	2.0	1.0
100 °C	k_g' (mol/m^2·s·Pa)	6.6E-7	2.5E-7	2.6
	[Am]	1.9E-2	6.5E-3	2.9
	γ_{Am}	1.9	2.1	0.9
	D_{CO2} (m^2/s)	1.1E-9	7.8E-10	1.3
	γ_{CO2}	1.6	1.8	0.9

8.3.3 Sensitivity Analysis

The sensitivity of the developed model to various parameters at 40 °C is portrayed in Figure 8.15. The effect of the change in parameter i on the liquid mass transfer coefficient is represented by $d\ln(k_g')/d\ln i$. At very low equilibrium CO_2 partial pressure (P_{CO2}^*), or very low CO_2 loading, the power to which k_g' is dependent on

$k_{2MPZ-2MPZ}$ is around 0.5, as expected from the expression based on the PFO assumption (Eq. (8.47)). At very lean loading range, the amine concentration is much higher than the total CO_2 concentration, therefore vast majority of CO_2 is absorbed through carbamate formation catalyzed by 2MPZ itself (Reaction (8.35)). As CO_2 loading increases, the dependence of $k_g^{'}$ on $k_{2MPZ-2MPZ}$ decays as free amine concentration decreases and the importance of diffusion grows. Since the concentration of $2MPZCOO^-$ increases with loading, the importance of Reaction (8.36) increases, which is reflected by the increasing dependence of $k_g^{'}$ on $k_{2MPZCOO^--2MPZ}$, which decreases again at rich end. The dependence of $k_g^{'}$ on bicarbonate formation rate constant, $k_{2,2MPZ}$, increases with loading as free amine gets depleted. This indicates that the bicarbonate formation reactions are only important at rich loading due to the much slower reaction rate compared to carbamate formation at 40 °C. As to diffusivity, $k_g^{'}$ has the same dependence on D_{Am} and D_{CO_2} at very lean loading, both close to the power of 0.26. The power for D_{Am} increases with CO_2 loading and approaches 0.34 at rich loading, while the dependence on D_{CO_2} decreases to 0.17 at higher loading. Interesting enough, the sum of the power of D_{Am} and D_{CO_2} is equal to the sum of the power of $k_{2MPZ-2MPZ}$ and $k_{2MPZCOO^--2MPZ}$ at very lean loading and remains around 0.5 throughout the loading range. The physical liquid film mass transfer coefficient k_l^0 has little impact on $k_g^{'}$ at very lean loading, however the dependence of $k_g^{'}$ on k_l^0 increases dramatically from the lean loading to the rich loading.

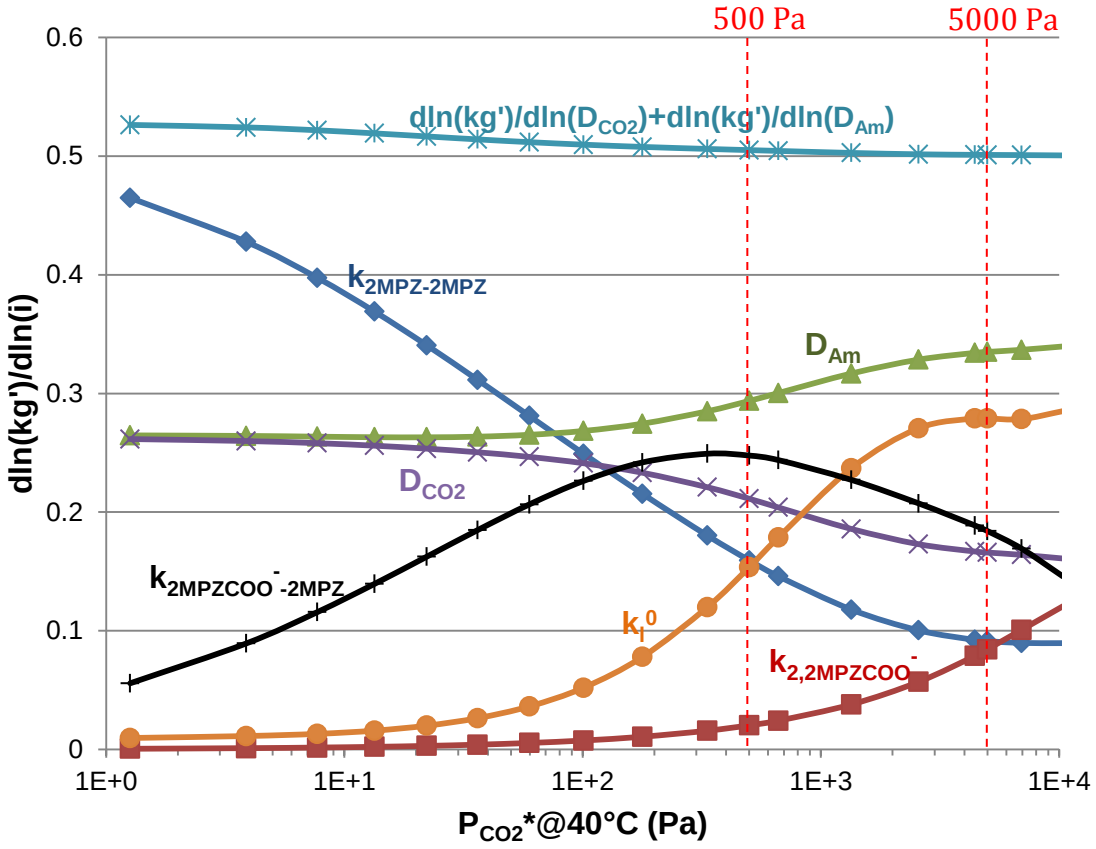

Figure 8.15: Sensitivity of $k_g^{'}$ to different parameters for 8 m 2MPZ at 40 °C.

According to Eq. (8.47), $d\ln\left(k_g^{'}\right)/d\ln D_{CO_2}$ should be equal to 0.5 at very lean loading when the PFO assumption is valid. The difference between the model and the theory is related to the way Aspen Plus® makes use of the user-defined binary diffusion coefficients for CO_2 and all the other species (Eq. (8.5) and Eq. (8.7)) and calculates film thickness. Strictly speaking, D_{CO_2} used in Eq. (8.47) refers to the effective diffusivity of CO_2, $D_{CO_2,eff}$, defined in the following equation:

$$N_i = -c_t D_{i,eff} \nabla x_i \text{, i = 1, 2, …, n} \tag{8.48}$$

in which c_t is the total concentration in molarity.

The following expression for $D_{i,eff}$ is obtained with the insertion of the Maxwell-Stefan equation into Eq. (8.48) (Taylor and Krishna 1993)

$$\frac{1}{D_{i,eff}} = \sum_{\substack{j=1 \\ j\neq i}}^{n} \frac{x_j}{D_{ij}} \left(1 - \frac{x_i N_j}{x_j N_i} \right) \tag{8.49}$$

According to Eq. (8.49), the relationship between $D_{CO_2,eff}$ and the binary diffusion coefficient, D_{CO_2}, implemented in Aspen is as follows:

$$D_{CO_2,eff} = D_{CO_2} \Bigg/ \left(\left(1 - x_{CO_2}\right) - x_{CO_2} \sum_{\substack{j=1 \\ j\neq CO_2}}^{n} \frac{N_j}{N_{CO_2}} \right) \tag{8.50}$$

Based upon the correlation above, $D_{CO_2,eff}$ is not simply proportional to D_{CO_2} because N_{CO_2} is a function of D_{CO_2} according to (8.17) and the fluxes of all other species, and N_j is a function of D_{Am}. N_j / N_{CO_2} is also dictated by the reaction stoichiometry in the liquid film. All the complexity resulted in that $D_{CO_2,eff}$ is dependent upon both D_{Am} and D_{CO_2} as seen in the sensitivity analysis in this study. However, an explicit analytical expression for Eq. (8.50) in terms of D_{Am} and D_{CO_2} is hard to derive.

The film thickness is calculated in Aspen Plus® as the ratio of the average mass transfer coefficient and the average diffusivity in the liquid.

$$\delta_{film} = \frac{\overline{D}}{\overline{k}} \tag{8.51}$$

where

$$\overline{D} = \frac{\sum_{i=1}^{nc-1} \sum_{k=i+1}^{nc} \left(x_i + \beta\right)\left(x_i + \beta\right) D_{ik}}{\sum_{i=1}^{nc-1} \sum_{k=i+1}^{nc} \left(x_i + \beta\right)\left(x_i + \beta\right)} \tag{8.52}$$

$$\overline{k} = \frac{\sum_{i=1}^{nc-1} \sum_{k=i+1}^{nc} \left(x_i + \beta\right)\left(x_i + \beta\right) \kappa_{ik}}{\sum_{i=1}^{nc-1} \sum_{k=i+1}^{nc} \left(x_i + \beta\right)\left(x_i + \beta\right)} \tag{8.53}$$

where β is a weighting parameter and set to a very smaller value in this case. Consequently, $\overline{D}$ and $\bar{k}$ is weighted by composition only. Since the mole fraction of CO_2 in the solution is very small compared to other species, the average diffusivity and the average mass transfer coefficient is essentially equal to, respectively, D_{Am} and k_{Am}. As a consequence of that, δ_{film} is only proportional to $D_{Am}^{0.5}$. Nonetheless, the classic film theory shows that δ_{film} should be dependent on D_{CO_2} as well. The way the film thickness is computed therefore affects the calculation of N_{CO_2}, and alters the dependence of flux N_{CO_2} on D_{Am} and D_{CO_2}. The relationship between the true value and the regressed value for $k_{2MPZ-2MPZ}$ can be approximated by the following equation:

$$k_{2MPZ-2MPZ}(true) = \left(\frac{D_{Am}}{D_{CO_2}}\right)^{0.5} k_{2MPZ-2MPZ}(regressed) \tag{8.54}$$

The ratio of the binary diffusion coefficients for non-CO_2 species and CO_2 used in this work is relatively constant at 0.6 at relevant conditions.

The sensitivity analysis is also done for 100 °C, as presented in Figure 8.16. The analysis cannot be accomplished at very high loading due to convergence issues. The dependence of $k_g^{'}$ on $k_{2MPZ-2MPZ}$ quickly drops to an insignificant level as CO_2 loading increases, while that on $k_{2MPZCOO^{-}-2MPZ}$ is very small. This suggests that carbamate formation reactions do not affect mass transfer at rich loading. The effect of $k_{2,2MPZCOO^{-}}$ on $k_g^{'}$ increases very slightly with loading. The dependence on D_{Am} is found to remain relatively constant with loading. D_{Am} dominates the mass transfer throughout the loading range and the power of it varies between 0.4 and 0.5. On the contrary, $d\ln\left(k_g^{'}\right)/d\ln D_{CO_2}$ steadily decreases with loading. $k_g^{'}$ is strongly dependent upon k_l^0 in the entire loading range. Therefore the diffusion of reactants and products is the major factor that determines the mass transfer rate in the liquid film.

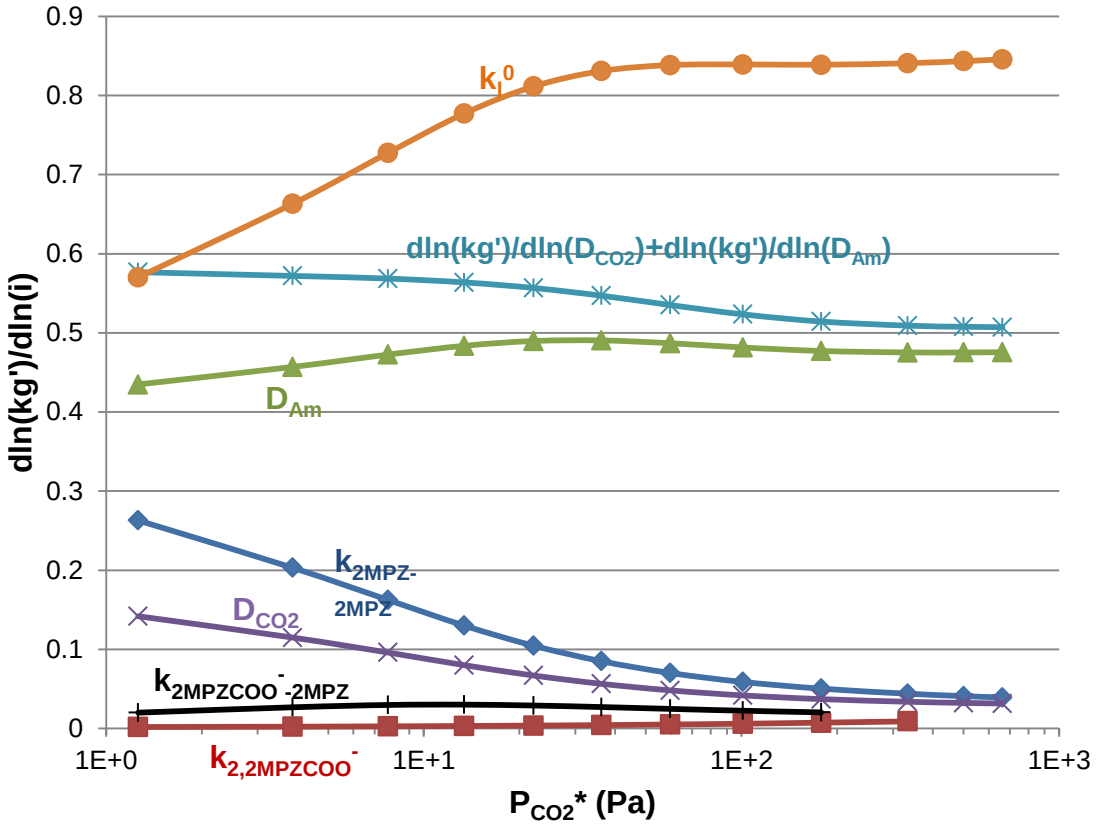

Figure 8.16: Sensitivity of $k_g^{'}$ to different parameters for 8 m 2MPZ at 100 °C.

The sensitivity of $k_g^{'}$ to $k_{2MPZ-2MPZ}$ and k_l^0 as a function of temperature at the lean and rich loading is shown in Figure 8.17. As can be seen from the figure, $k_g^{'}$ has a stronger dependence on $k_{2MPZ-2MPZ}$ and $k_{2MPZCOO^{-}-2MPZ}$ but a weaker dependence on k_l^0 at the lean loading than at the rich loading. Moreover, the dependence of $k_g^{'}$ on $k_{2MPZCOO^{-}-2MPZ}$ is greater than that on $k_{2MPZ-2MPZ}$. The dependence on $k_{2MPZ-2MPZ}$ and $k_{2MPZCOO^{-}-2MPZ}$ decreases with temperature but that on k_l^0 increases, and the mass transfer process becomes diffusion limited at high temperature. At 100 °C, $d\ln\left(k_g^{'}\right)/d\ln i$ at the lean and rich loading approaches same value, which means the value of loading is not important any more.

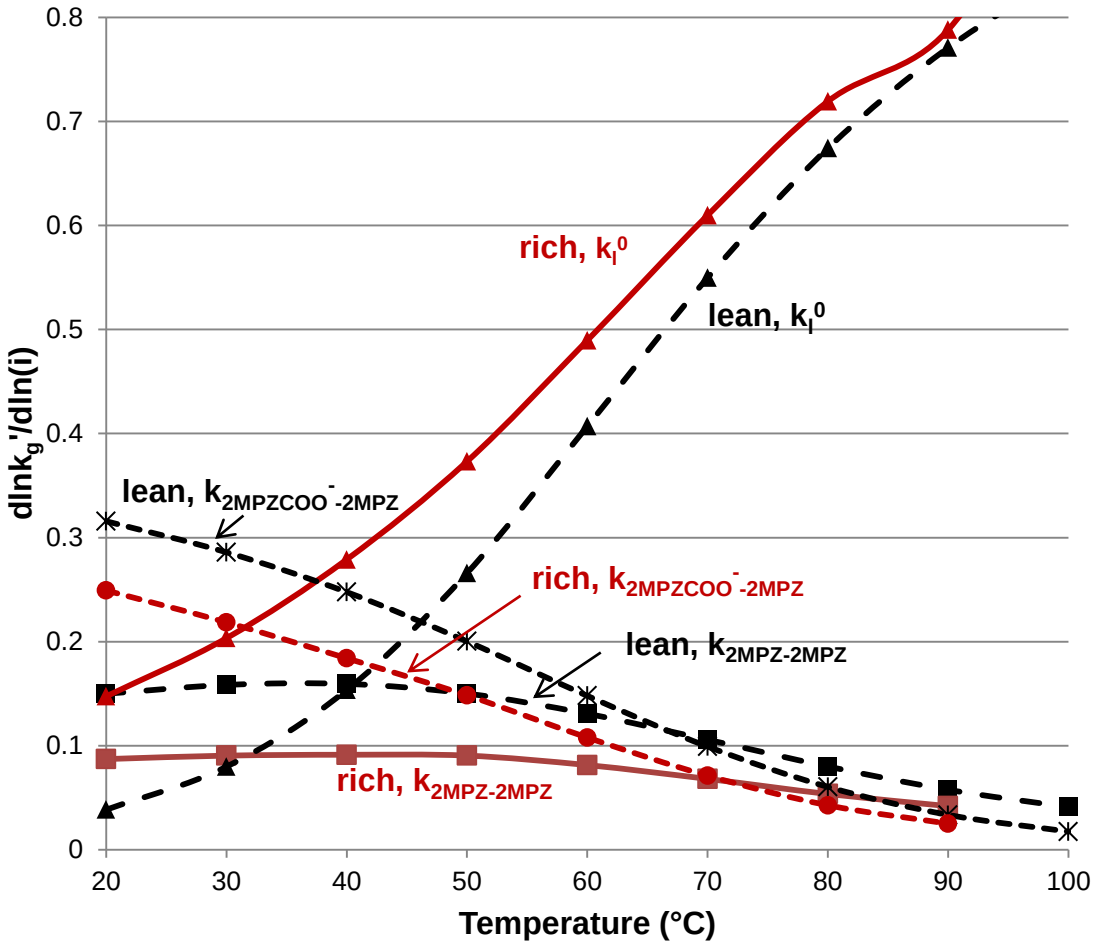

Figure 8.17: Sensitivity of the liquid film mass transfer coefficient to the kinetic rate constant $k_{2MPZ-2MPZ}$ and the physical liquid mass transfer coefficient (k_l^0) as a function of temperature for 8 m 2MPZ at $\alpha = 0.265$ (lean loading) and 0.356 mol/mol alkalinity (rich loading).

Unlike 8 m PZ, there are no solid solubility issues for 8 m 2MPZ at lower temperature, so it is possible to use the solvent in a cooler absorber. The lean and rich CO_2 loading corresponding to the equilibrium partial pressure of 500 and 5000 Pa at 25 °C are 0.304 and 0.400 mol/mol alkalinity, respectively. The richer lean loading and richer rich loading for 25 °C corresponds to a cyclic CO_2 capacity of 0.77 mol CO_2/kg

solvent, compared to 0.74 mol CO_2/kg solvent at 40 °C. The same sensitivity analysis as that shown in Figure 8.17 was also done for the lean and rich loading for 25 °C and the results are presented in Figure 8.18. The similar conclusions as for 40 °C can be drawn for the case of 25 °C.

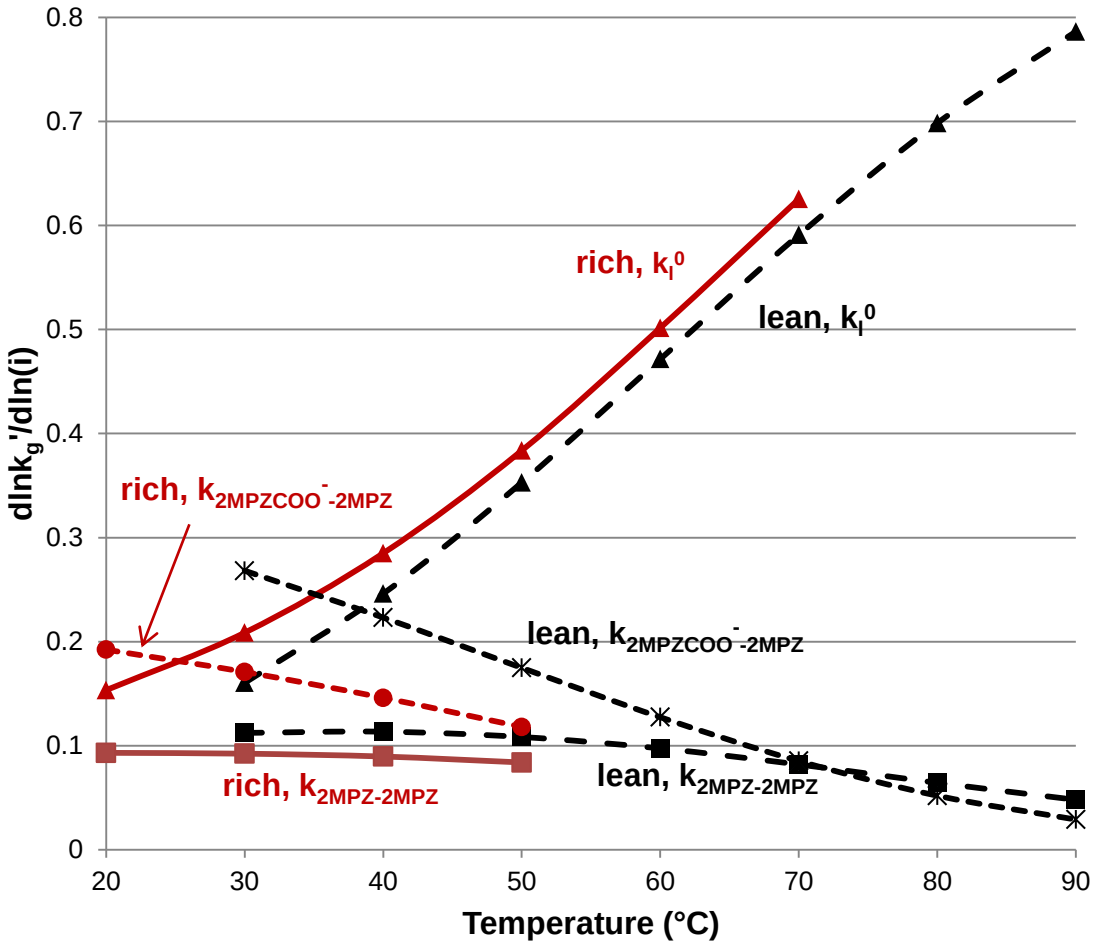

Figure 8.18: Sensitivity of the liquid film mass transfer coefficient to the kinetic rate constant $k_{2MPZ-2MPZ}$ and the physical liquid mass transfer coefficient (k_l^0) as a function of temperature for 8 m 2MPZ at α = 0.304 and 0.400 mol/mol alkalinity.

8.3.4 Film Profile of Concentration

The liquid film concentration profiles for 8 m 2MPZ at 40 °C and 100 °C and the lean and rich loading are shown in Figure 8.19 through Figure 8.22. The CO_2 partial pressure in the gas phase (P_{CO2}) used in this analysis is twice the equilibrium CO_2 partial pressure at corresponding temperature. Since the order of magnitude of the mole fraction of different species is very different, the mole fraction relative to the interface concentration, ($x_i - x_i^I$), is plotted to more clearly compare variation of concentration for all the species in the liquid film. The variation in concentration of H^+ and OH^- is extremely small compared to other species, so they are not shown in these figures.

At 40 °C and the lean loading (Figure 8.19), most of the change in CO_2 concentration occurs in a very thin boundary layer ($\delta < 0.005$), which is the reaction film. 2MPZ and $2MPZCOO^-$ are the main reactants that diffuse toward the interface to react with CO_2, and $2MPZ(COO^-)_2$, H2MPZCOO and $2MPZH^+$ are the major products that diffuse away from the interface.

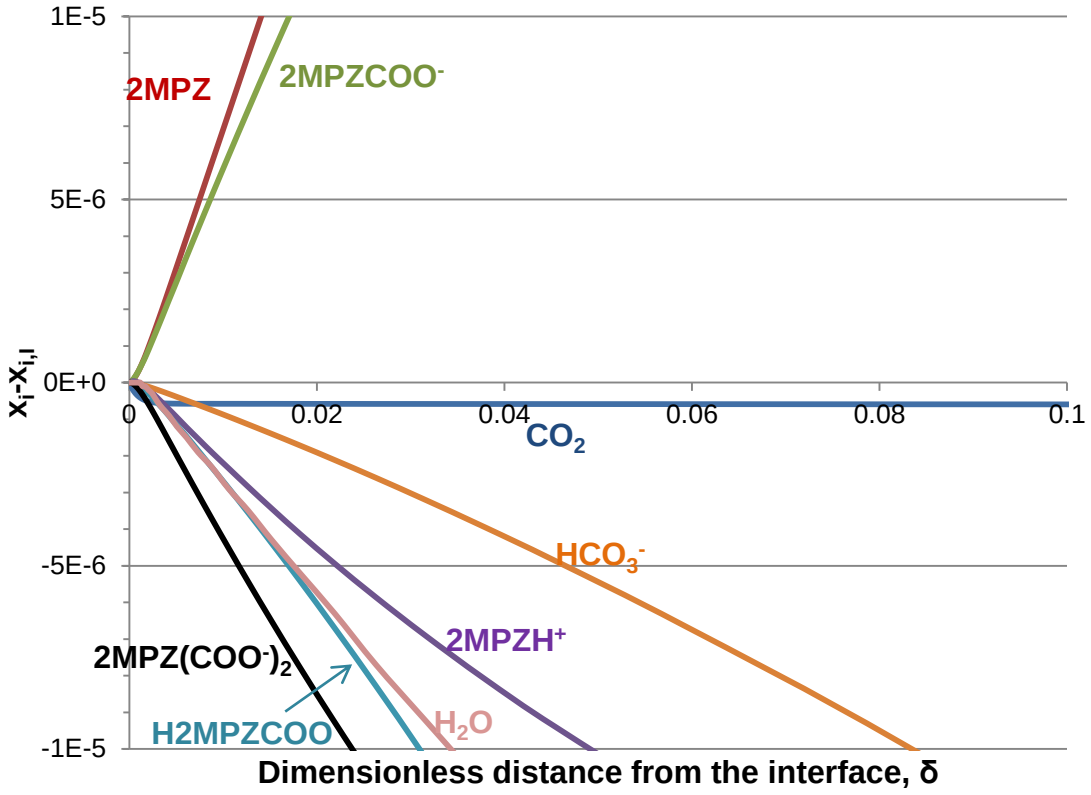

Figure 8.19: Calculated concentration profile relative to interface concentration ($x_i - x_i^I$) in the liquid film for 8 m 2MPZ at 40 °C, α = 0.265 CO_2 mol/mol alkalinity, P_{CO2}^*@40 °C = 500 Pa, $P_{CO2} = 2 \times P_{CO2}^*$. The total pressure in gas phase = 138 kPa (20psig).

At 40 °C and the rich loading (Figure 8.20), the majority of the decrease in CO_2 concentration still occurs in in a very thin layer. 2MPZ, $2MPZCOO^-$ and $2MPZH^+$ are all diffusing to the interface with $2MPZCOO^-$ being the most important reactant. H2MPZCOO is the most important product that transfers from the interface to the bulk. The flux of $2MPZ(COO^-)_2$ and HCO_3^- are also significant.

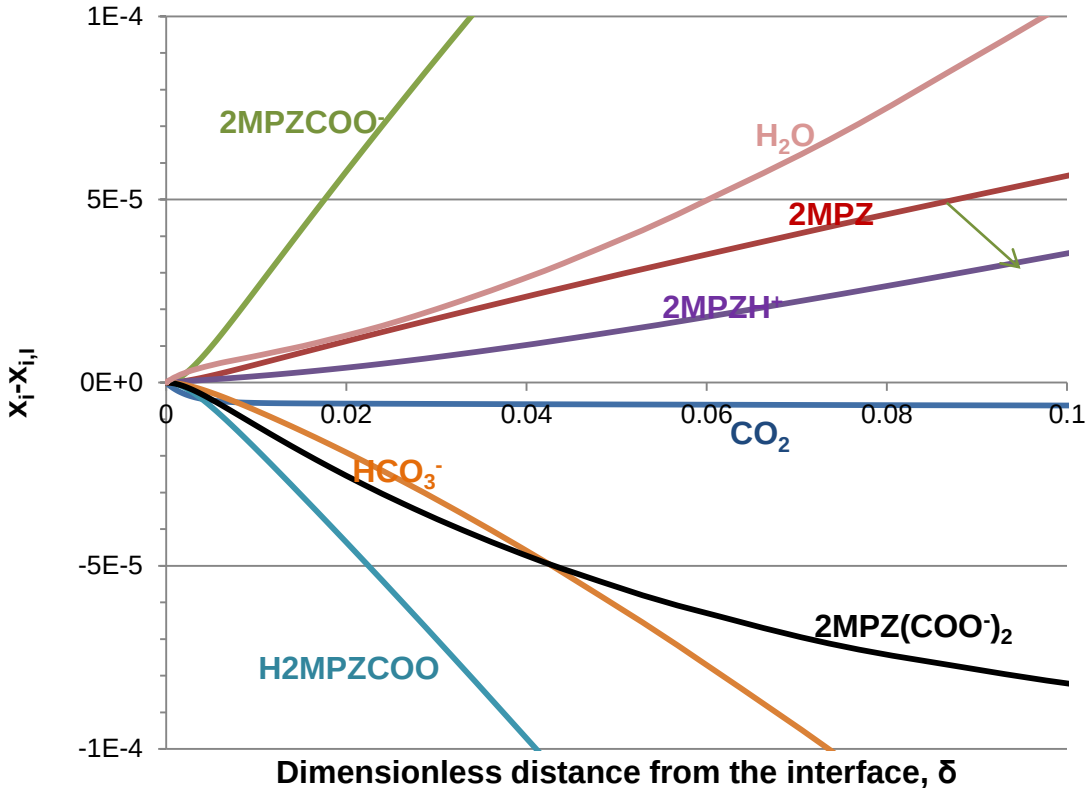

Figure 8.20: Calculated concentration profile relative to interface concentration ($x_i - x_i^I$) in the liquid film for 8 m 2MPZ at 40 °C, α = 0.356 CO_2 mol/mol alkalinity, P_{CO2}^*@40 °C = 5000 Pa, $P_{CO2} = 2 \times P_{CO2}^*$. The total pressure in gas phase = 276 kPa (40psig).

At 100 °C, a steady decrease in CO_2 concentration across the entire liquid film exists for both the lean and rich loading, as shown in Figure 8.21 and Figure 8.22. At the lean loading, a moderately sharp decrease in free CO_2 concentration in $0 < \delta < 0.005$ is observed, and an insignificant but steady decrease in CO_2 concentration over a broader film thickness is observed. This suggests that reaction still dominates the mass transfer of CO_2, but diffusion has an incremental effect on mass transfer at 100 °C. 2MPZ and $2MPZCOO^-$ are the main reactants, and H2MPZCOO and HCO_3^- are the main reaction products. $2MPZ(COO^-)_2$ is not as an important product as it is at 40 °C due to its

increased instability. At the rich loading (Figure 8.22), the diffusion of CO_2 becomes the dominant mechanism. $2MPZH^+$ changes from a product at the lean loading to a reactant at the rich loading, which is due to the depletion of 2MPZ. $2MPZ(COO^-)_2$ is found to form at the interface, and then be converted to other species near the interface. CO_2 is mainly absorbed through bicarbonate formation under the catalysis of 2MPZ and $2MPZCOO^-$.

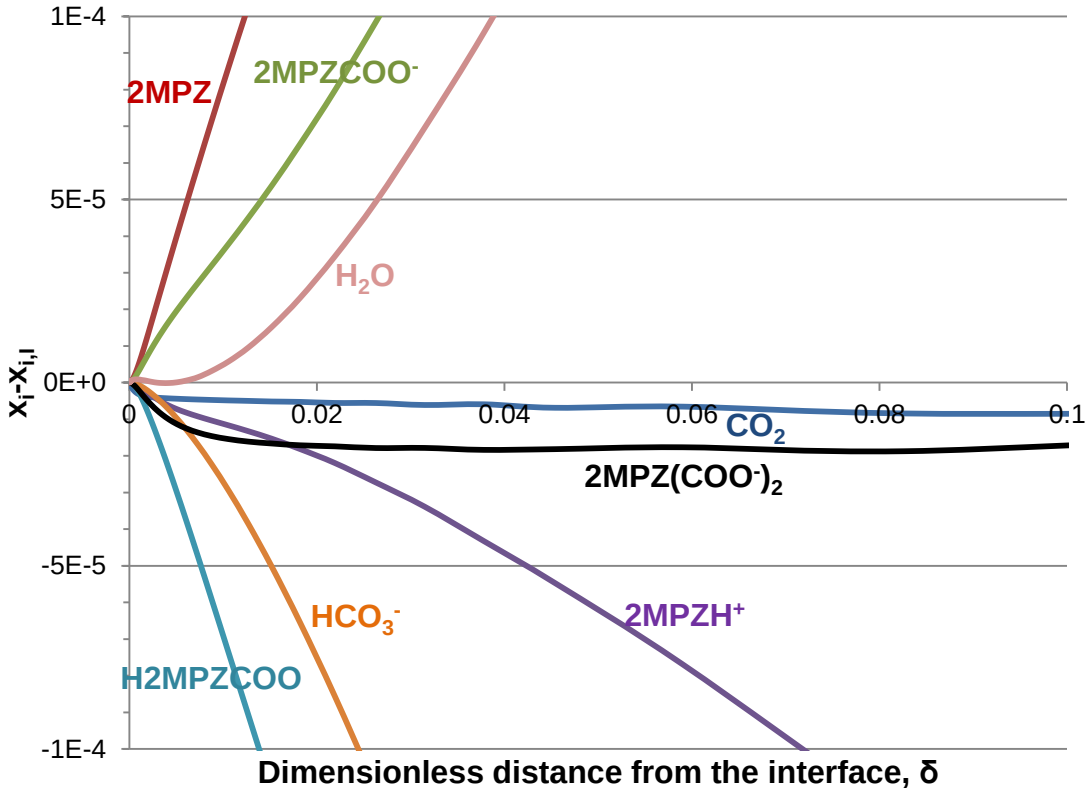

Figure 8.21: Calculated concentration profile relative to interface concentration ($x_i - x_i^I$) in the liquid film for 8 m 2MPZ at 100 °C, α = 0.265 CO_2 mol/mol alkalinity, P_{CO2}^*@40 °C = 500 Pa, $P_{CO2} = 2 \times P_{CO2}^*$. The total pressure in gas phase = 276 kPa (40psig).

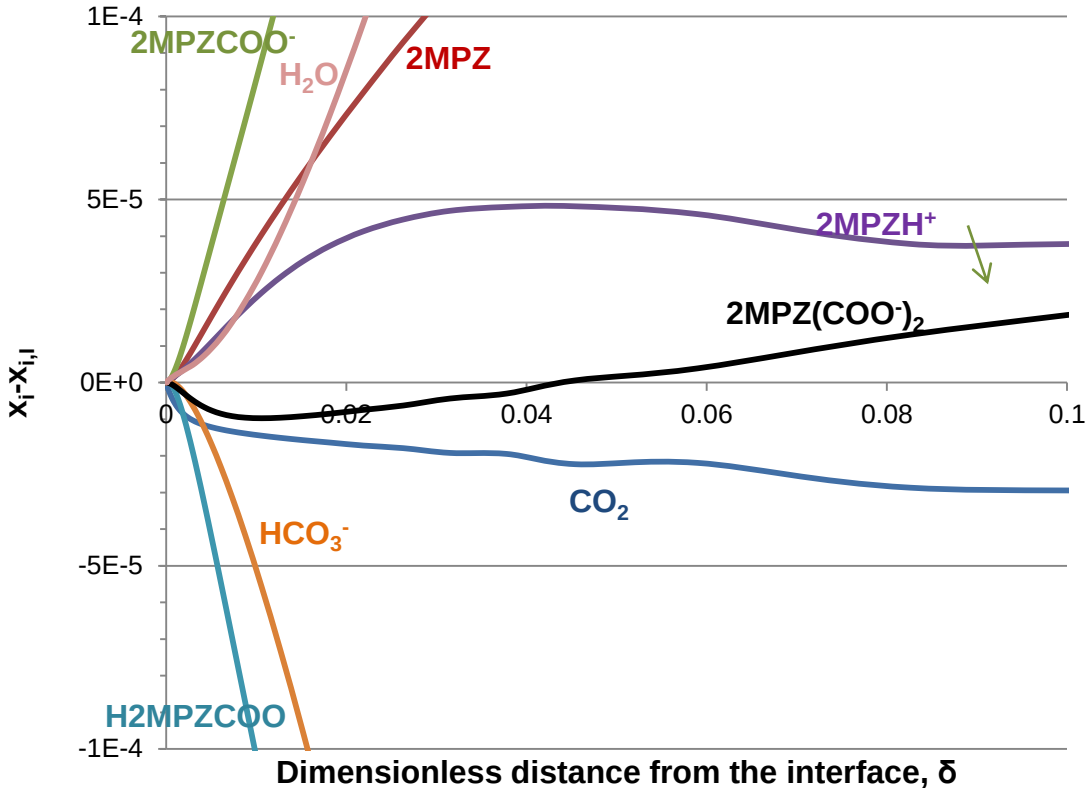

Figure 8.22: Calculated concentration profile relative to interface concentration ($x_i - x_i^I$) in the liquid film for 8 m 2MPZ at 100 °C, α = 0.356 CO_2 mol/mol alkalinity, P_{CO2}^*@40 °C = 5000 Pa, $P_{CO2} = 2 \times P_{CO2}^*$. The total pressure in gas phase = 276 kPa (40psig).

8.3.5 Bronsted Theory Revisited

Cullinane *et al.* (Cullinane and Rochelle 2006) reinterpreted the literature values for the kinetic rate constants of Morpholine (MOR), Diethanolamine (DEA), diisopropanolamine (DIPA) with termolecular mechanism. These constants are compared to the constant for 2MPZ obtained in this work (after correction) and that for MEA to validate the Bronsted theory, as shown in Table 8.8.

Table 8.8: Termolecular kinetic rate constants (k_{Am-Am}) for different amines at 25 °C.

Amine	MOR[a]	PZ[b]	2MPZ[c]	MEA[d]	DEA[e]	DIPA[f]
pKa	8.49	9.73	9.57	9.5	8.88	8.89
k_{Am-Am} at 25 ℃ ($m^6/kmol^2 \cdot s$)	1715	70100	44557	1713	315	147

a: (Alper 1990) ; b: (Cullinane and Rochelle 2006); c: This work; d: (Aboudheir, Tontiwachwuthikul et al. 2003); e: (Danckwerts 1979); f: (Littel, Versteeg et al. 1992).

A Bronsted plot for these rate constants is shown in Figure 8.23. It is found that linear correlations can be obtained for the cyclic amines and acyclic amines, respectively. The slopes of the two lines are both approximately equal to 1.4. Amine with high pKa enhances the reaction rate both as a base catalyst and a carbamate formation agent. Cyclic amines are faster than the acyclic amines at the same basic strength, which can be attributed to the open ring structure (Bishnoi 2000).

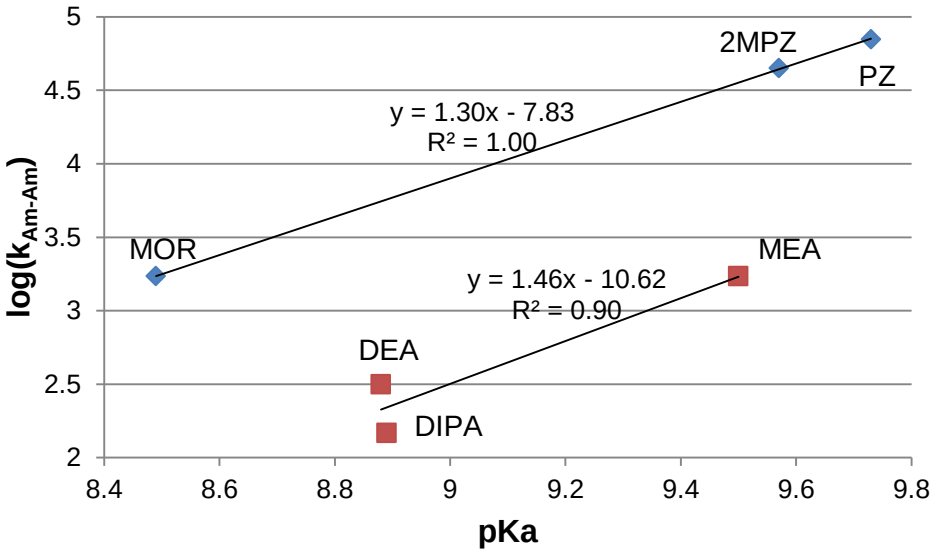

Figure 8.23: Relationship between the concentration-based termolecular reaction rate constants and the base strength of six amines at 25 °C.

8.4 PRACTICAL APPLICATION

The model developed in this work can be used to simulate large-scale CO_2 absorption/desorption processes. It is useful for column design and packing selection to analyze the performance of 2MPZ at typical industrial conditions involving treatment of flue gas from coal-fired power plants.

Figure 8.24 presents the variation of $k_g^{'}$ with k_l^0 at the rich CO_2 loading. A small driving force is used for the analysis since that is normally also the case in a real absorber, for which a pinch is sometimes approached. The value of k_l^0 for the WWC experiments for 2MPZ varies between 10^{-5} to 10^{-4} m/s. For an absorber or a stripper with structured packing, k_l^0 is typically in the range of 1×10^{-5} – 5×10^{-5} m/s. In this region, $k_g^{'}$ is not a strong function of k_l^0 at 40 °C and the PFO assumption applies. However, $k_g^{'}$ is more significantly affected by k_l^0 at 60 °C and 80 °C. The PFO region shifts to higher k_l^0 and becomes narrower as temperature increases.

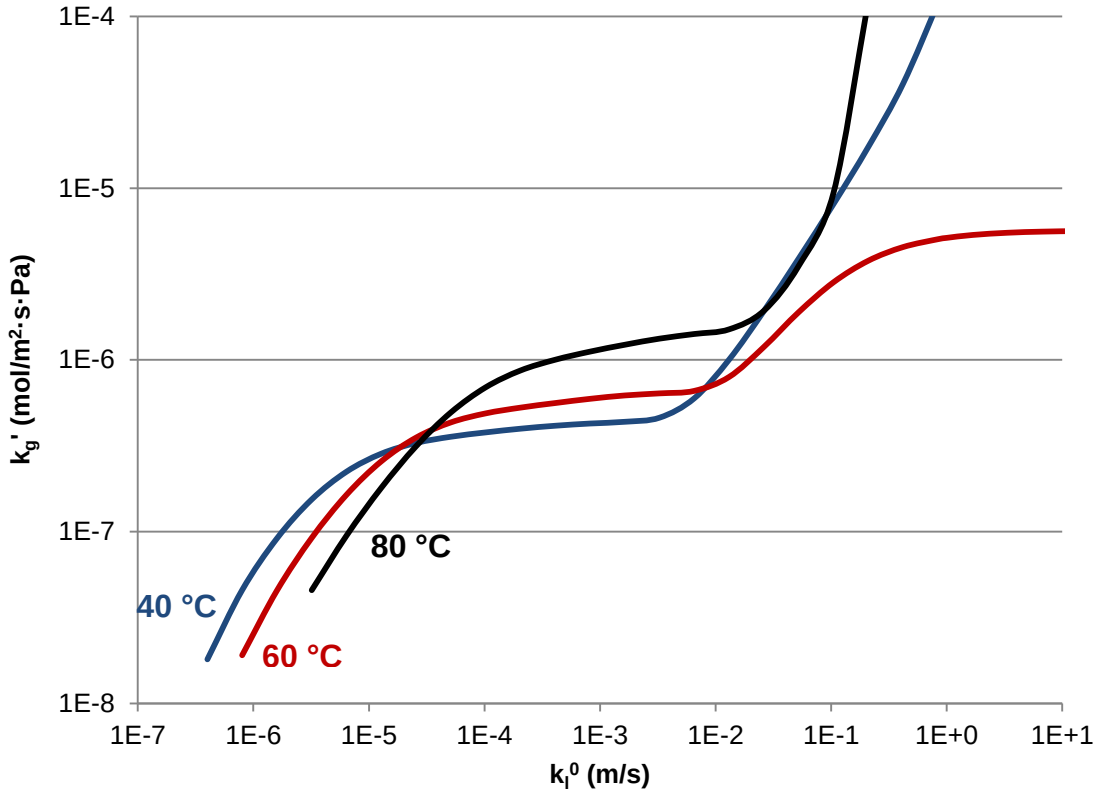

Figure 8.24: The effect of varying k_l^0 on the k_g' at varied temperature for 8 m 2MPZ, α = 0.356 CO_2 mol/mol alkalinity, P_{CO2}* = 5000 Pa at 40 °C, $P_{CO2,g} = 1.1 \times P_{CO2}$*.

The ratio of the overall mass transfer coefficient to the gas film mass transfer coefficient represents the contribution of gas film resistance to the overall resistance. This ratio as a function of CO_2 loading is shown in Figure 8.25. The values of k_l^0 and k_g used in the analysis are representative of industrial conditions. Again a low driving force is used. The ratio is not available for 100 °C at rich loading due to convergence issues. The gas film resistance is significant for 40 °C at lean loading because of the abundant free amine and fast chemical reactions in the liquid film. As amine concentration decreases at high loading, the percent gas film resistance drops to 10 – 25%

between the lean and the rich loading. At 100 °C, the gas film resistance is even less important.

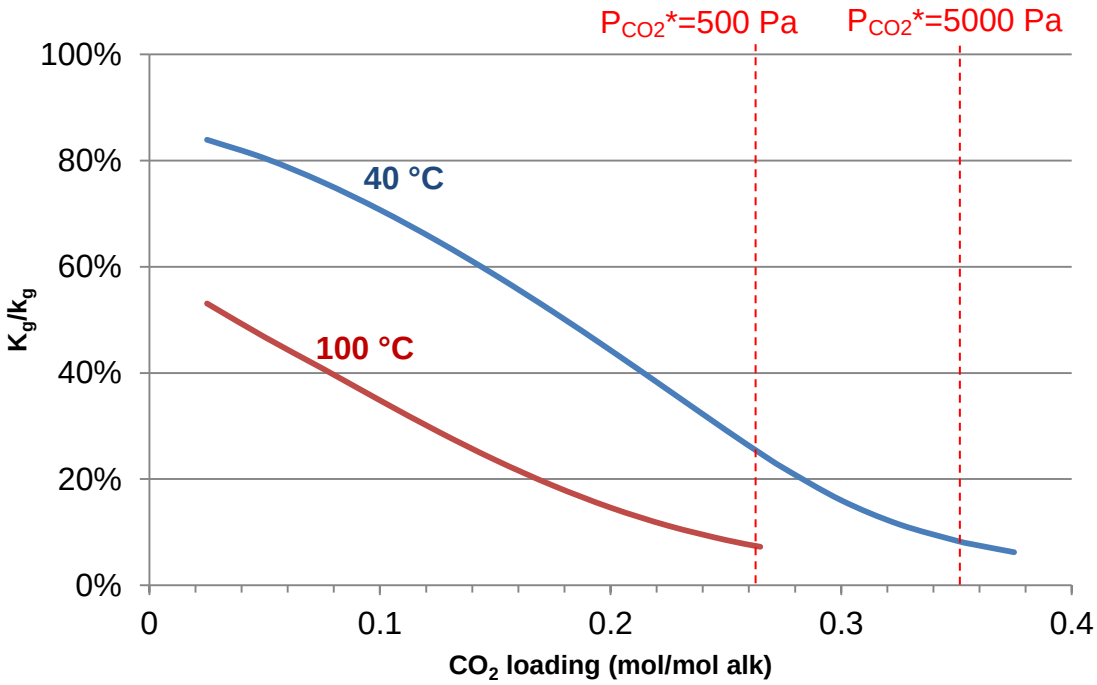

Figure 8.25: Contribution of the gas film resistance to the overall mass transfer in 8 m 2MPZ, $P_{CO2,g} = 1.1 \times P_{CO2}$*, $k_l^0 = 3.56 \times 10^{-5}$ m/s, $k_g = 0.02$ m/s.

8.5 CONCLUSIONS

The Wetted Wall Column was modeled in Aspen Plus® as a Radfrac column. The activity-based termolecular mechanism was used to describe the kinetic reactions between CO_2 and aqueous 2MPZ solution. The reaction rate constants are correlated with the Bronsted theory.

Most of the measured CO_2 fluxes at 40 °C – 100 °C and variable CO_2 loading were represented by the model within ±20% via the regression of two carbamate formation rate constants, one bicarbonate formation rate constant, and the temperature dependence of the diffusion coefficient of all the non-CO_2 species. The regressed

kinetic rate constant for carbamate formation between 2MPZ and CO_2 catalyzed by 2MPZ is 1.94×10^{10} kmol/m^3·s. The diffusion activation energy for the non-CO_2 species in 8 m 2MPZ at the rich loading is approximately 28 kJ/mol. The calculated liquid film mass transfer coefficients at 40 – 100 °C agree well with the measured values except at very lean loading. The pseudo-first-order approximation is found to be valid for 40 °C but not for 100 °C. The drop in liquid film transfer coefficient from the lean loading to the rich loading is mainly caused by the depletion of free amine.

The liquid film mass transfer coefficient is most sensitive to the reaction rate of carbamate formation at lean loading at 40 °C, with the overall power close to 0.5, whereas the dependence on bicarbonate formation is only significant at rich CO_2 loading. The overall dependence of $k_g^{'}$ on carbamate formation rate decreases with CO_2 loading. The dependence on diffusivity of CO_2 decreases with loading while the diffusivity of all other species increasingly affects the liquid mass transfer coefficient as loading increases. The sum of the powers of D_{CO_2} and D_{Am} is approximately constant at 0.5 throughout the lean and rich loading and approximately equal to the sum of the powers for the dependence of $k_g^{'}$ on $k_{2MPZ-2MPZ}$ and $k_{2MPZCOO^{-}-2MPZ}$ at very lean loading. The dependence of $k_g^{'}$ on physical liquid film mass transfer coefficient, k_l^0, is weak at lean loading but gets stronger at rich loading. At 100 °C, the dependence of $k_g^{'}$ on carbamate formation rate constant is much less and diminishes at rich loading. D_{Am} and k_l^0 dominate the mass transfer rate. $k_g^{'}$ at the lean and rich loading exhibits decreasing dependence on $k_{2MPZ-2MPZ}$ and $k_{2MPZCOO^{-}-2MPZ}$ but increasing dependence on k_l^0 with temperature.

The concentration profiles in the liquid film calculated for 40 °C and 100 °C at the lean and rich loading show that the mass transfer resistance from reaction dominates the mass transfer at low temperature, while the diffusivity of the reactants and products

determines the mass transfer to a greater extent at high temperature. 2MPZ is the most important reactant in the boundary layer at the lean loading but $2MPZCOO^-$ takes over at the rich loading. $2MPZH^+$ changes from a reactant at the lean loading to a product at the rich loading. H2MPZCOO and HCO_3^- are always important products in the operating loading range. $2MPZ(COO^-)_2$ is an important product at 40 °C but not at 100 °C.

The region where $k_g^{'}$ is independent of k_l^0 shifts to higher value of k_l^0 and narrows down with increased temperature. Over the operating CO_2 loading range, the contribution of the gas film resistance to the overall mass transfer resistance is less than 25 % and decreases with CO_2 loading and temperature.

Chapter 9: Conclusions and Recommendations

9.1 SUMMARY OF WORK COMPLETED

In this work 17 concentrated aqueous amine solutions, including primary amines, secondary amines, tertiary amines promoted with piperazine, hindered amine and piperazine derivatives were screened with a Wetted-Wall Column. The simultaneous characterization of CO_2 solubility and liquid mass transfer rates at variable temperature and CO_2 loading, and the subsequent estimation of heat of absorption and CO_2 capacity enable the comparison of different solvents. Quantitative ^{1}H and ^{13}C NMR studies were conducted to further understand the speciation in 2MPZ and the blend of PZ and 2MPZ, which were identified as two of the best solvents with respect to application in CO_2 capture. A rigorous ENRTL thermodynamic model was developed for 8 m 2MPZ through sequential data regression for binary and ternary systems. The rate data for 8 m 2MPZ were used for extraction of kinetic and diffusivity parameters by modeling the WWC in Aspen Plus®.

9.2 CONCLUSIONS

Amine Screening

A summary table is presented (Table 9.1) to show all the key results obtained from the amine screening experiments.

A semi-empirical CO_2 solubility model was developed based on experimental CO_2 solubility data and used for calculation of CO_2 capacity and heat of absorption of the amine solvents. These results are used along with the liquid film mass transfer coefficient as criteria to compare the amine solvents.

Table 9.1: Overview of the properties for all the amines tested. Results for PZ and MEA (Dugas and Rochelle 2009) are also included.

Amine	Lean/Rich loading (mol CO_2/mol alkalinity)	Cyclic CO_2 Capacity (mol/kg (water+amine))	$-\Delta H_{abs}$ @ $P^*_{CO_2}$ =1.5kPa (kJ/mol)	$k'_{g,avg}$ @40°C ($\times 10^7$mol/s·Pa·m^2)	$\frac{A_{packing}}{G_{fluegas}}$ (10^3 m^2/(m^3/s))
8 m PZ	0.31/0.39	0.79	70	8.5	1.8
3.75m 1-MPZ/3.75mPZ/0.5m 1,4-DMPZ	0.23/0.32	0.88	67	8.5	1.8
8 m 1-MPZ	0.16/0.26	0.83	67	8.4	1.8
5m MDEA/5 m PZ	0.21/0.35	0.99	70	8.3	1.8
4m 2-MPZ/4m PZ	0.30/0.39	0.84	70	7.1	2.1
7m/2m MDEA/PZ	0.13/0.28	0.8	68	6.9	2.2
8 m 2-MPZ	0.27/0.37	0.93	72	5.9	2.5
7.7 m HEP	0.15/0.24	0.68	69	5.3	2.8
7 m MEA	0.45/0.55	0.47	82	4.3	3.5
10 m DGA®	0.41/0.49	0.38	81	3.6	4.2
6 m AEP	0.26/0.32	0.66	72	3.5	4.3
8 m 2-PE	0.37/0.68	1.23	73	3.5	4.3
8 m MAPA	0.47/0.51	0.42	84	3.1	4.8
12 m EDA	0.44/0.50	0.78	81	2.5	6
4.8 m AMP	0.27/0.56	0.96	73	2.4	6.3

The primary amines, DGA®, MAPA and EDA, feature high heat of CO_2 absorption like MEA with values around 80 kJ/mol. The average heat of CO_2 absorption for all the PZ derivatives is around 70 kJ/mol, substantially less than the primary amines. The average heat of absorption for hindered amine ranges from 70-75 kJ/mol. Addition of MDEA to PZ slightly lowers the heat of CO_2 absorption. A greater heat of absorption will always enhance the energy performance with temperature swing regeneration.

The hindered amines, 4.8 m AMP and 8 m 2-PE, have high CO_2 capacity but low rate at rich loading. The primary amines have disadvantages of low capacity at operating loading range, although the capacity of EDA can be increased by increasing the amine concentration. Blending PZ with MDEA increases the CO_2 capacity of the solvent. The CO_2 capacity for 2-MPZ is slightly higher than PZ due to the moderately hindered amino group. Cyclic CO_2 capacity of amine from $P^*_{CO_2}$ = 0.5 kPa to $P^*_{CO_2}$ = 5 kPa at 40 °C decreases in the sequence of 8 m 2-PE > 5 m MDEA /5 m PZ > 4.8 m AMP > 8 m 2-MPZ > 3.75 m1-MPZ/ 3.75 m PZ/0.5 m 1,4-DMPZ > 4 m 2-MPZ/4 m PZ > 8 m 1-MPZ > 7 m MDEA/2 m PZ > 8 m PZ > 12 m EDA > 7.7 m HEP > 6 m AEP > 7 m MEA > 8 m MAPA > 10 m DGA®.

The liquid film mass transfer coefficient decreases in the order of 8 m PZ = 3.75 m 1-MPZ/3.75 m PZ/0.5 m 1,4-DMPZ > 8 m 1-MPZ > 5 m MDEA /5 m PZ > 4 m 2-MPZ/4 m PZ > 7 m MDEA/2 m PZ > 8 m 2-MPZ > 7.7 m HEP > 7 m MEA > 10 m DGA® > 8 m 2-PE = 6 m AEP > 8 m MAPA > 12 m EDA > 4.8 m AMP. The packing area required for 90% CO_2 removal of unit flue gas flow rate obtained through a simple design of isothermal absorber is inversely proportional to the measured liquid film mass transfer coefficient. Fast amines such as 5 m /5 m MDEA/PZ, only require 1/2 to 1/3 of the packing area that would be needed for slow solvents like DGA®, MAPA, and AMP.

With all the criteria taken into consideration, 2MPZ/PZ and 2MPZ are promising amine solvents because of their high absorption rate and high CO_2 capacity. MDEA/PZ is also a good solvent candidate for CO_2 capture, although its relatively low heat of absorption may make it less attractive.

Speciation

At 40 °C, more than 75% of the total dissolved CO_2 is converted to unhindered 2MPZ carbamate or its protonated form (2MPZCOO$^-$/H2MPZCOO) over the loading range of 0.10-0.37 mol CO_2/mol alkalinity (α). Hindered carbamate species are not found in the spectra. The amount of HCO_3^-/CO_3^{2-} and 2MPZ$(COO^-)_2$ is relatively small but steadily increases with CO_2 loading, accounting for 12% and 9 %, respectively, at α = 0.367. The fraction of the original 2MPZ that are converted to 2MPZCOO$^-$ /H2MPZCOO increases from 19% at α = 0.104 to 56% at α = 0.367.

Determination of the complete liquid composition for the 4 m 2MPZ / 4 m PZ over the loading range of 0 – 0.4 at 40 °C is limited by the extensive overlap of peaks in the NMR spectra. The equilibrium composition can only be determined for PZCOO$^-$ /HPZCOO, 2MPZCOO$^-$/H2MPZCOO and PZ$(COO^-)_2$ at lean loading. The ratios between them determined from ^{1}H NMR data are consistent with the values from ^{13}C NMR spectra. At lean loading, PZCOO$^-$/HPZCOO, 2MPZCOO$^-$/H2MPZCOO and PZ$(COO^-)_2$ are the major CO_2 sinks, contributing to roughly 50%, 40% and 10% of the total CO_2 absorption, respectively.

Thermodynamic Modeling

2MPZ and H2MPZCOO are modeled as a volatile and a nonvolatile Henry's component, respectively. pKa and volatility of 2MPZ in water is matched by the model. The predictions for CO_2 solubility and speciation agree well with the experimental data. The standard free energy of formation, the standard enthalpy of formation for all

carbamate species as well as binary interaction parameters adjusted during the data regression were mostly slightly or moderately correlated to each other. They all have small standard deviations compared to the final estimates. Average adjustment of 2.4% in rich CO_2 loading is allowed to properly represent the VLE data.

Calculated speciation by the model shows that 2MPZ is almost depleted at loading of 0.4 in 8 m 2MPZ at 40 °C. $2MPZCOO^-$ reaches maximum concentration around loading of 0.25 and diminishes at rich end. About 40% of the total 2MPZ is in the form of $2MPZH^+$ and the rest is H2MPZCOO at the CO_2 loading of 0.5. 2MPZ dicarbamate is relatively unimportant throughout the loading range, with the maximum concentration of 0.25 m. The amount of bicarbonate is significant starting at $\alpha = 0.3$ and accounted for 40% of the total dissolved CO_2 at $\alpha = 0.5$.

The predicted activity coefficients for ionic species decrease with CO_2 loading at 40 °C, while those for 2MPZ and CO_2 slightly increase. H2MPZCOO has the lowest activity coefficient among all the species, which might be related to the property of a zwitterion ion.

Reaction stoichiometry between 2MPZ and CO_2 is around 2 at lean loading range, but decreases all the way with loading to 0. Formation of H2MPZCOO prevails at medium loading. Bicarbonate formation buffered by 2MPZ and $2MPZCOO^-$ is the major reaction as the loading is above the lean loading.

Calculated heat of CO_2 absorption for 8 m 2MPZ is about 70 - 75 kJ/mol at the temperature of 120 – 140 °C, and it is a strong function of temperature over the range of 40 – 140 °C. An increase in heat of absorption with temperature is predicted as loading is above 0.25.

Kinetic Modeling

Most of the measured fluxes for 8 m 2MPZ at 40 °C – 100 °C and variable CO_2 loading in the WWC were matched by the kinetic model developed in Aspen Plus® within ±20% via the regression of three kinetic constants associated with carbamate and bicarbonate formation and one parameter associated with dependence of diffusivity on temperature. The calculated liquid film mass transfer coefficients at 40 – 100 °C agree well with the measured values except at very lean loading. The pseudo first order approximation is found to be valid for 40 °C but not for 100 °C. The drop in liquid film transfer coefficient from the lean condition to the rich condition is mainly caused by the depletion of free amine.

At 40 °C, the liquid film mass transfer coefficient ($k_g^{'}$) is dependent upon the reaction rate of carbamate formation at lean loading to the overall power of ~ 0.5, but the dependence decreases with loading. $k_g^{'}$ is only affected by bicarbonate formation at rich CO_2 loading. The dependence on diffusivity of CO_2 decreases with loading while that on the diffusivity of all other species increases with loading. The sum of the powers of D_{CO_2} and D_{Am} is approximately constant at 0.5 throughout the lean and rich loading and approximately equal to the sum of the powers of $k_{2MPZ-2MPZ}$ and $k_{2MPZCOO^{-}-2MPZ}$ at lean loading. The dependence of $k_g^{'}$ on physical liquid film mass transfer coefficient, k_l^0 is weak at lean loading but becomes much stronger at rich loading. At 100 °C, the dependence of $k_g^{'}$ on carbamate formation rate constant is much less and diminishes at rich loading; the mass transfer rate is mainly determined by D_{Am} and k_l^0. The dependence $k_g^{'}$ on the same parameter approaches the same value for the lean and rich loading.

The mass transfer of CO_2 in the liquid film becomes diffusion controlled as temperature increases from 40 °C to 100 °C. 2MPZ and $2MPZCOO^-$ are the most important reactant, and H2MPZCOO and HCO_3^- are the main products in the liquid film

at the lean and rich loading. $2MPZH^+$ changes from a reactant to a product as CO_2 loading increases. As CO_2 loading increases and free 2MPZ decreases, $2MPZH^+$ and $2MPZCOO^-$ change from products to reactants. HCO_3^- is not a significant product in the liquid film.

For 8 m 2MPZ, the pseudo-first order region, where the liquid film mass transfer coefficient is independent of the physical mass transfer coefficient (k_l^0), shifts to higher k_l^0 as temperature increases. Gas film resistance accounts for less than 25% of the total mass transfer resistance at the operating CO_2 loading range and practical conditions.

9.3 RECOMMENDATIONS FOR FUTURE WORK

9.3.1 Experimental

WWC Modification

Due to the constraint of the maximum total pressure allowable in the current WWC set up and the maximum CO_2 concentration that is measurable by the CO_2 analyzer, the capability of measuring CO_2 solubility and liquid mass transfer coefficient at high temperature and high loading is somewhat limited. The water saturator made of glass is the weak spot which cannot endure pressure greater than 100 psig. It may be redesigned and built with high strength materials such as stainless steel. However, a way needs to be figured out to tell the amount of water left in the saturator. A CO_2 analyzer with higher CO_2 range would also be necessary to expand the measurement range of the WWC setup.

The total pressure is currently adjusted with a needle valve, which is not a perfect choice for backpressure regulation. Minor liquid and gas leakage from the need valve was observed. The total pressure was found to fluctuate as the bypass valve is switched, so the adjustment in the needle valve was frequently required. Replacement with more

accurate back pressure regulator is suggested. In addition to that, digital pressure gauges would give a more accurate reading than the currently used pressure gauges.

The temperature control of the gas stream in the WWC was not closely monitored during the experiment and may not be precise. The adjustment in the temperature of water bath should be tried to find out the impact on the temperature of the gas stream upon entering the WWC.

The maximum temperature achievable by the current WWC setup is limited to below 120 °C due to the limitation of the heat pump and a substantial amount of heat loss. The length of time required to heat amine solution to relatively high temperature is also long, limiting the amount of measurements that can be done in a unit time. Additionally, the fluctuation in temperature was more significant at high temperature. A bigger oil bath, which can accommodate the solution reservoir and the WWC chamber, is expected to solve these problems.

Amine Screening

Based on the amine screening results, the following amine solvents should be considered for the future screening work: PZ/AMP with a ratio greater than 6m/4m to avoid solid solubility problem; 2-(isopropylamino)ethanol (IPAE) and its blend with PZ; morpholine promoted with PZ for their superior degradation resistance; aminoethoxyethylamine. A quick thermal stability test should be conducted though before any other rate and VLE measurement is carried out (Davis 2009). Hindered amine with good thermal stability blended with PZ should be pursued.

Hindered Amine Reaction Mechanism

Quantitative ^{13}C NMR spectroscopic study for $^{13}CO_2$ loaded moderately hindered amine solutions can be applied to further study the reaction mechanism and accurately quantify all the products. The speciation data can be incorporated into modeling work to

reveal the role of carbamate species in CO_2 absorption, especially in the reaction boundary layer.

9.3.2 Data Regression and Modeling

The accuracy of the model is partially determined by the amount and types of the relevant data included in data regression. Speciation data and VLE data spanning a broader range of loading and temperature are expected to improve the applicable range of the model. Accurate heat of absorption and heat capacity measurements at various temperature are also beneficial in deriving the temperature dependence of important thermodynamic parameters such as heat capacity and binary interaction parameter.

The measurement of Henry's constant of CO_2 in the new amine solvent would provide valuable information on CO_2 activity, which is also critical for accurate kinetic modeling. Amine vapor pressure at variable amine concentration, temperature and CO_2 loading would yield useful information on amine activity. Inclusion of CO_2 and amine activity coefficient data for 2MPZ loaded solution should be considered for refinement of the thermodynamic model, which will also further improve the kinetic model.

Diffusivity of CO_2 and all other species in amine solvents remains a challenging task. Although attempts had been made to measure the effective diffusion coefficient by diaphragm cell, data for concentrated amine solvent at various conditions is still lacking. More efficient techniques such as Taylor dispersion should be further explored for characterization of diffusion coefficient in concentrated amine solvents.

Viscosity of 2MPZ at variable concentration and temperature would improve the prediction of diffusion coefficients of CO_2 and other molecular and ionic species. These data can be incorporated into the kinetic model to calculate the mass transfer rate at different amine concentration.

Independent regression of important kinetic constants is difficult due to the complication of diffusivity and the limited availability of kinetic data. WWC is not suitable for measurements of very fast kinetics, therefore different techniques such as laminar jet are needed to obtain a comprehensive understanding of kinetic behavior of both unloaded and loaded amine solution. Conditions such as amine concentration and gaseous CO_2 partial pressure can also be carefully selected to emphasize certain reactions. For example, CO_2 absorption into concentrated unloaded amine solution could yield information on 2MPZ and CO_2 reaction; CO_2 absorption into acid neutralized 2MPZ solutions could provide kinetic information on the reaction between $2MPZH^+$ and CO_2.

As a superior solvent identified in this work, 2MPZ/PZ should receive further study. An attempt has been made in this work to combine the 2MPZ model with the PZ model to describe the thermodynamic and kinetic behavior of 2MPZ/PZ. However, the VLE data and speciation data from quantitative NMR cannot be fitted simultaneously. It has been found that the current PZ model ("Guy Fawkes") is not able to adequately fit the speciation data, therefore work is needed to further improve the PZ model by including the speciation data in regression. This will also help to better fit the amine volatility data for PZ and 2MPZ/PZ. Experiment-wise, the effect of the ratio between PZ and 2MPZ on rates and solid solubility should be systematically studied. More thorough data on density and viscosity of the blend at different amine concentration and CO_2 loading is necessary. Pilot plant test on 2MPZ/PZ should be considered, which can also be used to validate 2MPZ/PZ model.

The developed WWC model for 2MPZ can be scaled up to model industrial absorber and stripper. The performance of 2MPZ in a real process can thus be estimated and compared to other amine solvents. The results from the process modeling in turn

could be used for verification of the conclusions obtained in the bench-scale amine screening.

Appendix A: Foaming of Aqueous Piperazine and Monoethanolamine for CO_2 Capture

A.1 ABSTRACT

The cause of foaming in aqueous amines used for CO_2 absorption was investigated in this study. The effect on foaming of amine concentration and various additives, including electrolytes, liquid hydrocarbon, and degradation products, was measured by a standard method. Both aqueous piperazine (PZ) with 0.3 mole CO_2/mole alkalinity (αα) and 7 m monoethanolamine (MEA, α = 0.4)) were studied. Formaldehyde at 270 mM substantially increases foaming in PZ. PZ foamed after 163 hours of oxidative degradation, but this effect was greatly mitigated with an oxidation inhibitor. Silicone antifoam of 1 ppm reduced the foaminess by 20 times. The tendency of 8 m PZ to foam was increased by 40% with the addition of iron (II) up to a concentration of 1.5 mM, but dissolved iron had no significant effect on 7 m MEA. The tendency to foam and foam stability of 8 m PZ solutions was only slightly affected by 1 mM iron (III), 0.1% heptane in water, 5 mM of copper sulfate, or 100 mM of an oxidation inhibitor.

A.2 INTRODUCTION

Foaming is a problem that is widely encountered in gas treating plants and normally leads to serious consequences such as loss of absorption capacity, reduced mass transfer area and efficiency, and carryover of amine solution to the downstream plant. Foaming can be induced by various chemical contaminants including condensed liquid hydrocarbon, fine particulates like iron sulfide, additives containing surface active chemicals, and amine degradation products (Pauley, Hashemi et al. 1989; Pauley 1991; Stewart and Lanning 1994; Abdi and Meisen 2000; von Phul 2001; Spooner, Sheilan et al. 2006; Al-Dhafeeri 2007). Relatively few studies involving systematic and quantitative investigation of foaming in amine solutions have been published. Pauley

studied the effect of hydrocarbon and organic acids on the foaming tendency of monoethanolamine (MEA), methyldiethanolamine (MDEA), diethanolamine (DEA), and formulated MDEA (Pauley, Hashemi et al. 1989). All the contaminants investigated were found to increase the foaming tendency and foam stability of amine solutions to various extents. McCarthy and Trebble studied the foaming tendency of DEA solutions in the presence of various contaminants such as carboxylic acids (McCarthy and Trebble 1996). They found that only those carboxylic acids with more than five carbons substantially enhanced the foaminess compared to a clean DEA solution. Thitakamol and Veawab systematically investigated the effects of process parameters on foaming behavior of MEA, MDEA, and 2-Amino-2-Methyl-Propanol (AMP) and their mixtures (Thitakamol and Veawab 2008). Ranges of solution volume and gas flow rates were identified and used for measuring the foaminess coefficient. They found that most clean amine solutions did not foam, but the addition of degradation products or corrosion inhibitors increased the foaming tendency by up to 23%. The solution volume and gas flow rate used in our study is based on their recommendations.

Concentrated (8 m) PZ has been identified as a promising solvent for CO_2 capture from coal-fired flue gas(Freeman, Davis et al. 2010). It has high absorption capacity and a fast rate of reaction with CO_2 (Bishnoi and Rochelle 2000; Dugas and Rochelle 2009). Foaming was observed in earlier pilot plant experiments with K_2CO_3/PZ (Chen 2007). Foaming has also been observed in recent bench-scale measurements of oxidative degradation in PZ systems (Freeman and Rochelle 2009). This study focused on finding the main causes for PZ foaming. The results obtained will be used for further study of the foaming effect on the CO_2 capture process, and developing efficient means for foaming control.

A.3 EXPERIMENTAL METHODS

A.3.1 Experimental Setup

Foaming tests were performed using a standard test method for foaming of lubricating oils (ASTM D892) as modified by Thitakamol (Thitakamol and Veawab 2008). As shown in Figure A.1, the experimental setup included a 1000 ml graduated cylinder, a water bath equipped with an immersion digital temperature controller, a gas diffusing stone (1 in. diam., porous fused crystalline alumina, average pore size = 60 um, Fisher Scientific) and a gas flow rotameter. Nitrogen instead of air was used to bubble solutions in order to prevent oxidative degradation and minimize variation of CO_2 loading of tested solutions during the course of experiments.

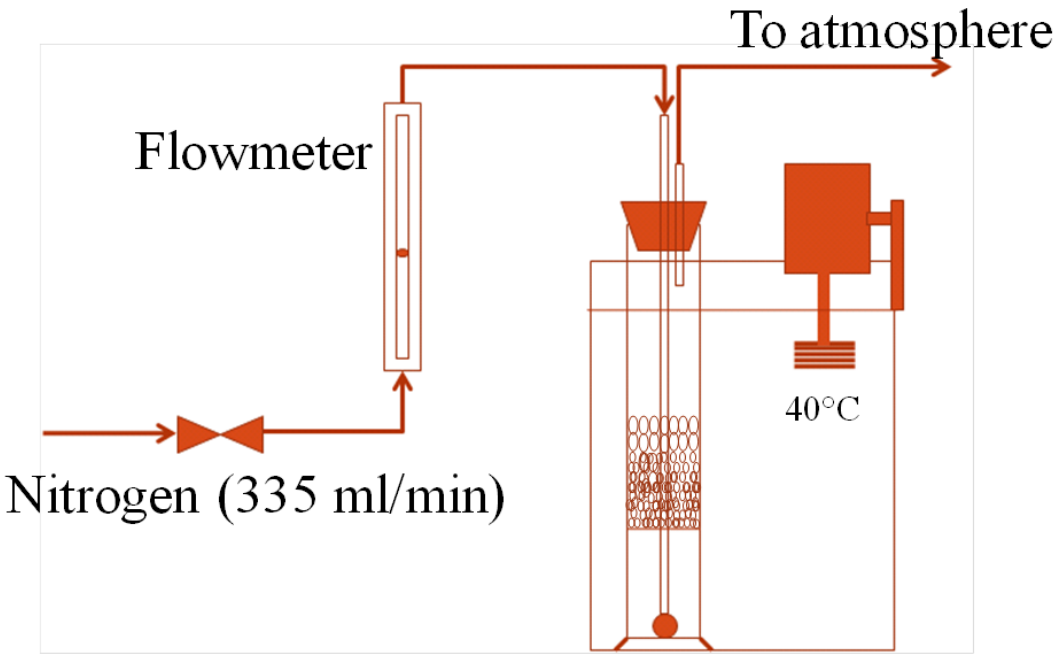

Figure A.1: Schematic diagram for foaming experimental setup

A.3.2 Materials

PZ (99%, Alfa Aesar) and MEA (99+%, Acros) were used without further purification. Amine solutions were prepared by dissolving amines in deionized water followed by sparging the solutions with CO_2 (99.99%) to achieve the desired loading. The typical solution compositions used in this study were 8 m PZ with $\alpha = 0.3$ (moles CO_2/mole alkalinity) and 7 m MEA with $\alpha = 0.4$.

Ferrous (II) sulfate (99%, Reagent A.C.S, Spectrum), ferric (III) chloride (Certified A.C.S, Fisher Chemical), cupric (II) sulfate (Analytical Reagent, Mallinckrodt), formaldehyde (37 wt % water solution, Certified A.C.S, Fisher Chemical), and formic acid (88 wt % water solution, Certified A.C.S, Fisher Chemical) were used without further purification. The antifoam was Q2-3183A obtained from Dow Corning, with silicone as the main component.

A.3.3 Experimental Procedure

A 1000 ml graduated cylinder containing 400 ml test solution was placed in the water bath that had been heated to 40 °C. The diffuser was immersed into the solution and the system was allowed approximately 20 minutes to reach thermal equilibrium. The initial solution volume was recorded. Then nitrogen was introduced to the graduated cylinder at a fixed flow rate of 2×10^{-3} m/s (with respect to the cross section area of the graduated cylinder). A stopwatch was used to track duration of bubbling time.

Since the interface between liquid and foam was hard to identify for most test solutions, the total volume of contents in the cylinder (liquid and foam), instead of the volume of foam only, was recorded every minute. Each foaming test was run for 25 minutes. The total volume seemed to be relatively constant 5 or 6 minutes after experiments were started, therefore the data recorded during the last 15 minutes was averaged and reported as the steady-state value.

Prior to testing each specific additive, neat amine solution (without any additive) was run as a base line. Since the results for neat solutions were not exactly the same each time, normalized foaminess was reported to compare different additives.

A.3.4 Data Analysis

By subtracting the original liquid volume from the total volume in the cylinder, the total gas volume contained in the foam was obtained. The foaminess (F, $m^2 \cdot s$) defined in this study was:

$$F = \frac{V_t - V_0}{G} = \frac{V_g}{G} \tag{A.1}$$

Where V_g is the total steady volume (m^3) of gas trapped in the liquid, V_0 is the original liquid volume (m^3), V_t is the total steady volume (m^3) of content in the cylinder during foaming, and G is the superficial velocity of gas (m/s). Note that the foaminess defined in this study is different from the foaminess coefficient reported by other literatures, which is the ratio of total foam volume to gas flow rate (Bikerman 1973; Thitakamol and Veawab 2008). The normalized foaminess (F^*) was obtained by dividing F by the foaminess of the neat amine solution (F_0):

$$F^* = \frac{F}{F_0} \tag{A.2}$$

The break time of foam (t, second) was defined as the period of time for foam to break completely after gas flow was discontinued. Break time was used to estimate foam stability.

A.4 RESULTS AND DISCUSSION

A.4.1 Amine concentration

Foaminess increased as PZ was varied from 2 m to 8 m at 40 ˚C with α = 0.3 (Figure 2). This is believed tobe mainly due to increased viscosity. As the viscosity of the bulk solution is increased, the drainage of liquid in foam films and the subsequent coalescence is retarded (Ivanov and Dimitrov 1988), which allows foam to propagate to a greater extent. Increase in ionic species with amine concentration might also contribute to the stabilization of foam through electrostatic repulsive forces (Exerowa, Kruglyakov et al. 1997). Attributed to the same reasons, the foam break time increased from 5 s to 29 s with 2 m to 8 m PZ, reflecting enhanced foam stability.

Freeman reported that viscosity of 7 m MEA at 0.4 loading is about 1 / 4 of that of 8 m PZ at 0.3 loading (Freeman, Dugas et al. 2010). Consistently, the foaminess for 7 m MEA solution, about 20×10^{-3} $m^2\cdot s\cdot$ s, is found to be much lower than that for 8 m PZ solution, around 80×10^{-3} $m^2\cdot s$ (Figure A.2).

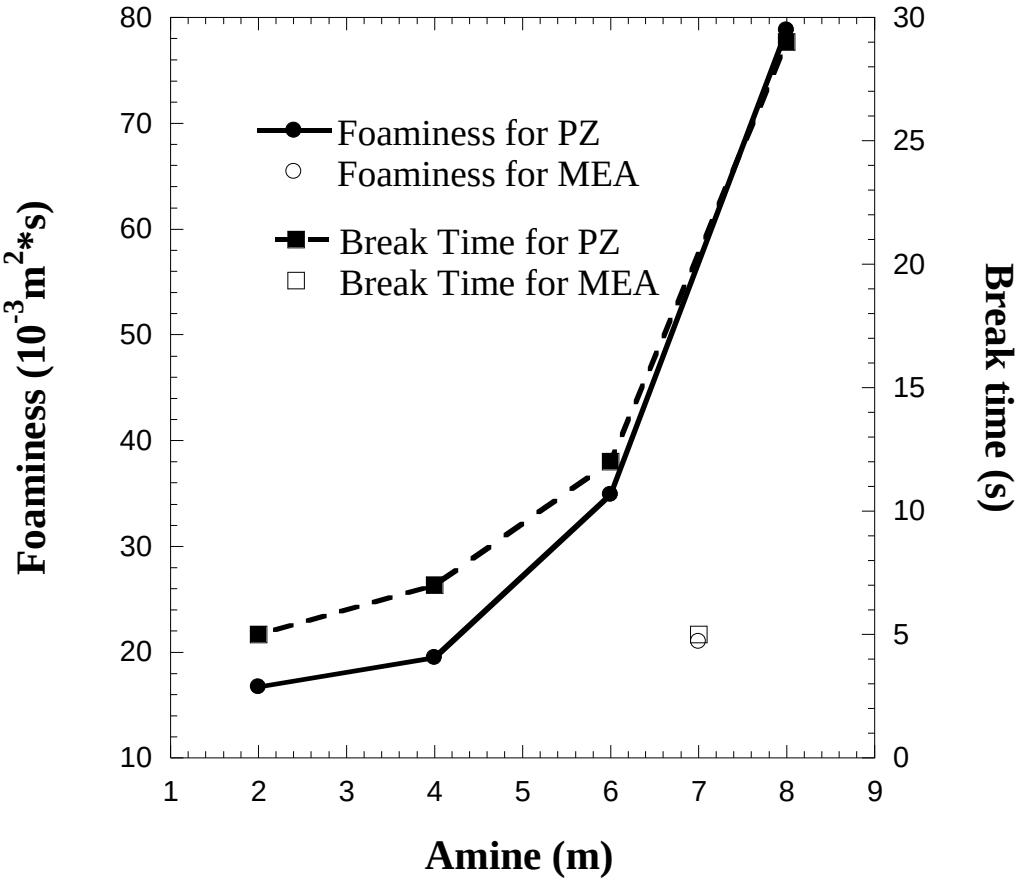

Figure A.2: Effect of amine concentration on foaminess and break time at 40 °C.

A.4.2 Oxidation Products

Freeman showed that formate is one of the primary oxidation products of PZ (Freeman, Davis et al. 2010). The mass balance between the loss of PZ and the increase of oxidation products was not achieved and formaldehyde is believed to be one of the important intermediate products of oxidation that has not been accounted for. Formic acid and formaldehyde were added to CO_2-loaded PZ solutions to study their effect on

foaminess. Foaminess increased only slightly from 81×10^{-3} $m^2\cdot s$ to 85×10^{-3} $m^2\cdot s$ with the addition of 0.5 M formic acid to 8 m PZ.

As shown in Figure A.3, the foaminess increased significantly with formaldehyde. With 270 mM formaldehyde, the volume of the foaming solution exceeded the limit of the graduated cylinder (1000 ml). Therefore the foaminess could only be estimated to be greater than 319×10^{-3} $m^2\cdot s$, more than 3 times greater than the original neat solution (indicated by the arrows in Figure A.3). In addition, the foam layer that formed had a break time greater than 300 s.

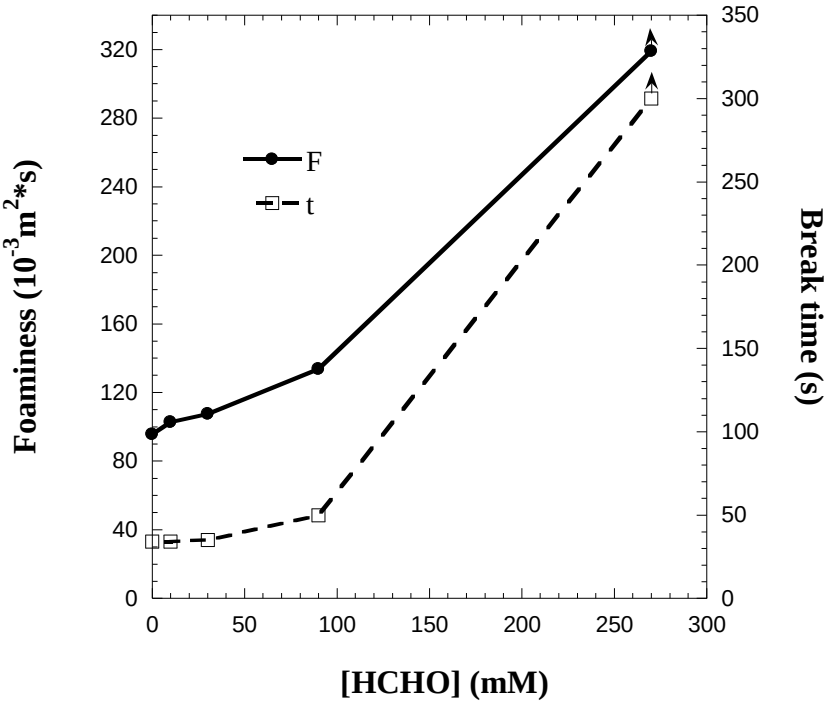

Figure A.3: Foaminess and break time as a function of formaldehyde concentration for 8 m PZ solution with α= 0.3 at 40 ºC. The value of F reported for [HCHO] = 270 mM is an estimation and less than the actual value.

The viscosity of PZ solutions with 270 mM formaldehyde was the same as that of neat solutions. Therefore viscosity does not play a role in increasing foaminess. Sandler reported a condensation reaction between formaldehyde and PZ (Sandler and Delgado 1969). The PZ solution was observed to turn slightly turbid as HCHO was added under stirring. The products, which may be oligimers or polymers, may be surface active and appear to enhance foam stability and increase foaminess. With 7 m MEA solution, the addition of 480 mM formaldehyde also caused a significant increase in foaming tendency.

A PZ solution with 5 mM Cu^{2+} that was oxidized at 55 ºC for over 4 weeks was found to foam like 8 m PZ with 270 mM formaldehyde. Unfortunately, analytical methods have not been developed to determine the formaldehyde in the oxidized solution.

A.4.3 Ferrous Ion

Steel materials are used for most gas treating facilities, making it necessary to study the effect of dissolved ferrous or ferric ions on foaming. A solution of 0.1 M $FeSO_4$ with 0.05 M H_2SO_4 was added to 8 m PZ solution under strong stirring at a rate of 1 drop/sec. The amount of Fe^{2+} in the amine solution was varied from 0 to 1.5 mM to cover the possible range of Fe^{2+} content in a real gas treating system. As shown in Figure A.4, the foaminess of the solution was increased by about 40% as Fe^{2+} was increased to 0.5 mM. Then the foaminess decreased slightly with further addition of Fe^{2+}. It was found that the amine solution turned from light yellow to dark orange as [Fe^{2+}] was gradually increased. Moreover, a layer of orange precipitation was visible on the bottom of the solution container after stirring was stopped. Du et al. and Gonzenbach et al. (Du, Bilbao-Montoya et al. 2003; Gonzenbach, Studart et al. 2006) suggested that if particles have the

correct range of surface energy, they could be favorably absorbed to the interface and form closely packed layer, thus preventing or reducing disproportionation and coalescence of bubbles. It was thus inferred that the fine particles composed of ferrous oxides or ferrous hydroxide in the amine solution might contribute to the increase of foaming tendency. When Fe^{2+} was greater than 0.5 mM, a foam layer of 3–4 mm in thickness remained on the top of the solutions, stable for at least 300 seconds after the gas flow was stopped.

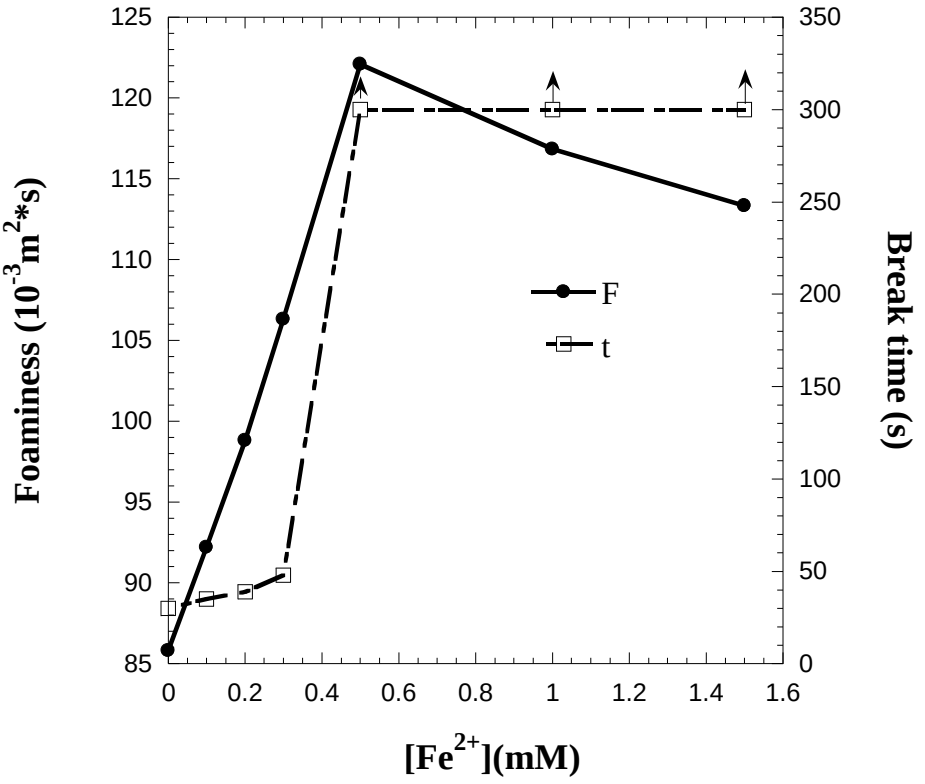

Figure A.4: Foaminess and break time as a function of $FeSO_4$ concentration for 8 m PZ solution with $\alpha = 0.3$ at 40 ºC.

The effect of Fe^{2+} on MEA solution was also studied, as shown in Figure A.5. A maximum in foaminess was observed as the [Fe^{2+}] was increased from 0 to 1 mM, but overall the foaming tendency of MEA solutions was not significantly changed by addition of Fe^{2+} based on the observation in this work.

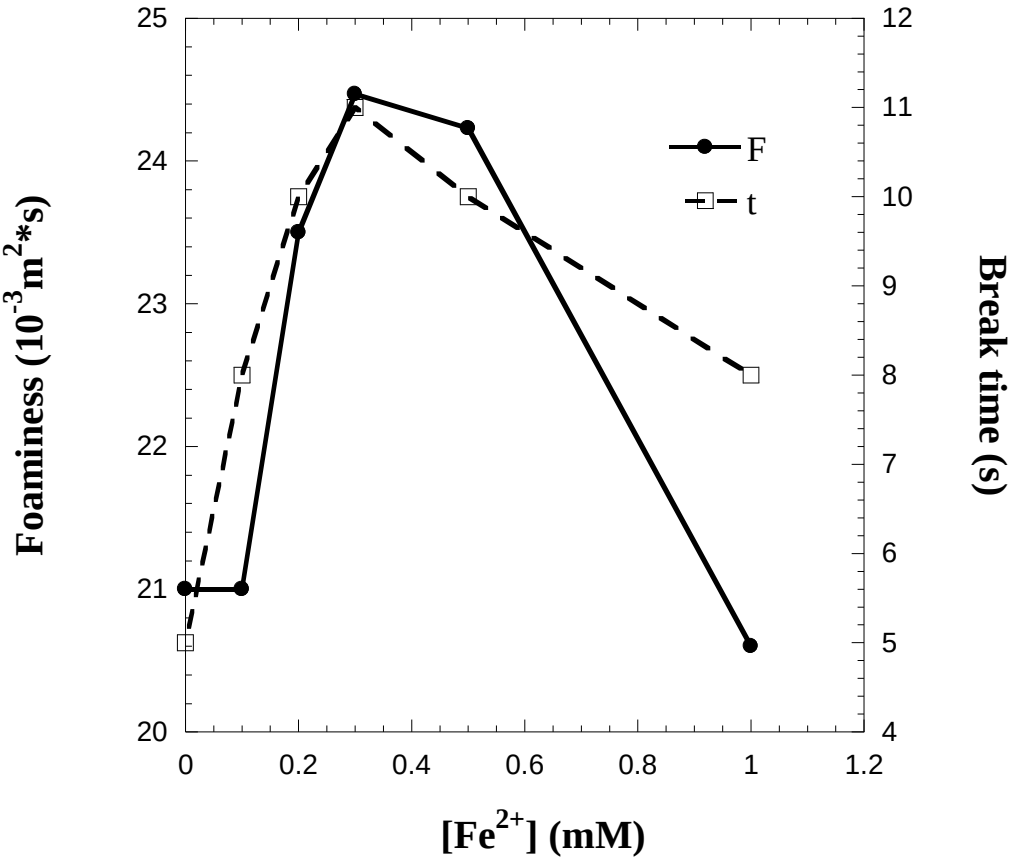

Figure A.5: Foaminess and break time as a function of $FeSO_4$ concentration for 7 m MEA solution with α= 0.4 at 40 ºC.a? ?

A.4.4 Ferric Ion

Dissolved Fe^{2+} can be easily oxidized to ferric ion, Fe^{3+}. Ferric chloride was added to neat amine solution to a concentration from 0.01–1 mM. The change in foaminess of PZ solutions due to the addition of Fe^{3+} is shown in Figure A.6. Foaminess increased slightly with Fe^{3+} concentration first, but peaked at 0.2 mM, then dropped and leveled off at higher concentrations. The ferric ion has a better solubility in amine solutions and may not be able to form fine particles to stabilized foam as ferrous ion did.

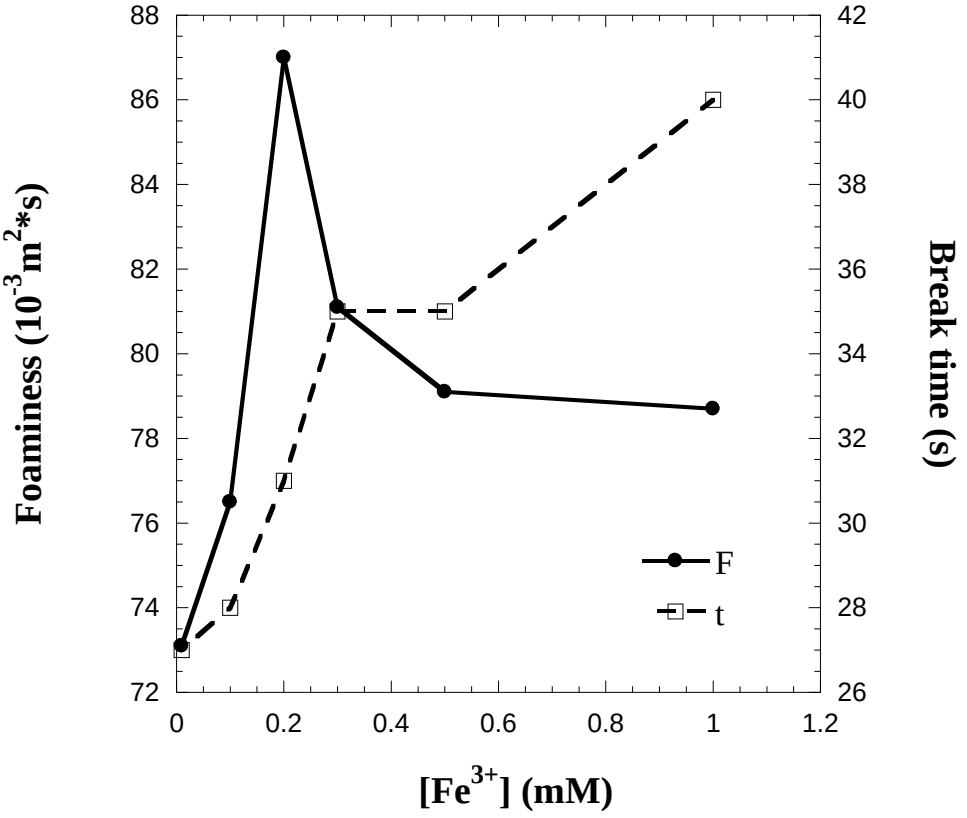

Figure A.6: Normalized foaminess and break time as a function of $FeCl_3$ concentration for 8 m PZ solution with α= 0.3 at 40 ºC.

A.4.5 Liquid hydrocarbon

Previous studies have suggested that hydrocarbon be an important cause of foaming observed in some plants (Pauley et al., 1989; Abdi, 2001; Al-Dhafeeri, 2007). Heptane was used in this work to study the effect of hydrocarbon on foaming. The solubility of heptane in pure water at 40 ºC is about 4.6×10^{-7} moles heptanes per mole water, which is calculated from the semi-empirical equation suggested by Marche and coworkers (Marche et al., 2003). It is difficult to add a small quantity of heptane below the solubility limit, so the starting molar ratio of heptane to water was 8.7×10^{-6} and gradually increased to 9×10^{-3}. As shown in Figure A.7, a very small quantity of heptane did not change the foaming tendency of PZ solution. As $n_{heptane}/n_{H2O}$ was increased to 9×10^{-3}, both foaming tendency and foam stability decreased and heptane started to act as a defoamer. At this concentration it could be observed that heptane droplets were dispersed in the solution. Wasan et al. suggested that oil droplets may enter liquid thin film, spread on the gas-aqueous liquid interface and act as a foam breaker (Wasan, Koczo et al. 1994).

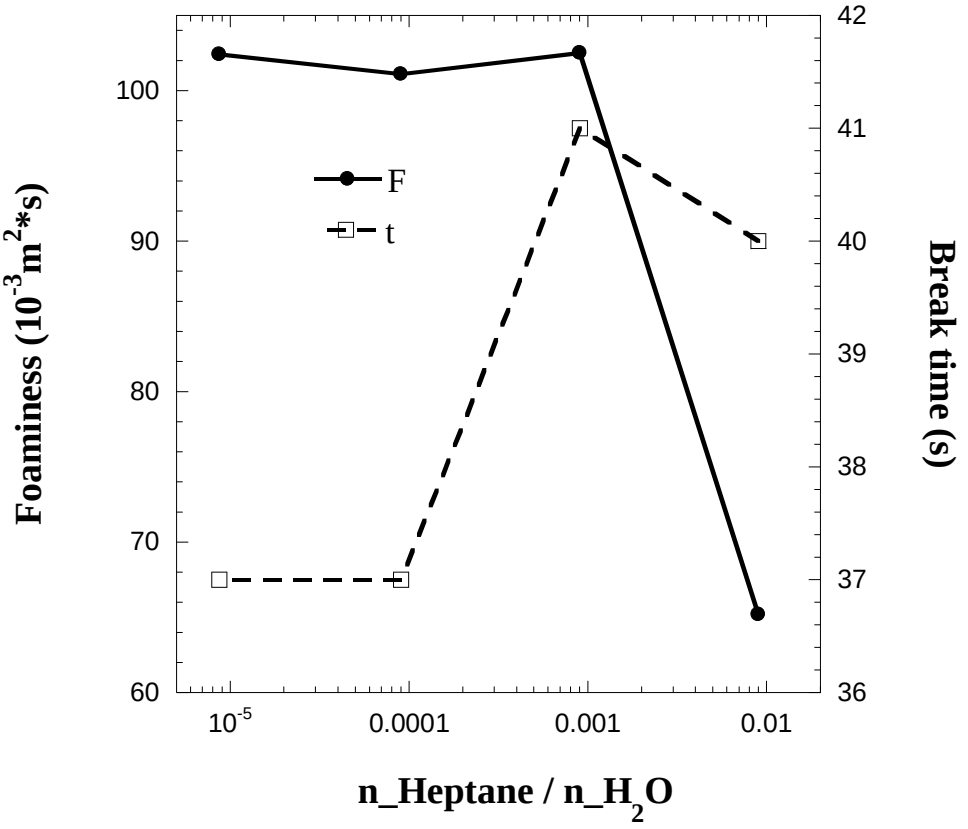

Figure A.7: Foaminess and break time as a function of molar ratio of heptane to water for 8 m PZ solution with α = 0.3 at 40 ºC.

A.4.6 Corrosion inhibitor and oxidation inhibitor

Copper (II) and vanadium (V) are common chemicals added as corrosion inhibitors to amine solutions. The proprietary oxidation inhibitor, "A", may be used used to curb amine oxidation. The effect of these additives on the foaming tendency of PZ is shown in Table A.1. The normalized foaminess, F^*, was found to be less than 1 with additions of corrosion or oxidation inhibitor, which means these inhibitors themselves do not contribute to foaming.

Table A.1: Effect of different chemical additives on normalized foaminess and break time for 8 m PZ solution with α= 0.3 at 40 ºC.

Additives to 8 m PZ, α=0.3	**$F^*=F/F_0$**	**t (s)**
Cu^{2+} (5mM)	0.98	30
Cu^{2+} (5mM) + Inhibitor "A" (100mM)	0.85	33
Cu^{2+} (5mM) +Inhibitor "A" (100mM)+Fe^{2+} (0.1mM)	0.90	35
V^{5+} (10mM)+ Fe^{2+} (0.1mM)	0.77	28

Although the addition of inhibitor A itself did not change the foaming tendency of the amine solution, it can retard the oxidation degradation process. If oxidation products are the main contributors to foaming, amine solution degraded in the presence of A should have a smaller foaming tendency than that of amine solution degraded without A. This is confirmed by foaming results of oxidatively degraded solutions, as shown in Table A.2. The amine solutions were degraded by the method of Sexton (Sexton 2008) at 55 °C under violent agitation in an environment of 98% O_2 and 2% CO_2 for a period of 70 or 163 hours prior to the foaming test. The addition of 100 mM Inhibitor A in PZ solutions was found to decrease foaminess from > 300 to 68 after 163 hours of oxidation.

Table A.2: Effect of inhibitor A on foaming tendency of degraded amine solution (8 m PZ, a=0.3, oxidized at 55 °C).

Additvies to 8 m PZ	**F (10^{-3} m^2 s)**	
	70-hour degradation	163-hour degradation
1 mM Fe^{2+}	85	>>300
1 mM Fe^{2+} + 100 mM A	92	68

A.4.7 Antifoam

The effectiveness of antifoam (Dow Corning, Q2-3183A) in eliminating foaming of PZ solutions was tested. The antifoam was added to the amine solution prior to the start of foaming test. As shown in Table A.3, as low as 1 ppm antifoam was sufficient to reduce the foaminess by 15 to 20 times as well as greatly destabilize the foam. One of the common theories about antifoaming mechanism suggests that antifoam oil can spread across interface, replace the original stabilizing agents and lead to film rupture (Pugh 1996). Strong correlation between antifoam efficiency and antifoam spreading has also been reported (Jha, Christiano et al. 2000).

Table A.3: Effect of antifoam on normalized foaminess with 8 m PZ at α= 0.3 containing Fe^{2+} or formaldehyde at 40 ºC.

Fe^{2+} (mM)	**HCHO (mM)**	**Antifoam (ppm)**	**$F^*=F/F_0$**	**T (s)**
0	0	0	1.00	34
1.5	0	0	1.32	>300
1.5	0	1	0.09	<2
0	270	0	3.33	N/A
0	270	1	0.18	20
0	270	2	0.12	<8

All the results for foaminess and foam stability are tabulated in Table A.4.

Table A.4: Summary of foaminess and break time measurements for PZ with α= 0.3 and MEA with α= 0.4 with different additives at 40 ºC.

Amine/m	**Additives/mM**	**Foaminess ($10^{-3}m^2$ s)**	**Break time (s)**	**Normalized foaminess F***
PZ/2	None	16.7	5	0.21
PZ/4	None	19.5	7	0.25
PZ/6	None	34.9	12	0.44

PZ/8	None	78.8	29	1.00
PZ/8	Fe^{3+}/0.01	73.1	27	1.00
PZ/8	Fe^{3+}/0.1	76.5	28	1.05
PZ/8	Fe^{3+}/0.2	87.0	31	1.19
PZ/8	Fe^{3+}/0.3	81.1	35	1.11
PZ/8	Fe^{3+}/0.5	79.1	35	1.08
PZ/8	Fe^{3+}/1	78.7	40	1.08
PZ/8	None	85.8	30	1.00
PZ/8	Fe^{2+}/0.1	92.2	35	1.07
PZ/8	Fe^{2+}/0.2	98.8	39	1.15
PZ/8	Fe^{2+}/0.3	106.3	48	1.24
PZ/8	Fe^{2+}/0.5	122.1	>300	1.42
PZ/8	Fe^{2+}/1.0	116.83	>300	1.36
PZ/8	Fe^{2+}/1.5	113.33	>300	1.32
PZ/8	Fe^{2+}/1.5 Antifoam/1ppm	7.5	<2	0.09
MEA/7	None	21.0	5	1.00
MEA/7	Fe^{2+}/0.001	20.5	6	0.98
MEA/7	Fe^{2+}/0.01	20.5	7	0.98
MEA/7	Fe^{2+}/0.1	21.0	8	1.00
MEA/7	Fe^{2+}/0.2	23.5	10	1.12
MEA/7	Fe^{2+}/0.3	24.47	11	1.17
MEA/7	Fe^{2+}/0.5	24.23	10	1.15
MEA/7	Fe^{2+}/1.0	20.6	8	0.98
PZ/8 degraded oxidatively	Cu^{2+} Inhibitor A	>303.5	>300	N/A
PZ/8	None	88.3	31	1.00
PZ/8	Cu^{2+}/5.0	86.3	30	0.98
PZ/8	Cu^{2+}/5.0 Inhibitor A/100	75.0	33	0.85
PZ/8	$CuSO_4$/5.0 Inhibitor A/100 $FeSO_4$/0.1	79.8	35	0.90
PZ/8	V^{5+}/10.0 Fe^{2+}/0.1	67.6	28	0.77
PZ/8	None	80.5	28	1.00

PZ/8	Formic Acid/500	85.1	30	1.06
PZ/8	None	95.8	34	1.00
PZ/8	Formaldehyde/10	102.8	34	1.07
PZ/8	Formaldehyde/30	107.4	35	1.12
PZ/8	Formaldehyde/90	133.6	50	1.39
PZ/8	Formaldehyde/270	>319	>300	3.33
PZ/8	Formaldehyde/270 Antifoam/1ppm	17.4	20	0.18
PZ/8	Formaldehyde/270 Antifoam/2ppm	12.0	15	0.12
PZ/8	None	95.0	34	1.00
PZ/8	Heptane/40 ppm	102.4	34	1.08
PZ/8	Heptane/430 ppm	101.1	35	1.06
PZ/8	Heptane/430 ppm	102.5	50	1.08
PZ/8	Heptane/40850 ppm	65.2	N/A	0.69

A.5 CONCLUSIONS

Formaldehyde at 270 and 500 mM, respectively, was found to dramatically increase the foaminess of 8 m PZ and 7 m MEA. Inhibitor A (100 mM) reduced foaminess when 8 m PZ was exposed to 98% O_2 and 2% CO_2 for 163 hours. Foaming was effectively inhibited by the addition of 1 ppm silicone-based antifoam (Dow Corning Q2-3183A). A higher concentration of piperazine has a higher foaming tendency, probably resulting from increased viscosity. The presence of 1 mM Fe^{2+} in solution increased the foaming tendency of PZ solution by up to 40%, but it does not significantly affect foaming of MEA solution. Fe^{3+} up to 1 mM only slightly changes foaminess of PZ solution. Addition of corrosion inhibitor Cu^{2+} or V^{5+} and oxidation inhibitor A did not increase foaming. Formic acid at a concentration of 0.5 M had no effect on the foaming tendency of PZ solutions. Heptane has a negligible effect on PZ solutions as $n_{hep}/n_{H2O} < 9\times10^{-4}$, but it can destabilize foam as n_{hep}/n_{H2O} is increased above 9×10^{-3}. Although some

additives tested in this study did not affect foaming tendency by themselves, the possibility that they could act as foaming promoters when other contaminants are present in the solutions is not excluded.

Appendix B: Detailed ^{1}H and ^{13}C NMR Spectra

B.1 2MPZ

Table B.1: Chemical shift (ppm) of various species in the down filed of ^{13}C NMR spectra for 8 m 2MPZ at varied loading.

	Species			
CO_2 loading (mol/mol alk)	2MPZCOO$^-$	HCO_3^-/CO_3^{2-}	2MPZ(COO$^-$)$_2$	
0.103	162.530	162.863	162.6	163.13
0.279	162.195	161.630	162.615	163.147
0.338	162.034	161.092	162.605	163.143

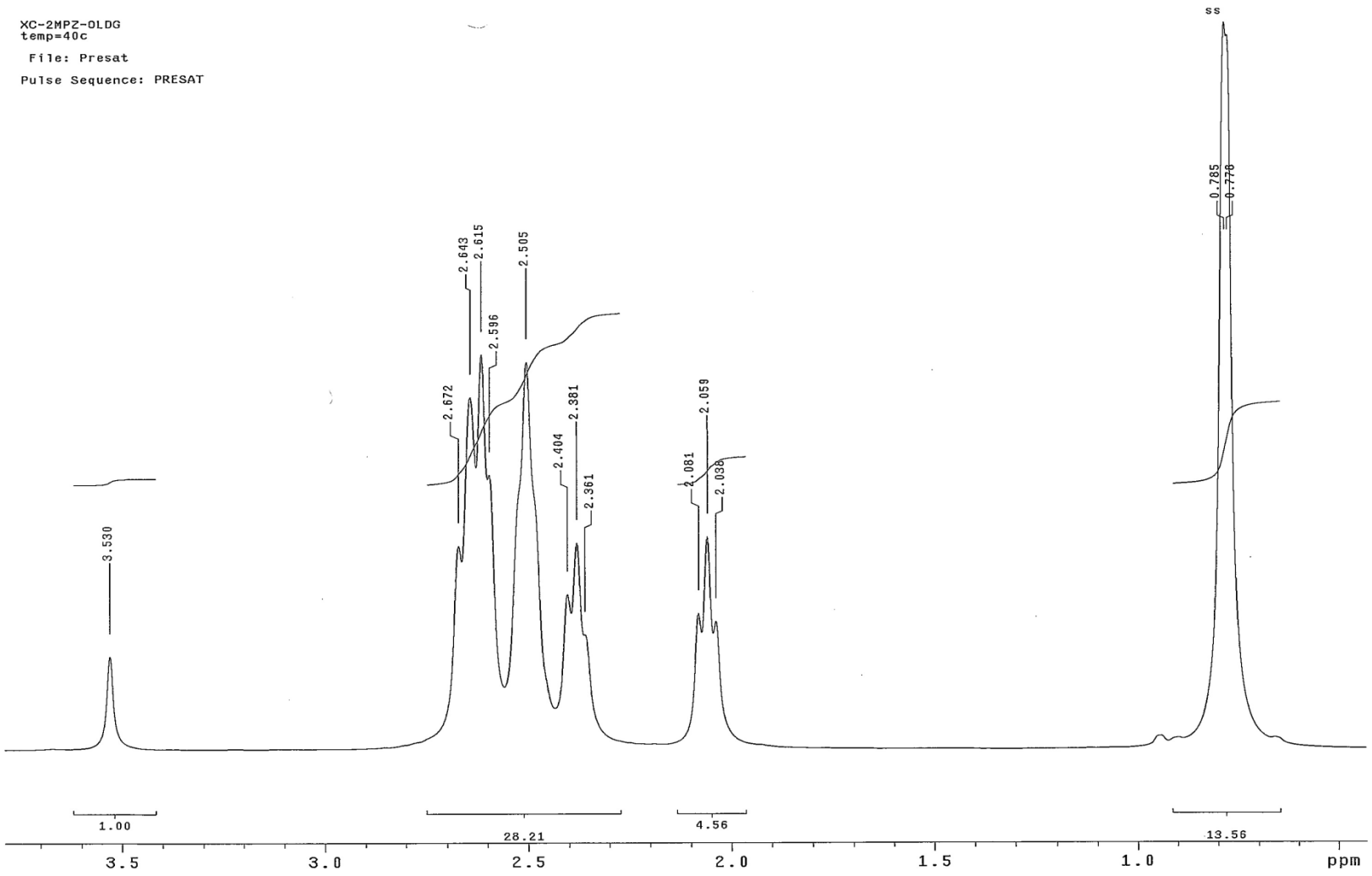

Figure B.1: ^{1}H NMR Spectrum for 8 m 2MPZ, Temperature (T) = 40 °C, CO_2 loading (α) = 0 mol CO_2/mol alkalinity.

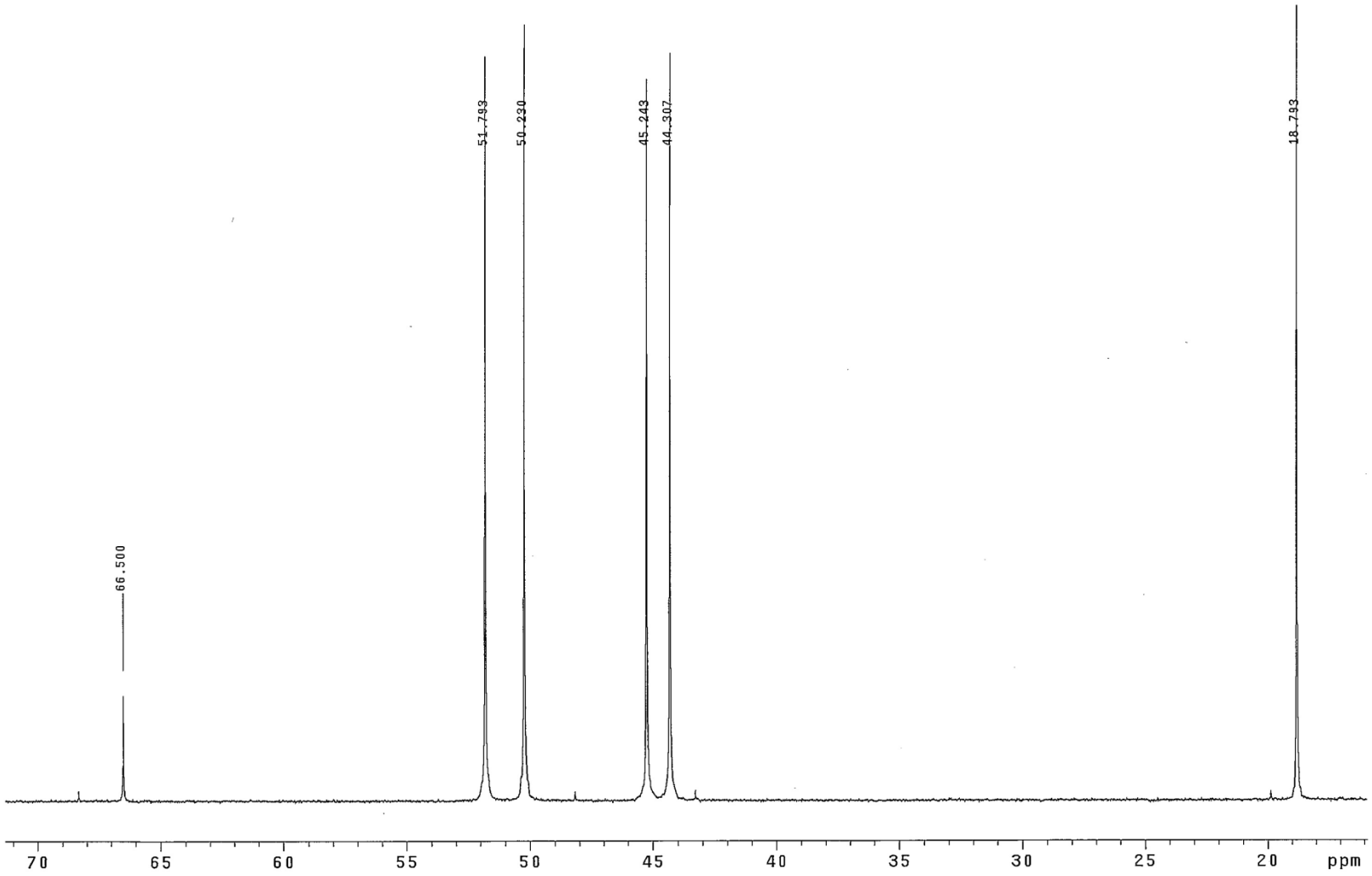

Figure B.2: ^{13}C NMR Spectrum for 8 m 2MPZ, T = 40 °C, α = 0 mol CO_2/mol alkalinity.

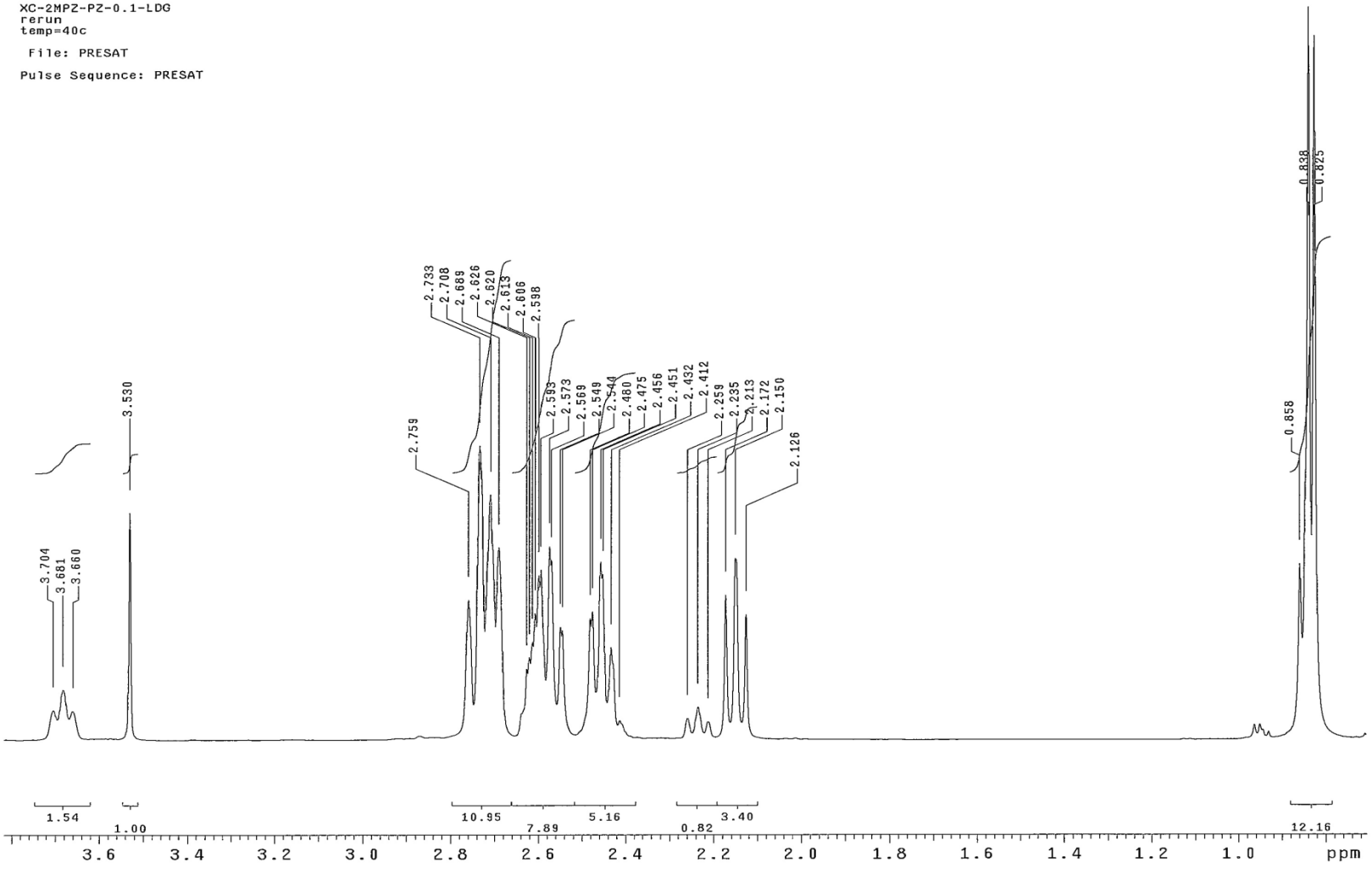

Figure B.3: ^{1}H NMR Spectrum for 8 m 2MPZ, Temp. = 40 °C, α = 0.104 mol CO_2/mol alkalinity.

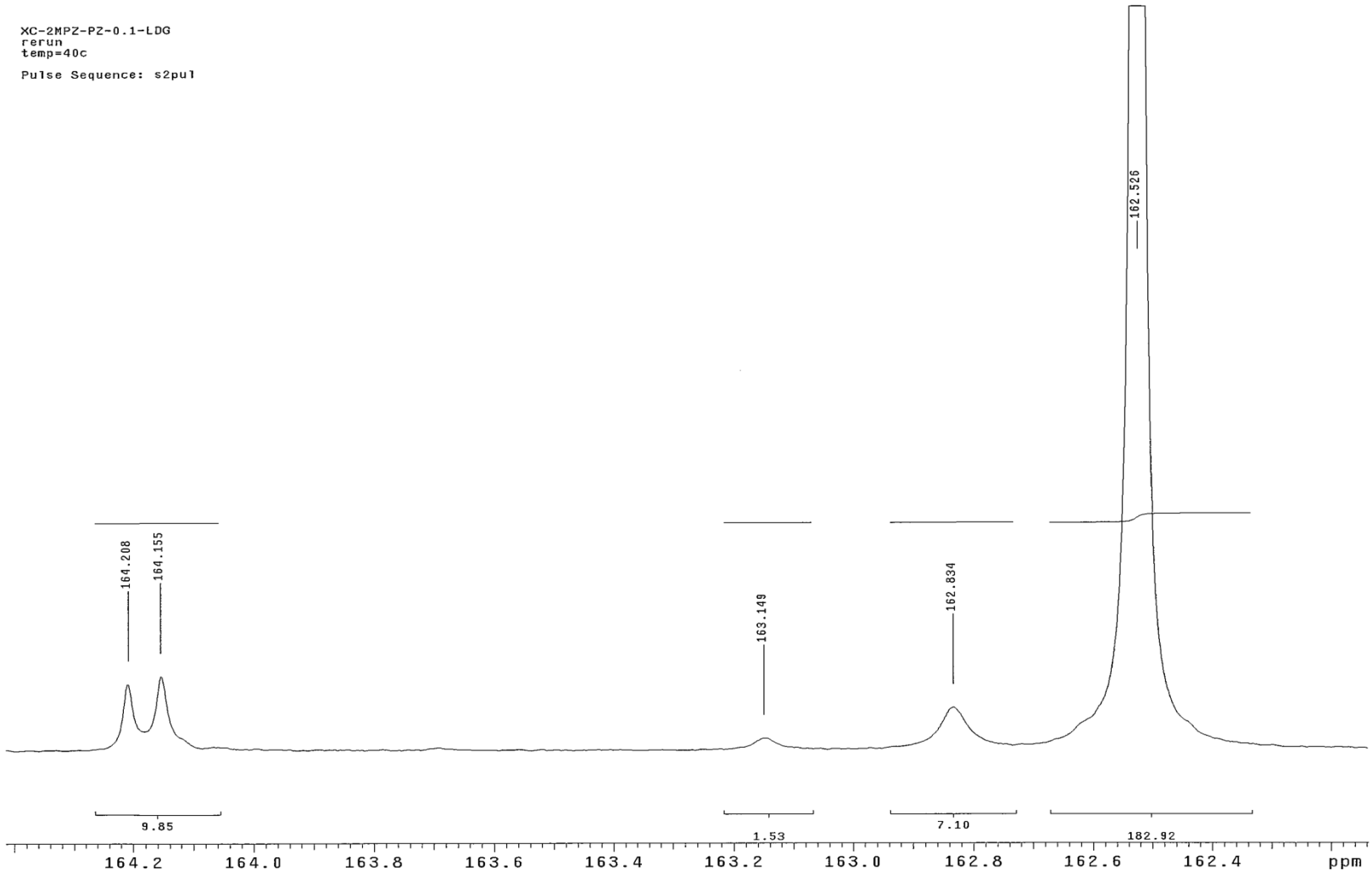

Figure B.4: ^{13}C NMR Spectrum for 8 m 2MPZ, T = 40 °C, α = 0.104 mol CO_2/mol alkalinity, δ = 160 – 165 ppm.

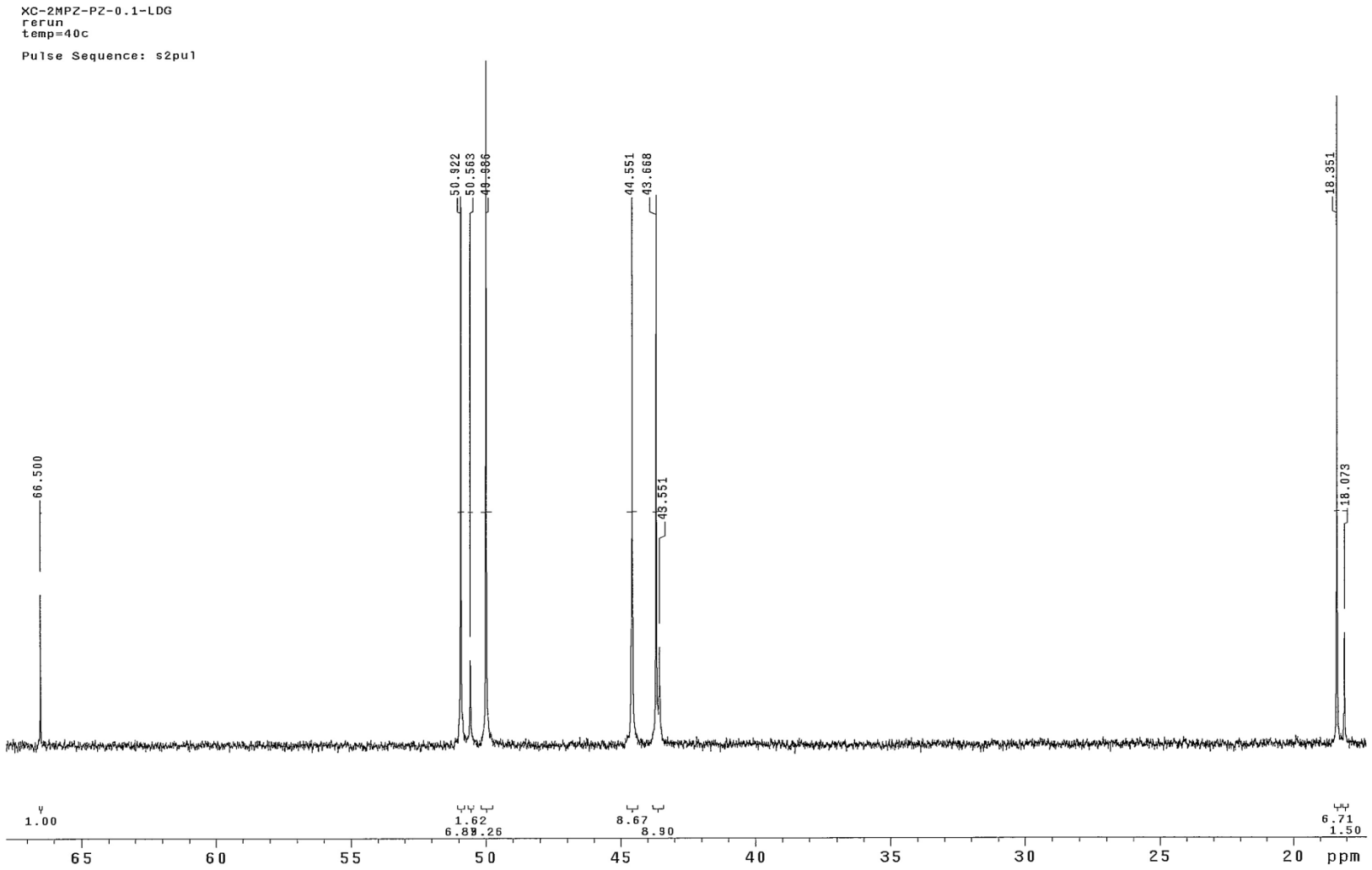

Figure B.5: ^{13}C NMR Spectrum for 8 m 2MPZ, T = 40 °C, α = 0.104 mol CO_2/mol alkalinity, δ = 15 – 70 ppm.

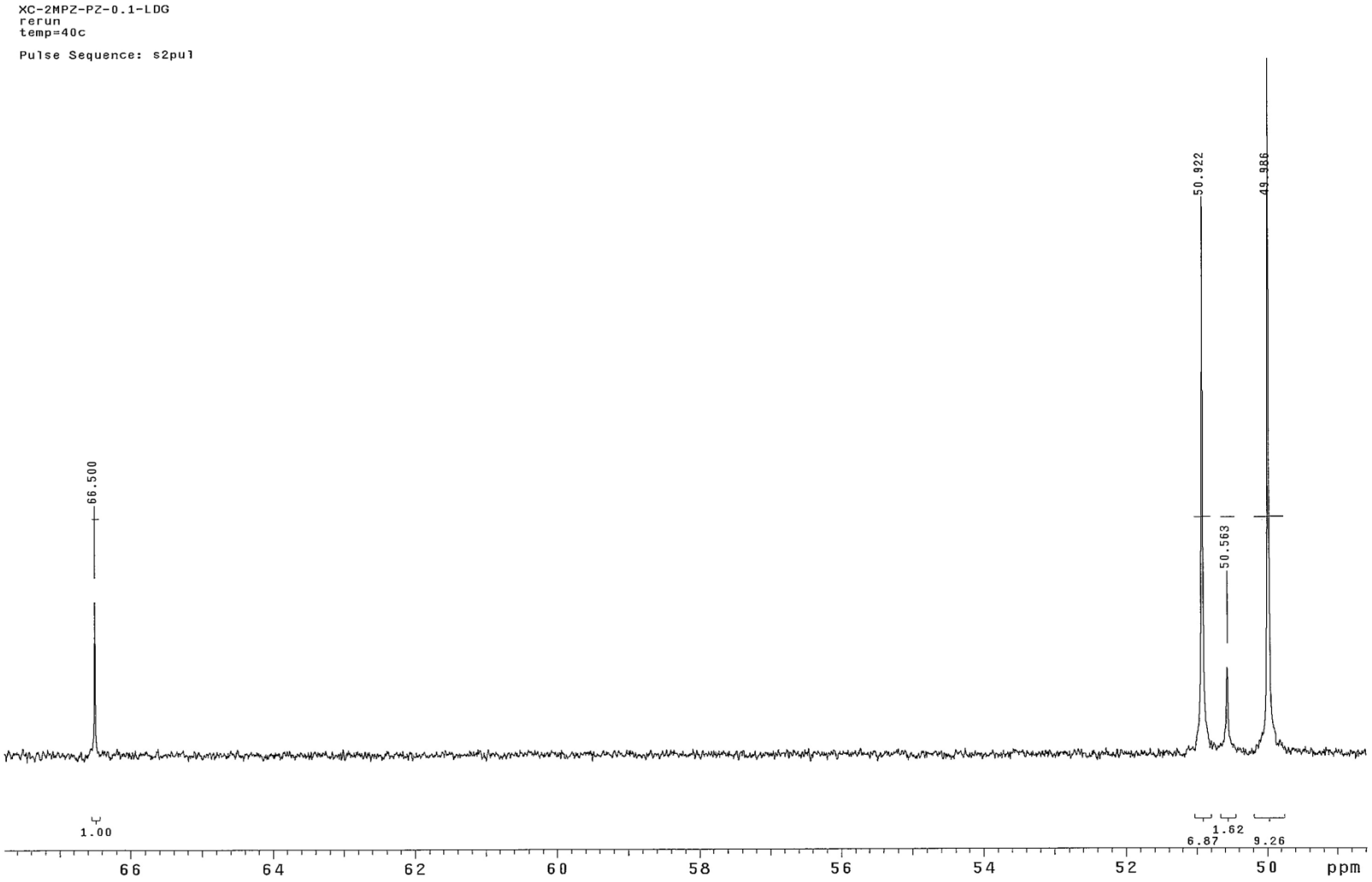

Figure B.6: ^{13}C NMR Spectrum for 8 m 2MPZ, T = 40 °C, α = 0.104 mol CO_2/mol alkalinity, δ = 50 – 70 ppm.

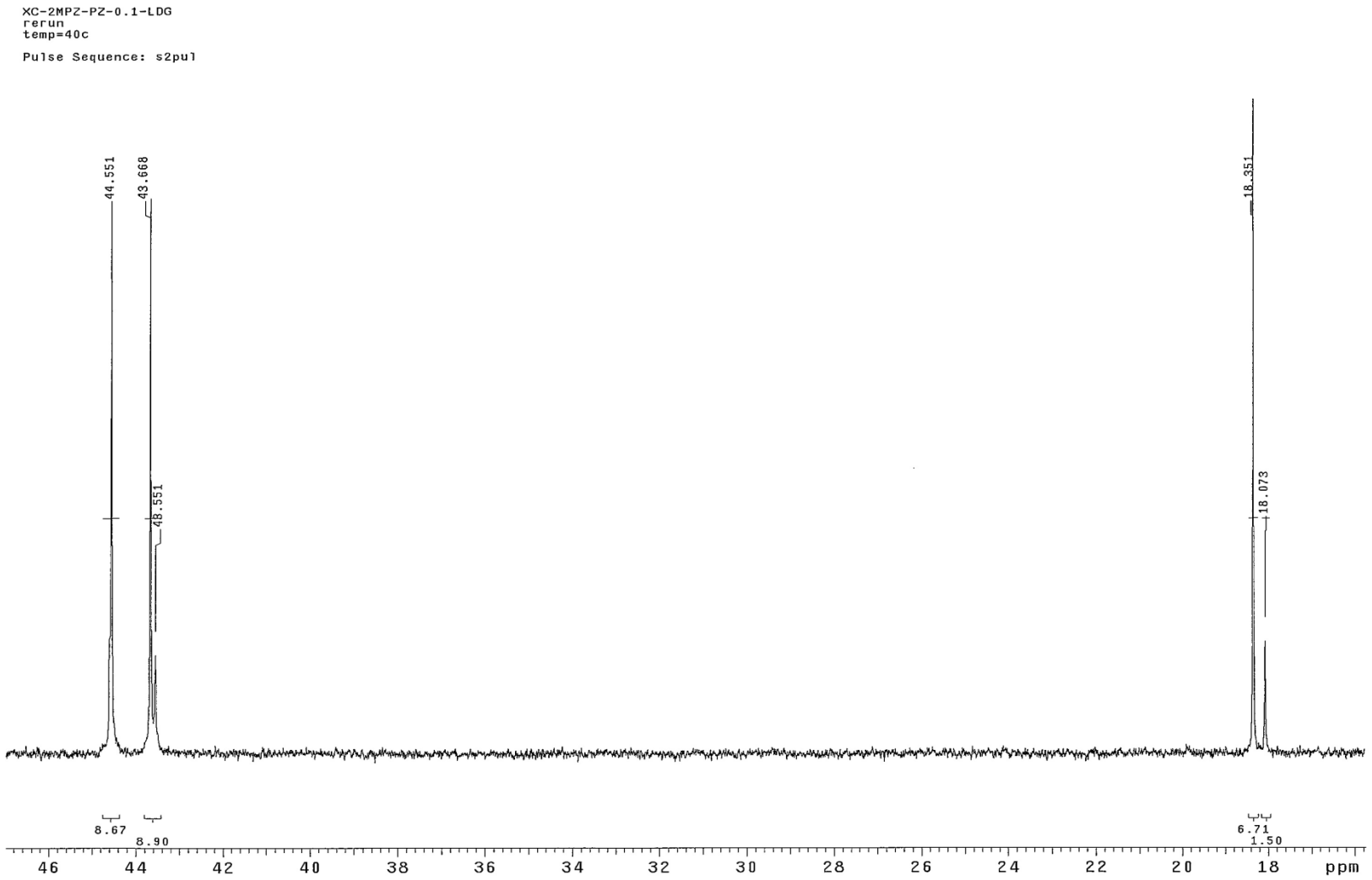

Figure B.7: ^{13}C NMR Spectrum for 8 m 2MPZ, T = 40 °C, α = 0.104 mol CO_2/mol alkalinity, δ = 15 – 46 ppm.

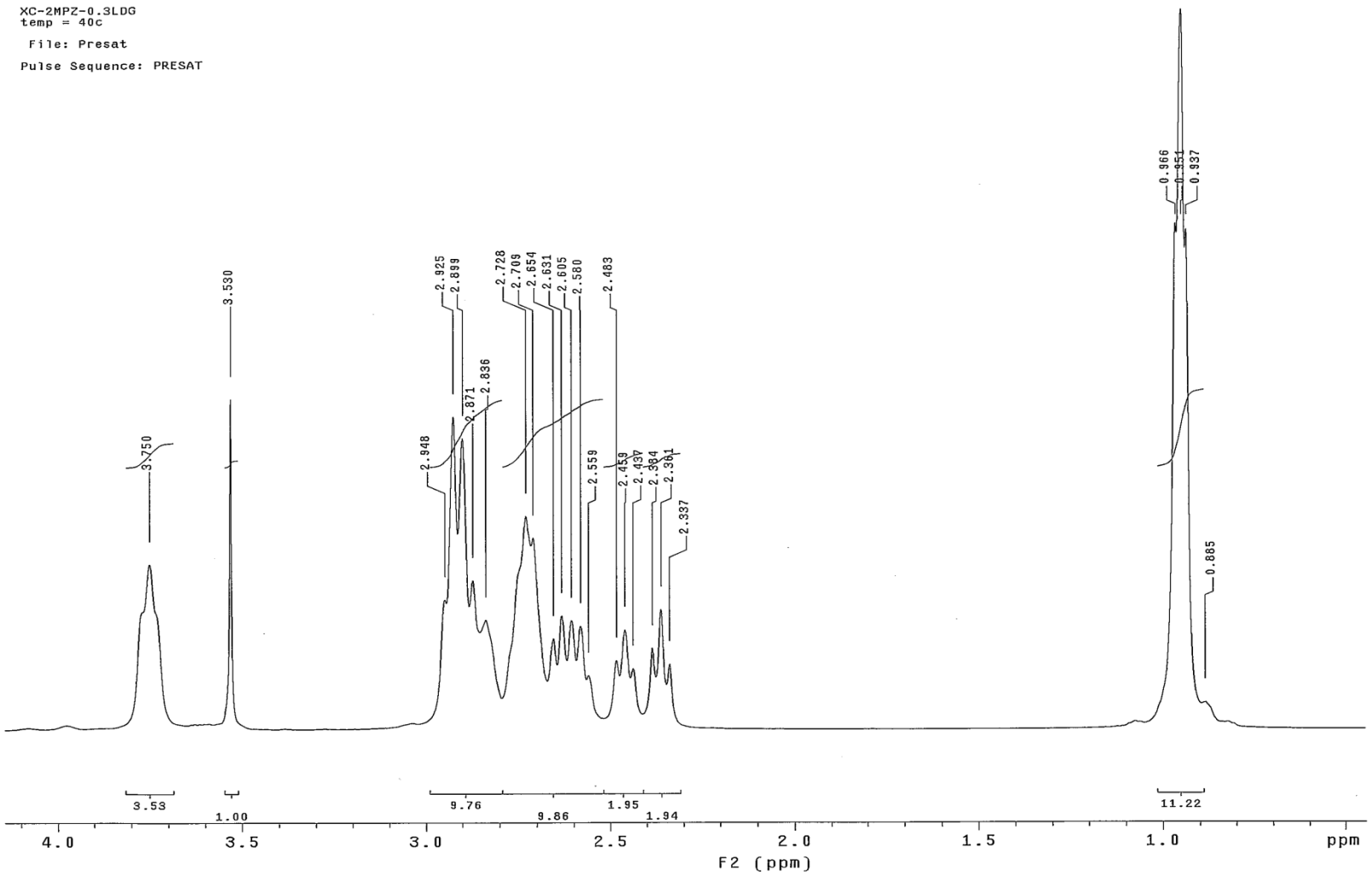

Figure B.8: ^{1}H NMR Spectrum for 8 m 2MPZ, T = 40 °C, α = 0.294 mol CO_2/mol alkalinity.

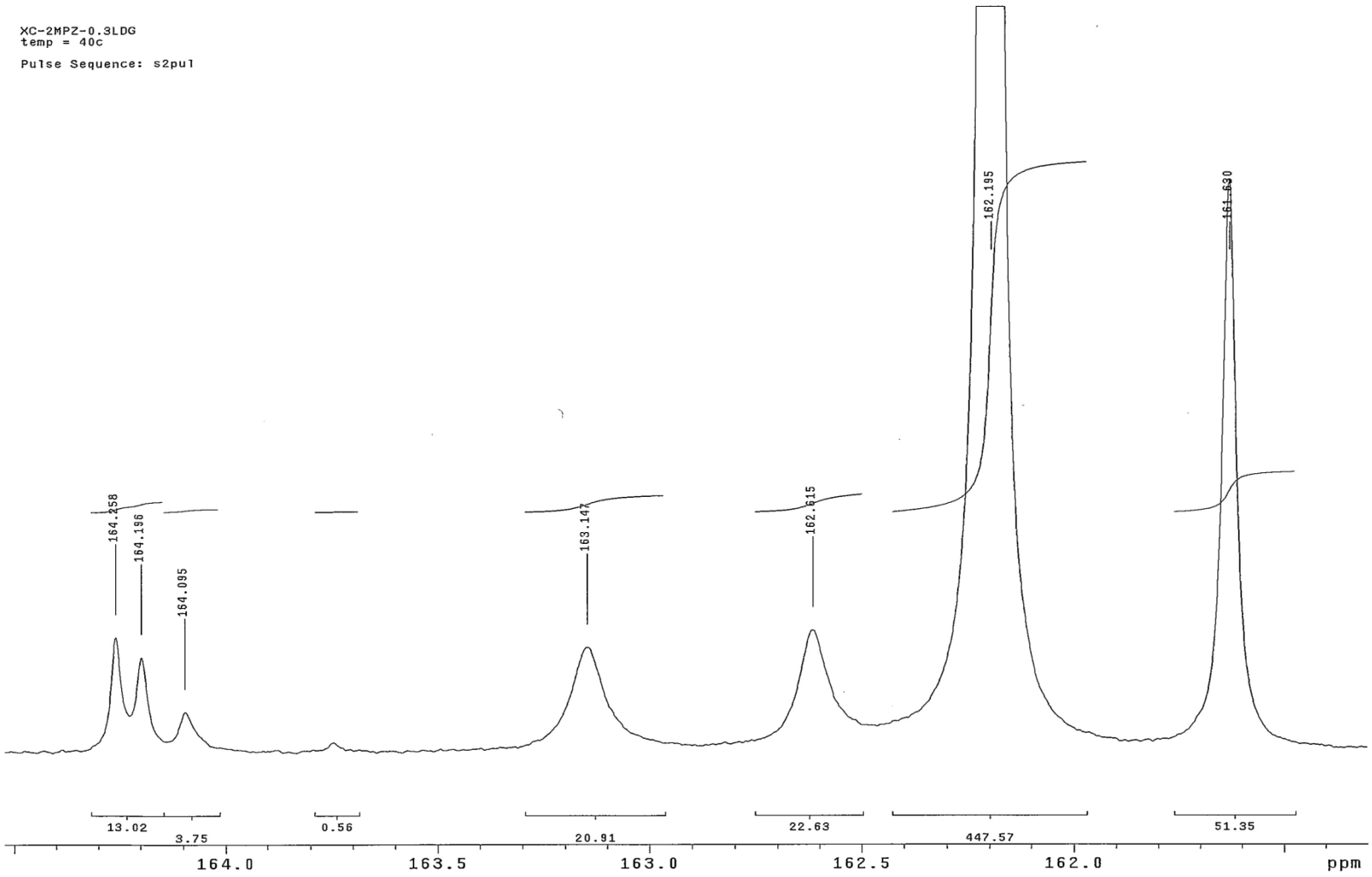

Figure B.9: ^{13}C NMR Spectrum for 8 m 2MPZ, T = 40 °C, α = 0. 294 mol CO_2/mol alkalinity, δ = 160 – 165 ppm.

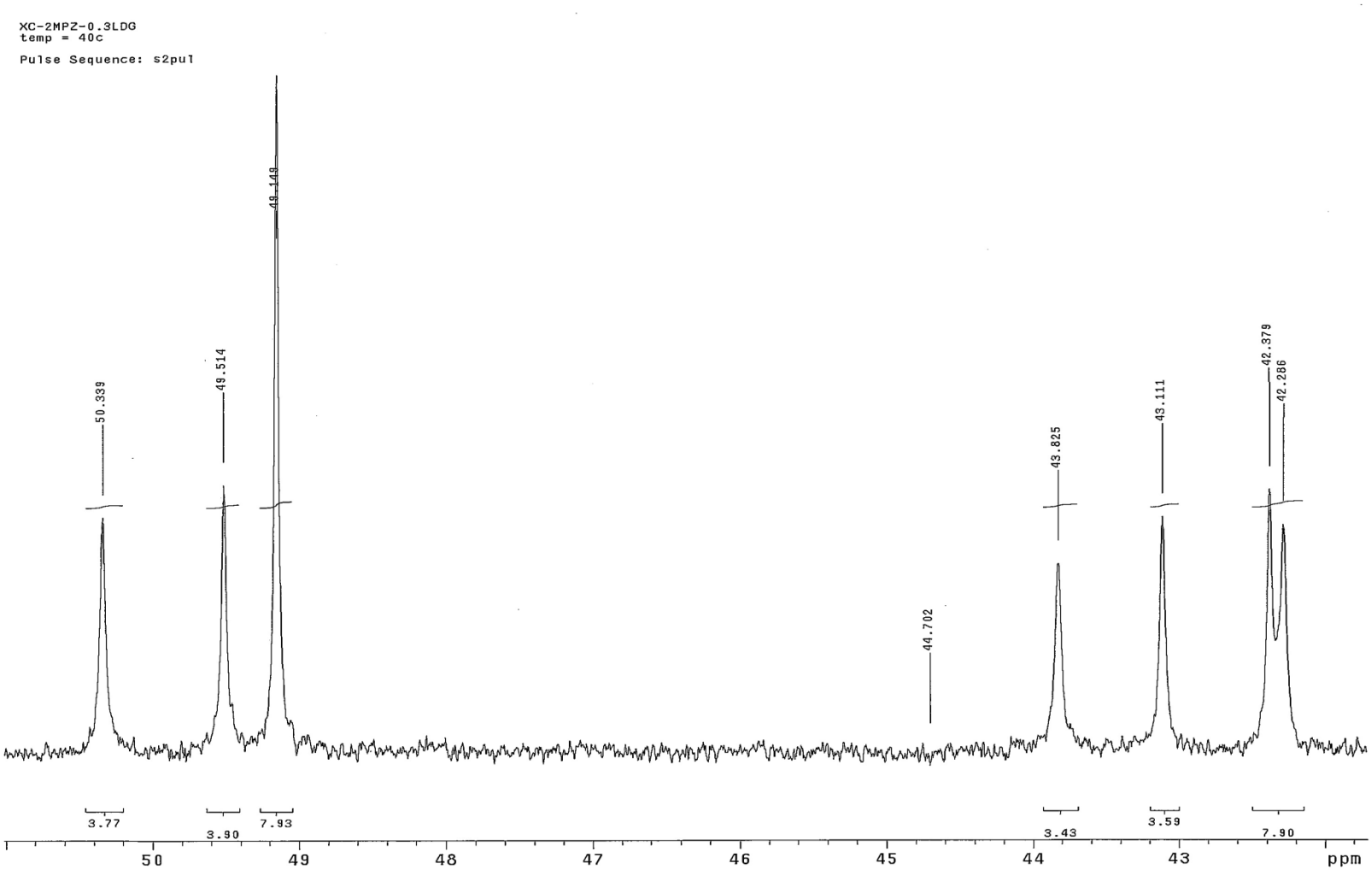

Figure B.10: ^{13}C NMR Spectrum for 8 m 2MPZ, T = 40 °C, α = 0. 294 mol CO_2/mol alkalinity, δ = 40 – 55 ppm.

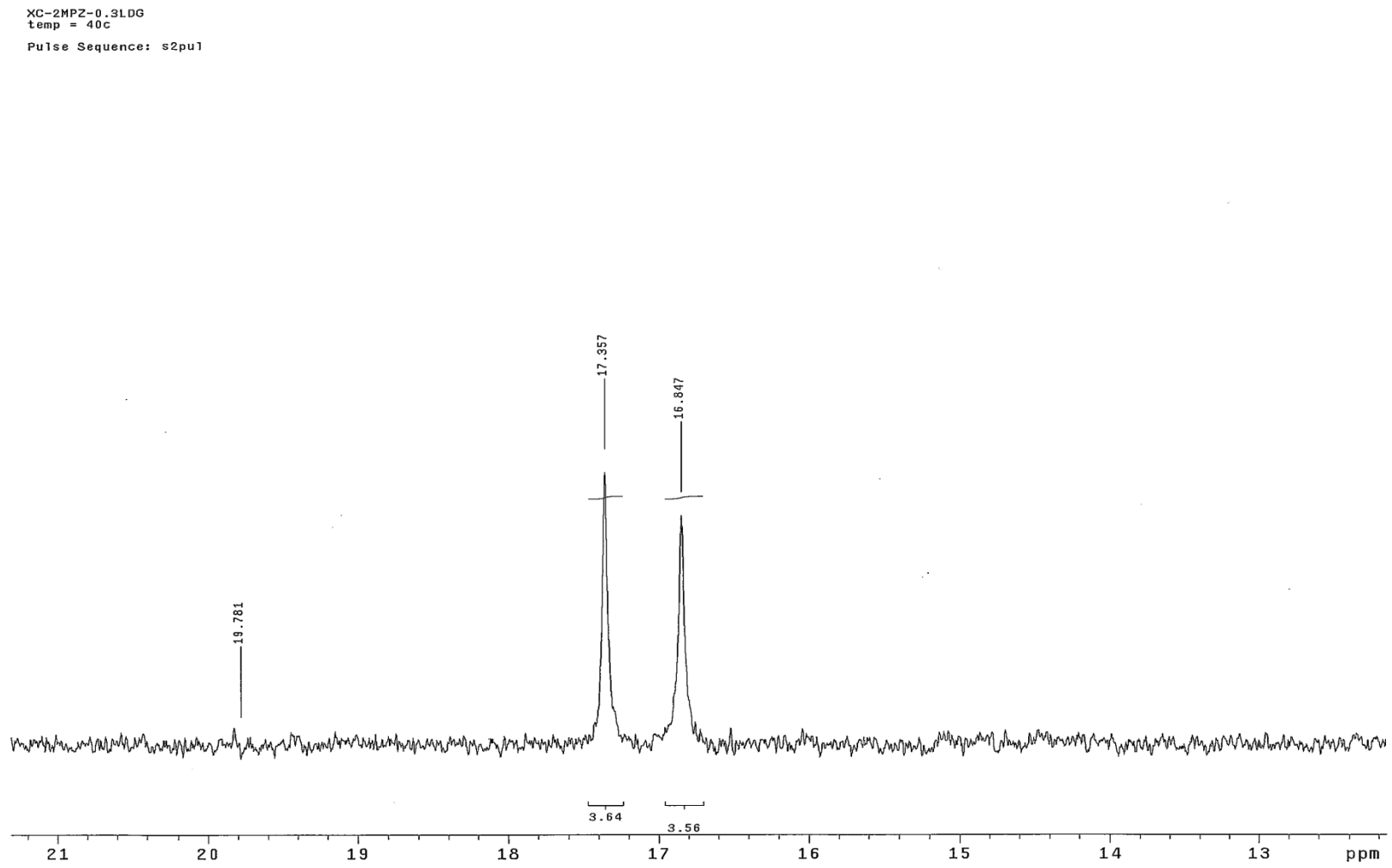

Figure B.11: ^{13}C NMR Spectrum for 8 m 2MPZ, T = 40 °C, α = 0. 294 mol CO_2/mol alkalinity, δ = 10 – 20 ppm.

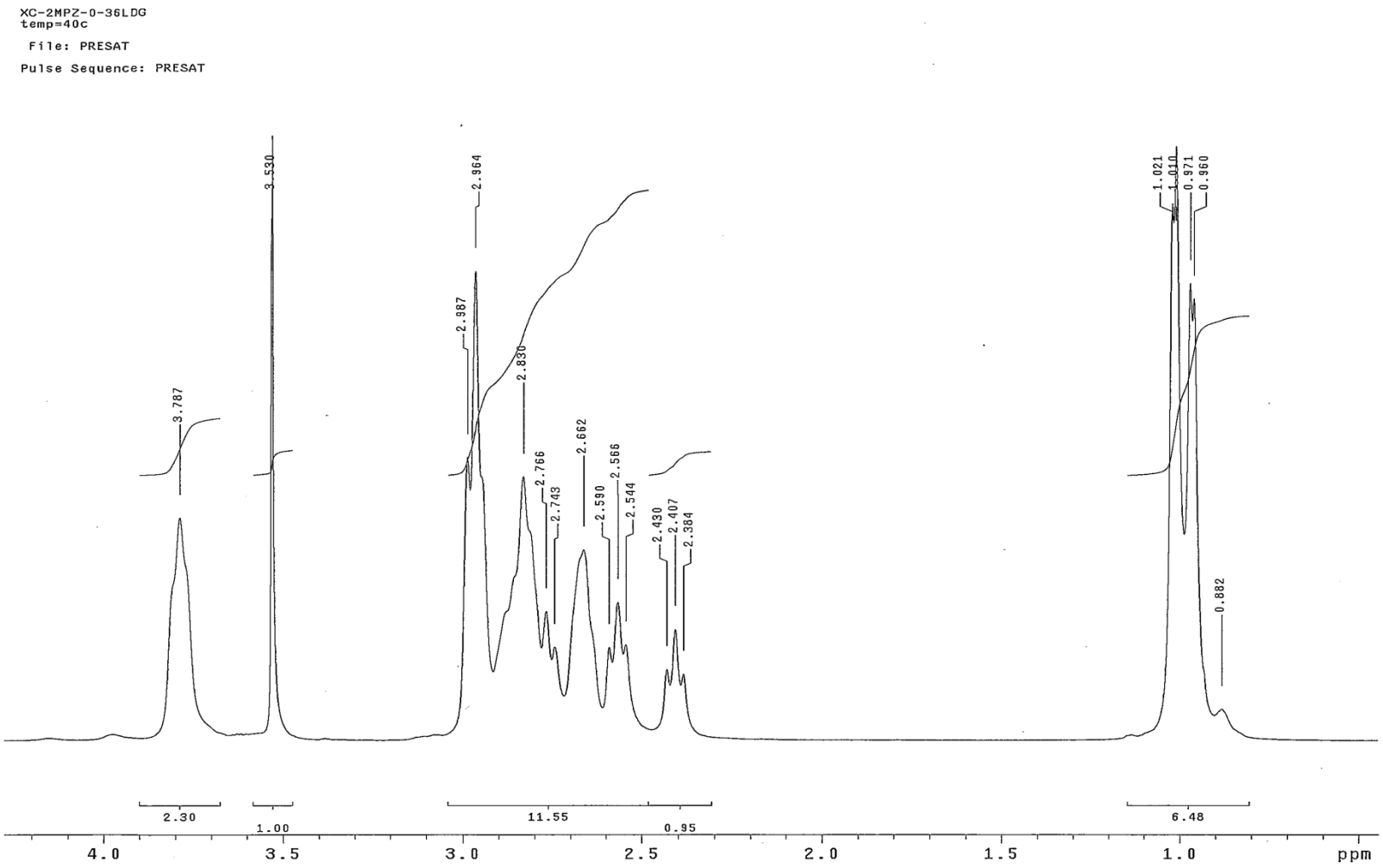

Figure B.12: ^{1}H NMR Spectrum for 8 m 2MPZ, T = 40 °C, α = 0.367 mol CO_2/mol alkalinity.

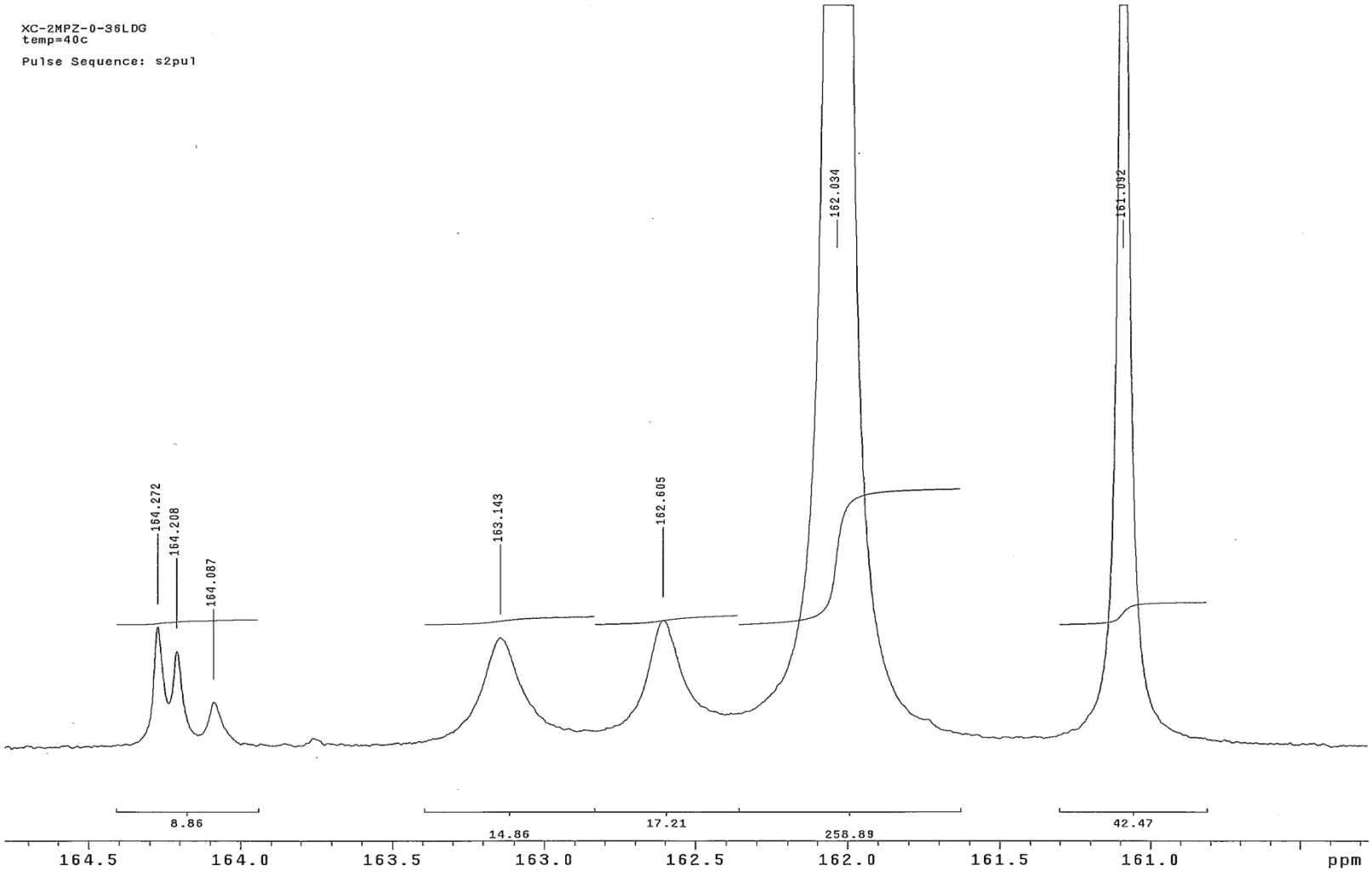

Figure B.13: ^{13}C NMR Spectrum for 8 m 2MPZ, T = 40 °C, α = 0.367 mol CO_2/mol alkalinity, δ = 160 – 165 ppm.

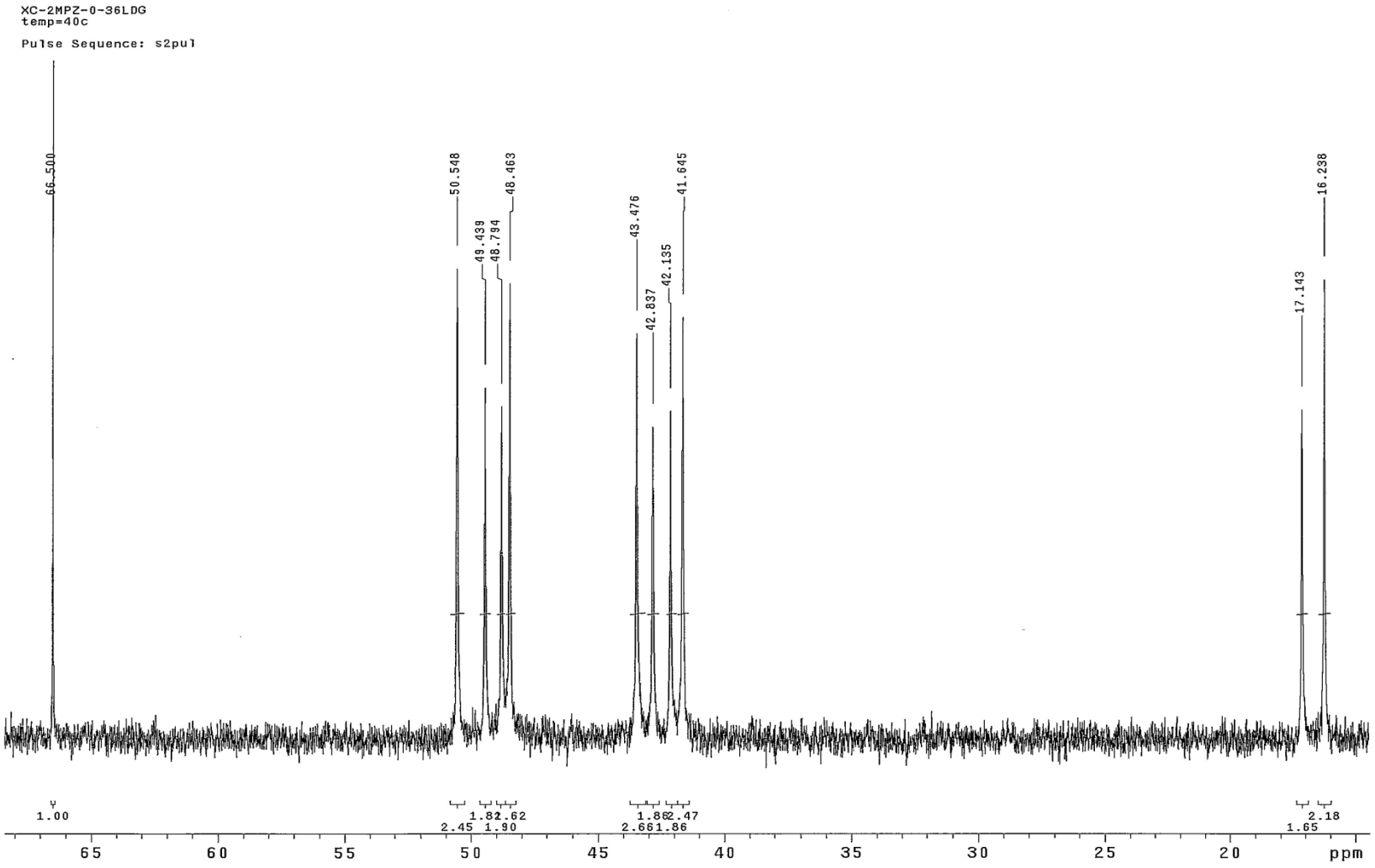

Figure B.14: ^{13}C NMR Spectrum for 8 m 2MPZ, T = 40 °C, α = 0.367 mol CO_2/mol alkalinity, δ = 15 – 70 ppm.

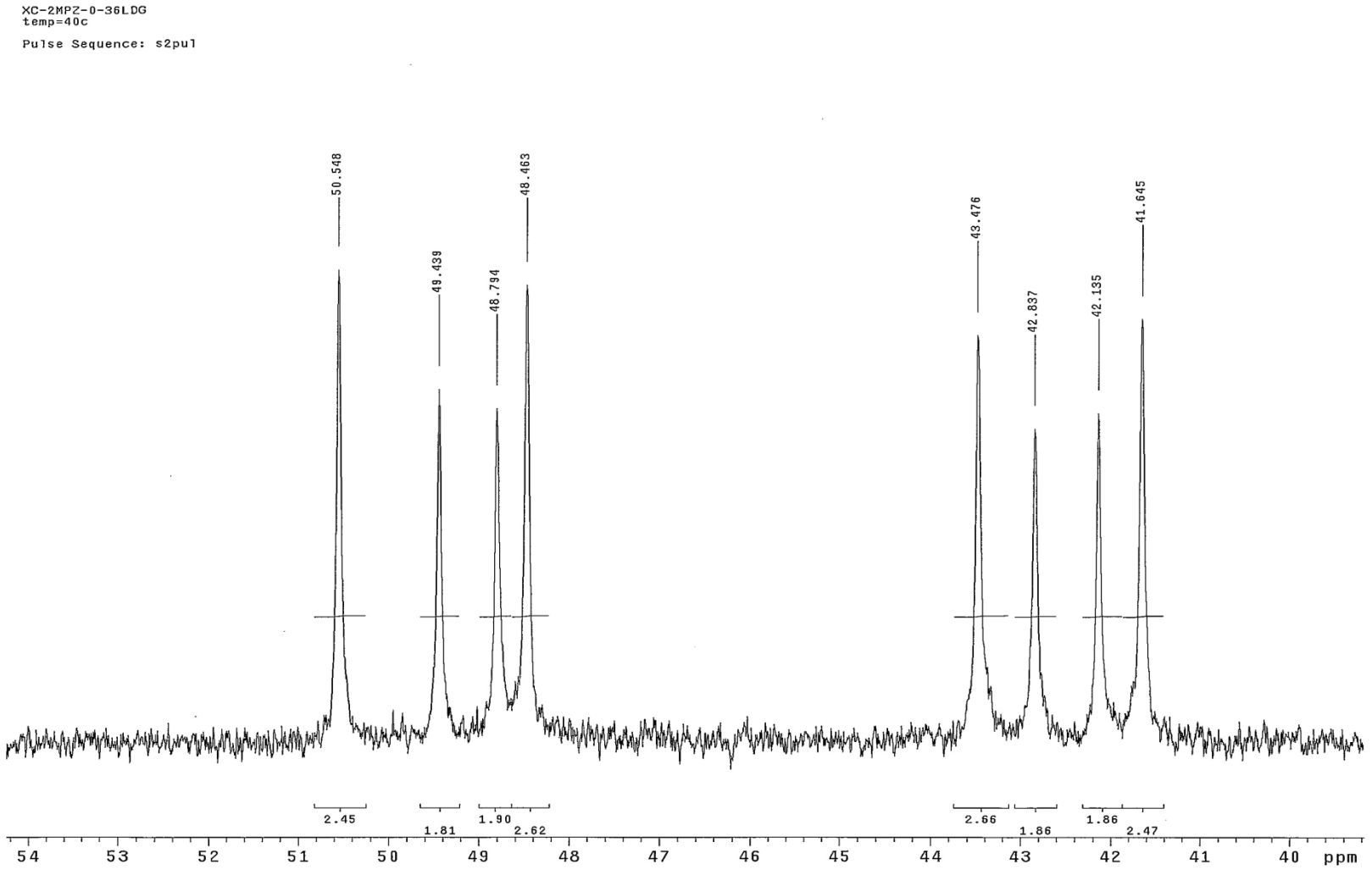

Figure B.15: ^{13}C NMR Spectrum for 8 m 2MPZ, T = 40 °C, α = 0.367 mol CO_2/mol alkalinity, δ = 40 – 55 ppm.

B.2 2MPZ/PZ BLEND

Table B.2: Chemical shift (ppm) of various species in the down filed of ^{13}C NMR spectra for 4 m 2MPZ / 4 m PZ at varied loading.

	Species					
CO_2 loading (mol/mol alk)	2MPZCOO$^-$	HCO_3^-/CO_3^{2-}	2MPZ(COO$^-$)$_2$		PZCOO$^-$	PZ(COO$^-$)$_2$
0.143	162.524	163.199	163.159	-	162.653	162.79
0.219	162.41	-	163.16	-	162.53	162.786
0.300	162.324	162.016	163.153	-	162.233	162.78
0.440	-	160.602	-	-	161.872	162.673

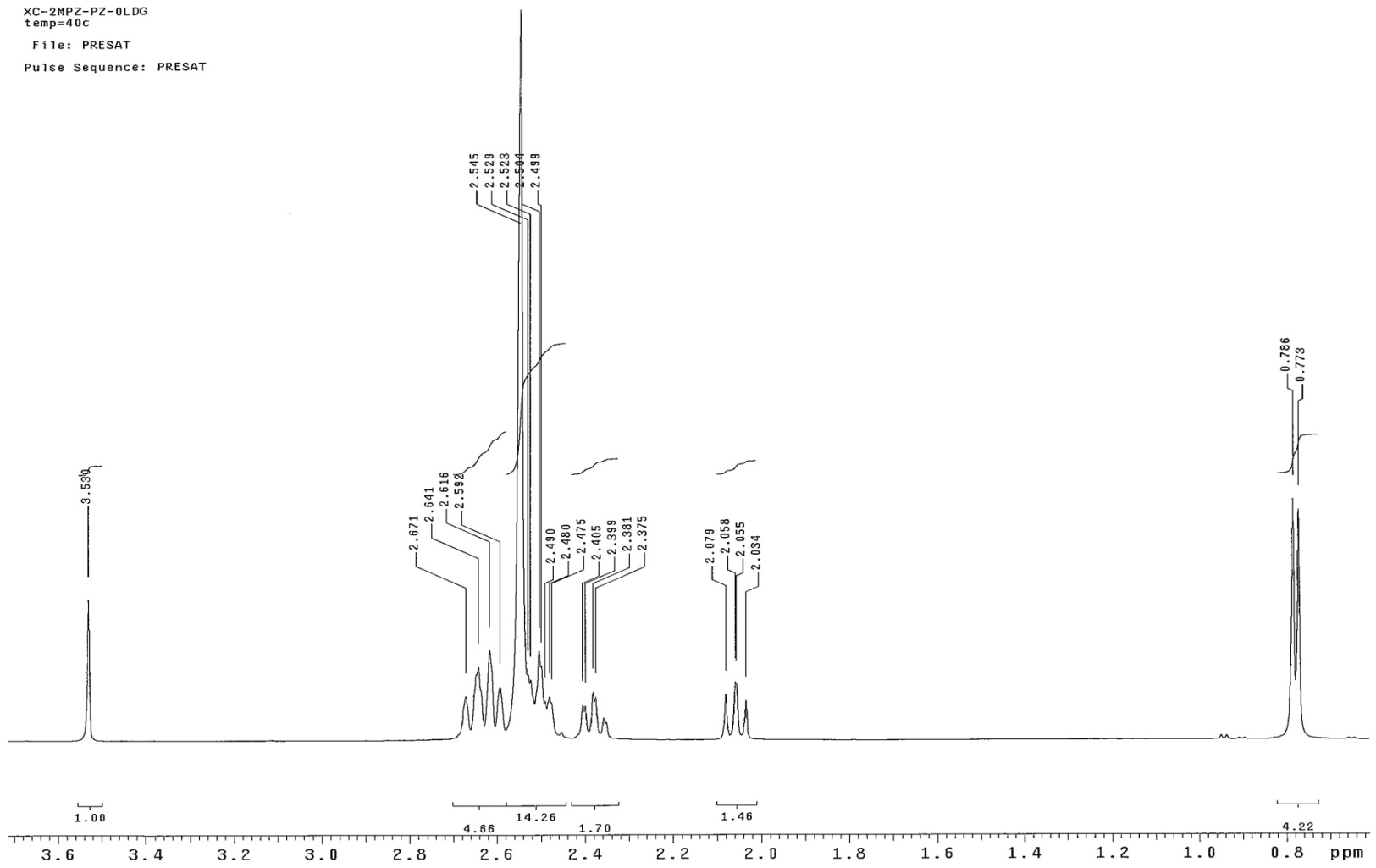

Figure B.16: ^{1}H NMR Spectrum for 4 m 2MPZ / 4 m PZ, T = 40 °C, α = 0 mol CO_2/mol alkalinity.

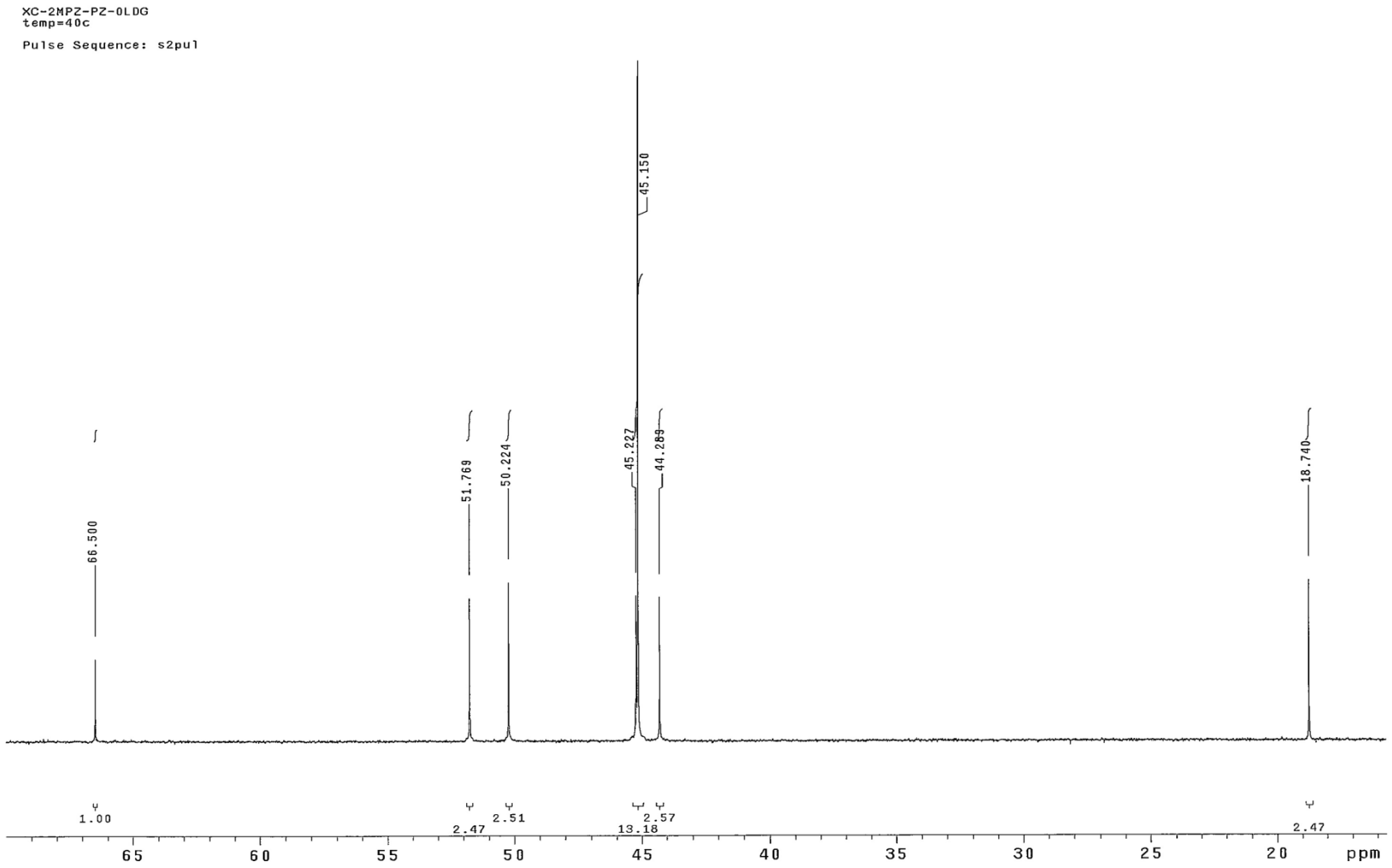

Figure B.17: ^{13}C NMR Spectrum for 4 m 2MPZ / 4 m PZ, T = 40 °C, α = 0 mol CO_2/mol alkalinity, δ = 40 – 55 ppm.

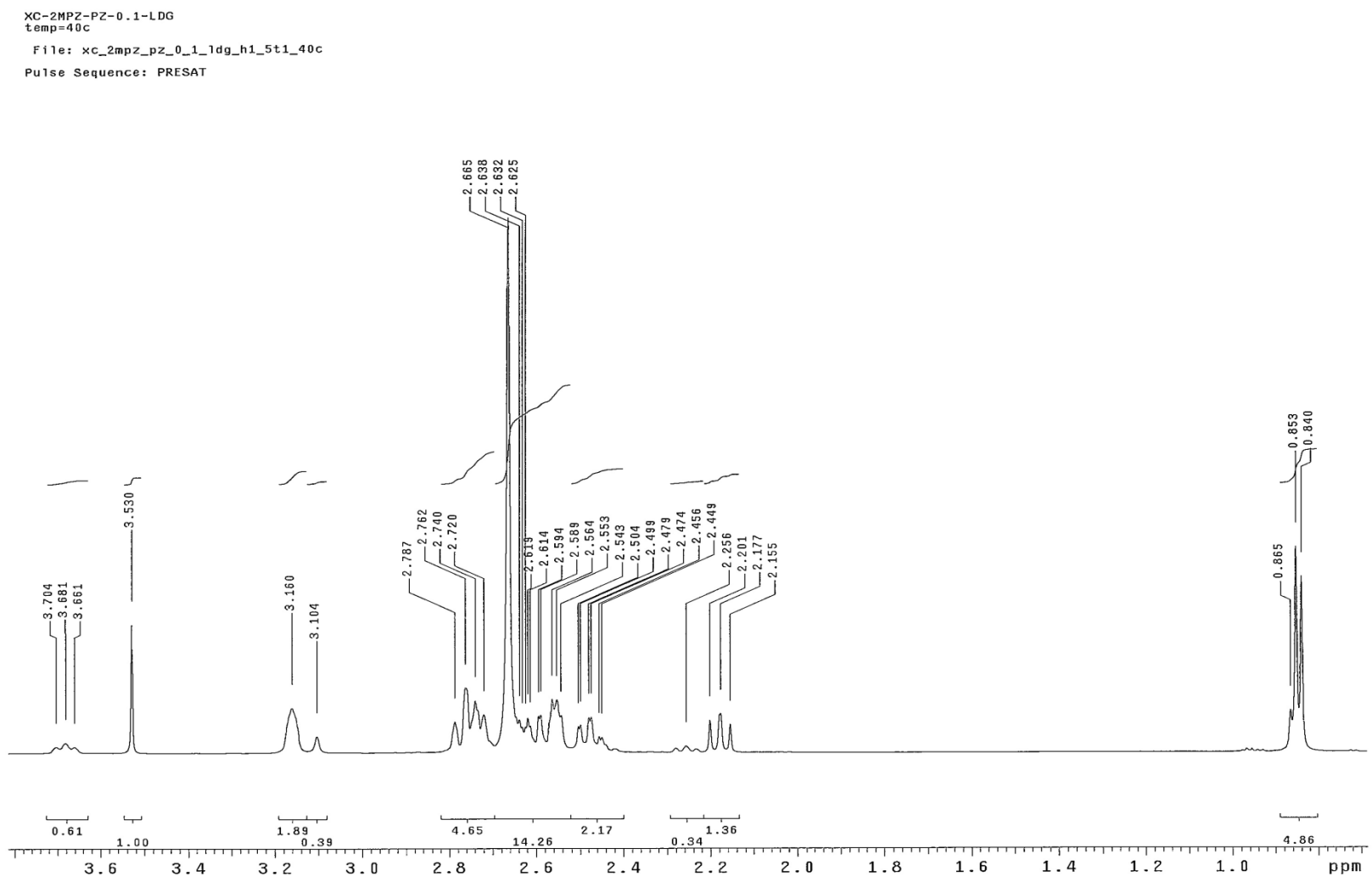

Figure B.18: ^{1}H NMR Spectrum for 4 m 2MPZ / 4 m PZ, T = 40 °C, α = 0.143 mol CO_2/mol alkalinity.

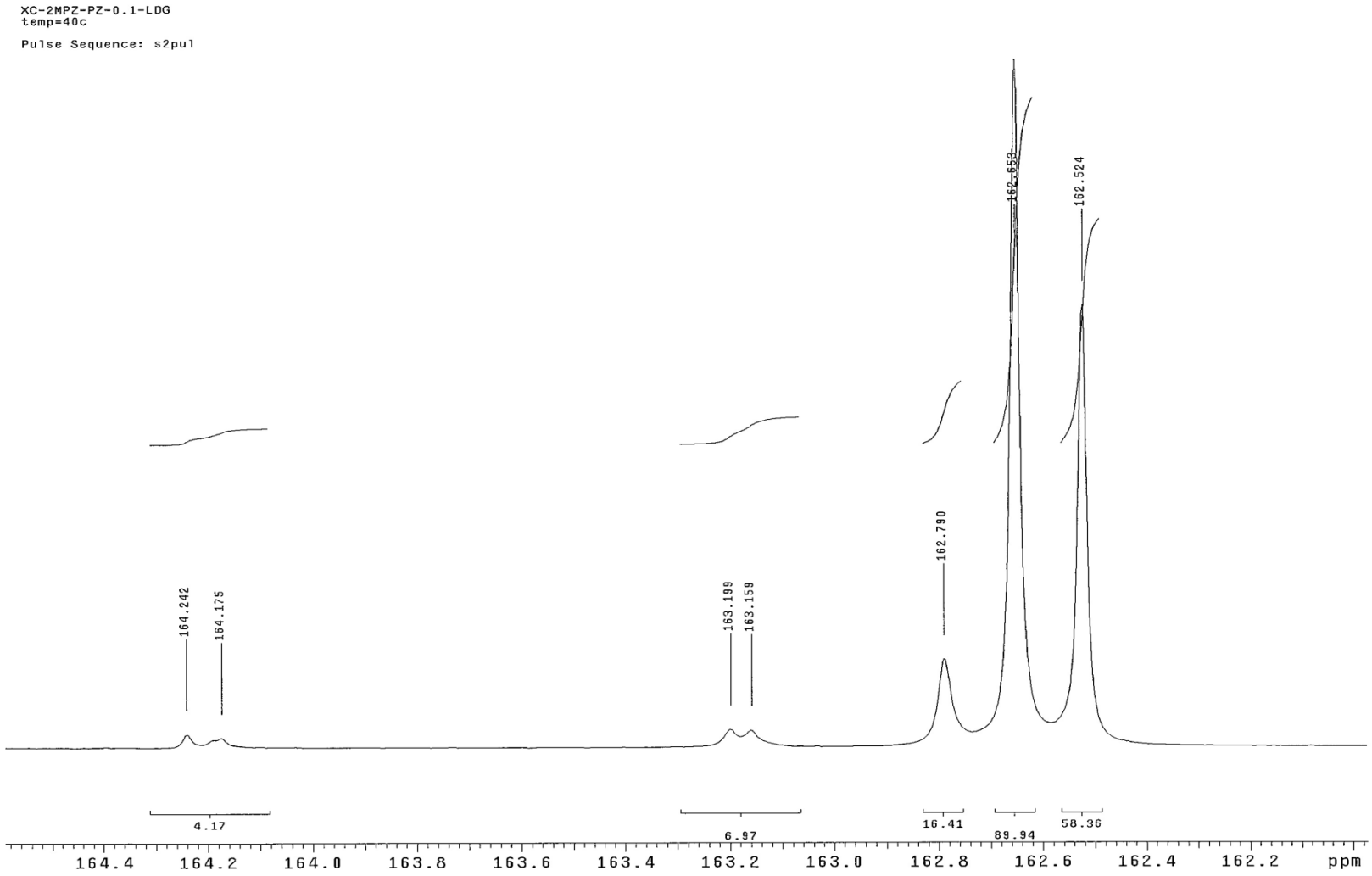

Figure B.19: ^{13}C NMR Spectrum for 4 m 2MPZ / 4 m PZ, T = 40 °C, α = 0.143 mol CO_2/mol alkalinity, δ = 160 – 165 ppm.

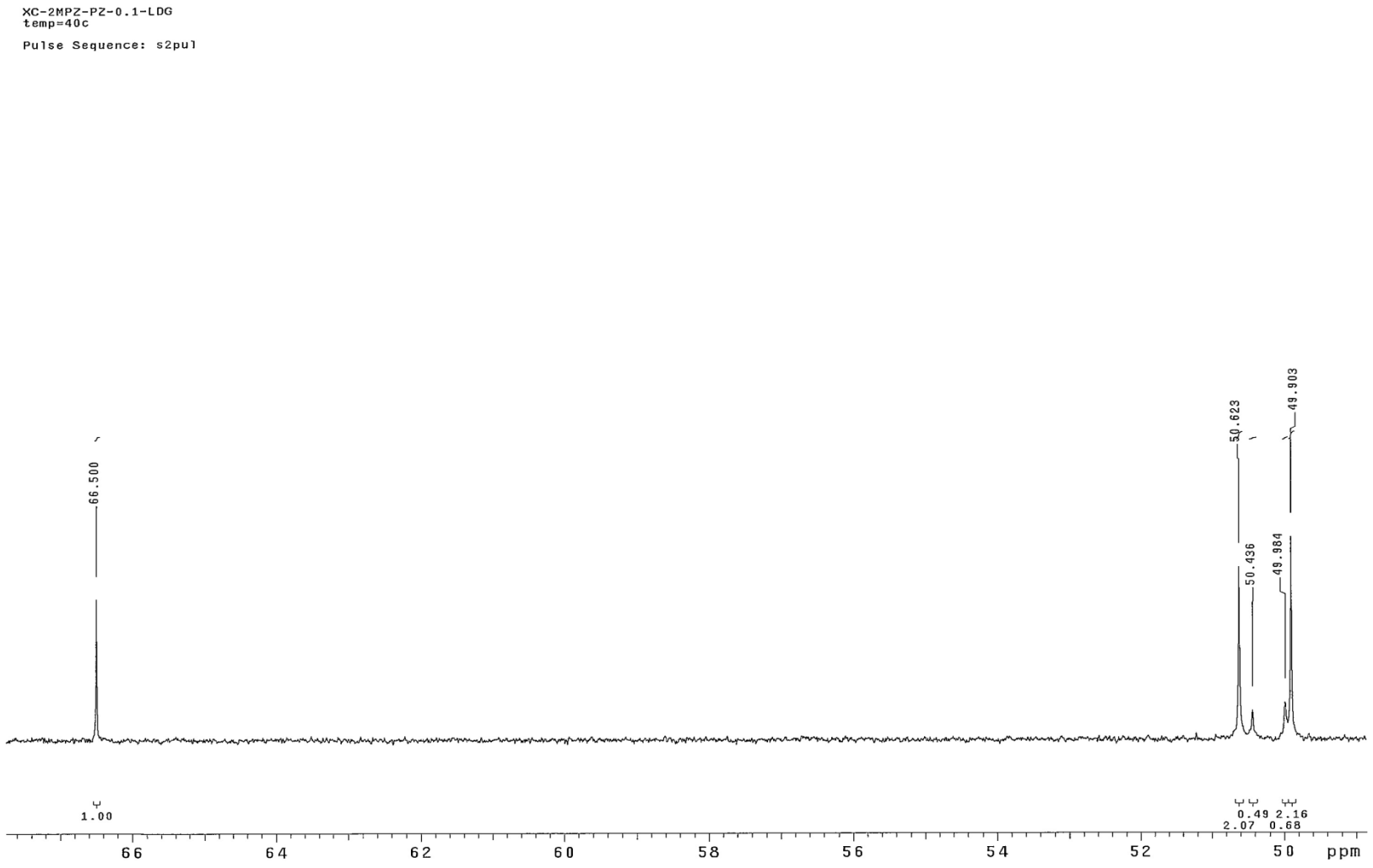

Figure B.20: ^{13}C NMR Spectrum for 4 m 2MPZ / 4 m PZ, T = 40 °C, α = 0.143 mol CO_2/mol alkalinity, δ = 45 – 70 ppm.

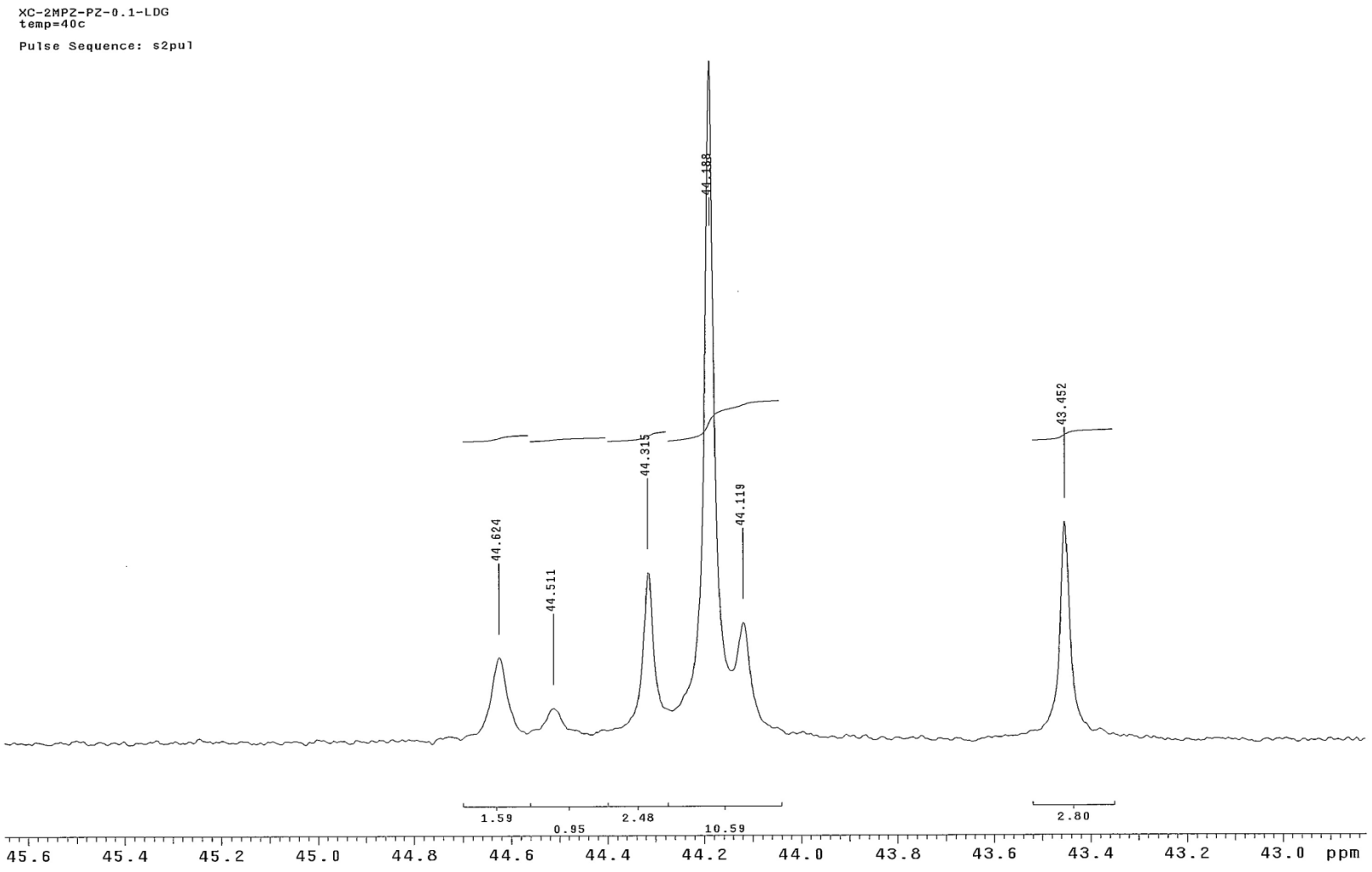

Figure B.21: ^{13}C NMR Spectrum for 4 m 2MPZ / 4 m PZ, T = 40 °C, α = 0.143 mol CO_2/mol alkalinity, δ = 40 – 45 ppm.

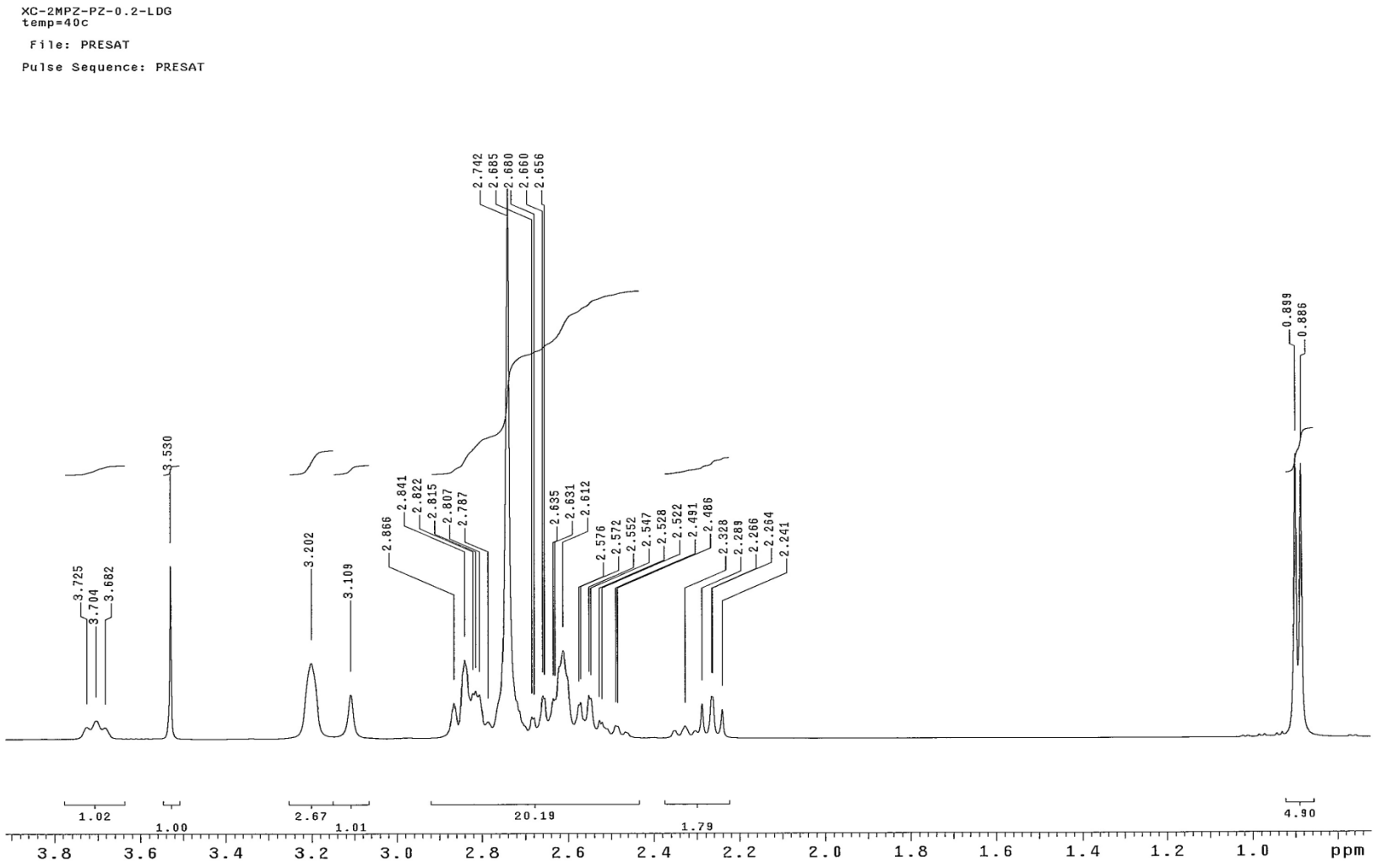

Figure B.22: ^{1}H NMR Spectrum for 4 m 2MPZ / 4 m PZ, T = 40 °C, α = 0.219 mol CO_2/mol alkalinity.

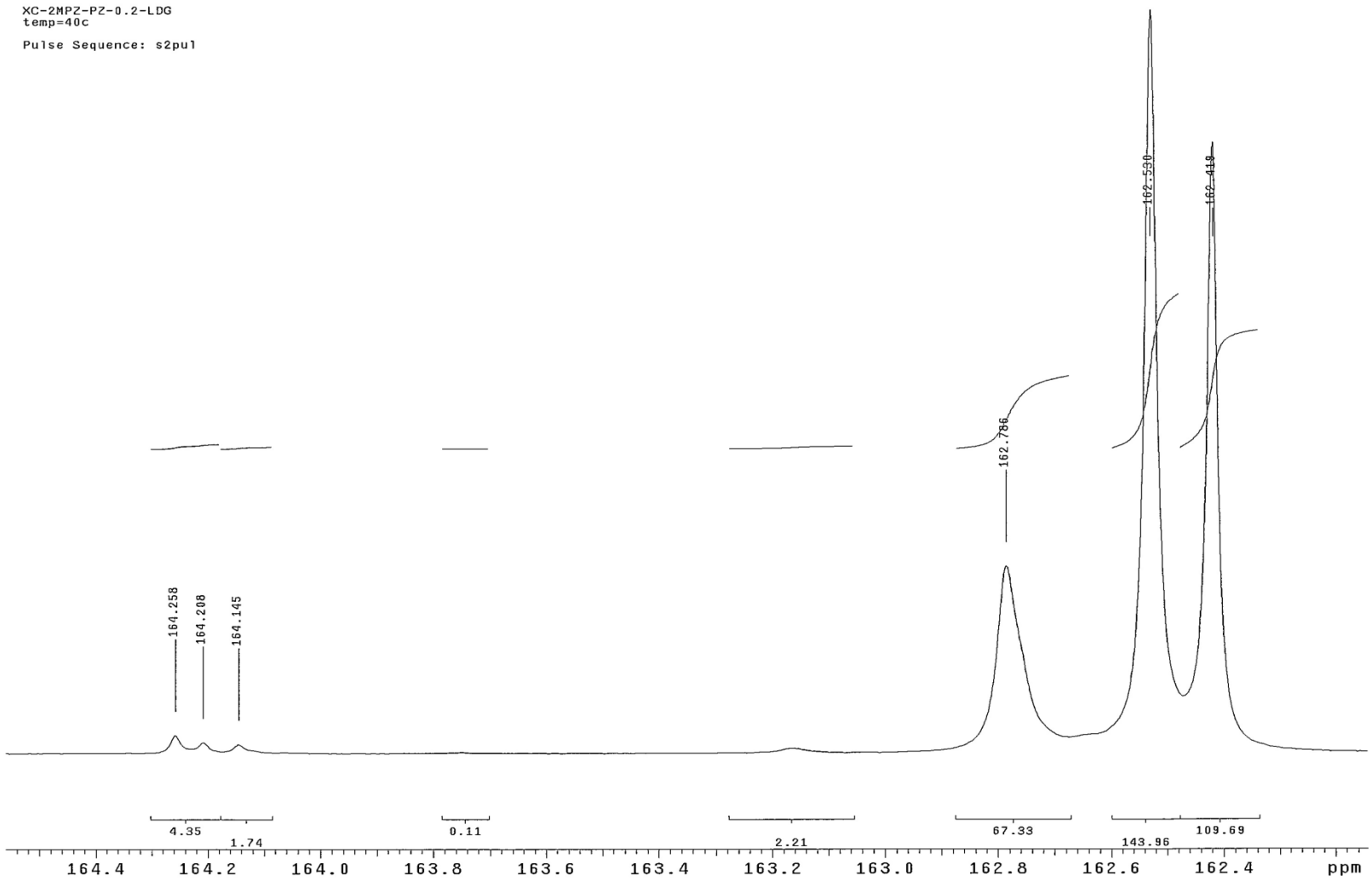

Figure B.23: ^{13}C NMR Spectrum for 4 m 2MPZ / 4 m PZ, T = 40 °C, α = 0.219 mol CO_2/mol alkalinity, δ = 160 – 165 ppm.

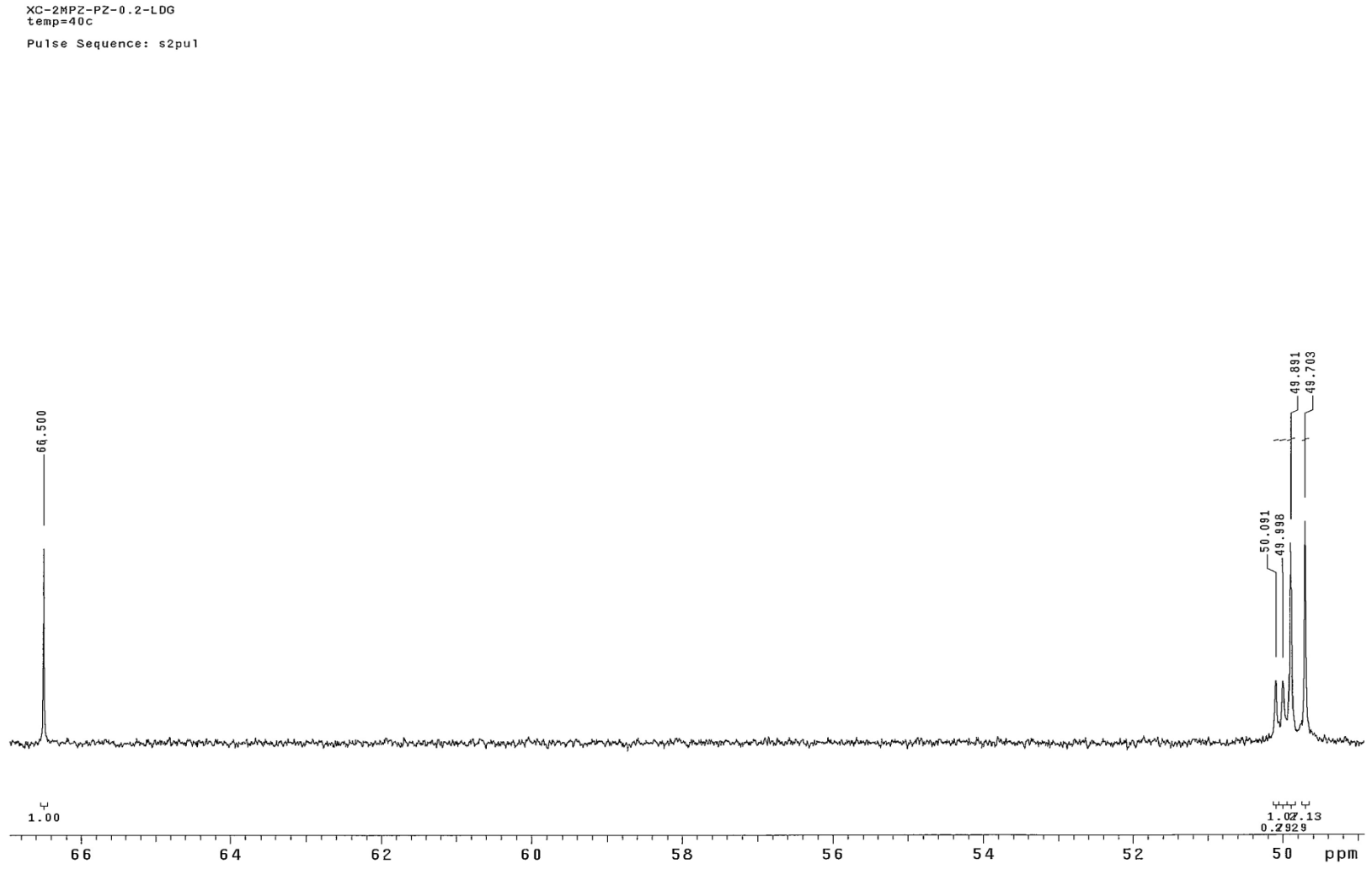

Figure B.24: ^{13}C NMR Spectrum for 4 m 2MPZ / 4 m PZ, T = 40 °C, α = 0.219 mol CO_2/mol alkalinity, δ = 50 – 70 ppm.

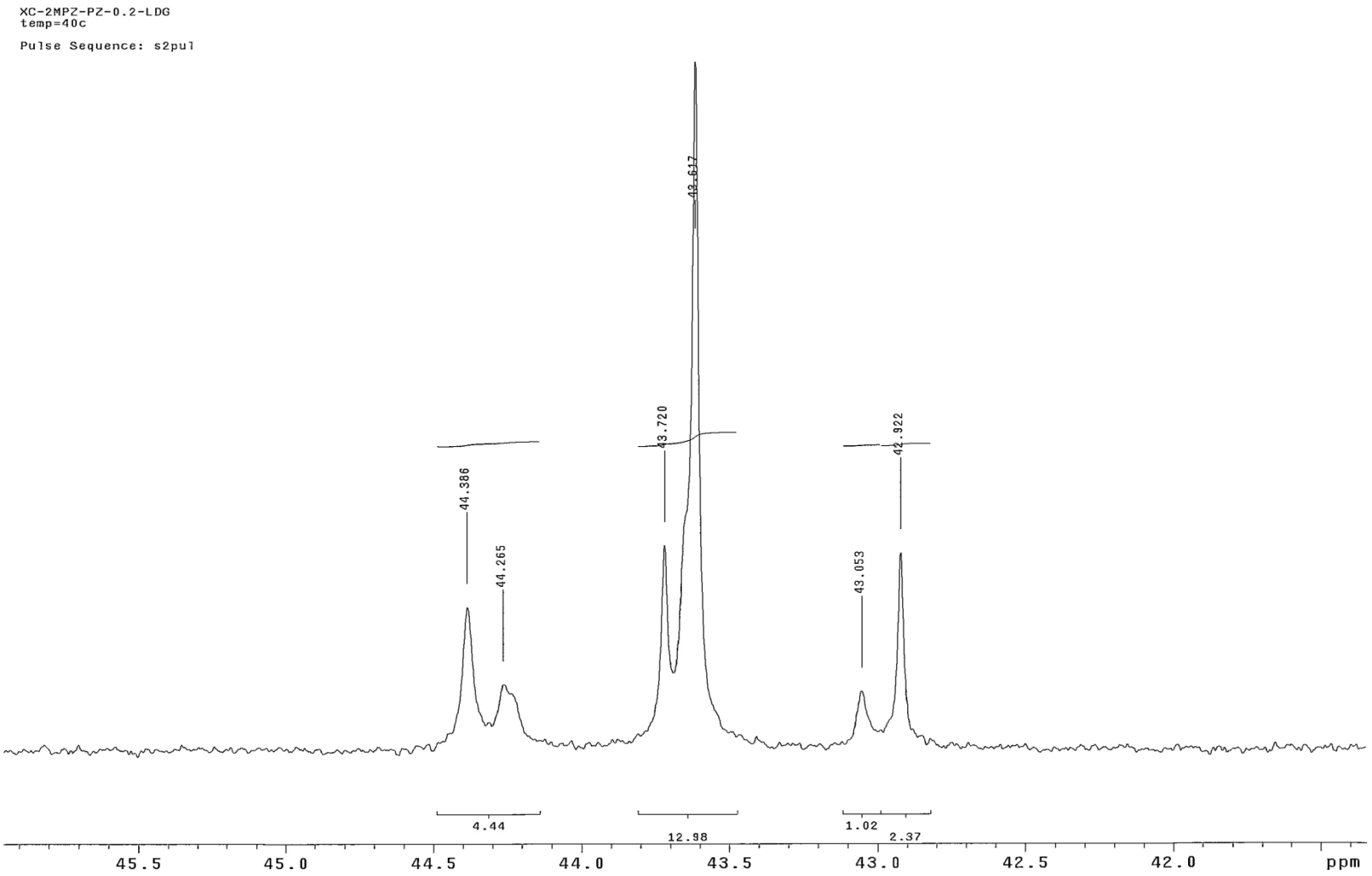

Figure B.25: ^{13}C NMR Spectrum for 4 m 2MPZ / 4 m PZ, T = 40 °C, α = 0.219 mol CO_2/mol alkalinity, δ = 40 –45 ppm.

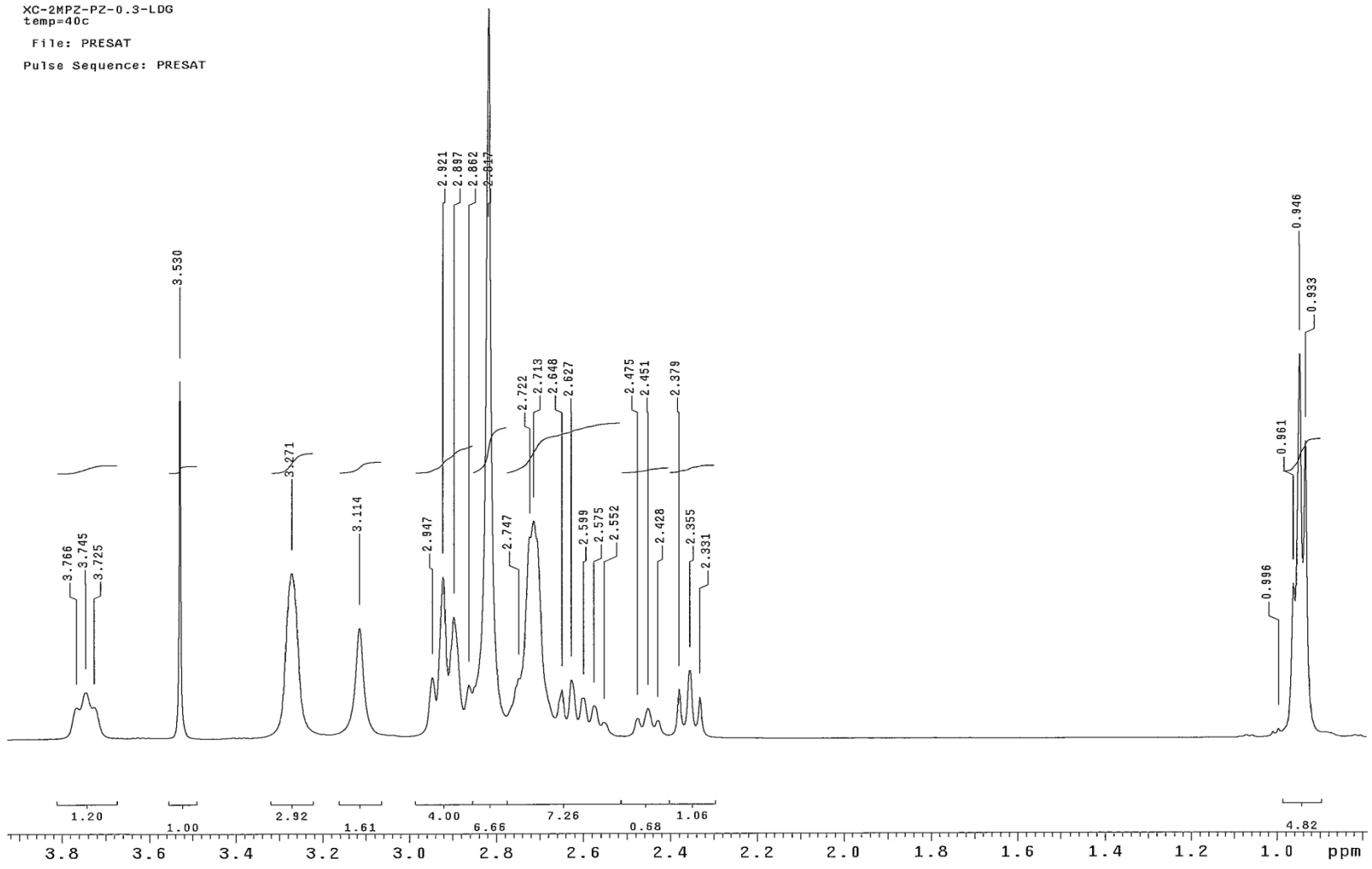

Figure B.26: ^{1}H NMR Spectrum for 4 m 2MPZ / 4 m PZ, T = 40 °C, α = 0.300 mol CO_2/mol alkalinity.

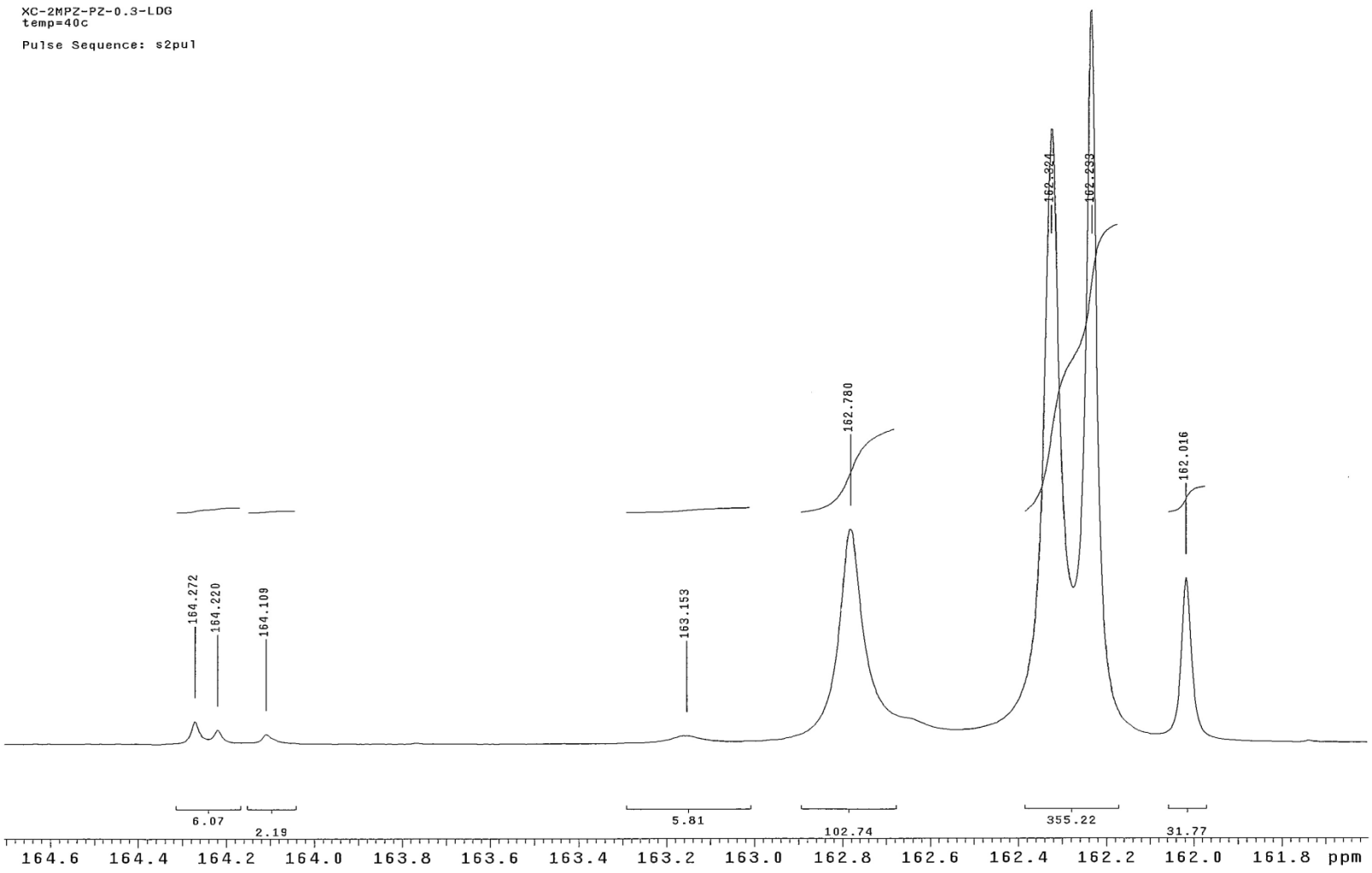

Figure B.27: ^{13}C NMR Spectrum for 4 m 2MPZ / 4 m PZ, T = 40 °C, α = 0.300 mol CO_2/mol alkalinity, δ = 160 – 165 ppm.

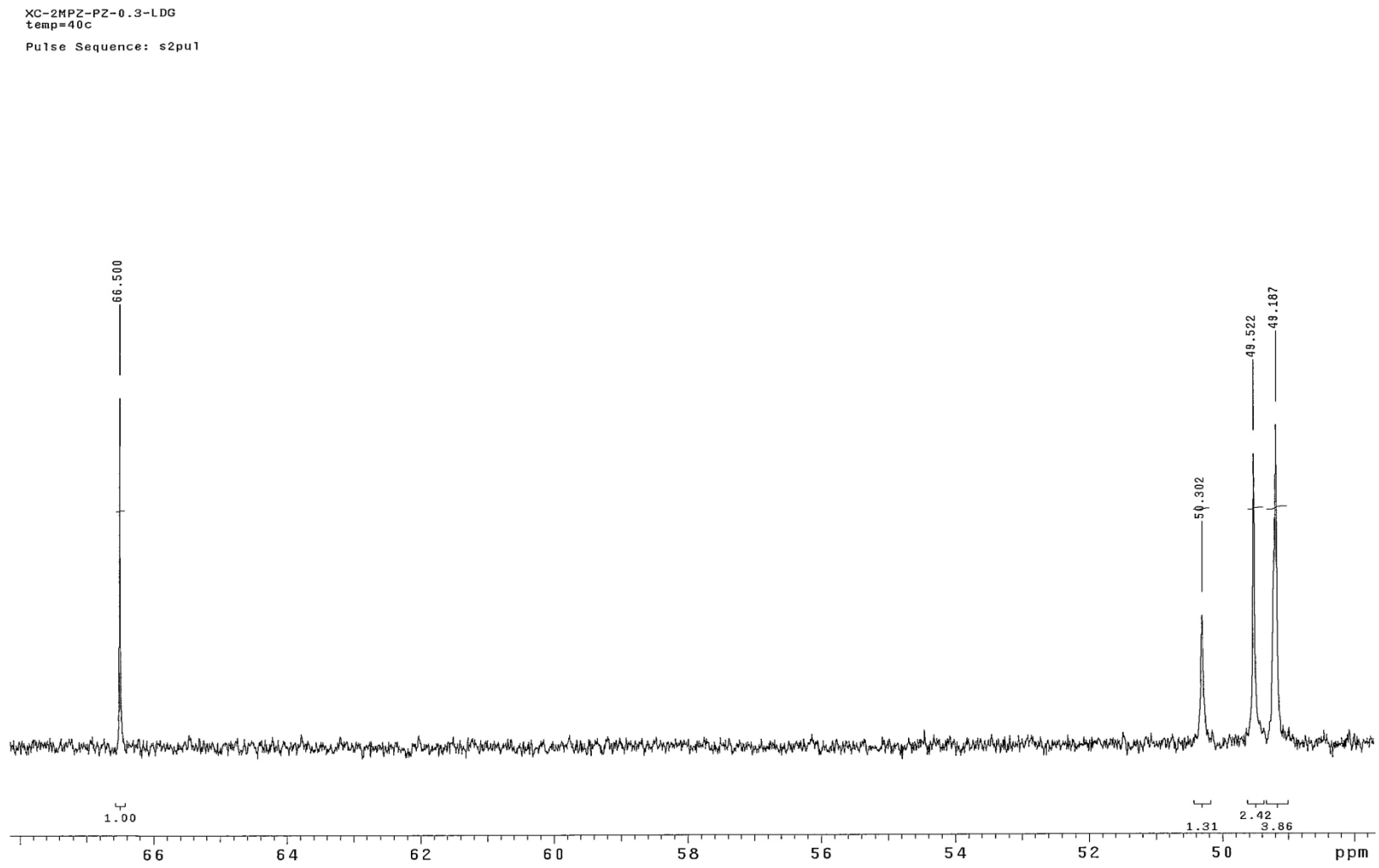

Figure B.28: ^{13}C NMR Spectrum for 4 m 2MPZ / 4 m PZ, T = 40 °C, α = 0.300 mol CO_2/mol alkalinity, δ = 45 – 70 ppm.

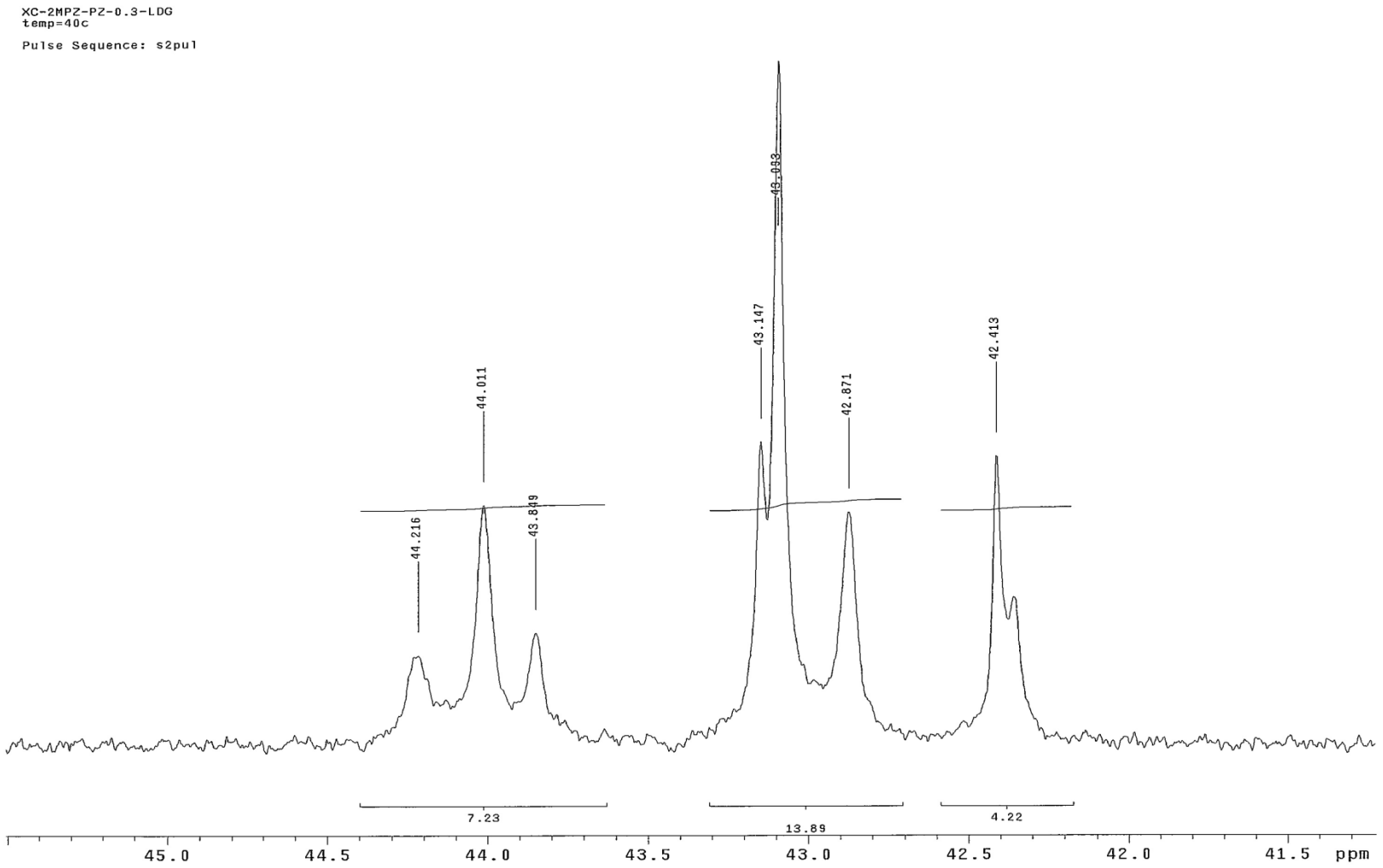

Figure B.29: ^{13}C NMR Spectrum for 4 m 2MPZ / 4 m PZ, T = 40 °C, α = 0.300 mol CO_2/mol alkalinity, δ = 40 – 45 ppm.

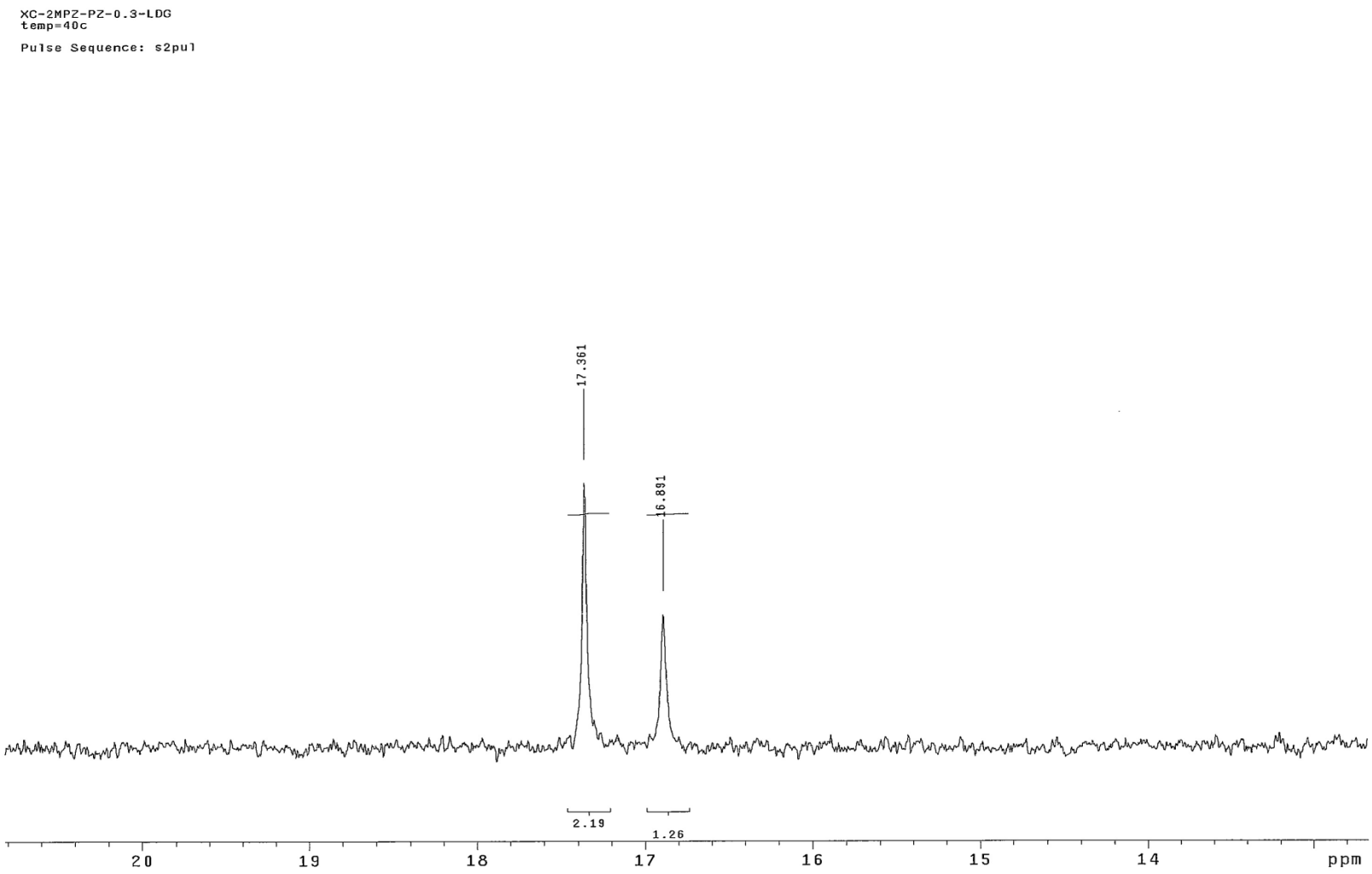

Figure B.30: ^{13}C NMR Spectrum for 4 m 2MPZ / 4 m PZ, T = 40 °C, α = 0.300 mol CO_2/mol alkalinity, δ = 10 – 20 ppm.

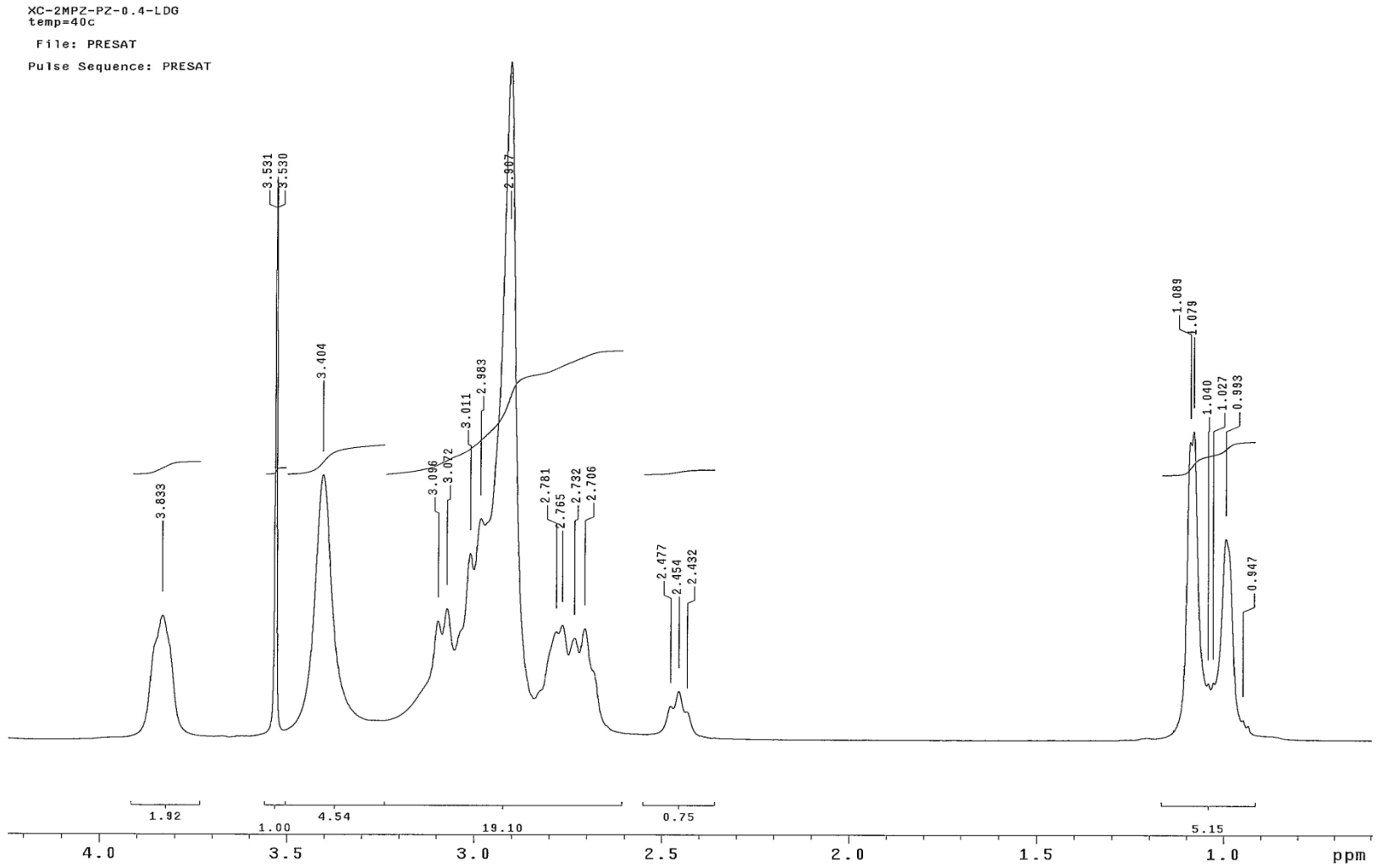

Figure B.31: ^{1}H NMR Spectrum for 4 m 2MPZ / 4 m PZ, T = 40 °C, α = 0.440 mol CO_2/mol alkalinity.

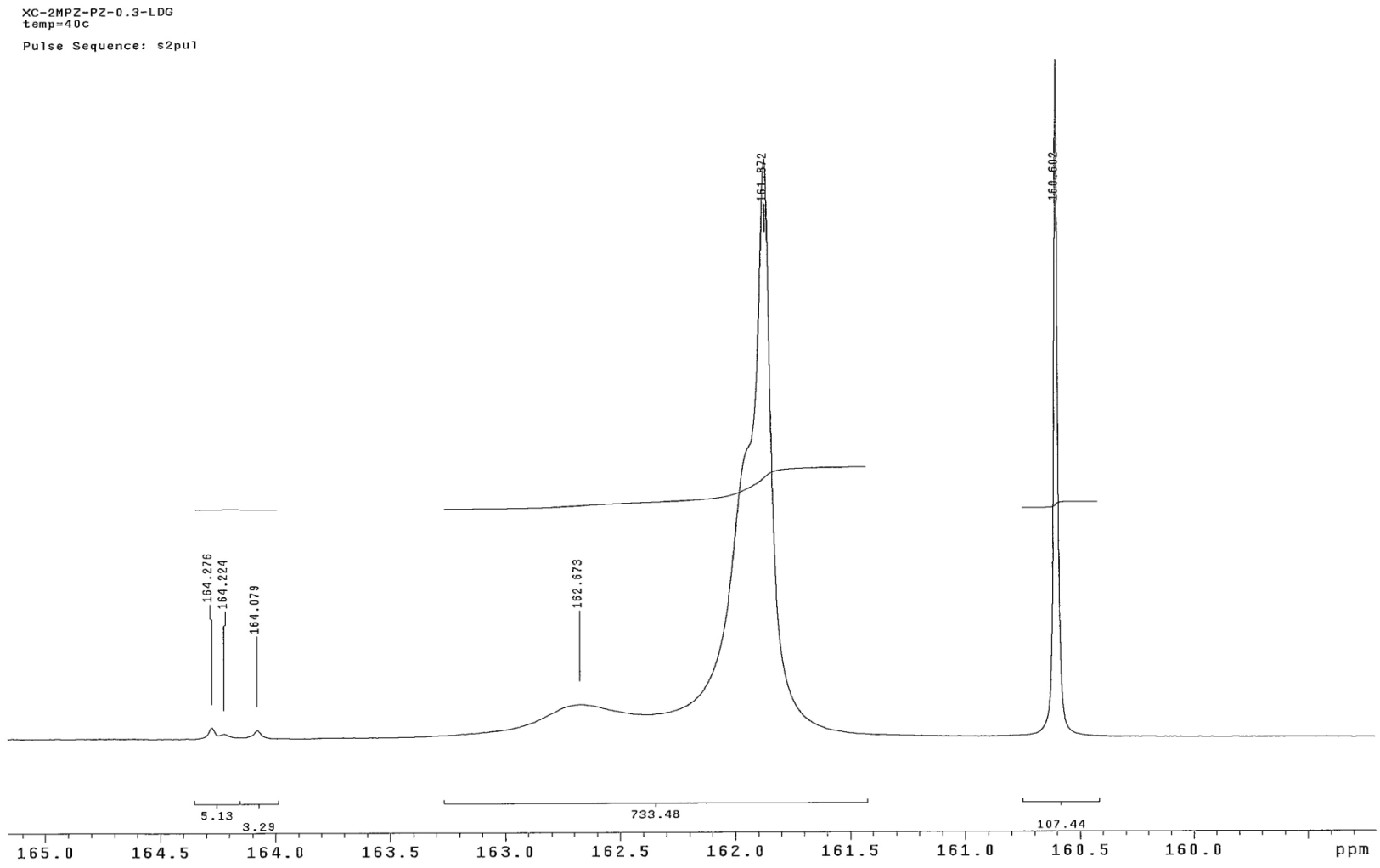

Figure B.32: ^{13}C NMR Spectrum for 4 m 2MPZ / 4 m PZ, T = 40 °C, α = 0.440 mol CO_2/mol alkalinity, δ = 160 –165 ppm.

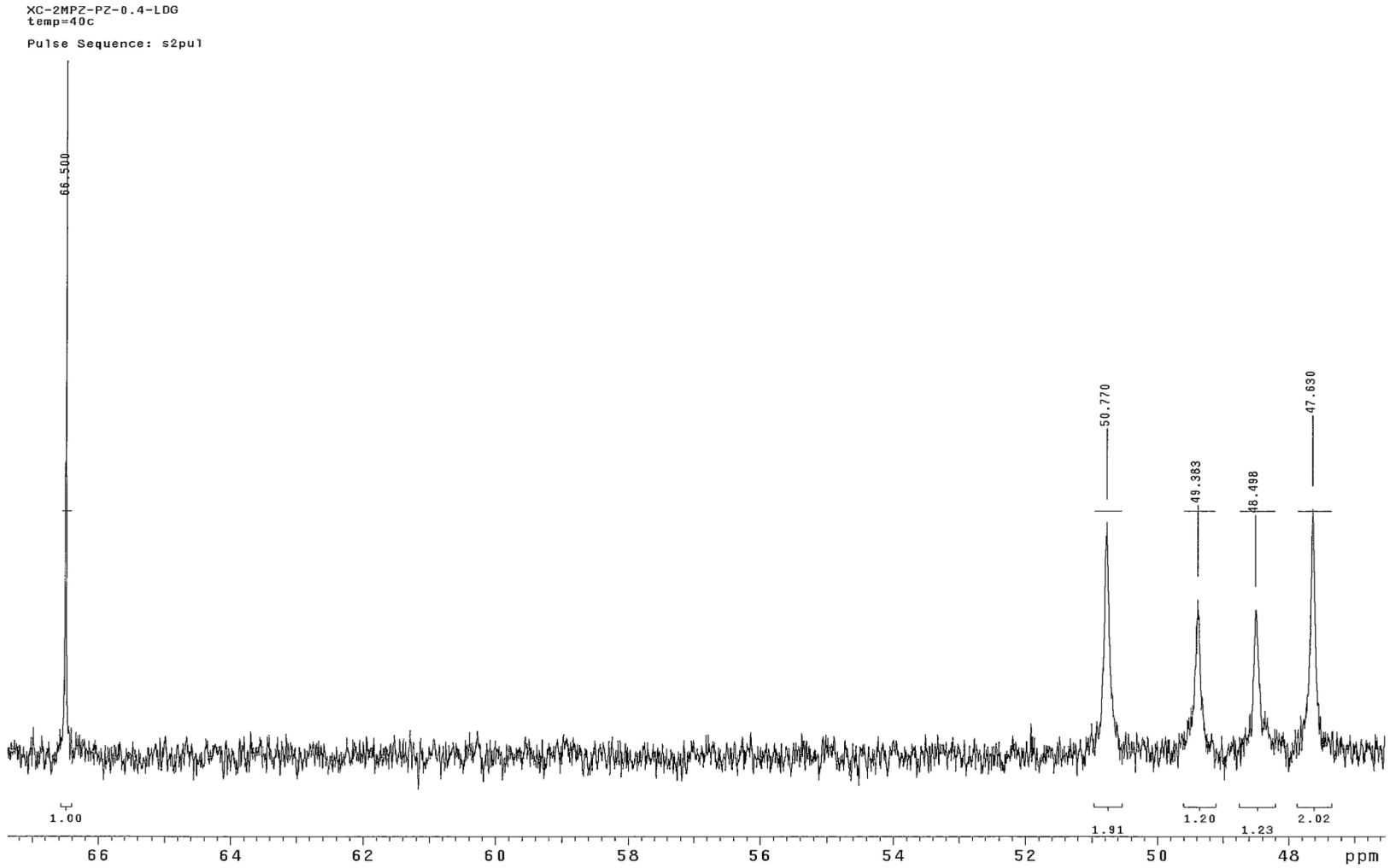

Figure B.33: ^{13}C NMR Spectrum for 4 m 2MPZ / 4 m PZ, T = 40 °C, α = 0.440 mol CO_2/mol alkalinity, δ = 45 – 70 ppm.

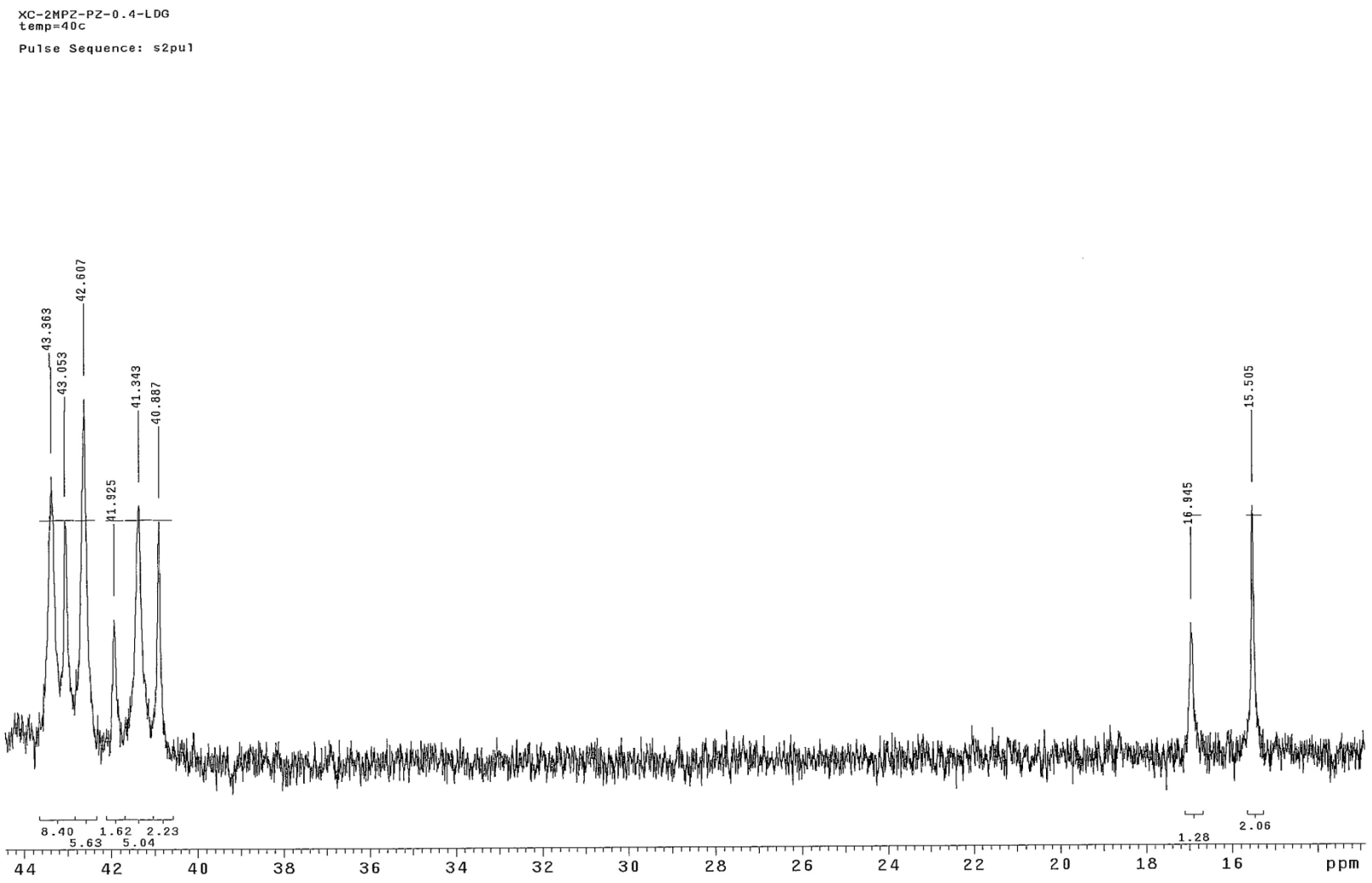

Figure B.34: ^{13}C NMR Spectrum for 4 m 2MPZ / 4 m PZ, T = 40 °C, α = 0.440 mol CO_2/mol alkalinity, δ = 15 – 45 ppm.

Appendix C: NMR on Degraded PZ

NMR and mass spectroscopy (MS) analysis were conducted on neat, formaldehyde-added and oxidatively degraded PZ aqueous solutions respectively in order to identify contaminants that account for increased foaming tendency of degraded PZ solutions. Most peaks in NMR spectrum were tentatively interpreted and correlated to different molecules. There were no additional peaks found in 2-week degraded PZ solutions. For another degraded PZ sample, NMR peaks with same position were found as seen in formaldehyde-added PZ, which may indicate that formaldehyde be the cause of increased foaming tendency. MS analysis seems not to render useful information on contaminants.

C.1 INTRODUCTION

Formaldehyde (HCHO) was reported to greatly increase foaming tendency of undegraded piperazine solutions. It was also found that degraded piperazine solutions have a serious foaming problem. Since HCHO is regarded as an important intermediate oxidation product of piperazine, it was hypothized that HCHO is the main reason that causes foaming of oxidatively degraded piperazine. To verify this hypothesis, ^{1}H &^{13}C NMR and MS anaylysis were performed on formaldehyde-added PZ samples as well as oxidated ones in order to identify different species given rise to by HCHO. All the spectrum were documented in this report and will be used as a reference for future work.

C.2 EXPERIMENTAL

Materials

The following materials were used in this study: PZ(anhydrous, 99%, Alfa Aesar), carbon dioxide (Coleman Intrument, 99.99%, Matheson), Deuterium oxide (≥99.9%,

Cambridge Isotopes), DSS (sodium 2,2-Dimethyl-2-silapentane-5-Sulfonate, 97%, Aldrich), deionized water (Millipore, Direct-Q).

Preparation of NMR samples

DSS was used as a reference for the NMR analysis. A solution of D_2O/DSS = 50/1 (w/w) was prepared beforehand. Then 0.5g of the D_2O/DSS solution was added to a 3.5g sample under well mixing. After that, experimental samples (approximately 1ml for each) were transferred into yellow top NMR sample tubes (5.00mm O.D. x 0.77 mm I.D. x 7 in. length, 300 mHz, WILMAD Labglass) and was submitted for analysis to the NMR laboratory at the Department of chemistry and Biochemistry, the University of Texas at Austin.

Mass spectroscopy analysis

Samples were diluted 50 times before being injected with a needle pump into a mass spectroscopy (Thermo Finnigan TSQ) located at the Department of Civil Engineering, the University of Texas at Austin. The injection rate was set at 50 ul/min.

C.3 RESULTS AND DISCUSSION

Molecular structure of different PZ species present in loaded PZ solution is illustrated in Figure C.1.

a)

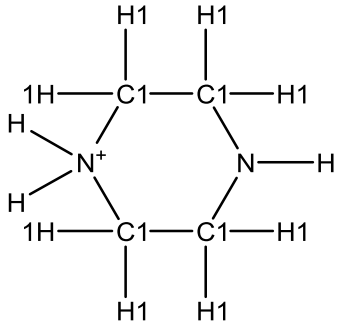

b)

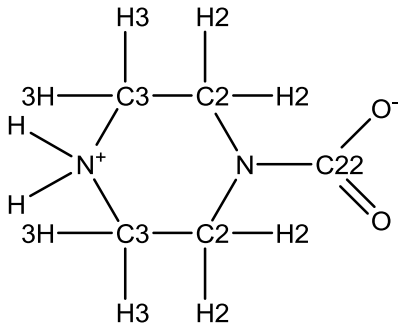

c)

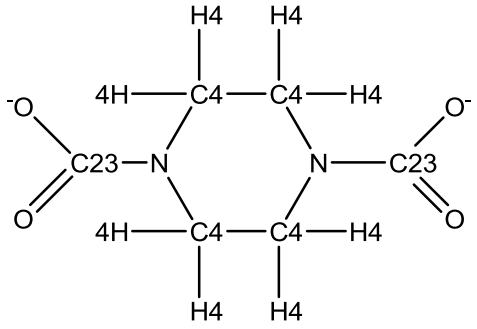

Figure C.1: Molecular structure and active nuclei of protons and carbons associated with a) PZ/PZH^+, b)$PZCOO^-$ /H^+PZCOO^-, c) $PZ(COO^-)_2$. Different types of nucleus are labeled with numbers to distinguish them.

Figure C.2 and Figure C.3 show ^1H NMR and ^{13}C NMR spectrum for 2m PZ without CO_2 loading respectively. The peaks are labeled with number of the corresponding nucleus. (NMR peak positions and areas are summarized in Appendix for all samples anaylized in this study.)

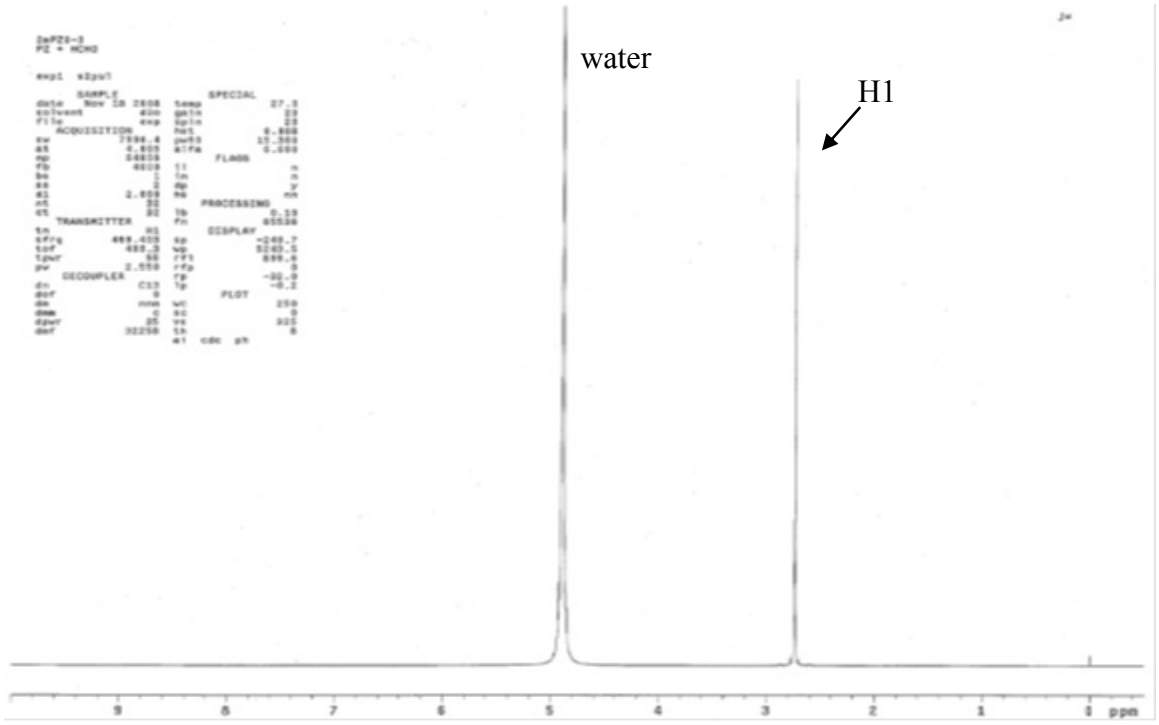

Figure C.2: ^{1}H NMR Spectrum of 2m PZ, α=0

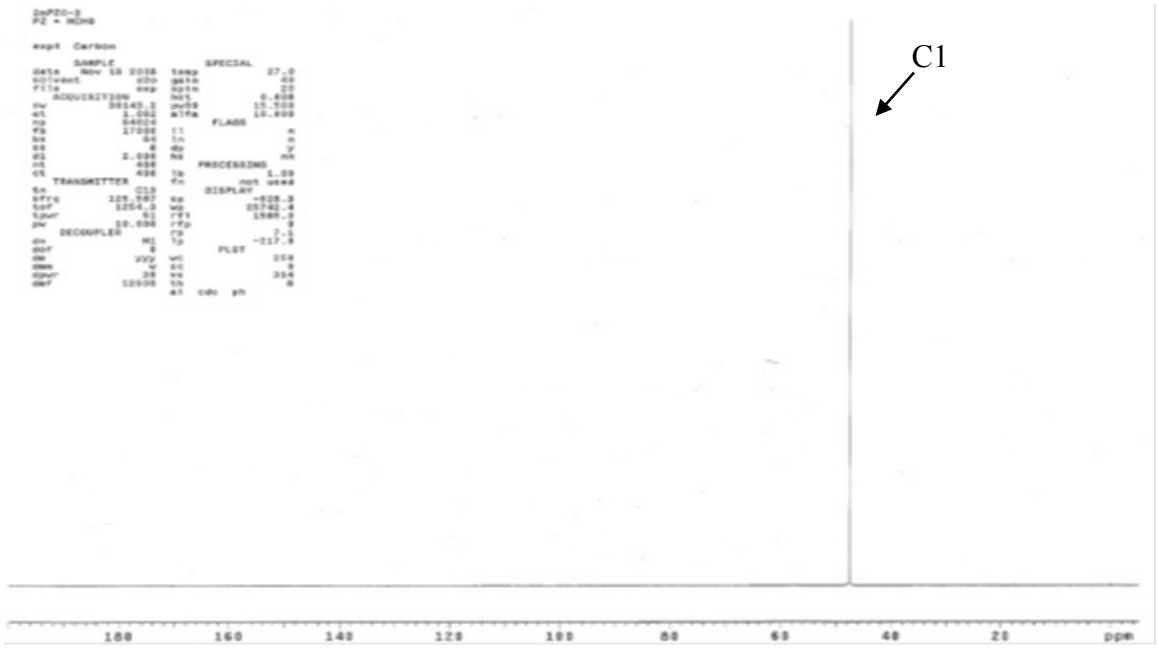

Figure C.3: ^{13}C NMR Spectrum of 2m PZ, α=0

As formaldehyde is added to PZ solutions, the speciation becomes complicate. Figure C.4 shows some of the possible molecular structures of products that could form as HCHO reacted with PZ as well as PZ carbamate.

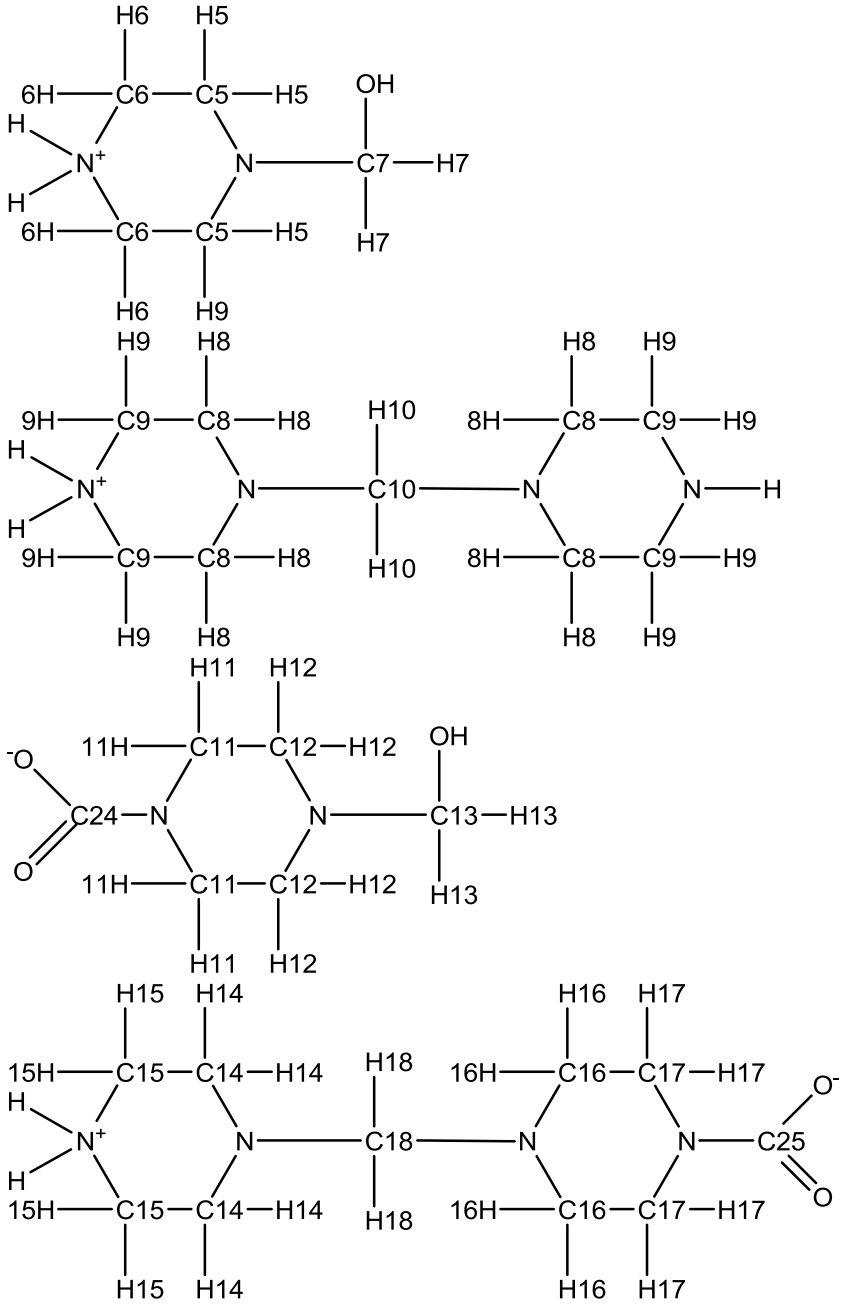

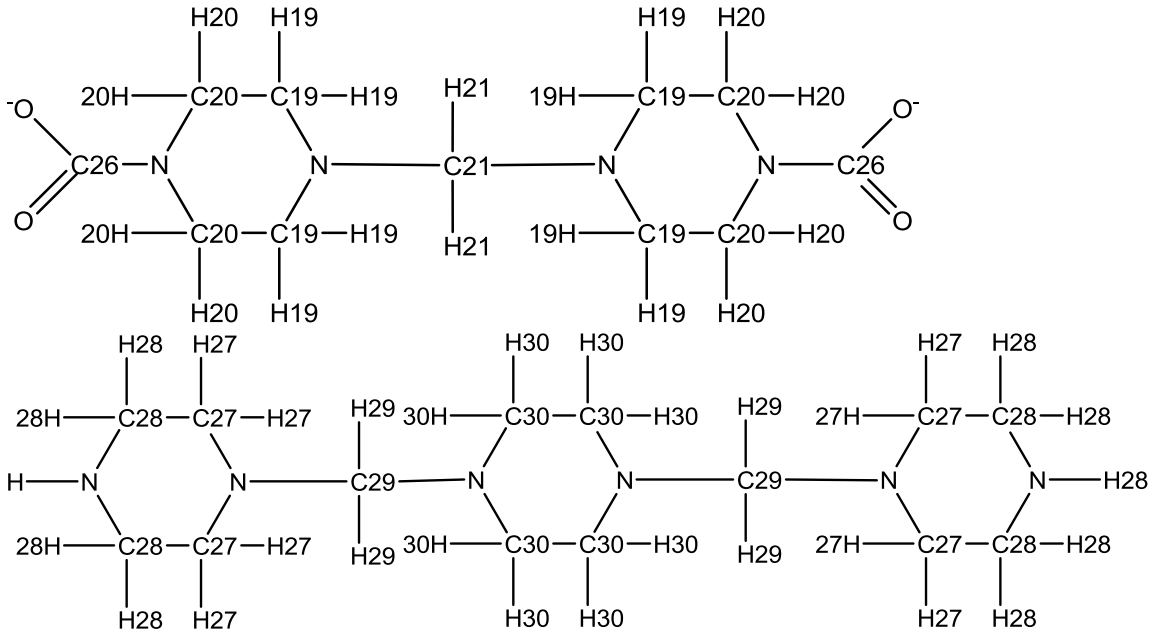

Figure C.4: Molecular structure and active nuclei of protons and carbons associated with products of CO_2 loaded PZ and formaldehyde.

Two samples of unloaded 2m PZ containing 325 mM and 743 mM HCHO were analyzed and the spectrum were shown in Figure C.5 ~ Figure C.17. The sample with 325 mM HCHO added is still clean solution while the one with 743 mM HCHO is milky white. As the ratio of HCHO to PZ is increased, the amount of pentamers (the last one in Figure C.4) was expected to increase. In the spectrum for these two samples, apparently the peaks whose area increases with HCHO concentration are associated with HCHO, methanol contained in HCHO solution or products of reactions that HCHO participated.

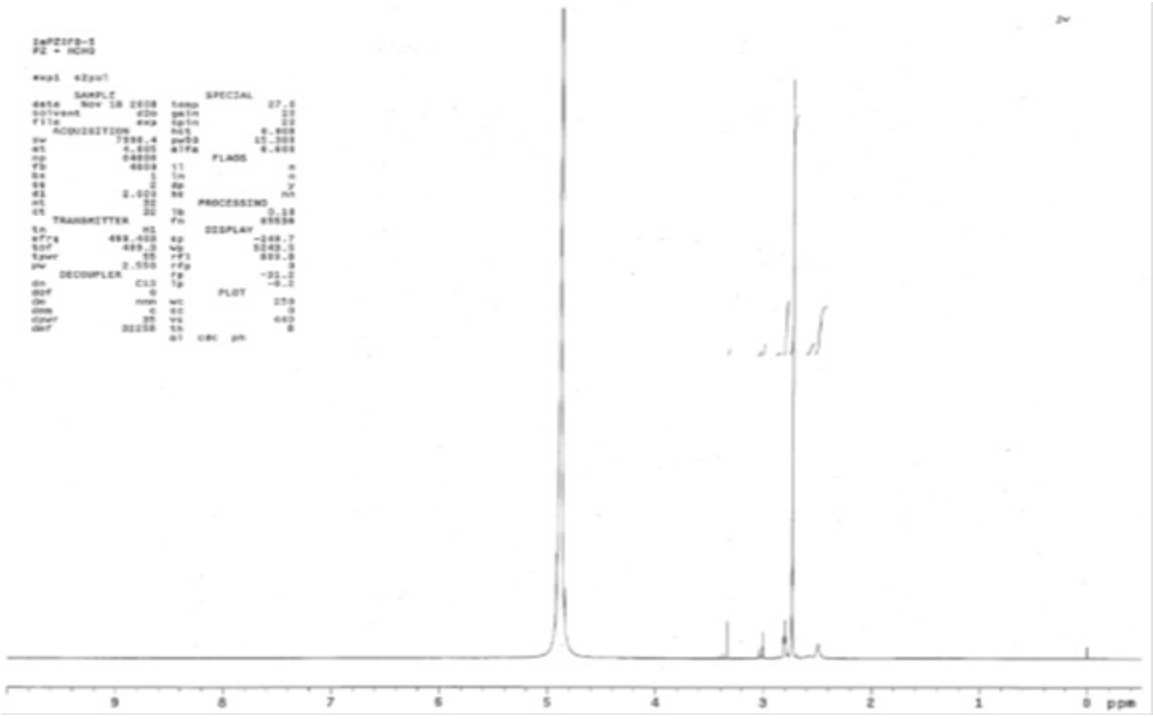

Figure C.5: ^{1}H NMR Spectrum of 2m PZ, α=0, [HCHO]=325mM (0-10 ppm)

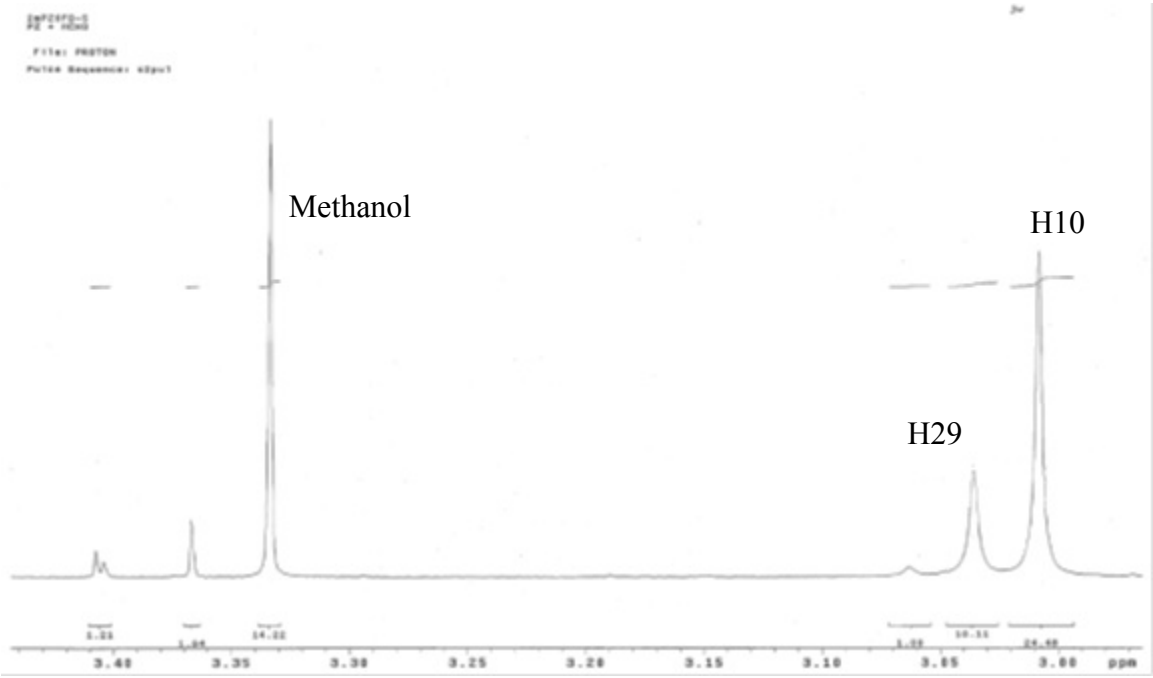

Figure C.6: ^{1}H NMR Spectrum of 2m PZ, α=0, [HCHO]=325mM (2.97-3.44 ppm)

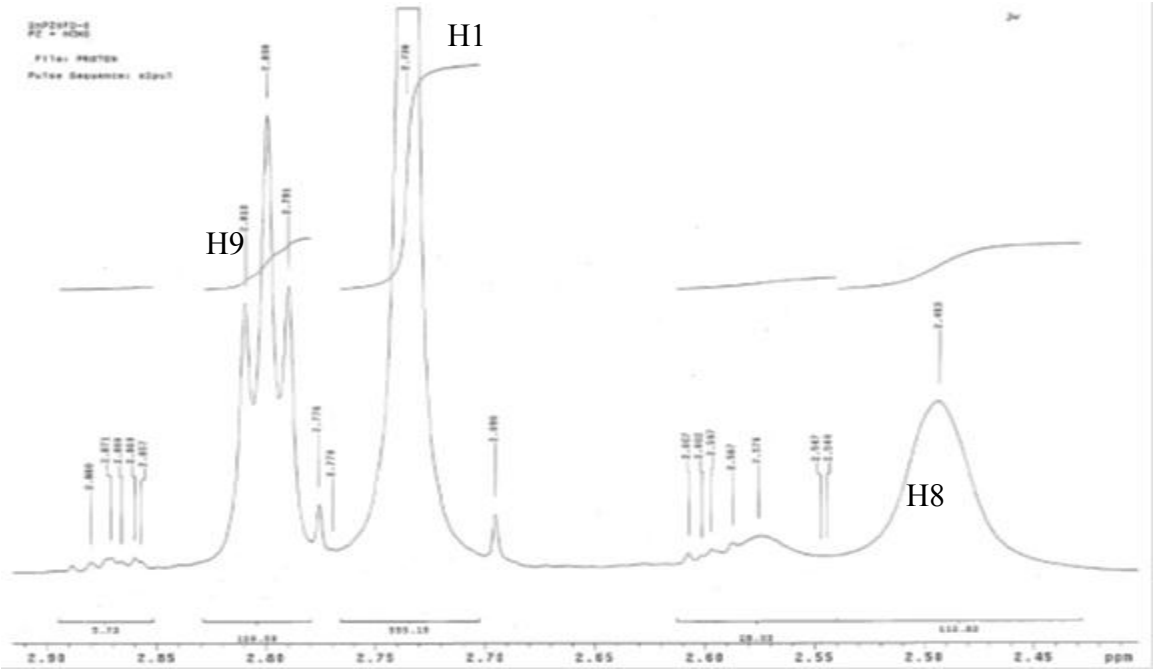

Figure C.7: ^{1}H NMR Spectrum of 2m PZ, α=0, [HCHO]=325mM (2.40-2.91 ppm)

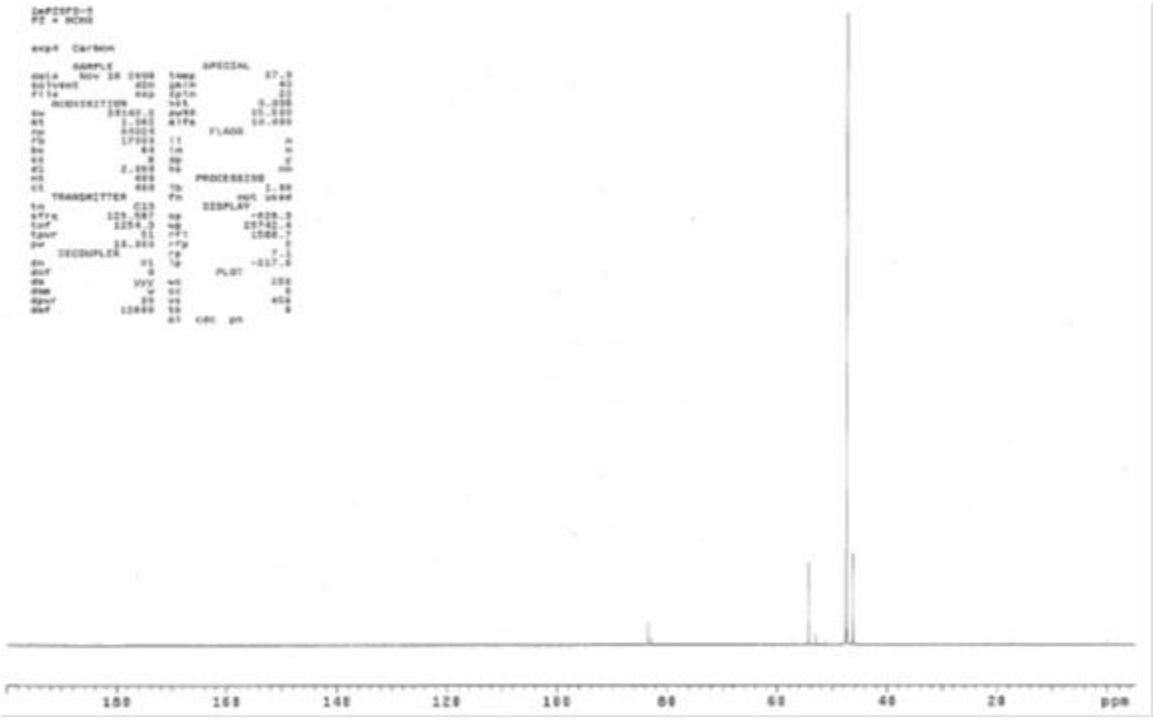

Figure C.8: ^{13}C NMR Spectrum of 2m PZ, α=0, [HCHO]=325mM (0-200 ppm)

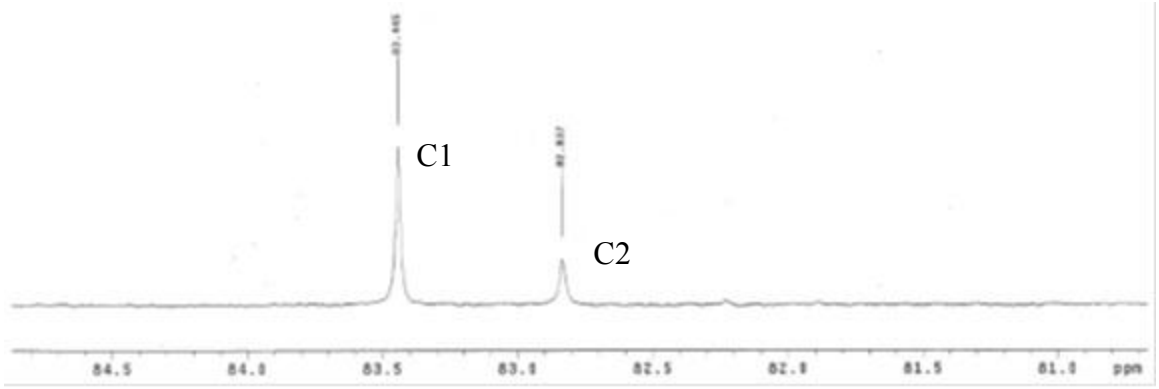

Figure C.9: ^{13}C NMR Spectrum of 2m PZ, α=0, [HCHO]=325mM (80.7-84.8 ppm)

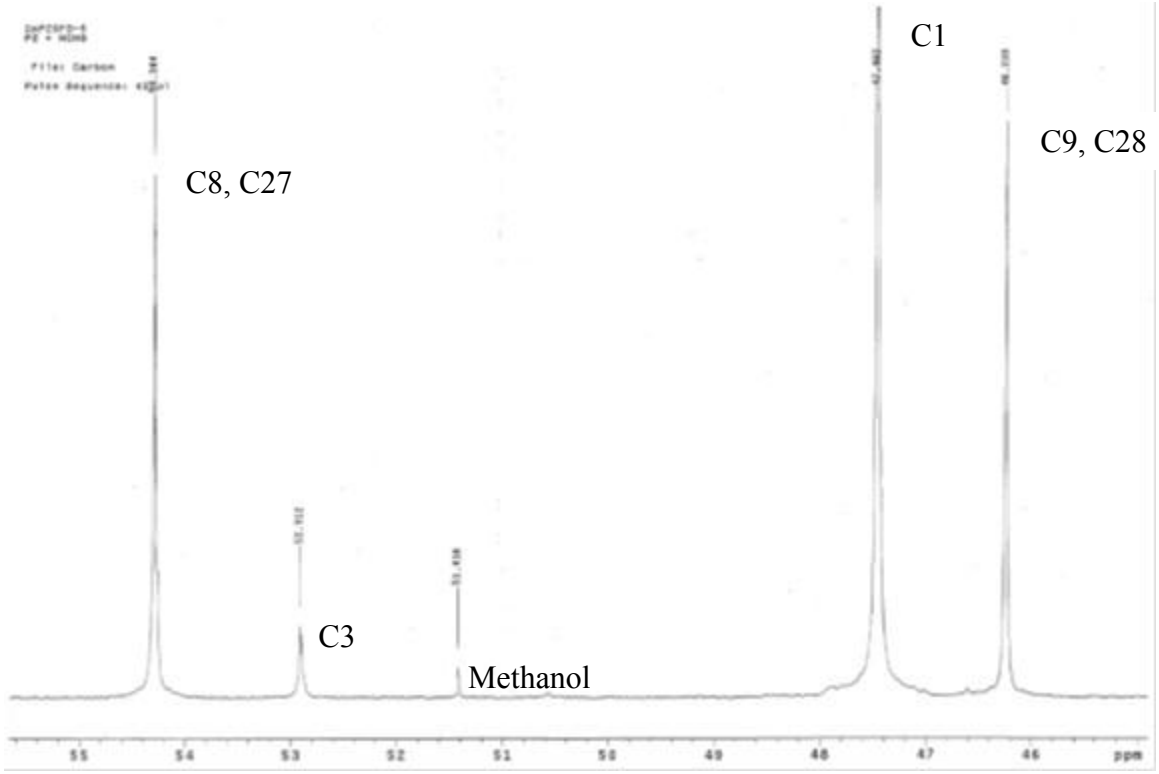

Figure C.10: ^{13}C NMR Spectrum of 2m PZ, α=0, [HCHO]=325mM (45.0-55.6 ppm)

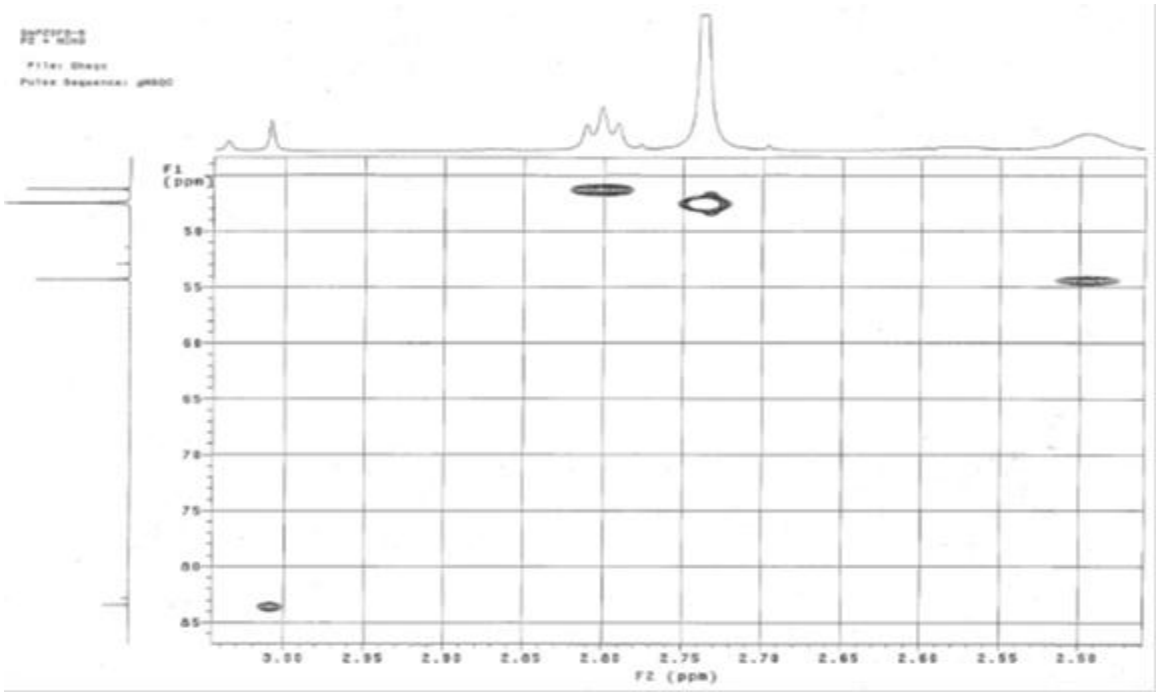

Figure C. 11: 2-D correlation NMR Spectrum of 2m PZ, α=0, [HCHO]=325mM

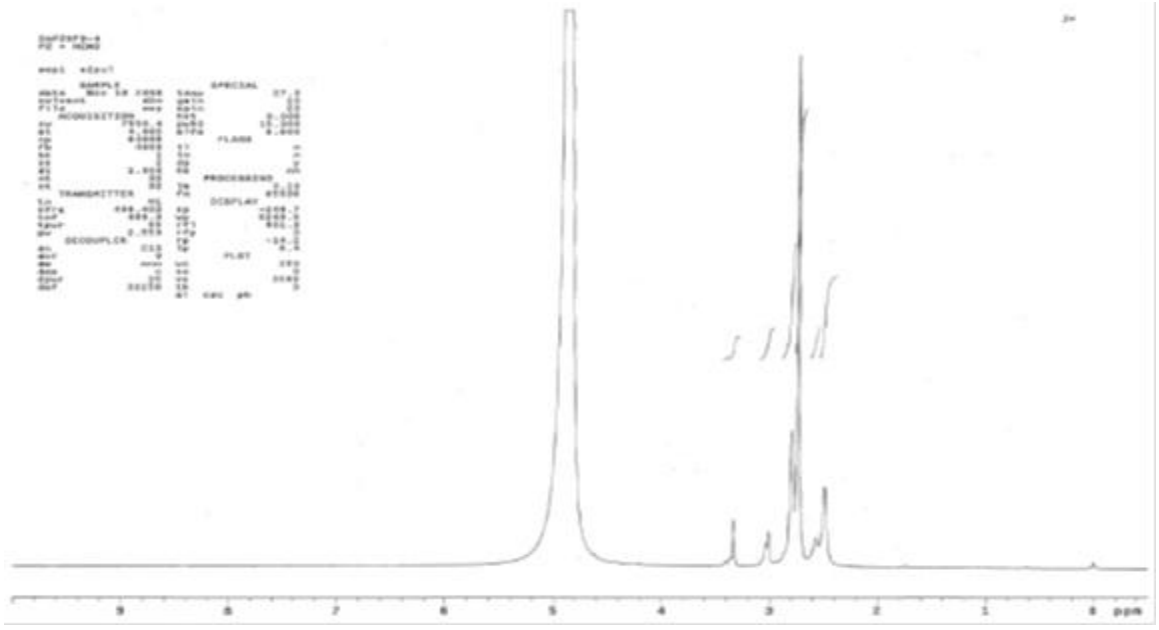

Figure C.12: ^{1}H NMR Spectrum of 2m PZ, α=0, [HCHO]=743mM (0-10 ppm)

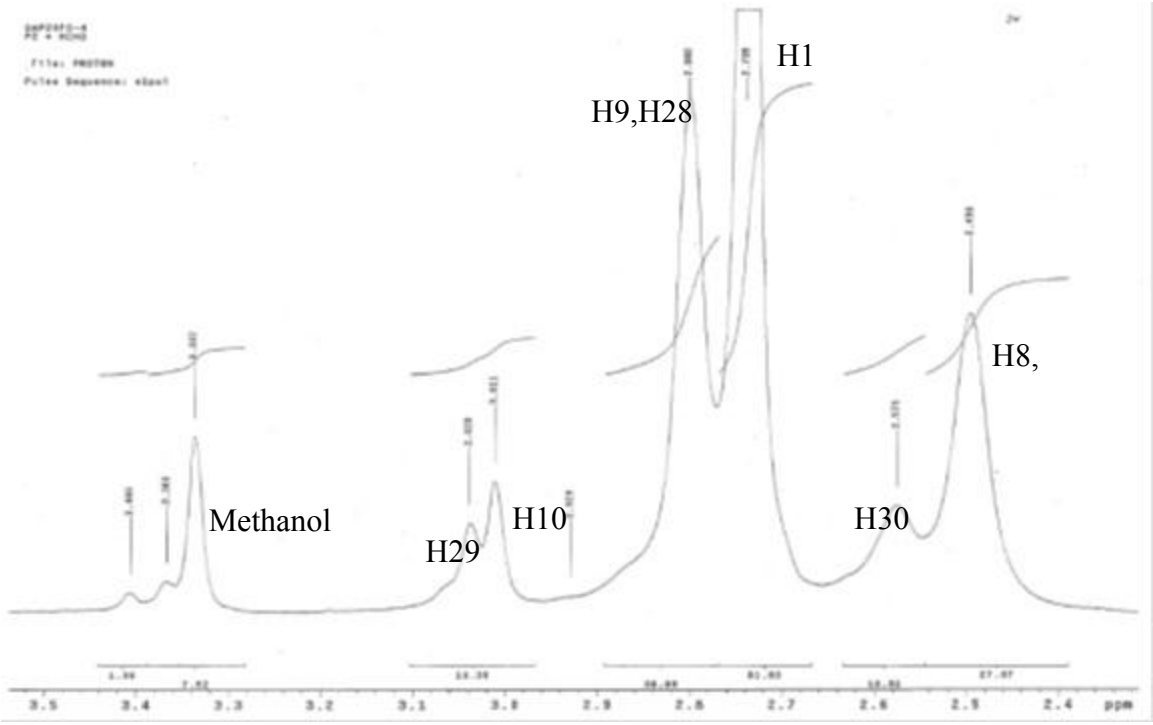

Figure C.13: ^{1}H NMR Spectrum of 2m PZ, α=0, [HCHO]=743mM (2.0-3.6 ppm)

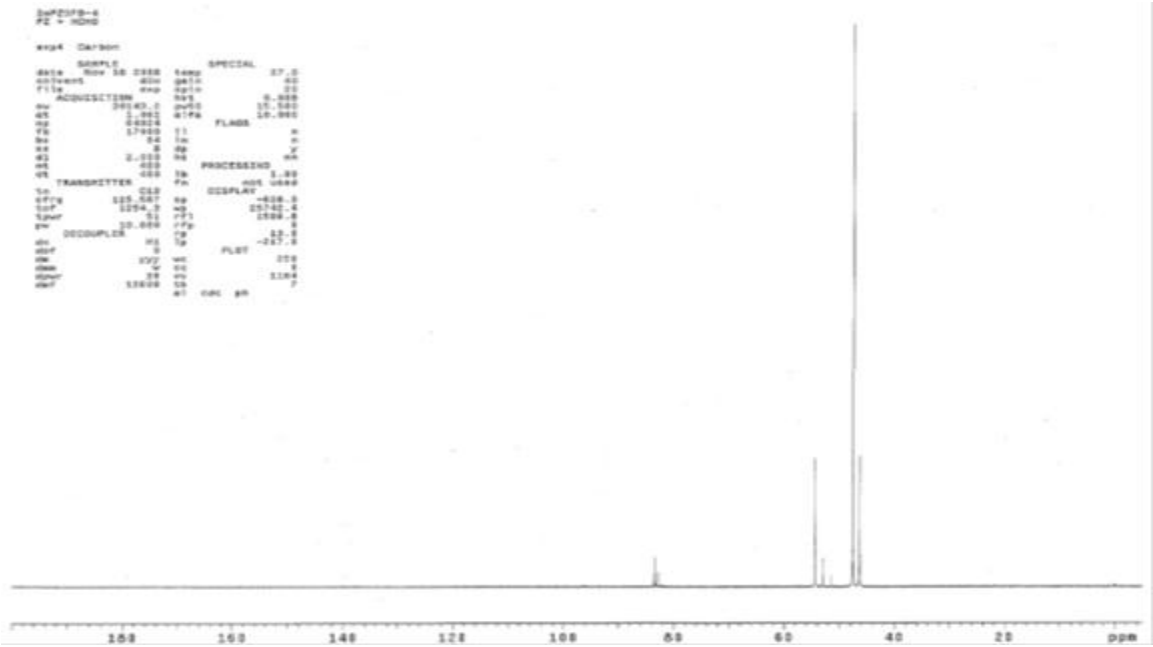

Figure C.14: ^{13}C NMR Spectrum of 2m PZ, α=0, [HCHO]=743mM (0-200 ppm)

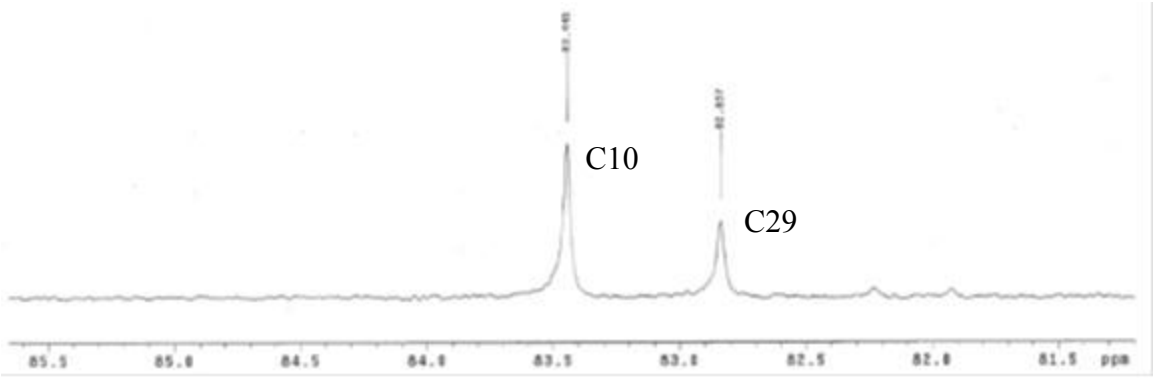

Figure C.15: ^{13}C NMR Spectrum of 2m PZ, α=0, [HCHO]=743mM (81.2-85.6 ppm)

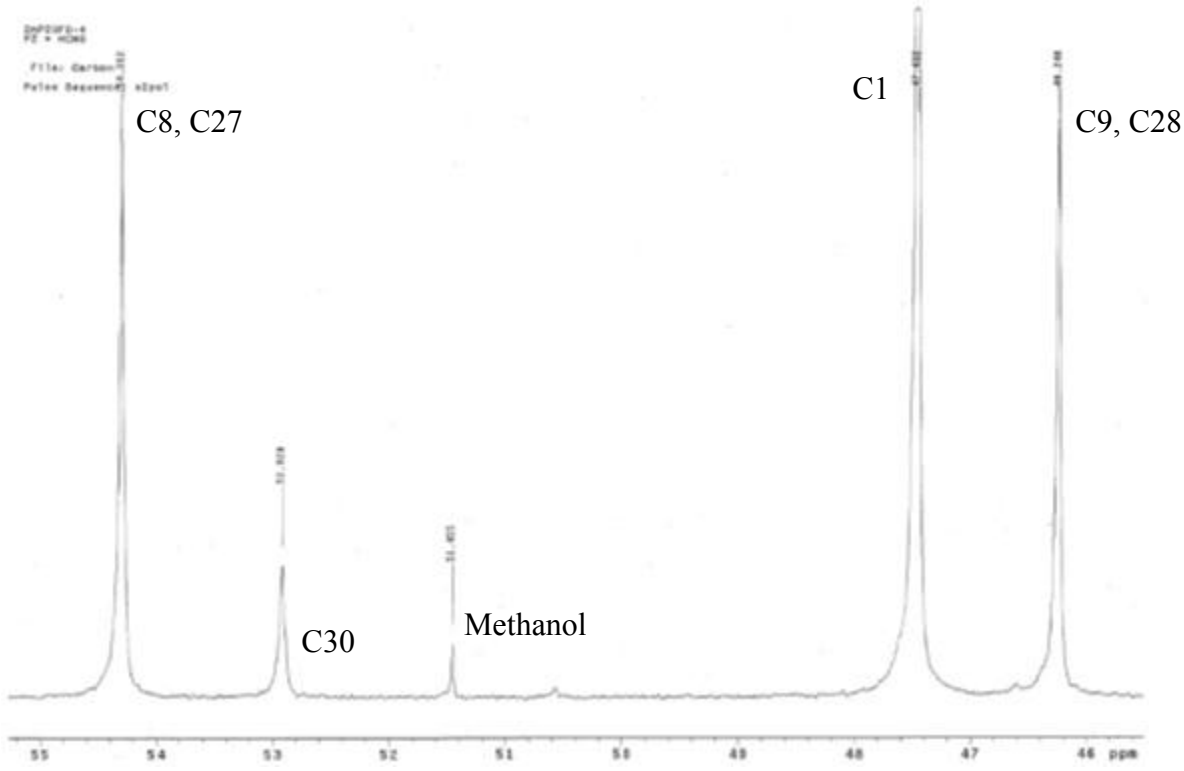

Figure C.16: ^{13}C NMR Spectrum of 2m PZ, α=0, [HCHO]=743mM (45.6-55.2 ppm)

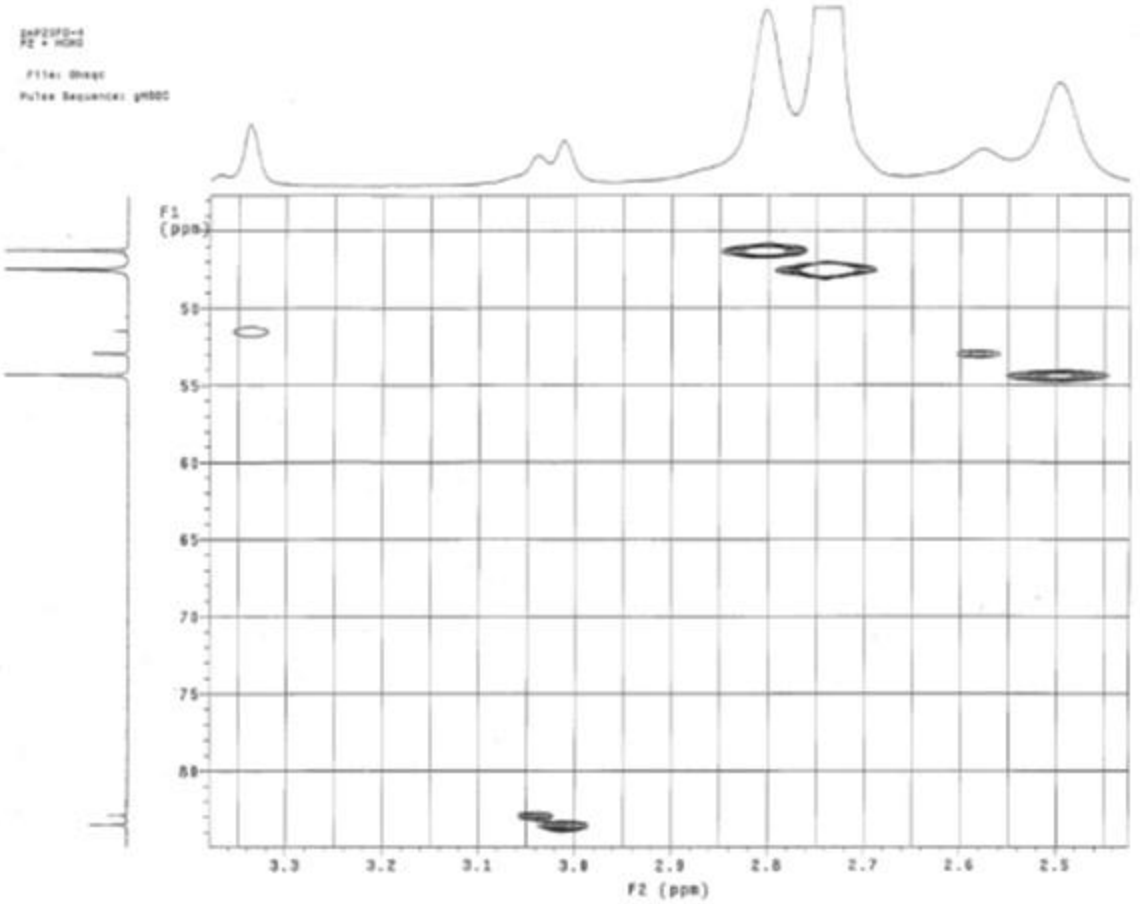

Figure C.17: 2-D correlation NMR Spectrum of 2m PZ, α=0, [HCHO]=743mM

The spectrum for 8m PZ with 0.3 loading was shown in Figure C.18 ~ Figure C.23.

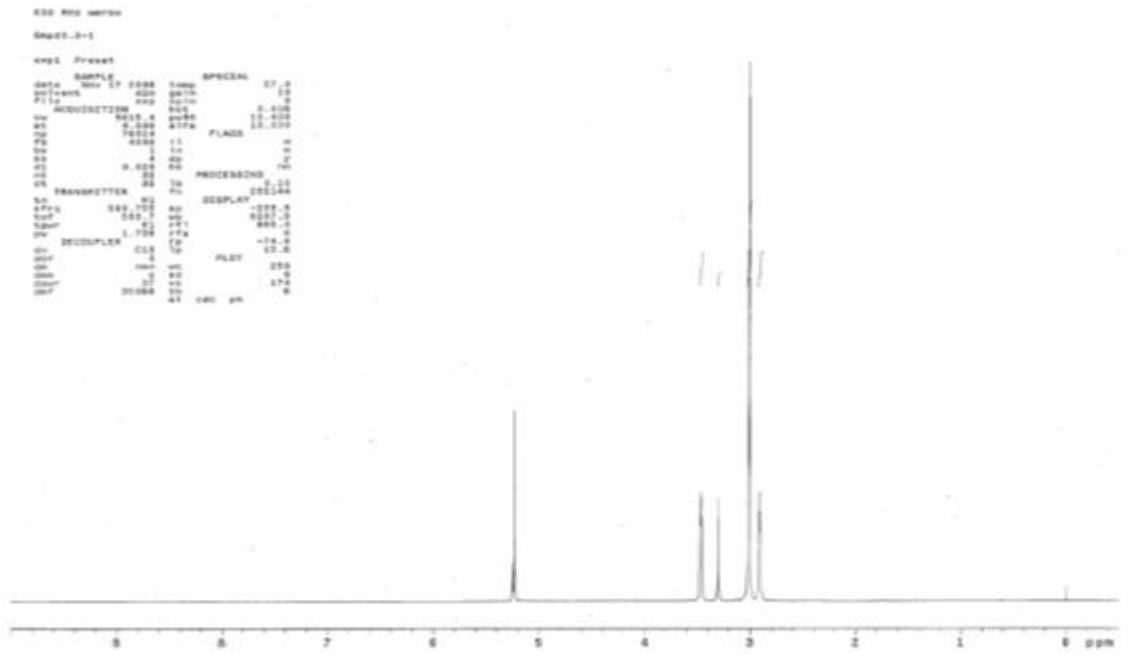

Figure C.18: ^{1}H NMR Spectrum of 8m PZ, α=0.3 (0-10 ppm)

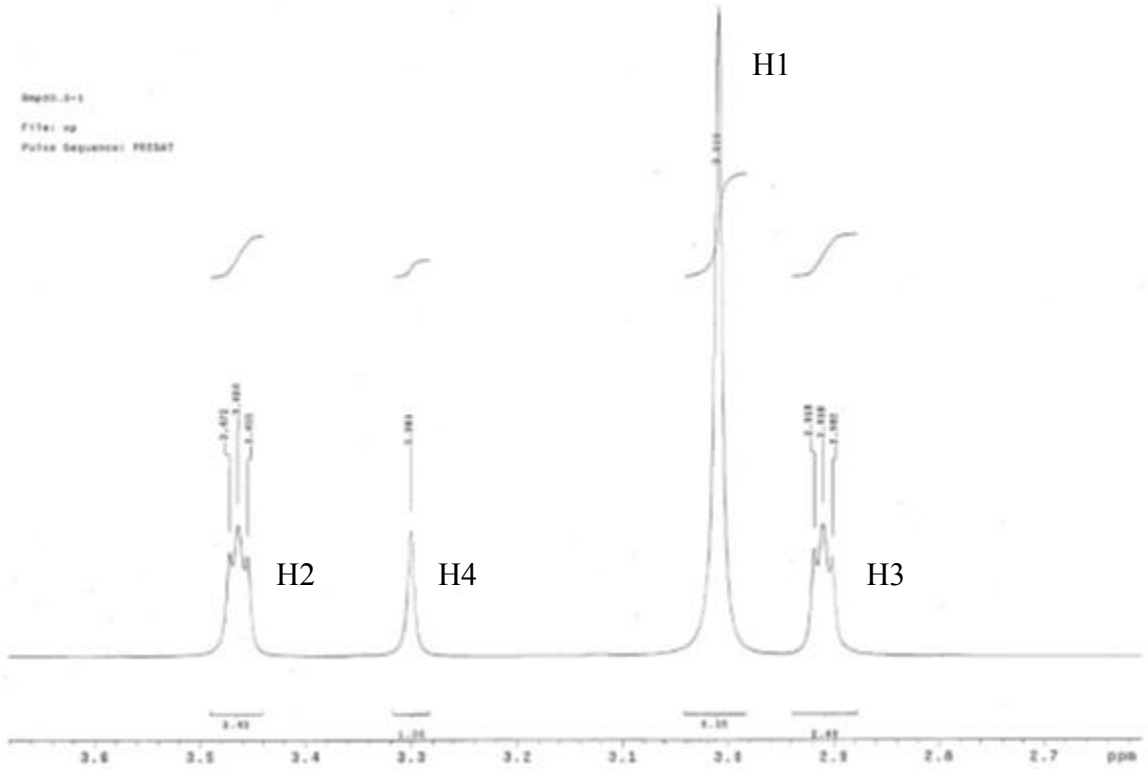

Figure C.19: ^{1}H NMR Spectrum of 8m PZ, α=0.3 (0-3.7 ppm)

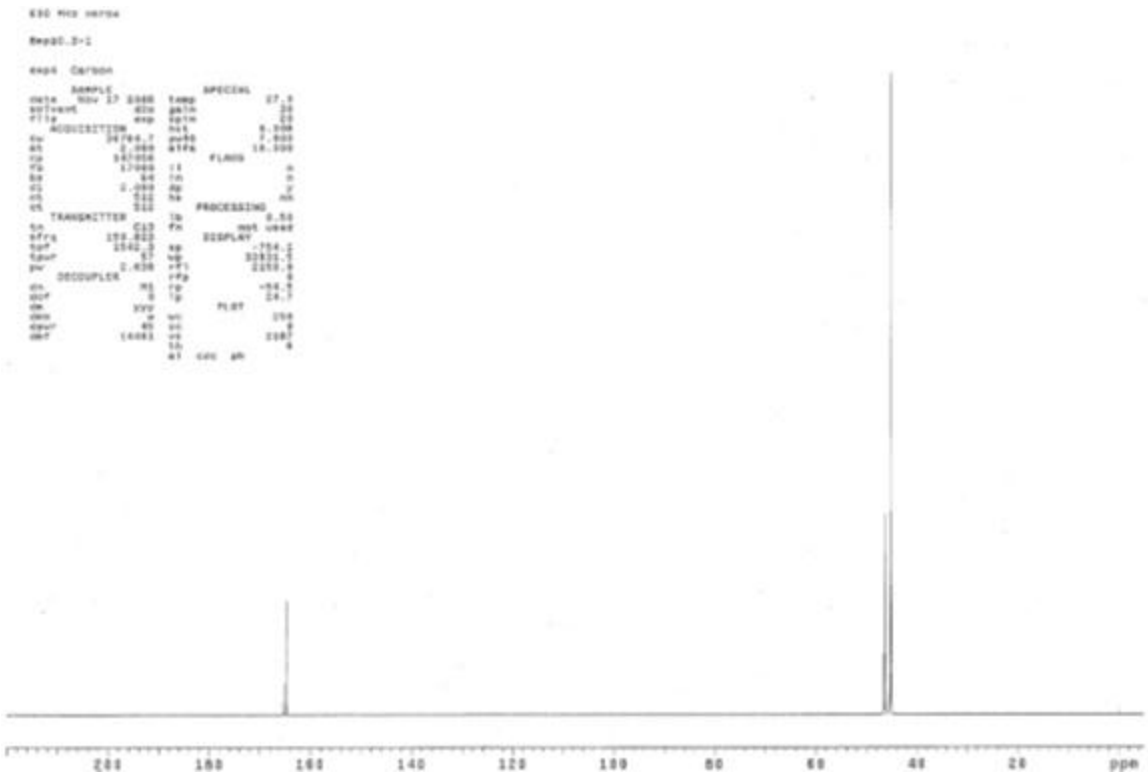

Figure C.20: ^{13}C NMR Spectrum of 8m PZ, α=0.3 (0-220 ppm)

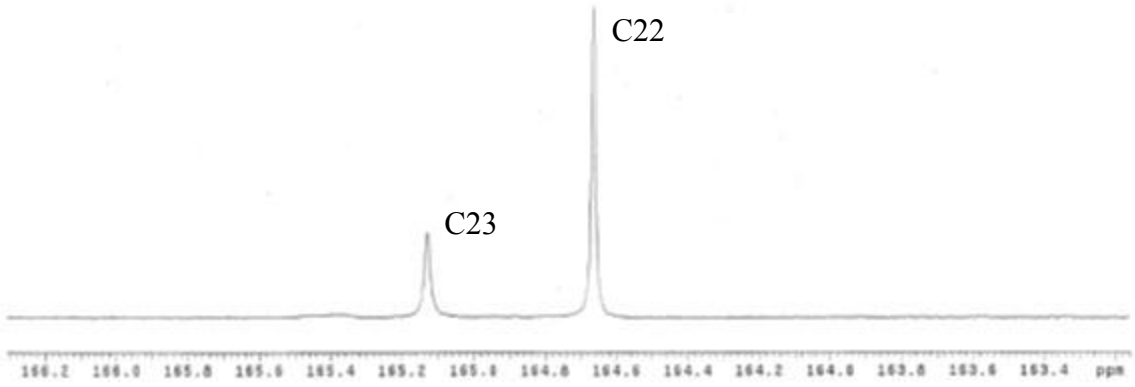

Figure C.21: ^{13}C NMR Spectrum of 8m PZ, α=0.3 (163.2-166.2 ppm)

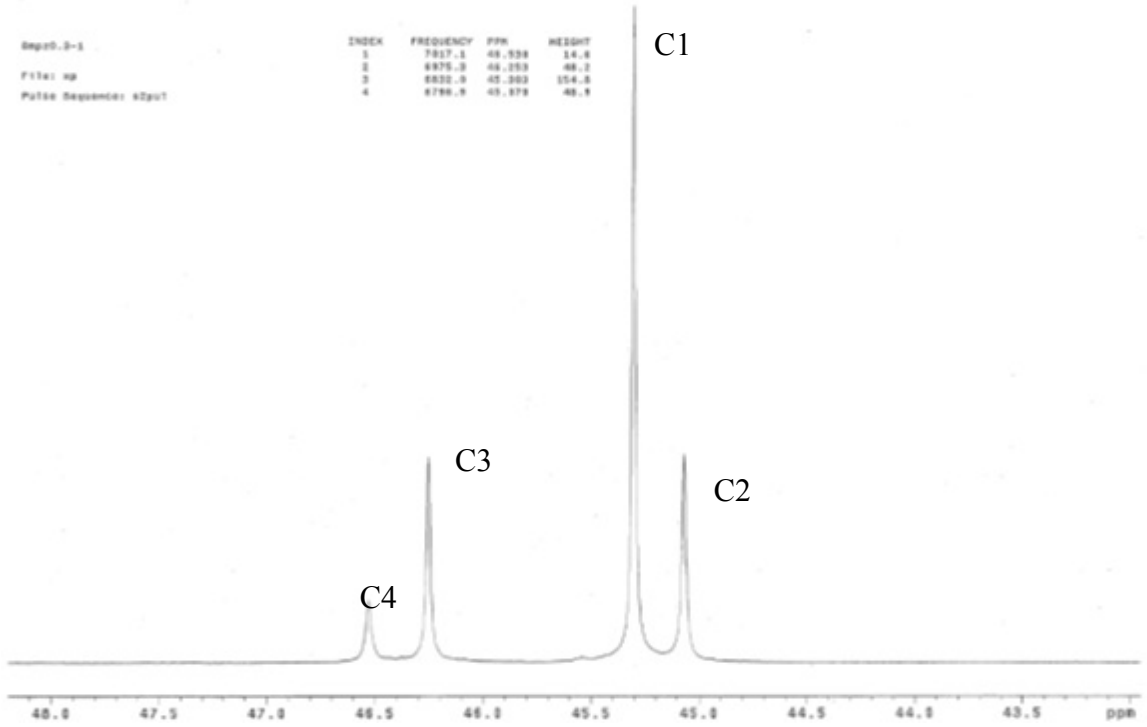

Figure C.22: ^{13}C NMR Spectrum of 8m PZ, α=0.3 (43.0-48.0 ppm)

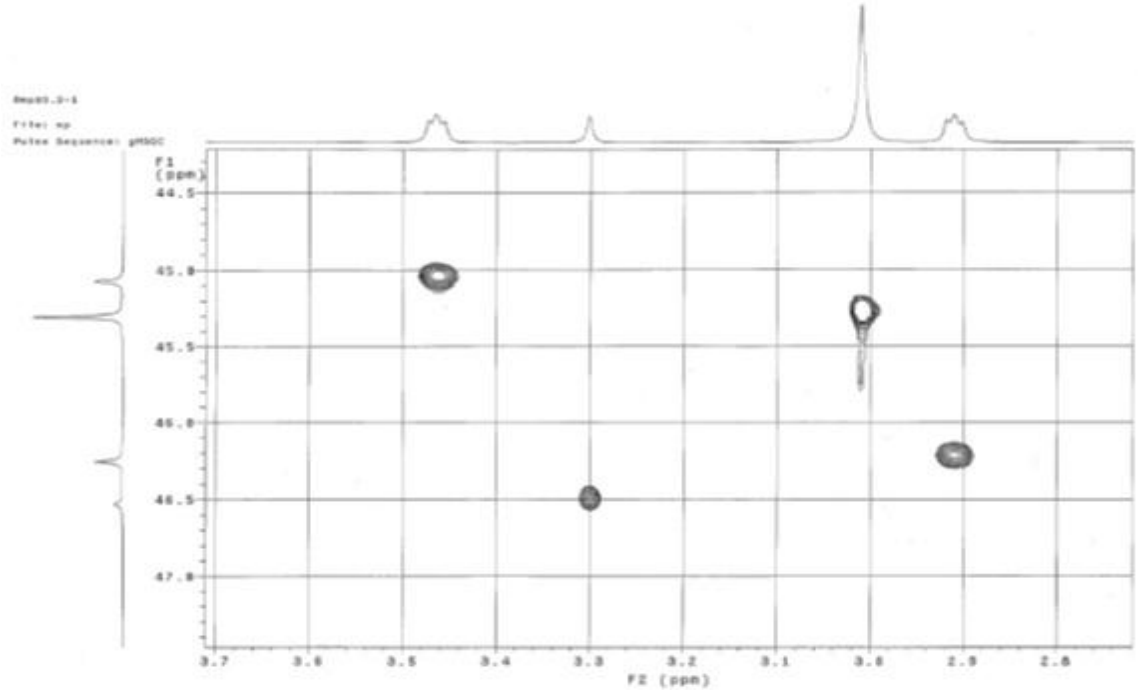

Figure C.23: 2D-correlation NMR Spectrum of 8m PZ, α=0.3

367 mM HCHO was added to loaded PZ solutions and the spectrum was shown in Figure C.24 ~ Figure C.31.

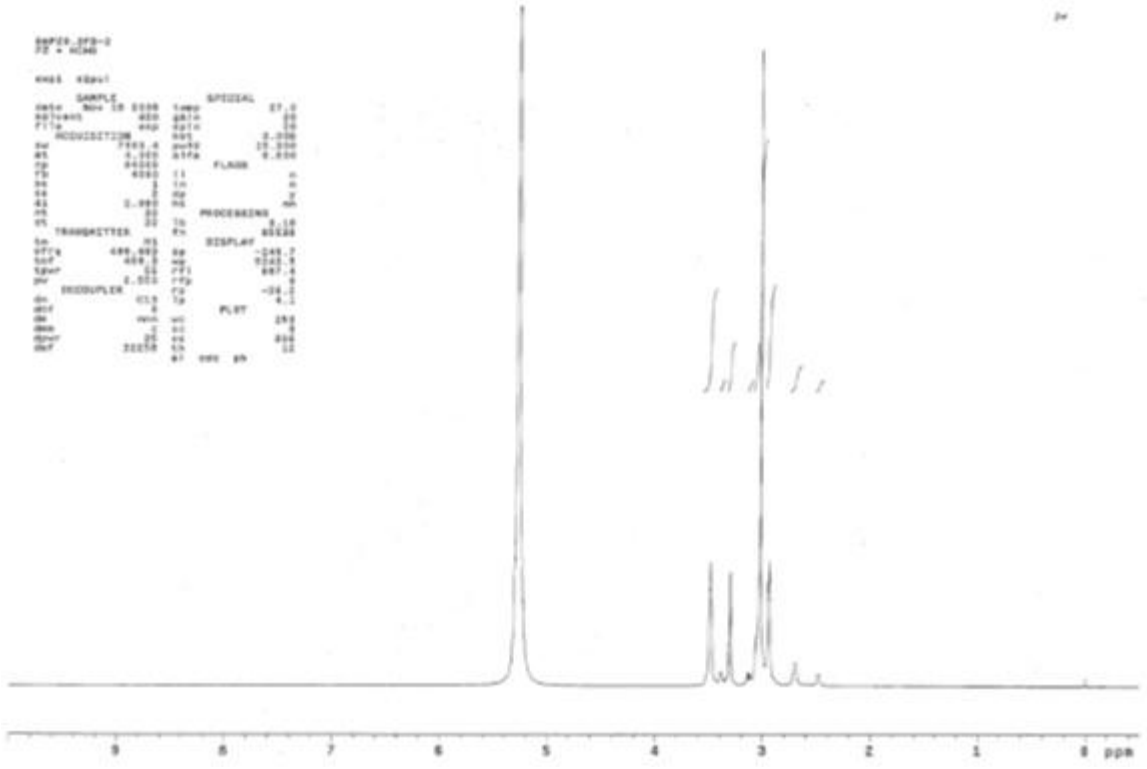

Figure C.24: ^{1}H NMR Spectrum of 8m PZ, α=0.3, [HCHO]=367mM (0-10 ppm)

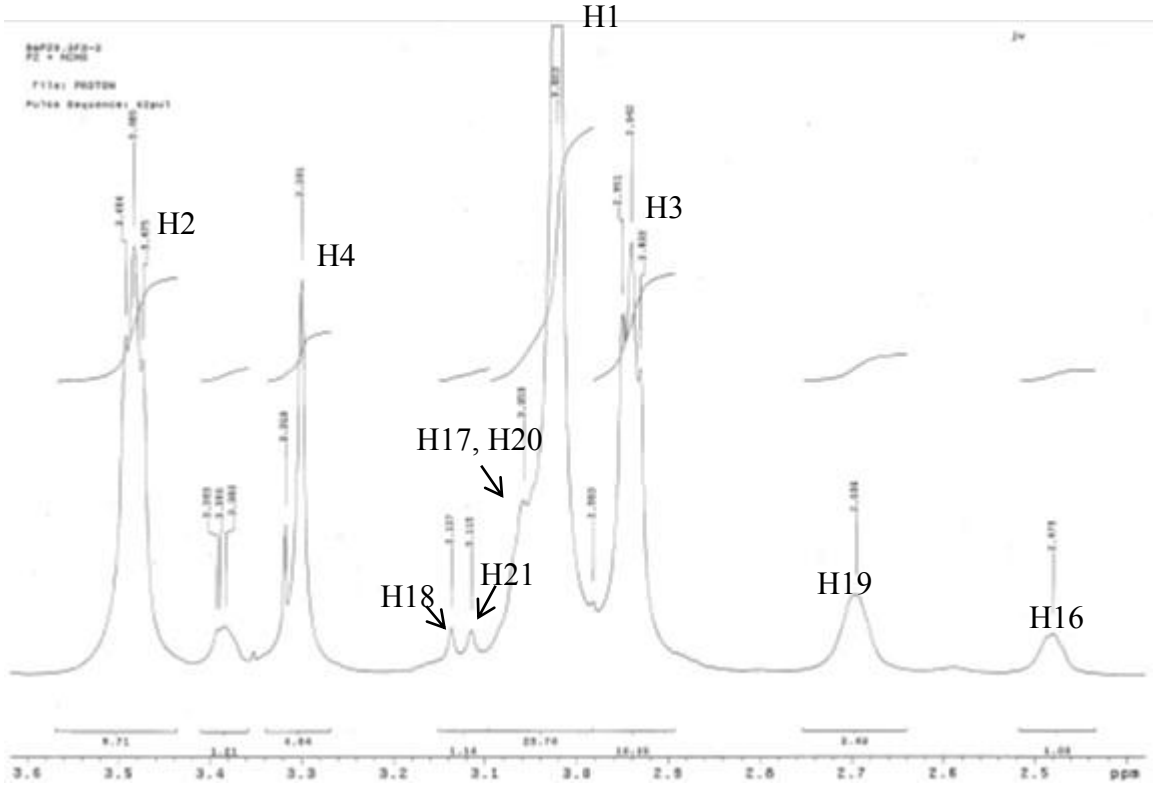

Figure C.25: ^{1}H NMR Spectrum of 8m PZ, α=0.3, [HCHO]=367mM (2.4-3.6 ppm)

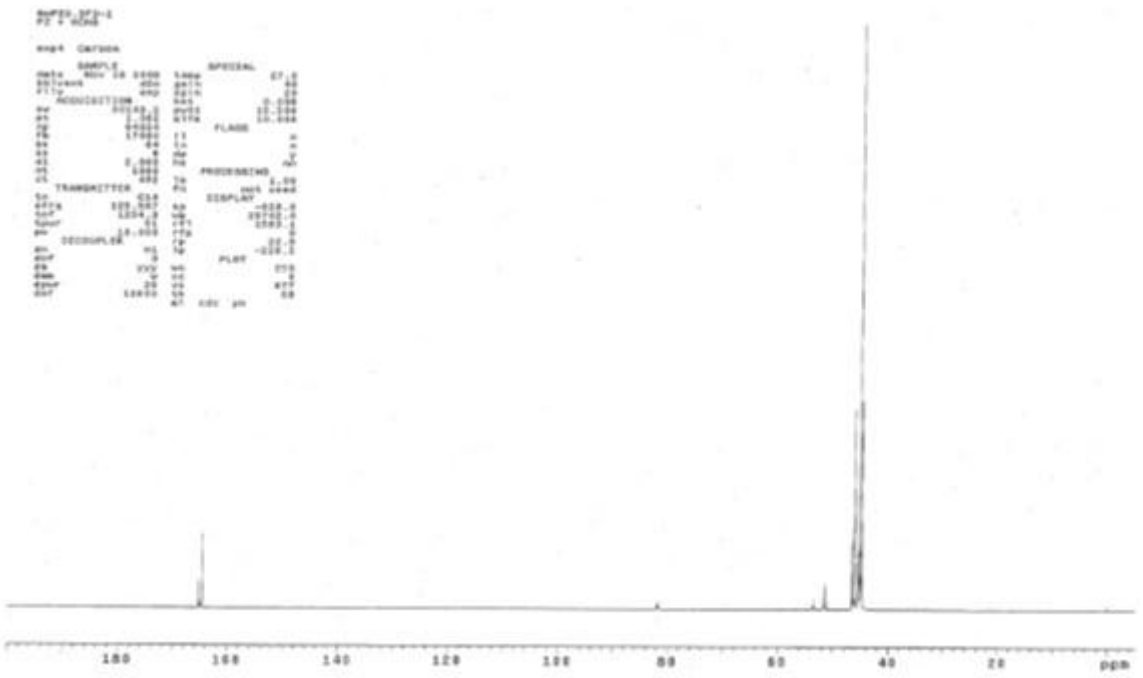

Figure C.26: ^{13}C NMR Spectrum of 8m PZ, α=0.3, [HCHO]=367mM (0-200 ppm)

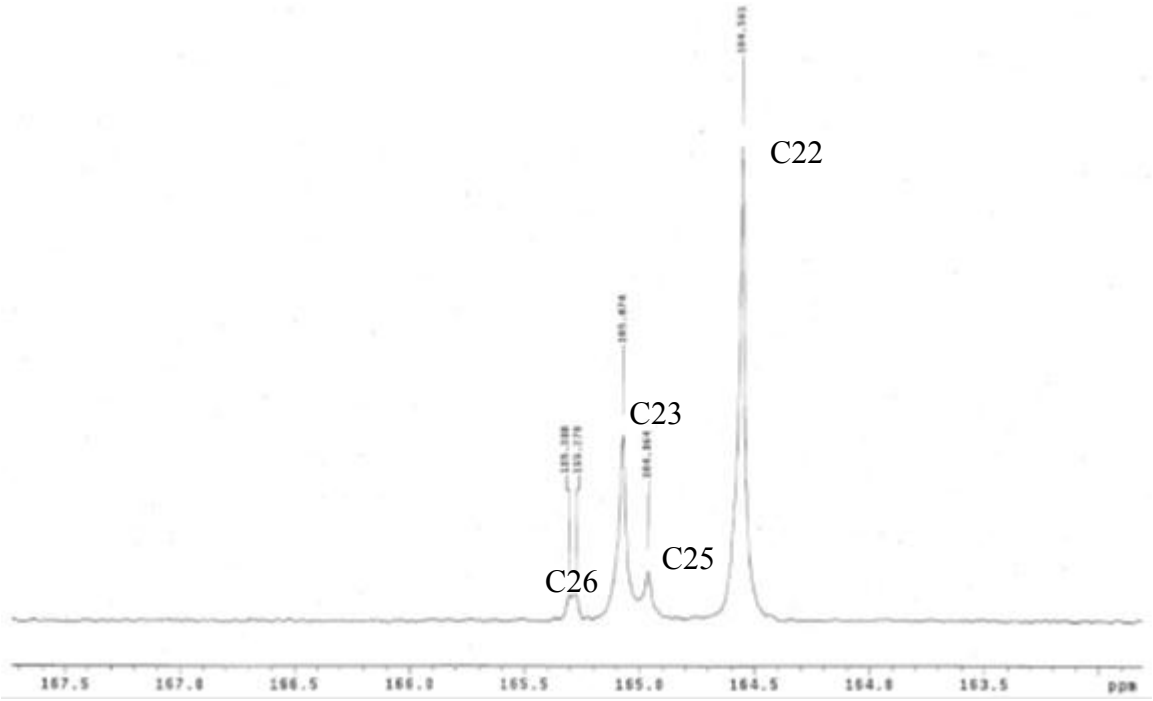

Figure C.27: ^{13}C NMR Spectrum of 8m PZ, α=0.3, [HCHO]=367mM (162.9-167.7 ppm)

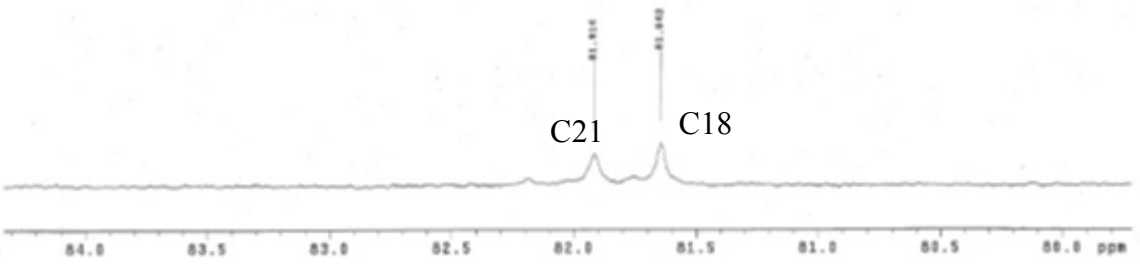

Figure C.28: ^{13}C NMR Spectrum of 8m PZ, α=0.3, [HCHO]=367mM (79.8-84.3 ppm)

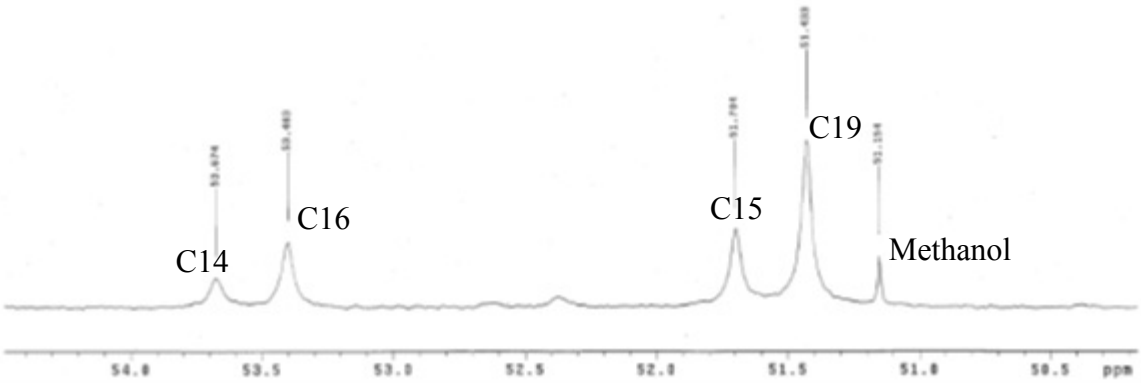

Figure C. 29: ^{13}C NMR Spectrum of 8m PZ, α=0.3, [HCHO]=367mM (50.2-55.0 ppm)

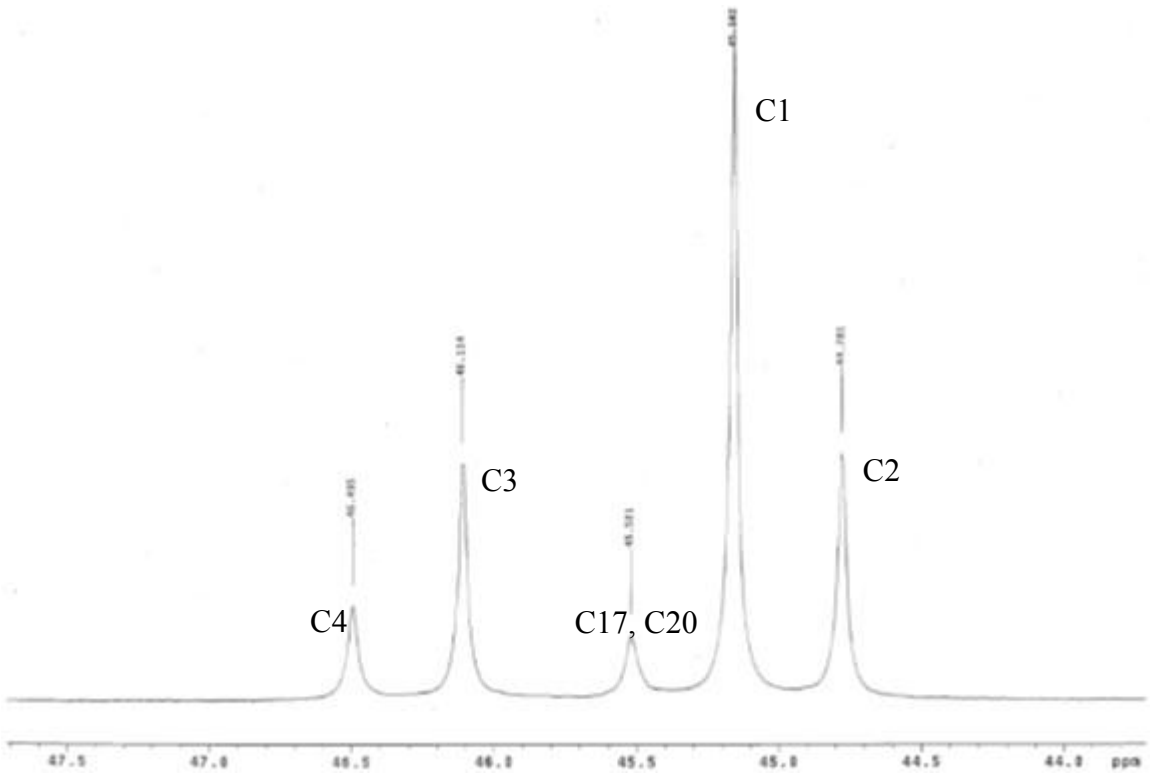

Figure C.30: ^{13}C NMR Spectrum of 8m PZ, α=0.3, [HCHO]=367mM (43.8-47.7 ppm)

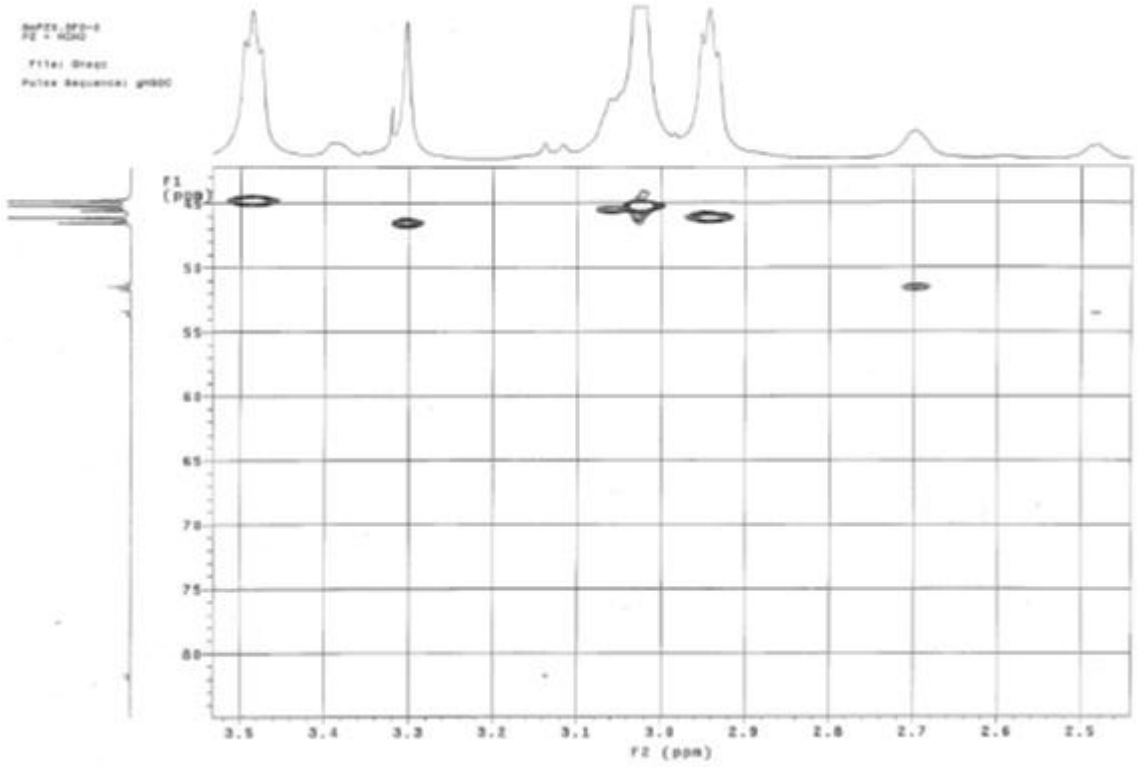

Figure C.31: 2D-correlation NMR Spectrum of 8m PZ, α=0.3, [HCHO]=367mM

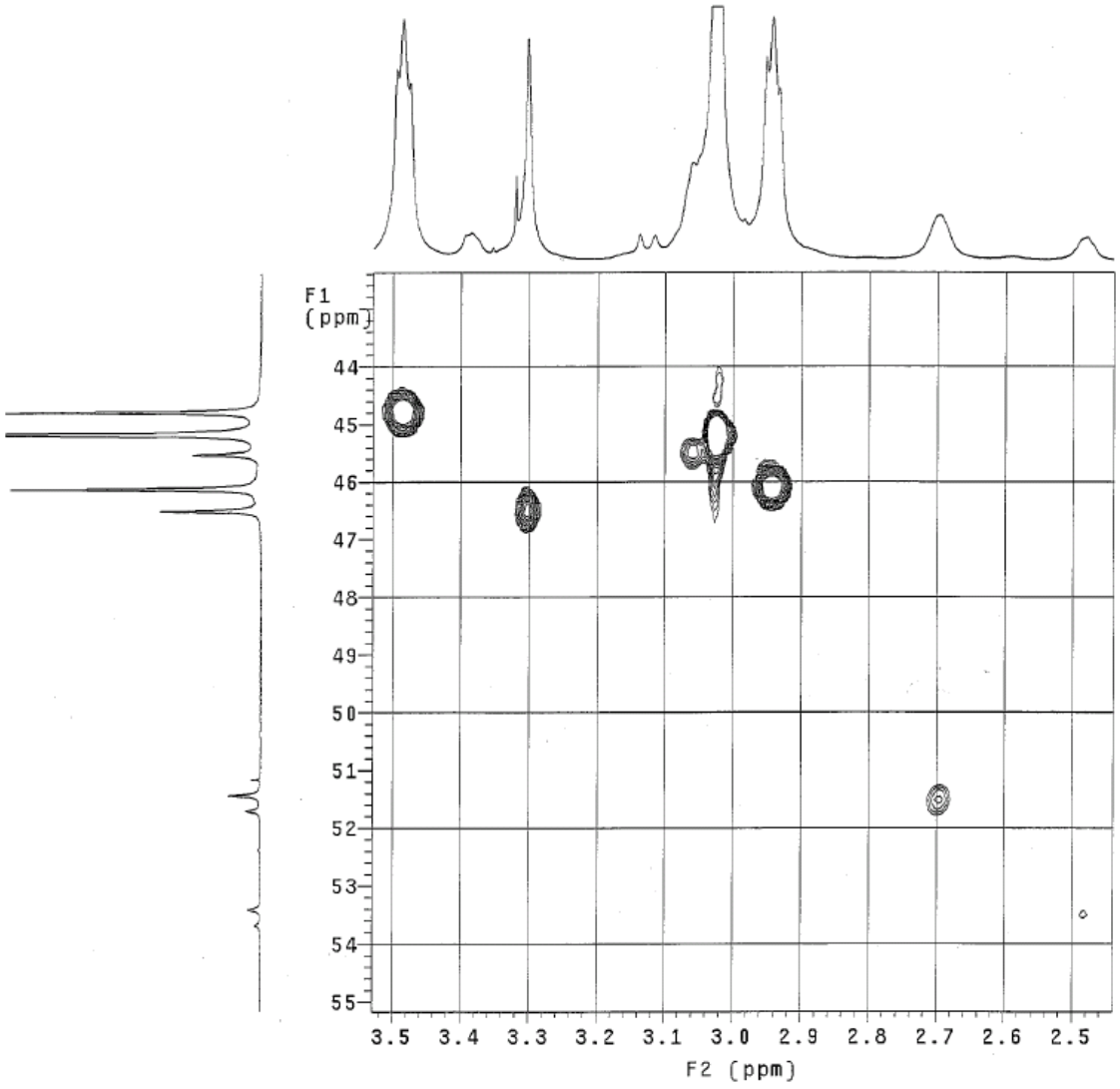

Figure C.32: 2D-correlation NMR Spectrum of 8m PZ, α=0.3, [HCHO]=367mM

Oxidatively degraded sample OE5 was used in this study for NMR and MS analysis. The foaming test showed that this sample had a much higher foaming tendency than undegraded PZ solution. Prior to the NMR analysis, 5 mM Na_2S was added to the sample to precipitate Fe^{2+} and reduce the interfering to NMR spectrum. The results were shown in

Figure C.33~Figure C.37.

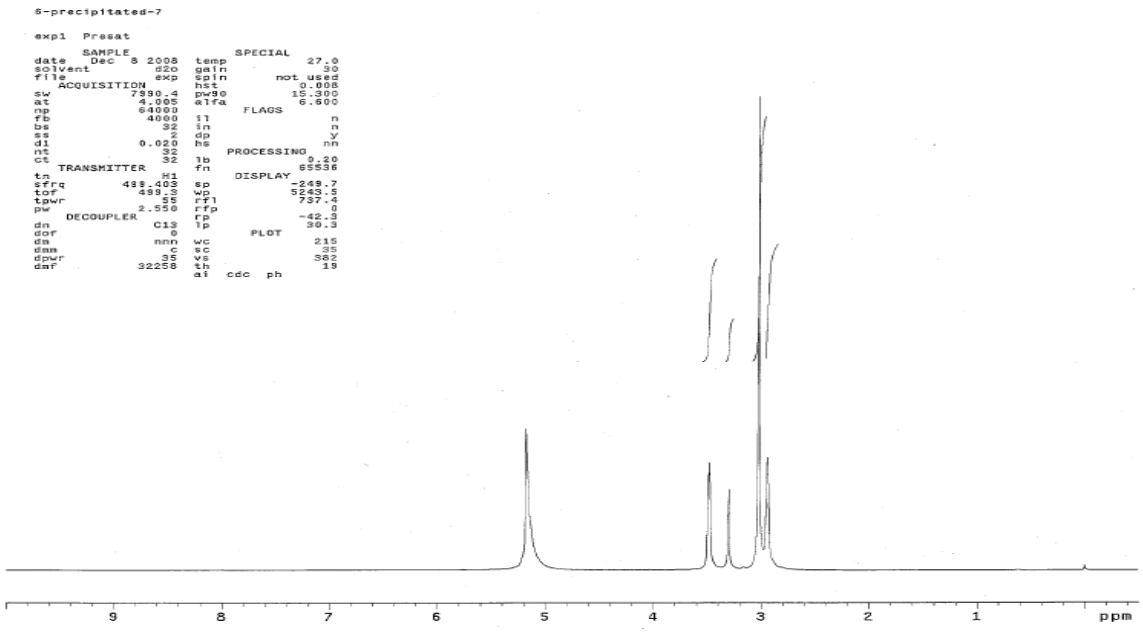

Figure C.33: ^{1}H NMR spectrum of degraded 8m PZ, 1mM Fe2+, 55°C, α =0.3, Fe^{2+} (OE5) was precipitated with 5mM Na_2S before NMR analysis. (0-10 ppm)

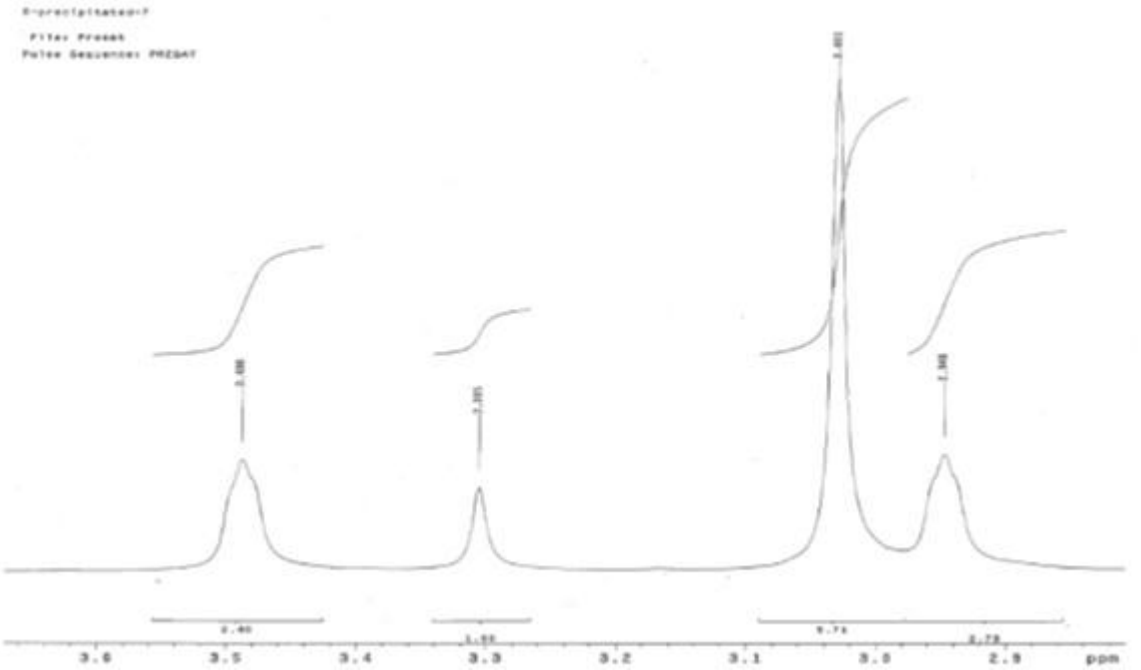

Figure C.34: ^{1}H NMR spectrum of degraded 8m PZ, 1mM Fe2+, 55°C, α =0.3, Fe^{2+} (OE5) was precipitated with 5mM Na_2S before NMR analysis. (2.82-3.66 ppm)

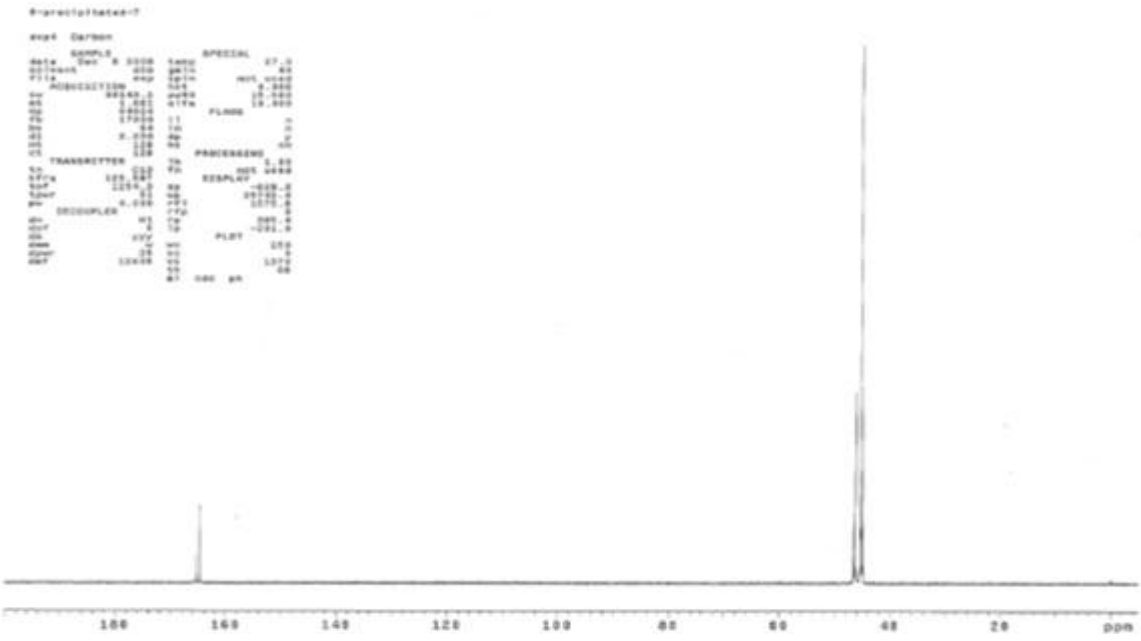

Figure C.35: ^{13}C NMR spectrum of degraded 8m PZ, 1mM Fe2+, 55°C, α =0.3, Fe^{2+} (OE5) was precipitated with 5mM Na_2S before NMR analysis. (0-200 ppm)

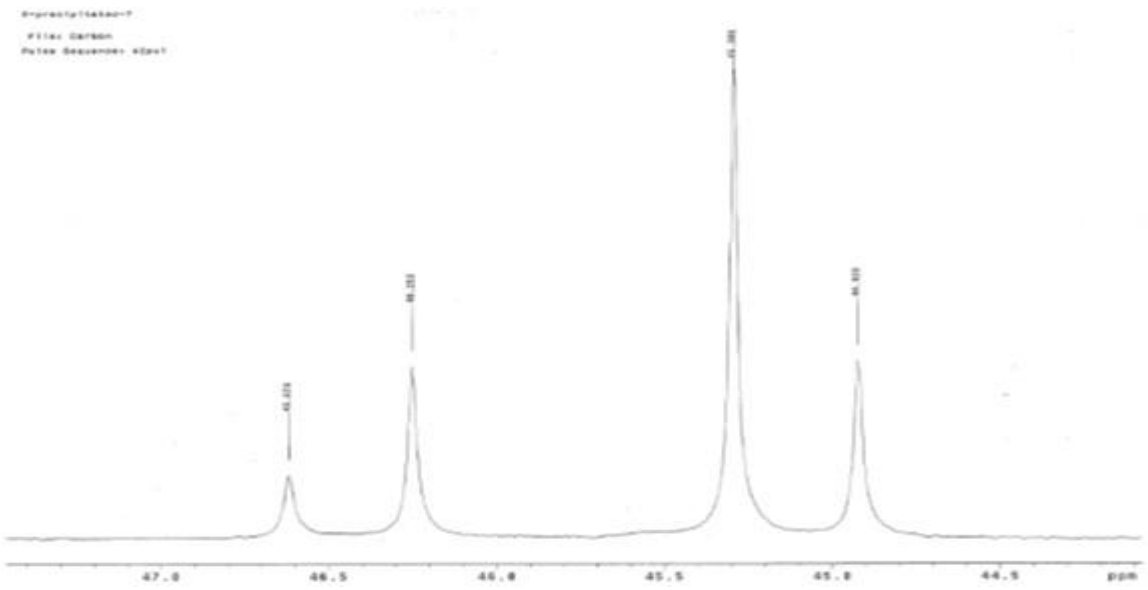

Figure C.36: ^{13}C NMR spectrum of degraded 8m PZ, 1mM Fe2+, 55°C, α =0.3, Fe^{2+} (OE5) was precipitated with 5mM Na_2S before NMR analysis. (44.1-47.4 ppm)

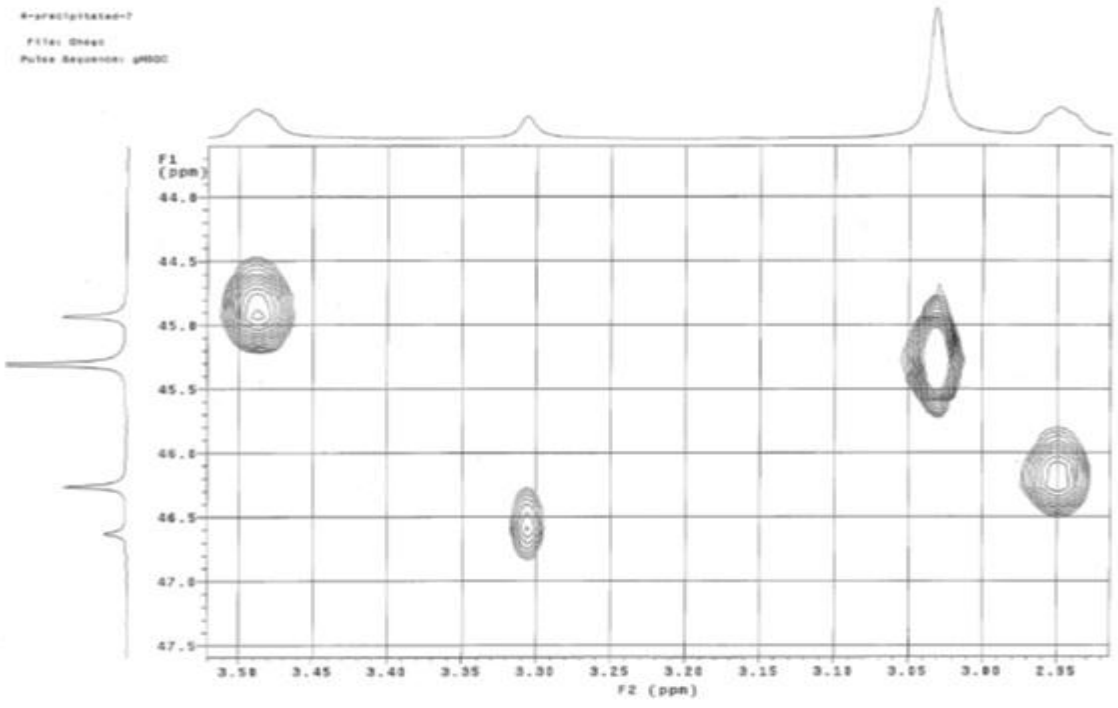

Figure C.37: 2D-correlation NMR spectrum of degraded 8m PZ, 1mM Fe2+, 55°C, α =0.3, Fe^{2+} (OE5) was precipitated with 5mM Na_2S before NMR analysis.

Unexpectedly, there were no interesting additional peaks found for OE5. All the major peaks that show up in the spectrum have the same peak position as those for the neat loaded PZ solution. Because OE5 is only degraded for a couple of weeks, the oxidation products might be present in such a small concentration that although they can significantly change the foaming property of the amine solution, they are not able to give rise to significant peaks on NMR spectrum.

Andrew Sexton had also done much NMR analysis for degraded PZ samples. The spectrum he got for degraded PZ solution was used here for comparison with the ones shown above. Figure C.38 ~ Figure C.42 gives the ^{1}H NMR spectrum of degraded 2.5m PZ with the presence of 5mM V. Those peaks which have same position as seen in this work are pinpointed with red arrows. Same peaks indicate that the degraded sample may have similar species as formaldehyde-added PZ. There are many small peaks in the ^{13}C NMR spectrum for this degraded sample and they are hard to be interpreted.

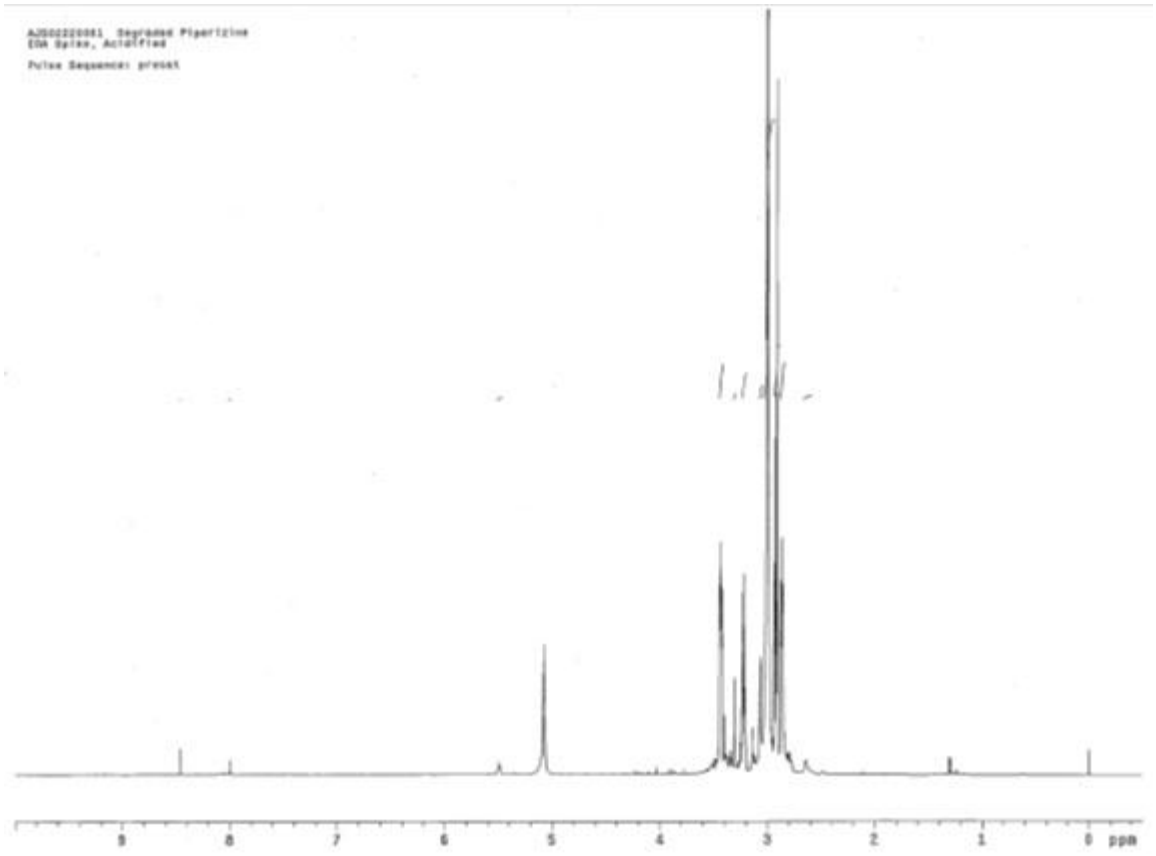

Figure C.38: ^{1}H NMR spectrum of degraded 2.5 m PZ, 5 mM V, 55^{o}C, α= 0.30, 1400 RPM (0~10 ppm)

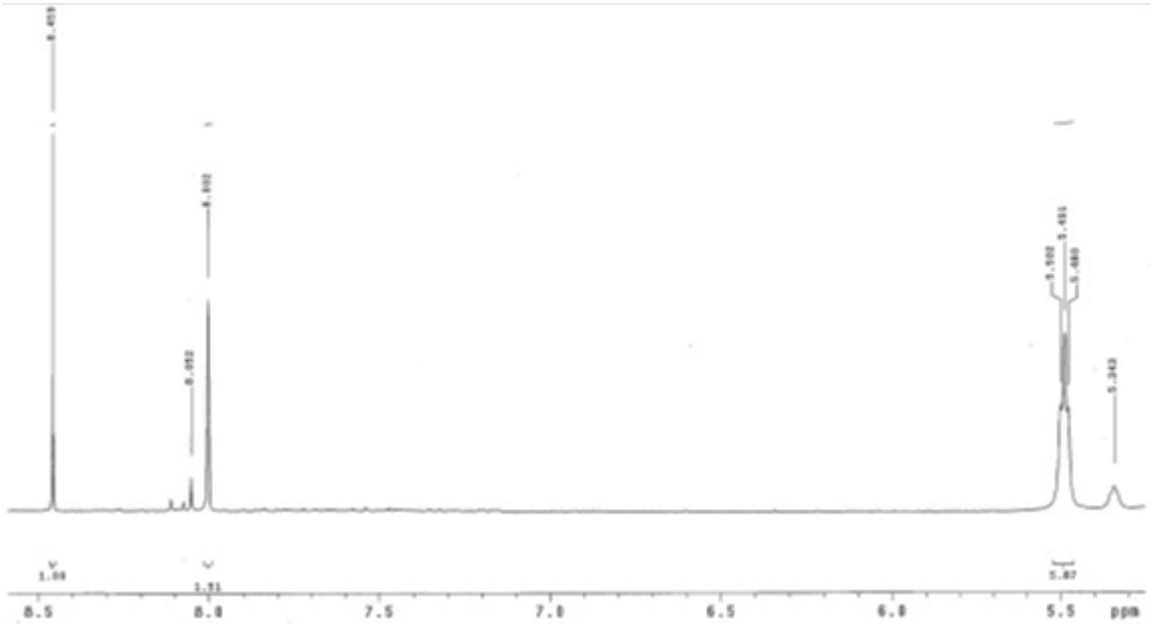

Figure C.39: ^{1}H NMR spectrum of degraded 2.5 m PZ, 5 mM V, 55^{o}C, α= 0.30, 1400 RPM (5.3~8.5 ppm)

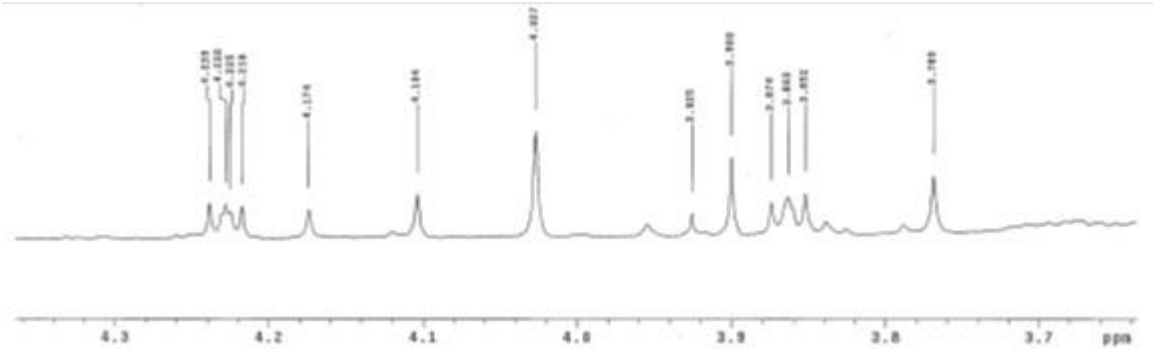

Figure C.40: ^{1}H NMR spectrum of degraded 2.5 m PZ, 5 mM V, 55^{o}C, α= 0.30, 1400 RPM (3.64~4.36 ppm

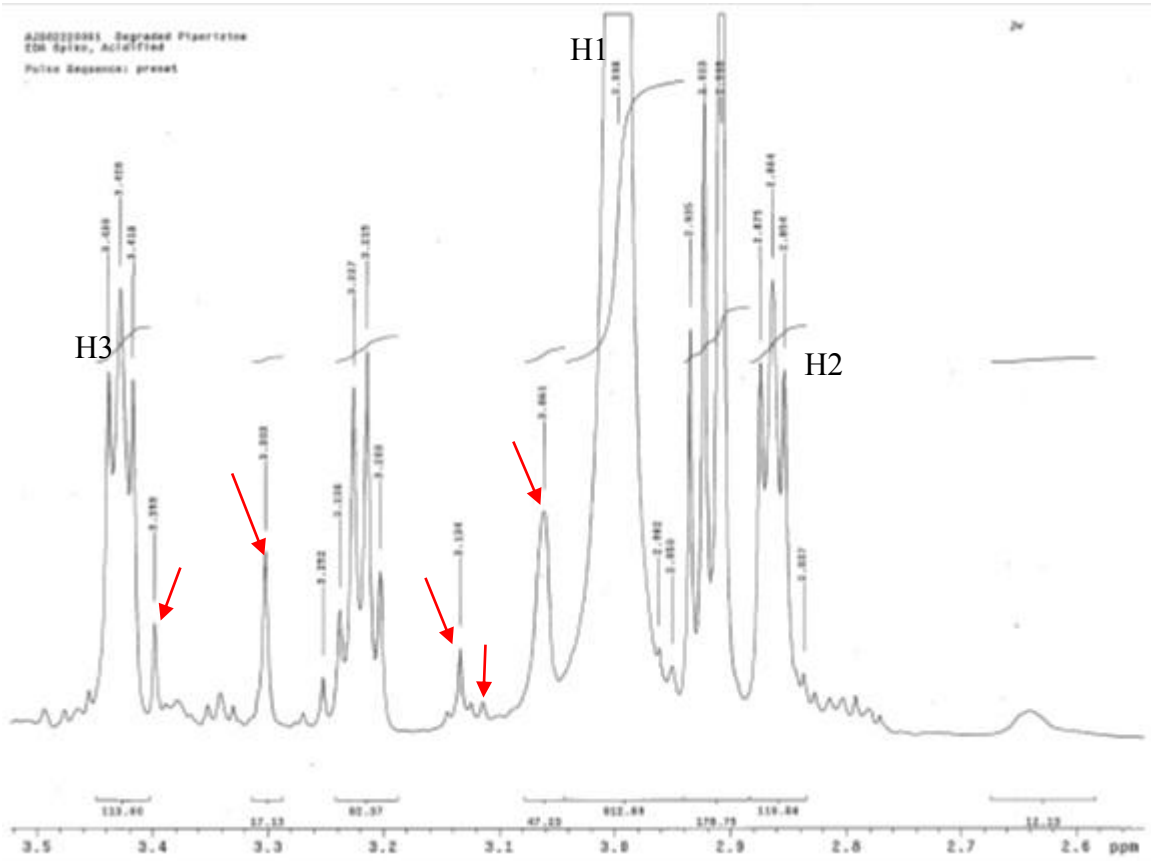

Figure C.41: ^{1}H NMR spectrum of degraded 2.5 m PZ, 5 mM V, 55^{o}C, α= 0.30, 1400 RPM (2.56~3.52 ppm)

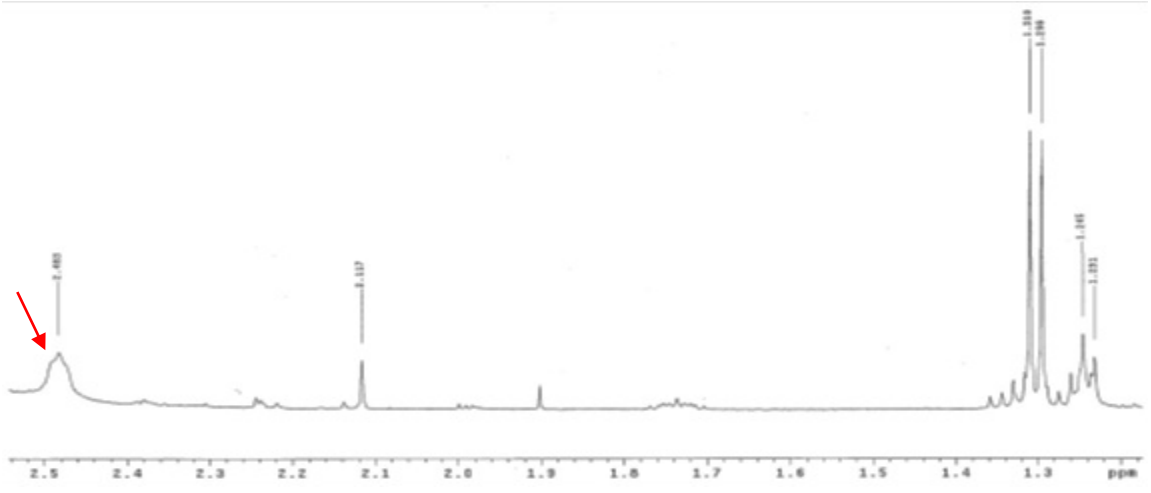

Figure C.42: ^{1}H NMR spectrum of degraded 2.5 m PZ, 5 mM V, 55^{o}C, α= 0.30, 1400 RPM (0~2.54 ppm)

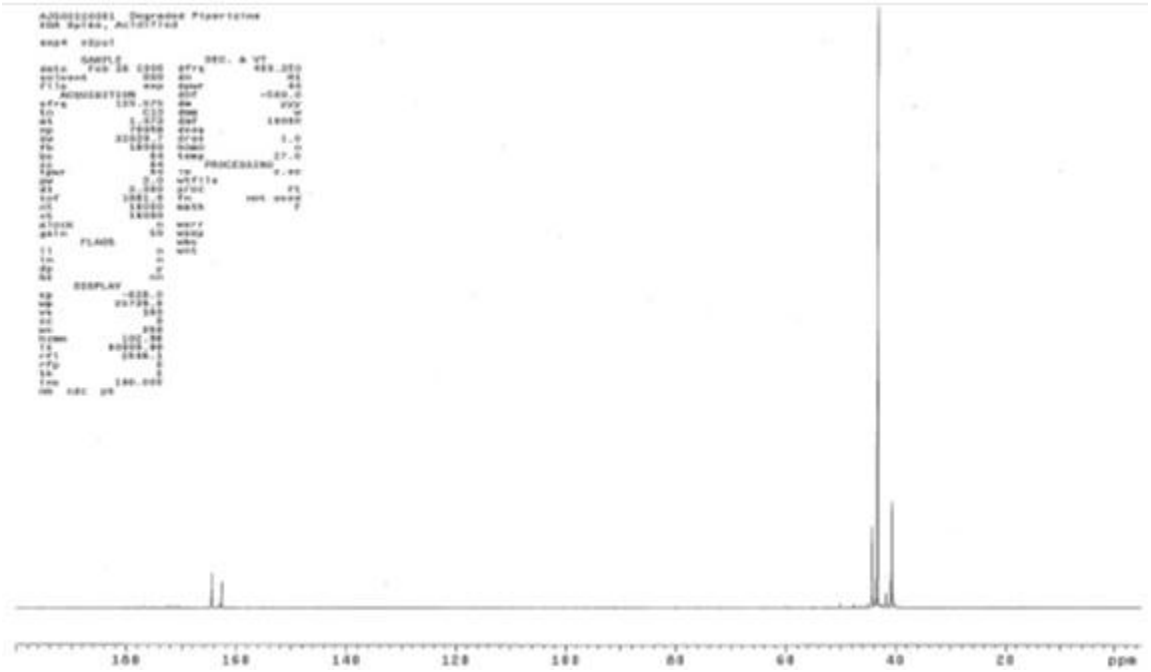

Figure C.43: ^{13}C NMR spectrum of degraded 2.5 m PZ, 5 mM V, 55^{o}C, α= 0.30, 1400 RPM (0~200 ppm)

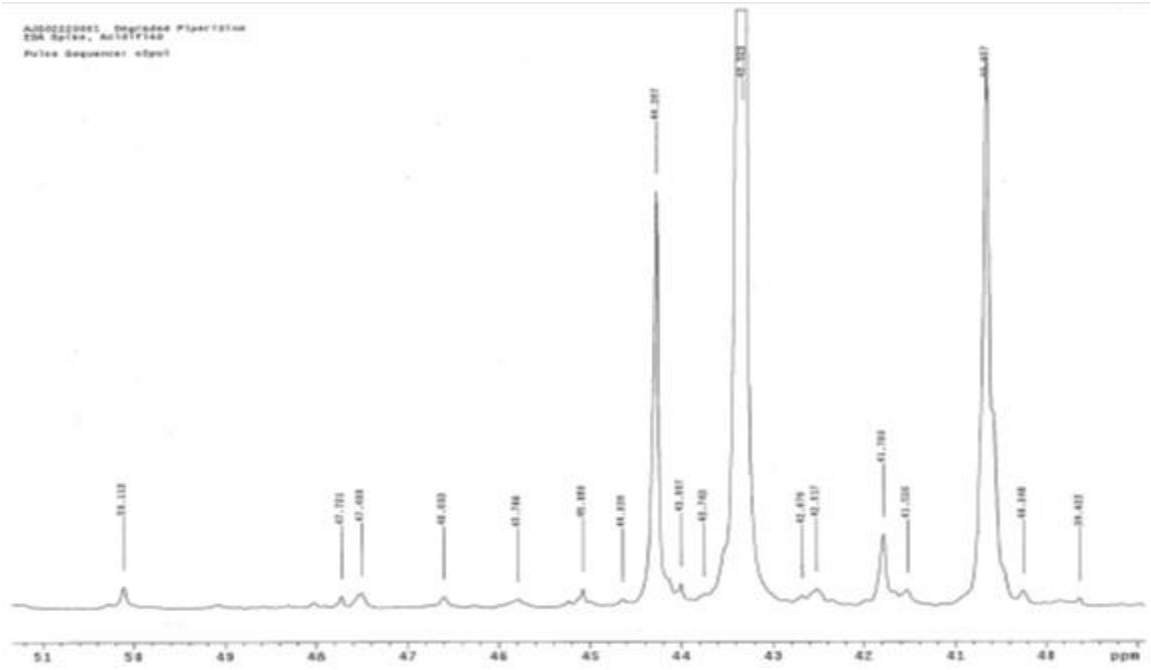

Figure C.44: ^{13}C NMR spectrum of degraded 2.5 m PZ, 5 mM V, 55^{o}C, α= 0.30, 1400 RPM (39~51 ppm)

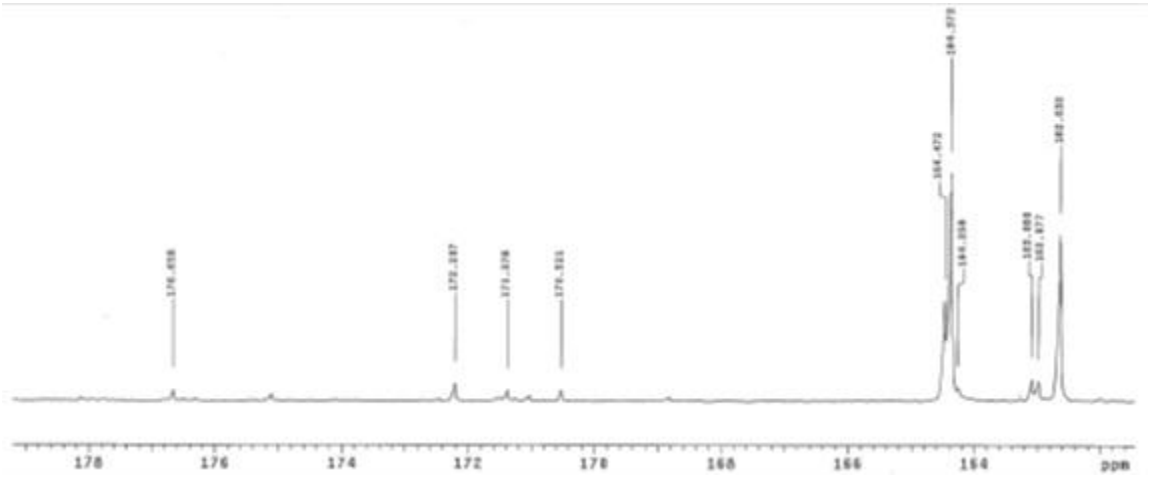

Figure C.45: ^{13}C NMR spectrum of degraded 2.5 m PZ, 5 mM V, 55°C, α= 0.30, 1400 RPM (162~178 ppm)

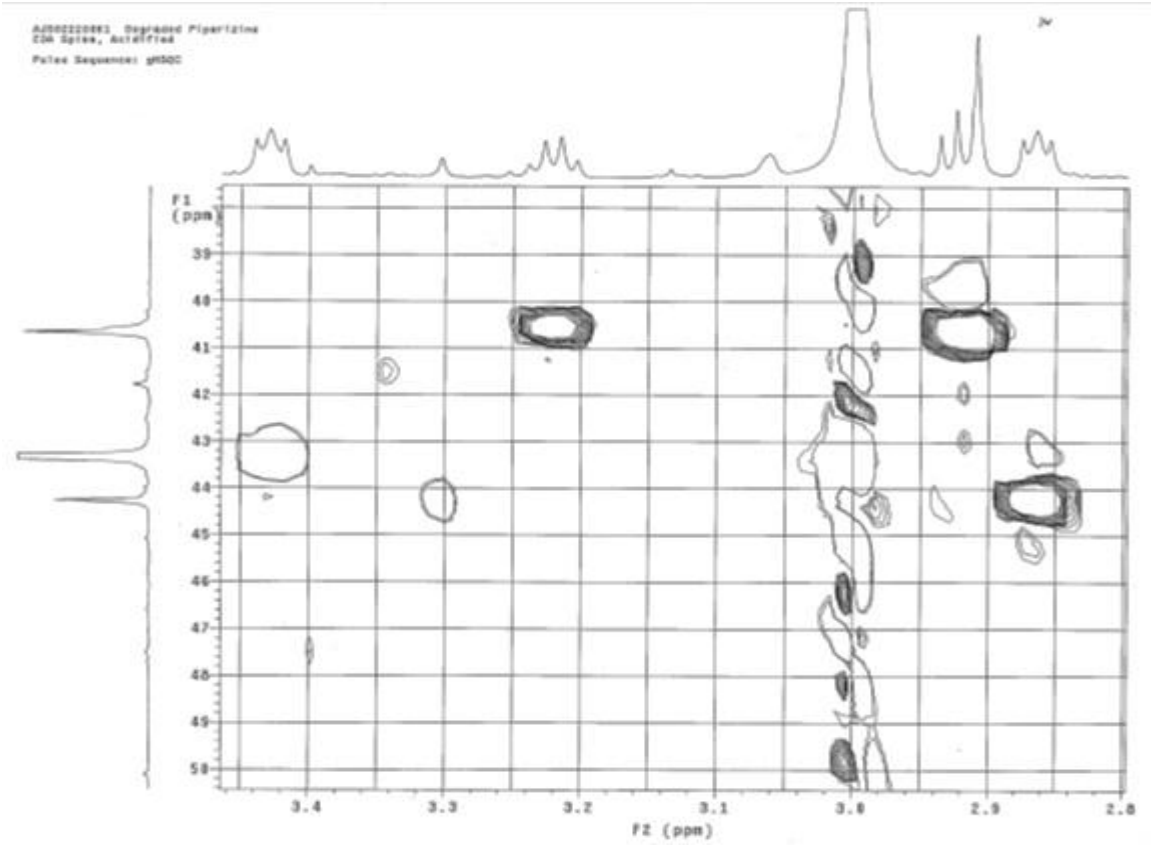

Figure C.46: 2-D correlation spectrum of degraded 2.5 m PZ, 5 mM V, 55°C, α= 0.30, 1400 RPM.

Mass spectroscopy was also tried to identify contaminants in the degraded sample OE4. Figure C.47, Figure C.48, Figure C.49 show the MS spectrum for neat PZ, degraded PZ solutions (OE4) and HCHO-added PZ respectively. For all the 3 samples, the only two peaks that consistently showed up in the spectrum are m/z=87 and m/z=70. Apparently the m/z=87 is corresponding to piperazine. Which species the peak of m/z=70 corresponds to is still unknown at this point. The fact that here are not extra significant peaks showing up in the MS spectrum for the degraded sample might be attributed to the detection limit of MS apparatus in this study.

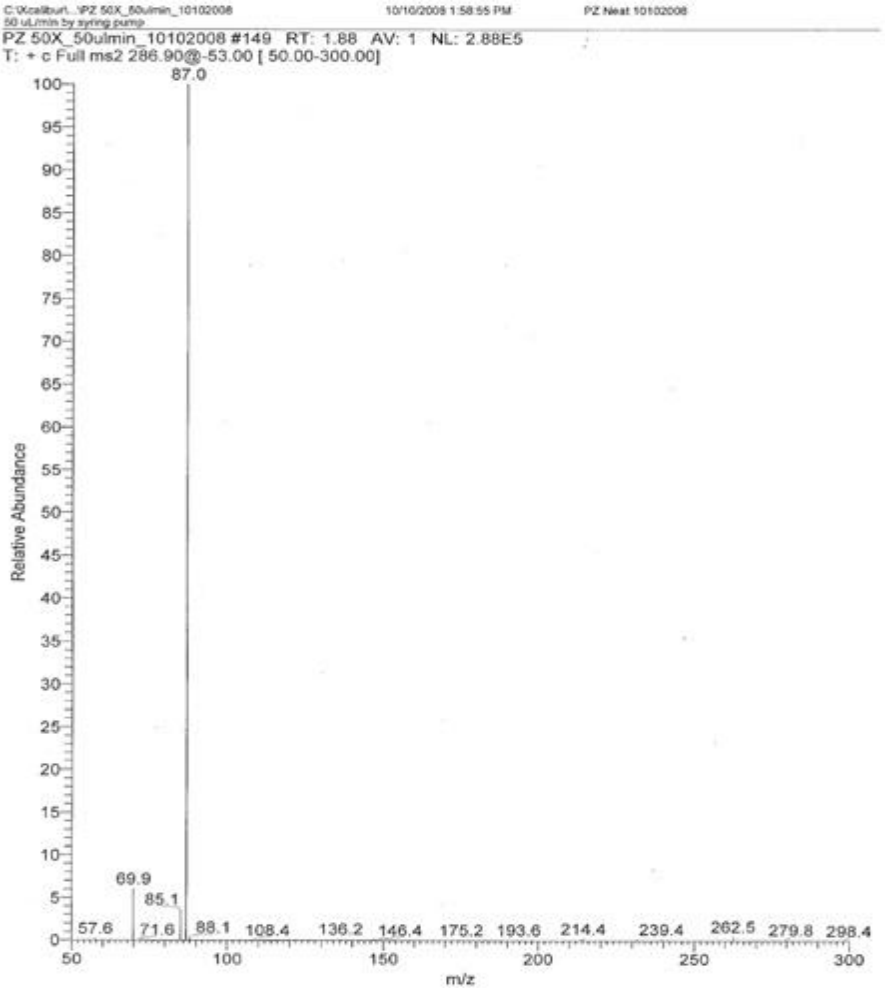

Figure C.47: Mass spectrum of 8m PZ, α =0.3.

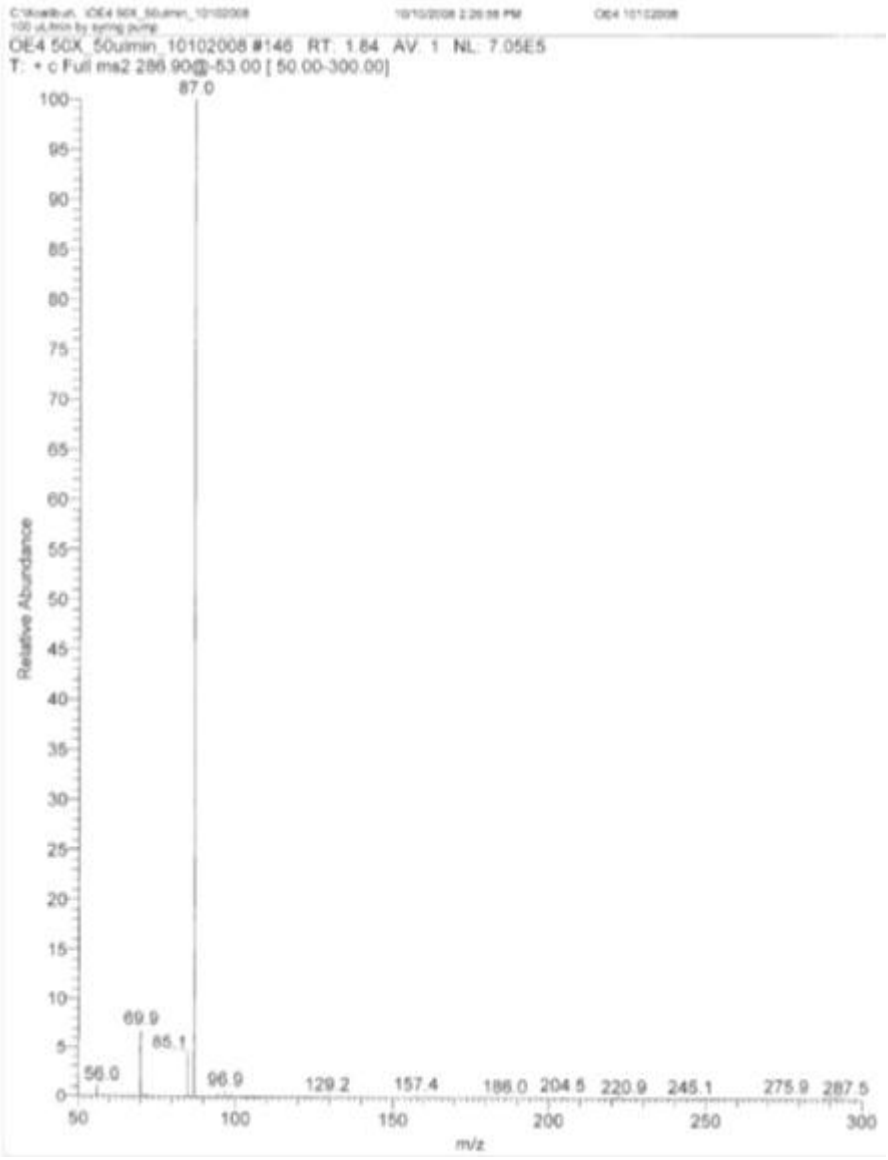

Figure C.48: Mass spectrum of oxidized PZ solution(OE4, 8m PZ, α =0.3, 5.0 mM Cu^{2+}, 0.1 mM Fe^{2+}, 100 mM "A", degraded at 55°C for ~4 weeks).

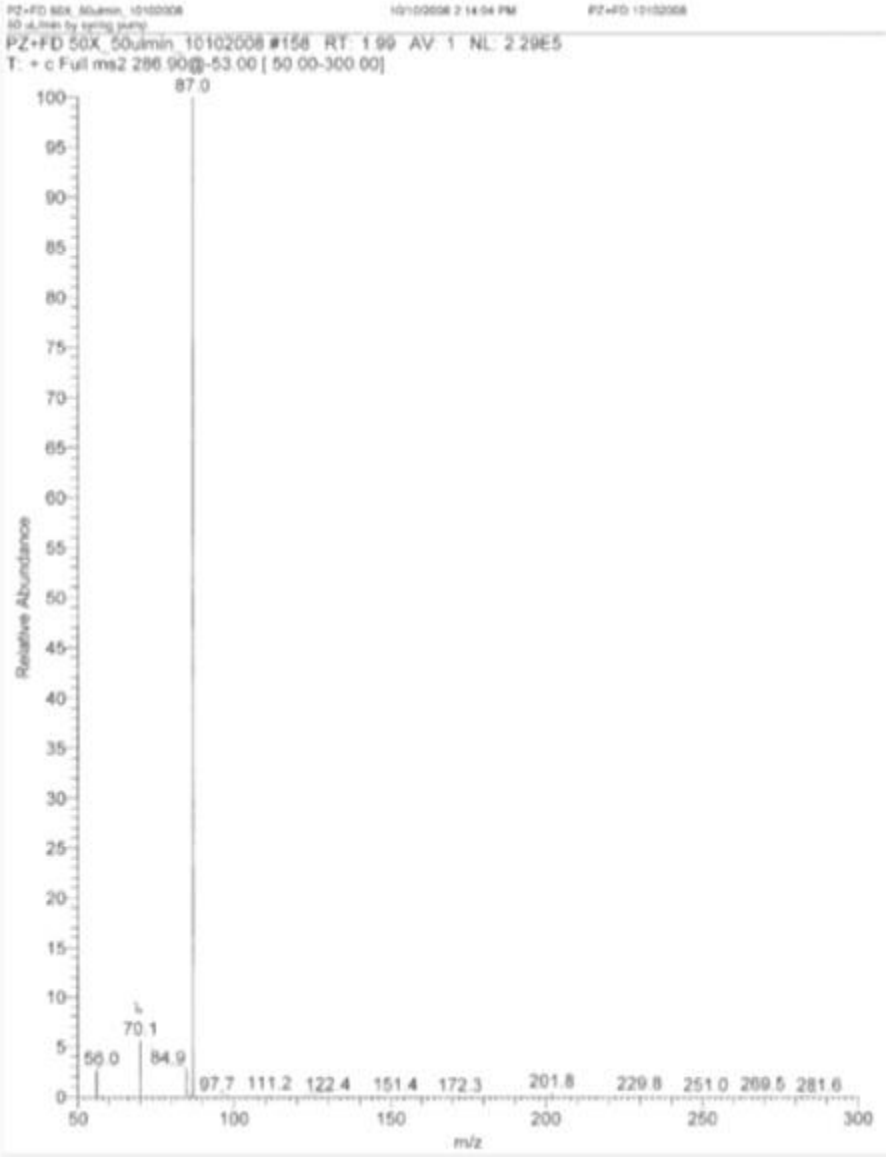

Figure C.49: Mass spectrum of 8m PZ, α =0.3, [HCHO]=270 mM

Summary

Speciation in formaldehyde-added PZ aqueous solution was studied by ^{1}H, ^{13}C and ^{1}H-^{13}C HSQC NMR analysis as well as mass spectroscopy. Trimer and pentamer, which are produced by condensation reaction between PZ and HCHO, were proposed to be the major new species upon addition of HCHO to PZ. 2.5m PZ degraded with the

presence of 5mM V was found to have similar NMR peaks as seen in HCHO-added PZ, indicating that HCHO could be an important intermediate oxidation product and the cause of increased foaming tendency.

Table C.1: NMR peaks summary for formaldehyde-added PZ and degraded PZ.

PZ Conc.	Loading	[HCHO]	Peak position	Type	Area
(m)	(mol/mol alk.)	(mM)	(ppm)		
2	0	0	2.737	^{1}H	
2	0	0	47.499	^{13}C	
2	0	325	3.408	^{1}H	1.21
			3.404		
			3.367		1.64
			3.334		14.22
			3.063		1.00
			3.036		10.11
			3.009		24.48
			2.880		5.73
			2.871		
			2.866		
			2.860		
			2.857		
			2.810		126.69
			2.800		
			2.791		
			2.776		
			2.736		555.15
			2.696		
			2.607		28.03
			2.597		
			2.587		
			2.576		
			2.493		112.82
			83.445	^{13}C	
			82.837		
			54.304		
			52.912		
			51.418		
			47.462		

			46.239		
2	0	743	3.406	^{1}H	1.00
			3.366		7.52
			3.337		
			3.039		10.36
			3.011		
			2.802		38.89
			2.739		81.83
			2.575		10.92
			2.496		27.07
			83.445	^{13}C	
			82.837		
			54.312		
			52.92		
			51.455		
			47.462		
			46.246		
8	0.3	0	3.472	^{1}H	2.4
			3.464		
			3.455		
			3.301		1.00
			3.010		6.05
			2.919		2.49
			2.910		
			2.902		
			165.129	^{13}C	
			164.664		
			46.53		
			46.253		
			45.303		
			45.07		
8	0.3	367	3.494	^{1}H	9.71
			3.485		
			3.475		
			3.393		1.21
			3.383		
			3.318		4.64
			3.301		
			3.137		1.14
			3.115		
			3.059		23.74
			3.023		

			2.983		10.05
			2.951		
			2.942		
			2.932		
			2.696		2.43
			2.479		1.00
			165.308	^{13}C	
			165.279		
			165.074		
			164.964		
			164.561		
			81.914		
			81.643		
			53.674		
			53.403		
			51.704		
			51.433		
			51.154		
			46.495		
			46.114		
			45.521		
			45.162		
			44.781		
8	0.3	1mM Fe^{2+}, degraded at 55 °C	3.488	^{1}H	2.4
			3.305		1
			3.031		5.71
			2.948		2.73
			165.264	^{13}C	
			164.744		
			46.620		
			46.253		
			45.301		
			44.928		
2.5	0.3	5 mM V, 55°C, 1400 RPM	8.459	^{1}H	1
			8.052		
			8.002		1.51
			5.502		5.87
			5.491		
			5.48		
			5.343		
			4.239		
			4.228		

			4.225		
			4.218		
			4.174		
			4.104		
			4.027		
			3.925		
			3.9		
			3.874		
			3.863		
			3.852		
			3.769		
			3.439		113.6
			3.428		
			3.418		
			3.398		
			3.303		17.13
			3.252		
			3.238		82.37
			3.227		
			3.215		
			3.203		
			3.134		
			3.061		47.23
			2.998		912.89
			2.962		
			2.95		
			2.935		178.75
			2.923		
			2.908		
			2.875		119.8
			2.864		
			2.854		
			2.483		12.13
			2.117		
			1.31		
			1.296		
			1.245		
			1.231		
			176.658	^{13}C	
			172.207		
			171.378		
			170.521		

			164.472		
			164.373		
			164.258		
			163.08		
			162.977		
			162.632		
			50.113		
			47.721		
			47.499		
			46.603		
			45.786		
			45.08		
			44.639		
			44.267		
			43.997		
			43.743		
			43.323		
			42.676		
			42.517		
			41.78		
			41.526		
			40.657		
			40.248		
			39.622		

Appendix D: Density and Viscosity Data

The following tables give the detailed density and viscosity data for 8 m 2MPZ and 4 m 2MPZ / 4 m PZ shown in Chapter 8. Both the measured value and the prediction from the empirical models (Eq. (8.1) and Eq. (8.2)) are tabulated. The viscosity of some other amines are also given.

Table D.1: Density data for 8 m 2MPZ.

Temp. (°C)	CO_2 loading (mol CO_2/mol alkalinity)	$\rho_{measured}$ (kg/m^3)	$\rho_{predicted}$ (kg/m^3)	Dev. (%)
20	0.00	1023.9	1016.2	-0.8%
	0.10	1057.9	1051.3	-0.6%
	0.15	1073.4	1067.5	-0.6%
	0.20	1089.5	1083.9	-0.5%
	0.25	1103.4	1098.6	-0.4%
	0.30	1117.6	1113.3	-0.4%
	0.35	1130.5	1127.3	-0.3%
	0.40	1143.0	1141.0	-0.2%
40	0.00	1008.3	1010.1	0.2%
	0.10	1044.3	1045.0	0.1%
	0.15	1060.5	1061.0	0.1%
	0.20	1077.2	1077.4	0.0%
	0.25	1091.7	1092.0	0.0%
	0.30	1106.6	1106.6	0.0%
	0.35	1119.7	1120.5	0.1%
	0.40	1132.4	1134.2	0.2%
60	0.00	992.3	1000.9	0.9%
	0.10	1030.0	1035.5	0.5%
	0.15	1046.9	1051.4	0.4%
	0.20	1064.5	1067.6	0.3%
	0.25	1079.6	1082.1	0.2%
	0.30	1094.8	1096.6	0.2%
	0.35	1108.3	1110.3	0.2%
	0.40	1118.6	1123.9	0.5%

Table D.2: Viscosity data for 8 m 2MPZ

Temp. (°C)	CO_2 loading (mol CO_2/mol alkalinity)	$\eta_{measured}$ (cP)	$\eta_{predicted}$ (cP)	Dev. (%)
40	0.00	8.6	8.3	-3.6%
	0.10	11.1	11.6	4.6%
	0.15	14.5	13.6	-5.7%
	0.20	16.2	16.3	0.7%
	0.25	18.3	19.3	5.4%
	0.30	22.2	23.0	3.2%
	0.35	28.8	27.2	-5.6%
	0.40	31.7	32.4	2.3%
50	0.00	5.3	5.6	4.8%
	0.10	7.4	8.0	8.0%
	0.15	10.0	9.4	-5.8%
	0.20	11.7	11.3	-3.0%
	0.25	14.1	13.4	-5.0%
	0.30	16.2	15.9	-1.9%
	0.35	18.1	18.9	4.2%
	0.40	22.8	22.4	-1.7%
60	0.00	4.1	3.9	-4.7%
	0.10	5.2	5.6	7.8%
	0.15	6.9	6.7	-3.1%
	0.20	8.3	8.1	-2.4%
	0.25	10.1	9.6	-4.8%
	0.30	10.7	11.4	7.0%
	0.35	12.6	13.5	7.1%
	0.40	16.7	15.9	-5.0%

Table D.3: Density data for 4 m 2MPZ / 4 m PZ.

Temp. (°C)	CO_2 loading (mol CO_2/mol alkalinity)	$\rho_{measured}$ (kg/m^3)	$\rho_{predicted}$ (kg/m^3)	Dev. (%)
20	0.15	1078.2	1075.3	-0.3%
	0.18	1093.8	1085.0	-0.8%
	0.25	1108.8	1107.0	-0.2%
	0.30	1122.7	1122.0	-0.1%
	0.34	1136.7	1133.6	-0.3%
	0.39	1150.6	1147.6	-0.3%
40	0.15	1065.1	1068.8	0.3%
	0.18	1081.7	1078.5	-0.3%
	0.25	1097.4	1100.3	0.3%
	0.30	1111.9	1115.2	0.3%
	0.34	1126.5	1126.8	0.0%
	0.39	1140.8	1140.8	0.0%
60	0.15	1053.1	1059.1	0.6%
	0.18	1070.3	1068.7	-0.1%
	0.25	1086.3	1090.3	0.4%
	0.30	1101.2	1105.1	0.4%
	0.34	1116	1116.5	0.0%
	0.39	1130.3	1130.4	0.0%

Table D.4: Viscosity data for 4 m 2MPZ / 4 m PZ

Temp. (°C)	CO_2 loading (mol CO_2/mol alkalinity)	$\eta_{measured}$ (cP)	$\eta_{predicted}$ (cP)	Dev. (%)
40	0.04	8.7	8.7	0.9%
	0.08	9.7	9.6	-0.6%
	0.11	10.9	10.5	-4.3%
	0.15	11.8	11.9	1.1%
	0.18	13.1	13.3	1.9%
	0.22	15.9	15.7	-1.5%
	0.24	17.0	17.1	0.8%
	0.28	20.3	20.6	1.5%
	0.3	24.1	22.7	-5.7%
50	0.04	5.9	6.1	2.8%
	0.08	6.7	6.7	0.2%
	0.11	7.6	7.3	-4.2%
	0.15	8.1	8.5	4.3%
	0.18	9.4	9.6	1.7%
	0.22	11.9	11.6	-2.3%
	0.24	12.5	12.8	2.5%
	0.28	15.7	16.0	2.0%
	0.3	16.9	17.9	6.2%
60	0.04	4.3	4.3	1.6%
	0.08	4.8	4.8	-1.4%
	0.11	5.6	5.3	-5.3%
	0.15	6.0	6.2	2.8%
	0.18	7.1	7.1	0.4%
	0.22	9.0	8.8	-2.0%
	0.24	9.4	9.9	5.0%
	0.28	13.1	12.7	-3.4%
	0.3	15.0	14.5	-3.8%

Table D.5: Viscosity data for 5 m PZ / 5 m MDEA

Temp. (°C)	CO_2 loading (mol CO_2/mol alkalinity)	$\eta_{measured}$ (cP)
40	0.18	11.8
	0.23	12.4
	0.28	13.1
	0.33	14.0
	0.37	15.2
60	0.18	6.5

	0.23	6.7
	0.28	7.1
	0.33	7.7
	0.37	8.3

Table D.6: Viscosity data for 12 m EDA at 40°C

Temp. (°C)	**CO_2 loading (mol CO_2/mol alkalinity)**	**$\eta_{measured}$ (cP)**
40	0.10	4.6
	0.22	6.5
	0.29	8.4
	0.36	9.6
	0.43	12.7
	0.49	14.2

Table D.7: Viscosity data for 10 m DGA® at 40°C

Temp. (°C)	**CO_2 loading (mol CO_2/mol alkalinity)**	**$\eta_{measured}$ (cP)**
40	0.21	5.9
	0.31	6.8
	0.40	8.3
	0.49	8.8

Table D.8: Viscosity data for 4.8 m AMP at 40°C

Temp. (°C)	**CO_2 loading (mol CO_2/mol alkalinity)**	**$\eta_{measured}$ (cP)**
40	0.15	2.7
	0.29	3.1
	0.45	3.6
	0.56	4.1

Appendix E: Fortran Subroutines

The Fortran subroutines used with the Aspen Plus® model in this work are shown below. These Fortran codes were originally developed from the templates provided by AspenTech and modified by the Rochelle's research group in the University of Texas at Austin. They were further adapted for the needs in this work.

E.1 MASS TRANSFER COEFFICIENT

```
      SUBROUTINE USRMTRFC (KSTG,    NCOMPS, IDX,      NBOPST, KPDIAG,
     1                     XCOMPB, FRATEL, YCOMPB, FRATEV, PRESS,
     2                     TLIQ,    TVAP,    AVMWLI, AVMWVA, VISCML,
     3                     DENMXL, SIGMAL, VISCMV, DENMXV, AREAIF,
     4                     PREK,    EXPKD,   COLTYP, USRCOR, TWRARA,
     5                     COLDIA, HTPACK, PACSIZ, SPAREA, CSIGMA,
     6                     PFACT,   PKPRMS, VOIDFR, IPAKAR, IPTYPE,
     7                     IVENDR, IPMAT,   IPSIZE, WEIRHT, DCAREA,
     8                     ARAACT, FLOPTH, NPASS,   WEIRL,   IFMETH,
     9                     SYSFAC, HOLEAR, ITTYPE, TRASPC, PITCH,
     A                     IPHASE, NINT,    INT,     NREAL,   REAL)
      IMPLICIT NONE
      INTEGER KSTG, NCOMPS, IDX(NCOMPS), NBOPST(6), KPDIAG,
     +          COLTYP, USRCOR, IPAKAR, IPTYPE, IVENDR, IPMAT,   IPSIZE,
     +          NPASS, IFMETH, ITTYPE, NINT, INT(NINT), IPHASE, NREAL
      REAL*8   XCOMPB(NCOMPS), FRATEL, YCOMPB(NCOMPS), FRATEV,
     +          PRESS, TLIQ, TVAP, AVMWLI, AVMWVA, VISCML, DENMXL,
     +          SIGMAL, VISCMV, DENMXV, AREAIF, PREK, EXPKD,
     +          TWRARA, COLDIA, HTPACK, PACSIZ, SPAREA, CSIGMA,
     +          PFACT,   PKPRMS(20), VOIDFR, WEIRHT, DCAREA, ARAACT,
     +          FLOPTH, WEIRL, SYSFAC, HOLEAR, TRASPC, PITCH,
     +          REAL(NREAL)
C***********************************************************************
C   LICENSED MATERIAL.   PROPERTY OF ASPEN TECHNOLOGY, INC.   TO BE        *
C   TREATED AS ASPEN TECH PROPRIETARY INFORMATION UNDER THE TERMS          *
C   OF THE ASPEN PLUS SUBSCRIPTION AGREEMENT.                              *
C***********************************************************************
C-----------------------------------------------------------------------
C            COPYRIGHT (C) 2004
C             ASPEN TECHNOLOGY, INC.
C             CAMBRIDGE, MA
C-----------------------------------------------------------------------
C
C       DESCRIPTION: User provided RateSep routine to calculate the
C                    liquid (IPHASE=0) and vapor (IPHASE=1) binary mass
C                    transfer coefficient parameters (PREK, EXPKD).
C
C       VARIABLES IN ARGUMENT LIST
C
C       VARIABLE I/O   TYPE    DIMENSION    DESCRIPTION AND RANGE
C       -------- ---   ----    ---------    ---------------------------------
```

```
C     KSTG       I    I          -         SEGMENT NUMBER
C     NCOMPS     I    I          -         NUMBER OF COMPONENTS
C     IDX        I    I       NCOMPS       COMPONENT INDEX VECTOR
C     NBOPST     I    I          6         PHYSICAL PROPERTY OPTION
C                                          SET BEAD POINTER
C     KPDIAG     I    I          -         PHYSICAL PROPERTY
C                                          DIAGOSTIC CODE
C     XCOMPB     I    R       NCOMPS       BULK LIQUID MOLE FRACTION
C     FRATEL     I    R          -         FLOW OF LIQUID (KMOL/SEC)
C     YCOMPB     I    R       NCOMPS       BULK VAPOR MOLE FRACTION
C     FRATEV     I    R          -         FLOW OF VAPOR (KMOL/SEC)
C     PRESS      I    R          -         PRESSURE (N/SQ.M)
C     TLIQ       I    R          -         LIQUID TEMPERATURE (K)
C     TVAP       I    R          -         VAPOR TEMPERATURE (K)
C     AVMWLI     I    R          -         AVERAGE MOLECULAR WEIGHT
C                                          OF LIQUID MIXTURE
C                                          (KG/KMOL)
C     AVMWVA     I    R          -         AVERAGE MOLECULAR WEIGHT
C                                          OF VAPOR MIXTURE (KG/KMOL)
C     VISCML     I    R          -         VISCOSITY OF LIQUID
C                                          (N-SEC/SQ.M)
C     DENMXL     I    R          -         DENSITY OF LIQUID MIXTURE
C                                          (KMOL/CU.M)
C     SIGMAL     I    R          -         SURFACE TENSION OF LIQUID
C                                          (N/M)
C     VISCMV     I    R          -         VISCOSITY OF VAPOR MIXTURE
C                                          (N-SEC/SQ.M)
C     DENMXV     I    R          -         DENSITY OF VAPOR MIXTURE
C                                          (KMOL/CU.M)
C     AREAIF     I    R          -         INTERFACIAL AREA
C                                          (SEE NOTE-1 BELOW)
C     PREK       O    R          -         BINARY MASS TRANSFER =
C     EXPRKD     O    R          -              PREK*DIFFUSIVITY**EXPKD
C                                          (SEE NOTE-2 BELOW)
C     COLTYP     I    I          -         TYPE OF COLUMN
C                                          1 = PACKED
C                                          2 = TRAY
C     USRCOR     I    I          -         CALCULATION METHOD (I.E.
C                                          CHOICE OF USER CORRELATION)
C                                            1   = USER1
C                                            2   = USER2
C                                            3   = USER3
C                                            4   = USER4
C     TWRARA     I    R          -         CROSS-SECTIONAL AREA OF
C                                          TOWER (SQ.M)
C     COLDIA     I    R          -         COLUMN DIAMETER (M)
C     HTPACK     I    R          -         HEIGHT OF PACKING IN THE
C                                          SEGMENT (M)
C     PACSIZ     I    R          -         SIZE OF PACKING (M)
C     SPAREA     I    R          -         SPECIFIC SURFACE AREA OF
C                                          PACKING (SQ.M/CU.M)
C     CSIGMA     I    R          -         CRITICAL SURFACE TENSION
C                                          OF PACKING MATERIAL (N/M)
C     PFACT      I    R          -         PACKING FACTOR (1/M)
C     PKPRMS     I    R         20         PACKING PARAMETERS
C                                          PKPRMS(1) = STICHLMAIR CONSTANT C1
C                                          PKPRMS(2) = STICHLMAIR CONSTANT C2
C                                          PKPRMS(3) = STICHLMAIR CONSTANT C3
```

```
C                                       PKPRMS(4) = CL IN BILLET 93
C                                       PKPRMS(5) = CV IN BILLET 93
C                                       PKPRMS(6) = B IN BRF 85
C                                       PKPRMS(7) = S IN BRF 85
C                                       PKPRMS(8) = H IN BRF 85
C                                       PKPRMS(9) = Fse IN BRF 92
C                                       PKPRMS(10) = CE IN BRF 92
C                                       PKPRMS(11) = THETA IN BRF 92
C     VOIDFR     I     R          -        VOID FRACTION OF PACKING
C     IPAKAR     I     I          -       PACKING ARRANGEMENT
C                                         1 = RANDOM
C                                         2 = STRUCTURED
C     IPTYPE     I     I          -       PACKING TYPE
C                                       See IPTYPE in packsr.f
C     IVENDR     I     I          -       PACKING VENDOR CODE
C     IPMAT      I     I          -       PACKING MATERIAL CODE
C     IPSIZE     I     I          -       PACKING SIZE CODE
C     WEIRHT     I     R          -       AVERAGE WEIR HEIGHT (M)
C     DCAREA     I     R          -       TOTAL AREA OF DOWNCOMER
C                                       ON TRAY (SQ.M)
C     ARAACT     I     R          -       TOTAL ACTIVE AREA AVAILABLE
C                                       ON TRAY (SQ.M)
C     FLOPTH     I     R          -       AVERAGE FLOWPATH LENGTH (M)
C     NPASS      I     I          -       NUMBER OF TRAY PASSES
C     WEIRL      I     R          -       AVERAGE WEIRH LENGTH (M)
C     IFMETH     I     I          -       FLOODING CALCULATION
C                                       METHOD; REQUIRED FOR SIEVE
C                                       TRAY
C     SYSFAC     I     R          -       SYSTEM FACTOR; REQUIRED FOR
C                                       SIEVE TRAY
C     HOLEAR     I     R          -       HOLE AREA/ACTIVE AREA; REQUIRED
C                                       FOR SIEVE TRAY
C     ITTYPE     I     I          -       TRAY TYPE
C                                         1 - BUBBLE CAPS
C                                         2 - SIEVE
C                                         3 - GLITSCH BALLAST
C                                         4 - KOCH FLEXITRAY
C                                         5 - NUTTER FLOAT VALVE
C     TRASPC     I     R          -       TRAY SPACING (M)
C     PITCH      I     R          -       SIEVE TRAY HOLE PITCH (M)
C     IPHASE     I     I          -       PHASE QUALIFIER
C                                       0 = LIQUID
C                                       1 = VAPOR
C     NINT       I     I          -       Size of INT
C     INT        I/O   I        NINT      User correlation INT array
C     NREAL      I     I          -       Size of REAL
C     REAL       I/O   I       NREAL      User correlation REAL array
C
C    NOTE-1:
C         SPECIFIC INTERFACIAL AREA "AREAIF" HAS THE FOLLOWING UNITS.
C           FOR PACKED COLUMNS, THE UNITS IS "SQ.M/CU.M OF PACKING"
C           FOR TRAY COLUMNS, THE UNITS IS "SQ.M/SQ.M ACTIVE TRAY AREA"
C
C    NOTE-2:
C         BINMTP = PREK * DIFFUSIVITY**EXPKD
C         BINARY MASS TRANSFER COEFFCIENTS "BINMTP" HAVE UNITS (KMOL/SEC)
C         DIFFUSIVITY HAVE UNITS (SQ.M/SEC)
C         BINMTP HAS MOLAR DENSITY AND INTERFACIAL AREA INCLUDED
```

```
C
C***********************************************************************
C       Declare local variables used in the user correlations
C
        REAL*8 RS_BennettHL
        REAL*8 RS_BennettA
        REAL*8 RS_BennettC
        REAL*8 ScLB,    ScVB,    rhoLms, rhoVms, ReLPrm,
     +         dTemp,   uL,      uV,     Fs,     QL,
     +         C,       alphae, hL,      ShLB,   ReV,
     +         vel,     hydia,   qsoln,  w,      dtempa
C
C       Instead of computing BINMTP from diffusivity as in RATEFRAC
C       compute PREK and EXPKD for RateSep
C
        IF (COLTYP .EQ. 1) THEN
C
C**** PACKED COLUMN
c
c       This is the begining of the Dugas Modification
c
          IF (USRCOR .EQ. 9) THEN
C
            IF (IPHASE.EQ.0) THEN
C
C               Liquid phase
C
              qsoln = FRATEL / DENMXL / 10000
C               The factor of 10000 is needed since the simulation has 100x diamter (100x flow).
C
              w = 0.03958407
C               w is the circumfrence of the column in meters.   Diamter of WWC is 0.0126m
C
              dTemp = 3**0.3333 * 2**0.5 / 3.1416**0.5
              dTemp = dTemp * qsoln**.3333*0.091**.5*w**.6667/0.003852
              dTemp = dTemp * (9.81*DENMXL/VISCML*AVMWLI)**.1667
C               The proceeding equation is a simplification of the equaitons in Cullinane's thesis,
c               pages 57-60.   The simplification for theta is used to allow the form Aspen requires.
c               The constants 0.091, 0.003852, and 9.81 refer to the height of the WWC, the area of the
c               WWC and acceleration due to gravity.
c
C               CONVERT K FROM M/S TO KMOL/S
              dTemp = dTemp * TWRARA * HTPACK * AREAIF * DENMXL
C               This is the conversion used in the Onda mass transfer routine

              PREK   = dtemp * 1.0
              EXPKD = 0.5D0
C
            ELSE
C
C               Vapor phase
C
C               From Pacheco's correlation:   R*T*kg*d/DCO2=1.075(Re*Sc*d/h)^0.85
C               Simplified, this gives RTkg=1.075*DCO2^.15*d^.7*(v/h)^.85
C
              vel = FRATEV / TWRARA / DENMXV
              hydia   = 0.0044D0
C               This corresponds to the estimated hydraulic diameter of the WWC, 0.44cm.
```

```
c
                  dTemp = 1.075D0 * hydia ** 0.7D0
                  dTemp = dTemp *(vel / (0.091D0)) ** 0.85D0
C                  The constant, 0.091, corresponds to the height of the WWC.    Aspen has a argument for the
C                  height of a stage but nothing for the # of stages.    Therefore the total height was hardwired.
C
                  dTemp = dTemp * DENMXV * AREAIF * TWRARA * HTPACK
C                  This time the number of stages is not need bc this mass tranfer coeffient is the moles reacted by stage
C                  Note: this correlation results in a MT value (in mol/s) 100 times greater than the calculated excel value
due to 10x diameter.
C
                  PREK = dtemp
                  EXPKD = 0.15D0
C
               END IF
C               END OF IF (IPHASE)
C
            END IF
C           END OF IF (USRCOR)
c
C       This is the end of the Dugas Modification
C
            IF (USRCOR .EQ. 1) THEN
C               user subroutine example for packed column: Onda 68
C
C               Onda, K., Takeuchi, H. and Okumoto, Y., "Mass Transfer
C                 Coefficients between Gas and Liquid Phases in Packed
C                 Columns", J. Chem. Eng. Jap., 1, (1968) P56
C
               IF (IPHASE.EQ.0) THEN
C
C                  Liquid phase
C
                  rhoLms = DENMXL * AVMWLI
                  uL = FRATEL / TWRARA / DENMXL
                  ReLPrm = rhoLms * uL / VISCML / AREAIF
                  dTemp = (rhoLms/9.81D0/VISCML)**(0.33333333D0)
                  dTemp = 0.0051D0 * (ReLPrm**(0.66666667D0))
     +                  *((SPAREA*PACSIZ)**(0.4D0)) / dTemp
C
C                  CONVERT K FROM M/S TO KMOL/S
                  dTemp = dTemp * TWRARA * HTPACK * AREAIF * DENMXL
C
C                  COMPOSITION INDEPENDENT PART OF SCHMIDT NUMBER
                  ScLB = VISCML / rhoLms
C
                  PREK   = dTemp / DSQRT(ScLB)
                  EXPKD = 0.5D0
C
               ELSE
C
C                  Vapor phase
C
                  rhoVms = DENMXV * AVMWVA
                  uV = FRATEV / TWRARA / DENMXV
                  ReV = rhoVms * uV / VISCMV / SPAREA
                  dTemp = SPAREA*PACSIZ
                  dTemp = dTemp * dTemp
```

```
                  IF (PACSIZ .GE. 0.015D0) THEN
                     dTemp = 5.23D0 / dTemp
                  ELSE
                     dTemp = 2.0D0 / dTemp
                  END IF
               dTemp = dTemp * (ReV**(0.7D0)) * SPAREA
C
C               CONVERT K FROM M/S TO KMOL/S
               dTemp = dTemp * TWRARA * HTPACK * AREAIF * DENMXV
C
C               COMPOSITION INDEPENDENT PART OF SCHMIDT NUMBER
               ScVB = VISCMV / rhoVms
C
               PREK = dTemp * ScVB ** 0.33333333D0
               EXPKD = 0.66666667D0
            END IF
C            END OF IF (IPHASE)
C
         END IF
C         END OF IF (USRCOR)
C
      ELSE IF (COLTYP .EQ. 2) THEN
C
C**** TRAY COLUMN
C
         IF (USRCOR .EQ. 1) THEN
C            user subroutine example for tray column: AIChE 58
C
C            AIChE, Bubble Tray Design Manual: Prediction of Fractionation
C              Efficiency, New York, 1958
C
C            For bubble cap, valve, and sieve trays
C
            IF (IPHASE.EQ.0) THEN
C
C               Liquid phase
C
               rhoVms = DENMXV * AVMWVA
               rhoLms = DENMXL * AVMWLI
               uV = FRATEV /DENMXV /ARAACT
               Fs = uV * DSQRT(rhoVms)
               C = 0.5D0 + 0.438D0 * DEXP(-137.8 * WEIRHT)
               QL = FRATEL/DENMXL
               ALPHAE = DEXP(-12.55D0*(uV*DSQRT(RHOVMS/DABS(RHOLMS-
     1                    RHOVMS)))**0.91D0)
               hL =ALPHAE*(WEIRHT + C*(QL/WEIRL/ALPHAE)**0.67D0)
               dTemp = 19700.0D0 *(0.4D0*Fs+0.17D0) * hL
     +                    * ARAACT * DENMXL
C
               PREK = dTemp
               EXPKD = 0.5D0
C
            ELSE
C
C               Vapor phase
C
               rhoVms = DENMXV * AVMWVA
               uV = FRATEV /DENMXV /ARAACT
```

```
                Fs = uV * DSQRT(rhoVms)
                QL = FRATEL/DENMXL
                dTemp = 0.776 + 4.57*WEIRHT - 0.238*Fs
     +                  + 104.8*QL/WEIRL
                dTemp = dTemp * uV * ARAACT * DENMXV
C
C                COMPOSITION INDEPENDENT PART OF SCHMIDT NUMBER
                ScVB = VISCMV / rhoVms
C
                PREK = dTemp /DSQRT(ScVB)
                EXPKD = 0.5D0
              END IF
C              END OF IF (IPHASE)
C
            END IF
C           END OF IF (USRCOR)
C
             END IF
C         END OF IF (COLTYP)
C
          RETURN
          END
```

E.2 AREA/VOLUME IN THE WWC MODEL

```
      SUBROUTINE AREA     (KSTG,    NCOMPS, IDX,      NBOPST, KPDIAG,
     1                     XCOMPB, FRATEL, YCOMPB, FRATEV, PRESS,
     2                     TLIQ,    TVAP,    AVMWLI, AVMWVA, VISCML,
     3                     DENMXL, SIGMAL, VISCMV, DENMXV, AREAIF,
     4                     COLTYP, USRCOR, TWRARA, COLDIA, HTPACK,
     5                     PACSIZ, SPAREA, CSIGMA, PFACT,   PKPRMS,
     6                     VOIDFR, IPAKAR, IPTYPE, IVENDR, IPMAT,
     7                     IPSIZE, WEIRHT, DCAREA, ARAACT, FLOPTH,
     8                     NPASS,   WEIRL,   IFMETH, SYSFAC, HOLEAR,
     9                     ITTYPE, TRASPC, PITCH,   NINT,    INT,
     A                      NREAL,   REAL)
      IMPLICIT NONE
      INTEGER KSTG, NCOMPS, IDX(NCOMPS), NBOPST(6), KPDIAG,
     +          COLTYP, USRCOR, IPAKAR, IPTYPE, IVENDR, IPMAT,   IPSIZE,
     +          NPASS, IFMETH, ITTYPE, NINT, INT(NINT), NREAL
      REAL*8   XCOMPB(NCOMPS), FRATEL, YCOMPB(NCOMPS), FRATEV,
     +          PRESS, TLIQ, TVAP, AVMWLI, AVMWVA, VISCML, DENMXL,
     +          SIGMAL, VISCMV, DENMXV, AREAIF, TWRARA, COLDIA,
     +          HTPACK, PACSIZ, SPAREA, CSIGMA, PFACT, PKPRMS(20),
     +          VOIDFR, WEIRHT, DCAREA, ARAACT, FLOPTH, WEIRL,
     +          SYSFAC, HOLEAR, TRASPC, PITCH, REAL(NREAL)
C***********************************************************************
C  LICENSED MATERIAL.   PROPERTY OF ASPEN TECHNOLOGY, INC.   TO BE        *
C  TREATED AS ASPEN TECH PROPRIETARY INFORMATION UNDER THE TERMS        *
C  OF THE ASPEN PLUS SUBSCRIPTION AGREEMENT.                                *
C***********************************************************************
C-----------------------------------------------------------------------
C           COPYRIGHT (C) 2004
C            ASPEN TECHNOLOGY, INC.
C            CAMBRIDGE, MA
C-----------------------------------------------------------------------
C
C      DESCRIPTION: User provided RateSep routine to calculate the
C                   specific interface area AREAIF (see NOTE-1).
C
C      VARIABLES IN ARGUMENT LIST
C
C      VARIABLE I/O   TYPE    DIMENSION    DESCRIPTION AND RANGE
C      -------- ---   ----    ---------    ---------------------------------
C      KSTG       I     I          -         SEGMENT NUMBER
C      NCOMPS     I     I          -         NUMBER OF COMPONENTS
C      IDX        I     I        NCOMPS      COMPONENT INDEX VECTOR
C      NBOPST     I     I          6         PHYSICAL PROPERTY OPTION
C                                           SET BEAD POINTER
C      KPDIAG     I     I          -         PHYSICAL PROPERTY
C                                           DIAGOSTIC CODE
C      XCOMPB     I     R        NCOMPS      BULK LIQUID MOLE FRACTION
C      FRATEL     I     R          -         FLOW OF LIQUID (KMOL/SEC)
C      YCOMPB     I     R        NCOMPS      BULK VAPOR MOLE FRACTION
C      FRATEV     I     R          -         FLOW OF VAPOR (KMOL/SEC)
C      PRESS      I     R          -         PRESSURE (N/SQ.M)
C      TLIQ       I     R          -         LIQUID TEMPERATURE (K)
C      TVAP       I     R          -         VAPOR TEMPERATURE (K)
C      AVMWLI     I     R          -         AVERAGE MOLECULAR WEIGHT
C                                           OF LIQUID MIXTURE
C                                           (KG/KMOL)
```

```
C     AVMWVA    I    R          -        AVERAGE MOLECULAR WEIGHT
C                                      OF VAPOR MIXTURE (KG/KMOL)
C     VISCML    I    R          -       VISCOSITY OF LIQUID
C                                      (N-SEC/SQ.M)
C     DENMXL    I    R          -       DENSITY OF LIQUID MIXTURE
C                                      (KMOL/CU.M)
C     SIGMAL    I    R          -       SURFACE TENSION OF LIQUID
C                                      (N/M)
C     VISCMV    I    R          -       VISCOSITY OF VAPOR MIXTURE
C                                      (N-SEC/SQ.M)
C     DENMXV    I    R          -       DENSITY OF VAPOR MIXTURE
C                                      (KMOL/CU.M)
C     AREAIF    O    R          -       INTERFACIAL AREA
C                                      (SEE NOTE-1 BELOW)
C     COLTYP    I    I          -       TYPE OF COLUMN
C                                      1 = PACKED
C                                      2 = TRAY
C     USRCOR    I    I          -       CALCULATION METHOD (I.E.
C                                      CHOICE OF USER CORRELATION)
C                                        1 = USER1
C                                        2 = USER2
C                                        3 = USER3
C                                        4 = USER4
C     TWRARA    I    R          -       CROSS-SECTIONAL AREA OF
C                                      TOWER (SQ.M)
C     COLDIA    I    R          -       COLUMN DIAMETER (M)
C     HTPACK    I    R          -       HEIGHT OF PACKING IN THE
C                                      SEGMENT (M)
C     PACSIZ    I    R          -       SIZE OF PACKING (M)
C     SPAREA    I    R          -       SPECIFIC SURFACE AREA OF
C                                      PACKING (SQ.M/CU.M)
C     CSIGMA    I    R          -       CRITICAL SURFACE TENSION
C                                      OF PACKING MATERIAL (N/M)
C     PFACT     I    R          -       PACKING FACTOR (1/M)
C     PKPRMS    I    R          20      PACKING PARAMETERS
C                                      PKPRMS(1) = STICHLMAIR CONSTANT C1
C                                      PKPRMS(2) = STICHLMAIR CONSTANT C2
C                                      PKPRMS(3) = STICHLMAIR CONSTANT C3
C                                      PKPRMS(4) = CL IN BILLET 93
C                                      PKPRMS(5) = CV IN BILLET 93
C                                      PKPRMS(6) = B IN BRF 85
C                                      PKPRMS(7) = S IN BRF 85
C                                      PKPRMS(8) = H IN BRF 85
C                                      PKPRMS(9) = Fse IN BRF 92
C                                      PKPRMS(10) = CE IN BRF 92
C                                      PKPRMS(11) = THETA IN BRF 92
C     VOIDFR    I    R          -       VOID FRACTION OF PACKING
C     IPAKAR    I    I          -       PACKING ARRANGEMENT
C                                        1 = RANDOM
C                                        2 = STRUCTURED
C     IPTYPE    I    I          -       PACKING TYPE
C                                      See IPTYPE in packsr.f
C     IVENDR    I    I          -       PACKING VENDOR CODE
C     IPMAT     I    I          -       PACKING MATERIAL CODE
C     IPSIZE    I    I          -       PACKING SIZE CODE
C     WEIRHT    I    R          -       AVERAGE WEIR HEIGHT (M)
C     DCAREA    I    R          -       TOTAL AREA OF DOWNCOMER
C                                      ON TRAY (SQ.M)
```

```
C       ARAACT     I     R          -        TOTAL ACTIVE AREA AVAILABLE
C                                          ON TRAY (SQ.M)
C       FLOPTH     I     R          -        AVERAGE FLOWPATH LENGTH (M)
C       NPASS      I     I          -        NUMBER OF TRAY PASSES
C       WEIRL      I     R          -        AVERAGE WEIRH LENGTH (M)
C       IFMETH     I     I          -        FLOODING CALCULATION
C                                          METHOD; REQUIRED FOR SIEVE
C                                          TRAY
C       SYSFAC     I     R          -        SYSTEM FACTOR; REQUIRED FOR
C                                          SIEVE TRAY
C       HOLEAR     I     R          -        HOLE AREA/ACTIVE AREA; REQUIRED
C                                          FOR SIEVE TRAY
C       ITTYPE     I     I          -        TRAY TYPE
C                                           1 - BUBBLE CAPS
C                                           2 - SIEVE
C                                           3 - GLITSCH BALLAST
C                                           4 - KOCH FLEXITRAY
C                                           5 - NUTTER FLOAT VALVE
C       TRASPC     I     R          -        TRAY SPACING (M)
C       PITCH      I     R          -        SIEVE TRAY HOLE PITCH (M)
C       NINT       I     I          -        Size of INT
C       INT        I/O   I          NINT     User correlation INT array
C       NREAL      I     I          -        Size of REAL
C       REAL       I/O   I          NREAL    User correlation REAL array
C
C       NOTE-1:
C            SPECIFIC INTERFACIAL AREA "AREAIF" HAS THE FOLLOWING UNITS.
C             FOR PACKED COLUMNS, THE UNITS IS "SQ.M/CU.M OF PACKING"
C             FOR TRAY COLUMNS, THE UNITS IS "SQ.M/SQ.M ACTIVE TRAY AREA"
C
C***********************************************************************
C       Declare local variables used in the user correlations
C
      REAL*8 WeL,    dTemp,   uV,      rhoVms,
     +       uL,     rhoLms, ReL,    FrL,     uL2,
     +       ReV,    d,      Wprime,
     +       AREAE, At, hp, Ft, Fse, ap,
     +       S, cosg, pi, theta
C
C       Compute specific interface area as described above
C       Check COLTYP/USRCOR if providing multiple area correlations
C
      IF (COLTYP .EQ. 1) THEN
C
C**** PACKED COLUMN
C
         IF (USRCOR .EQ. 1) THEN
C            user subroutine example for packed column: Onda 68
C
C            Onda, K., Takeuchi, H. and Okumoto, Y., "Mass Transfer
C              Coefficients between Gas and Liquid Phases in Packed
C              Columns", J. Chem. Eng. Jap., 1, (1968) p. 56
C
             rhoLms = DENMXL * AVMWLI
             uL = FRATEL / TWRARA / DENMXL
             uL2 = uL * uL
             ReL = rhoLms * uL / VISCML / SPAREA
             FrL = SPAREA * uL2 / 9.81D0
```

```
C            WHERE 9.81D0 IS GRAVITY CONSTANT IN M/S**2
             WeL      = rhoLms * uL2 / SIGMAL / SPAREA
             dTemp = -1.45D0*((CSIGMA/SIGMAL)**0.75D0)
     +                     *(ReL**0.1D0)*(FrL**(-0.05D0))
     +                     *(WeL**0.2D0)
             dTemp = 1.D0 - DEXP(dTemp)

             AREAIF = SPAREA*dTemp

C            Uses specific area of the packing for both random and structured

           ELSEIF (USRCOR .EQ. 2) THEN

             AREAIF = SPAREA   !(sq.m/cu.m)

C            Uses the Rocha-Bravo-Fair (1992) Model as defined in Aspen Plus

           ELSEIF (USRCOR .EQ. 3) THEN

             IF (SIGMAL .GE. 0.055) THEN
                cosg = 5.211*(10**(-16.835 * SIGMAL))
             ELSE
                cosg = 0.9
             END IF

             pi       = 3.141592654
             theta    = PKPRMS(11)*pi/180

             rhoLms   = DENMXL * AVMWLI
             uL       = FRATEL / TWRARA / DENMXL
             uL2      = uL * uL
             S        = PKPRMS(7)

             WeL      = uL2 * rhoLms * S / SIGMAL
             FrL      = uL2 / (S * 9.81D0)
             ReL      = uL * S * rhoLms / VISCML
             Ft       = (29.12*((WeL*FrL)**0.15)*(S**0.359))/(ReL**0.2)
     +                        /(VOIDFR**0.6)/(dsin(theta)**0.3)
     +                        /(1-(0.93*cosg))


             Fse      = PKPRMS(9) !Surface enhancement factor
             ap       = SPAREA   !Specific area of packing
C            At       = TWRARA   (cross sectional area of column)
C            hp       = HTPACK   (height of packing)

             AREAIF   = Ft*Fse*ap

             IF (IPSIZE .eq. 606 .AND. IPTYPE .eq. 701) THEN
                AREAIF = AREAIF*1.147643+172.01
             ELSE
                AREAIF = AREAIF
             END IF

C            AREAIF = dsin(PKPRMS(11)*Pi)
C            WRITE (*,*) denmxl, avmwli, fratel, twrara, S

           Elseif (USRCOR .EQ. 9) THEN
```

```
            AREAIF = 325.78D0

c           Actual wetted are of the WWC is 38.52cm2.
c           Column diamter is listed as 0.128655m (a factor of 10 bigger than the area which matches gas flow area) and
height as 9.1cm.
c           This gives a surface area of 325.444m2/m3 for the Aspen Simulations.

            END IF
C           END OF IF (USRCOR)
C
         ELSE IF (COLTYP .EQ. 2) THEN
C
C**** TRAY COLUMN
C
            IF (USRCOR .EQ. 1) THEN
C              user subroutine example for tray column: Scheffe-Weiland 87
C
C              Scheffe, R.D. and Weiland, R.H., "Mass Transfer
C              Characteristics of Valve Trays." Ind. Eng. Chem. Res.
C              26, (1987) p. 228
C
C              The original paper only mentioned valve tray.
C              It is also used for bubble-cap tray and sieve tray.
C
C              CHARACTERISTIC LENGTH IS ALWAYS 1 METER.
               d = 1.0D0
               rhoLms = DENMXL * AVMWLI
               rhoVms = DENMXV * AVMWVA
               uL = FRATEL / TWRARA / DENMXL
               uV = FRATEV / TWRARA / DENMXV
               ReL = rhoLms * uL * d / VISCML
               ReV = rhoVms * uV * d / VISCMV
               Wprime = WEIRHT / d
               AREAIF = 0.27D0 * ReV**0.375D0 * ReL**0.247D0
               AREAIF = AREAIF * Wprime**0.515
            END IF
C           END OF IF (USRCOR)
C
            END IF
C        END OF IF (COLTYP)
C
         RETURN
         END
```

E.3 DENSITY

```
C Log keyword added
C
C$ #1 BY: PING LI 14-MAY-2004 USER ROUTINE FOR MIXTURE PROPERTIES USING
C$                                MIXING RULE
C ========================cvs revision history=======================
      SUBROUTINE VL2U2 (T, P, X, N, IDX, XMW, SG, VLSTD, VL2U2A,
     *                  VI, DVI, DPVI, KSW, KOP, NDS, KDIAG,
     *                  VMX, DVMX, DPVMX, KER )
C***********************************************************************
C     Template for VL2U2 routine for mixture liquid molar volume
C     and its temperature, pressure derivatives
C
C     VMX is the calculated liquid mixture molar volume (output)
C
C     DVMX is the temperature derivative of VMX (output)
C
C     DPVMX is the pressure derivative of VMX (output)
C
C     All input and output in this user routine are in SI Units
C      with Gas constant = 8314.33
C
C***********************************************************************
C     ARGUMENT LIST VARIABLES:
C
C        VARIABLE I/O TYPE-SPEC DIMENSION      DESCRIPTION AND RANGE
C
C         T          I   REAL*8              OPERATING TEMPERATURE
C         P          I   REAL*8              OPERATING PRESSURE
C         Z          I   REAL*8     N        COMPONENT MOLE FRACTION VECTOR
C         N          I   INTEGER             NUMBER OF COMPONENTS IN MIXTURE
C         IDX        I   INTEGER    N        VECTOR OF COMPONENT POINTERS
C         XMW        I   REAL*8     NCC      MOLECULAR WEIGHT FOR EACH COMPONENT
C         SG         I   REAL*8     NCC      SPECIFIC GRAVITY FOR EACH COMPONENT
C         VLSTD      I   REAL*8     NCC      STD. LIQUID VOLUME FOR EACH COMPONENT
C         VL2U2A     I   REAL*8     5,NCC    USER DEFIND PARAMETER FOR THIS MODEL
C         VI         I   REAL*8     N        PURE LIQUID MOLAR VOLUME
C         DVI        I   REAL*8     N        TEMPERATURE DERIVATIVE OF VI
C         DPVI       I   REAL*8     N        PRESSURE DERIVATIVE OF VI
C         KSW        I   INTEGER    3        CALCULATION CODE
C                                            KSW(1) FOR PROPERTY
C                                            KSW(2) FOR TEMP. DERIVATIVE
C                                            KSW(3) FOR PRES. DERIVATIVE
C                                            VALUE = 1: CALCULATE
C                                            VALUE = 0: DO NOT CALCULATE
C         KOP        I   INTEGER    10       MODEL OPTION CODE
C         NDS        I   INTEGER             DATA SET NUMBER
C         KDIAG      I   INTEGER             MESSAGE PRINTING CODE
C                                            IF .GE. 2: PRINT ERROR MESSAGES
C                                            IF .GE. 3: PRINT WARNING MSGS.
C         VMX        O   REAL*8              LIQUID MOLAR VOLUME [CUM/KGMOL]
C         DVMX       O   REAL*8              TEMPERATURE DERIVATIVE OF VMX [CUM/KGMOL-K]
C         DPVMX      O   REAL*8              PRESSURE DERIVATIVE OF VMX [CUM/KGMOL-PA]
C         KER        O   INTEGER             ERROR RETURN CODE
C
C***********************************************************************
      IMPLICIT NONE
```

```
#include "dms_global.cmn"
C
C       DECLARE VARIABLES USED IN DIMENSIONING
C
        INTEGER N
C
C       DECLARE ARGUMENTS
C
        INTEGER IDX(N), KSW(3), KOP, NDS, KDIAG, KER
        INTEGER DMS_KCCIDC
        INTEGER IWATER, IPZCOO, ICO2, IPZCOO2, IHPZCOO, IHCO3
        INTEGER IPZH, IPZ, ICO3, IMDEA, IMDEAH
            INTEGER I2MPZ,I2MPZH,I2MPZCOO,IOOC2MPZ
            INTEGER IH2MPZCOO,IOOC2MPZH,I2MPZCOO2
        REAL*8 X(N), T, P, XMW(N), SG(1), VLSTD(1), VL2U2A(5,1),
     .           VI(N), DVI(N), DPVI(N), VMX, DVMX, DPVMX
        REAL*8 WATER, PZCOO, CO2, PZCOO2, HPZCOO, HCO3, PZH, PZ
            REAL*8 MDEA, MDEAH, CO3
CC          COEFFICIENTS FOR PZ
        REAL*8 A1, B1, C1, D1, E1, F1

CC          COEFFICIENTS FOR 2MPZ
            REAL*8 A2, B2, C2, D2, E2, F2

CC          COEFFICIENTS FOR PZ
            REAL*8 A3, B3, C3, D3, E3, F3

            REAL*8 XPZCOO2, X2MPZCOO2
        REAL*8 AA, BB, ML, LDG, RHOX
        REAL*8 PPUTL_AVEMW,MWT,MWH2O
            REAL*8 XPZT,X2MPZT,XCO2T,XH2O,XMDEAT,XAMINE

            REAL*8 VH2O,V2MPZ,VBLEND,VPZ,V2
C
C       DECLARE LOCAL VARIABLES
C
        INTEGER IPROG(2)
C
C         DATA STATEMENTS
C
        DATA IPROG /4HVL2U, 4H2     /
C
C       BEGIN EXECUTABLE CODE
C
C
C          Molar volume calculated from the regressed data using a correlation for PZ
C          5m 7m 8m 9m
C          JORGE M. PLAZA 08/05/09
C
C       VALUES OBTAINED FROM THE DENSITY REGRESSION
C
        INTEGER I
        REAL*8 SUM, DSUM, DPSUM
        SUM = 0D0
        DSUM = 0D0
        DPSUM = 0D0

C
```

```
C       CALCULATE AVERAGE MW
C
        MWT = PPUTL_AVEMW (N, IDX, X)
C
C     INDEX VALUES FOR COMPONENTS IN SIMULATION
C
        IWATER = DMS_KCCIDC('H2O')
        IPZCOO = DMS_KCCIDC('PZCOO-')
        ICO2 = DMS_KCCIDC('CO2')
        IPZCOO2 = DMS_KCCIDC('PZCOO-2')
        IHPZCOO = DMS_KCCIDC('HPZCOO')
        IHCO3   = DMS_KCCIDC('HCO3-')
        IPZH = DMS_KCCIDC('PZH+')
        IPZ = DMS_KCCIDC('PZ')
            ICO3 = DMS_KCCIDC('CO3--')
            IMDEA = DMS_KCCIDC('C5H13-01')
            IMDEAH = DMS_KCCIDC('C5H14-01')

        I2MPZ = DMS_KCCIDC('2MPZ')
        I2MPZCOO = DMS_KCCIDC('2MPZCOO')
        IOOC2MPZ = DMS_KCCIDC('OOC2MPZ')
        I2MPZCOO2 = DMS_KCCIDC('2MPZCOO2')
        IH2MPZCOO = DMS_KCCIDC('H2MPZCOO')
        IOOC2MPZH   = DMS_KCCIDC('OOC2MPZH')
        I2MPZH = DMS_KCCIDC('2MPZH+')

C
        MWH2O = XMW(IWATER)

C       ASSIGNMENT OF INDEX NUMBERS FOR SPECIES PRESENT
C
        DO 50 I = 1, N
        IF (IDX(I). EQ. IWATER) IWATER = I
        IF (IDX(I). EQ. IPZCOO) IPZCOO = I
        IF (IDX(I). EQ. ICO2) ICO2 = I
        IF (IDX(I). EQ. IPZCOO2) IPZCOO2 = I
        IF (IDX(I). EQ. IHPZCOO) IHPZCOO = I
        IF (IDX(I). EQ. IHCO3) IHCO3 = I
        IF (IDX(I). EQ. IPZH) IPZH = I
        IF (IDX(I). EQ. IPZ) IPZ = I
            IF (IDX(I). EQ. ICO3) ICO3 = I
            IF (IDX(I). EQ. IMDEA) IMDEA = I
            IF (IDX(I). EQ. IMDEAH) IMDEAH = I

        IF (IDX(I). EQ. I2MPZ) I2MPZ = I
        IF (IDX(I). EQ. I2MPZCOO2) I2MPZCOO2 = I
        IF (IDX(I). EQ. I2MPZCOO) I2MPZCOO = I
        IF (IDX(I). EQ. IOOC2MPZ) IOOC2MPZ = I
        IF (IDX(I). EQ. IH2MPZCOO) IH2MPZCOO = I
        IF (IDX(I). EQ. IOOC2MPZH) IOOC2MPZH = I
        IF (IDX(I). EQ. I2MPZH) I2MPZH = I

   50 CONTINUE
C
C       MOLAR VOLUME OF WATER
C
        VH2O = VI(IWATER)
C
```

```
C       LOADING CALCULATIONS
C
        XH2O = X(IWATER)
        XPZCOO2                 = 2D0*X(IPZCOO2)
        X2MPZCOO2               = 2D0*X(I2MPZCOO2)
        XCO2T =       X(ICO2)+X(IHCO3)+X(ICO3)
       .                +X(IPZCOO)+X(IHPZCOO)+XPZCOO2
      .+X(I2MPZCOO)+X(IOOC2MPZ)+X(IH2MPZCOO)+X(IOOC2MPZH)+X2MPZCOO2
        XPZT = X(IPZCOO)+X(IPZCOO2)+X(IHPZCOO)+X(IPZH)+X(IPZ)
            XMDEAT = X(IMDEA) + X(IMDEAH)
        X2MPZT=X(I2MPZ)+X(I2MPZH)+X(I2MPZCOO)+X(IOOC2MPZ)+X(IH2MPZCOO)
      .+X(IOOC2MPZH)+X(I2MPZCOO2)
        LDG = XCO2T/2D0/(XPZT + X2MPZT)
C
C       DENSITY CALCULATION
C           PZ
            VPZ=VH2O*MWT/MWH2O/(0.0407*XCO2T/MWT*1D3+0.008*XPZT/MWT*1D3+0.991)
C           2MPZ
            V2MPZ=VH2O*MWT/MWH2O/(0.0407*XCO2T/MWT*1D3+1.018039)



C           2MPZ-PZ BLEND

            VBLEND=VH2O*MWT/MWH2O/(0.040447*XCO2T/MWT*1D3+1.02475)

C         AA = A*XCO2T + B*XAMINE + C*(XCO2T / XAMINE) + D
C         BB = DLOG(AA)
C         RHOX = (E + F*T)*BB
C
            IF (X2MPZT .LE. 1D-10) THEN
                    VMX = VPZ
            ELSE IF (XPZT .LE. 1D-10) THEN
                    VMX = V2MPZ
            ELSE
                    VMX = VBLEND
            END IF

C
C     VMX
        IF (KSW(1) .EQ. 1) VMX = VMX
C     dVMX/dT
        IF (KSW(2) .EQ. 1) DVMX = DSUM
C     dVMX/dP
        IF (KSW(3) .EQ. 1) DPVMX = DPSUM
C
  200 CONTINUE
        RETURN
        END
```

E.4 VISCOSITY

```
C Log keyword added
C
C$ #1 BY: PING LI 14-MAY-2004 USER ROUTINE FOR MIXTURE PROPERTIES USING
C$                                MIXING RULE
C ========================cvs revision history=======================
      SUBROUTINE MUL2U2 (T, P, X, N, IDX, XMW, SG, VLSTD, MULU2A,
     *                   MUI, DMUI, DPMUI, KSW, KOP, NDS, KDIAG,
     *                   MUMX, DMUMX, DPMUMX, KER )
C***********************************************************************
C       Template for MUL2U2 routine for mixture liquid viscosity
C       and its temperature, pressure derivatives
C
C       MUMX is the calculated liquid mixture viscosity (output)
C
C       DMUMX is the temperature derivative of MUMX (output)
C
C       DPMUMX is the pressure derivative of MUMX (output)
C
C       All input and output in this user routine are in SI Units
C        with Gas constant = 8314.33
C
C***********************************************************************
C       ARGUMENT LIST VARIABLES:
C
C          VARIABLE I/O TYPE-SPEC DIMENSION       DESCRIPTION AND RANGE
C
C           T          I    REAL*8               OPERATING TEMPERATURE
C           P          I    REAL*8               OPERATING PRESSURE
C           Z          I    REAL*8     N          COMPONENT MOLE FRACTION VECTOR
C           N          I    INTEGER              NUMBER OF COMPONENTS IN MIXTURE
C           IDX        I    INTEGER    N         VECTOR OF COMPONENT POINTERS
C           XMW        I    REAL*8     NCC       MOLECULAR WEUGHT FOR EACH COMPONENT
C           SG         I    REAL*8     NCC       SPECIFIC GRAVITY FOR EACH COMPONENT
C           VLSTD      I    REAL*8     NCC       STD. LIQUID VOLUME FOR EACH COMPONENT
C           MULU2A     I    REAL*8     5,NCC     USER DEFIND PARAMETER FOR THIS MODEL
C           MUI        I    REAL*8     N         PURE LIQUID VISCOSITY
C           DMUI       I    REAL*8     N          TEMPERATURE DERIVATIVE OF MUI
C           DPMUI      I    REAL*8     N          PRESSURE DERIVATIVE OF MUI
C           KSW        I    INTEGER    3          CALCULATION CODE
C                                        KSW(1) FOR PROPERTY
C                                        KSW(2) FOR TEMP. DERIVATIVE
C                                        KSW(3) FOR PRES. DERIVATIVE
C                                        VALUE = 1: CALCULATE
C                                        VALUE = 0: NO CALCULATION
C           KOP        I    INTEGER              OPTION CODE
C           NDS        I    INTEGER              DATA SET NUMBER
C           KDIAG      I    INTEGER               MESSAGE PRINTING CODE
C                                        IF .GE. 2: PRINT ERROR MESSAGES
C                                        IF .GE. 3: PRINT WARNING MSGS.
C           MUMX       O    REAL*8                LIQUID VISCOSITY
C           DMUMX      O    REAL*8                TEMPERATURE DERIVATIVE OF MUMX
C           DPMUMX     O    REAL*8                PRESSURE DERIVATIVE OF MUMX
C           KER        O    INTEGER              ERROR RETURN CODE
C
C***********************************************************************
      IMPLICIT NONE
```

```
#include "dms_global.cmn"
C
C       DECLARE VARIABLES USED IN DIMENSIONING
C
        INTEGER N
C
C       DECLARE ARGUMENTS
C
        INTEGER IDX(N), KSW(3), KOP, NDS, KDIAG, KER
        INTEGER DMS_KCCIDC
        INTEGER IWATER,
       .                IPZH, IPZ, IPZCOO, IPZCOO2, IHPZCOO,
       .                IMDEA, IMDEAH
            INTEGER ICO2, ICO3, IHCO3
        INTEGER I2MPZ,I2MPZCOO,IOOC2MPZ,IH2MPZCOO,IOOC2MPZH,
       .                I2MPZCOO2,I2MPZH
        REAL*8       X(N), T, P, XMW(N), SG(1), VLSTD(1), MULU2A(5,1),
       .                MUI(N), DMUI(N), DPMUI(N), MUMX, DMUMX, DPMUMX
        REAL*8   WATER, PZ, PZH, PZCOO, PZCOO2, HPZCOO
            REAL*8   CO2, HCO3, CO3, MDEA, MDEAH
        REAL*8   A1, B1, C1, D1, E1, F1, G1
            REAL*8  A2, B2, C2, D2, E2, F2, G2
        REAL*8       A3,B3,C3,D3,E3,F3,G3
            REAL*8   XPZCOO2,X2MPZCOO2, LDG
        REAL*8   XH2O, XCO2T, XPZT, X2MPZT, XMDEAT
            REAL*8  XWPZ, XW2MPZ, XWMDEA, XWAMINE
            REAL*8   MWPZ, MW2MPZ, MWH2O, MWCO2, MWT, MWMDEA
        REAL*8       MUBLEND, MUPZ, MU2MPZ, MUH2O
            REAL*8  AA, BB
CCCC   PARAMETERS FOR VISCOSITY MODEL (FREEMAN 2011 PAGE 127)
            REAL*8  PHIPZ1,PHIPZ2,PHI2MPZ1,PHI2MPZ2,PHIBLD1,PHIBLD2
            REAL*8  PZA1,PZB1,PZB2,PZC1,PZC2,PZD1,PZD2
            REAL*8  MPZA1,MPZB1,MPZB2,MPZC1,MPZC2,MPZD1,MPZD2
            REAL*8  BLDA1,BLDB1,BLDB2,BLDC1,BLDC2,BLDD1,BLDD2
C
C       DECLARE LOCAL VARIABLES
C
        INTEGER IPROG(2)
C
C        DATA STATEMENTS
C
        DATA IPROG /4HMUL2, 4HU2   /
C
C       BEGIN EXECUTABLE CODE
C
C       Viscosity is calculated from the regressed data using Weiland et al.1998 FOR PZ
C       5m, 7m, 9m.
C       JORGE M. PLAZA 05/04/09
C
C       VALUES OBTAINED FROM THE VISCOSITY REGRESSION
        INTEGER I
        REAL*8 SUM, DSUM, DPSUM
        SUM = 0D0
        DSUM = 0D0
        DPSUM = 0D0
        A1 = -0.015584757D0
        B1 = 0.043257306D0
        C1 = 0.049806214D0
```

```
      D1 = -0.018606132D0
      E1 = 0.046802557D0
           F1 = 0.176347466D0
           G1 = 3525.98334
C
           A2 = -0.004854379D0
           B2 = 0.020405406D0
           C2 = -0.041480506D0
           D2 = 0.184019437D0
           E2 = 2820.988726D0
C
            A3 = -0.015584757D0
      B3 = 0.043257306D0
      C3 = 0.049806214D0
      D3 = -0.018606132D0
      E3 = 0.046802557D0
           F3 = 0.176347466D0
           G3 = 3525.98334

           PZA1=    1.723D0
           PZB1=    2.63D0
           PZB2=    -778D0
           PZC1=    -1.019D0
           PZC2=    355.2D0
           PZD1=    -0.527D0
           PZD2=    169.3D0

C
           MPZA1= -4.63443D0
           MPZB1= -3.76473D0
           MPZB2= 1586.582D0
           MPZC1= 0D0
           MPZC2= 506.099D0
           MPZD1= 1.171451D0
           MPZD2= -410.978D0
C
           BLDA1= -3.43354D0
           BLDB1= 25.57663D0
           BLDB2= -7123.72D0
           BLDC1= 0D0
           BLDC2= 406.9763D0
           BLDD1= -5.75002D0
           BLDD2= 1636.09D0
C     INDEX VALUES FOR COMPONENTS IN SIMULATION
C
      IWATER = DMS_KCCIDC('H2O')
      IPZCOO = DMS_KCCIDC('PZCOO-')
      ICO2 = DMS_KCCIDC('CO2')
      IPZCOO2 = DMS_KCCIDC('PZCOO-2')
      IHPZCOO = DMS_KCCIDC('HPZCOO')
      IHCO3   = DMS_KCCIDC('HCO3-')
      IPZH = DMS_KCCIDC('PZH+')
      IPZ = DMS_KCCIDC('PZ')
            ICO3 = DMS_KCCIDC('CO3--')
            IMDEA = DMS_KCCIDC('C5H13-01')
           IMDEAH = DMS_KCCIDC('C5H14-01')
C
      I2MPZ = DMS_KCCIDC('2MPZ')
```

```
      I2MPZCOO = DMS_KCCIDC('2MPZCOO')
      IOOC2MPZ = DMS_KCCIDC('OOC2MPZ')
      I2MPZCOO2 = DMS_KCCIDC('2MPZCOO2')
      IH2MPZCOO = DMS_KCCIDC('H2MPZCOO')
      IOOC2MPZH   = DMS_KCCIDC('OOC2MPZH')
      I2MPZH = DMS_KCCIDC('2MPZH+')
C
C
C       ASSIGNMENT OF INDEX NUMBERS FOR SPECIES PRESENT
C
      DO 50 I = 1, N
      IF (IDX(I). EQ. IWATER) IWATER = I

      IF (IDX(I). EQ. ICO2) ICO2 = I
      IF (IDX(I). EQ. IHCO3) IHCO3 = I
          IF (IDX(I). EQ. ICO3) ICO3 = I

      IF (IDX(I). EQ. IPZCOO2) IPZCOO2 = I
      IF (IDX(I). EQ. IHPZCOO) IHPZCOO = I
      IF (IDX(I). EQ. IPZCOO) IPZCOO = I
      IF (IDX(I). EQ. IPZH) IPZH = I
      IF (IDX(I). EQ. IPZ) IPZ = I

          IF (IDX(I). EQ. IMDEA) IMDEA = I
          IF (IDX(I). EQ. IMDEAH) IMDEAH = I
C
      IF (IDX(I). EQ. I2MPZ) I2MPZ = I
      IF (IDX(I). EQ. I2MPZCOO2) I2MPZCOO2 = I
      IF (IDX(I). EQ. I2MPZCOO) I2MPZCOO = I
      IF (IDX(I). EQ. IOOC2MPZ) IOOC2MPZ = I
      IF (IDX(I). EQ. IH2MPZCOO) IH2MPZCOO = I
      IF (IDX(I). EQ. IOOC2MPZH) IOOC2MPZH = I
      IF (IDX(I). EQ. I2MPZH) I2MPZH = I

   50 CONTINUE
C
C VISCOSITY OF WATER
C
      MUH2O = MUI(IWATER)
C
C LOADING CALCULATIONS
C
      XPZCOO2              = 2D0*X(IPZCOO2)
      X2MPZCOO2            = 2D0*X(I2MPZCOO2)
      XCO2T =       X(ICO2)+X(IHCO3)+X(ICO3)
     .              +X(IPZCOO)+X(IHPZCOO)+XPZCOO2
     .+X(I2MPZCOO)+X(IOOC2MPZ)+X(IH2MPZCOO)+X(IOOC2MPZH)+X2MPZCOO2
      XPZT = X(IPZCOO)+X(IPZCOO2)+X(IHPZCOO)+X(IPZH)+X(IPZ)
          XMDEAT = X(IMDEA) + X(IMDEAH)
      X2MPZT=X(I2MPZ)+X(I2MPZH)+X(I2MPZCOO)+X(IOOC2MPZ)+X(IH2MPZCOO)
     .+X(IOOC2MPZH)+X(I2MPZCOO2)
      LDG = XCO2T/2D0/(XPZT + X2MPZT)
C
C       AMINE MASS FRACTION CALCULATION
C
      MWPZ = 86.14D0
      MWCO2 = 44.01D0
      MWH2O = 18.02D0
```

```
            MWMDEA = 119.163D0
            MW2MPZ=100.16D0
          XH2O = X(IWATER)
          MWT = XCO2T*MWCO2 + XPZT*MWPZ + XH2O*MWH2O + X2MPZT*MW2MPZ
          XWPZ = (XPZT*MWPZ)/MWT
C           XWMDEA = (XMDEAT*MWMDEA)/MWT
            XW2MPZ=(X2MPZT*MW2MPZ)/MWT
            XWAMINE = XWPZ + XW2MPZ
C
C
C       PZ VISCOSITY CALCULATION
C
            PHIPZ1= PZB1*XCO2T/MWT*1D3+PZC1*XPZT/MWT*1D3
     .+PZD1*XCO2T/MWT*1D3*XPZT/MWT*1D3
            PHIPZ2= PZB2*XCO2T/MWT*1D3+PZC2*XPZT/MWT*1D3
     .+PZD2*XCO2T/MWT*1D3*XPZT/MWT*1D3
            MUPZ=MUH2O*EXP(PZA1+PHIPZ1+PHIPZ2/T)


C           2MPZ VISCOSITY CALCULATION
            PHI2MPZ1=       MPZB1*XCO2T/MWT*1D3+MPZC1*X2MPZT/MWT*1D3
     .+MPZD1*XCO2T/MWT*1D3*X2MPZT/MWT*1D3
            PHI2MPZ2= MPZB2*XCO2T/MWT*1D3+MPZC2*X2MPZT/MWT*1D3
     .+MPZD2*XCO2T/MWT*1D3*X2MPZT/MWT*1D3
            MU2MPZ=MUH2O*EXP(MPZA1+PHI2MPZ1+PHI2MPZ2/T)


C           MU2MPZ=0D0
C           2MPZ-PZ BLEND VISCOSITY CALCULATION
            PHIBLD1=        BLDB1*XCO2T/MWT*1D3+BLDC1*(X2MPZT+XPZT)/MWT*1D3
     .+BLDD1*XCO2T/MWT*1D3*(X2MPZT+XPZT)/MWT*1D3
            PHIBLD2= BLDB2*XCO2T/MWT*1D3+BLDC2*(X2MPZT+XPZT)/MWT*1D3
     .+BLDD2*XCO2T/MWT*1D3*(X2MPZT+XPZT)/MWT*1D3
            MUBLEND=MUH2O*EXP(BLDA1+PHIBLD1+PHIBLD2/T)
C           MUPZ=(A2+B2*XWPZ+C2*LDG+D2*XWPZ*LDG)*DEXP(E2/T)
C           MUPZ=MUPZ/DEXP(E2/313.15D0)
C           MU2MPZ=
C           MU2MPZ=
            IF (XW2MPZ .LE. 1D-10) THEN
                  MUMX = MUPZ
            ELSE IF (XWPZ .LE. 1D-10) THEN
                  MUMX = MU2MPZ
            ELSE
                  MUMX = MUBLEND
            END IF
C
C     MUMX
          IF (KSW(1) .EQ. 1) THEN
          MUMX = MUMX
          END IF
C     dMUMX/dT
          IF (KSW(2) .EQ. 1) DMUMX = DSUM
C     dMUMX/dP
          IF (KSW(3) .EQ. 1) DPMUMX = DPSUM
C
  200 CONTINUE
          RETURN
          END
```

E.5 DIFFUSIVITY

```
C Log keyword added
C
C$ #1 BY: SUPHAT WATANASIRI 09-SET-2007 USER ROUTINE FOR LIQUID BINARY
C                                        DIFFUSION COEFFICIENTS
C
C ========================cvs revision history=======================
      SUBROUTINE DL0U ( T, P, X, N, IDX, IRW, IIW, KCALC, KOP,
     *                  NDS, KDIAG, QBIN, KER )
C**********************************************************************
C     Template for DL0U routine for binary liquid diffusion coefficients
C     STUB ROUTINE
C
C     T = temperature
C     P = pressure (system)
C     X(N) = mole fraction
C     N = number of components present in X
C     IDX(N) = index of component present
C     IRW = real work area index
C     IIW = integer work area index
C     KCALC = calculation code (0=do not calculate, 1 = calculate)
C     KOP(10) = model option code
C     NDS = data set number
C     KDIAG = diagnostic message level
C     QBIN(N,N) = results. Binary diffusion coeffcients.
C     QBIN(i,j) is binary diffusion coefficient of component i in component j
C     KER = error return code (0 = no error)
C     All input and output in this user routine are in SI Units
C     with Gas constant = 8314.33
C**********************************************************************
C
      IMPLICIT NONE
C
C     DECLARE VARIABLES USED IN DIMENSIONING
C
      INTEGER N
#include "dms_global.cmn"
#include "dms_errout.cmn"
#include "ppexec_user.cmn"
#include "dms_maxwrt.cmn"
#include "dms_plex.cmn"
C
C     DECLARE ARGUMENTS
C
      INTEGER IDX(N), IRW, IIW, KCALC, KOP, NDS, KDIAG, KER
          INTEGER IWATER, IPZCOO, ICO2, IPZCOO2, IHPZCOO, IHCO3
          INTEGER IPZH, IPZ, ICO3, IMDEA, IMDEAH, IN2, IO2
          INTEGER I2MPZ, I2MPZH, I2MPZCOO, IOOC2MPZ
          INTEGER IH2MPZCOO, IOOC2MPZH,I2MPZCOO2
          INTEGER DMS_KCCIDC, DMS_IFCMNC
      REAL*8 X(N), QBIN(N,N), T, P
          REAL*8 WATER, PZCOO, CO2, PZCOO2, HPZCOO, HCO3, PZH, PZ
          REAL*8 CO3, MDEA, MDEAH,MPZ,MPZH,MPZCOO,OOCMPZ
          REAL*8 HMPZCOO,OOCMPZH,MPZCOO2
          REAL*8 LDG, XPZCOO2, X2MPZCOO2,XCO2T, XPZT, XMDEAT,X2MPZT
          REAL*8 MWPZ, MWCO2, MWH2O, MWMDEA, XH2O, MWT, XWPZ, XWMDEA
          REAL*8 MW2MPZ,XW2MPZ, XWAMINE
```

```
      REAL*8 IOND, CO2D, MDEAD, PZD, MPZD, XMOLT, CO2DW
      REAL*8 MA, MB, MC, MD, ME, MUMX, MUMX1
      REAL*8 A, E, BB, THET, C, MU0, MUW, R, HG
      Real*8 VISC, LVISC, VM, B(1)
      EQUIVALENCE (B(1), IB(1))
      integer nbopst(6), name(2), USRPAR1,USRPAR2,USRPAR3, USRPAR4
      CHARACTER*256 BUFFER(1)
C
C     DECLARE LOCAL VARIABLES
C
      INTEGER IPROG(2), I, J, K
C
C      DATA STATEMENTS
C
      DATA IPROG /4HDL0U, 4H      /
C
C     BEGIN EXECUTABLE CODE
C       DIFFUSIVITIES CALCULATED BY (...) METHOD
C       VALUES OBTAINED FROM THE DIFFUSIVITY REGRESSION
      KER = 0
      IF (KCALC .EQ. 0) RETURN
c
C       INDEX VALUES FOR COMPONENTS IN SIMULATION
C
      IWATER = DMS_KCCIDC('H2O')
      IPZCOO = DMS_KCCIDC('PZCOO-')
      ICO2 = DMS_KCCIDC('CO2')
      IPZCOO2 = DMS_KCCIDC('PZCOO-2')
      IHPZCOO = DMS_KCCIDC('HPZCOO')
      IHCO3   = DMS_KCCIDC('HCO3-')
      IPZH = DMS_KCCIDC('PZH+')
      IPZ = DMS_KCCIDC('PZ')
      ICO3 = DMS_KCCIDC('CO3--')
      IMDEA = DMS_KCCIDC('C5H13-01')
      IMDEAH = DMS_KCCIDC('C5H14-01')
      IN2 = DMS_KCCIDC('N2')
      IO2 = DMS_KCCIDC('O2')
      I2MPZ = DMS_KCCIDC('2MPZ')
      I2MPZH = DMS_KCCIDC('2MPZH+')
      I2MPZCOO = DMS_KCCIDC('2MPZCOO')
      IOOC2MPZ = DMS_KCCIDC('OOC2MPZ')
      IH2MPZCOO = DMS_KCCIDC('H2MPZCOO')
      IOOC2MPZH = DMS_KCCIDC('OOC2MPZH')
      I2MPZCOO2 = DMS_KCCIDC('2MPZCOO2')

C
C
C       ASSIGNMENT OF INDEX NUMBERS FOR SPECIES PRESENT
C
      DO 50 I = 1, N
      IF (IDX(I). EQ. IWATER) IWATER = I
      IF (IDX(I). EQ. IPZCOO) IPZCOO = I
      IF (IDX(I). EQ. ICO2) ICO2 = I
      IF (IDX(I). EQ. IPZCOO2) IPZCOO2 = I
      IF (IDX(I). EQ. IHPZCOO) IHPZCOO = I
      IF (IDX(I). EQ. IHCO3) IHCO3 = I
      IF (IDX(I). EQ. IPZH) IPZH = I
      IF (IDX(I). EQ. IPZ) IPZ = I
```

```
            IF (IDX(I). EQ. ICO3) ICO3 = I
            IF (IDX(I). EQ. IMDEA) IMDEA = I
            IF (IDX(I). EQ. IMDEAH) IMDEAH = I
            IF (IDX(I). EQ. IN2) IN2 = I
            IF (IDX(I). EQ. IO2) IO2 = I
            IF (IDX(I). EQ. I2MPZ) I2MPZ = I
            IF (IDX(I). EQ. I2MPZH) I2MPZH = I
            IF (IDX(I). EQ. I2MPZCOO) I2MPZCOO = I
            IF (IDX(I). EQ. IOOC2MPZ) IOOC2MPZ = I
            IF (IDX(I). EQ. IH2MPZCOO) IH2MPZCOO = I
            IF (IDX(I). EQ. IOOC2MPZH) IOOC2MPZH = I
            IF (IDX(I). EQ. I2MPZCOO2) I2MPZCOO2 = I
   50 CONTINUE
C
C           LOADING CALCULATION
            XPZCOO2 = 2D0*X(IPZCOO2)
            X2MPZCOO2 = 2D0*X(I2MPZCOO2)
            XCO2T = X(IPZCOO)+X(ICO2)+XPZCOO2+X(IHPZCOO)+X(IHCO3)
     .      +X(I2MPZCOO)+X(IOOC2MPZ)+X2MPZCOO2+X(IH2MPZCOO)+X(IOOC2MPZH)
            XPZT = X(IPZCOO)+X(IPZCOO2)+X(IHPZCOO)+X(IPZH)+X(IPZ)
            X2MPZT = X(I2MPZCOO)+X(IH2MPZCOO)+X(IOOC2MPZ)+X(IOOC2MPZH)
     .      +X(I2MPZCOO2)+X(I2MPZH)+X(I2MPZ)
            XMDEAT = X(IMDEA)+X(IMDEAH)
            LDG = XCO2T/(2D0*XPZT + 2D0*X2MPZT)
C
C
C           AMINE MASS FRACTION CALCULATION
C
            MWPZ = 86.14D0
            MWCO2 = 44.01D0
            MWH2O = 18D0
            MWMDEA = 119.163D0
            MW2MPZ = 100.16D0
            XH2O = X(IWATER)
            MWT = XCO2T*MWCO2 + XPZT*MWPZ + XH2O*MWH2O + X2MPZT*MW2MPZ
            XWPZ = (XPZT*MWPZ)/MWT
            XW2MPZ = (X2MPZT*MW2MPZ)/MWT
            XWMDEA = (XMDEAT*MWMDEA)/MWT
            XWAMINE = XWPZ + XW2MPZ

c           Viscosity of solution from Aspen
            call PPUTL_GOPSET ( NBOPST , NAME )
c
            CALL PPMON_VISCL (T, P, X, N, IDX, NBOPST, KDIAG, VISC, KER)
            LVISC = VISC
            MUMX = LVISC
C
C     Viscosity of water according to Likhachev E.R. Technical Physics, Vol. 48 N0.4 2003 pp. 514-515
C     Viscosity in Pa-s
      E = 4.753D0
      MU0 = 0.000024055D0
      THET = 139.7D0
           A = 0.000442D0
           BB = 0.0009565D0
           C = 0.0124D0
           R = 0.008314D0
           P = P / 100000D0
           HG = A * P +((E - BB * P)/(R * (T - THET - C * P)))
```

```
            MUW = MU0 * EXP(HG)

C           USRPAR1, USRPAR2 & USRPAR3 STORE THE POSITION OF REGRESSES PARAMETERS FOR
DIFF. CORRELATION
C           THEY REFER TO THE VALUES SPECIFIED IN PROPERTY-PARAMETER-USRDEF

          USRPAR1 = DMS_IFCMNC('USRPAR1')
            USRPAR2 = DMS_IFCMNC('USRPAR2')
            USRPAR3 = DMS_IFCMNC('USRPAR3')
            USRPAR4 = DMS_IFCMNC('USRPAR4')
C
C       DIFFUSIVITY OF CO2 IN WATER
          CO2DW = 0.00000235D0 * EXP(-2119D0 / T)
C
C       DIFFUSIVITY OF CO2 IN SOLUTION BASED ON VERSTEEG, 2003
          CO2D = CO2DW * (MUW / MUMX)**(0.8D0)*B(USRPAR4+IDX(ICO2))
C
C       DIFFUSIVITY OF AMINE IN WATER


            VM = 129.371D0
          PZD = 8.2D-10*313.15D0/303.15D0*(T/313.15D0)**B(USRPAR2+IDX(ICO2))
          PZD = B(USRPAR1+IDX(ICO2))*PZD*((MUMX*1.0D3)
         .      **B(USRPAR3+IDX(ICO2)))

C           MPZD = 0.0000000004D0*((T/313.15D0))
C       MPZD = MPZD*((MUMX/0.0155D0)**-0.72D0)
C
C
C       ASSIGNING VALUES IN THE DIFFUSIVITY MATRIX
C
C
          DO 200 I = 1, N
            DO 100 J = 1, N
              IF (I.EQ.J) THEN
                QBIN(I,J) = 0D0
              ELSE
                QBIN(I,J) = PZD
                IF (I.EQ.ICO2)QBIN(I,J) = CO2D
                IF (J.EQ.ICO2)QBIN(I,J) = CO2D
                IF (I.EQ.IN2)QBIN(I,J) = CO2D
                IF (J.EQ.IN2)QBIN(I,J) = CO2D
              END IF
  100       CONTINUE
  200     CONTINUE

c
C           WRITE VARIABLES TO HISTORY FILE
C
C            THE WRITE TO UNIT USER_NHSTRY WRITES TO THE HISTORY FILE
            WRITE (BUFFER, *) 'Executed fortran subroutine'
            CALL DMS_WRTALN(USER_NHSTRY, BUFFER(1))
            WRITE (BUFFER, *) 'Pressure ', P
            CALL DMS_WRTALN(USER_NHSTRY, BUFFER(1))
            WRITE (BUFFER, *) 'Temperature ', T
            CALL DMS_WRTALN(USER_NHSTRY, BUFFER(1))
            WRITE (BUFFER, *) 'LVISC ', LVISC
            CALL DMS_WRTALN(USER_NHSTRY, BUFFER(1))
```

```
            WRITE (BUFFER, *) ' '
            CALL DMS_WRTALN(USER_NHSTRY, BUFFER(1))

C 999       RETURN
        END
```

E.6 NMR DATA REGRESSION

```
C$ May 30, 2000 suphat from Jon hillier.   calculate bubble pressure
c           used with testdrs.inp
C$ #1 BY: SUPHAT DATE: 12-MAY-1995 DRS USER ROUTINE EXAMPLE
C$
C$ #5 BY: SUPHAT DATE: 12-APR-1993 ADD RIAZI FOR DRSEX14.INP
C$ #4 BY: LOCKE DATE: 13-APR-1992 CHANGES FOR PLEXIFICATION
C$ #3 BY: SUPHAT DATE: 8-FEB-1990 CHANGE COMMENTS
C$ #2 BY: SUPHAT DATE: 9-OCT-1989 ADD EXAMPLE
C$ #1 BY: SUPHAT DATE: 26-JUL-1989 NEW FOR DRS UPGRADE
      SUBROUTINE DRUSR0 (T, P, X, Y, NCP, IDX, NBOPST, KDIAG,
     1                   ITYPE, PROP, KER)
C
C-----------------------------------------------------------------------
C            COPYRIGHT (C) 1989
C             ASPEN TECHNOLOGY, INC.
C             CAMBRIDGE, MA
C-----------------------------------------------------------------------
C
C     MODULE TITLE: GENERIC USER PROPERTY VS. STATE VARIABLES
C
C     VARIABLES USED:
C
C      VARIABLES IN ARGUMENT LIST - NONE
C
C      IMPORTANT INTERNAL VARIABLES
C
C       VARIABLE  I/O   TYPE      DIMENSION      DESCRIPTION AND RANGE
C
C            T       I     R*8         -           TEMPERATURE, K
C
C            P       I     R*8         -           PRESSURE, PASCAL
C
C            X       I     R*8         NCP         LIQUID MOLE FRAC VECTOR
C
C            Y       I     R*8         NCP         VAPOR MOLE FRAC VECTOR
C
C            NCP     I     I           -           NO. OF COMPONENT PRESENT
C
C            IDX     I     I           NCP         COMPONENT INDEX VECTOR
C
C            NBOPST I      I           6           OPTION SET BEAD
C
C            KDIAG  I      I           -           PROPERTY DIAGNOSTIC CODE
C
C            ITYPE  I      I           -           TYPE OF PROPERTY
C                                                   (SEE ABOVE)
C
C            PROP    O     R*8         1           CALCULATED PURE COMP
C                                                  PROPERTY
C                                      NCP         CALCULATED PARTIAL PROP
C                                      1           CALCULATED MIXTURE PROP
C
C            KER     O     I           -           ERROR RETURN CODE
C
C     ERROR CONDITIONS: NONE
C
```

```
C       SUBROUTINES CALLED:
C
C       FILES:
C
C          SPECIFICATIONS, DECLARATIONS, DATA STATEMENTS, ETC.
C
       IMPLICIT NONE
C
#include "dms_global.cmn"
#include "dms_rglob.cmn"
#include "dms_ncomp.cmn"
C
#include "shs_stwork.cmn"
#include "dms_stwkwk.cmn"

       EQUIVALENCE (NCPM, STWKWK_NCPMOO)
       EQUIVALENCE (PCALC, STWKWK_PCALC)
C
#include "dms_plex.cmn"
       EQUIVALENCE (IB(1), B(1))
C
C       DECLARE ARGUMENTS
C
       INTEGER IDX(1),NBOPST(1),      NCP,     KDIAG, ITYPE,
      +           KER,     I, DMS_IFCMNC
       REAL*8 X(1),   Y(1),   PROP(1), T, P, MEATOT, CO2TOT,
      +           MEAH, MEACOO, CO3HCO3, OBJFUN, AA, BB, CC,
      +                    PZTOT, PZH, HPZCOO, PZCOO2, MPZTOT
C
C       DECLARE LOCAL VARIABLES
C
       INTEGER IPROG(2),LDRU1,LDRU2,addValue,caseValue,idValue
       REAL*8 B(1), SVEC(30), TOL, SPEC1,
      +         SPEC2, GUESS, RETN(1000), total
       INTEGER NSUBS, IXTYPE, KODE, NPKODE, MAXIT,
      +           IRETN(6), JRES,KRESLT, lcflag, lmsg, lpmsg,
      +                   kphase, idxsub(1)
C
       REAL*8 XT, XL, XS, S2TL, TL2AL, HMX, DHMX
       INTEGER IDXT, IDXL ,IDXS, KH, N, KBASE,
      1           NL, NS, NT
       DIMENSION XT(33), IDXT(33), XL(33), IDXL(33),
      1             XS(33), IDXS(33)
       INTEGER KPPMON(4), KENTHL(5), IFPTR
C
       INTEGER IOLI, NPHASE, MXIT, LODIAG, NV, IDXV(1),
      1           NBOPSTS
            REAL*8   HDUM, XV(1), SF, VF, LF, T2A
            REAL*8   XMEA,XMEAH,XTEMP(33),XMEACOO,XCO2,XCO3,XHCO3
            REAL*8   XH2O, XPZ, XPZH, XPZH2, XPZCOO, XPZCOO2
            REAL*8   XHPZCOO
            REAL*8   X2MPZ,X2MPZH,X2MPZCOO,XOOC2MPZ,X2MPZCOO2
            REAL*8   XH2MPZCOO,XOOC2MPZH

C
C       DECLARE LOCAL VARIABLES
C         IMEA STORES THE ALIAS OF MEA (8 CHARACTERS)
C         IMEAH STORES THE ALIAS OF MEAH+ (8 CHARACTERS)
```

```
C          AND SO ON...
C
      INTEGER NCPM, J, II, FRMULA, LFRMULA,
     .                  LIDSCC, IMEA(2), IMEAH(2),
     .           IMEACOO(2), ICO2(2), ICO3(2), IHCO3(2), Z,
     .           IH2O(2), IPZ(2), IPZH(2), IPZH2(2), IPZCOO(2),
     .           IPZCOO2(2), IHPZCOO(2),
     .           I2MPZ(2),I2MPZH(2),I2MPZCOO(2),IOOC2MPZ(2),
     .           I2MPZCOO2(2),IH2MPZCOO(2),IOOC2MPZH(2)
C
      REAL*8 PCALC,YTEMP(33),PRES,PPTEMP(33),ZTEMP(33),RecT

c           #include "dms_initv.cmn"
#include "dms_ipoff1.cmn"
#include "dms_ipoff4.cmn"
c           #include "ppexec_user.cmn"
C
C       DATA STATEMENTS
C
      DATA IPROG/4HDRUS, 4HR0   /
      DATA KPPMON / 4HPPMO, 4HN      ,2*4H      /
      DATA KENTHL / 4HPPMO, 4HN_EN, 4HTHL , 2*4H      /
C
      DATA IMEA     /4HC2H7, 4HNO   /,
     .      IH2O     /4HH2O , 4H      /,
     .      IMEAH   /4HC2H8, 4HNO+ /,
     .      IMEACOO/4HC3H6, 4HNO3-/,
     .      ICO2     /4HCO2 , 4H      /,
     .      ICO3     /4HCO3-, 4H2     /,
     .      IHCO3    /4HHCO3, 4H-     /,
     .      IPZ      /4HC4H1, 4H0N2 /,
     .      IPZH     /4HC4H1, 4H1N2 /,
     .      IPZH2    /4HC4H1, 4H2N2 /,
     .      IPZCOO /4HC5H9, 4HN2O2/,
     .      IPZCOO2/4HC6H8, 4HN2O4/,
     .      IHPZCOO/4HC5H1, 4H0N2O/
     .      I2MPZ   /4H2MPZ, 4H      /,
     .      I2MPZH     /4H2MPZ, 4HH+   /,
     .      I2MPZCOO     /4H2MPZ, 4HCOO /,
     .      IOOC2MPZ     /4HOOC2, 4HMPZ /,
     .      I2MPZCOO2     /4H2MPZ, 4HCOO2/,
     .      IH2MPZCOO     /4HH2MP, 4HZCOO/,
     .      IOOC2MPZH     /4HOOC2, 4HMPZH/
C
C   STATEMENT FUNCTIONS FOLLOW
C
      FRMULA(I,J) = LFRMULA + 3*(J - 1) + I
           LIDSCC = DMS_IFCMNC('IDSCC')
c           IDSCC(I,J)= LIDSCC + 3*(J-1) + I

C
C       BEGIN EXECUTABLE CODE
C
C   SET PLEX OFFSETS
C
      LDRU1 = IPOFF1_IPOFF1(102)
      LDRU2 = IPOFF1_IPOFF1(103)
      LFRMULA = IPOFF4_IPOFF4(1)
```

```
C
C
================================================================================
C
C      Set Case Value for NMR or DHabs code
C      caseValue = 15 for NMR code only
C      caseValue = 7 for DHabs code only
C
       addValue = 1D0
       caseValue = 0D0
       idValue = 0D0

       DO I=1,NCP

            IF (IDX(I).ne.0) THEN
            caseValue = caseValue + addValue
            idValue = IDX(I) + idValue
       ENDIF

            addValue = addValue*2

            END DO
C           write (user_nhstry,*) ' '
C          write(user_nhstry,*) 'Final idValue ' ,idValue
C          write (user_nhstry,*) ' '

C
C
================================================================================
C
       IF (idValue.EQ.46) THEN
C
C              PZ & 2MPZ NMR Data
C      Convert Mole fractions to total mole fractions
C
C                        X(1) = PZ
C                        X(2) = 2MPZ
C                        X(3) = CO2
C                        X(4) = H2O
C
       PZTOT = X(1)
            MPZTOT = X(2)
       CO2TOT = X(3)

C
C      Convert to SVEC components according to the SPECIES list
C
       XTEMP(1)=1D0-PZTOT-MPZTOT-CO2TOT
       XTEMP(2)=CO2TOT
C        XTEMP(3)=0D0
C        XTEMP(4)=0D0
C        XTEMP(5)=0D0
C        XTEMP(6)=0D0
       XTEMP(17)=PZTOT
            XTEMP(26)=MPZTOT
C
C
================================================================================
```

```
C
C       The following code calls the FLash subroutine.
C
                        TOTAL = 0D0
                        DO 299 I=1, NCOMP_NCC+9
                                SVEC(I) = 0D0
  299           CONTINUE
C
C                       NCP is the number of components specified in the DRS component list.
C
            DO 300 I = 1, NCP
                        SVEC(I) = XTEMP(I)
                        TOTAL = SVEC(I) + TOTAL
C
  300       CONTINUE
C
                        SVEC(17) = XTEMP(17)
C
                        TOTAL = SVEC(17) + TOTAL
                       SVEC(26)= XTEMP(26)
                       TOTAL = SVEC(26) + TOTAL
C
C
C           write (user_nhstry,*) ' '
C           write (user_nhstry,*) 'total ',total
            SVEC(NCOMP_NCC+1) = TOTAL
            svec(ncomp_ncc+2) = t
            svec(ncomp_ncc+3) = P
C
C                       do 98 i = 1, ncomp_ncc+9
C            write(user_nhstry,*) 'svec(ncomp_ncc) ' ,svec(i),i
C   98       continue

                        NSUBS = 1
                        IXTYPE = 1
                        KODE = 5
                        NPKODE = 2
                        MAXIT = 30
                        TOL = 1E-4
                        SPEC1 = T
                        SPEC2= 0.0001
                        GUESS = P
                        JRES= 0
                        KRESLT = 1
          KPHASE = 2
          idxsub(1) = 1
C
C
            CALL FLSH_FLASH (SVEC, NSUBS, IDXSUB, IXTYPE, NBOPST, KODE,
       +    NPKODE, KPHASE, MAXIT, TOL, SPEC1,SPEC2, GUESS, LMSG, LPMSG,
       +    JRES, KRESLT, RETN, IRETN, LCFLAG)

C
C
C           write (user_nhstry,*) ' '
C                write(user_nhstry,*) 'lcflag ',lcflag
C
C           do 99 i = 1, ncomp_ncc+9
```

```
C                write(user_nhstry,*) 'svec(ncomp_ncc) ' ,svec(i)
C   99      continue

C
C       GET CALCULATED PRESSURE
C
        PRES = PCALC

C          write (user_nhstry,*) 'PCALC, [Pa]', PCALC
C
C       GET VAPOR MOLE FRACTIONS
C
        DO I = 1, NCP
           YTEMP(I) = 0D0
        END DO

C          write (user_nhstry,*) ' '
        DO I = 1, NCPM
          YTEMP(i) = B(STWKWK_LRSTW+(STWORK_MY+I-1))
C
C          FIND CO2
C
          IF (IB(FRMULA(1,I)).EQ.ICO2(1) .AND.
     .          IB(FRMULA(2,I)).EQ.ICO2(2)) THEN
            PPTEMP(I) = PRES*YTEMP(i)
C              write (user_nhstry,*) 'YTEMP-CO2, i', YTEMP(i), i
C              write (user_nhstry,*) 'PPTEMP-CO2,[Pa] ',PPTEMP(i), i
          ENDIF
        END DO
C
C       ================================================================>
C
C       The following code is to get true species.
C
        CALL PPSTUB_GETTRU ( NT, IDXT, XT, NL, IDXL, XL, NS, IDXS, XS,
     1                       S2TL, TL2AL )
C
C          write (user_nhstry,*) ' '
C          do 101 I = 1, NL
C               write(user_nhstry,*) 'XL ' ,XL(I), I, IDXL(I)
C   101    continue

C
C     The Following Code retrieves the liquid phase mole fractions
C
        XMEA = 0D0
        XH2O = 0D0
        XMEAH = 0D0
        XMEACOO = 0D0
        XCO2 = 0D0
        XCO3 = 0D0
        XHCO3 = 0D0
        XPZ = 0D0
        XPZH = 0D0
        XPZH2 = 0D0
        XPZCOO = 0D0
        XPZCOO2 = 0D0
        XHPZCOO = 0D0
```

```
            X2MPZ= 0D0
            X2MPZH= 0D0
            X2MPZCOO= 0D0
            XOOC2MPZ= 0D0
            X2MPZCOO2= 0D0
            XH2MPZCOO= 0D0
            XOOC2MPZH= 0D0
c
C       write (user_nhstry,*) 'XH2O TRUE ',XH2O
C
C        write (user_nhstry,*) ' '
       DO I = 1, NL
          IF (IB(FRMULA(1,IDXL(I))) .EQ. IMEA(1). AND.
     .        IB(FRMULA(2,IDXL(I))).EQ.IMEA(2)) THEN
             XMEA = XL(I)
C               write (user_nhstry,*) 'XMEA TRUE ',XMEA
          ELSE IF (IB(FRMULA(1,IDXL(I))) .EQ. IH2O(1). AND.
     .        IB(FRMULA(2,IDXL(I))).EQ.IH2O(2)) THEN
             XH2O = XL(I)*(18.01528/1000)
C               write (user_nhstry,*) 'XH2O TRUE ',XH2O
          ELSE IF (IB(FRMULA(1,IDXL(I))) .EQ. IMEAH(1). AND.
     .               IB(FRMULA(2,IDXL(I))).EQ.IMEAH(2)) THEN
             XMEAH = XL(I)
C               write (user_nhstry,*) 'XMEAH TRUE ', XMEAH
          ELSE IF (IB(FRMULA(1,IDXL(I))) .EQ. IMEACOO(1). AND.
     .               IB(FRMULA(2,IDXL(I))).EQ.IMEACOO(2)) THEN
             XMEACOO = XL(I)
C               write (user_nhstry,*) 'XMEACOO TRUE ', XMEACOO
          ELSE IF (IB(FRMULA(1,IDXL(I))) .EQ. ICO2(1). AND.
     .               IB(FRMULA(2,IDXL(I))).EQ.ICO2(2)) THEN
             XCO2 = XL(I)
C               write (user_nhstry,*) 'XCO2 TRUE ', XCO2
          ELSE IF (IB(FRMULA(1,IDXL(I))) .EQ. ICO3(1). AND.
     .               IB(FRMULA(2,IDXL(I))).EQ.ICO3(2)) THEN
             XCO3 = XL(I)
C               write (user_nhstry,*) 'XCO3 TRUE ', XCO3
          ELSE IF (IB(FRMULA(1,IDXL(I))) .EQ. IHCO3(1). AND.
     .               IB(FRMULA(2,IDXL(I))).EQ.IHCO3(2)) THEN
             XHCO3 = XL(I)
C               write (user_nhstry,*) 'XHCO3 TRUE ', XHCO3
                    ELSE IF (IB(FRMULA(1,IDXL(I))) .EQ. IPZ(1). AND.
     .               IB(FRMULA(2,IDXL(I))).EQ.IPZ(2)) THEN
             XPZ = XL(I)
C               write (user_nhstry,*) 'XPZ TRUE ', XPZ
          ELSE IF (IB(FRMULA(1,IDXL(I))) .EQ. IPZH(1). AND.
     .               IB(FRMULA(2,IDXL(I))).EQ.IPZH(2)) THEN
             XPZH = XL(I)
C               write (user_nhstry,*) 'XPZH TRUE ', XPZH
          ELSE IF (IB(FRMULA(1,IDXL(I))) .EQ. IPZH2(1). AND.
     .               IB(FRMULA(2,IDXL(I))).EQ.IPZH2(2)) THEN
             XPZH2 = XL(I)
C               write (user_nhstry,*) 'XPZH2 TRUE ', XPZH2
          ELSE IF (IB(FRMULA(1,IDXL(I))) .EQ. IPZCOO(1). AND.
     .               IB(FRMULA(2,IDXL(I))).EQ.IPZCOO(2)) THEN
             XPZCOO = XL(I)
C               write (user_nhstry,*) 'XPZCOO TRUE ', XPZCOO
          ELSE IF (IB(FRMULA(1,IDXL(I))) .EQ. IPZCOO2(1). AND.
     .               IB(FRMULA(2,IDXL(I))).EQ.IPZCOO2(2)) THEN
```

```
            XPZCOO2 = XL(I)
C               write (user_nhstry,*) 'XPZCOO2 TRUE ', XPZCOO2
          ELSE IF (IB(FRMULA(1,IDXL(I))) .EQ. IHPZCOO(1). AND.
     .               IB(FRMULA(2,IDXL(I))).EQ.IHPZCOO(2)) THEN
            XHPZCOO = XL(I)
C               write (user_nhstry,*) 'XHPZCOO TRUE ', XHPZCOO
           ELSE IF (IB(LIDSCC+2*(IDXL(I)-1)+1) .EQ. I2MPZ(1). AND.
     .               IB(LIDSCC+2*(IDXL(I)-1)+2).EQ.I2MPZ(2)) THEN
            X2MPZ = XL(I)
C               write (user_nhstry,*) 'X2MPZ TRUE ', XPZ
          ELSE IF (IB(LIDSCC+2*(IDXL(I)-1)+1) .EQ. I2MPZH(1). AND.
     .               IB(LIDSCC+2*(IDXL(I)-1)+2).EQ.I2MPZH(2)) THEN
            X2MPZH = XL(I)
C               write (user_nhstry,*) 'XPZH TRUE ', XPZH
          ELSE IF (IB(LIDSCC+2*(IDXL(I)-1)+1) .EQ. I2MPZCOO(1). AND.
     .               IB(LIDSCC+2*(IDXL(I)-1)+2).EQ.I2MPZCOO(2)) THEN
            X2MPZCOO = XL(I)
C               write (user_nhstry,*) 'XPZH2 TRUE ', XPZH2
          ELSE IF (IB(LIDSCC+2*(IDXL(I)-1)+1) .EQ. IOOC2MPZ(1). AND.
     .               IB(LIDSCC+2*(IDXL(I)-1)+2).EQ.IOOC2MPZ(2)) THEN
            XOOC2MPZ = XL(I)
C               write (user_nhstry,*) 'XPZCOO TRUE ', XPZCOO
          ELSE IF (IB(LIDSCC+2*(IDXL(I)-1)+1) .EQ. I2MPZCOO2(1). AND.
     .               IB(LIDSCC+2*(IDXL(I)-1)+2).EQ.I2MPZCOO2(2)) THEN
            X2MPZCOO2 = XL(I)
C               write (user_nhstry,*) 'XPZCOO2 TRUE ', XPZCOO2
          ELSE IF (IB(LIDSCC+2*(IDXL(I)-1)+1) .EQ. IH2MPZCOO(1). AND.
     .               IB(LIDSCC+2*(IDXL(I)-1)+2).EQ.IH2MPZCOO(2)) THEN
            XH2MPZCOO = XL(I)
C               write (user_nhstry,*) 'XHPZCOO TRUE ', XHPZCOO
          ELSE IF (IB(LIDSCC+2*(IDXL(I)-1)+1) .EQ. IOOC2MPZH(1). AND.
     .               IB(LIDSCC+2*(IDXL(I)-1)+2).EQ.IOOC2MPZH(2)) THEN
            XOOC2MPZH = XL(I)
C               write (user_nhstry,*) 'XHPZCOO TRUE ', XHPZCOO
          ENDIF
        END DO
C       ===================================================================<
C
C
C       Property Function
C
              PROP(1) = (XOOC2MPZ+XOOC2MPZH)/(X2MPZCOO+XH2MPZCOO)
C
C         write (user_nhstry,*) ' '
C          write (user_nhstry,*) 'prop(1) ',prop(1)
C          write (user_nhstry,*) ' '

           ENDIF
C
C
=================================================================================
C
        IF (idValue.EQ.69) THEN
C
C             PZ & 2MPZ NMR Data
C       Convert Mole fractions to total mole fractions
C
C                       X(1) = PZ
```

```
C                       X(2) = 2MPZ
C                       X(3) = CO2
C                       X(4) = H2O
C            X(5) = PZ/H
C
       PZTOT = X(1)
            MPZTOT = X(2)
       CO2TOT = X(3)

C
C       Convert to SVEC components according to the SPECIES list
C
       XTEMP(1)=1D0-PZTOT-MPZTOT-CO2TOT
       XTEMP(2)=CO2TOT
C        XTEMP(3)=0D0
C        XTEMP(4)=0D0
C        XTEMP(5)=0D0
C        XTEMP(6)=0D0
       XTEMP(17)=PZTOT
            XTEMP(26)=MPZTOT
C
C
================================================================================
C
C       The following code calls the FLash subroutine.
C
                        TOTAL = 0D0
                        DO 221 I=1, NCOMP_NCC+9
                                SVEC(I) = 0D0
  221           CONTINUE
C
C                       NCP is the number of components specified in the DRS component list.
C
            DO 301 I = 1, NCP
                         SVEC(I) = XTEMP(I)
                         TOTAL = SVEC(I) + TOTAL
C
  301       CONTINUE
C
                         SVEC(17) = XTEMP(17)
C
                         TOTAL = SVEC(17) + TOTAL
                        SVEC(26)= XTEMP(26)
                        TOTAL = SVEC(26) + TOTAL
C
C
C           write (user_nhstry,*) ' '
C           write (user_nhstry,*) 'total ',total
            SVEC(NCOMP_NCC+1) = TOTAL
            svec(ncomp_ncc+2) = t
            svec(ncomp_ncc+3) = P
C
C                       do 98 i = 1, ncomp_ncc+9
C            write(user_nhstry,*) 'svec(ncomp_ncc) ' ,svec(i),i
C   98       continue

                        NSUBS = 1
                        IXTYPE = 1
```

```
                    KODE = 5
                    NPKODE = 2
                    MAXIT = 30
                    TOL = 1E-4
                    SPEC1 = T
                    SPEC2= 0.0001
                    GUESS = P
                    JRES= 0
                    KRESLT = 1
      KPHASE = 2
      idxsub(1) = 1
C
C
        CALL FLSH_FLASH (SVEC, NSUBS, IDXSUB, IXTYPE, NBOPST, KODE,
     +  NPKODE, KPHASE, MAXIT, TOL, SPEC1,SPEC2, GUESS, LMSG, LPMSG,
     +  JRES, KRESLT, RETN, IRETN, LCFLAG)

C
C
C       write (user_nhstry,*) ' '
C            write(user_nhstry,*) 'lcflag ',lcflag
C
C       do 99 i = 1, ncomp_ncc+9
C            write(user_nhstry,*) 'svec(ncomp_ncc) ' ,svec(i)
C 99    continue

C
C     GET CALCULATED PRESSURE
C
      PRES = PCALC

C       write (user_nhstry,*) 'PCALC, [Pa]', PCALC
C
C     GET VAPOR MOLE FRACTIONS
C
      DO I = 1, NCP
         YTEMP(I) = 0D0
      END DO

C       write (user_nhstry,*) ' '
      DO I = 1, NCPM
        YTEMP(i) = B(STWKWK_LRSTW+(STWORK_MY+I-1))
C
C       FIND CO2
C
        IF (IB(FRMULA(1,I)).EQ.ICO2(1) .AND.
     .       IB(FRMULA(2,I)).EQ.ICO2(2)) THEN
          PPTEMP(I) = PRES*YTEMP(i)
C           write (user_nhstry,*) 'YTEMP-CO2, i', YTEMP(i), i
C           write (user_nhstry,*) 'PPTEMP-CO2,[Pa] ',PPTEMP(i), i
        ENDIF
      END DO
C
C     ================================================================>
C
C     The following code is to get true species.
C
      CALL PPSTUB_GETTRU ( NT, IDXT, XT, NL, IDXL, XL, NS, IDXS, XS,
```

```
     1                  S2TL, TL2AL )
C
C         write (user_nhstry,*) ' '
C         do 101 I = 1, NL
C              write(user_nhstry,*) 'XL ' ,XL(I), I, IDXL(I)
C   101    continue

C
C     The Following Code retrieves the liquid phase mole fractions
C
          XMEA = 0D0
          XH2O = 0D0
          XMEAH = 0D0
          XMEACOO = 0D0
          XCO2 = 0D0
          XCO3 = 0D0
          XHCO3 = 0D0
          XPZ = 0D0
          XPZH = 0D0
          XPZH2 = 0D0
          XPZCOO = 0D0
          XPZCOO2 = 0D0
          XHPZCOO = 0D0
               X2MPZ= 0D0
               X2MPZH= 0D0
               X2MPZCOO= 0D0
               XOOC2MPZ= 0D0
               X2MPZCOO2= 0D0
               XH2MPZCOO= 0D0
               XOOC2MPZH= 0D0
c
C        write (user_nhstry,*) 'XH2O TRUE ',XH2O
C
C         write (user_nhstry,*) ' '
          DO I = 1, NL
             IF (IB(FRMULA(1,IDXL(I))) .EQ. IMEA(1). AND.
     .          IB(FRMULA(2,IDXL(I))).EQ.IMEA(2)) THEN
                XMEA = XL(I)
C                  write (user_nhstry,*) 'XMEA TRUE ',XMEA
             ELSE IF (IB(FRMULA(1,IDXL(I))) .EQ. IH2O(1). AND.
     .          IB(FRMULA(2,IDXL(I))).EQ.IH2O(2)) THEN
                XH2O = XL(I)*(18.01528/1000)
C                  write (user_nhstry,*) 'XH2O TRUE ',XH2O
             ELSE IF (IB(FRMULA(1,IDXL(I))) .EQ. IMEAH(1). AND.
     .                IB(FRMULA(2,IDXL(I))).EQ.IMEAH(2)) THEN
                XMEAH = XL(I)
C                  write (user_nhstry,*) 'XMEAH TRUE ', XMEAH
             ELSE IF (IB(FRMULA(1,IDXL(I))) .EQ. IMEACOO(1). AND.
     .                IB(FRMULA(2,IDXL(I))).EQ.IMEACOO(2)) THEN
                XMEACOO = XL(I)
C                  write (user_nhstry,*) 'XMEACOO TRUE ', XMEACOO
             ELSE IF (IB(FRMULA(1,IDXL(I))) .EQ. ICO2(1). AND.
     .                IB(FRMULA(2,IDXL(I))).EQ.ICO2(2)) THEN
                XCO2 = XL(I)
C                  write (user_nhstry,*) 'XCO2 TRUE ', XCO2
             ELSE IF (IB(FRMULA(1,IDXL(I))) .EQ. ICO3(1). AND.
     .                IB(FRMULA(2,IDXL(I))).EQ.ICO3(2)) THEN
                XCO3 = XL(I)
```

```
C               write (user_nhstry,*) 'XCO3 TRUE ', XCO3
              ELSE IF (IB(FRMULA(1,IDXL(I))) .EQ. IHCO3(1). AND.
     .                 IB(FRMULA(2,IDXL(I))).EQ.IHCO3(2)) THEN
                 XHCO3 = XL(I)
C               write (user_nhstry,*) 'XHCO3 TRUE ', XHCO3
                      ELSE IF (IB(FRMULA(1,IDXL(I))) .EQ. IPZ(1). AND.
     .                 IB(FRMULA(2,IDXL(I))).EQ.IPZ(2)) THEN
                 XPZ = XL(I)
C               write (user_nhstry,*) 'XPZ TRUE ', XPZ
              ELSE IF (IB(FRMULA(1,IDXL(I))) .EQ. IPZH(1). AND.
     .                 IB(FRMULA(2,IDXL(I))).EQ.IPZH(2)) THEN
                 XPZH = XL(I)
C               write (user_nhstry,*) 'XPZH TRUE ', XPZH
              ELSE IF (IB(FRMULA(1,IDXL(I))) .EQ. IPZH2(1). AND.
     .                 IB(FRMULA(2,IDXL(I))).EQ.IPZH2(2)) THEN
                 XPZH2 = XL(I)
C               write (user_nhstry,*) 'XPZH2 TRUE ', XPZH2
              ELSE IF (IB(FRMULA(1,IDXL(I))) .EQ. IPZCOO(1). AND.
     .                 IB(FRMULA(2,IDXL(I))).EQ.IPZCOO(2)) THEN
                 XPZCOO = XL(I)
C               write (user_nhstry,*) 'XPZCOO TRUE ', XPZCOO
              ELSE IF (IB(FRMULA(1,IDXL(I))) .EQ. IPZCOO2(1). AND.
     .                 IB(FRMULA(2,IDXL(I))).EQ.IPZCOO2(2)) THEN
                 XPZCOO2 = XL(I)
C               write (user_nhstry,*) 'XPZCOO2 TRUE ', XPZCOO2
              ELSE IF (IB(FRMULA(1,IDXL(I))) .EQ. IHPZCOO(1). AND.
     .                 IB(FRMULA(2,IDXL(I))).EQ.IHPZCOO(2)) THEN
                 XHPZCOO = XL(I)
C               write (user_nhstry,*) 'XHPZCOO TRUE ', XHPZCOO
               ELSE IF (IB(LIDSCC+2*(IDXL(I)-1)+1) .EQ. I2MPZ(1). AND.
     .                 IB(LIDSCC+2*(IDXL(I)-1)+2).EQ.I2MPZ(2)) THEN
                 X2MPZ = XL(I)
C               write (user_nhstry,*) 'X2MPZ TRUE ', XPZ
              ELSE IF (IB(LIDSCC+2*(IDXL(I)-1)+1) .EQ. I2MPZH(1). AND.
     .                 IB(LIDSCC+2*(IDXL(I)-1)+2).EQ.I2MPZH(2)) THEN
                 X2MPZH = XL(I)
C               write (user_nhstry,*) 'XPZH TRUE ', XPZH
              ELSE IF (IB(LIDSCC+2*(IDXL(I)-1)+1) .EQ. I2MPZCOO(1). AND.
     .                 IB(LIDSCC+2*(IDXL(I)-1)+2).EQ.I2MPZCOO(2)) THEN
                 X2MPZCOO = XL(I)
C               write (user_nhstry,*) 'XPZH2 TRUE ', XPZH2
              ELSE IF (IB(LIDSCC+2*(IDXL(I)-1)+1) .EQ. IOOC2MPZ(1). AND.
     .                 IB(LIDSCC+2*(IDXL(I)-1)+2).EQ.IOOC2MPZ(2)) THEN
                 XOOC2MPZ = XL(I)
C               write (user_nhstry,*) 'XPZCOO TRUE ', XPZCOO
              ELSE IF (IB(LIDSCC+2*(IDXL(I)-1)+1) .EQ. I2MPZCOO2(1). AND.
     .                 IB(LIDSCC+2*(IDXL(I)-1)+2).EQ.I2MPZCOO2(2)) THEN
                 X2MPZCOO2 = XL(I)
C               write (user_nhstry,*) 'XPZCOO2 TRUE ', XPZCOO2
              ELSE IF (IB(LIDSCC+2*(IDXL(I)-1)+1) .EQ. IH2MPZCOO(1). AND.
     .                 IB(LIDSCC+2*(IDXL(I)-1)+2).EQ.IH2MPZCOO(2)) THEN
                 XH2MPZCOO = XL(I)
C               write (user_nhstry,*) 'XHPZCOO TRUE ', XHPZCOO
              ELSE IF (IB(LIDSCC+2*(IDXL(I)-1)+1) .EQ. IOOC2MPZH(1). AND.
     .                 IB(LIDSCC+2*(IDXL(I)-1)+2).EQ.IOOC2MPZH(2)) THEN
                 XOOC2MPZH = XL(I)
C               write (user_nhstry,*) 'XHPZCOO TRUE ', XHPZCOO
              ENDIF
```

```
      END DO
C     ================================================================<
C
C
C     Property Function
C
            PROP(1) = (X2MPZCOO2)/(X2MPZCOO+XH2MPZCOO)
C
C       write (user_nhstry,*) ' '
C         write (user_nhstry,*) 'prop(1) ',prop(1)
C         write (user_nhstry,*) ' '

          ENDIF
C
C
================================================================================
C
================================================================================
C
      IF (idValue.EQ.71) THEN
C
C           PZ & 2MPZ NMR Data
C     Convert Mole fractions to total mole fractions
C
C                     X(1) = PZ
C                     X(2) = 2MPZ
C                     X(3) = CO2
C                     X(4) = H2O
C          X(5) = PZ/H2
C
      PZTOT = X(1)
          MPZTOT = X(2)
      CO2TOT = X(3)

C
C     Convert to SVEC components according to the SPECIES list
C
      XTEMP(1)=1D0-PZTOT-MPZTOT-CO2TOT
      XTEMP(2)=CO2TOT
C       XTEMP(3)=0D0
C       XTEMP(4)=0D0
C       XTEMP(5)=0D0
C       XTEMP(6)=0D0
      XTEMP(17)=PZTOT
          XTEMP(26)=MPZTOT
C
C
================================================================================
C
C     The following code calls the FLash subroutine.
C
                    TOTAL = 0D0
                    DO 222 I=1, NCOMP_NCC+9
                            SVEC(I) = 0D0
  222       CONTINUE
C
C                   NCP is the number of components specified in the DRS component list.
C
```

```
          DO 302 I = 1, NCP
                       SVEC(I) = XTEMP(I)
                       TOTAL = SVEC(I) + TOTAL
C
  302     CONTINUE
C
                       SVEC(17) = XTEMP(17)
C
                       TOTAL = SVEC(17) + TOTAL
                      SVEC(26)= XTEMP(26)
                      TOTAL = SVEC(26) + TOTAL
C
C
C          write (user_nhstry,*) ' '
C          write (user_nhstry,*) 'total ',total
           SVEC(NCOMP_NCC+1) = TOTAL
           svec(ncomp_ncc+2) = t
           svec(ncomp_ncc+3) = P
C
C                       do 98 i = 1, ncomp_ncc+9
C           write(user_nhstry,*) 'svec(ncomp_ncc) ' ,svec(i),i
C   98       continue

                      NSUBS = 1
                      IXTYPE = 1
                      KODE = 5
                      NPKODE = 2
                      MAXIT = 30
                      TOL = 1E-4
                      SPEC1 = T
                      SPEC2= 0.0001
                      GUESS = P
                      JRES= 0
                      KRESLT = 1
         KPHASE = 2
         idxsub(1) = 1
C
C
           CALL FLSH_FLASH (SVEC, NSUBS, IDXSUB, IXTYPE, NBOPST, KODE,
     +     NPKODE, KPHASE, MAXIT, TOL, SPEC1,SPEC2, GUESS, LMSG, LPMSG,
     +     JRES, KRESLT, RETN, IRETN, LCFLAG)

C
C
C          write (user_nhstry,*) ' '
C               write(user_nhstry,*) 'lcflag ',lcflag
C
C          do 99 i = 1, ncomp_ncc+9
C               write(user_nhstry,*) 'svec(ncomp_ncc) ' ,svec(i)
C   99     continue

C
C       GET CALCULATED PRESSURE
C
        PRES = PCALC

C          write (user_nhstry,*) 'PCALC, [Pa]', PCALC
C
```

```
C       GET VAPOR MOLE FRACTIONS
C
        DO I = 1, NCP
           YTEMP(I) = 0D0
        END DO

C          write (user_nhstry,*) ' '
        DO I = 1, NCPM
          YTEMP(i) = B(STWKWK_LRSTW+(STWORK_MY+I-1))
C
C          FIND CO2
C
          IF (IB(FRMULA(1,I)).EQ.ICO2(1) .AND.
     .         IB(FRMULA(2,I)).EQ.ICO2(2)) THEN
            PPTEMP(I) = PRES*YTEMP(i)
C              write (user_nhstry,*) 'YTEMP-CO2, i', YTEMP(i), i
C              write (user_nhstry,*) 'PPTEMP-CO2,[Pa] ',PPTEMP(i), i
          ENDIF
        END DO
C
C       ================================================================>
C
C       The following code is to get true species.
C
        CALL PPSTUB_GETTRU ( NT, IDXT, XT, NL, IDXL, XL, NS, IDXS, XS,
     1                       S2TL, TL2AL )
C
C          write (user_nhstry,*) ' '
C          do 101 I = 1, NL
C               write(user_nhstry,*) 'XL ' ,XL(I), I, IDXL(I)
C   101    continue

C
C       The Following Code retrieves the liquid phase mole fractions
C
        XMEA = 0D0
        XH2O = 0D0
        XMEAH = 0D0
        XMEACOO = 0D0
        XCO2 = 0D0
        XCO3 = 0D0
        XHCO3 = 0D0
        XPZ = 0D0
        XPZH = 0D0
        XPZH2 = 0D0
        XPZCOO = 0D0
        XPZCOO2 = 0D0
        XHPZCOO = 0D0
             X2MPZ= 0D0
             X2MPZH= 0D0
             X2MPZCOO= 0D0
             XOOC2MPZ= 0D0
             X2MPZCOO2= 0D0
             XH2MPZCOO= 0D0
             XOOC2MPZH= 0D0
c
C          write (user_nhstry,*) 'XH2O TRUE ',XH2O
C
```

```
C       write (user_nhstry,*) ' '
      DO I = 1, NL
        IF (IB(FRMULA(1,IDXL(I))) .EQ. IMEA(1). AND.
     .      IB(FRMULA(2,IDXL(I))).EQ.IMEA(2)) THEN
          XMEA = XL(I)
C           write (user_nhstry,*) 'XMEA TRUE ',XMEA
        ELSE IF (IB(FRMULA(1,IDXL(I))) .EQ. IH2O(1). AND.
     .      IB(FRMULA(2,IDXL(I))).EQ.IH2O(2)) THEN
          XH2O = XL(I)*(18.01528/1000)
C           write (user_nhstry,*) 'XH2O TRUE ',XH2O
        ELSE IF (IB(FRMULA(1,IDXL(I))) .EQ. IMEAH(1). AND.
     .           IB(FRMULA(2,IDXL(I))).EQ.IMEAH(2)) THEN
          XMEAH = XL(I)
C           write (user_nhstry,*) 'XMEAH TRUE ', XMEAH
        ELSE IF (IB(FRMULA(1,IDXL(I))) .EQ. IMEACOO(1). AND.
     .           IB(FRMULA(2,IDXL(I))).EQ.IMEACOO(2)) THEN
          XMEACOO = XL(I)
C           write (user_nhstry,*) 'XMEACOO TRUE ', XMEACOO
        ELSE IF (IB(FRMULA(1,IDXL(I))) .EQ. ICO2(1). AND.
     .           IB(FRMULA(2,IDXL(I))).EQ.ICO2(2)) THEN
          XCO2 = XL(I)
C           write (user_nhstry,*) 'XCO2 TRUE ', XCO2
        ELSE IF (IB(FRMULA(1,IDXL(I))) .EQ. ICO3(1). AND.
     .           IB(FRMULA(2,IDXL(I))).EQ.ICO3(2)) THEN
          XCO3 = XL(I)
C           write (user_nhstry,*) 'XCO3 TRUE ', XCO3
        ELSE IF (IB(FRMULA(1,IDXL(I))) .EQ. IHCO3(1). AND.
     .           IB(FRMULA(2,IDXL(I))).EQ.IHCO3(2)) THEN
          XHCO3 = XL(I)
C           write (user_nhstry,*) 'XHCO3 TRUE ', XHCO3
                ELSE IF (IB(FRMULA(1,IDXL(I))) .EQ. IPZ(1). AND.
     .           IB(FRMULA(2,IDXL(I))).EQ.IPZ(2)) THEN
          XPZ = XL(I)
C           write (user_nhstry,*) 'XPZ TRUE ', XPZ
        ELSE IF (IB(FRMULA(1,IDXL(I))) .EQ. IPZH(1). AND.
     .           IB(FRMULA(2,IDXL(I))).EQ.IPZH(2)) THEN
          XPZH = XL(I)
C           write (user_nhstry,*) 'XPZH TRUE ', XPZH
        ELSE IF (IB(FRMULA(1,IDXL(I))) .EQ. IPZH2(1). AND.
     .           IB(FRMULA(2,IDXL(I))).EQ.IPZH2(2)) THEN
          XPZH2 = XL(I)
C           write (user_nhstry,*) 'XPZH2 TRUE ', XPZH2
        ELSE IF (IB(FRMULA(1,IDXL(I))) .EQ. IPZCOO(1). AND.
     .           IB(FRMULA(2,IDXL(I))).EQ.IPZCOO(2)) THEN
          XPZCOO = XL(I)
C           write (user_nhstry,*) 'XPZCOO TRUE ', XPZCOO
        ELSE IF (IB(FRMULA(1,IDXL(I))) .EQ. IPZCOO2(1). AND.
     .           IB(FRMULA(2,IDXL(I))).EQ.IPZCOO2(2)) THEN
          XPZCOO2 = XL(I)
C           write (user_nhstry,*) 'XPZCOO2 TRUE ', XPZCOO2
        ELSE IF (IB(FRMULA(1,IDXL(I))) .EQ. IHPZCOO(1). AND.
     .           IB(FRMULA(2,IDXL(I))).EQ.IHPZCOO(2)) THEN
          XHPZCOO = XL(I)
C           write (user_nhstry,*) 'XHPZCOO TRUE ', XHPZCOO
         ELSE IF (IB(LIDSCC+2*(IDXL(I)-1)+1) .EQ. I2MPZ(1). AND.
     .           IB(LIDSCC+2*(IDXL(I)-1)+2).EQ.I2MPZ(2)) THEN
          X2MPZ = XL(I)
C           write (user_nhstry,*) 'X2MPZ TRUE ', XPZ
```

```
          ELSE IF (IB(LIDSCC+2*(IDXL(I)-1)+1) .EQ. I2MPZH(1). AND.
     .                IB(LIDSCC+2*(IDXL(I)-1)+2).EQ.I2MPZH(2)) THEN
             X2MPZH = XL(I)
C               write (user_nhstry,*) 'XPZH TRUE ', XPZH
          ELSE IF (IB(LIDSCC+2*(IDXL(I)-1)+1) .EQ. I2MPZCOO(1). AND.
     .                IB(LIDSCC+2*(IDXL(I)-1)+2).EQ.I2MPZCOO(2)) THEN
             X2MPZCOO = XL(I)
C               write (user_nhstry,*) 'XPZH2 TRUE ', XPZH2
          ELSE IF (IB(LIDSCC+2*(IDXL(I)-1)+1) .EQ. IOOC2MPZ(1). AND.
     .                IB(LIDSCC+2*(IDXL(I)-1)+2).EQ.IOOC2MPZ(2)) THEN
             XOOC2MPZ = XL(I)
C               write (user_nhstry,*) 'XPZCOO TRUE ', XPZCOO
          ELSE IF (IB(LIDSCC+2*(IDXL(I)-1)+1) .EQ. I2MPZCOO2(1). AND.
     .                IB(LIDSCC+2*(IDXL(I)-1)+2).EQ.I2MPZCOO2(2)) THEN
             X2MPZCOO2 = XL(I)
C               write (user_nhstry,*) 'XPZCOO2 TRUE ', XPZCOO2
          ELSE IF (IB(LIDSCC+2*(IDXL(I)-1)+1) .EQ. IH2MPZCOO(1). AND.
     .                IB(LIDSCC+2*(IDXL(I)-1)+2).EQ.IH2MPZCOO(2)) THEN
             XH2MPZCOO = XL(I)
C               write (user_nhstry,*) 'XHPZCOO TRUE ', XHPZCOO
          ELSE IF (IB(LIDSCC+2*(IDXL(I)-1)+1) .EQ. IOOC2MPZH(1). AND.
     .                IB(LIDSCC+2*(IDXL(I)-1)+2).EQ.IOOC2MPZH(2)) THEN
             XOOC2MPZH = XL(I)
C               write (user_nhstry,*) 'XHPZCOO TRUE ', XHPZCOO
          ENDIF
        END DO
C       ======================================================================<
C
C
C       Property Function
C
              PROP(1) = (XPZCOO+XHPZCOO)/(X2MPZCOO+XH2MPZCOO)
C
C          write (user_nhstry,*) ' '
C            write (user_nhstry,*) 'prop(1) ',prop(1)
C            write (user_nhstry,*) ' '

             ENDIF
C            C
================================================================================
C
        IF (idValue.EQ.70) THEN
C
C             PZ & 2MPZ NMR Data
C       Convert Mole fractions to total mole fractions
C
C                       X(1) = PZ
C                       X(2) = 2MPZ
C                       X(3) = CO2
C                       X(4) = H2O
C            X(5) = H/PZCOO
C
        PZTOT = X(1)
            MPZTOT = X(2)
        CO2TOT = X(3)

C
C       Convert to SVEC components according to the SPECIES list
```

```
C
      XTEMP(1)=1D0-PZTOT-MPZTOT-CO2TOT
      XTEMP(2)=CO2TOT
C       XTEMP(3)=0D0
C       XTEMP(4)=0D0
C       XTEMP(5)=0D0
C       XTEMP(6)=0D0
      XTEMP(17)=PZTOT
          XTEMP(26)=MPZTOT
C
C
================================================================================
C
C      The following code calls the FLash subroutine.
C
                    TOTAL = 0D0
                    DO 223 I=1, NCOMP_NCC+9
                              SVEC(I) = 0D0
  223       CONTINUE
C
C                   NCP is the number of components specified in the DRS component list.
C
         DO 303 I = 1, NCP
                     SVEC(I) = XTEMP(I)
                     TOTAL = SVEC(I) + TOTAL
C
  303     CONTINUE
C
                     SVEC(17) = XTEMP(17)
C
                     TOTAL = SVEC(17) + TOTAL
                    SVEC(26)= XTEMP(26)
                    TOTAL = SVEC(26) + TOTAL
C
C
C          write (user_nhstry,*) ' '
C          write (user_nhstry,*) 'total ',total
           SVEC(NCOMP_NCC+1) = TOTAL
           svec(ncomp_ncc+2) = t
           svec(ncomp_ncc+3) = P
C
C                    do 98 i = 1, ncomp_ncc+9
C           write(user_nhstry,*) 'svec(ncomp_ncc) ' ,svec(i),i
C   98       continue

                    NSUBS = 1
                    IXTYPE = 1
                    KODE = 5
                    NPKODE = 2
                    MAXIT = 30
                    TOL = 1E-4
                    SPEC1 = T
                    SPEC2= 0.0001
                    GUESS = P
                    JRES= 0
                    KRESLT = 1
         KPHASE = 2
         idxsub(1) = 1
```

```
C
C
            CALL FLSH_FLASH (SVEC, NSUBS, IDXSUB, IXTYPE, NBOPST, KODE,
     +      NPKODE, KPHASE, MAXIT, TOL, SPEC1,SPEC2, GUESS, LMSG, LPMSG,
     +      JRES, KRESLT, RETN, IRETN, LCFLAG)

C
C
C           write (user_nhstry,*) ' '
C                write(user_nhstry,*) 'lcflag ',lcflag
C
C           do 99 i = 1, ncomp_ncc+9
C                write(user_nhstry,*) 'svec(ncomp_ncc) ' ,svec(i)
C   99      continue

C
C       GET CALCULATED PRESSURE
C
        PRES = PCALC

C           write (user_nhstry,*) 'PCALC, [Pa]', PCALC
C
C       GET VAPOR MOLE FRACTIONS
C
        DO I = 1, NCP
           YTEMP(I) = 0D0
        END DO

C           write (user_nhstry,*) ' '
        DO I = 1, NCPM
          YTEMP(i) = B(STWKWK_LRSTW+(STWORK_MY+I-1))
C
C           FIND CO2
C
          IF (IB(FRMULA(1,I)).EQ.ICO2(1) .AND.
     .          IB(FRMULA(2,I)).EQ.ICO2(2)) THEN
            PPTEMP(I) = PRES*YTEMP(i)
C               write (user_nhstry,*) 'YTEMP-CO2, i', YTEMP(i), i
C               write (user_nhstry,*) 'PPTEMP-CO2,[Pa] ',PPTEMP(i), i
          ENDIF
        END DO
C
C       ================================================================>
C
C       The following code is to get true species.
C
        CALL PPSTUB_GETTRU ( NT, IDXT, XT, NL, IDXL, XL, NS, IDXS, XS,
     1                       S2TL, TL2AL )
C
C           write (user_nhstry,*) ' '
C           do 101 I = 1, NL
C                write(user_nhstry,*) 'XL ' ,XL(I), I, IDXL(I)
C   101     continue

C
C       The Following Code retrieves the liquid phase mole fractions
C
        XMEA = 0D0
```

```
      XH2O = 0D0
      XMEAH = 0D0
      XMEACOO = 0D0
      XCO2 = 0D0
      XCO3 = 0D0
      XHCO3 = 0D0
      XPZ = 0D0
      XPZH = 0D0
      XPZH2 = 0D0
      XPZCOO = 0D0
      XPZCOO2 = 0D0
      XHPZCOO = 0D0
           X2MPZ= 0D0
           X2MPZH= 0D0
           X2MPZCOO= 0D0
           XOOC2MPZ= 0D0
           X2MPZCOO2= 0D0
           XH2MPZCOO= 0D0
           XOOC2MPZH= 0D0
c
C       write (user_nhstry,*) 'XH2O TRUE ',XH2O
C
C         write (user_nhstry,*) ' '
      DO I = 1, NL
         IF (IB(FRMULA(1,IDXL(I))) .EQ. IMEA(1). AND.
     .        IB(FRMULA(2,IDXL(I))).EQ.IMEA(2)) THEN
            XMEA = XL(I)
C              write (user_nhstry,*) 'XMEA TRUE ',XMEA
         ELSE IF (IB(FRMULA(1,IDXL(I))) .EQ. IH2O(1). AND.
     .        IB(FRMULA(2,IDXL(I))).EQ.IH2O(2)) THEN
            XH2O = XL(I)*(18.01528/1000)
C              write (user_nhstry,*) 'XH2O TRUE ',XH2O
         ELSE IF (IB(FRMULA(1,IDXL(I))) .EQ. IMEAH(1). AND.
     .              IB(FRMULA(2,IDXL(I))).EQ.IMEAH(2)) THEN
            XMEAH = XL(I)
C              write (user_nhstry,*) 'XMEAH TRUE ', XMEAH
         ELSE IF (IB(FRMULA(1,IDXL(I))) .EQ. IMEACOO(1). AND.
     .              IB(FRMULA(2,IDXL(I))).EQ.IMEACOO(2)) THEN
            XMEACOO = XL(I)
C              write (user_nhstry,*) 'XMEACOO TRUE ', XMEACOO
         ELSE IF (IB(FRMULA(1,IDXL(I))) .EQ. ICO2(1). AND.
     .              IB(FRMULA(2,IDXL(I))).EQ.ICO2(2)) THEN
            XCO2 = XL(I)
C              write (user_nhstry,*) 'XCO2 TRUE ', XCO2
         ELSE IF (IB(FRMULA(1,IDXL(I))) .EQ. ICO3(1). AND.
     .              IB(FRMULA(2,IDXL(I))).EQ.ICO3(2)) THEN
            XCO3 = XL(I)
C              write (user_nhstry,*) 'XCO3 TRUE ', XCO3
         ELSE IF (IB(FRMULA(1,IDXL(I))) .EQ. IHCO3(1). AND.
     .              IB(FRMULA(2,IDXL(I))).EQ.IHCO3(2)) THEN
            XHCO3 = XL(I)
C              write (user_nhstry,*) 'XHCO3 TRUE ', XHCO3
                    ELSE IF (IB(FRMULA(1,IDXL(I))) .EQ. IPZ(1). AND.
     .              IB(FRMULA(2,IDXL(I))).EQ.IPZ(2)) THEN
            XPZ = XL(I)
C              write (user_nhstry,*) 'XPZ TRUE ', XPZ
         ELSE IF (IB(FRMULA(1,IDXL(I))) .EQ. IPZH(1). AND.
     .              IB(FRMULA(2,IDXL(I))).EQ.IPZH(2)) THEN
```

```
            XPZH = XL(I)
C               write (user_nhstry,*) 'XPZH TRUE ', XPZH
          ELSE IF (IB(FRMULA(1,IDXL(I))) .EQ. IPZH2(1). AND.
     .               IB(FRMULA(2,IDXL(I))).EQ.IPZH2(2)) THEN
            XPZH2 = XL(I)
C               write (user_nhstry,*) 'XPZH2 TRUE ', XPZH2
          ELSE IF (IB(FRMULA(1,IDXL(I))) .EQ. IPZCOO(1). AND.
     .               IB(FRMULA(2,IDXL(I))).EQ.IPZCOO(2)) THEN
            XPZCOO = XL(I)
C               write (user_nhstry,*) 'XPZCOO TRUE ', XPZCOO
          ELSE IF (IB(FRMULA(1,IDXL(I))) .EQ. IPZCOO2(1). AND.
     .               IB(FRMULA(2,IDXL(I))).EQ.IPZCOO2(2)) THEN
            XPZCOO2 = XL(I)
C               write (user_nhstry,*) 'XPZCOO2 TRUE ', XPZCOO2
          ELSE IF (IB(FRMULA(1,IDXL(I))) .EQ. IHPZCOO(1). AND.
     .               IB(FRMULA(2,IDXL(I))).EQ.IHPZCOO(2)) THEN
            XHPZCOO = XL(I)
C               write (user_nhstry,*) 'XHPZCOO TRUE ', XHPZCOO
           ELSE IF (IB(LIDSCC+2*(IDXL(I)-1)+1) .EQ. I2MPZ(1). AND.
     .               IB(LIDSCC+2*(IDXL(I)-1)+2).EQ.I2MPZ(2)) THEN
            X2MPZ = XL(I)
C               write (user_nhstry,*) 'X2MPZ TRUE ', XPZ
          ELSE IF (IB(LIDSCC+2*(IDXL(I)-1)+1) .EQ. I2MPZH(1). AND.
     .               IB(LIDSCC+2*(IDXL(I)-1)+2).EQ.I2MPZH(2)) THEN
            X2MPZH = XL(I)
C               write (user_nhstry,*) 'XPZH TRUE ', XPZH
          ELSE IF (IB(LIDSCC+2*(IDXL(I)-1)+1) .EQ. I2MPZCOO(1). AND.
     .               IB(LIDSCC+2*(IDXL(I)-1)+2).EQ.I2MPZCOO(2)) THEN
            X2MPZCOO = XL(I)
C               write (user_nhstry,*) 'XPZH2 TRUE ', XPZH2
          ELSE IF (IB(LIDSCC+2*(IDXL(I)-1)+1) .EQ. IOOC2MPZ(1). AND.
     .               IB(LIDSCC+2*(IDXL(I)-1)+2).EQ.IOOC2MPZ(2)) THEN
            XOOC2MPZ = XL(I)
C               write (user_nhstry,*) 'XPZCOO TRUE ', XPZCOO
          ELSE IF (IB(LIDSCC+2*(IDXL(I)-1)+1) .EQ. I2MPZCOO2(1). AND.
     .               IB(LIDSCC+2*(IDXL(I)-1)+2).EQ.I2MPZCOO2(2)) THEN
            X2MPZCOO2 = XL(I)
C               write (user_nhstry,*) 'XPZCOO2 TRUE ', XPZCOO2
          ELSE IF (IB(LIDSCC+2*(IDXL(I)-1)+1) .EQ. IH2MPZCOO(1). AND.
     .               IB(LIDSCC+2*(IDXL(I)-1)+2).EQ.IH2MPZCOO(2)) THEN
            XH2MPZCOO = XL(I)
C               write (user_nhstry,*) 'XHPZCOO TRUE ', XHPZCOO
          ELSE IF (IB(LIDSCC+2*(IDXL(I)-1)+1) .EQ. IOOC2MPZH(1). AND.
     .               IB(LIDSCC+2*(IDXL(I)-1)+2).EQ.IOOC2MPZH(2)) THEN
            XOOC2MPZH = XL(I)
C               write (user_nhstry,*) 'XHPZCOO TRUE ', XHPZCOO
          ENDIF
        END DO
C     ================================================================<
C
C
C       Property Function
C
            PROP(1) = (XPZCOO2)/(X2MPZCOO+XH2MPZCOO)
C
C         write (user_nhstry,*) ' '
C          write (user_nhstry,*) 'prop(1) ',prop(1)
C          write (user_nhstry,*) ' '
```

```
            ENDIF
C       ================================================================<
C           C
            IF (idValue.EQ.20) THEN
C
C           DHabs Only Data
C
C       Convert to SVEC components according to the SPECIES list
C
C       X(1) = PZ
C       X(2) = CO2
C       X(3) = H2O
C
        XTEMP(1)=X(3)
        XTEMP(2)=X(2)
        XTEMP(3)=0D0
        XTEMP(17)=X(1)
C
C
================================================================================
C
C       The following code calls the FLash subroutine.
C
                        TOTAL = 0D0
                        DO 296 I=1, NCOMP_NCC+9
                                SVEC(I) = 0D0
  296           CONTINUE
C
            DO 340 I = 1, NCP
                        SVEC(I) = XTEMP(I)
                        TOTAL = SVEC(I) + TOTAL
C
  340       CONTINUE

                        SVEC(17) = XTEMP(17)

                        TOTAL = SVEC(17) + TOTAL

C
C           write (user_nhstry,*) ' '
C           write (user_nhstry,*) 'total ',total
            SVEC(NCOMP_NCC+1) = TOTAL
            svec(ncomp_ncc+2) = t
            svec(ncomp_ncc+3) = P
C
C                       do 92 i = 1, ncomp_ncc+9
C             write(user_nhstry,*) 'svec(ncomp_ncc) ' ,svec(i),i
C   92        continue
C
C           THE FOLLOWING DO LOOP FLASHES THE SAME STREAM TWICE AT T AND T+1
C           TO GET THE PARTIAL PRESSURE OF CO2 FOR DHABS CALCULATION.
C
          DO 230 z = 1,2
C
                        NSUBS = 1
                        IXTYPE = 1
                        KODE = 5
```

```
                    NPKODE = 2
                    MAXIT = 30
                    TOL = 1E-4
                    SPEC1 = T
                    SPEC2= 0.0001
                    GUESS = P
                    JRES= 0
                    KRESLT = 1
        KPHASE = 2
        idxsub(1) = 1
C
C
          CALL FLSH_FLASH (SVEC, NSUBS, IDXSUB, IXTYPE, NBOPST, KODE,
     +    NPKODE, KPHASE, MAXIT, TOL, SPEC1,SPEC2, GUESS, LMSG, LPMSG,
     +    JRES, KRESLT, RETN, IRETN, LCFLAG)

C
C
C         write (user_nhstry,*) ' '
C         write(user_nhstry,*) 'lcflag ',lcflag
C
C         do 97 i = 1, ncomp_ncc+9
C           write(user_nhstry,*) 'svec(ncomp_ncc) ' ,svec(i)
C 97      continue

C
C      GET CALCULATED PRESSURE
C
       PRES = PCALC

C        write (user_nhstry,*) 'PCALC, [Pa]', PCALC
C
C      GET VAPOR MOLE FRACTIONS
C
       DO I = 1, NCP
          YTEMP(I) = 0D0
       END DO

C        write (user_nhstry,*) ' '
       DO I = 1, NCPM
         YTEMP(i) = B(STWKWK_LRSTW+(STWORK_MY+I-1))
C
C         FIND CO2
C
         IF (IB(FRMULA(1,I)).EQ.ICO2(1) .AND.
     .        IB(FRMULA(2,I)).EQ.ICO2(2)) THEN
           PPTEMP(I) = PRES*YTEMP(i)
           ZTEMP(Z) = PPTEMP(I)
C            write (user_nhstry,*) 'YTEMP-CO2, i', YTEMP(i), i
C            write (user_nhstry,*) 'PPTEMP-CO2,[Pa] ',PPTEMP(i), i
C            write (user_nhstry,*) 'ZTEMP-CO2,[Pa] ',ZTEMP(Z), Z
         ENDIF
       END DO
C
       t = t + 0.10
C
  230 END DO
C
```

```
C       PUT T BACK TO WHERE IT WAS T-1

        t = t - 0.10
c
c       CALCULATE RECIPICAL TEMPERATURE DIFFERENCE

        RecT = (1/(T+0.10))-(1/(T))
C         write (user_nhstry,*) 'RecT ',RecT
C
C       CALCULATE -DHABS IN kJ/mol
C
        PROP(1) = -0.008314*(log(ZTEMP(2)/ZTEMP(1))/RecT)
C
C       PROP(1) = 1D0
C
C
C         write (user_nhstry,*) ' '
C            write (user_nhstry,*) 'prop(1) ',prop(1)
C            write (user_nhstry,*) ' '

                        ENDIF
C
C
================================================================================
C
                        IF (idValue.EQ.44) THEN
C
C               PZ Only NMR Data
C       Convert Mole fractions to total mole fractions
C
C                       X(1) = PZ
C                       X(2) = CO2
C                       X(3) = H/PZCOO
C                       X(4) = H2O
C
        PZTOT = X(1)
        CO2TOT = X(2)
C
C       Convert to SVEC components according to the SPECIES list
C
        XTEMP(1)=1D0-PZTOT-CO2TOT
        XTEMP(2)=CO2TOT
        XTEMP(3)=0D0
        XTEMP(4)=0D0
        XTEMP(5)=0D0
        XTEMP(6)=0D0
        XTEMP(17)=PZTOT
C
C
================================================================================
C
C       The following code calls the FLash subroutine.
C
                        TOTAL = 0D0
                        DO 279 I=1, NCOMP_NCC+9
                                SVEC(I) = 0D0
  279           CONTINUE
C
```

```
C                       NCP is the number of components specified in the DRS component list.
C
          DO 305 I = 1, NCP
                        SVEC(I) = XTEMP(I)
                        TOTAL = SVEC(I) + TOTAL
C
  305     CONTINUE
C
                        SVEC(17) = XTEMP(17)
C
                        TOTAL = SVEC(17) + TOTAL
C
C
C         write (user_nhstry,*) ' '
C         write (user_nhstry,*) 'total ',total
          SVEC(NCOMP_NCC+1) = TOTAL
          svec(ncomp_ncc+2) = t
          svec(ncomp_ncc+3) = P
C
C                       do 92 i = 1, ncomp_ncc+9
C          write(user_nhstry,*) 'svec(ncomp_ncc) ' ,svec(i),i
C   92      continue

                      NSUBS = 1
                      IXTYPE = 1
                      KODE = 5
                      NPKODE = 2
                      MAXIT = 30
                      TOL = 1E-4
                      SPEC1 = T
                      SPEC2= 0.0001
                      GUESS = P
                      JRES= 0
                      KRESLT = 1
        KPHASE = 2
        idxsub(1) = 1
C
C
          CALL FLSH_FLASH (SVEC, NSUBS, IDXSUB, IXTYPE, NBOPST, KODE,
     +    NPKODE, KPHASE, MAXIT, TOL, SPEC1,SPEC2, GUESS, LMSG, LPMSG,
     +    JRES, KRESLT, RETN, IRETN, LCFLAG)

C
C
C         write (user_nhstry,*) ' '
C              write(user_nhstry,*) 'lcflag ',lcflag
C
C         do 94 i = 1, ncomp_ncc+9
C              write(user_nhstry,*) 'svec(ncomp_ncc) ' ,svec(i)
C   94    continue

C
C      GET CALCULATED PRESSURE
C
       PRES = PCALC

C         write (user_nhstry,*) 'PCALC, [Pa]', PCALC
C
```

```
C       GET VAPOR MOLE FRACTIONS
C
        DO I = 1, NCP
           YTEMP(I) = 0D0
        END DO

C          write (user_nhstry,*) ' '
        DO I = 1, NCPM
          YTEMP(i) = B(STWKWK_LRSTW+(STWORK_MY+I-1))
C
C          FIND CO2
C
          IF (IB(FRMULA(1,I)).EQ.ICO2(1) .AND.
     .         IB(FRMULA(2,I)).EQ.ICO2(2)) THEN
            PPTEMP(I) = PRES*YTEMP(i)
C               write (user_nhstry,*) 'YTEMP-CO2, i', YTEMP(i), i
C               write (user_nhstry,*) 'PPTEMP-CO2,[Pa] ',PPTEMP(i), i
          ENDIF
        END DO
C
C       ================================================================>
C
C       The following code is to get true species.
C
        CALL PPSTUB_GETTRU ( NT, IDXT, XT, NL, IDXL, XL, NS, IDXS, XS,
     1                       S2TL, TL2AL )
C
C          write (user_nhstry,*) ' '
C          do 106 I = 1, NL
C               write(user_nhstry,*) 'XL ' ,XL(I), I, IDXL(I)
C   106    continue

C
C       The Following Code retrieves the liquid phase mole fractions
C
        XMEA = 0D0
        XH2O = 0D0
        XMEAH = 0D0
        XMEACOO = 0D0
        XCO2 = 0D0
        XCO3 = 0D0
        XHCO3 = 0D0
        XPZ = 0D0
        XPZH = 0D0
        XPZH2 = 0D0
        XPZCOO = 0D0
        XPZCOO2 = 0D0
        XHPZCOO = 0D0
c
C         write (user_nhstry,*) 'XH2O TRUE ',XH2O
C
C          write (user_nhstry,*) ' '
        DO I = 1, NL
           IF (IB(FRMULA(1,IDXL(I))) .EQ. IMEA(1). AND.
     .          IB(FRMULA(2,IDXL(I))).EQ.IMEA(2)) THEN
              XMEA = XL(I)
C                write (user_nhstry,*) 'XMEA TRUE ',XMEA
           ELSE IF (IB(FRMULA(1,IDXL(I))) .EQ. IH2O(1). AND.
```

```
     .          IB(FRMULA(2,IDXL(I))).EQ.IH2O(2)) THEN
                XH2O = XL(I)*(18.01528/1000)
C                  write (user_nhstry,*) 'XH2O TRUE ',XH2O
              ELSE IF (IB(FRMULA(1,IDXL(I))) .EQ. IMEAH(1). AND.
     .                 IB(FRMULA(2,IDXL(I))).EQ.IMEAH(2)) THEN
                XMEAH = XL(I)
C                  write (user_nhstry,*) 'XMEAH TRUE ', XMEAH
              ELSE IF (IB(FRMULA(1,IDXL(I))) .EQ. IMEACOO(1). AND.
     .                 IB(FRMULA(2,IDXL(I))).EQ.IMEACOO(2)) THEN
                XMEACOO = XL(I)
C                  write (user_nhstry,*) 'XMEACOO TRUE ', XMEACOO
              ELSE IF (IB(FRMULA(1,IDXL(I))) .EQ. ICO2(1). AND.
     .                 IB(FRMULA(2,IDXL(I))).EQ.ICO2(2)) THEN
                XCO2 = XL(I)
C                  write (user_nhstry,*) 'XCO2 TRUE ', XCO2
              ELSE IF (IB(FRMULA(1,IDXL(I))) .EQ. ICO3(1). AND.
     .                 IB(FRMULA(2,IDXL(I))).EQ.ICO3(2)) THEN
                XCO3 = XL(I)
C                  write (user_nhstry,*) 'XCO3 TRUE ', XCO3
              ELSE IF (IB(FRMULA(1,IDXL(I))) .EQ. IHCO3(1). AND.
     .                 IB(FRMULA(2,IDXL(I))).EQ.IHCO3(2)) THEN
                XHCO3 = XL(I)
C                  write (user_nhstry,*) 'XHCO3 TRUE ', XHCO3
                     ELSE IF (IB(FRMULA(1,IDXL(I))) .EQ. IPZ(1). AND.
     .                IB(FRMULA(2,IDXL(I))).EQ.IPZ(2)) THEN
                XPZ = XL(I)
C                  write (user_nhstry,*) 'XPZ TRUE ', XPZ
              ELSE IF (IB(FRMULA(1,IDXL(I))) .EQ. IPZH(1). AND.
     .                 IB(FRMULA(2,IDXL(I))).EQ.IPZH(2)) THEN
                XPZH = XL(I)
C                  write (user_nhstry,*) 'XPZH TRUE ', XPZH
              ELSE IF (IB(FRMULA(1,IDXL(I))) .EQ. IPZH2(1). AND.
     .                 IB(FRMULA(2,IDXL(I))).EQ.IPZH2(2)) THEN
                XPZH2 = XL(I)
C                  write (user_nhstry,*) 'XPZH2 TRUE ', XPZH2
              ELSE IF (IB(FRMULA(1,IDXL(I))) .EQ. IPZCOO(1). AND.
     .                 IB(FRMULA(2,IDXL(I))).EQ.IPZCOO(2)) THEN
                XPZCOO = XL(I)
C                  write (user_nhstry,*) 'XPZCOO TRUE ', XPZCOO
              ELSE IF (IB(FRMULA(1,IDXL(I))) .EQ. IPZCOO2(1). AND.
     .                 IB(FRMULA(2,IDXL(I))).EQ.IPZCOO2(2)) THEN
                XPZCOO2 = XL(I)
C                  write (user_nhstry,*) 'XPZCOO2 TRUE ', XPZCOO2
              ELSE IF (IB(FRMULA(1,IDXL(I))) .EQ. IHPZCOO(1). AND.
     .                 IB(FRMULA(2,IDXL(I))).EQ.IHPZCOO(2)) THEN
                XHPZCOO = XL(I)
C                  write (user_nhstry,*) 'XHPZCOO TRUE ', XHPZCOO
              ENDIF
            END DO
C     ==========================================================================<
C
C
C       Property Function
C
                PROP(1) = (XPZCOO +XHPZCOO)/XH2O
C
C           write (user_nhstry,*) ' '
C            write (user_nhstry,*) 'prop(1) ',prop(1)
```

```
C           write (user_nhstry,*) ' '

              ENDIF
C
C
C
================================================================================
C
                        IF (idValue.EQ.77) THEN
C
C             PZ Only NMR Data
C       Convert Mole fractions to total mole fractions
C
C                       X(1) = PZ/H
C                       X(2) = H/PZCOO
C                       X(3) = PZCOO2
C                       X(4) = CO3/HCO3
C                       X(5) = H2O
C
        PZTOT = X(1) + X(2) + X(3)
        CO2TOT = X(2) + 2*X(3) + X(4)
C
C       Convert to SVEC components according to the SPECIES list
C
        XTEMP(1)=1D0-PZTOT-CO2TOT
        XTEMP(2)=CO2TOT
        XTEMP(3)=0D0
        XTEMP(4)=0D0
        XTEMP(5)=0D0
        XTEMP(6)=0D0
        XTEMP(17)=PZTOT
C
C
================================================================================
C
C       The following code calls the FLash subroutine.
C
                        TOTAL = 0D0
                        DO 229 I=1, NCOMP_NCC+9
                                SVEC(I) = 0D0
  229           CONTINUE
C
C                       NCP is the number of components specified in the DRS component list.
C
            DO 307 I = 1, NCP
                         SVEC(I) = XTEMP(I)
                         TOTAL = SVEC(I) + TOTAL
C
  307       CONTINUE
C
                         SVEC(17) = XTEMP(17)
C
                         TOTAL = SVEC(17) + TOTAL
C
C
C           write (user_nhstry,*) ' '
C           write (user_nhstry,*) 'total ',total
              SVEC(NCOMP_NCC+1) = TOTAL
```

```
            svec(ncomp_ncc+2) = t
            svec(ncomp_ncc+3) = P
C
C                       do 97 i = 1, ncomp_ncc+9
C           write(user_nhstry,*) 'svec(ncomp_ncc) ' ,svec(i),i
C   97      continue

                        NSUBS = 1
                        IXTYPE = 1
                        KODE = 5
                        NPKODE = 2
                        MAXIT = 30
                        TOL = 1E-4
                        SPEC1 = T
                        SPEC2= 0.0001
                        GUESS = P
                        JRES= 0
                        KRESLT = 1
          KPHASE = 2
          idxsub(1) = 1
C
C
            CALL FLSH_FLASH (SVEC, NSUBS, IDXSUB, IXTYPE, NBOPST, KODE,
     +      NPKODE, KPHASE, MAXIT, TOL, SPEC1,SPEC2, GUESS, LMSG, LPMSG,
     +      JRES, KRESLT, RETN, IRETN, LCFLAG)

C
C           write (user_nhstry,*) ' '
C                write(user_nhstry,*) 'lcflag ',lcflag
C
C           do 97 i = 1, ncomp_ncc+9
C                write(user_nhstry,*) 'svec(ncomp_ncc) ' ,svec(i)
C   97      continue

C
C       GET CALCULATED PRESSURE
C
        PRES = PCALC

C           write (user_nhstry,*) 'PCALC, [Pa]', PCALC
C
C       GET VAPOR MOLE FRACTIONS
C
        DO I = 1, NCP
           YTEMP(I) = 0D0
        END DO

C           write (user_nhstry,*) ' '
        DO I = 1, NCPM
          YTEMP(i) = B(STWKWK_LRSTW+(STWORK_MY+I-1))
C
C         FIND CO2
C
          IF (IB(FRMULA(1,I)).EQ.ICO2(1) .AND.
     .        IB(FRMULA(2,I)).EQ.ICO2(2)) THEN
            PPTEMP(I) = PRES*YTEMP(i)
C               write (user_nhstry,*) 'YTEMP-CO2, i', YTEMP(i), i
C               write (user_nhstry,*) 'PPTEMP-CO2,[Pa] ',PPTEMP(i), i
```

```
          ENDIF
        END DO
C
C       ===============================================================>
C
C       The following code is to get true species.
C
        CALL PPSTUB_GETTRU ( NT, IDXT, XT, NL, IDXL, XL, NS, IDXS, XS,
     1                       S2TL, TL2AL )
C
C         write (user_nhstry,*) ' '
C         do 107 I = 1, NL
C              write(user_nhstry,*) 'XL ' ,XL(I), I, IDXL(I)
C   107    continue

C
C     The Following Code retrieves the liquid phase mole fractions
C
        XMEA = 0D0
        XH2O = 0D0
        XMEAH = 0D0
        XMEACOO = 0D0
        XCO2 = 0D0
        XCO3 = 0D0
        XHCO3 = 0D0
        XPZ = 0D0
        XPZH = 0D0
        XPZH2 = 0D0
        XPZCOO = 0D0
        XPZCOO2 = 0D0
        XHPZCOO = 0D0
c
C         write (user_nhstry,*) 'XH2O TRUE ',XH2O
C
C         write (user_nhstry,*) ' '
        DO I = 1, NL
           IF (IB(FRMULA(1,IDXL(I))) .EQ. IMEA(1). AND.
     .          IB(FRMULA(2,IDXL(I))).EQ.IMEA(2)) THEN
              XMEA = XL(I)
C                write (user_nhstry,*) 'XMEA TRUE ',XMEA
           ELSE IF (IB(FRMULA(1,IDXL(I))) .EQ. IH2O(1). AND.
     .          IB(FRMULA(2,IDXL(I))).EQ.IH2O(2)) THEN
              XH2O = XL(I)
C                write (user_nhstry,*) 'XH2O TRUE ',XH2O
           ELSE IF (IB(FRMULA(1,IDXL(I))) .EQ. IMEAH(1). AND.
     .                IB(FRMULA(2,IDXL(I))).EQ.IMEAH(2)) THEN
              XMEAH = XL(I)
C                write (user_nhstry,*) 'XMEAH TRUE ', XMEAH
           ELSE IF (IB(FRMULA(1,IDXL(I))) .EQ. IMEACOO(1). AND.
     .                IB(FRMULA(2,IDXL(I))).EQ.IMEACOO(2)) THEN
              XMEACOO = XL(I)
C                write (user_nhstry,*) 'XMEACOO TRUE ', XMEACOO
           ELSE IF (IB(FRMULA(1,IDXL(I))) .EQ. ICO2(1). AND.
     .                IB(FRMULA(2,IDXL(I))).EQ.ICO2(2)) THEN
              XCO2 = XL(I)
C                write (user_nhstry,*) 'XCO2 TRUE ', XCO2
           ELSE IF (IB(FRMULA(1,IDXL(I))) .EQ. ICO3(1). AND.
     .                IB(FRMULA(2,IDXL(I))).EQ.ICO3(2)) THEN
```

```
            XCO3 = XL(I)
C               write (user_nhstry,*) 'XCO3 TRUE ', XCO3
          ELSE IF (IB(FRMULA(1,IDXL(I))) .EQ. IHCO3(1). AND.
     .              IB(FRMULA(2,IDXL(I))).EQ.IHCO3(2)) THEN
            XHCO3 = XL(I)
C               write (user_nhstry,*) 'XHCO3 TRUE ', XHCO3
                    ELSE IF (IB(FRMULA(1,IDXL(I))) .EQ. IPZ(1). AND.
     .              IB(FRMULA(2,IDXL(I))).EQ.IPZ(2)) THEN
            XPZ = XL(I)
C               write (user_nhstry,*) 'XPZ TRUE ', XPZ
          ELSE IF (IB(FRMULA(1,IDXL(I))) .EQ. IPZH(1). AND.
     .              IB(FRMULA(2,IDXL(I))).EQ.IPZH(2)) THEN
            XPZH = XL(I)
C               write (user_nhstry,*) 'XPZH TRUE ', XPZH
          ELSE IF (IB(FRMULA(1,IDXL(I))) .EQ. IPZH2(1). AND.
     .              IB(FRMULA(2,IDXL(I))).EQ.IPZH2(2)) THEN
            XPZH2 = XL(I)
C               write (user_nhstry,*) 'XPZH2 TRUE ', XPZH2
          ELSE IF (IB(FRMULA(1,IDXL(I))) .EQ. IPZCOO(1). AND.
     .              IB(FRMULA(2,IDXL(I))).EQ.IPZCOO(2)) THEN
            XPZCOO = XL(I)
C               write (user_nhstry,*) 'XPZCOO TRUE ', XPZCOO
          ELSE IF (IB(FRMULA(1,IDXL(I))) .EQ. IPZCOO2(1). AND.
     .              IB(FRMULA(2,IDXL(I))).EQ.IPZCOO2(2)) THEN
            XPZCOO2 = XL(I)
C               write (user_nhstry,*) 'XPZCOO2 TRUE ', XPZCOO2
          ELSE IF (IB(FRMULA(1,IDXL(I))) .EQ. IHPZCOO(1). AND.
     .              IB(FRMULA(2,IDXL(I))).EQ.IHPZCOO(2)) THEN
            XHPZCOO = XL(I)
C               write (user_nhstry,*) 'XHPZCOO TRUE ', XHPZCOO
          ENDIF
        END DO
C       ================================================================<
C
C
C       Property Function
C
              PROP(1) = XCO2 + XCO3 + XHCO3
C
C           write (user_nhstry,*) ' '
C             write (user_nhstry,*) 'prop(1) ',prop(1)
C             write (user_nhstry,*) ' '

              ENDIF
C
        RETURN
#undef P_NPOFF1
        END
```

Appendix F: Detailed WWC data

Table F.1: Detailed WWC data for 8 m 2MPZ.

CO_2 Loading	T	P_{tot}	Q_{liquid}	Q_{gas}	$Q_{gas,wet}$	$P_{CO2,in,dry}$	$P_{CO2,in,wet}$	$P_{CO2,out,dry}$	$P_{CO2,out,wet}$	P_{CO2}*	$(P_{CO2}-P_{CO2}^{*})_{LM}$	N_{CO2}	k_l^0	k_g	K_g	k_g'	K_g/k_g'
mol/mol_{alk}	℃	psig	ml/s	StdL/min	StdL/min	Pa	Pa	Pa	Pa	Pa	Pa	$mol/s \cdot m^2$	m/s	$mol/s \cdot Pa \cdot m^2$	$mol/s \cdot Pa \cdot m^2$	$mol/s \cdot Pa \cdot m^2$	%
0.102	40	20	4	5.0	5.2	0	0	9	8	307	-303	-3.47E-5	2.70E-5	4.57E-6	3.69E-6	1.92E-5	19%
						5	5	11	11		-299	-2.50E-5					
						10	10	13	13		-296	-1.37E-5					
						20	19	17	16		-289	1.21E-5					
						25	24	19	18		-286	2.54E-5					
						30	29	22	21		-282	3.39E-5					
0.102	60	20	4	5.0	5.5	0	0	48	44	85	-60	-1.93E-4	4.35E-5	4.83E-6	3.16E-6	9.14E-6	35%
						30	27	62	57		-41	-1.30E-4					
						60	55	76	70		-22	-6.45E-5					
						120	110	105	96		17	6.05E-5					
						150	137	120	110		37	1.20E-4					
						180	165	136	125		57	1.77E-4					
0.102	80	40	4	5.0	5.7	0	0	305	267	592	-445	-7.81E-4	6.61E-5	3.21E-6	2.13E-6	6.33E-6	34%
						300	262	530	463		-214	-5.89E-4					
						600	525	670	586		-26	-1.79E-4					
						900	787	783	685		137	3.00E-4					
						1200	1049	920	804		319	7.17E-4					
						1500	1312	1060	927		503	1.13E-3					
0.102	100	40	4	5.0	6.8	0	0	1690	1236	2679	-1998	-4.33E-3	9.58E-5	3.76E-6	2.17E-6	5.13E-6	42%
						1500	1097	2510	1835		-1174	-2.59E-3					
						3000	2194	3300	2413		-365	-7.68E-4					
						4500	3291	4110	3006		454	9.99E-4					
						6000	4388	4910	3591		1269	2.79E-3					
						7500	5485	5740	4198		2097	4.51E-3					
0.154	40	20	4	5.0	5.2	0	0	21	20	42	-31	-8.36E-5	2.44E-5	4.57E-6	2.58E-6	5.92E-6	44%
						15	15	30	29		-19	-6.14E-5					
						30	29	35	34		-10	-2.02E-5					
						60	58	48	46		9	4.92E-5					
						75	73	62	60		24	5.37E-5					

						90	87	70	68		35	7.99E-5				
0.154	60	40	4	5.0	5.3	0	0	147	139	290	-213	-3.76E-4	3.91E-5	2.98E-6	1.87E-6	5.02E-6	37%
						100	95	215	204		-134	-2.94E-4					
						200	189	246	233		-77	-1.18E-4					
						400	379	358	339		67	1.08E-4					
						500	474	400	379		131	2.56E-4					
						600	568	453	429		201	3.76E-4					
0.154	80	40	4	5.0	5.7	0	0	945	826	1801	-1346	-2.42E-3	5.90E-5	3.21E-6	1.81E-6	4.15E-6	44%
						500	437	1240	1084		-1006	-1.90E-3					
						1000	874	1480	1294		-696	-1.23E-3					
						3000	2623	2550	2230		604	1.15E-3					
						3500	3060	2810	2457		925	1.77E-3					
						4000	3497	3140	2745		1284	2.20E-3					
0.154	100	40	4	5.0	6.8	0	0	3750	2742	7394	-5917	-9.61E-3	8.50E-5	3.76E-6	1.64E-6	2.91E-6	56%
						2500	1828	5300	3876		-4464	-7.17E-3					
						5000	3656	6900	5046		-2989	-4.87E-3					
						15000	10969	13500	9872		2993	3.84E-3					
						17500	12797	14700	10750		4299	7.17E-3					
						20000	14625	16100	11774		5687	9.99E-3					
0.203	40	20	4	5.0	5.2	0	0	45	44	122	-99	-1.82E-4	2.22E-5	4.57E-6	1.74E-6	2.81E-6	62%
						50	48	77	75		-60	-1.09E-4					
						100	97	107	104		-22	-2.83E-5					
						200	194	171	166		57	1.17E-4					
						250	242	207	201		98	1.74E-4					
						300	291	244	236		140	2.26E-4					
0.203	60	40	4	5.0	5.3	0	0	330	313	861	-693	-8.45E-4	3.54E-5	2.98E-6	1.35E-6	1.35E-10	100%
						300	284	560	530		-442	-6.66E-4					
						600	568	732	693		-224	-3.38E-4					
						1200	1137	1090	1032		219	2.82E-4					
						1500	1421	1275	1208		445	5.76E-4					
						1800	1705	1435	1359		656	9.35E-4					
0.203	80	40	4	5.0	5.7	0	0	1740	1521	4063	-3243	-4.46E-3	5.32E-5	3.21E-6	1.38E-6	2.42E-6	57%
						1500	1312	2680	2343		-2195	-3.02E-3					
						3000	2623	3590	3139		-1163	-1.51E-3					
						6000	5246	5550	4853		973	1.15E-3					
						7500	6558	6440	5631		1996	2.71E-3					
						9000	7869	7330	6409		3017	4.28E-3					
0.203	100	60	4	5.0	6.2	0	0	7700	6185	18648	-15348	-1.44E-2	7.64E-5	2.54E-6	9.41E-7	1.49E-6	63%
						5000	4016	11100	8916		-12016	-1.14E-2					

						10000	8032	14200	11406		-8822	-7.87E-3				
						30000	24097	28100	22571		4644	3.56E-3				
						35000	28113	31100	24980		7794	7.31E-3				
						40000	32129	34200	27470		10987	1.09E-2				
0.253	40	40	4	5.0	5.1	0	0	118	116	324	-262	-3.02E-4	2.01E-5	2.87E-6	1.17E-6	1.98E-6	59%
						100	98	190	186		-178	-2.30E-4					
						200	196	245	240		-104	-1.15E-4					
						400	392	365	358		49	8.96E-5					
						500	490	440	431		135	1.54E-4					
						600	588	508	498		216	2.36E-4					
0.253	60	40	4	5.0	5.3	0	0	780	739	2255	-1861	-2.00E-3	3.20E-5	2.98E-6	1.07E-6	1.67E-6	64%
						750	710	1310	1241		-1261	-1.43E-3					
						1500	1421	1780	1686		-693	-7.17E-4					
						2500	2368	2420	2292		68	2.05E-4					
						3250	3078	2970	2813		682	7.17E-4					
						4000	3789	3490	3306		1277	1.31E-3					
0.253	80	60	4	5.0	5.5	0	0	3650	3314	9715	-7943	-6.85E-3	4.81E-5	2.28E-6	8.57E-7	1.37E-6	62%
						4000	3632	6200	5630		-5018	-4.13E-3					
						8000	7264	8950	8127		-1989	-1.78E-3					
						16000	14528	14300	12984		3992	3.19E-3					
						20000	18160	16800	15254		6890	6.00E-3					
						24000	21792	19450	17661		9867	8.54E-3					
0.300	40	20	4	5.0	5.2	0	0	155	150	961	-884	-6.26E-4	1.83E-5	4.57E-6	7.44E-7	8.89E-7	84%
						300	291	420	407		-610	-4.84E-4					
						600	581	670	649		-344	-2.83E-4					
						1200	1163	1160	1124		182	1.61E-4					
						1500	1454	1415	1371		450	3.43E-4					
						1800	1744	1670	1618		719	5.25E-4					
0.300	60	40	4	5.0	5.3	0	0	1250	1184	4874	-4255	-3.20E-3	2.92E-5	2.98E-6	7.35E-7	9.76E-7	75%
						2000	1894	2700	2557		-2634	-1.79E-3					
						4000	3789	4300	4073		-936	-7.68E-4					
						8000	7577	7300	6914		2356	1.79E-3					
						10000	9471	8880	8411		4044	2.87E-3					
						12000	11366	10350	9803		5674	4.23E-3					
0.300	80	60	4	5.0	5.5	0	0	5700	5176	22060	-19357	-1.07E-2	4.39E-5	2.28E-6	5.57E-7	7.37E-7	76%
						10000	9080	13400	12167		-11367	-6.38E-3					
						20000	18160	20900	18977		-3476	-1.69E-3					
						30000	27240	29000	26332		4711	1.88E-3					
						40000	36320	36100	32779		12405	7.32E-3					

						50000	45400	43900	39861		20445	1.14E-2					
0.365	40	40	4	5.0	5.1	0	0	585	574	4732	-4439	-1.50E-3	1.61E-5	2.87E-6	3.28E-7	3.70E-7	89%
						1000	980	1480	1451		-3511	-1.23E-3					
						2000	1961	2300	2255		-2621	-7.68E-4					
						6000	5883	5800	5686		1049	5.12E-4					
						7000	6863	6750	6618		2006	6.40E-4					
						8000	7843	7670	7520		2947	8.45E-4					
0.365	60	60	4	5.0	5.2	0	0	2900	2788	22414	-20989	-5.44E-3	2.57E-5	2.16E-6	2.45E-7	2.76E-7	89%
						5000	4806	7150	6873		-16553	-4.03E-3					
						10000	9613	11400	10959		-12116	-2.62E-3					
						30000	28839	29200	28070		6032	1.50E-3					
						35000	33645	33600	32299		10544	2.62E-3					
						40000	38452	38100	36625		15106	3.56E-3					

Table F.2: Detailed WWC data for 4 m PZ / 4 m 2MPZ.

CO_2 Loading	**T**	**P_{tot}**	**Q_{liquid}**	**Q_{gas}**	**$Q_{gas,wet}$**	**$P_{CO2,in,dry}$**	**$P_{CO2,in,wet}$**	**$P_{CO2,out,dry}$**	**$P_{CO2,out,wet}$**	**P_{CO2}***	**$(P_{CO2}-P_{CO2}^{*})_{LM}$**	**N_{CO2}**	**k_l^0**	**k_g**	**K_g**	**k_g'**	**K_g/k_g'**
mol/mol_{alk}	℃	psig	ml/s	StdL/min	StdL/min	Pa	Pa	Pa	Pa	Pa	Pa	$mol/s \cdot m^2$	m/s	$mol/s \cdot Pa \cdot m^2$	$mol/s \cdot Pa \cdot m^2$	$mol/s \cdot Pa \cdot m^2$	%
0.158	40	20	4	5.0	5.2	0	0	13	13	22.5	-15	-5.33E-5	2.61E-5	4.57E-6	3.87E-6	2.53E-5	15%
						10	10	18	17		-8	-3.23E-5					
						20	19	23	22		-1	-1.21E-5					
						30	29	27	26		5	1.09E-5					
						40	39	29	28		10	4.64E-5					
						50	48	34	32		17	6.66E-5					
0.158	60	20	4	5.0	5.5	0	0	87	80	169	-125	-3.51E-4	4.05E-5	4.83E-6	2.73E-6	6.28E-6	43%
						80	73	126	115		-73	-1.86E-4					
						120	110	150	137		-44	-1.21E-4					
						240	220	214	196		38	1.05E-4					
						280	257	235	215		65	1.81E-4					
						320	293	259	237		94	2.46E-4					
0.158	80	40	4	5.0	5.7	0	0	595	520	1026	-735	-1.52E-3	5.94E-5	3.21E-6	2.11E-6	6.16E-6	34%
						500	437	850	743		-417	-8.96E-4					
						1000	874	1105	966		-99	-2.69E-4					
						1500	1312	1330	1163		202	4.35E-4					

						2000	1749	1560	1364		506	1.13E-3					
						2500	2186	1825	1596		830	1.73E-3					
0.158	100	40	4	5.0	6.8	0	0	2540	1857	4189	-3170	-6.51E-3	8.35E-5	3.76E-6	2.04E-6	4.46E-6	46%
						2000	1463	3600	2633		-2087	-4.10E-3					
						4000	2925	4820	3525		-932	-2.10E-3					
						6000	4388	5830	4263		126	4.35E-4					
						8000	5850	7070	5170		1291	2.38E-3					
						10000	7313	8070	5901		2348	4.94E-3					
0.232	40	20	4	5.0	5.2	0	0	53	51	111	-83	-2.14E-4	2.21E-5	4.57E-6	2.30E-6	4.63E-6	50%
						25	24	61	59		-68	-1.45E-4					
						50	48	76	74		-49	-1.05E-4					
						150	145	130	126		23	8.07E-5					
						175	170	149	144		45	1.05E-4					
						200	194	168	163		66	1.29E-4					
0.232	60	40	4	5.0	5.3	0	0	305	289	635	-476	-7.81E-4	3.25E-5	2.98E-6	1.71E-6	4.01E-6	43%
						200	189	440	417		-319	-6.15E-4					
						400	379	520	493		-194	-3.07E-4					
						800	758	735	696		88	1.66E-4					
						1000	947	836	792		226	4.20E-4					
						1200	1137	962	911		378	6.09E-4					
0.232	80	40	4	5.0	5.7	0	0	1650	1443	3632	-2850	-4.23E-3	4.57E-5	3.21E-6	1.50E-6	2.82E-6	53%
						1500	1312	2600	2273		-1797	-2.82E-3					
						3000	2623	3430	2999		-806	-1.10E-3					
						5000	4372	4680	4092		589	8.20E-4					
						6500	5683	5560	4861		1605	2.41E-3					
						8000	6995	6450	5640		2627	3.97E-3					
0.232	100	60	4	5.0	6.2	0	0	7350	5904	15746	-12564	-1.38E-2	6.16E-5	2.54E-6	1.10E-6	1.94E-6	57%
						5000	4016	10400	8354		-9395	-1.01E-2					
						10000	8032	13700	11004		-6108	-6.93E-3					
						25000	20081	22900	18394		3422	3.93E-3					
						30000	24097	26600	21366		6895	6.37E-3					
						35000	28113	28800	23133		9664	1.16E-2					
0.281	40	20	4	5.0	5.2	0	0	68	66	332	-298	-2.74E-4	1.94E-5	4.57E-6	1.36E-6	1.94E-6	70%
						100	97	168	163		-200	-2.74E-4					
						200	194	240	233		-118	-1.61E-4					
						400	388	382	370		46	7.27E-5					
						500	485	456	442		130	1.78E-4					
						600	581	530	514		214	2.83E-4					
0.281	60	40	4	5.0	5.3	0	0	750	710	2012	-1631	-1.92E-3	2.74E-5	2.98E-6	1.14E-6	1.85E-6	62%

						500	474	1035	980		-1268	-1.37E-3					
						1000	947	1390	1317		-867	-9.99E-4					
						2500	2368	2380	2254		295	3.07E-4					
						3000	2841	2700	2557		677	7.68E-4					
						3500	3315	3020	2860		1059	1.23E-3					
0.281	80	40	4	5.0	5.7	0	0	3060	2676	8583	-7162	-7.84E-3	3.70E-5	3.21E-6	1.07E-6	1.61E-6	67%
						3000	2623	5050	4415		-5010	-5.25E-3					
						6000	5246	7090	6199		-2834	-2.79E-3					
						12000	10492	11400	9968		1633	1.54E-3					
						15000	13115	13450	11760		3815	3.97E-3					
						18000	15738	15450	13509		5971	6.53E-3					
0.330	40	40	4	5.0	5.1	0	0	288	282	1010	-861	-7.37E-4	1.69E-5	2.87E-6	8.05E-7	1.12E-6	72%
						300	294	490	480		-618	-4.86E-4					
						600	588	700	686		-371	-2.56E-4					
						1500	1471	1365	1338		391	3.46E-4					
						1800	1765	1605	1574		655	4.99E-4					
						2100	2059	1820	1784		905	7.17E-4					
0.330	60	40	4	5.0	5.3	0	0	1420	1345	5388	-4683	-3.64E-3	2.26E-5	2.98E-6	7.69E-7	1.04E-6	74%
						1500	1421	2580	2444		-3430	-2.77E-3					
						3000	2841	3640	3448		-2230	-1.64E-3					
						8000	7577	7360	6971		1870	1.64E-3					
						9500	8998	8480	8032		3102	2.61E-3					
						11000	10418	9800	9282		4438	3.07E-3					
0.330	80	60	4	5.0	5.5	0	0	6250	5675	23950	-20985	-1.17E-2	2.91E-5	2.28E-6	5.57E-7	7.37E-7	76%
						5000	4540	10000	9080		-17039	-9.38E-3					
						10000	9080	13900	12621		-13019	-7.32E-3					
						30000	27240	29200	26513		2912	1.50E-3					
						35000	31780	33000	29964		6882	3.75E-3					
						40000	36320	36700	33323		10802	6.19E-3					
0.391	40	40	4	5.0	5.1	0	0	860	843	5440	-5007	-2.20E-3	1.40E-5	2.87E-6	3.73E-7	4.29E-7	87%
						2000	1961	2330	2284		-3315	-8.45E-4					
						4000	3922	4200	4118		-1418	-5.12E-4					
						8000	7843	7700	7549		2253	7.68E-4					
						10000	9804	9370	9187		4048	1.61E-3					
						12000	11765	11180	10961		5914	2.10E-3					
0.391	60	60	4	5.0	5.2	0	0	3800	3653	22831	-20952	-7.12E-3	1.74E-5	2.16E-6	2.50E-7	2.83E-7	88%
						5000	4806	7350	7065		-16870	-4.40E-3					
						10000	9613	11600	11151		-12433	-3.00E-3					
						30000	28839	29100	27974		5564	1.69E-3					

						35000	33645	33600	32299		10126	2.62E-3					
						40000	38452	38200	36721		14738	3.37E-3					

Table F.3: Detailed WWC data for 3.75 m PZ / 3.75 m 1-MPZ /0.5 m 1,4-DMPZ.

CO_2 Loading	T	P_{tot}	Q_{liquid}	Q_{gas}	$Q_{gas,wet}$	$P_{CO2,in,dry}$	$P_{CO2,in,wet}$	$P_{CO2,out,dry}$	$P_{CO2,out,wet}$	P_{CO2}*	$(P_{CO2}-P_{CO2}^{*})_{LM}$	N_{CO2}	k_l^0	k_g	K_g	k_g'	K_g/k_g'
mol/mol_{alk}	℃	psig	ml/s	StdL/min	StdL/min	Pa	Pa	Pa	Pa	Pa	Pa	mol/s·m^2	m/s	mol/s·Pa·m^2	mol/s·Pa·m^2	mol/s·Pa·m^2	%
0.209	40	20	4	5.0	5.2	4	4	116	112	307	-245	-4.51E-4	-	4.57E-6	1.61E-6	2.48E-6	65%
						60	58	139	134		-209	-3.15E-4					
						111	108	170	164		-170	-2.31E-4					
						359	347	343	330		31	7.21E-5					
						461	447	418	403		116	1.84E-4					
						512	497	456	440		159	2.36E-4					
0.209	60	20	4	5.0	5.5	17	15	630	569	1713	-1403	-2.44E-3	-	4.83E-6	1.67E-6	2.55E-6	65%
						674	618	1070	957		-915	-1.49E-3					
						1318	1208	1480	1346		-432	-6.06E-4					
						2026	1857	1985	1809		119	2.10E-4					
						2703	2478	2450	2240		639	1.04E-3					
						3375	3094	2920	2666		1154	1.88E-3					
0.209	80	40	4	5.0	5.7	0	0	3256	2847	7966	-6438	-8.34E-3	-	3.21E-6	1.24E-6	2.01E-6	62%
						3393	2967	5298	4632		-4110	-4.88E-3					
						6711	5868	7434	6500		-1763	-1.85E-3					
						16326	14275	13839	12101		5145	6.37E-3					
						19493	17044	15972	13965		7432	9.02E-3					
						22622	19780	17968	15710		9636	1.19E-2					
0.209	100	60	4	5.0	6.2	51	41	11579	9301	29161	-24195	-2.16E-2	-	2.54E-6	8.65E-7	1.31E-6	66%
						11894	9554	19173	15400		-16512	-1.36E-2					
						22038	17701	26259	21092		-9666	-7.91E-3					
						42324	33996	40638	32641		4121	3.16E-3					
											#DIV/0!	0.00E+0					
											#DIV/0!	0.00E+0					
0.249	40	20	4	5.0	5.2	55	53	227	220	840	-700	-6.94E-4	-	4.57E-6	9.73E-7	1.24E-6	79%
						289	280	404	391		-502	-4.62E-4					
						617	598	677	656		-212	-2.41E-4					

						1308	1268	1208	1171		377	4.05E-4				
						1679	1627	1511	1464		703	6.79E-4				
						2047	1984	1805	1749		1022	9.80E-4				
0.249	60	30	4	5.0	5.4	62	58	1075	1006	3795	-3240	-3.18E-3	-	3.69E-6	1.07E-6	1.50E-6	71%
						1325	1239	2135	1997		-2155	-2.54E-3					
						2681	2507	3080	2881		-1090	-1.25E-3					
						6655	6225	5957	5571		2086	2.19E-3					
						8042	7521	6942	6493		3185	3.45E-3					
						9336	8732	7887	7377		4223	4.54E-3					
0.249	80	40	4	5.0	5.7	38	33	4963	4339	16816	-14524	-1.26E-2	-	3.21E-6	8.37E-7	1.13E-6	74%
						5618	4912	8946	7822		-10381	-8.52E-3					
						11085	9692	12930	11305		-6283	-4.73E-3					
						32161	28121	29055	25404		9884	7.96E-3					
						37176	32505	32757	28642		13666	1.13E-2					
						42379	37054	36559	31966		17571	1.49E-2					
0.290	40	40	4	5.0	5.1	26	26	582	570	2121	-1809	-1.42E-3	-	2.87E-6	6.94E-7	9.15E-7	76%
						698	684	999	979		-1284	-7.71E-4					
						1365	1338	1526	1496		-701	-4.13E-4					
						4125	4044	3655	3583		1682	1.20E-3					
						4811	4717	4210	4128		2289	1.54E-3					
						5490	5382	4719	4627		2867	1.97E-3					
0.290	60	40	4	5.0	5.3	38	36	2588	2451	9926	-8626	-6.53E-3	-	2.98E-6	6.76E-7	8.74E-7	77%
						3431	3250	4849	4593		-5980	-3.63E-3					
						6862	6499	7526	7128		-3102	-1.70E-3					
						19908	18855	17775	16836		7876	5.46E-3					
						23075	21855	20267	19196		10543	7.19E-3					
						26053	24676	22713	21512		13105	8.55E-3					
0.320	40	40	4	5.0	5.1	226	222	950	931	4480	-3893	-1.85E-3	-	2.87E-6	4.68E-7	5.59E-7	84%
						1961	1922	2386	2339		-2343	-1.09E-3					
						3997	3918	4099	4019		-510	-2.61E-4					
						9313	9131	8494	8328		4237	2.10E-3					
						11273	11053	10158	9959		6009	2.86E-3					
						13309	13049	11916	11683		7866	3.57E-3					
0.320	60		4	5.0	5.4	185	173	2850	2665	18984	-17535	-2.54E-2	-	3.69E-6	4.46E-7	5.08E-7	88%
						5669	5302	7394	6916		-12858	-1.64E-2					
						11030	10317	12087	11305		-8163	-1.01E-2					
						31551	29510	30104	28157		9834	1.38E-2					
						36973	34581	35021	32755		14665	1.86E-2					
						41841	39135	39112	36582		18846	2.60E-2					

Table F.4: Detailed WWC data for 5 m PZ / 5 m MDEA.

CO_2 Loading	T	P_{tot}	Q_{liquid}	Q_{gas}	$Q_{gas,wet}$	$P_{CO2,in,dry}$	$P_{CO2,in,wet}$	$P_{CO2,out,dry}$	$P_{CO2,out,wet}$	P_{CO2}*	$(P_{CO2}-P_{CO2}^{*})_{LM}$	N_{CO2}	k_l^0	k_g	K_g	k_g'	K_g/k_g'
mol/mol$_{alk}$	℃	psig	ml/s	StdL/min	StdL/min	Pa	Pa	Pa	Pa	Pa	Pa	mol/s·m^2	m/s	mol/s·Pa·m^2	mol/s·Pa·m^2	mol/s·Pa·m^2	%
0.18	40	20	4	5.0	5.2	0	0	64	62	237	-204	-2.58E-4	2.67E-5	4.57E-6	1.37E-6	1.96E-6	70%
						50	48	107	104		-159	-2.30E-4					
						100	97	145	141		-117	-1.82E-4					
						300	291	280	271		43	8.07E-5					
						350	339	318	308		86	1.29E-4					
						400	388	360	349		130	1.61E-4					
0.18	60	40	4	5.0	5.3	0	0	555	526	1447	-1164	-1.42E-3	4.02E-5	2.98E-6	1.26E-6	2.18E-6	58%
						500	474	910	862		-763	-1.05E-3					
						1000	947	1190	1127		-403	-4.87E-4					
						2000	1894	1806	1711		347	4.97E-4					
						2500	2368	2150	2036		743	8.96E-4					
						3000	2841	2450	2320		1114	1.41E-3					
0.18	80	40	4	5.0	5.7	0	0	2500	2186	6731	-5567	-6.40E-3	-	3.21E-6	1.09E-6	1.65E-6	66%
						2500	2186	4100	3585		-3803	-4.10E-3					
						5000	4372	5750	5028		-2014	-1.92E-3					
						10000	8744	9200	8044		1638	2.05E-3					
						12500	10929	10970	9592		3487	3.92E-3					
						15000	13115	12850	11235		5390	5.51E-3					
0.18	100	60	4	5.0	6.2	0	0	9050	7269	26717	-22890	-1.70E-2	-	2.54E-6	6.72E-7	9.14E-7	74%
						10000	8032	15900	12771		-16200	-1.11E-2					
						20000	16064	22400	17992		-9657	-4.50E-3					
						40000	32129	37650	30241		4401	4.40E-3					
						50000	40161	46200	37109		11853	7.12E-3					
						60000	48193	53700	43133		18833	1.18E-2					
0.23	40	20	4	5.0	5.2	0	0	175	170	641	-552	-7.06E-4	2.60E-5	4.57E-6	1.19E-6	1.61E-6	74%
						250	242	340	330		-353	-3.63E-4					
						500	485	535	518		-139	-1.41E-4					
						1500	1454	1310	1270		717	7.67E-4					
						1750	1696	1480	1434		918	1.09E-3					
						2000	1938	1655	1604		1122	1.39E-3					
0.23	60	40	4	5.0	5.3	0	0	1200	1137	3698	-3095	-3.07E-3	3.92E-5	2.98E-6	9.04E-7	1.30E-6	70%

						1000	947	1720	1629		-2394	-1.84E-3					
						2000	1894	2520	2387		-1544	-1.33E-3					
						5000	4736	4720	4470		899	7.17E-4					
						6000	5683	5470	5181		1722	1.36E-3					
						7000	6630	6060	5740		2460	2.41E-3					
0.23	80	60	4	5.0	5.5	0	0	5100	4631	16942	-14504	-9.57E-3	-	2.28E-6	6.37E-7	8.84E-7	72%
						6000	5448	9250	8399		-9946	-6.10E-3					
						12000	10896	13650	12394		-5261	-3.10E-3					
						24000	21792	22450	20384		4106	2.91E-3					
						30000	27240	27400	24879		9066	4.88E-3					
						36000	32688	31200	28329		13449	9.00E-3					
0.28	40	40	4	5.0	5.1	0	0	700	686	2163	-1798	-1.79E-3	2.51E-5	2.87E-6	8.36E-7	1.18E-6	71%
						500	490	950	931		-1441	-1.15E-3					
						1000	980	1220	1196		-1071	-5.63E-4					
						2500	2451	2410	2363		241	2.30E-4					
						3000	2941	2820	2765		686	4.61E-4					
						3500	3431	3150	3088		1088	8.96E-4					
0.28	60	40	4	5.0	5.3	0	0	2050	1942	8769	-7758	-5.25E-3	3.82E-5	2.98E-6	6.45E-7	8.23E-7	78%
						3000	2841	4200	3978		-5339	-3.07E-3					
						6000	5683	6670	6317		-2757	-1.72E-3					
						15000	14207	13850	13118		4873	2.94E-3					
						18000	17048	16300	15438		7445	4.35E-3					
						21000	19890	18350	17380		9812	6.79E-3					
0.33	40	40	4	5.0	5.1	0	0	650	637	3158	-2827	-1.66E-3	2.43E-5	2.87E-6	4.90E-7	5.91E-7	83%
						1000	980	1300	1275		-2027	-7.68E-4					
						2000	1961	2140	2098		-1127	-3.58E-4					
						6000	5883	5590	5481		2518	1.05E-3					
						7000	6863	6420	6294		3413	1.49E-3					
						8000	7843	7100	6961		4229	2.30E-3					
0.33	40	40	4	5.0	5.1	0	0	580	569	3542	-3249	-1.49E-3	2.43E-5	2.87E-6	5.21E-7	6.37E-7	82%
						1000	980	1650	1618		-2228	-1.66E-3					
						2000	1961	2260	2216		-1450	-6.66E-4					
						6000	5883	5350	5245		2005	1.66E-3					
						7000	6863	6420	6294		3028	1.49E-3					
						8000	7843	7320	7177		3959	1.74E-3					
0.33	40	60	4	5.0	5.2	0	0	3830	3682	18253	-16343	-7.18E-3	3.65E-5	2.16E-6	3.89E-7	4.74E-7	82%
						3000	2884	5680	5460		-14042	-5.02E-3					
						6000	5768	8050	7738		-11472	-3.84E-3					
						21000	20187	20800	19995		1836	3.75E-4					

						24000	23071	23100	22206		4371	1.69E-3					
						27000	25955	25500	24513		6956	2.81E-3					
0.37	40	40	4	5.0	5.1	0	0	960	941	6592	-6109	-2.46E-3	2.31E-5	2.87E-6	3.59E-7	4.10E-7	87%
						1500	1471	2100	2059		-4821	-1.54E-3					
						3000	2941	3450	3382		-3425	-1.15E-3					
						8500	8334	8210	8049		1595	7.43E-4					
						10000	9804	9600	9412		3012	1.02E-3					
						11500	11275	10930	10716		4398	1.46E-3					
0.37	60	60	4	5.0	5.2	0	0	4400	4230	28209	-26037	-8.25E-3	3.49E-5	2.16E-6	3.01E-7	3.50E-7	86%
						10000	9613	12600	12112		-17316	-4.87E-3					
						20000	19226	21250	20427		-8368	-2.34E-3					
						50000	48064	47100	45277		18426	5.44E-3					
						60000	57677	55500	53352		27248	8.43E-3					
						70000	67290	64300	61811		36273	1.07E-2					

Table F.5: Detailed WWC data for 2 m PZ / 7 m MDEA.

CO_2 Loading	**T**	**P_{tot}**	**Q_{liquid}**	**Q_{gas}**	**$Q_{gas,wet}$**	**$P_{CO2,in,dry}$**	**$P_{CO2,in,wet}$**	**$P_{CO2,out,dry}$**	**$P_{CO2,out,wet}$**	**P_{CO2}***	**$(P_{CO2}-P_{CO2}^{*})_{LM}$**	**N_{CO2}**	**k_l^0**	**k_g**	**K_g**	**k_g'**	**K_g/k_g'**
mol/mol_{alk}	℃	psig	ml/s	StdL/min	StdL/min	Pa	Pa	Pa	Pa	Pa	Pa	$mol/s \cdot m^2$	m/s	$mol/s \cdot Pa \cdot m^2$	$mol/s \cdot Pa \cdot m^2$	$mol/s \cdot Pa \cdot m^2$	%
0.027	80	20	4	4.5	5.6	0	0	525	421	1273	-1048	-1.91E-3	-	4.98E-6	1.78E-6	2.77E-6	64%
						800	642	1050	842		-525	-9.08E-4					
						1600	1283	1700	1363		37	-3.63E-4					
						2400	1925	2150	1724		545	9.08E-4					
						3200	2566	2625	2105		1046	2.09E-3					
						4000	3208	3250	2606		1615	2.72E-3					
0.027	100	20	4	3.0	5.2	0	0	2500	1441	5212	-4453	-6.05E-3	-	4.70E-6	1.21E-6	1.63E-6	74%
						3000	1729	4350	2507		-3077	-3.27E-3					
						6000	3458	6660	3839		-1556	-1.60E-3					
						9000	5188	8920	5141		-44	1.94E-4					
						12000	6917	11100	6398		1430	2.18E-3					
						15000	8646	13700	7897		3044	3.15E-3					
0.093	40	20	4	5.0	5.2	0	0	40	39	189	-169	-1.61E-4	3.55E-5	4.57E-6	1.21E-6	1.65E-6	74%
						50	48	96	93		-117	-1.86E-4					
						100	97	127	123		-78	-1.09E-4					

						300	291	268	260		85	1.29E-4					
						350	339	313	303		131	1.49E-4					
						400	388	348	337		172	2.10E-4					
0.093	60	40	4	5.0	5.3	0	0	425	403	1247	-1033	-1.09E-3	-	2.98E-6	1.08E-6	1.69E-6	64%
						500	474	772	731		-636	-6.97E-4					
						1000	947	1110	1051		-244	-2.82E-4					
						1500	1421	1445	1369		146	1.41E-4					
						2000	1894	1770	1676		531	5.89E-4					
						2500	2368	2110	1998		924	9.99E-4					
0.093	80	40	4	5.0	5.7	0	0	1705	1491	5623	-4839	-4.37E-3	-	3.21E-6	8.89E-7	1.23E-6	72%
						2000	1749	3120	2728		-3361	-2.87E-3					
						4000	3497	4660	4074		-1822	-1.69E-3					
						7000	6120	6825	5967		416	4.48E-4					
						9000	7869	8350	7301		1948	1.66E-3					
						11000	9618	9800	8569		3444	3.07E-3					
0.093	100	60	4	5.0	6.2	0	0	5800	4659	19779	-17346	-1.09E-2	-	2.54E-6	5.84E-7	7.58E-7	77%
						10000	8032	13000	10442		-10496	-5.62E-3					
						20000	16064	20700	16627		-3426	-1.31E-3					
						30000	24097	28900	23213		3859	2.06E-3					
						40000	32129	36600	29398		10928	6.37E-3					
						50000	40161	44500	35743		18083	1.03E-2					
0.166	40	40	4	5.0	5.1	0	0	245	240	953	-827	-6.27E-4	-	2.87E-6	7.56E-7	1.03E-6	74%
						400	392	555	544		-481	-3.97E-4					
						800	784	835	819		-151	-8.96E-5					
						1200	1177	1135	1113		190	1.66E-4					
						1600	1569	1440	1412		533	4.10E-4					
						2000	1961	1750	1716		880	6.40E-4					
0.166	60	40	4	5.0	5.3	0	0	1140	1080	4411	-3846	-2.92E-3	-	2.98E-6	7.38E-7	9.81E-7	75%
						2000	1894	2600	2463		-2220	-1.54E-3					
						4000	3789	4145	3926		-551	-3.71E-4					
						6000	5683	5700	5399		1124	7.68E-4					
						8000	7577	7200	6819		2770	2.05E-3					
						10000	9471	8725	8264		4429	3.27E-3					
0.166	80	60	4	5.0	5.5	0	0	4325	3927	17638	-15592	-8.11E-3	-	2.28E-6	5.23E-7	6.79E-7	77%
						5000	4540	8050	7309		-11659	-5.72E-3					
						10000	9080	12100	10987		-7565	-3.94E-3					
						30000	27240	28000	25424		8662	3.75E-3					
						40000	36320	35600	32325		16604	8.25E-3					
						50000	45400	42800	38862		24347	1.35E-2					

0.237	40	40	4	5.0	5.1	0	0	520	510	2839	-2576	-1.33E-3	-	2.87E-6	5.01E-7	6.07E-7	83%
						1000	980	1320	1294		-1697	-8.19E-4					
						2000	1961	2150	2108		-802	-3.84E-4					
						4000	3922	3800	3726		981	5.12E-4					
						5000	4902	4640	4549		1881	9.22E-4					
						6000	5883	5460	5353		2770	1.38E-3					
0.237	60	40	4	5.0	5.3	0	0	2375	2249	13493	-12334	-6.08E-3	-	2.98E-6	4.58E-7	5.41E-7	85%
						6000	5683	7070	6696		-7292	-2.74E-3					
						12000	11366	12350	11697		-1957	-8.96E-4					
						18000	17048	17400	16480		3263	1.54E-3					
						24000	22731	22600	21405		8558	3.59E-3					
						30000	28414	27500	26046		13703	6.40E-3					
0.273	60	60	4	5.0	5.2	0	0	3600	3461	19590	-17804	-6.75E-3	-	2.16E-6	3.71E-7	4.48E-7	83%
						10000	9613	11500	11055		-9237	-2.81E-3					
						20000	19226	20200	19418		-256	-3.75E-4					
						30000	28839	28600	27493		8558	2.62E-3					
						40000	38452	36500	35087		17124	6.56E-3					
						50000	48064	44800	43066		25895	9.75E-3					
0.286	40	40	4	5.0	5.1	0	0	850	833	5261	-4832	-2.18E-3	-	2.87E-6	4.10E-7	4.78E-7	86%
						2000	1961	2475	2427		-3061	-1.22E-3					
						4000	3922	4150	4069		-1264	-3.84E-4					
						9000	8824	8425	8260		3273	1.47E-3					
						12000	11765	11025	10809		6013	2.50E-3					
						15000	14706	13650	13383		8767	3.46E-3					

Table F.6: Detailed WWC data for 8 m N-methylpiperazine.

CO_2 Loading	**T**	**P_{tot}**	**Q_{liquid}**	**Q_{gas}**	**$Q_{gas,wet}$**	**$P_{CO2,in,dry}$**	**$P_{CO2,in,wet}$**	**$P_{CO2,out,dry}$**	**$P_{CO2,out,wet}$**	**P_{CO2}***	**$(P_{CO2}-P_{CO2}^{*})_{LM}$**	**N_{CO2}**	**k_l^0**	**k_g**	**K_g**	**k_g'**	**K_g/k_g'**
mol/mol_{alk}	℃	psig	ml/s	StdL/min	StdL/min	Pa	Pa	Pa	Pa	Pa	Pa	$mol/s \cdot m^2$	m/s	$mol/s \cdot Pa \cdot m^2$	$mol/s \cdot Pa \cdot m^2$	$mol/s \cdot Pa \cdot m^2$	%
0.10	40	20	4	5.0	5.2	0	0	31	30	96	-80	-1.25E-4	-	4.57E-6	1.48E-6	2.19E-6	68%
						50	48	71	69		-36	-8.48E-5					
						100	97	95	92		-	2.02E-5					
						200	194	159	154		76	1.66E-4					
						250	242	208	202		125	1.70E-4					

						300	291	245	237		167	2.22E-4					
0.10	60	40	4	5.0	5.3	0	0	280	265	616	-471	-7.17E-4	-	2.98E-6	1.75E-6	4.24E-6	41%
						200	189	458	434		-287	-6.61E-4					
						400	379	513	486		-178	-2.89E-4					
						800	758	728	690		104	1.84E-4					
						1000	947	830	786		242	4.35E-4					
						1200	1137	933	884		380	6.84E-4					
0.10	80	40	4	5.0	5.7	0	0	1730	1513	3655	-2832	-4.43E-3	-	3.21E-6	1.55E-6	3.00E-6	52%
						1000	874	2300	2011		-2163	-3.33E-3					
						2000	1749	2930	2562		-1462	-2.38E-3					
						4000	3497	3980	3480		-166	5.12E-5					
						5000	4372	4700	4109		576	7.68E-4					
						6000	5246	5270	4608		1245	1.87E-3					
0.10	100	60	4	5.0	6.2	0	0	6200	4980	12836	-10143	-1.16E-2	-	2.54E-6	1.16E-6	2.14E-6	54%
						5000	4016	9200	7390		-6998	-7.87E-3					
						10000	8032	12400	9960		-3758	-4.50E-3					
						30000	24097	24800	19920		9012	9.74E-3					
						35000	28113	27950	22450		12228	1.32E-2					
						40000	32129	30000	24097		14918	1.87E-2					
0.15	40	20	4	5.0	5.2	0	0	90	87	346	-300	-3.63E-4	-	4.57E-6	1.49E-6	2.21E-6	67%
						100	97	189	183		-203	-3.59E-4					
						200	194	258	250		-122	-2.34E-4					
						600	581	526	510		197	2.99E-4					
						700	678	594	576		278	4.28E-4					
						800	775	665	644		360	5.45E-4					
0.15	60	40	4	5.0	5.3	0	0	840	796	2145	-1717	-2.15E-3	-	2.98E-6	1.25E-6	2.15E-6	58%
						500	474	1160	1099		-1335	-1.69E-3					
						1000	947	1470	1392		-958	-1.20E-3					
						3000	2841	2700	2557		542	7.68E-4					
						3500	3315	3060	2898		946	1.13E-3					
						4000	3789	3360	3182		1317	1.64E-3					
0.15	80	60	4	5.0	5.5	0	0	4300	3904	10095	-7984	-8.07E-3	-	2.28E-6	9.75E-7	1.70E-6	57%
						4000	3632	6500	5902		-5246	-4.69E-3					
						8000	7264	9070	8236		-2311	-2.01E-3					
						16000	14528	14390	13066		3653	3.02E-3					
						20000	18160	16850	15300		6531	5.91E-3					
						24000	21792	18900	17161		9188	9.57E-3					
0.15	100	60	4	5.0	6.8	0	0	11800	9478	33012	-28006	-2.43E-2	-	2.54E-6	7.42E-7	1.05E-6	71%
						10000	8032	18100	14538		-21563	-1.67E-2					

						20000	16064	24900	20000		-14893	-1.01E-2					
						60000	48193	56300	45221		13641	7.62E-3					
						70000	56226	62400	50121		20006	1.57E-2					
						80000	64258	68300	54860		26267	2.41E-2					
0.20	40	20	4	5.0	5.2	0	0	280	271	1321	-1180	-1.13E-3	-	4.57E-6	9.55E-7	1.21E-6	79%
						300	291	535	518		-912	-9.49E-4					
						600	581	740	717		-669	-5.65E-4					
						1500	1454	1460	1415		112	1.61E-4					
						1800	1744	1710	1657		378	3.63E-4					
						2100	2035	1960	1900		644	5.65E-4					
0.20	60	40	4	5.0	5.3	0	0	1800	1705	6413	-5517	-4.61E-3	-	2.98E-6	8.00E-7	1.09E-6	73%
						2500	2368	3550	3362		-3525	-2.69E-3					
						5000	4736	5360	5077		-1500	-9.22E-4					
						10000	9471	9250	8761		2688	1.92E-3					
						12500	11839	11080	10494		4722	3.64E-3					
						15000	14207	12840	12161		6719	5.53E-3					
0.20	80	60	4	5.0	5.5	0	0	6900	6265	25303	-22022	-1.29E-2	-	2.28E-6	5.52E-7	7.28E-7	76%
						10000	9080	13900	12621		-14380	-7.32E-3					
						20000	18160	21300	19340		-6535	-2.44E-3					
						40000	36320	37900	34413		10033	3.94E-3					
						50000	45400	44800	40678		17631	9.76E-3					
						60000	54480	52200	47397		25472	1.46E-2					
0.26	40	40	4	5.0	5.1	0	0	920	902	5547	-5083	-2.36E-3	-	2.87E-6	4.12E-7	4.81E-7	86%
						2000	1961	2480	2431		-3345	-1.23E-3					
						4000	3922	4180	4098		-1535	-4.61E-4					
						8000	7843	7620	7471		2105	9.73E-4					
						10000	9804	9400	9216		3956	1.54E-3					
						12000	11765	11100	10883		5766	2.30E-3					
0.26	60	60	4	5.0	5.2	0	0	4400	4230	22950	-20763	-8.25E-3	-	2.16E-6	3.35E-7	3.96E-7	84%
						5000	4806	7700	7402		-16812	-5.06E-3					
						10000	9613	11700	11247		-12502	-3.19E-3					
						35000	33645	33200	31915		9805	3.37E-3					
						40000	38452	37550	36096		14292	4.59E-3					
						45000	43258	41750	40134		18702	6.09E-3					

Table F.7: Detailed WWC data for 8 m 2-piperidineethanol.

CO_2 Loading	T	P_{tot}	Q_{liquid}	Q_{gas}	$Q_{gas,wet}$	$P_{CO2,in,dry}$	$P_{CO2,in,wet}$	$P_{CO2,out,dry}$	$P_{CO2,out,wet}$	P_{CO2}*	$(P_{CO2}-P_{CO2}^{*})_{LM}$	N_{CO2}	k_l^0	k_g	K_g	k_g'	K_g/k_g'
mol/mol_{alk}	℃	psig	ml/s	StdL/min	StdL/min	Pa	Pa	Pa	Pa	Pa	Pa	$mol/s \cdot m^2$	m/s	$mol/s \cdot Pa \cdot m^2$	$mol/s \cdot Pa \cdot m^2$	$mol/s \cdot Pa \cdot m^2$	%
0.205	40	40	4	5.0	5.1	0	0	45	44	120	-96	-1.15E-4	-	2.87E-6	1.23E-6	2.14E-6	57%
						40	39	70	69		-65	-7.68E-5					
						80	78	96	94		-33	-4.10E-5					
						120	118	123	121		#NUM!	-7.68E-6					
						160	157	146	143		29	3.58E-5					
						200	196	169	166		60	7.94E-5					
0.202	60	40	4	5.0	5.3	0	0	300	284	923	-772	-7.68E-4	-	2.98E-6	1.05E-6	1.61E-6	65%
						300	284	552	523		-510	-6.45E-4					
						600	568	698	661		-306	-2.51E-4					
						900	852	918	869		-62	-4.61E-5					
						1200	1137	1125	1066		176	1.92E-4					
						1500	1421	1337	1266		416	4.17E-4					
0.215	80	60	4	5.0	5.5	0	0	1690	1535	4908	-4093	-3.17E-3	-	2.28E-6	8.00E-7	1.23E-6	65%
						2000	1816	3090	2806		-2565	-2.04E-3					
						4000	3632	4520	4104		-1022	-9.76E-4					
						6000	5448	5820	5285		453	3.38E-4					
						8000	7264	7180	6519		1960	1.54E-3					
						10000	9080	8480	7700		3436	2.85E-3					
0.199	100	80	4	5.0	5.9	0	0	6550	5533	20933	-18025	-9.69E-3	-	1.92E-6	5.35E-7	7.42E-7	72%
						10000	8448	13600	11489		-10894	-5.33E-3					
						20000	16896	21500	18163		-3364	-2.22E-3					
						30000	25343	28700	24245		3835	1.92E-3					
						40000	33791	36200	30581		11176	5.62E-3					
						50000	42239	43100	36410		18237	1.02E-2					
0.360	40	40	4	5.0	5.1	0	0	117	115	454	-394	-3.00E-4	-	2.87E-6	7.31E-7	9.81E-7	75%
						150	147	226	222		-268	-1.95E-4					
						300	294	337	330		-141	-9.47E-5					
						450	441	451	442		-12	-2.56E-6					
						600	588	562	551		115	9.73E-5					
						750	735	686	673		249	1.64E-4					
0.367	60	60	4	5.0	5.2	0	0	990	952	3502	-3001	-1.86E-3	-	2.16E-6	5.99E-7	8.29E-7	72%
						1500	1442	2070	1990		-1772	-1.07E-3					
						3000	2884	3120	2999		-558	-2.25E-4					
						4500	4326	4280	4114		713	4.12E-4					
						6000	5768	5370	5162		1947	1.18E-3					
						7500	7210	6500	6248		3203	1.87E-3					

0.375	80	60	4	5.0	5.5	0	0	3850	3496	15368	-13545	-7.22E-3	-	2.28E-6	5.29E-7	6.88E-7	77%
						7000	6356	9150	8308		-7996	-4.03E-3					
						14000	12712	14600	13257		-2373	-1.13E-3					
						21000	19068	20170	18314		3309	1.56E-3					
						28000	25424	25750	23381		8996	4.22E-3					
						35000	31780	30700	27875		14371	8.07E-3					
0.360	100	80	4	5.0	5.9	0	0	14200	11996	61569	-55355	-2.10E-2	-	1.92E-6	3.46E-7	4.22E-7	82%
						20000	16896	28800	24330		-40844	-1.30E-2					
						40000	33791	45200	38184		-25518	-7.69E-3					
						60000	50687	62000	52376		-10014	-2.96E-3					
						80000	67582	78500	66315		5355	2.22E-3					
						100000	84478	95900	81014		21130	6.06E-3					
0.514	40	40	4	5.0	5.1	0	0	200	196	1531	-1431	-5.12E-4	-	2.87E-6	3.64E-7	4.17E-7	87%
						500	490	645	632		-968	-3.71E-4					
						1000	980	1070	1049		-516	-1.79E-4					
						1500	1471	1500	1471		#DIV/0!	0.00E+0					
						2000	1961	1940	1902		400	1.54E-4					
						2500	2451	2380	2333		860	3.07E-4					
0.524	60	60	4	5.0	5.2	0	0	1500	1442	8922	-8180	-2.81E-3	-	2.16E-6	3.49E-7	4.16E-7	84%
						3000	2884	4060	3903		-5513	-1.99E-3					
						6000	5768	6590	6335		-2861	-1.11E-3					
						9000	8652	8950	8604		-294	9.37E-5					
						12000	11535	11570	11122		2401	8.06E-4					
						15000	14419	14080	13535		5042	1.72E-3					
0.525	80	60	4	5.0	5.5	0	0	5900	5357	36111	-33361	-1.11E-2	-	2.28E-6	3.10E-7	3.59E-7	86%
						15000	13620	17900	16253		-21147	-5.44E-3					
						30000	27240	31300	28420		-8267	-2.44E-3					
						45000	40860	44400	40315		4471	1.13E-3					
						60000	54480	57600	52301		17256	4.50E-3					
						75000	68100	69800	63378		29565	9.76E-3					
0.684	40	60	4	5.0	5.1	0	0	550	542	5377	-5101	-1.03E-3	-	2.09E-6	1.75E-7	1.91E-7	92%
						2000	1971	2250	2218		-3281	-4.68E-4					
						4000	3943	4100	4041		-1384	-1.87E-4					
						6000	5914	5940	5855		507	1.12E-4					
						8000	7885	7750	7639		2383	4.68E-4					
						10000	9857	9650	9512		4305	6.56E-4					
0.695	60	80	4	5.0	5.2	0	0	2750	2666	25231	-23873	-4.07E-3	-	1.69E-6	1.43E-7	1.56E-7	92%
						10000	9695	11200	10858		-14947	-1.78E-3					
						20000	19389	20200	19583		-5744	-2.96E-4					

						30000	29084	29500	28599		3605	7.40E-4					
						40000	38779	38900	37712		13007	1.63E-3					
						50000	48473	48000	46534		22259	2.96E-3					
0.635	80	80	4	5.0	5.4	0	0	8600	7976	82091	-78035	-1.27E-2		1.76E-6	1.54E-7	1.69E-7	91%
						30000	27823	34800	32274		-52011	-7.10E-3					
						60000	55646	62400	57871		-25316	-3.55E-3					
						90000	83468	90200	83654		1468	-2.96E-4					
						100000	92743	100500	93206		10882	-7.39E-4					
						110000	102017	110600	102573		20203	-8.87E-4					

Table F.8: Detailed WWC data for 4.8 m AMP.

CO_2 Loading	**T**	**P_{tot}**	**Q_{liquid}**	**Q_{gas}**	**$Q_{gas,wet}$**	**$P_{CO2,in,dry}$**	**$P_{CO2,in,wet}$**	**$P_{CO2,out,dry}$**	**$P_{CO2,out,wet}$**	**P_{CO2}***	**$(P_{CO2}-P_{CO2}^{*})_{LM}$**	**N_{CO2}**	**k_l^0**	**k_g**	**K_g**	**k_g'**	**K_g/k_g'**
mol/mol_{alk}	℃	psig	ml/s	StdL/min	StdL/min	Pa	Pa	Pa	Pa	Pa	Pa	$mol/s \cdot m^2$	m/s	$mol/s \cdot Pa \cdot m^2$	$mol/s \cdot Pa \cdot m^2$	$mol/s \cdot Pa \cdot m^2$	%
0.150	40	40	4	5.0	5.1	0	0	27	26	139	-125	-6.91E-5	-	2.87E-6	5.61E-7	6.97E-7	80%
						60	59	75	74		-73	-3.84E-5					
						120	118	125	123		-19	-1.28E-5					
						180	176	172	169		33	2.05E-5					
						240	235	224	220		88	4.10E-5					
						300	294	267	262		138	8.45E-5					
0.150	60	40	4	5.0	5.3	0	0	210	199	977	-874	-5.38E-4	-	2.98E-6	6.23E-7	7.87E-7	79%
						500	474	610	578		-449	-2.82E-4					
						2000	1894	1800	1705		819	5.12E-4					
						3000	2841	2580	2444		1658	1.08E-3					
						4000	3789	3430	3249		2532	1.46E-3					
						5000	4736	4160	3940		3345	2.15E-3					
0.150	80	60	4	5.0	5.5	0	0	1160	1053	4849	-4301	-2.18E-3	-	2.28E-6	5.16E-7	6.66E-7	77%
						2000	1816	2730	2479		-2688	-1.37E-3					
						4000	3632	4330	3932		-1060	-6.19E-4					
						6000	5448	5880	5339		543	2.25E-4					
						8000	7264	7390	6710		2126	1.14E-3					
						10000	9080	8960	8136		3739	1.95E-3					
0.150	100	60	4	5.0	6.2	0	0	3700	2972	18525	-16996	-6.93E-3	-	2.54E-6	3.93E-7	4.65E-7	85%
						10000	8032	12000	9639		-9667	-3.75E-3					

						20000	16064	20300	16305		-2338	-5.62E-4					
						30000	24097	28900	23213		5117	2.06E-3					
						40000	32129	37400	30041		12531	4.87E-3					
						50000	40161	45900	36868		19944	7.68E-3					
0.285	40	40	4	5.0	5.1	0	0	80	78	524	-484	-2.05E-4	-	2.87E-6	4.12E-7	4.81E-7	86%
						150	147	204	200		-350	-1.38E-4					
						300	294	334	327		-213	-8.71E-5					
						450	441	461	452		-77	-2.82E-5					
						600	588	591	579		60	2.30E-5					
						750	735	719	705		196	7.94E-5					
0.294	60	60	4	5.0	5.2	0	0	805	774	3814	-3412	-1.51E-3	-	2.16E-6	4.43E-7	5.57E-7	79%
						1500	1442	1990	1913		-2128	-9.18E-4					
						3000	2884	3210	3086		-825	-3.94E-4					
						4500	4326	4390	4220		457	2.06E-4					
						6000	5768	5600	5383		1754	7.50E-4					
						7500	7210	6770	6508		3031	1.37E-3					
0.297	80	60	4	5.0	5.5	0	0	3100	2815	18147	-16700	-5.82E-3	-	2.28E-6	3.45E-7	4.07E-7	85%
						6000	5448	8150	7400		-11696	-4.03E-3					
						12000	10896	13250	12031		-6667	-2.35E-3					
						18000	16344	18200	16526		-1711	-3.75E-4					
						24000	21792	23400	21247		3365	1.13E-3					
						30000	27240	28500	25878		8393	2.81E-3					
0.296	100	60	4	5.0	6.2	0	0	8600	6908	63557	-60037	-1.61E-2	-	2.54E-6	2.68E-7	3.00E-7	89%
						20000	16064	26300	21125		-44915	-1.18E-2					
						40000	32129	44300	35583		-29668	-8.06E-3					
						60000	48193	62200	49960		-14462	-4.12E-3					
						70000	56226	71000	57029		-6922	-1.87E-3					
						80000	64258	79800	64097		617	3.75E-4					
0.449	40	40	4	5.0	5.1	0	0	190	186	2078	-1983	-4.86E-4	-	2.87E-6	2.14E-7	2.32E-7	93%
						1000	980	1080	1059		-1058	-2.05E-4					
						2000	1961	1990	1951		-122	2.56E-5					
						3000	2941	2920	2863		823	2.05E-4					
						4000	3922	3850	3775		1769	3.84E-4					
						5000	4902	4790	4696		2720	5.38E-4					
0.449	60	60	4	5.0	5.2	0	0	1550	1490	11744	-10982	-2.91E-3	-	2.16E-6	2.67E-7	3.04E-7	88%
						4000	3845	5050	4855		-7383	-1.97E-3					
						8000	7690	8600	8267		-3758	-1.12E-3					
						12000	11535	11950	11487		-232	9.37E-5					
						16000	15381	15550	14948		3416	8.43E-4					

						20000	19226	19000	18264		6990	1.87E-3					
0.449	80	60	4	5.0	5.5	0	0	5400	4903	50999	-48506	-1.01E-2	-	2.28E-6	1.99E-7	2.18E-7	91%
						25000	22700	27500	24970		-27148	-4.69E-3					
						50000	45400	50600	45945		-5322	-1.13E-3					
						65000	59020	64100	58202		7605	1.69E-3					
						75000	68100	73500	66738		16410	2.81E-3					
						85000	77180	82300	74728		24935	5.07E-3					
0.561	40	40	4	5.0	5.1	0	0	320	314	5405	-5247	-8.15E-4	-	2.87E-6	1.58E-7	1.67E-7	94%
						2000	1961	2180	2137		-3355	-4.58E-4					
						4000	3922	4130	4049		-1419	-3.31E-4					
						6000	5883	5980	5863		468	5.09E-5					
						8000	7843	7830	7677		2354	4.33E-4					
						10000	9804	9740	9549		4271	6.62E-4					
0.603	60	60	4	5.0	5.2	0	0	2450	2355	30215	-29021	-4.59E-3	-	2.16E-6	1.47E-7	1.58E-7	93%
						15000	14419	16000	15381		-15310	-1.87E-3					
						30000	28839	30000	28839		#DIV/0!	0.00E+0					
						45000	43258	44000	42297		12556	1.87E-3					
						60000	57677	57900	55659		26440	3.94E-3					
						75000	72097	71900	69117		40373	5.81E-3					

Table F.9: Detailed WWC data for 5 m PZ with 70% of the total alkalinity neutralized with H_2SO_4.

CO_2 Loading	T	P_{tot}	Q_{liquid}	Q_{gas}	$Q_{gas,wet}$	$P_{CO2,in,dry}$	$P_{CO2,in,wet}$	$P_{CO2,out,dry}$	$P_{CO2,out,wet}$	P_{CO2}*	$(P_{CO2}-P_{CO2}^*)_{LM}$	N_{CO2}	k_l^0	k_g	K_g	k_g'	K_g/k_g'
mol/mol$_{alk}$	℃	psig	ml/s	StdL/min	StdL/min	Pa	Pa	Pa	Pa	Pa	Pa	mol/s·m^2	m/s	mol/s·Pa·m^2	mol/s·Pa·m^2	mol/s·Pa·m^2	%
0.00	22	20	4	5.0	5.1	0	0	0	0	0	#DIV/0!	0.00E+0	-	4.46E-6	2.95E-7	3.16E-7	93%
						1000	990	957	957		973	1.34E-4					
						1500	1484	1400	1400		1442	3.42E-4					
						2000	1979	1835	1835		1906	5.89E-4					
						2500	2474	2306	2306		2389	6.84E-4					
						3000	2969	2780	2780		2873	7.70E-4					
-	40	20	4	5.0	5.2	0	0	11	11	128	-122	-4.68E-5	-	4.57E-6	2.69E-7	2.86E-7	94%
						500	485	463	463		346	9.04E-5					
						1000	969	910	910		811	2.47E-4					
						1500	1454	1375	1375		1286	3.27E-4					
						2000	1938	1818	1818		1749	5.02E-4					
						2500	2423	2285	2285		2225	5.73E-4					
-	60	20	4	5.0	5.5	0	0	26	26	692	-679	-1.16E-4	-	4.83E-6	2.07E-7	2.16E-7	96%
						500	458	474	474		-226	-7.02E-5					
						1000	917	909	909		221	3.24E-5					
						1500	1375	1344	1344		668	1.35E-4					
						2000	1833	1777	1777		1113	2.47E-4					
						2500	2292	2219	2219		1563	3.21E-4					
-	81	40	4	5.0	5.7	0	0	94	94	1678	-1631	-2.74E-4	-	3.21E-6	1.72E-7	1.82E-7	95%
						500	437	504	504		-1207	-1.96E-4					
						1000	874	927	927		-777	-1.56E-4					
						1500	1312	1332	1332		-356	-5.89E-5					
						3000	2623	2563	2563		915	1.75E-4					
						2500	2186	2162	2162		496	6.92E-5					
						15000	14419	16000	15381		-15310	-1.87E-3					
						30000	28839	30000	28839		#DIV/0!	0.00E+0					
						45000	43258	44000	42297		12556	1.87E-3					
						60000	57677	57900	55659		26440	3.94E-3					
						75000	72097	71900	69117		40373	5.81E-3					

Appendix G: Tabulated Model Predictions

G.1 Equilibrium CO_2 Partial Pressure and Speciation

The equilibrium CO_2 partial pressure, speciation and reaction stoichiometry for 8 m 2MPZ with variable temperature and loading as predicted from the ENRTL model presented in Chapter 7 is tabulated as follows.

Table G.1: Predictions for CO_2 solubility in 8 m 2MPZ.

Loading (mol/mol alk.)	P_{CO2}* (Pa)						
	40 ℃	60 ℃	80 ℃	100 ℃	120 ℃	140 ℃	160 ℃
0.025	1.26187	10.0221	60.2893	289.0939	1151.484	3938.047	11872.02
0.050	3.86872	30.4227	181.1668	859.1482	3378.233	11389.43	33796.05
0.075	7.71288	60.0694	354.6301	1667.139	6496.964	21698.34	63751.28
0.100	13.4154	103.0741	601.4065	2797.448	10798.9	35773.11	104395.9
0.125	22.2093	167.1523	957.7968	4386.029	16723.02	54941.07	159669
0.150	36.3062	265.1632	1479.607	6624.964	24846.76	80904.21	234709.8
0.175	59.8425	419.4329	2256.63	9803.723	36001.89	116016.5	336561.5
0.200	101.1748	671.1465	3439.372	14364.43	51384.71	163613.7	475007.2
0.225	178.6097	1099.047	5276.534	20959.01	72642.74	228127.5	662986.3
0.250	334.5791	1851.482	8150.31	30452.74	101822.5	315094.6	916894.8
0.275	665.1638	3177.718	12562.53	43838.82	141257.3	430909.8	1257353
0.300	1346.923	5393.932	19018.38	62112.52	193564.9	583816.2	1711840
0.325	2575.669	8745.597	27919.48	86336.53	262170.8	785240	2320542
0.350	4438.394	13359.84	39705.64	118142.7	352688	1053852	3149032
0.375	6967.652	19463.16	55332.16	160820.5	475744.6	1423391	4314575
0.400	10375.84	27802.97	77153.2	221585.9	653196.1	1959768	6048587
0.425	15424.78	40486.36	111124.3	317629.5	934838.6	2804064	8881396
0.450	24616.69	64064.46	175120.2	498599.4	1454270	4298974	14544500
0.475	50271.64	129953.4	350833.2	969508.5	2670175	7441195	14884160
0.500	401200	799567.1	1578570	3145622	6560098	17072820	15135910

Table G.2: Predictions for speciation in 8 m 2MPZ at 40 °C.

Loading	Mole Fraction										
(mol/mol alk.)	2MPZ	2MPZCOO$^-$	H2MPZCOO	2MPZ(COO$^-$)$_2$	2MPZH$^+$	HCO_3^-	CO_3^{2-}	CO_2	H^+	OH^-	H_2O
0.000	1.26E-1	0.00E+0	0.00E+0	0.00E+0	8.33E-5	0.00E+0	0.00E+0	0.00E+0	4.66E-15	8.33E-5	8.74E-1
0.005	1.23E-1	1.18E-3	2.46E-7	1.39E-7	1.34E-3	9.07E-6	6.90E-5	2.17E-10	3.95E-14	1.58E-5	8.74E-1
0.010	1.21E-1	2.40E-3	9.93E-7	6.66E-7	2.63E-3	1.87E-5	1.00E-4	7.27E-10	7.98E-14	9.89E-6	8.74E-1
0.015	1.18E-1	3.61E-3	2.36E-6	1.69E-6	3.91E-3	2.87E-5	1.30E-4	1.44E-9	1.23E-13	7.74E-6	8.74E-1
0.020	1.16E-1	4.83E-3	4.49E-6	3.29E-6	5.20E-3	3.90E-5	1.60E-4	2.32E-9	1.69E-13	6.63E-6	8.74E-1
0.025	1.13E-1	6.04E-3	7.60E-6	5.56E-6	6.49E-3	4.97E-5	1.91E-4	3.33E-9	2.17E-13	5.95E-6	8.74E-1
0.030	1.11E-1	7.24E-3	1.19E-5	8.56E-6	7.78E-3	6.07E-5	2.24E-4	4.46E-9	2.69E-13	5.50E-6	8.74E-1
0.035	1.08E-1	8.45E-3	1.76E-5	1.24E-5	9.06E-3	7.22E-5	2.57E-4	5.71E-9	3.25E-13	5.17E-6	8.74E-1
0.040	1.06E-1	9.64E-3	2.51E-5	1.71E-5	1.03E-2	8.41E-5	2.93E-4	7.06E-9	3.84E-13	4.93E-6	8.74E-1
0.045	1.03E-1	1.08E-2	3.47E-5	2.28E-5	1.16E-2	9.65E-5	3.29E-4	8.51E-9	4.47E-13	4.74E-6	8.74E-1
0.050	1.01E-1	1.20E-2	4.68E-5	2.95E-5	1.29E-2	1.09E-4	3.67E-4	1.01E-8	5.14E-13	4.59E-6	8.74E-1
0.055	9.85E-2	1.32E-2	6.17E-5	3.74E-5	1.42E-2	1.23E-4	4.07E-4	1.18E-8	5.85E-13	4.47E-6	8.73E-1
0.060	9.60E-2	1.44E-2	7.99E-5	4.65E-5	1.55E-2	1.37E-4	4.47E-4	1.35E-8	6.61E-13	4.36E-6	8.73E-1
0.065	9.35E-2	1.55E-2	1.02E-4	5.70E-5	1.68E-2	1.52E-4	4.89E-4	1.55E-8	7.42E-13	4.27E-6	8.73E-1
0.070	9.11E-2	1.67E-2	1.29E-4	6.88E-5	1.80E-2	1.67E-4	5.32E-4	1.75E-8	8.29E-13	4.19E-6	8.73E-1
0.075	8.86E-2	1.78E-2	1.60E-4	8.21E-5	1.93E-2	1.83E-4	5.77E-4	1.98E-8	9.21E-13	4.11E-6	8.73E-1
0.080	8.61E-2	1.89E-2	1.98E-4	9.70E-5	2.06E-2	2.00E-4	6.22E-4	2.21E-8	1.02E-12	4.04E-6	8.73E-1
0.085	8.37E-2	2.01E-2	2.41E-4	1.14E-4	2.18E-2	2.18E-4	6.68E-4	2.47E-8	1.12E-12	3.97E-6	8.73E-1
0.090	8.13E-2	2.12E-2	2.92E-4	1.32E-4	2.31E-2	2.37E-4	7.15E-4	2.75E-8	1.23E-12	3.91E-6	8.73E-1

0.095	7.89E-2	2.23E-2	3.51E-4	1.52E-4	2.43E-2	2.56E-4	7.63E-4	3.05E-8	1.35E-12	3.84E-6	8.73E-1
0.100	7.64E-2	2.33E-2	4.19E-4	1.75E-4	2.56E-2	2.77E-4	8.11E-4	3.38E-8	1.48E-12	3.78E-6	8.73E-1
0.105	7.41E-2	2.44E-2	4.97E-4	1.99E-4	2.68E-2	2.99E-4	8.59E-4	3.73E-8	1.61E-12	3.71E-6	8.73E-1
0.110	7.17E-2	2.54E-2	5.86E-4	2.26E-4	2.80E-2	3.22E-4	9.08E-4	4.11E-8	1.76E-12	3.65E-6	8.73E-1
0.115	6.93E-2	2.65E-2	6.86E-4	2.55E-4	2.92E-2	3.47E-4	9.57E-4	4.53E-8	1.91E-12	3.58E-6	8.73E-1
0.120	6.70E-2	2.75E-2	7.99E-4	2.86E-4	3.04E-2	3.73E-4	1.01E-3	4.99E-8	2.07E-12	3.51E-6	8.73E-1
0.125	6.46E-2	2.85E-2	9.26E-4	3.20E-4	3.16E-2	4.01E-4	1.05E-3	5.49E-8	2.24E-12	3.44E-6	8.73E-1
0.130	6.23E-2	2.94E-2	1.07E-3	3.56E-4	3.28E-2	4.30E-4	1.10E-3	6.03E-8	2.43E-12	3.36E-6	8.72E-1
0.135	6.00E-2	3.04E-2	1.23E-3	3.96E-4	3.39E-2	4.62E-4	1.15E-3	6.63E-8	2.62E-12	3.29E-6	8.72E-1
0.140	5.78E-2	3.13E-2	1.40E-3	4.38E-4	3.51E-2	4.95E-4	1.20E-3	7.29E-8	2.83E-12	3.21E-6	8.72E-1
0.145	5.55E-2	3.22E-2	1.60E-3	4.82E-4	3.62E-2	5.31E-4	1.25E-3	8.01E-8	3.05E-12	3.13E-6	8.72E-1
0.150	5.33E-2	3.31E-2	1.81E-3	5.30E-4	3.73E-2	5.70E-4	1.29E-3	8.80E-8	3.29E-12	3.05E-6	8.72E-1
0.155	5.11E-2	3.39E-2	2.04E-3	5.81E-4	3.84E-2	6.11E-4	1.34E-3	9.68E-8	3.54E-12	2.97E-6	8.72E-1
0.160	4.89E-2	3.47E-2	2.30E-3	6.35E-4	3.94E-2	6.55E-4	1.38E-3	1.06E-7	3.80E-12	2.88E-6	8.72E-1
0.165	4.68E-2	3.55E-2	2.57E-3	6.93E-4	4.04E-2	7.03E-4	1.43E-3	1.17E-7	4.09E-12	2.80E-6	8.72E-1
0.170	4.47E-2	3.62E-2	2.87E-3	7.54E-4	4.14E-2	7.54E-4	1.47E-3	1.29E-7	4.39E-12	2.71E-6	8.72E-1
0.175	4.26E-2	3.69E-2	3.20E-3	8.18E-4	4.24E-2	8.09E-4	1.51E-3	1.42E-7	4.72E-12	2.62E-6	8.72E-1
0.180	4.06E-2	3.76E-2	3.55E-3	8.86E-4	4.34E-2	8.69E-4	1.55E-3	1.57E-7	5.06E-12	2.53E-6	8.72E-1
0.185	3.86E-2	3.82E-2	3.92E-3	9.57E-4	4.43E-2	9.34E-4	1.59E-3	1.74E-7	5.43E-12	2.44E-6	8.72E-1
0.190	3.66E-2	3.88E-2	4.32E-3	1.03E-3	4.52E-2	1.01E-3	1.63E-3	1.92E-7	5.83E-12	2.35E-6	8.71E-1
0.195	3.47E-2	3.94E-2	4.75E-3	1.11E-3	4.60E-2	1.08E-3	1.66E-3	2.13E-7	6.25E-12	2.26E-6	8.71E-1
0.200	3.28E-2	3.99E-2	5.21E-3	1.19E-3	4.69E-2	1.17E-3	1.70E-3	2.36E-7	6.71E-12	2.16E-6	8.71E-1
0.205	3.09E-2	4.04E-2	5.70E-3	1.28E-3	4.77E-2	1.26E-3	1.73E-3	2.63E-7	7.20E-12	2.07E-6	8.71E-1
0.210	2.91E-2	4.08E-2	6.22E-3	1.37E-3	4.84E-2	1.36E-3	1.76E-3	2.93E-7	7.73E-12	1.98E-6	8.71E-1
0.215	2.73E-2	4.12E-2	6.77E-3	1.47E-3	4.92E-2	1.47E-3	1.79E-3	3.27E-7	8.30E-12	1.89E-6	8.71E-1

0.220	2.56E-2	4.15E-2	7.35E-3	1.57E-3	4.99E-2	1.59E-3	1.82E-3	3.65E-7	8.91E-12	1.80E-6	8.71E-1
0.225	2.40E-2	4.18E-2	7.96E-3	1.67E-3	5.06E-2	1.73E-3	1.84E-3	4.10E-7	9.58E-12	1.70E-6	8.70E-1
0.230	2.23E-2	4.20E-2	8.61E-3	1.78E-3	5.12E-2	1.88E-3	1.87E-3	4.60E-7	1.03E-11	1.61E-6	8.70E-1
0.235	2.08E-2	4.22E-2	9.29E-3	1.89E-3	5.18E-2	2.04E-3	1.89E-3	5.19E-7	1.11E-11	1.52E-6	8.70E-1
0.240	1.93E-2	4.23E-2	1.00E-2	2.01E-3	5.24E-2	2.22E-3	1.90E-3	5.86E-7	1.19E-11	1.44E-6	8.70E-1
0.245	1.78E-2	4.24E-2	1.07E-2	2.13E-3	5.29E-2	2.43E-3	1.92E-3	6.64E-7	1.29E-11	1.35E-6	8.70E-1
0.250	1.64E-2	4.24E-2	1.15E-2	2.26E-3	5.34E-2	2.66E-3	1.93E-3	7.54E-7	1.39E-11	1.27E-6	8.69E-1
0.255	1.51E-2	4.23E-2	1.23E-2	2.38E-3	5.38E-2	2.91E-3	1.95E-3	8.58E-7	1.50E-11	1.18E-6	8.69E-1
0.260	1.39E-2	4.21E-2	1.32E-2	2.51E-3	5.43E-2	3.19E-3	1.95E-3	9.80E-7	1.62E-11	1.11E-6	8.69E-1
0.265	1.27E-2	4.19E-2	1.41E-2	2.65E-3	5.46E-2	3.51E-3	1.96E-3	1.12E-6	1.75E-11	1.03E-6	8.69E-1
0.270	1.16E-2	4.16E-2	1.50E-2	2.78E-3	5.50E-2	3.86E-3	1.96E-3	1.28E-6	1.89E-11	9.55E-7	8.68E-1
0.275	1.05E-2	4.13E-2	1.60E-2	2.91E-3	5.53E-2	4.25E-3	1.96E-3	1.47E-6	2.05E-11	8.85E-7	8.68E-1
0.280	9.56E-3	4.09E-2	1.69E-2	3.05E-3	5.56E-2	4.68E-3	1.96E-3	1.69E-6	2.21E-11	8.19E-7	8.67E-1
0.285	8.67E-3	4.04E-2	1.80E-2	3.17E-3	5.58E-2	5.16E-3	1.95E-3	1.95E-6	2.39E-11	7.56E-7	8.67E-1
0.290	7.84E-3	3.98E-2	1.90E-2	3.30E-3	5.60E-2	5.69E-3	1.94E-3	2.24E-6	2.58E-11	6.98E-7	8.66E-1
0.295	7.09E-3	3.92E-2	2.01E-2	3.41E-3	5.62E-2	6.26E-3	1.93E-3	2.57E-6	2.79E-11	6.43E-7	8.66E-1
0.300	6.41E-3	3.86E-2	2.12E-2	3.52E-3	5.63E-2	6.89E-3	1.91E-3	2.95E-6	3.01E-11	5.93E-7	8.65E-1
0.305	5.79E-3	3.78E-2	2.23E-2	3.61E-3	5.64E-2	7.57E-3	1.89E-3	3.37E-6	3.23E-11	5.46E-7	8.65E-1
0.310	5.23E-3	3.71E-2	2.35E-2	3.69E-3	5.65E-2	8.30E-3	1.87E-3	3.84E-6	3.47E-11	5.04E-7	8.64E-1
0.315	4.73E-3	3.63E-2	2.46E-2	3.76E-3	5.66E-2	9.08E-3	1.85E-3	4.36E-6	3.72E-11	4.65E-7	8.63E-1
0.320	4.28E-3	3.54E-2	2.58E-2	3.81E-3	5.66E-2	9.92E-3	1.82E-3	4.94E-6	3.98E-11	4.30E-7	8.62E-1
0.325	3.88E-3	3.46E-2	2.70E-2	3.85E-3	5.67E-2	1.08E-2	1.79E-3	5.57E-6	4.24E-11	3.98E-7	8.61E-1
0.330	3.52E-3	3.37E-2	2.82E-2	3.87E-3	5.67E-2	1.17E-2	1.76E-3	6.25E-6	4.51E-11	3.68E-7	8.61E-1
0.335	3.20E-3	3.28E-2	2.94E-2	3.88E-3	5.67E-2	1.27E-2	1.73E-3	6.99E-6	4.78E-11	3.42E-7	8.60E-1
0.340	2.91E-3	3.18E-2	3.07E-2	3.87E-3	5.67E-2	1.37E-2	1.70E-3	7.78E-6	5.05E-11	3.18E-7	8.59E-1

0.345	2.65E-3	3.09E-2	3.19E-2	3.84E-3	5.67E-2	1.47E-2	1.67E-3	8.62E-6	5.33E-11	2.96E-7	8.58E-1
0.350	2.42E-3	2.99E-2	3.32E-2	3.80E-3	5.66E-2	1.58E-2	1.63E-3	9.52E-6	5.61E-11	2.76E-7	8.57E-1
0.355	2.21E-3	2.90E-2	3.44E-2	3.75E-3	5.66E-2	1.69E-2	1.60E-3	1.05E-5	5.89E-11	2.58E-7	8.56E-1
0.360	2.02E-3	2.80E-2	3.57E-2	3.69E-3	5.66E-2	1.81E-2	1.56E-3	1.15E-5	6.17E-11	2.42E-7	8.54E-1
0.365	1.85E-3	2.70E-2	3.69E-2	3.61E-3	5.65E-2	1.92E-2	1.52E-3	1.25E-5	6.45E-11	2.26E-7	8.53E-1
0.370	1.69E-3	2.61E-2	3.82E-2	3.52E-3	5.65E-2	2.04E-2	1.48E-3	1.37E-5	6.73E-11	2.12E-7	8.52E-1
0.375	1.55E-3	2.51E-2	3.95E-2	3.43E-3	5.64E-2	2.16E-2	1.44E-3	1.48E-5	7.02E-11	1.99E-7	8.51E-1
0.380	1.42E-3	2.41E-2	4.08E-2	3.33E-3	5.64E-2	2.28E-2	1.40E-3	1.61E-5	7.31E-11	1.87E-7	8.50E-1
0.385	1.31E-3	2.31E-2	4.20E-2	3.22E-3	5.63E-2	2.40E-2	1.36E-3	1.74E-5	7.61E-11	1.76E-7	8.49E-1
0.390	1.20E-3	2.21E-2	4.33E-2	3.10E-3	5.62E-2	2.53E-2	1.31E-3	1.88E-5	7.92E-11	1.65E-7	8.47E-1
0.395	1.10E-3	2.11E-2	4.46E-2	2.98E-3	5.62E-2	2.66E-2	1.27E-3	2.04E-5	8.24E-11	1.55E-7	8.46E-1
0.400	1.01E-3	2.01E-2	4.59E-2	2.85E-3	5.61E-2	2.78E-2	1.22E-3	2.20E-5	8.57E-11	1.46E-7	8.45E-1
0.405	9.20E-4	1.91E-2	4.71E-2	2.72E-3	5.61E-2	2.91E-2	1.18E-3	2.37E-5	8.92E-11	1.37E-7	8.44E-1
0.410	8.41E-4	1.81E-2	4.84E-2	2.58E-3	5.60E-2	3.04E-2	1.13E-3	2.56E-5	9.30E-11	1.28E-7	8.42E-1
0.415	7.67E-4	1.71E-2	4.97E-2	2.45E-3	5.59E-2	3.17E-2	1.08E-3	2.77E-5	9.70E-11	1.20E-7	8.41E-1
0.420	6.98E-4	1.62E-2	5.09E-2	2.31E-3	5.59E-2	3.30E-2	1.03E-3	3.00E-5	1.01E-10	1.12E-7	8.40E-1
0.425	6.34E-4	1.52E-2	5.22E-2	2.17E-3	5.58E-2	3.44E-2	9.76E-4	3.25E-5	1.06E-10	1.04E-7	8.39E-1
0.430	5.73E-4	1.41E-2	5.35E-2	2.02E-3	5.57E-2	3.57E-2	9.23E-4	3.53E-5	1.12E-10	9.65E-8	8.37E-1
0.435	5.16E-4	1.31E-2	5.48E-2	1.88E-3	5.57E-2	3.70E-2	8.69E-4	3.86E-5	1.18E-10	8.92E-8	8.36E-1
0.440	4.63E-4	1.21E-2	5.60E-2	1.74E-3	5.56E-2	3.84E-2	8.13E-4	4.23E-5	1.25E-10	8.21E-8	8.35E-1
0.445	4.13E-4	1.11E-2	5.73E-2	1.59E-3	5.55E-2	3.97E-2	7.56E-4	4.66E-5	1.33E-10	7.51E-8	8.34E-1
0.450	3.65E-4	1.01E-2	5.85E-2	1.45E-3	5.55E-2	4.10E-2	6.97E-4	5.16E-5	1.43E-10	6.82E-8	8.32E-1
0.455	3.20E-4	9.14E-3	5.98E-2	1.30E-3	5.54E-2	4.24E-2	6.37E-4	5.78E-5	1.55E-10	6.14E-8	8.31E-1
0.460	2.77E-4	8.13E-3	6.11E-2	1.16E-3	5.53E-2	4.37E-2	5.75E-4	6.54E-5	1.69E-10	5.47E-8	8.30E-1
0.465	2.37E-4	7.13E-3	6.23E-2	1.01E-3	5.53E-2	4.51E-2	5.11E-4	7.50E-5	1.88E-10	4.80E-8	8.28E-1

0.470	1.99E-4	6.13E-3	6.36E-2	8.69E-4	5.52E-2	4.64E-2	4.46E-4	8.76E-5	2.13E-10	4.14E-8	8.27E-1
0.475	1.62E-4	5.14E-3	6.48E-2	7.26E-4	5.51E-2	4.78E-2	3.79E-4	1.05E-4	2.47E-10	3.47E-8	8.26E-1
0.480	1.28E-4	4.15E-3	6.60E-2	5.85E-4	5.51E-2	4.91E-2	3.10E-4	1.31E-4	2.97E-10	2.81E-8	8.24E-1
0.485	9.57E-5	3.17E-3	6.72E-2	4.46E-4	5.50E-2	5.04E-2	2.40E-4	1.71E-4	3.77E-10	2.16E-8	8.23E-1
0.490	6.55E-5	2.22E-3	6.84E-2	3.11E-4	5.49E-2	5.17E-2	1.70E-4	2.45E-4	5.23E-10	1.52E-8	8.22E-1
0.495	3.87E-5	1.34E-3	6.95E-2	1.87E-4	5.49E-2	5.29E-2	1.04E-4	4.07E-4	8.43E-10	9.18E-9	8.21E-1
0.500	1.89E-5	6.62E-4	7.03E-2	9.25E-5	5.48E-2	5.38E-2	5.19E-5	8.24E-4	1.66E-9	4.55E-9	8.19E-1

Table G.3: Predictions for activity coefficients in 8 m 2MPZ at 40 °C.

Loading	Activity Coefficient										
(mol/mol alk.)	2MPZ	2MPZCOO-	H2MPZCOO	$2MPZ(COO^-)_2$	$2MPZH^+$	HCO_3^-	CO_3^{2-}	CO_2	H^+	OH^-	H_2O
0.000	1.636	-	-	-	4.255	-	-	-	4.404	4.255	0.966
0.005	1.642	1.709	0.980	1.769	1.707	1.709	1.769	1.611	3.416	3.403	0.966
0.010	1.648	1.545	0.801	1.261	1.544	1.545	1.261	1.614	3.038	3.029	0.966
0.015	1.655	1.430	0.660	0.984	1.429	1.430	0.984	1.618	2.768	2.761	0.966
0.020	1.662	1.339	0.548	0.803	1.338	1.339	0.803	1.621	2.553	2.547	0.966
0.025	1.668	1.263	0.458	0.674	1.263	1.263	0.674	1.625	2.374	2.368	0.966
0.030	1.675	1.199	0.386	0.578	1.199	1.198	0.578	1.629	2.219	2.214	0.966
0.035	1.681	1.142	0.327	0.503	1.142	1.142	0.503	1.634	2.084	2.079	0.967
0.040	1.687	1.092	0.279	0.442	1.092	1.091	0.442	1.638	1.964	1.959	0.967
0.045	1.693	1.047	0.240	0.393	1.047	1.046	0.393	1.643	1.857	1.852	0.968
0.050	1.699	1.007	0.207	0.352	1.007	1.006	0.352	1.648	1.760	1.756	0.969
0.055	1.704	0.970	0.180	0.318	0.970	0.969	0.318	1.653	1.673	1.668	0.969
0.060	1.710	0.937	0.157	0.289	0.937	0.935	0.289	1.658	1.593	1.589	0.970

0.065	1.716	0.906	0.137	0.264	0.906	0.904	0.264	1.664	1.520	1.516	0.971
0.070	1.721	0.878	0.121	0.242	0.878	0.875	0.242	1.669	1.454	1.449	0.972
0.075	1.726	0.852	0.107	0.223	0.852	0.849	0.223	1.675	1.392	1.388	0.973
0.080	1.731	0.827	0.095	0.207	0.828	0.824	0.207	1.681	1.336	1.332	0.974
0.085	1.736	0.805	0.085	0.192	0.805	0.801	0.192	1.687	1.284	1.280	0.975
0.090	1.741	0.784	0.077	0.179	0.784	0.779	0.179	1.693	1.236	1.231	0.976
0.095	1.745	0.764	0.069	0.168	0.765	0.759	0.168	1.699	1.191	1.187	0.977
0.100	1.750	0.746	0.062	0.158	0.746	0.740	0.158	1.705	1.149	1.145	0.979
0.105	1.754	0.728	0.057	0.149	0.729	0.721	0.149	1.711	1.111	1.107	0.980
0.110	1.759	0.712	0.052	0.141	0.713	0.704	0.141	1.717	1.075	1.071	0.981
0.115	1.763	0.696	0.047	0.133	0.697	0.688	0.133	1.724	1.042	1.038	0.982
0.120	1.767	0.682	0.043	0.126	0.683	0.672	0.126	1.730	1.011	1.007	0.984
0.125	1.770	0.668	0.040	0.120	0.669	0.657	0.120	1.737	0.982	0.978	0.985
0.130	1.774	0.655	0.037	0.115	0.656	0.643	0.115	1.743	0.955	0.951	0.987
0.135	1.778	0.642	0.034	0.110	0.644	0.629	0.110	1.750	0.930	0.926	0.988
0.140	1.781	0.630	0.032	0.105	0.632	0.616	0.105	1.756	0.907	0.903	0.989
0.145	1.785	0.618	0.030	0.101	0.620	0.603	0.101	1.763	0.885	0.881	0.991
0.150	1.788	0.607	0.028	0.097	0.610	0.590	0.097	1.770	0.865	0.861	0.992
0.155	1.791	0.597	0.026	0.094	0.599	0.578	0.094	1.776	0.846	0.842	0.994
0.160	1.795	0.586	0.025	0.090	0.589	0.566	0.090	1.783	0.828	0.824	0.996
0.165	1.798	0.576	0.023	0.087	0.579	0.554	0.087	1.790	0.811	0.807	0.997
0.170	1.801	0.566	0.022	0.085	0.570	0.543	0.085	1.796	0.796	0.792	0.999
0.175	1.804	0.557	0.021	0.082	0.561	0.532	0.082	1.803	0.782	0.778	1.001
0.180	1.807	0.548	0.020	0.080	0.552	0.521	0.080	1.810	0.768	0.764	1.002
0.185	1.810	0.539	0.019	0.077	0.543	0.510	0.077	1.817	0.756	0.752	1.004

0.190	1.813	0.530	0.018	0.075	0.535	0.499	0.075	1.824	0.745	0.741	1.006
0.195	1.816	0.521	0.018	0.073	0.527	0.488	0.073	1.830	0.734	0.730	1.008
0.200	1.819	0.512	0.017	0.072	0.519	0.477	0.072	1.837	0.724	0.720	1.010
0.205	1.822	0.504	0.016	0.070	0.511	0.467	0.070	1.844	0.715	0.711	1.011
0.210	1.825	0.495	0.016	0.068	0.503	0.456	0.068	1.851	0.707	0.703	1.013
0.215	1.828	0.487	0.015	0.067	0.495	0.445	0.067	1.858	0.700	0.695	1.015
0.220	1.831	0.479	0.015	0.066	0.487	0.435	0.066	1.864	0.693	0.688	1.018
0.225	1.834	0.471	0.014	0.064	0.480	0.424	0.064	1.871	0.687	0.682	1.020
0.230	1.838	0.462	0.014	0.063	0.472	0.414	0.063	1.878	0.681	0.676	1.022
0.235	1.841	0.454	0.014	0.062	0.465	0.403	0.062	1.885	0.676	0.671	1.024
0.240	1.845	0.446	0.013	0.061	0.457	0.393	0.061	1.891	0.672	0.667	1.026
0.245	1.848	0.438	0.013	0.060	0.450	0.382	0.060	1.898	0.668	0.663	1.029
0.250	1.852	0.430	0.013	0.059	0.442	0.372	0.059	1.904	0.665	0.660	1.031
0.255	1.856	0.421	0.013	0.058	0.435	0.361	0.058	1.911	0.663	0.658	1.033
0.260	1.860	0.413	0.012	0.057	0.427	0.351	0.057	1.917	0.661	0.656	1.036
0.265	1.865	0.405	0.012	0.056	0.419	0.340	0.056	1.923	0.660	0.654	1.039
0.270	1.869	0.397	0.012	0.055	0.412	0.330	0.055	1.929	0.660	0.654	1.041
0.275	1.874	0.389	0.012	0.055	0.404	0.320	0.055	1.935	0.660	0.653	1.044
0.280	1.879	0.380	0.012	0.054	0.397	0.309	0.054	1.941	0.661	0.654	1.047
0.285	1.885	0.372	0.012	0.053	0.389	0.299	0.053	1.947	0.662	0.655	1.049
0.290	1.890	0.364	0.012	0.053	0.381	0.289	0.053	1.952	0.664	0.656	1.052
0.295	1.896	0.357	0.011	0.052	0.374	0.280	0.052	1.957	0.666	0.658	1.055
0.300	1.903	0.349	0.011	0.051	0.366	0.270	0.051	1.962	0.669	0.661	1.058
0.305	1.909	0.341	0.011	0.051	0.358	0.261	0.051	1.967	0.673	0.664	1.061
0.310	1.916	0.334	0.011	0.051	0.350	0.253	0.051	1.971	0.677	0.668	1.064

0.315	1.923	0.327	0.011	0.050	0.343	0.244	0.050	1.976	0.682	0.672	1.068
0.320	1.930	0.320	0.011	0.050	0.335	0.236	0.050	1.980	0.688	0.677	1.071
0.325	1.938	0.314	0.010	0.050	0.327	0.228	0.050	1.984	0.693	0.682	1.074
0.330	1.946	0.308	0.010	0.049	0.320	0.221	0.049	1.987	0.700	0.687	1.077
0.335	1.954	0.302	0.010	0.049	0.312	0.214	0.049	1.991	0.706	0.693	1.081
0.340	1.962	0.296	0.010	0.049	0.305	0.207	0.049	1.994	0.714	0.699	1.084
0.345	1.971	0.291	0.010	0.049	0.297	0.201	0.049	1.997	0.721	0.706	1.088
0.350	1.980	0.286	0.009	0.049	0.290	0.195	0.049	2.000	0.729	0.712	1.091
0.355	1.989	0.281	0.009	0.049	0.283	0.190	0.049	2.003	0.737	0.720	1.095
0.360	1.998	0.277	0.009	0.049	0.275	0.184	0.049	2.006	0.746	0.727	1.098
0.365	2.007	0.273	0.009	0.049	0.268	0.179	0.049	2.009	0.755	0.735	1.102
0.370	2.017	0.269	0.008	0.050	0.261	0.175	0.050	2.012	0.764	0.743	1.105
0.375	2.027	0.265	0.008	0.050	0.254	0.170	0.050	2.014	0.774	0.751	1.109
0.380	2.037	0.262	0.008	0.050	0.248	0.166	0.050	2.017	0.784	0.760	1.113
0.385	2.047	0.258	0.008	0.051	0.241	0.162	0.051	2.019	0.794	0.768	1.117
0.390	2.057	0.256	0.007	0.051	0.234	0.159	0.051	2.021	0.805	0.777	1.120
0.395	2.067	0.253	0.007	0.052	0.228	0.155	0.052	2.023	0.816	0.787	1.124
0.400	2.078	0.250	0.007	0.052	0.221	0.152	0.052	2.026	0.827	0.796	1.128
0.405	2.088	0.248	0.007	0.053	0.215	0.149	0.053	2.028	0.838	0.806	1.132
0.410	2.099	0.246	0.006	0.053	0.209	0.147	0.053	2.030	0.850	0.816	1.136
0.415	2.110	0.244	0.006	0.054	0.203	0.144	0.054	2.032	0.862	0.826	1.140
0.420	2.121	0.242	0.006	0.055	0.197	0.142	0.055	2.033	0.874	0.836	1.144
0.425	2.132	0.241	0.006	0.055	0.192	0.139	0.055	2.035	0.887	0.846	1.148
0.430	2.144	0.239	0.006	0.056	0.186	0.137	0.056	2.037	0.900	0.857	1.152
0.435	2.155	0.238	0.005	0.057	0.180	0.135	0.057	2.039	0.913	0.868	1.156

0.440	2.167	0.237	0.005	0.058	0.175	0.133	0.058	2.040	0.926	0.879	1.160
0.445	2.178	0.236	0.005	0.059	0.170	0.132	0.059	2.042	0.940	0.890	1.164
0.450	2.190	0.235	0.005	0.060	0.165	0.130	0.060	2.043	0.954	0.902	1.168
0.455	2.202	0.234	0.005	0.061	0.160	0.129	0.061	2.045	0.968	0.913	1.173
0.460	2.214	0.233	0.005	0.062	0.155	0.127	0.062	2.046	0.982	0.925	1.177
0.465	2.226	0.233	0.004	0.063	0.150	0.126	0.063	2.047	0.997	0.937	1.181
0.470	2.238	0.233	0.004	0.064	0.146	0.125	0.064	2.049	1.012	0.949	1.185
0.475	2.250	0.232	0.004	0.065	0.141	0.124	0.065	2.050	1.027	0.962	1.189
0.480	2.263	0.232	0.004	0.067	0.137	0.123	0.067	2.051	1.043	0.974	1.194
0.485	2.275	0.232	0.004	0.068	0.133	0.122	0.068	2.052	1.058	0.987	1.198
0.490	2.287	0.232	0.004	0.070	0.129	0.121	0.070	2.052	1.074	0.999	1.202
0.495	2.299	0.233	0.004	0.071	0.125	0.121	0.071	2.053	1.089	1.012	1.206
0.500	2.310	0.233	0.004	0.072	0.122	0.120	0.072	2.052	1.102	1.022	1.208

Table G.4: Reaction stoichiometry normalized to CO_2 in 8 m 2MPZ at 40 °C.

Loading	Stoichiometry										
(mol/mol alk.)	2MPZ	2MPZCOO-	H2MPZCOO	$2MPZ(COO^-)_2$	$2MPZH^+$	HCO_3^-	CO_3^{2-}	CO_2	H^+	OH^-	H_2O
0	-1.97E+0	8.17E-1	2.58E-5	7.24E-8	1.19E+0	6.17E-3	1.77E-1	2.77E-8	7.05E-12	1.02E-2	-1.91E-1
0.025	-2.03E+0	9.59E-1	2.86E-3	2.10E-3	1.02E+0	8.26E-3	2.54E-2	8.89E-7	4.45E-11	-3.81E-4	0.00E+0
0.050	-2.14E+0	9.36E-1	1.14E-2	6.02E-3	1.07E+0	1.34E-2	2.68E-2	1.34E-6	6.02E-11	-1.34E-4	0.00E+0
0.075	-1.99E+0	9.00E-1	2.57E-2	1.16E-2	1.03E+0	1.29E-2	3.86E-2	1.93E-6	7.71E-11	-6.43E-5	0.00E+0
0.100	-1.95E+0	8.44E-1	5.84E-2	1.95E-2	9.74E-1	1.95E-2	3.90E-2	3.25E-6	1.30E-10	-6.49E-5	-6.49E-2
0.125	-1.84E+0	7.59E-1	1.08E-1	3.16E-2	9.49E-1	2.53E-2	4.43E-2	4.43E-6	1.27E-10	-6.33E-5	-6.33E-2
0.150	-1.80E+0	6.67E-1	1.80E-1	4.00E-2	9.33E-1	3.33E-2	4.00E-2	6.67E-6	2.00E-10	-6.67E-5	-6.67E-2
0.175	-1.62E+0	5.62E-1	2.62E-1	5.00E-2	7.50E-1	4.37E-2	3.12E-2	6.25E-6	2.50E-10	-1.25E-4	-1.25E-1

0.200	-1.49E+0	3.90E-1	3.83E-1	6.49E-2	6.49E-1	7.14E-2	2.60E-2	2.60E-5	3.90E-10	-6.49E-5	-1.30E-1
0.225	-1.26E+0	2.40E-1	4.73E-1	8.38E-2	4.79E-1	1.02E-1	1.80E-2	3.59E-5	5.39E-10	-5.99E-5	-1.20E-1
0.250	-1.04E+0	0.00E+0	6.10E-1	9.76E-2	3.66E-1	1.83E-1	1.22E-2	7.32E-5	6.10E-10	-6.10E-5	-1.83E-1
0.275	-7.79E-1	-3.25E-1	7.79E-1	1.10E-1	1.95E-1	3.31E-1	-6.49E-3	1.30E-4	1.30E-9	-5.84E-5	-3.25E-1
0.300	-4.97E-1	-4.91E-1	8.59E-1	7.36E-2	6.13E-2	4.97E-1	-1.23E-2	3.07E-4	1.84E-9	-3.68E-5	-4.91E-1
0.325	-3.05E-1	-7.14E-1	9.74E-1	2.60E-2	6.49E-2	7.14E-1	-2.60E-2	5.19E-4	2.60E-9	-2.60E-5	-7.14E-1
0.350	-1.83E-1	-7.84E-1	1.04E+0	-3.92E-2	-6.53E-2	8.49E-1	-3.27E-2	7.84E-4	2.61E-9	-1.31E-5	-8.49E-1
0.375	-1.06E-1	-7.45E-1	9.93E-1	-7.45E-2	-6.21E-2	9.31E-1	-3.10E-2	6.21E-4	2.48E-9	-6.21E-6	-8.69E-1
0.400	-6.74E-2	-7.35E-1	9.80E-1	-9.80E-2	-6.13E-2	9.80E-1	-3.06E-2	1.23E-3	2.45E-9	-6.13E-6	-9.80E-1
0.425	-4.36E-2	-7.48E-1	9.98E-1	-1.06E-1	-6.23E-2	9.98E-1	-3.74E-2	2.49E-3	6.23E-9	-6.23E-6	-9.98E-1
0.450	-4.15E-2	-8.98E-1	1.04E+0	-1.31E-1	-6.91E-2	1.17E+0	-5.53E-2	4.84E-3	1.38E-8	-6.22E-6	-1.11E+0
0.475	-2.42E-2	-7.52E-1	9.70E-1	-1.09E-1	-6.06E-2	1.03E+0	-4.85E-2	1.82E-2	3.03E-8	-4.85E-6	-9.70E-1
0.500	-1.17E-2	-4.10E-1	4.56E-1	-5.73E-2	-6.51E-2	5.86E-1	-3.19E-2	5.15E-1	9.77E-7	-2.87E-6	-9.77E-1

G.2 LIQUID MASS TRANSFER COEFFICIENT

The liquid film mass transfer coefficients listed in the table are the average of the calculated values for the inlet gaseous CO_2 partial pressure $P_{CO2,g}$ = 0, 0.3, 0.6, 1.4, 1.7 and 2.0 × P_{CO2}*.

Table G.5: Equilibrium CO_2 partial pressure (P_{CO2}*, Pa) and liquid film mass transfer coefficient (kg', mol/s·Pa·m^2) for 8 m 2MPZ with variable loading and temperature.

Loading	Temperature							
	40 ℃		60 ℃		80 ℃		100 ℃	
(mol/mol alk.)	P_{CO2}*	k_g'	P_{CO2}*	k_g'	P_{CO2}*	k_g'	P_{CO2}*	k_g'
0.025	1.26E+0	9.20E-6	1.00E+1	1.34E-5	6.03E+1	1.79E-5	2.89E+2	1.62E-5
0.050	3.87E+0	8.43E-6	3.04E+1	1.21E-5	1.81E+2	1.51E-5	8.58E+2	1.20E-5
0.075	7.70E+0	7.53E-6	6.00E+1	1.06E-5	3.54E+2	1.24E-5	1.67E+3	8.89E-6
0.100	1.34E+1	6.60E-6	1.03E+2	9.08E-6	6.00E+2	9.97E-6	2.79E+3	6.48E-6
0.125	2.22E+1	5.67E-6	1.67E+2	7.59E-6	9.56E+2	7.74E-6	4.38E+3	4.66E-6
0.150	3.62E+1	4.77E-6	2.65E+2	6.18E-6	1.48E+3	5.82E-6	6.61E+3	3.32E-6
0.175	5.97E+1	3.92E-6	4.19E+2	4.87E-6	2.25E+3	4.23E-6	9.78E+3	2.34E-6
0.200	1.01E+2	3.12E-6	6.70E+2	3.68E-6	3.43E+3	2.97E-6	1.43E+4	1.64E-6
0.225	1.78E+2	2.39E-6	1.10E+3	2.66E-6	5.26E+3	2.03E-6	2.09E+4	1.15E-6
0.250	3.34E+2	1.74E-6	1.85E+3	1.82E-6	8.13E+3	1.37E-6	3.04E+4	8.08E-7
0.265	5.00E+2	1.40E-6	2.55E+3	1.43E-6	1.05E+4	1.08E-6	3.78E+4	6.59E-7
0.275	6.63E+2	1.19E-6	3.17E+3	1.21E-6	1.25E+4	9.31E-7	4.38E+4	5.76E-7
0.300	1.34E+3	7.84E-7	5.38E+3	8.10E-7	1.90E+4	6.52E-7	6.20E+4	4.19E-7
0.325	2.57E+3	5.26E-7	8.73E+3	5.66E-7	2.79E+4	4.71E-7	8.62E+4	-
0.350	4.43E+3	3.70E-7	1.33E+4	4.10E-7	3.96E+4	3.45E-7	1.18E+5	-
0.356	5.00E+3	3.41E-7	1.47E+4	3.80E-7	4.31E+4	3.19E-7	1.28E+5	-
0.375	6.96E+3	2.68E-7	1.94E+4	3.00E-7	5.53E+4	2.57E-7	1.61E+5	-
0.400	1.04E+4	1.94E-7	2.78E+4	2.14E-7	7.71E+4	2.16E-7	2.21E+5	-

Appendix H: Nomenclature

A	area
a	activity
$A_{packing}$	packing area
c	Molar concentration
C_p^{ig}	ideal gas heat capacity
$C_p^{\infty,aq}$	aqueous infinite dilution heat capacity
d	diameter
D	diffusion coefficient
D_{Am}	Binary diffusion coefficient of all non-CO_2 components in any other component
D_{CO_2}	Binary diffusion coefficient of CO_2 with respect to any other component
$D_{CO_2,eff}$	Effective diffusion coefficient of CO_2
E	enhancement factor or activation energy
E_D	diffusion activation energy
f	fugacity
g	gravity
g^*	Molar Gibbs free energy
g_{ji}	interaction energy between species i and j
G_i^0	standard free energy of formation of component i
$G_{fluegas}$	volumetric flow rate of flue gas
h	height
Ha	Hatta number
H_i^0	standard enthalpy of formation of component i
H_{i,H_2O}	Henry's constant of component i in water
k_2	second-order reaction rate constant

$k_{2,b}$	rate constant for bicarbonate formation catalyzed by base b
K_g	overall mass transfer coefficient
k_g	gas film mass transfer coefficient
$k_g^{'}$	liquid film mass transfer coefficient
k_l^0	physical liquid film mass transfer coefficient
k_f	forward reaction rate constant
k_r	reverse reaction rate constant
k_{Am-b}	rate constant for termolecular reaction (Am + CO_2 + base)
K_{eq}	activity-based equilibrium constant
N	flux
N_{CO_2}	CO_2 flux
P	pressure
$P_{CO_2}^*$	equilibrium CO_2 partial pressure of loaded amine solution
$P_{CO_2,g}$	CO_2 partial pressure in gas
Q	liquid volumetric flow rate
R	gas constant
r_{CO_2}	reaction rate of CO_2
Re	Reynolds number
Sc	Schmidt number
Sh	Sherwood number
T	temperature
u	velocity
v	volume flow rate
V	volume
V_m	molar volume
W	circumference

x	mol fraction

Greek symbols

α	CO_2 loading
κ	binary mass transfer coefficient
δ	chemical shift in NMR, or film thickness, or dimensionless distance in liquid film
ρ	density
$\overline{\rho}$	molar density
η	viscosity or dimensionless penetration distance
γ	activity coefficient
τ	time of exposure
τ_{ij}	binary interaction parameters between component i and j
μ	Viscosity or chemical potential
ΔH_{abs}	enthalpy of CO_2 absorption
ϕ_i	fugacity coefficient of component i
Θ	dimensionless driving force

References

Abdi, M. A. and A. Meisen (2000). Amine Degradation: Problems, Review of Research Achievements, Recovery Techniques. Proceedings of the 2nd International Oil, Gas and Petrochemical Conference. Tehran, Iran.

Aboudheir, A., P. Tontiwachwuthikul, et al. (2003). "Kinetics of the reactive absorption of carbon dioxide in high CO2-loaded, concentrated aqueous monoethanolamine solutions." Chemical Engineering Science 58(23-24): 5195-5210.

Al-Dhafeeri, M. A. (2007). "Identifying sources key to detailed troubleshooting of amine foaming." Oil and Gas Journal 105(32): 56.

Al-Juaied, M. (2004). Caron dioxide Removal from Natural Gas by Membranes in the Presence of Heavy Hydrocarbons and by Aqueous Diglycolamine®/Morpholine. Department of Chemical Engineering. Austin, TX, The University of Texas at Austin. Ph. D. Dissertation.

Al-Juaied, M. and G. T. Rochelle (2006). "Thermodynamics and Equilibrium Solubility of Carbon Dioxide in Diglycolamine/Morpholine/Water." Journal of Chemical & Engineering Data 51(2): 708-717.

Alper, E. (1990). "Kinetics of reactions of carbon dioxide with diglycolamine and morpholine." The Chemical Engineering Journal 44(2): 107-111.

Alper, E. (1990). "Reaction mechanism and kinetics of aqueous solutions of 2-amino-2-methyl-1-propanol and carbon dioxide." Industrial & Engineering Chemistry Research 29(8): 1725-8.

Alstom (2001). Engineering feasibility and economics of CO2 capture on an existing coal-fired power plant. Report no. PPL-01-CT-09 to Ohio Department of Development, Columbus, OH and US Department of Energy/NETL, Pittsburgh, PA.

Alstom (2011). "CCS with the Alstom Chilled Ammonia Process Development Program –Field Pilot Results." Energy Procedia 4(4): 273–281.

Aroua, M. K., M. Z. Haji-Sulaiman, et al. (2002). "Modelling of carbon dioxide absorption in aqueous solutions of AMP and MDEA and their blends using Aspenplus." Separation and Purification Technology 29(2): 153-162.

Asprion, N. and W. M. a. C. Pantelides (2006). Simulation of mass transfer in reactive absorption. Computer Aided Chemical Engineering, Elsevier. Volume 21**:** 119-124.

Attalla, M. (2008). Postcombustion carbon dioxide capture research program at CSIRO, Australia, American Chemical Society.

Austgen, D. M., G. T. Rochelle, et al. (1989). "Model of vapor-liquid equilibria for aqueous acid gas-alkanolamine systems using the electrolyte-NRTL equation." Industrial & Engineering Chemistry Research 28(7): 1060-73.

Ballard, M., M. Bown, et al. (2011). "NMR studies of mixed amines." Energy Procedia 4: 291-298.

Barth, D., C. Tondre, et al. (1984). "Kinetics and mechanisms of the reactions of carbon dioxide with alkanolamines: a discussion concerning the cases of MDEA and DEA." Chemical Engineering Science 39(12): 1753-1757.

Barth, D., C. Tondre, et al. (1986). "Stopped-flow investigations of the reaction kinetics of carbon dioxide with some primary and secondary alkanolamines in aqueous solutions." International Journal of Chemical Kinetics 18(4): 445-457.

Barzagli, F., F. Mani, et al. (2010). "Continuous cycles of CO2 absorption and amine regeneration with aqueous alkanolamines: a comparison of the efficiency between pure and blended DEA, MDEA and AMP solutions by 13C NMR spectroscopy." Energy Environ. Sci. 3(6): 772-779.

Bikerman, J. J. (1973). Applied Physics and Engineering, No. 10: Foams. [Physicochemical Aspects].

Bindwal, A. B., P. D. Vaidya, et al. (2011). "Kinetics of carbon dioxide removal by aqueous diamines." Chemical Engineering Journal 169(1-3): 144-150.

Bishnoi, S. (2000). Carbon dioxide absorption and solution equilibrium in piperazine activated methyldiethanolamine Department of Chemical Engineering. Austin, TX, the University of Texas at Austin. Ph.D.

Bishnoi, S. (2000). Carbon dioxide absorption and solution equilibrium in piperazine activated methyldiethanolamine Department of Chemical Engineering. Austin, TX, the University of Texas at Austin. Ph.D. Dissertation.

Bishnoi, S. and G. T. Rochelle (2000). "Absorption of carbon dioxide into aqueous piperazine: reaction kinetics, mass transfer and solubility." Chemical Engineering Science 55(22): 5531-5543.

Bishnoi, S. and G. T. Rochelle (2000). "Physical and chemical solubility of carbon dioxide in aqueous methyldiethanolamine." Fluid Phase Equilibria 168(2): 241-258.

Bishnoi, S. and G. T. Rochelle (2002). "Absorption of carbon dioxide in aqueous piperazine/methyldiethanolamine." AIChE Journal 48(12): 2788-2799.

Blauwhoff, P. M. M., G. F. Versteeg, et al. (1984). "A study on the reaction between carbon dioxide and alkanolamines in aqueous solutions." Chemical Engineering Science 39(2): 207-25.

Boden, T., G. Marland, et al. (2009). Global CO2 Emissions from Fossil-Fuel Burning, Cement Manufacture and Gas Flaring: 1751-2006. Oak Ridge, Tennessee, Carbon Dioxide Information Analysis Center, Oak Ridge National Laboratory.

Bottinger, W., M. Maiwald, et al. (2008). "Online NMR Spectroscopic Study of Species Distribution in MDEA-H2O-CO2 and MDEA-PIP-H2O-CO2." Ind. Eng. Chem. Res. 47(20): 7917-7926.

Böttinger, W., M. Maiwald, et al. (2008). "Online NMR spectroscopic study of species distribution in MEA-H2O-CO2 and DEA-H2O-CO2." Fluid Phase Equilibria 263(2): 131-143.

Bougie, F. and M. C. Iliuta (2009). "Kinetics of absorption of carbon dioxide into aqueous solutions of 2-amino-2-hydroxymethyl-1,3-propanediol." Chemical Engineering Science 64(1): 153-162.

Bougie, F., J. Lauzon-Gauthier, et al. (2009). "Acceleration of the reaction of carbon dioxide into aqueous 2-amino-2-hydroxymethyl-1,3-propanediol solutions by piperazine addition." Chemical Engineering Science 64(9): 2011-2019.

Bronsted, J. N. (1928). "Acid and Basic Catalysis." Chemical Reviews 5(3): 231-338.

Caplow, M. (1968). "Kinetics of carbamate formation and breakdown." Journal of the American Chemical Society 90(24): 6795-803.

Chakraborty, A. K., G. Astarita, et al. (1986). "CO2 absorption in aqueous solutions of hindered amines." Chemical Engineering Science 41(4): 997-1003.

Chang, L.-C., T.-I. Lin, et al. (2004). "Mutual Diffusion Coefficients of Some Aqueous Alkanolamines Solutions." Journal of Chemical & Engineering Data 50(1): 77-84.

Chen, C.-C., H. I. Britt, et al. (1982). "Local composition model for excess Gibbs energy of electrolyte systems. Part I: Single solvent, single completely dissociated electrolyte systems." AIChE Journal 28(4): 588-596.

Chen, C.-C. and L. B. Evans (1986). "A local composition model for the excess Gibbs energy of aqueous electrolyte systems." AIChE Journal 32(3): 444-454.

Chen, C., A. B. Rao, et al. (2003). Comparative assessment of CO2 capture options for existing coal-fired power plants. the Second National Conference on Carbon Sequestration. Alexandria, VA, USA.

Chen, E. (2007). Carbon dioxide absorption into piperazine promoted potassium carbonate using structured packing. Austin, TX, the University of Texas at Austin. Ph.D. Dissertation.

Chilton, T. H. and A. P. Colburn (1934). "Mass Transfer (Absorption) Coefficients Prediction from Data on Heat Transfer and Fluid Friction." Industrial & Engineering Chemistry 26(11): 1183-1187.

Choi, W.-J., K.-C. Cho, et al. (2007). "Removal of carbon dioxide by absorption into blended amines: kinetics of absorption into aqueous AMP/HMDA, AMP/MDEA, and AMP/piperazine solutions." Green Chemistry 9(6): 594-598.

Chowdhury, F. A., H. Okabe, et al. (2011). "Synthesis and selection of hindered new amine absorbents for CO2 capture." Energy Procedia 4: 201-208.

Ciftja, A. F., A. Hartono, et al. (2011). "Study on carbamate stability in the Amp/CO2/H2O system from 13C-NMR spectroscopy." Energy Procedia 4: 614-620.

Crooks, J. E. and J. P. Donnellan (1989). "Kinetics and mechanism of the reaction between carbon dioxide and amines in aqueous solution." Journal of the Chemical Society, Perkin Transactions 2: Physical Organic Chemistry (1972-1999)(4): 331-3.

Cullinane, J. T. (2005). Thermodynamics and Kinetics of Aqueous Piperazine with Potassium Carbonate for Carbon Dioxide Absorption. Chemical Engineering. Austin, TX, The University of Texas at Austin. Ph. D.

Cullinane, J. T. (2005). Thermodynamics and Kinetics of Aqueous Piperazine with Potassium Carbonate for Carbon Dioxide Absorption. Chemical Engineering. Austin, TX, The University of Texas at Austin. Ph. D. Dissertation.

Cullinane, J. T. and G. T. Rochelle (2005). "Thermodynamics of aqueous potassium carbonate, piperazine, and carbon dioxide." Fluid Phase Equilibria 227(2): 197-213.

Cullinane, J. T. and G. T. Rochelle (2006). "Kinetics of Carbon Dioxide Absorption into Aqueous Potassium Carbonate and Piperazine." Industrial & Engineering Chemistry Research 45(8): 2531-2545.

da Silva, E. F. and H. F. Svendsen (2006). "Study of the Carbamate Stability of Amines Using ab Initio Methods and Free-Energy Perturbations." Industrial & Engineering Chemistry Research 45(8): 2497-2504.

Danckwerts, P. V. (1951). "Significance of Liquid-Film Coefficients in Gas Absorption." Industrial & Engineering Chemistry 43(6): 1460-1467.

Danckwerts, P. V. (1970). Gas-Liquid Reactions. New York, McGraw-Hill Book Co.

Danckwerts, P. V. (1979). "The reaction of carbon dioxide with ethanolamines." Chemical Engineering Science 34(4): 443-6.

Danckwerts, P. V. (1979). "The reaction of CO2 with ethanolamines." Chemical Engineering Science 34(4): 443-446.

Dang, H. (2000). CO2 absorption rate and solubility in monoethanolamine/piperazine/water. Chemical Engineering. Austin, TX, The University of Texas at austin. M.S.E**:** 129.

Dash, S. K., A. Samanta, et al. (2011). "Absorption of carbon dioxide in piperazine activated concentrated aqueous 2-amino-2-methyl-1-propanol solvent." Chemical Engineering Science In Press, Corrected Proof.

Davis, J. D. (2009). Thermal Degradation of Aqueous Amines Used for Carbon Dioxide Capture. Department of Chemical Engineering. Austin, TX, The University of Texas at Austin. Ph. D. Dissertation.

Derks, P. W. J., J. A. Hogendoorn, et al. (2009). "Experimental and theoretical study of the solubility of carbon dioxide in aqueous blends of piperazine and N-methyldiethanolamine." Journal of Chemical Thermodynamics 42(1): 151-163.

Derks, P. W. J., T. Kleingeld, et al. (2006). "Kinetics of absorption of carbon dioxide in aqueous piperazine solutions." Chemical Engineering Science 61(20): 6837-6854.

Du, Z., M. P. Bilbao-Montoya, et al. (2003). "Outstanding Stability of Particle-Stabilized Bubbles." Langmuir 19(8): 3106-3108.

Dubois, L. and D. Thomas (2011). "Carbon dioxide absorption into aqueous amine based solvents: Modeling and absorption tests." Energy Procedia 4: 1353-1360.

Dugas, R. (2009). Absorption, desorption and mass transfer of carbon dioxide into monoethanolamine and piperazine. Chemical Engineering. Austin, the University of Texas at Austin. Ph. D.

Dugas, R. (2009). Carbon Dioxide Absorption, Desorption, and Diffusion in Aqueous Piperazine and Monoethanolamine. Chemical Engineering. Austin, TX, the University of Texas at Austin. Ph.D. Dissertation.

Dugas, R. and G. Rochelle (2009). "Absorption and desorption rates of carbon dioxide with monoethanolamine and piperazine." Energy Procedia 1(1): 1163-1169.

Edali, M., A. Aboudheir, et al. (2009). "Kinetics of carbon dioxide absorption into mixed aqueous solutions of MDEA and MEA using a laminar jet apparatus and a numerically solved 2D absorption rate/kinetics model." International Journal of Greenhouse Gas Control 3(5): 550-560.

Edali, M., R. Idem, et al. (2010). "1D and 2D absorption-rate/kinetic modeling and simulation of carbon dioxide absorption into mixed aqueous solutions of MDEA and PZ in a laminar jet apparatus." International Journal of Greenhouse Gas Control 4(2): 143-151.

EIA (2010). "Annual Energy Review 2009 (August 2010)." U.S. Energy Information Administration.

EIA (2011). "Emission of Greenhouse Gases in the United States." U.S. Energy Information Administration.

EPA (2011). "INVENTORY OF U.S. GREENHOUSE GAS EMISSIONS AND SINKS: 1990 – 2009." U.S. Environmental Protection Agency.

Ermatchkov, V., Á. P.-S. Kamps, et al. (2003). "Chemical equilibrium constants for the formation of carbamates in (carbon dioxide + piperazine + water) from 1H-NMR-spectroscopy." The Journal of Chemical Thermodynamics 35(8): 1277-1289.

Etheridge, D. M., L. P. Steele, et al. (1998). Historical CO2 record from the Law Dome DE08, DE08-2, and DSS ice cores. Aspendale, Victoria, Australia, Division of Atmospheric Research, CSIRO.

Exerowa, D., P. M. Kruglyakov, et al. (1997). Foam and Foam Films: Theory, Experiment, Application.

Fan, G.-j., A. G. H. Wee, et al. (2009). "NMR Studies of Amine Species in MEA-CO2-H2O System: Modification of the Model of Vapor-Liquid Equilibrium (VLE)." Ind. Eng. Chem. Res. FIELD Full Journal Title:Industrial & Engineering Chemistry Research 48(5): 2717-2720.

Figueroa, J. D., T. Fout, et al. (2008). "Advances in CO_2 capture technology—The U.S. Department of Energy's Carbon Sequestration Program." International Journal of Greenhouse Gas Control 2(1): 9-20.

Frailie, P. (2011). Modeling MDEA/PZ Thermodynamics, Hydraulics, and Kinetics. First Quarterly Progress Report 2011, Luminant Carbon Management Program, The University of Texas at Austin, Austin, TX.

Frailie, P., J. Plaza, et al. (2011). "Modeling piperazine thermodynamics." Energy Procedia 4: 35-42.

Freeman, S. (2011). Thermal Degradation and Oxidation of Aqueous Piperazine for Carbon Dioxide Capture. Department of Chemical Engineering. Austin, TX, The University of Texas at Austin. Ph. D. Dissertation.

Freeman, S. and G. T. Rochelle (2009). Degradation of concentrated aqueous PZ in CO_2 capture. The 5th Trondheim Conference on CO_2 Capture, Transport and Storage. Trondheim, Norway.

Freeman, S. A., J. Davis, et al. (2010). "Degradation of aqueous piperazine in carbon dioxide capture." International Journal of Greenhouse Gas Control 4(5): 756-761.

Freeman, S. A., R. Dugas, et al. (2009). "Carbon dioxide capture with concentrated, aqueous piperazine." Energy Procedia 1(1): 1489-1496.

Freeman, S. A., R. Dugas, et al. (2010). "Carbon dioxide capture with concentrated, aqueous piperazine." International Journal of Greenhouse Gas Control 4(2): 119-124.

Freguia, S. and G. T. Rochelle (2003). "Modeling of CO2 capture by aqueous monoethanolamine." AIChE Journal 49(7): 1676-1686.

Gibbins, R. I. C. J., et al. (2005). Maximising the effectiveness of post-combustion CO_2 capture systems. Proceedings of the 7th International Conference on Greenhouse Gas Control Technologies.

Glasscock, D. A. (1990). Modeling and Experimental Study of Carbon Dioxide Absorption into Aqueous Alkanolamines. Department of Chemical Engineering. Austin, TX, The University of Texas at Austin. Ph.D. Dissertation.

Glasscock, D. A. and G. T. Rochelle (1989). "Numerical simulation of theories for gas absorption with chemical reaction." AIChE Journal 35(8): 1271-81.

Gonzenbach, U. T., A. R. Studart, et al. (2006). "Ultrastable particle-stabilized foams." Angewandte Chemie, International Edition 45(21): 3526-3530.

Goto, K., F. A. Chowdhury, et al. (2011). "Development of a low cost CO2 capture system with a novel absorbent under the COCS project." Energy Procedia 4: 253-258.

Hamborg, E. S., J. P. M. Niederer, et al. (2007). "Dissociation Constants and Thermodynamic Properties of Amino Acids Used in CO2 Absorption from (293 to 353) K." Journal of Chemical & Engineering Data 52(6): 2491-2502.

Hansen, J. E., R. Ruedy, et al. (2009). Global Annual Temperature Anomalies (Land + Ocean) (1880-2008). New York, NY, NASA Goddard Institute for Space Studies.

Hartono, A. (2009). Characterization of diethylenetriamine (DETA) as absorbent for CO_2. Chemical Engineering. Trondheim, Norway, Norwegian University of Science and Technology. Ph. D. Dissertation.

Hartono, A., U. E. Aronu, et al. (2011). "Liquid speciation study in amine amino acid salts for CO2 absorbent with ^{13}C-NMR." Energy Procedia 4: 209-215.

Haszeldine, R. S. (2009). "Carbon capture and storage: How green can black be?" Science (Washington, DC, U. S.) FIELD Full Journal Title:Science (Washington, DC, United States) 325(5948): 1647-1652.

Hessen, E. T., T. Haug-Warberg, et al. (2011). "The refined e-NRTL model applied to CO2-H2O-alkanolamine systems." Chemical Engineering Science 65(11): 3638-3648.

Hetzer, H. B., R. A. Robinson, et al. (1968). "Dissociation constants of piperazinium ion and related thermodynamic quantities from 0 to 50.deg." The Journal of Physical Chemistry 72(6): 2081-2086.

Higbie, R. (1935). "The Rate of Absorption of a Pure Gas Into a Still Liquid During Short Periods of Exposure." Trans. Am. Inst. Chem. Engrs. 31: 365-389.

Hilliard, M. D. (2008). A Predictive Thermodynamic Model for an Aqueous Blend of Potassium Carbonate, Piperazine, and Monoethanolamine for Carbon Dioxide Capture from Flue Gas. Department of Chemical Engineering. Austin, TX, The University of Texas at Austin. Ph.D. Dissertation.

Hobler, T. (1966). Mass Transfer and Absorbers Pergamon Press.

Holst, J. v., G. F. Versteeg, et al. (2009). "Kinetic study of CO2 with various amino acid salts in aqueous solution." Chemical Engineering Science 64(1): 59-68.

Hook, R. J. (1997). "An Investigation of Some Sterically Hindered Amines as Potential Carbon Dioxide Scrubbing Compounds." Industrial & Engineering Chemistry Research 36(5): 1779-1790.

House, K. Z., C. F. Harvey, et al. (2009). "The energy penalty of post-combustion CO2 capture & storage and its implications for retrofitting the U.S. installed base." Energy & Environmental Science 2(2): 193-205.

Idem, R., M. Wilson, et al. (2005). "Pilot Plant Studies of the CO2 Capture Performance of Aqueous MEA and Mixed MEA/MDEA Solvents at the University of Regina CO2 Capture Technology Development Plant and the Boundary Dam CO2 Capture Demonstration Plant." Industrial & Engineering Chemistry Research 45(8): 2414-2420.

IEA (2000). Leading options for the capture of CO_2 emissions at power stations. report PH3/14, Feb. 2000, IEA Greenhouse Gas R&D Programme, Cheltenham, UK.

IEA (2004). Improvements in power generation with postcombustion capture of CO_2. report PH4/33, Nov, 2004, IEA Greenhouse Gas R&D Programme, Cheltenham, UK.

IEA (2010). "CO_2 Emissions from Fuel Combustion Highlights (2010 Edition)." International Energy Agency.

IPCC (2005). "Carbon Dioxide Capture and Storage - Bert Metz, Ogunlade Davidson, Heleen de Coninck, Manuela Loos and Leo Meyer (Eds.) " Cambridge University Press, UK: 431.

IPCC (2010). "Climate Change 2007: The Physical Science Basis. Contribution of Working Group I to the Fourth Assessment Report of the Intergovernmental Panel on Climate Change. S. Solomon , D. Qin, M. Manning, Z. Chen, M. Marquis, K.B. Averyt, M. Tignor and H.L. Miller (eds.)." Cambridge University Press. Cambridge, United Kingdom.

Ivanov, I. and D. Dimitrov (1988). "Thin film drainage." Surfactant Science Series 29(Thin Liq. Films): 379-96.

Jakobsen, J. P., E. F. da Silva, et al. (2008). "NMR study and quantum mechanical calculations on the 2-[(2-aminoethyl)amino]-ethanol-H2O-CO2 system." Journal of Magnetic Resonance 191(2): 304-314.

Jakobsen, J. P., J. Krane, et al. (2005). "Liquid-Phase Composition Determination in CO_2-H_2O-Alkanolamine Systems: An NMR Study." Industrial & Engineering Chemistry Research 44(26): 9894-9903.

Jha, B. K., S. P. Christiano, et al. (2000). "Silicone Antifoam Performance: Correlation with Spreading and Surfactant Monolayer Packing." Langmuir 16(26): 9947-9954.

Keeling, R. F., S. C. Piper, et al. (2009). Atmospheric CO2 values (ppmv) derived from in situ air samples collected at Mauna Loa, Hawaii, USA. La Jolla, California USA, Carbon Dioxide Research Group, Scripps Institution of Oceanography (SIO), University of California

Kent, R. L. and B. Eisenberg (1976). "Better data for amine treating." Hydrocarbon Processing (1966-2001) 55(2): 87-90.

Khalili, F., A. Henni, et al. (2009). "pKa Values of Some Piperazines at (298, 303, 313, and 323) K." J. Chem. Eng. Data(54): 2914–2917.

Kierzkowska-Pawlak, H. and A. Chacuk (2011). "Kinetics of CO2 desorption from aqueous N-methyldiethanolamine solutions." Chemical Engineering Journal 168(1): 367-375.

King, C. J. (1966). "Turbulent Liquid Phase Mass Transfer at a Free Gas-Liquid Interface." Ind. Eng. Chem. Fund 5(1): 1-8.

Knudsen, J. N., J. N. Jensen, et al. (2009). "Experience with CO2 capture from coal flue gas in pilot-scale: testing of different amine solvents." Energy Procedia 1(1): 783-790.

Ko, J.-J. and M.-H. Li (2000). "Kinetics of absorption of carbon dioxide into solutions of N-methyldiethanolamine+water." Chemical Engineering Science 55(19): 4139-4147.

Kohl, A. L. and R. B. Nielsen (1997). Gas Purification. Houston, TX, USA, Gulf Professional Publishing.

Konduru, P. B., P. D. Vaidya, et al. (2010). "Kinetics of Removal of Carbon Dioxide by Aqueous Solutions of N,N-Diethylethanolamine and Piperazine." Environmental Science & Technology 44(6): 2138-2143.

Koskela, H. and T. Vaananen (2002). "Quantitative determination of alphatic hydrocarbon compounds by 2D NMR." Magnetic Resonance in Chemistry 40: 705-715.

Krishna, R. (1977). "A generalized film model for mass transfer in non-ideal fluid mixtures." Chemical Engineering Science 32(6): 659-667.

Krishna, R. and G. L. Standart (1976). "A multicomponent film model incorporating a general matrix method of solution to the Maxwell-Stefan equations." AIChE Journal 22(2): 383-389.

Krishna, R. and J. A. Wesselingh (1997). "The Maxwell-Stefan approach to mass transfer." Chemical Engineering Science 52(6): 861-911.

Kucka, L., I. Muller, et al. (2003). "On the modelling and simulation of sour gas absorption by aqueous amine solutions." Chemical Engineering Science 58(16): 3571-3578.

Kucka, L., J. Richter, et al. (2003). "Determination of gas-liquid reaction kinetics with a stirred cell reactor." Separation and Purification Technology 31(2): 163-175.

Lewis, W. K. and W. G. Whitman (1924). "Principles of Gas Absorption." Industrial & Engineering Chemistry 16: 1215-1220.

Li, M.-H. and B.-C. Chang (1994). "Solubilities of Carbon Dioxide in Water + Monoethanolamine + 2-Amino-2-methyl-1-propanol." Journal of Chemical and Engineering Data 39(3): 448-52.

Littel, R. J., W. P. M. Van Swaaij, et al. (1990). "Kinetics of carbon dioxide with tertiary amines in aqueous solution." AIChE Journal 36(11): 1633-40.

Littel, R. J., G. F. Versteeg, et al. (1992). "Kinetics of CO2 with primary and secondary amines in aqueous solutions--I. Zwitterion deprotonation kinetics for DEA and DIPA in aqueous blends of alkanolamines." Chemical Engineering Science 47(8): 2027-2035.

Liu, Y., L. Zhang, et al. (1999). "Representing Vapor-Liquid Equilibrium for an Aqueous MEA-CO_2 System Using the Electrolyte Nonrandom-Two-Liquid Model." Industrial & Engineering Chemistry Research 38(5): 2080-2090.

Luthi, D., M. Le Floch, et al. (2008). "High-resolution carbon dioxide concentration record 650,000-800,000 years before present." Nature 453(7193): 379-82.

Ma'mun, S., H. F. Svendsen, et al. (2006). "Selection of new absorbents for carbon dioxide capture." Energy Conversion and Management 48(1): 251-258.

Maloney, M. D., R. A. Gardiner, et al. (2010). "Post combustion carbon capture by solvent scrubbing - demonstration and verification." Int. Tech. Conf. Clean Coal Fuel Syst. 35: 987-998.

Mandal, B. P. and S. S. Bandyopadhyay (2006). "Absorption of carbon dioxide into aqueous blends of 2-amino-2-methyl-1-propanol and monoethanolamine." Chemical Engineering Science 61(16): 5440-5447.

Mandal, B. P., A. K. Biswas, et al. (2003). "Absorption of carbon dioxide into aqueous blends of 2-amino-2-methyl-1-propanol and diethanolamine." Chemical Engineering Science 58(18): 4137-4144.

Mangalapally, H. P. and H. Hasse (2011). "Pilot Plant Experiments for Post Combustion Carbon Dioxide Capture by Reactive Absorption with Novel Solvents." Energy Procedia 4(4): 1-8.

Martin, J. L., F. D. Otto, et al. (1978). "Solubility of hydrogen sulfide and carbon dioxide in a diglycolamine solution." Journal of Chemical and Engineering Data 23(2): 163-4.

McCarthy, J. and M. A. Trebble (1996). "An experimental investigation into the foaming tendency of diethanolamine gas sweetening solutions." Chemical engineering communications(Print) 144: 159-171.

Mimura, T., T. Nojo, et al. (2003). Recent developments in flue gas CO2 recovery technology. Greenhouse Gas Control Technologies

Proceedings of the 6th International Conference on Greenhouse Gas Control Technologies (GHGT-6), Kyoto, Japan, Elsevier Science Ltd, Oxford, UK.

Mshewa, M. M. (1995). Carbon Dioxide Desorption/Absorption with Aqueous Mixtures of Methyldiethanolamine and Diethanolamine at 40 to 120C. Chemical Engineering. Austin, TX, The University of Texas at Austin. Ph. D.

Mshewa, M. M. (1995). Carbon Dioxide Desorption/Absorption with Aqueous Mixtures of Methyldiethanolamine and Diethanolamine at 40 to 120C. Chemical Engineering. Austin, TX, The University of Texas at Austin. Ph. D. Dissertation.

NETL (2002). Advanced fossil power systems comparison study. Final report prepared for NETL by E.L. Parsons (NETL, Morgantown, WV), W.W. Shelton and J.L. Lyons (EG&G Technical Services, Inc., Morgantown, WV), December.

Nguyen, T. (2010). Amine Volatility, First Quarterly Progress Report 2010, Luminant Carbon Management Program. The University of Texas at Austin.

Notz, R., N. Asprion, et al. (2006). "Selection and pilot plant tests of new absorbents for post combustion carbon dioxide capture." Inst. Chem. Eng. Symp. Ser. 152: 132-141.

Okoye, C. I. (2005). Carbon Dioxide Solubility and Absorption Rate in Monoethanolamine/Piperazine/H2O. Chemical Engineering. Austin, TX, The University of Texas at Austin. Ph. D.

Orr, J. F. M. (2009). "CO_2 capture and storage: are we ready?" Energy & Environmental Science 2(5): 449-458.

Oyenekan, B. A. and G. T. Rochelle (2006). "Energy Performance of Stripper Configurations for CO_2 Capture by Aqueous Amines." Industrial & Engineering Chemistry Research 45(8): 2457-2464.

Pacheco, M. A. (1998). Mass Transfer, Kinetics and Rate-based Modeling of Reactive Absorption. Chemical Engineering. Austin, TX, The University of Texas at Austin. Ph. D.

Pacheco, M. A. (1998). Mass Transfer, Kinetics and Rate-based Modeling of Reactive Absorption. Chemical Engineering. Austin, TX, The University of Texas at Austin. Ph.D. Dissertation.

Park, J.-Y., S. J. Yoon, et al. (2003). "Effect of Steric Hindrance on Carbon Dioxide Absorption into New Amine Solutions: Thermodynamic and Spectroscopic Verification through Solubility and NMR Analysis." Environmental Science and Technology 37(8): 1670-1675.

Park, J.-Y., S. J. Yoon, et al. (2003). "Effect of Steric Hindrance on Carbon Dioxide Absorption into New Amine Solutions: Thermodynamic and Spectroscopic Verification through Solubility and NMR Analysis." Environ. Sci. Technol. FIELD Full Journal Title:Environmental Science and Technology 37(8): 1670-1675.

Park, S.-W., Y.-S. Son, et al. (2008). "Absorption of Carbon Dioxide into Aqueous Solution of Sodium Glycinate." Separation Science and Technology 43(11): 3003-3019.

Parsons Infrastructure & Technology Group, I. (2002). Updated cost and performance estimates for fossil fuel power plants with CO_2 removal. Report under Contract No. DE-AM26-99FT40465 to U.S.DOE/NETL, Pittsburgh, PA, and EPRI, Palo Alto, CA.

Paul, S., A. K. Ghoshal, et al. (2008). "Absorption of Carbon Dioxide into Aqueous Solutions of 2-Piperidineethanol: Kinetics Analysis." Industrial & Engineering Chemistry Research 48(3): 1414-1419.

Paul, S., A. K. Ghoshal, et al. (2009). "Absorption of Carbon Dioxide into Aqueous Solutions of 2-Piperidineethanol: Kinetics Analysis." Industrial & Engineering Chemistry Research 48(3): 1414-1419.

Paul, S., A. K. Ghoshal, et al. (2009). "Kinetics of absorption of carbon dioxide into aqueous solution of 2-(1-piperazinyl)-ethylamine." Chemical Engineering Science 64(2): 313-321.

Paul, S., A. K. Ghoshal, et al. (2009). "Kinetics of absorption of carbon dioxide into aqueous solution of 2-(1-piperazinyl)ethylamine." Chemical Engineering Science 64(2): 313-321.

Paul, S., A. K. Ghoshal, et al. (2009). "Kinetics of absorption of carbon dioxide into aqueous solutions of 2-amino-2-hydroxymethyl-1,3-propanediol." Separation and Purification Technology 68(3): 422-427.

Pauley, C. R. (1991). "Face the facts about amine foaming." Chemical Engineering Progress 87(7): 33-8.

Pauley, C. R., R. Hashemi, et al. (1989). "Analysis of foaming mechanisms in amine plants." Proceedings - Laurance Reid Gas Conditioning Conference: 219-47.

Pauley, C. R., R. Hashemi, et al. (1989). "Ways to control amine unit foaming offered." Oil & Gas Journal 87(50): 67-75.

Pigford, R. L. (1941). Counter-Diffusion in a Wetted Wall Column. Chemistry. Urbana, The University of Illinois. Ph. D. Thesis**:** 107.

Pitzer, K. S. (1973). "Thermodynamics of electrolytes. I. Theoretical basis and general equations." The Journal of Physical Chemistry 77(2): 268-277.

Plaza, J. M., E. Chen, et al. Pilot plant studies of CO2 capture using concentrated piperazine, American Chemical Society.

Plaza, J. M., D. V. Wagener, et al. (2009). "Modeling CO2 capture with aqueous monoethanolamine." Energy Procedia 1(1): 1171-1178.

Posey, M. L. (1996). Thermodynamic Model for Acid Gas Loaded Aqueous Alkanolamine Solutions. Department of Chemical Engineering. Austin, TX, The University of Texas at Austin. Ph. D. Dissertation.

Pugh, R. J. (1996). "Foaming, foam films, antifoaming and defoaming." Advances in Colloid and Interface Science 64: 67-142.

Puxty, G., R. Rowland, et al. (2009). "Carbon Dioxide Postcombustion Capture: A Novel Screening Study of the Carbon Dioxide Absorption Performance of 76 Amines." Environmental Science & Technology 43(16): 6427-6433.

Puxty, G., R. Rowland, et al. (2010). "Comparison of the rate of CO2 absorption into aqueous ammonia and monoethanolamine." Chemical Engineering Science 65(2): 915-922.

Ramachandran, N., A. Aboudheir, et al. (2006). "Kinetics of the Absorption of CO2 into Mixed Aqueous Loaded Solutions of Monoethanolamine and Methyldiethanolamine." Industrial & Engineering Chemistry Research 45(8): 2608-2616.

Rao, A. B. and E. S. Rubin (2002). "A Technical, Economic, and Environmental Assessment of Amine-Based CO2 Capture Technology for Power Plant Greenhouse Gas Control." Environmental Science & Technology 36(20): 4467-4475.

Renon, H. and J. M. Prausnitz (1968). "Local Compositions in Thermodynamic Excess Functions for Liquid Mixtures." AIChE Journal 14(1): 135-144.

Robinson, K., A. McCluskey, et al. (2011). "The effect molecular structural variations has on the CO2 absorption characteristics of heterocyclic amines." Energy Procedia 4: 224-231.

Rochelle, G., E. Chen, et al. "Aqueous piperazine as the new standard for CO_2 capture technology " Chemical Engineering Journal In press.

Rochelle, G. T. (2009). "Amine Scrubbing for CO2 Capture." Science (Washington, DC, United States) 325(5948): 1652-1654.

Rochelle, G. T., S. Bishnoi, et al. (2001). Research Needs for CO_2 Capture from Flue Gas by Aqueous Absorption/Stripping. Final report for P.O. No. DE-AF26-99FT01029. F. E. T. C. U.S. Department of Energy, Pittsburgh, PA 15236. Austin, Texas 78712, The University of Texas at Austin.

Rowland, R., Q. Yang, et al. (2011). "Amine mixtures and the effect of additives on the CO2 capture rate." Energy Procedia 4: 195-200.

Rubin, E. S., C. Chen, et al. (2007). "Cost and performance of fossil fuel power plants with CO2 capture and storage." Energy Policy 35(9): 4444-4454.

Saha, A. K. and S. S. Bandyopadhyay (1995). "Kinetics of absorption of CO_2 into aqueous solutions of 2-amino-s-methyl-1-propanol." Chemical Engineering Science 50(22): 3587-98.

Samanta, A. and S. S. Bandyopadhyay (2007). "Kinetics and modeling of carbon dioxide absorption into aqueous solutions of piperazine." Chemical Engineering Science 62(24): 7312-7319.

Samanta, A. and S. S. Bandyopadhyay (2009). "Absorption of carbon dioxide into aqueous solutions of piperazine activated 2-amino-2-methyl-1-propanol." Chemical Engineering Science 64(6): 1185-1194.

Samanta, A. and S. S. Bandyopadhyay (2011). "Absorption of carbon dioxide into piperazine activated aqueous N-methyldiethanolamine." Chemical Engineering Journal In Press.

Sandler, S. R. and M. L. Delgado (1969). "Reinvestigation of the Reaction of Piperazine with Aldehydes." Journal of Polymer Science: Part A-1 7: 1373-1378.

Sartori, G. and D. W. Savage (1983). "Sterically hindered amines for carbon dioxide removal from gases." Industrial & Engineering Chemistry Fundamentals 22(2): 239-49.

SDBS (2011). Spectral Database for Organic Compounds SDBS, National Institute of Advanced Industrial Science and Technology (Japan).

Seiersten, M. (2001). Material selection for separation, transportation and disposal of CO_2. Proceedings Corrosion 2001, National Association of Corrosion Engineers.

Sexton, A. (2008). Amine oxidation in CO_2 capture processes. Department of Chemical Engineering. Austin, TX, the University of Texas at Austin. Ph.D. Dissertation.

Shoulder, B. (2011). Personal Communication. Department of Chemistry and Biochemistry, The University of Texas at Austin, Austin, TX.

Simbeck, D. R. (2002). New power plant CO2 mitigation costs. Mountain View, California, SFA Pacific, Inc.

Simbeck, D. R. a. M. M. (2001). Existing coal power plant retrofit CO2 control options analysis. Proceedings of the 5th International Conference on Greenhouse Gas Control Technologies, Cairns, Australia, CSIRO Publishing, Collingwood, Vic., Australia.

Simons, K., W. Brilman, et al. (2011). "Kinetics of CO2 Absorption in Aqueous Sarcosine Salt Solutions: Influence of Concentration, Temperature, and CO2 Loading." Industrial & Engineering Chemistry Research 49(20): 9693-9702.

Singh, D., E. Croiset, et al. (2003). "Techno-economic study of CO2 capture from an existing coal-fired power plant: MEA scrubbing vs. O2/CO2 recycle combustion." Energy Conversion and Management 44(19): 3073-3091.

Singh, P., D. W. F. Brilman, et al. (2009). "Solubility of CO_2 in aqueous solution of newly developed absorbents." Energy Procedia 1(1): 1257-1264.

Singh, P., J. P. M. Niederer, et al. (2007). "Structure and activity relationships for amine based CO_2 absorbents-I." International Journal of Greenhouse Gas Control 1(1): 5-10.

Singh, P., J. P. M. Niederer, et al. (2009). "Structure and activity relationships for amine-based CO_2 absorbents-II." Chemical Engineering Research and Design 87(2): 135-144.

Snijder, E. D., M. J. M. te Riele, et al. (1993). "Diffusion coefficients of several aqueous alkanolamine solutions." Journal of Chemical & Engineering Data 38(3): 475-480.

Soave, G. (1972). "Equilibrium Constants for Modified Redlich Kwong Equation of State." Chemical Engineering Science 27: 1196-1203.

Spooner, B., M. Sheilan, et al. (2006). "Iron Sulphides-Friend or Foe?" Proceedings of the Laurance Reid Gas Conditioning Conference 2006: 109.

Stephens, E. J. and G. A. Morris (1951). "Determination of Liquid Film Absorption Coefficients." Chem. Eng. Progr 47: 232.

Stewart, E. J. and R. A. Lanning (1994). "Reduce Amine Plant Solvent Losses." Hydrocarbon Processing 73(5): 67-81.

Stobbs, R. and P. Clark (2005). Canadian Clean Power Coalition: The Evaluation of Options for CO2 Capture From Existing and New Coal-Fired Power Plants. Proceedings of 7th International Conference on Greenhouse Gas Control Technologies, Elsevier Science, Oxford, UK.

Suda, T., T. Iwaki, et al. (1996). "Facile determination of dissolved species in CO2-Amine-H2O system by NMR spectroscopy." Chem. Lett. FIELD Full Journal Title:Chemistry Letters(9): 777-778.

Sun, W.-C., C.-B. Yong, et al. (2005). "Kinetics of the absorption of carbon dioxide into mixed aqueous solutions of 2-amino-2-methyl-l-propanol and piperazine." Chemical Engineering Science 60(2): 503-516.

Taylor, R. and R. Krishna (1993). Multicomponent Mass Transfer. New York, John Wiley & Sons, Inc.

Thitakamol, B. and A. Veawab (2008). "Foaming Behavior in CO_2 Absorption Process Using Aqueous Solutions of Single and Blended Alkanolamines." Industrial & Engineering Chemistry Research 47(1): 216-225.

Tobiesen, F. A., H. F. Svendsen, et al. (2007). "Experimental validation of a rigorous absorber model for CO2 postcombustion capture." AIChE Journal 53(4): 846-865.

Vaidya, P. D. and E. Y. Kenig (2007). "Acceleration of CO2 Reaction with N,N-Diethylethanolamine in Aqueous Solutions by Piperazine." Industrial & Engineering Chemistry Research 47(1): 34-38.

Vaidya, P. D. and E. Y. Kenig (2007). "Gas-Liquid reaction Kinetics: A Review of Determination Methods." Chemical Engineering Communications 194(12): 1543-1565.

Versteeg, G. F., L. A. J. Van Dijck, et al. (1996). On the Kinetics Between CO_2 and Alkanolamines Both in Aqueous and Non-Aqueous Solutions. an Overview, Taylor & Francis. 144**:** 113 - 158.

Versteeg, G. F. and W. P. M. Van Swaaij (1988). "On the kinetics between carbon dioxide and alkanolamines both in aqueous and non-aqueous solutions - II. Tertiary amines." Chemical Engineering Science 43(3): 587-91.

Versteeg, G. F. and W. P. M. van Swaaij (1988). "On the kinetics between CO2 and alkanolamines both in aqueous and non-aqueous solutions--I. Primary and secondary amines." Chemical Engineering Science 43(3): 573-585.

Versteeg, G. F. and W. Van Swaalj (1988). "Solubility and diffusivity of acid gases (carbon dioxide, nitrous oxide) in aqueous alkanolamine solutions." Journal of Chemical & Engineering Data 33(1): 29-34.

von Phul, S. A. (2001). "Sweetening Process Foaming and Abatement." Proceedings of the Laurance Reid Gas Conditioning Conference: 251-280.

Wasan, D. T., K. Koczo, et al. (1994). "Mechanisms of aqueous foam stability and antifoaming action with and without oil:A thin-film approach." Advances in Chemistry Series 242(Foams: Fundamentals and Applications in the Petroleum Industry): 47-114.

Wilke, C. R. and P. Chang (1955). "Correlation of diffusion coefficients in dilute solutions." AIChE Journal 1(2): 264-270.

Wilson, G. M. (1964). "Vapor-Liquid Equilibrium. XI. A New Expression for the Excess Free Energy of Mixing." J. Am. Chem. Soc. 86(2): 127-130.

Xu, G., C. Zhang, et al. (1992). "Kinetics study on absorption of carbon dioxide into solutions of activated methyldiethanolamine." Industrial & Engineering Chemistry Research 31(3): 921-7.

Xu, Q. and G. Rochelle (2011). "Total pressure and CO2 solubility at high temperature in aqueous amines." Energy Procedia 4: 117-124.

Xu, S., Y. W. Wang, et al. (1993). "Kinetics of the reaction of carbon dioxide with aqueous 2-piperidineethanol solutions." AIChE Journal 39(10): 1721-5.

Yamada, H., S. Shimizu, et al. (2010). "Prediction of the Basicity of Aqueous Amine Solutions and the Species Distribution in the Amin-H_2O-CO_2 System Using the COSMO-RS Method." Industrial & Engineering Chemistry Research(49): 2449-2455.

Yamada, H., S. Shimizu, et al. (2010). "Prediction of the Basicity of Aqueous Amine Solutions and the Species Distribution in the Amine-H2O-CO2 System Using the COSMO-RS Method." Ind. Eng. Chem. Res. FIELD Full Journal Title:Industrial & Engineering Chemistry Research 49(5): 2449-2455.

Yang, Q., M. Bown, et al. (2009). "A carbon-13 NMR study of carbon dioxide absorption and desorption with aqueous amine solutions." Energy Procedia FIELD Full Journal Title:Energy Procedia 1(1): 955-962.

Yokoyama, K., S. Takamoto, et al. (2011). "Hitachi's carbon dioxide scrubbing technology with new absorbent for coal-fired power plants." Energy Procedia 4(4): 245-252.

Yoon, J.-H., J.-I. Baek, et al. (2003). "Kinetics of removal of carbon dioxide by aqueous 2-amino-2-methyl-1,3-propanediol." Chemical Engineering Science 58(23-24): 5229-5237.

Yoon, S. J. and H. Lee (2003). "Substituent effect in amine-CO2 interaction investigated by NMR and IR spectroscopies." Chem. Lett. 32(4): 344-345.

Zhang, P., Y. Shi, et al. (2007). "Kinetics region and model for mass transfer in carbon dioxide absorption into aqueous solution of 2-amino-2-methyl-1-propanol." Separation and Purification Technology 56(3): 340-347.

Zhang, X., C.-F. Zhang, et al. (2001). "A Kinetics Study on the Absorption of Carbon Dioxide into a Mixed Aqueous Solution of Methyldiethanolamine and Piperazine." Industrial & Engineering Chemistry Research 40(17): 3785-3791.

Zhang, Y. and C.-C. Chen (2011). "Thermodynamic Modeling for CO2 Absorption in Aqueous MDEA Solution with Electrolyte NRTL Model." Industrial & Engineering Chemistry Research 50(1): 163-175.

Vita

Xi Chen was born in Fujian, China in 1981 to Lianghua Chen and Hongyu Fan. After graduating from the 1st high school of Xianyou in 1998, he enrolled at Tsinghua University in Beijing, P.R. China. He received his B.E. in Chemical Engineering in 2002 and M.S. in Materials Science in 2005. After that, he was accepted to the graduate Chemical Engineering program in The University of Texas at Austin. Upon completing master degree work in August 2008, he joined Dr. Gary T. Rochelle's research group to pursue his Ph.D. degree. He has accepted full-time employment with Alstom Power in Knoxville, TN.

Permanent email: chenxi02@gmail.com

This dissertation was typed by the author.